DEUTSCHES ELEKTRONEN-SYNCHROTRON **DESY**

DESY 79/48
August 1979

Proceedings of the
STUDY OF AN ep FACILITY FOR EUROPE
DESY Hamburg, April 2 and 3, 1979

U. Amaldi
(Editor)

NOTKESTRASSE 85 · 2 HAMBURG 52

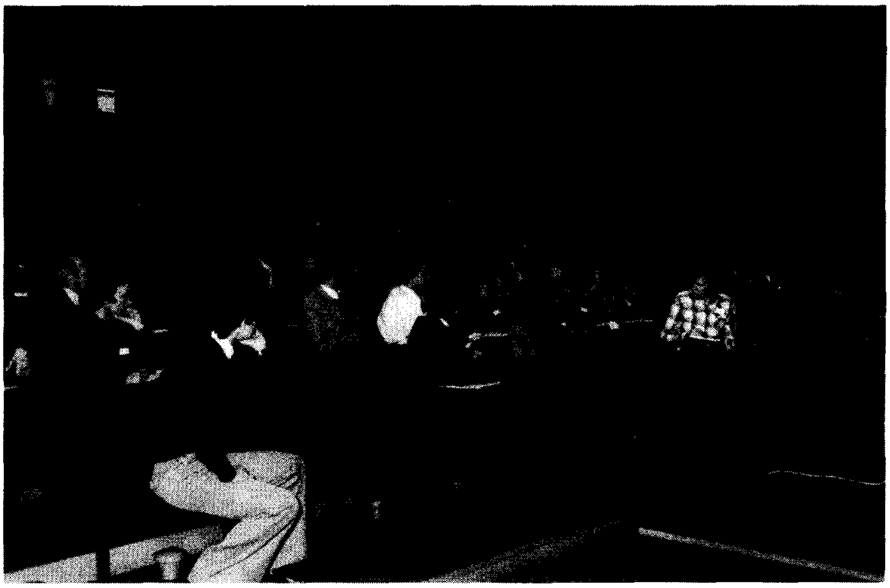

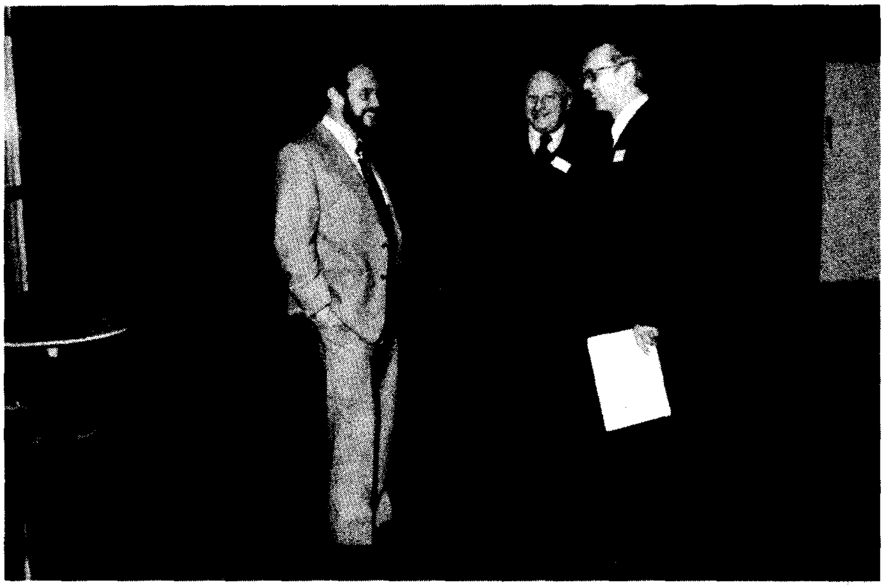

CONTENT

GENERALITIES ON THE STUDY OF AN ELECTRON-PROTON FACILITY FOR EUROPE

Ugo Amaldi

CERN, Geneva

In September 1978 the European Committee for Future Accelerators decided to organize, in collaboration with DESY, a study of the physics interest and of the technical feasibility of an electron-proton facility to complement the European program, which in the eighties will be centered around the electron-positron storage ring LEP. The following Organizing Committee was formed, under the chairmanship of M. Vivargent: A. Bohr, N. Cabibbo, M. Jacob, J. Mulvey, J. Perez y Jorba, A. Salam, H. Schopper, J.J. Thresher, B.H. Wiik and A. Zichichi. P. von Handel and myself agreed to act as organizational and scientific secretaries, respectively.

In Europe electron-proton colliders have been studied with great interest since many years. In DESY first reports were published in 1972-73(1) and in October 1973 a special seminar was organized in Hamburg(2). Electron-proton facilities were later considered at the Rutherford Laboratory(3) and at CERN(4). More recently the physics of such machines was discussed in detail by C.H. Llewellyn-Smith and B.H. Wiik(5), and a comprehensive report was issued by a working group set up by ECFA, with a strong CERN participation, to study the interest and the feasibility of colliding electrons with the protons circulating in the CERN SPS(6). The work was concluded by an ECFA Study Week on Electron-Proton Storage Rings organized by the Rutherford Laboratory at Milton Hill House, Steventon

(10-14 October 1977). The outcome of all this work, the "CHEEP report" of reference 6, covers theoretical, experimental and technical aspects and has been extensively used in the present study of an Electron-Proton Facility for Europe.

Our study aimed to reassess the physics relevance and the technical problems of an electron-proton project, taking into account the new high energy machines that will be available in the eighties: LEP in primis, together with the Proton-Antiproton Collider, the Energy Doubler, Isabelle, and UNK. The main project under consideration was PROPER, the electron-proton facility obtainable by constructing a superconducting storage ring for protons in the tunnel of PETRA. This would allow the collision of polarized electrons (and positrons) of about 20 GeV with protons of about 300 GeV. At the same time, the physics groups were required by ECFA to consider also the interest in colliding the protons of the CERN SPS (maximum energy about 400 GeV) with the electrons and the positrons of LEP (maximum energy about 100 GeV). For this reason many reports and discussions appearing in these proceedings consider ep collisions ranging from about (20 + 300) GeV to about (100 + 400) GeV. However, the lack of time did not allow a careful consideration of the higher energy possibilities, and studies are continuing while this volume is appearing.

The time scale of the study was relatively short: four months between the first meeting of the Organizing Committee and the two days of presentation and discussion in Hamburg, on the 2nd and 3rd of April 1979. It was in fact decided to have an early meeting for the first open discussions and to continue later going deeper into the problems, if so decided by DESY and ECFA. The program of the meeting is reproduced in the tables.

FIRST DAY : technical aspects

Rapporteur	Discussion Leader	Topic
K. Steffen K. Hübner	G.-A. Voss	ep projects under discussion possibilities and limitations of ep machines
A.V. Tollestrup W. Sampson J. Pérot L. Resegotti	H. Schopper	superconducting magnets
H. Hahn B. Montague D.B. Thomas A.V. Tollestrup G.-A. Voss	H. Schopper	panel discussion on technical problems

The first day of the meeting was devoted to the technical aspects. K. Steffen reviewed the ep projects under discussion and K. Hübner discussed the possibilities and limitations of these colliders. Other contributions were presented in this session and appear in the proceedings. In the next session four speakers presented the status of the art of making superconducting magnets in various laboratories. A.V. Tollestrup spoke of the Fermilab magnets, W. Sampson discussed the solutions adopted at Brookhaven, J. Pérot (Saclay) spoke for the GESSS collaboration and E. Resegotti reviewed the lines followed at CERN. Various technical aspects were clarified in a lively panel discussion chaired by H. Schopper.

SECOND DAY : physics issues

Rapporteur	Discussion Leader	Topic
R.J. Cashmore	L.M. Sehgal	new currents and new particles
C.T. Sachrajda	D.H. Perkins	large q^2 physics and hadron structure
W. Hoogland	M. Greco	small q^2 physics and photoproduction
R. Turlay	K. Tittel	detectors for charged current events
P.G. Innocenti	M. Holder	detectors for neutral current events

For the physics subjects, discussed on the second day, a different format was chosen. The arguments presented had been prepared during the previous months in five working groups, each one organized by a Discussion Leader and a Rapporteur. The first three subjects refer to the physics potentials of an electron-proton machine and, when possible, to the comparison with similar physics that could be produced at other types of accelerators. The two subjects "new currents and new particles" and "large q^2 physics and hadron structure" had already been treated by Llewellyn-Smith and Wiik[(5)] and by the CHEEP report[(6)], so that the main point here was to review these on the basis of the latest experimental and theoretical acquisitions. The third subject, "small q^2 physics and photoproduction", had never been examined in depth before and, albeit not the main argument in favour of this kind of accelerator, it was felt worthwhile to go carefully into it. The written report appearing in the proceedings shows that this was indeed done.

The detector problems were, somewhat arbitrarily, divided between two groups. It has to be stressed that the CHEEP report describes only a non-magnetic detector that can be fitted into the SPS tunnel, so that the groups had ample space for considering more ambituous detectors. The written reports show, not only that the groups have looked into the feasibility of various magnetic detectors, but also that new insight has been gained on how to deal with the particular kinematics of the reactions, particularly in the case of charged current events having an undetectable neutrino in the final state.

In these proceedings, for every session of the meeting we reproduce (i) the talk of the Rapporteur, (ii) a summary of the discussion (that was recorded during the meeting), (iii) the comments of the Discussion Leader on the subject discussed and, when it was felt useful, a list of the problems that are still open. In some cases some particularly interesting individual contributions have also been included.

Since no list of "generally agreed" conclusions can give full justice to a very open discussion meeting, all this material is offered to the attention of the European physicists as a faithful collection of the arguments that have been put forward and are relevant to the choice of an electron-proton facility as an essential part of the European high energy physics program in the eighties. After the meeting, the Discussion Leaders and the Rapporteurs discussed the outcome of the meeting. Their preliminary conclusions were presented by me at the Plenary ECFA meeting held at DESY on May 11, 1979. They can be summarized as follows:

a) the technical problems connected with the mass production of superconducting magnets are about to be solved in the States for fields around 5 Tessla. Higher fields can now also be envisaged;

b) the physics argument presented and discussed at the meeting confirmed that an electron-proton collider is ideal for studying strong interactions;

c) such a machine provides a unique opening on new phenomena, particularly in the field of weak interactions: new charged intermediate bosons, right-handed weak currents, new leptons, subquarks, etc. This opening would be favoured by energies somewhat higher than the "standard" PROPER energy: (17.5 + 280) GeV;

d) a high degree of polarization of the electron and positron beams is essential for the study of weak interactions;

e) at the meeting it was shown that detectors can be built to reveal and accurately measure the kinematical variables of neutral current <u>and</u> charged current events;

f) an electron-proton facility is complementary to the other accelerators that will be working in the eighties and, together with LEP, will offer to the European physicists a rich and balanced program.

After the meeting, ECFA and DESY agreed with the positive spirit of these conclusions and decided to pursue the study.

The merit of the perfect organization of the meeting goes to Peter von Handel and to the enthousiastic staff around him. I am also very grateful to Mrs. M. Stuckenberg, who took care of the printing of the proceedings.

REFERENCES

(1) H. Gerke, H. Wiedemann, G. Wolf, Int. Bericht DESY H-72/22.

M. Tigner, DESY Techn. Notiz 2/73.

(2) Proceedings of the Seminar on e-p and e-e Storage Rings, DESY 73/66.

(3) "A Feasibility Report for Colliding Beam Facilities - EPIC", Rutherford Laboratory Report RL-74-124, 1976.

(4) "The Physics Interest of a 10 TeV Proton Synchrotron, 400 x 400 GeV^2 Proton Storage Rings and Electron-Proton Storage Rings", CERN Yellow Report 76-12.

(5) C.H. Llewellyn-Smith and B.H. Wiik, "Physics with Large Electron-Proton Colliding Beams", DESY 77/38 (June 1977).

(6) J. Ellis, B.H. Wiik and K. Hübner (editors), "CHEEP, an e-p Facility in the SPS", CERN Yellow Report 78-02 (1978).

SESSION ON MACHINE PROBLEMS

Discussion Leader: G. A. Voss

Scientific Secretary: R. Kose

ep PROJECTS UNDER DISCUSSION

by

K. Steffen

List of ep projects and references

A list of the seven ep projects under discussion, including e- and p-energies, CM energy and design luminosity, is given in Tab. 1.
Tab. 2 gives the references used in preparing the subsequent summary description of the individual projects.

Table 1 Current ep colliding beam proposals

Proposal	E_e [GeV]	E_p [GeV]	$\sqrt{S}$ [GeV]	L_{max} [cm^{-2} sec^{-1}]
UNK	20	3000	490	10^{32}
CERN	80 (LEP)	270 (SPS)	294	$1.7 \cdot 10^{32}$
FERMILAB	11.5	1000 (ED)	214	10^{32}
ISABELLE	15	400	155	$0.5 \cdot 10^{32}$
DESY	17.5 (PETRA) [→45?]	280	140 [→225?]	$4 \cdot 10^{32}$
SLAC-LRL	15 (PEP)	300	134	10^{32}
TRISTAN	16	70/200	67/113	$0.6 \cdot 10^{32}$

Table 2 ep References

UNK	L. Fedotov (rapporteur): IEEE Transact. on Nucl. Science, Vol. NS-24, No. 3, p. 1900 (June 1977)
CERN	A. Hutton: CERN-ISR-TH/79-13 (March 1979)
FERMILAB	A. Ruggiero: Report on group study on ep colliding beam facility, Batavia (April 1978)
ISABELLE	Proposal BNL 50648, Brookhaven (April 1977)
DESY	E. Dasskowski et al.: DESY 78/02 (January 1978)
SLAC-LRL	A. Garren et al.: Proceedings of the 1979 National Accelerator Conference, San Francisco (March 1979)
TRISTAN	S. Kamada et al.: IEEE Transact. on Nuclear Science, Vo. NS-24, No.3, p. 1194 (June 1977)

U N K ep project (Serpuchov; design to be finished this year)

Proton accel. to 1.5 GeV in FAST BOOSTER	$1.7 \cdot 10^{12}$ ppp rep. freq. 20 Hz
Proton accel. to 70 GeV in U-70 SYNCHROTRON	injected: 30 pulses in 15 sec $N_p = 5 \cdot 10^{13}$, $\varepsilon = 2 \cdot 10^{-6}$ m at 70 GeV: beam debunched and picked up by sawtooth rf with $h = 1$, $f_{rf} = 200$ kHz, $U_{rf} = 17$ kV bunch length $2\ \sigma_S = 150$ m
Proton accel. to 200 GeV in UNK iron ring (1st stage) (aperture 10 x 5 cm^2) ($B_{mag} = 16.7$ kG)	injected: 64 x 1 bunch $N_{p,tot} = 3 \cdot 10^{15}$ accel. with $f_{rf} = 1$ MHz, i.e. 64 bunches, 300 m apart
Proton accel. to 2.7 - 3 TeV in UNK supercond. ring (2nd stage) (aperture 7 x 6 cm^2) ($B_{mag} = 4.5 - 5$ T; NbTi coils)	accel. of the 64 bunches, i. e. $3 \cdot 10^{15}$ protons with $f_{rf} = 1$ MHz in 30 min to 3000 GeV
Electron accel. to 20 GeV in UNK iron ring (1st stage) (operable with polarised electrons)	e injected from either - a 2 - 3 GeV electron synchrotron or - collected at 10 - 20 GeV from internal target, bombarded with small portions of 3000 GeV protons up to $N_{e,tot} = 3 \cdot 10^{14}$

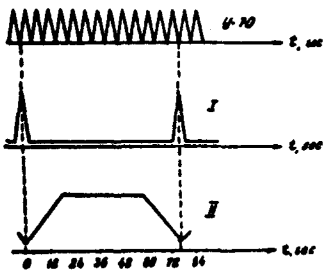

Fig. 1. Operational modes of the UNK

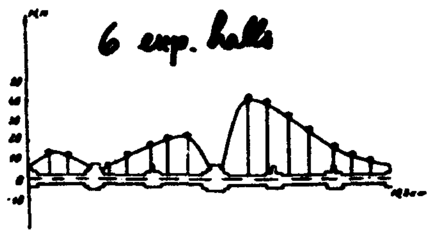

Fig. 3. Elevations of the UNK

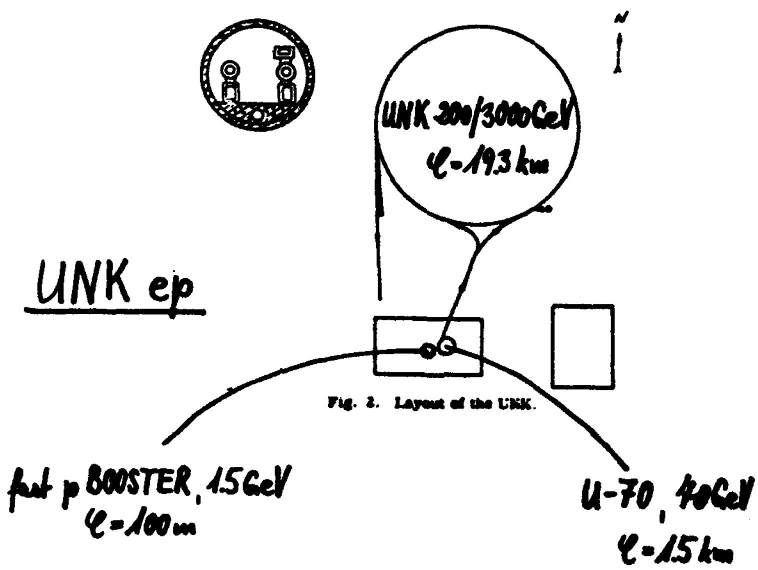

Fig. 2. Layout of the UNK.

C E R N   ep project - one ep insertion (SPS bypass toward LEP)

Proton accel. to 130 - 270 GeV in SPS ($\phi \sim 6.9$ km)

$N_p = 4 \cdot 10^{11}$ per bunch

$n_b = \begin{cases} 50 & \text{in dedicated mode} \\ (10) & \text{in parasitic mode} \end{cases}$

$\varepsilon_x = 20 \cdot 10^{-6}/\beta\gamma$; $\varepsilon_z = 10 \cdot 10^{-6}/\beta\gamma$ [m]

β_x^*, β_z^* optimized as fcts. of E

Electron accel. to 20 - 80 GeV in LEP ($\phi \sim 30.6$ km)

in dedicated mode:

$n_b = 220^*$; N_e optimised as fct. of E

in parasitic mode:

$n_b = (4)$; $N_e = (1.5 \cdot 10^{12} \times E_e/80$ GeV)

$\varepsilon_x = 6.9 \cdot 10^{-8}$ m) independent of E

$\varepsilon_z = 4.3 \cdot 10^{-9}$ m) (wigglers!)

* Comment: $n_b = 220$ is the optimum for all energies since HOM losses and ΔQ_p get smaller for smaller N_e per bunch.

For optimization of parameters, equal tune shifts in x and z (A. Hutton):

$$\frac{\beta_{ex}}{\beta_{ez}} = \left(\frac{\varepsilon_{ex}}{\varepsilon_{ez}} \frac{\varepsilon_{px}^2}{\varepsilon_{pz}^2}\right)^{1/3} ; \qquad \frac{\beta_{px}}{\beta_{pz}} = \left(\frac{\varepsilon_{ex}^2}{\varepsilon_{ez}^2} \frac{\varepsilon_{px}}{\varepsilon_{pz}}\right)^{1/3}$$

max. luminosity L [cm^{-2} sec^{-1}]

	in dedicated mode	in parasitic mode
for ΔQ_p = 0,01	$1.7 \cdot 10^{32}$	$2.8 \cdot 10^{30}$
for ΔQ_p = 0.005	$0.9 \cdot 10^{32}$	$0.8 \cdot 10^{30}$

LEP ep Luminosity

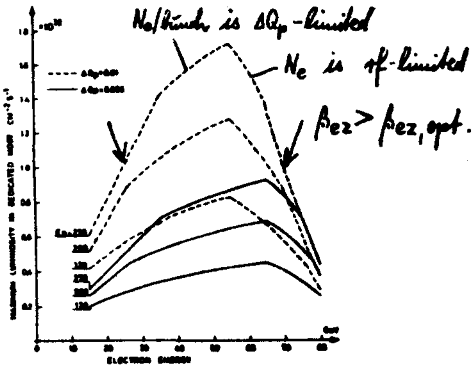

Fig. 4. Maximum luminosity in dedicated mode.

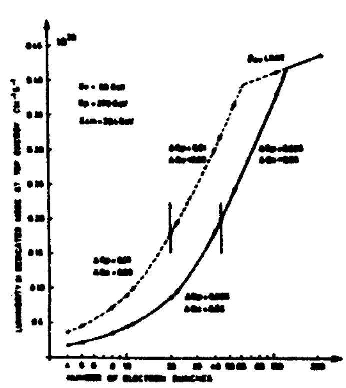

Fig. 3. Luminosity at top energy as a function of the number of electron bunches.

FERMILAB ep project - one ep insertion

(E. D. to be ready 1981)

Proton accel. to 8 GeV in BOOSTER	$2 \cdot 10^{13}$ ppp with $\varepsilon = 1.5 \cdot 10^{-6}$ m at 8 GeV
Proton accel. to 100 GeV in MAIN RING	
Proton accel. to 1000 GeV in ENERGY DOUBLER (E. D.)	No. of pulses from main ring: 1 rf stacking: 10 $I_p = 0.15$ /1.5 A N_p per bunch /$2 \cdot 10^{11}$ $N_{p,tot}$ /$2 \cdot 10^{14}$ $n_b = 1113$ $f_{rf} = 53.1$ MHz; $U_{rf} = 1$ MV at 1000 GeV: $\varepsilon_{x,z} = 1.3 \cdot 10^{-8}$ m $\sigma_S = 50$ cm $\sigma_E/E = 1.2 \cdot 10^{-4}$ $\varepsilon_S =$ /3.8 eV s
Electron accel. to 75 MeV in e-LINAC	specs: rep. freq. 15 Hz pulse length 2 µsec $I_{pulse} = 400$ mA in $\varepsilon = 25 \cdot 10^{-6}$ and $\frac{\sigma_E}{E} = 0.5$ %

Electron accel. to 750 MeV
in ECR
(separate function)

$N_e = 1.1 \cdot 10^{12}$ adiab. captured into 24 bunches with $f_{rf} = 53.1$ MHz; $h = 24$; $U_{rf} = 40$ kV

at 750 MeV:

$\sigma_S = 36$ cm

$\frac{\sigma_E}{E} = 8.5 \cdot 10^{-4}$

$\varepsilon_S = 0.0024$ eV s

rep. freq. 3 Hz

Electron accel. to 4 GeV
in BOOSTER
(combined fct.;
$\alpha_x = -2$, $\alpha_z = 1$, $\alpha_S = 5$)

rep. freq. 15 Hz (i. e. 4 out of 5 cycles without beam)

$f_{rf} = 53.1$ MHz; $h = 84$; $U_{rf} = 1.2$ MV

$n_b = 24$ (60 empty suppressed buckets)

at 4 GeV:

$\varepsilon = 0.5 \quad 10^{-6}$ m;

$\varepsilon_S = 0.0024$ eV s

$\sigma_S = 17.4$ cm

$\frac{\sigma_E}{E} = 5 \cdot 10^{-4}$

Electron accel. to 11.5 GeV
in MAIN RING

injected: 46 pulses of 24 bunches each

$n_b = 1113$

$I_e = 380$ mA

$N_{e,tot} = 5 \cdot 10^{13}$

N_e per bunch: $5 \cdot 10^{10}$

$f_{rf} = 53.1$ MHz; $U_{rf} = 4$ MV

at 11.5 GeV:

rad. loss 2.7 MeV/turn

$P_{syn} = 1$ MW

$$\varepsilon_x = 0.2 \cdot 10^{-6}\ \text{m}$$
$$\varepsilon_z = 0.42 \cdot 10^{-6}\ \text{m}$$
$$\sigma_S = 13\ \text{cm}$$
$$\frac{\sigma_E}{E} = 6 \cdot 10^{-4}$$

Interaction data

	e	p	
crossing angle	2 mrad, horizontal		
β_x^*	0.35 m	5 m	
β_z^*	0.30 m	5 m	
$\Delta\gamma$	0.02	0.001	← small!
L	$\sim 10^{32}\ \text{cm}^{-2}\ \text{sec}^{-1}$		

FERMILAB ep scheme

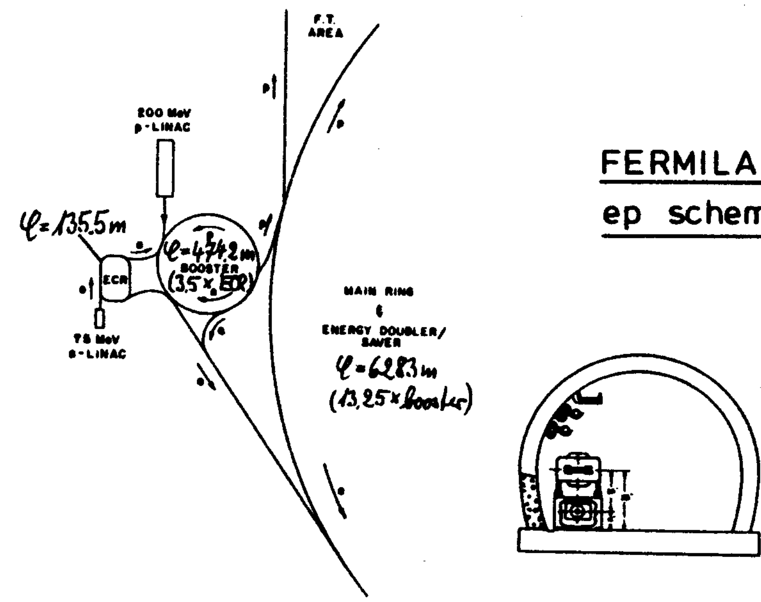

Fig. II-1. The e-p Scheme Layout

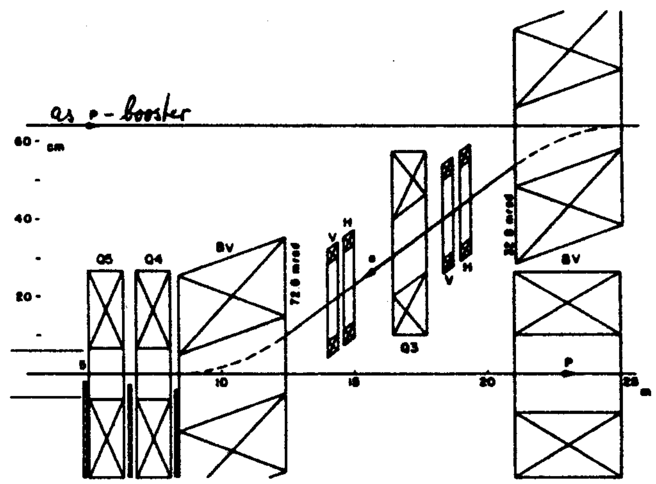

Fig. VIII-1. Half of the e-p Colliding Region.

I S A B E L L E ep project

The 2 x 400 GeV pp rings are to be finished end of 1983, "a later ep addition is desirable".

Planned:	2 ep insertions
15 GeV e-ring	1/2 above, 1/2 below p-ring; 2 crossings. In the other 4 pp-halls, the e-ring bulges out to a distance of 6 m. Vertical ring separation 90 cm. Small vertical crossing angle. $L \sim 0.5 \cdot 10^{32}\ cm^{-2}\ sec^{-1}$ with 6 MW rf at 15 GeV; a higher L is possible at lower energies.
As an alternative:	
electron ring 4 - 20 GeV	separately housed with one ep-insertion only

ISABELLE

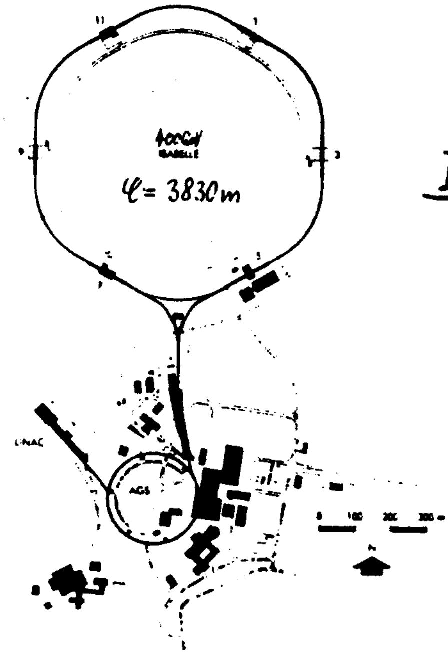

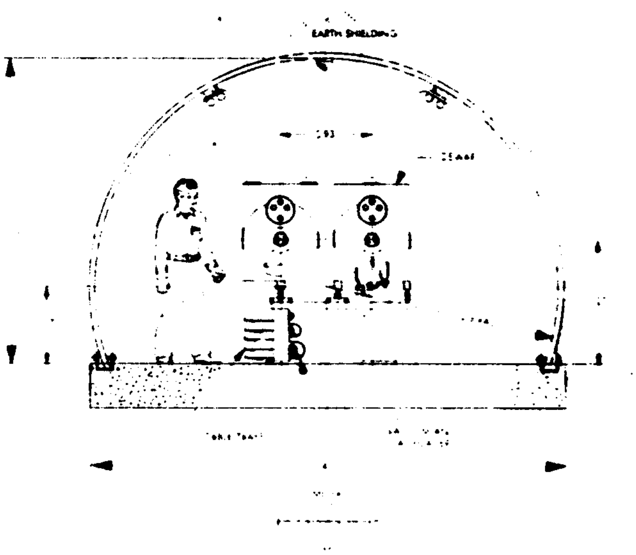

T R I S T A N ep project (hoped to be started in 1982)

Proton accel. to 12 GeV in KEK PS	$5 \cdot 10^{12}$ ppp; cycle time 2 sec $n_b = 9$; $h = 9$
Proton accel. to 70 GeV in TRISTAN, RING I ($\gamma_T = 20$)	$h = 54$ (6 x KEK) $= n_b$; $U_{rf} = 100$ kV only 9 consecutive bunches filled cycle time 22 sec (accel. 10 sec) 120 pulses 44 min. total
Proton storage at 70 GeV in TRISTAN, RING II (iron magnets, 18.6 kG)	$N_p = 6 \cdot 10^{14}$; $I_p = 14$ A; $n_b = 54$ coasting proton beam
Alternative:	accelerate bunched beam in ring II (i. e. use ring I for electrons only)
Electron accel. to 2.5 GeV in e-LINAC	$I_e = 50$ mA pulse length 1.7 sec; rep. rate 50 Hz
Electron accel. to 16 GeV in TRISTAN, RING I	$N_e = 8 \cdot 10^{12}$; $I_e = 200$ mA injected in 32 linac pulses ($\eta = 0.5$) with repetit. rate 6/sec $h = 3232$; $n_b = 54$; $f_{rf} = 47$ MHz; $U_{rf} = 71$ MV At 16 GeV: 47 MeV/turn $P_{syn} = 9.4$ MW $P_{cav} = 5$ MW

Interaction data

	e	p	e	p
	straight crossing		curved crossing	
crossing angle	4 mrad		0	
β_x^* [m]	1.5	5.0	1.5	5.0
β_z^* [m]	1.0	1.0	0.6	1.0
interaction length	1.2 m		1.8 m	
$\Delta\nu_z$	0.056	$\leq$ 0.0005	0.057	$\leq$ 0.0005
L [cm^{-2} sec^{-1}]	$3 \cdot 10^{31}$		$6 \cdot 10^{31}$	

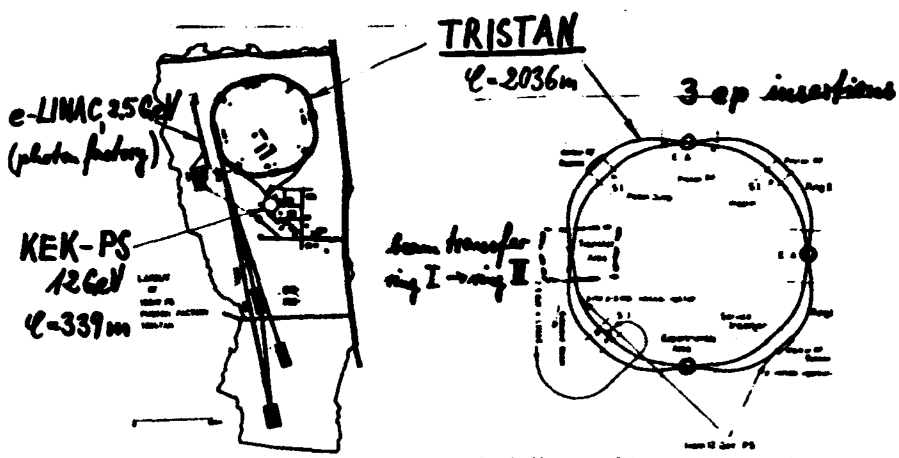

Fig.1 A general layout of TRISTAN

Fig.2 Allocation of intersecting and service insertions

<u>S L A C - L R L</u> ep project (PEP to be finished end of this year)

Proton accel. to 50 MeV in <u>p-LINAC</u>	I_p = 100 mA
Proton accel. to 5 GeV/c (4.15 GeV) in <u>BOOSTER SYNCHR.</u> (ϕ = 122.2 m)	injected: single turn, adiabatic pickup $0.83 \cdot 10^{12}$ ppp f_{rf} = 4.82 MHz at 5 GeV/c repetition period 5 sec
Proton accel. to 300 GeV in supercond. <u>p-RING</u> (C = 2000 m = 18 x booster = 18 x booster syn.) (B_{mag} = 73 kG!) ($r_{apert.}$ = 2.5 cm; β = 1100 m) (l_{dipole} = 4.5 m; l_{quad} = 2.5 m)	injected: 18 pulses in 1.5 min $N_p = 1.5 \cdot 10^{13}$; n_b = 36; 2 rf systems: one for accel., one for final bunching $\varepsilon_{x,z} = 1.6 \quad 10^{-8}$m; ε_l = 0.025 m ε_l = 0.025 m σ_l = 30 cm $\frac{\sigma_E}{E} = 1 \cdot 10^{-3}$
Electron accel. to 15 GeV in <u>PEP</u> ($r_{aperture}$ = 3 cm; β = 900 m)	$N_e = 0.8 \cdot 10^{13}$; n_b = 36 P_{rf} = 12 MW $\varepsilon_{x,z} = 3.1 \cdot 10^{-8}$ m ε_l = 0.034 m σ_l = 1.2 cm $\frac{\sigma_E}{E} = 1 \cdot 10^{-3}$

Interaction data

	e	p
crossing angle	2 mrad, vertical (as small as possible)	
β_x^* [m]	0.5	1.0
β_z^* [m]	1.25	1.9
$\Delta\nu_x/\Delta\nu_z$	0.054/0.049	0.004/0.005
L [cm^{-2} sec^{-1}]	$1 \cdot 10^{32}$	

PEP ep scheme

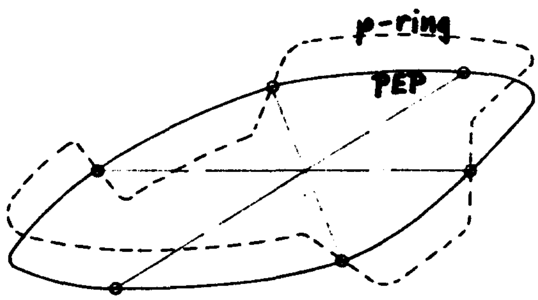

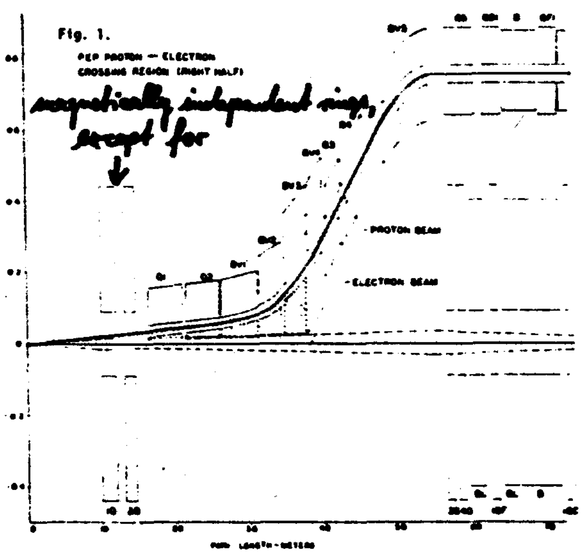

PETRA ep project

Proton accel. to 50 MeV in proton linac	50 mA, > $8 \cdot 10^{11}$ p
Proton accel. to 5 GeV/c in DESY	$\alpha = 0.03$; transition at 5.4 GeV/c $8 \cdot 10^{11}$ p in 8 bunches 5 sec accel. time f_{rf} 2.4 → 8 MHz
rebunching into single bunch	$f_{rf} = 1$ MHz: $n = 8 \rightarrow n = 1$
Proton accel. to 40 GeV/c	quads weak → $\alpha = 0.05$ trans. at 4.1 GeV/c "rf bypass" (8 to) 67 bunches 5 min filling time 3 min accel. time (eddy currents!) $f_{rf} = 8$ MHz
Proton accel. to 280 GeV/c in the supercond. p-ring	$\alpha = 0.003$; trans. at 17.1 GeV/c (8 to) 64 bunches 5 min accel. time $f_{rf} = 8$ MHz bunch length 1 m at 100 kV
bunch compression	bunch length → 0.6 m; $\frac{\Delta p}{p} \rightarrow 0.03$ % $f_{rf} = 128$ MHz

PETRA is filled with electrons during p-bunch compression.

Total filling time < 15 min

PETRA ep project

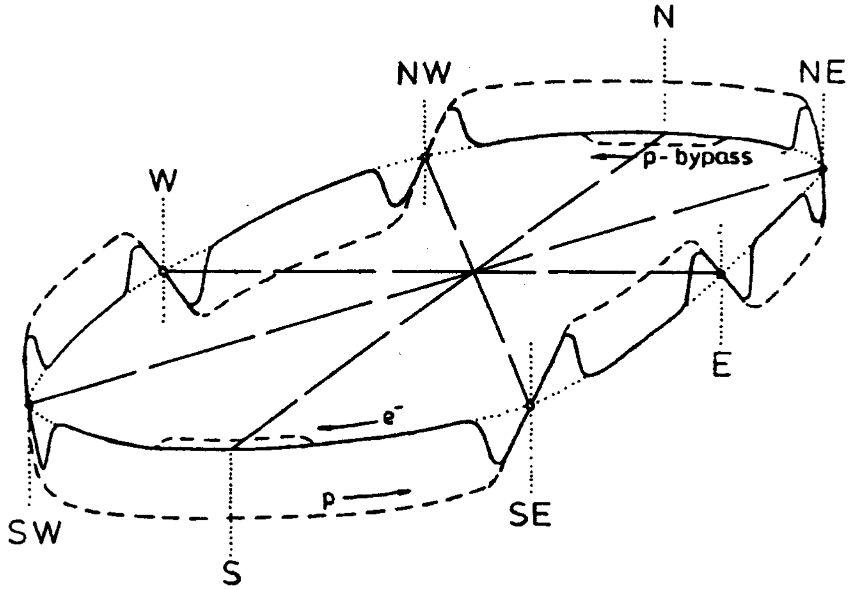

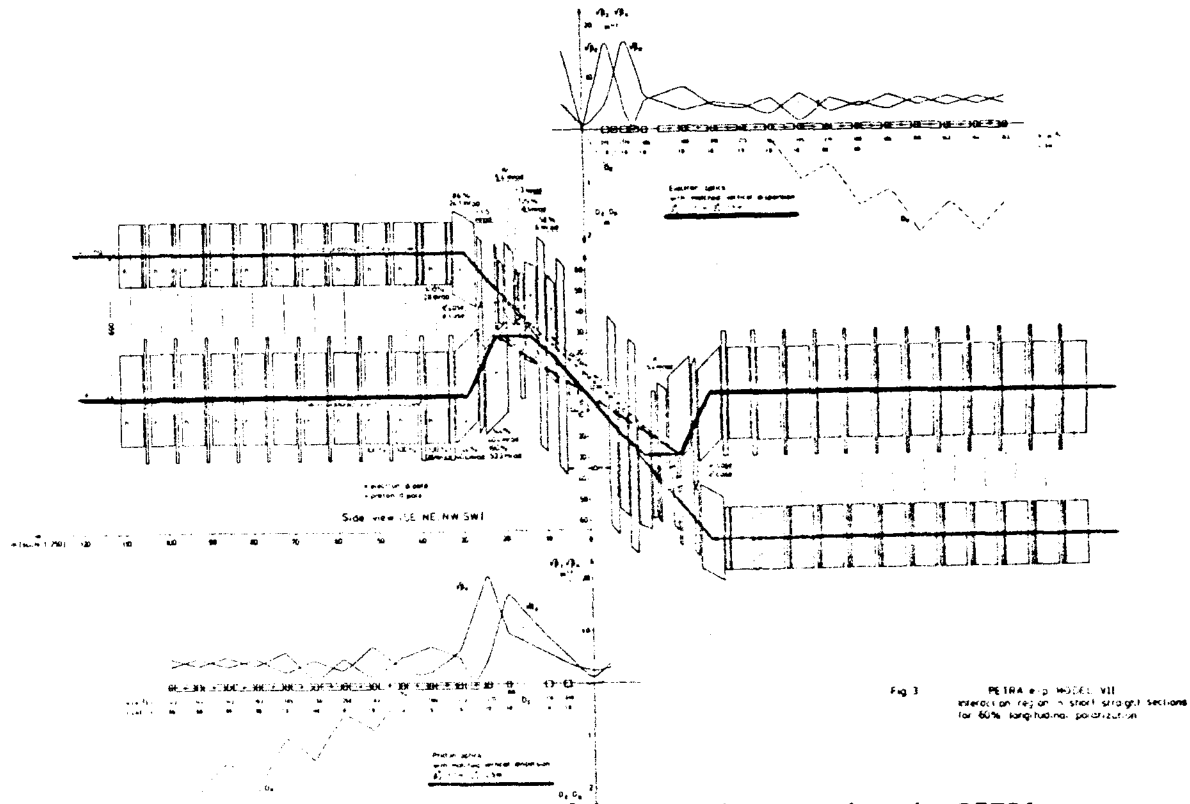

ep interaction in PETRA

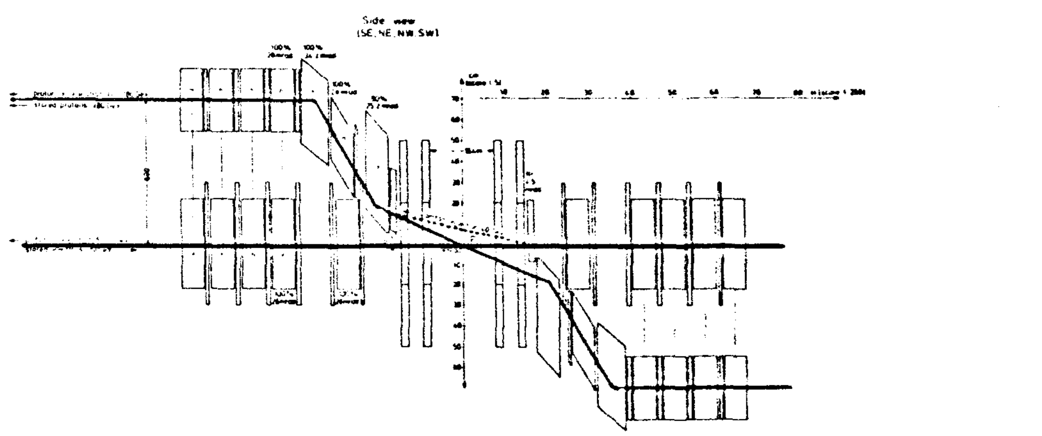

e^+e^- interaction

in PETRA, undistorted by superposed proton ring.

Fig 4 PETRA e-p colliding beam facility 20/280 GeV MODEL VII Short straight section e^+-e^- interaction

PETRA ep project

Luminosity per I.P versus Energy

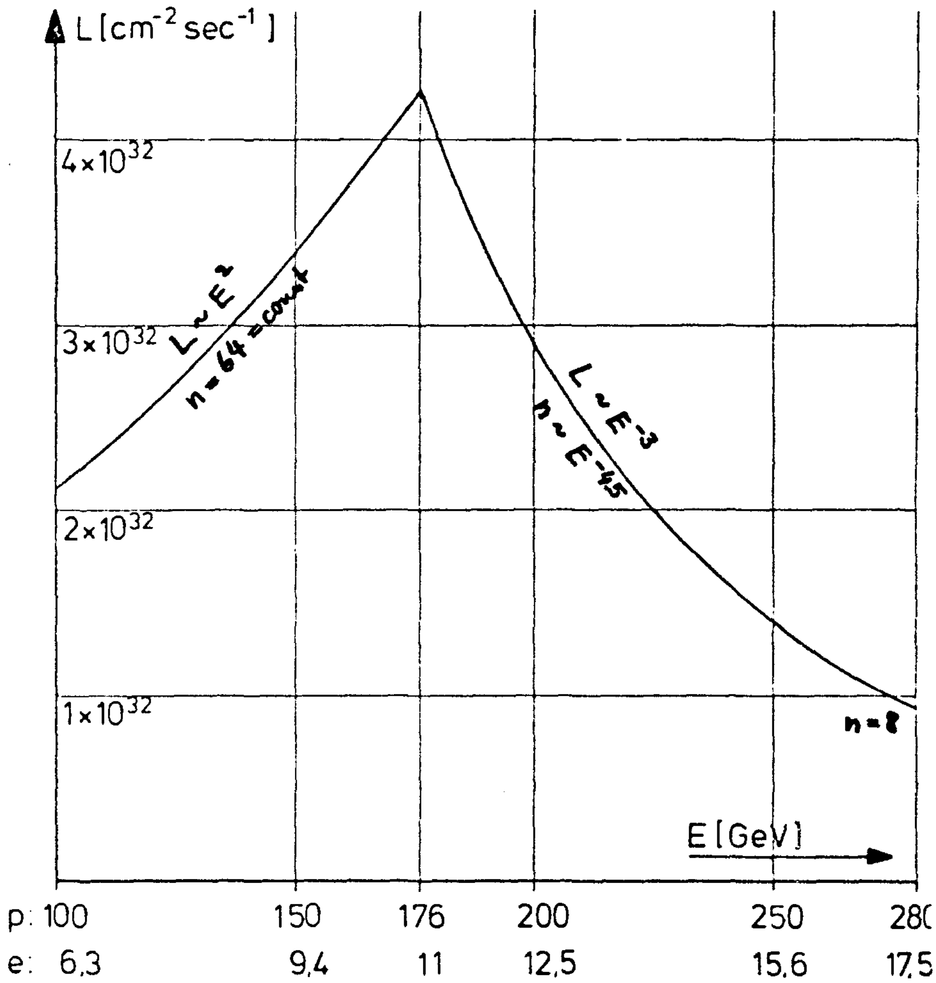

Now proposed and being studied:

PETRA 45 — 45 GeV electron S.R. in PETRA tunnel

Principle: Very low β^* — through very small insertion quads that are very close to the I.P.

Very small ε — through very strong focusing ring lattice

Very small electron current at same ΔQ and L

i.e. very small beam power

Luminosity:

$$L = \frac{c}{2\, r_e^2} \frac{n_b (\Delta Q)^2\, \varepsilon (1 + K) \gamma^2}{R\, \beta_z^*}$$

Beam-beam effect:

$$\Delta Q = \frac{r_e}{2\pi} \frac{N}{n_b\, \varepsilon\, \gamma}$$

The possibility of PETRA 45 ep is being investigated. It will necessitate the addition of a separate ~ 30 GeV proton booster ring that, independent of energy, is now being considered as a basic improvement to the PETRA ep system.

29134

PETRA

UPDATED VERSION OF THE PETRA PROPOSAL

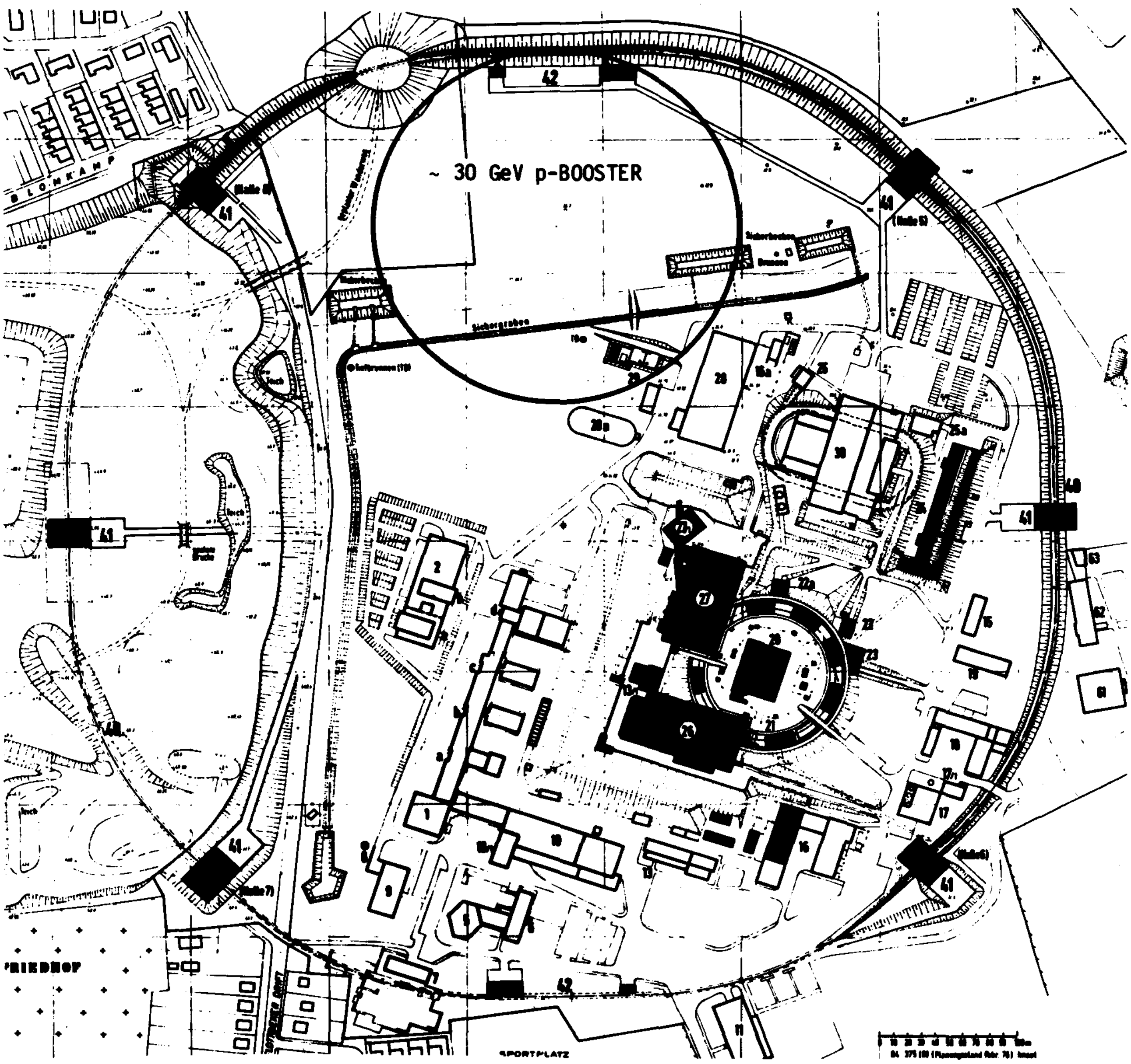

DEUTSCHES ELEKTRONEN-SYNCHROTRON DESY

HAMBURG, FEBRUARY 1976

ep interactions region geometries with and without longitudinal electron spin orientation

For the discussion of electron spin orientation we assume that the equilibrium spin direction in the ring is vertical. This is the case in a plane ring with radiative polarization as well as in a very high energy ring where beam polarization is maintained with the aid of two "siberian snakes", as shown in fig. 2.

Fig. 1 gives a survey of the types of ep interaction region geometries that, to the author, appear most interesting. The crossings shown at the right side occur at a vertical slope that is chosen as to have a longitudinal spin orientation at the interaction point, while the corresponding geometries shown at the left side have the vertical electron spin orientation at the I.P. Solutions IIA) have a "plane" proton ring, with the electron ring being alternately above and below, while solutions IIB) have a "flat" electron ring and a proton ring of alternating location.

Common bending magnets for the separation of electrons and protons greatly facilitate the technical design of an ep interaction region; they cannot be used in the schemes B1) and A2), and the author, therefore, would prefer the scheme B2) if the problem of synchrotron radiation background generated by bending the electrons can be overcome.

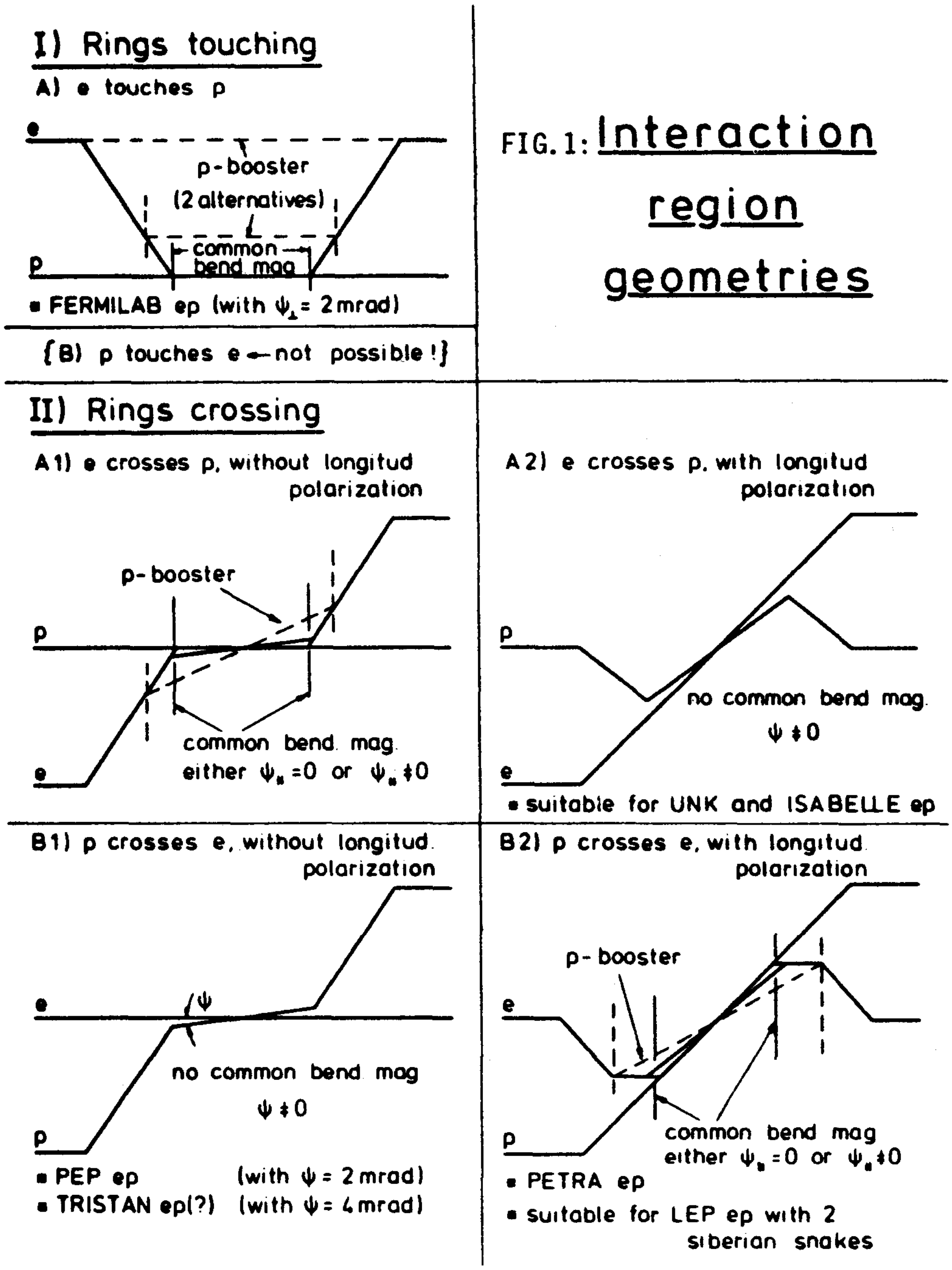

I) Rings touching
A) e touches p
e
p-booster
(2 alternatives)
common bend mag
p
▪ FERMILAB ep (with $\psi_\perp$ = 2 mrad)
{B) p touches e ← not possible !}
FIG. 1: Interaction region geometries
II) Rings crossing
A1) e crosses p, without longitud polarization
p-booster
p
common bend mag
either $\psi_\parallel$ = 0 or $\psi_\parallel \neq 0$
e
A2) e crosses p, with longitud polarization
p
no common bend mag
$\psi \neq 0$
e
▪ suitable for UNK and ISABELLE ep
B1) p crosses e, without longitud polarization
e
ψ
no common bend mag
$\psi \neq 0$
p
▪ PEP ep (with ψ = 2 mrad)
▪ TRISTAN ep(?) (with ψ = 4 mrad)
B2) p crosses e, with longitud polarization
p-booster
e
p
common bend mag
either $\psi_\parallel$ = 0 or $\psi_\parallel \neq 0$
▪ PETRA ep
▪ suitable for LEP ep with 2 siberian snakes

FIG.2: e RING WITH SIBERIAN SNAKES OF THE 1st and 2nd KIND (SCHEMATIC).

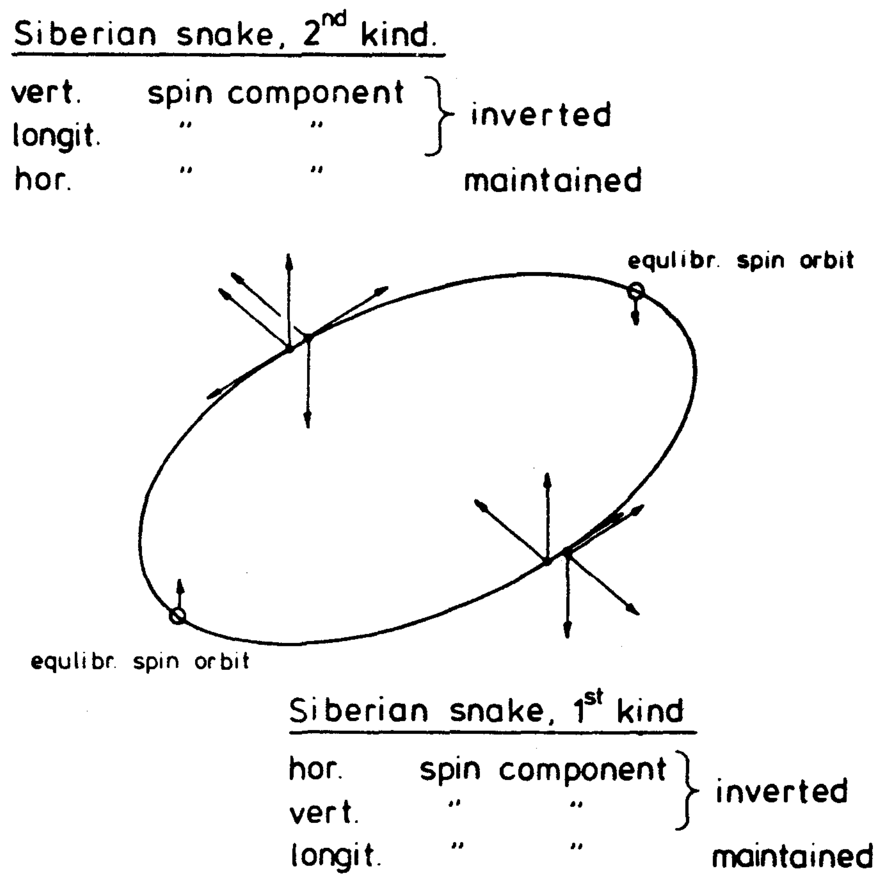

Discussion

Ting:

I would like some comment from you with regard to the calculations of luminosity. You mentioned on the TRISTAN project they use as an injector a 1.5 GeV linac and they have a luminosity of $6 \cdot 10^{32}$. The PEP project which has SLAC as an injector has a luminosity of 10^{32}. The project at DESY which has a complicated injector has a higher luminosity of $4 \cdot 10^{32}$. I wonder how you would explain that.

Answer:

The luminosity is probably more a question of the ΔQ limits which have been assumed.

Ting:

$4 \cdot 10^{32}$ is a very, very nice number. Is there some safety factor in this?

Answer:

The next talk of Hübner will deal with the limitations and clearly the question of space charge limits is at the bottom of all this. We will hear then how optimistic or pessimistic these numbers are. The DESY project assumes a ΔQ of 0.01 for protons and 0.05 for electrons.

Vivargent:

The e^+- e^- project with the mini beta insertion reaches 45 GeV. What will be the length of the free space on either side of the crossing point?

Answer:

About 60 cm.

Vivargent:

Did you give some luminosity value?

Answer:

No, not yet. It may be a little below 10^{32}.

Schopper:

Do all these projects assume bunched proton beams?

Answer:

All except one. There is a coasting proton beam in TRISTAN as an alternative.

Voss:

How good is the vacuum in the FERMI Lab. machine and what kind of life times are expected for electrons?

Answer:

At 12 GeV the pressure due to synchrotron radiation outgassing is expected to be 10^{-7} Torr, the corresponding life time is 50 minutes.

Adams:

What happened to the CHEEP project? I did not see it on the list.

Answer:

I was under the impression that this project was withdrawn some time last year, and I have been presenting only subjects that are still considered. Of course the CHEEP report is at the basis of much of the work done during this study.

2nd July 1979

REVIEW OF DESIGN CRITERIA FOR e p MACHINES *

K. Hübner, CERN, Geneva

1. Introduction

The design of an ep machine is challenging because not only problems common to electron and proton rings have to be tackled but also a number of problems particular to ep. The main emphasis of this review is on topics concerning ep though questions common to other machines are also touched upon. It is hoped that this summary provides a useful reminder of effects which have to be taken into account, though no claim is made that the list is exhaustive. The limitations on size and energy imposed by present knowledge are discussed, and numerical values are given assuming an isomagnetic electron ring. Most of these limits are of a more technical nature, and means might be found in future to remove or surmount them, if enough effort is made. Remedies already exist in some cases, where the limits presented below have only the function of warnings that things may get more complicated from a certain point onwards. All that is said in the following applies for electrons and positrons though only the term electron is used throughout the paper.

2. Energy and Size

There are a number of effects which link size and energy of the electron ring.

2.1 Chromaticity correction

Since the focussing properites of the magnetic structure depend on

---

* Talk given at the ECFA ep Study, DESY, Hamburg, April 1979

particle energy, chromatic effects due to the energy spread become important in high-energy rings, particularly if the beam is focussed strongly at the interaction points by means of low β insertions[1]. Present techniques provide correction for relative spreads $\Delta E/E$ up to 0.01, maybe 0.02 in future. Since the relative spread σ_E/E in the beam should be smaller than $\Delta E/E$ by a factor ≈ 10 if a good lifetime is required, we obtain

$$\sigma_E/E \leq 2\cdot 10^{-3} \quad . \tag{1}$$

The relative energy spread in an isomagnetic machine[2] is

$$\frac{\sigma_E}{E} = \frac{E_e}{m_e c^2}\sqrt{\frac{C_q}{J_E\cdot\rho_e}} \tag{2}$$

where $C_q = 3.84\ 10^{-13}$ m, $J_E = 2$ and ρ_e the bending radius. According to (2) the spread will become excessive at high energies if ρ_e is not increased. If we impose (1) we obtain from (2)

$$\rho_e(\mathrm{m}) \geq 200\left[E_e(\mathrm{GeV})/30\right]^2 \tag{3}$$

where we have normalized to the PETRA bending radius (ρ = 192 m). This limit is plotted as curve I in Fig. 1.

2.2 Transverse polarization

In order to maximize the benefit for physics from an ep facility, polarized electron beams are required[3]. Beam polarization has been obtained in small e^+e^- storage rings, and there is strong incentive to achieve it also in larger rings[4]. In a machine various ways of obtaining polarized beams exist: radiative polarization[5], injection of pre-polarized beams, and polarization by a laser[6,7].

If the ring parameters are chosen appropriately radiative polarization will take place, leading to a gradual build-up of spin polarization. In the absence of depolarizing effects, the beam becomes polarized with a time constant τ_p[8]

$$\frac{1}{\tau_p} = C_p E^5 \frac{\oint \left|\frac{1}{\rho_e{}^3}\right| ds}{\oint ds} \qquad (4)$$

$$C_p = \frac{5\sqrt{3}}{8} \frac{\hbar c^2 r_e}{(m_e c^2)^6} = \frac{1}{98.7} \; s^{-1} GeV^{-5} m^3$$

and the approach to equilibrium polarization is given by

$$P = P_e(1 - \exp(-t/\tau_p)) \qquad (5)$$

where

$$P_e = \frac{8}{5\sqrt{3}} \frac{\oint \frac{1}{\rho_e{}^3} ds}{\oint \left|\frac{1}{\rho_e{}^3}\right| ds} \qquad (6)$$

If a polarization time is required which is smaller than the beam lifetime, say 30 min, we can calculate an upper limit on ρ_e from (4). For an isomagnetic machine with $R_e/\rho_e = \oint ds/2\pi\rho_e \cong 2$ (PETRA)

$$\rho_e(m) \leq 200 \left[E_e(GeV)/15\right]^{5/3} \qquad (7)$$

The line II in Fig. 1 corresponds to this limit.

If ρ_e is much larger, the natural polarization time will become inconveniently long and must be reduced by introducing wiggler magnets which enhance the term $|1|\rho_e^3|$ in (4)[9,10,11]. However, inspection of (6) shows that reverse bending in wigglers reduces the equilibrium polarization from its maximum value (92.4%). A better solution is to introduce a series of positive "kinks" in the orbit avoiding reverse bends altogether[12].

If the radiative polarization cannot be enhanced sufficiently, the beams must be either injected in an already polarized state or they have to be polarized by a laser. The former requires either an extremely tight control of the depolarizing resonances during acceleration after injection, or a powerful injector capable of providing the pre-polarized beams at operating energy. Neither of these two propositions is very attractive. Polarization by laser works via spin-dependent Compton scattering of the photons on the electrons. It is promising but has not yet been used.

2.3 Depolarization

The most troublesome depolarization resonances occur when the number of spin precessions ν per revolution

$$\nu = \gamma_e \cdot (g-2)/2 = a \cdot E_e/m_e c^2 \tag{8}$$

becomes an integer

$$\nu = k \tag{9}$$

where g is the gyromagnetic ratio of the electron. These resonances are caused mainly by the radial magnetic fields, encountered by the particles travelling on an orbit displaced vertically in the quadrupoles.

These numerous resonances can be very strong and alignment of the orbit to make them harmless for particles crossing them is rather difficult[13], though not hopeless[14]. From (8) and (9) it can be inferred that these resonances occur at intervals of $m_e c^2/a$ = 440 MeV on the energy scale. The best way to avoid them is to put the operating energy between two resonances. This introduces immediately two requirements: the energy spread σ_E in the beam and the width of the resonances must be much smaller than 440 MeV.

The first requirement sets a lower limit on the bending radius. Imposing (somewhat arbitrarily)

$$8\sigma_E \leq m_e c^2/a = 440 \text{ MeV} \tag{10}$$

we find for an isomagnetic machine by virtue of (2)

$$\rho_e(\text{m}) \geq 200 \left[E_e(\text{GeV})/30\right]^4 \tag{11}$$

which is shown as curve III in Fig. 1.

The requirement on the width of the resonances puts a constraint on the admissible k^{th} Fourier component of the vertical closed orbit y

$$y = y_k \sin(k \cdot c \cdot t/R_e) \quad . \tag{12}$$

In order that the k^{th} and the $(k+1)^{th}$ resonances are distinct and well separated[13] the inequality

$$y_k \ll R_e/(E_e \cdot a/m_e \cdot c^2) \tag{13}$$

must hold. Measurements in the SPS indicate that $y_k \simeq 0.1$ mm can be achieved provided that k is sufficiently far from the betatron tune of the machine[15]. For this value of y_k and a safety factor 10 in (13) we obtain from (13)

$$\rho_e(m) \geq 200 \left[E_e(\text{GeV})/33\right]^3 \tag{14}$$

If this holds, the integer resonances are well separated. Comparing (14) with (11) shows that (11) is the more stringent criterion in the range we are interested in. Thus, the limit according to (14) is not shown in Fig. 1 because it is automatically fulfilled if line III, corresponding to (11), is not crossed.

If the last criterion (11) cannot be met and, furthermore, if the depolarization time on these resonances is too short, the design of the ring must incorporate a so-called "Siberian Snake" which removes the spin resonances altogether[16,11]. This device has a number of disadvantages but they are certainly not insurmountable[17]; the equilibrium polarization is likely to be lower, and a variable orbit geometry in the snake is needed if operation over a wide range of energy is wanted. Since installation of only one of these snakes suppresses the radiative polarization, two of them must be installed[18] if radiative polarization is to be maintained.

Avoiding the integer spin resonances is only a necessary and not a sufficient criterion for obtaining polarization. All other depolarizing mechanisms must be scrutinized carefully, as has been done for PETRA[19], CHEEP[20] and PEP[21], to make sure that the depolarization time τ_d is indeed much longer than the polarization time τ_p, at least over wide intervals in the operating range. Otherwise, the equilibrium polarization P_e is reduced by a factor[14,19]

$$\frac{\tau_d}{\tau_d + \tau_p} \tag{15}$$

because (5) has to be replaced by

$$P = \frac{\tau_d}{\tau_d + \tau_p} \cdot P_e \cdot \left\{ 1 - \exp\left[- \left(\frac{1}{\tau_p} + \frac{1}{\tau_d} \right) t \right] \right\} \tag{16}$$

if $\tau_p << \tau_d$ is not fulfilled.

Examination of the ratio τ_p/τ_d for these effects[19] studied for PETRA seems to indicate that $\tau_p/\tau_d << 1$ can be expected in an isomagnetic machine, provided that inequality (11) is fulfilled. The only exception seems to be the depolarization by direct vertical quantum excitation[22,23] where

$$\tau_p/\tau_d \sim Q_z^2 \tag{17}$$

This effect could be bothersome in rings with a very high vertical betatron tune Q_z.

In general, the beam-beam interaction is not expected to depolarize the beam if it is so weak that it has no adverse effect on the beam lifetime[24]. However, its influence on spin resonances should be examined in detail[14,25,26] if operation close to the beam-beam limit is planned.

2.4 Summary

Table I summarizes the formulae.

Table I. Limitations on bending radius in an isomagnetic electron ring

Chromaticity				
$\rho_e(m) \geq 200 \left[E_e(GeV)/30\right]^2$	for	σ_E/E	$\leq$	$2 \cdot 10^{-3}$
Polarization				
$\rho_e(m) \leq 200 \left[E_e(GeV)/15\right]^{5/3}$	for	τ_p	$\leq$	30 min
Depolarization				
$\rho_e(m) \geq 200 \left[E(GeV)/30\right]^4$	for	$8\sigma_E$	$\leq$	440 MeV

Fig. 1 gives a synopsis of the limitations in the ρ_e, E_e plane. Although it is no more than indicative even for an isomagnetic ring, it provides some useful guidance. Below curve I, the energy spread σ_E/E in the beam becomes larger than $2 \cdot 10^{-3}$, and chromaticity correction with present techniques becomes very difficult. Above curve II, the radiative polarization becomes very slow and means to speed it up must be applied. Below curve III, depolarization by integer spin resonances becomes very strong. They must be fought with special tricks such as the "Siberian Snake".

According to Fig. 1, PETRA and PEP are in the "good" region up to $\approx$ 30 GeV, whereas a special effort would be needed in a machine like LEP if polarized beams were to be provided[17].

If the same tunnel were used to house the electron and the proton rings, the proton energies shown in Fig. 2 could be obtained for a magnetic field of 5T in the magnets of the proton ring. The resulting maximum centre-of-mass energy squared is shown in Fig. 3.

The last two diagrams are certainly not complete because effects proper to the proton ring may introduce new limitations, though it seems that proton rings are less demanding as far as the choice of bending radius and energy is concerned[27].

3. Coasting versus bunched proton beams

This topical question has not yet found an answer. The luminosity can be made virtually the same for bunched and coasting protons.

In the latter case many more protons are needed, and the filling time will be longer or a more powerful injector is needed in comparison to the bunched beam. The safe disposal of the high-intensity proton beam needs attention[27,28] and shielding is more difficult.

However, the advantages of the coasting beam also deserve consideration: it is expected to be more stable (no synchrotron motion, no problems with RF noise[29,30]), and no synchronization between e-ring and p-ring is required, which could limit the operating range in energy with bunched beams; stochastic cooling[31] may be applied more easily to the coasting than to the bunched proton beam[32].

For a cold bore vacuum system, the power loss of the proton bunch by unavoidable corrugations of the vacuum chamber must be considered. The power deposited per metre is given by[33]

$$p_{pm} = k_b \, e^2 \, N_p^2 \, f_o \, k'_{pm} \qquad (18)$$

where k_b is the number of bunches, N_p the number of protons per bunch and f_o the revolution frequency. The parameter k'_{pm} is the energy deposited on average per running metre of the vacuum chamber by a single proton riding in a bunch which has a total charge of one Coulomb.

In order to illustrate the effect we calculate this loss for PROPER assuming it has a PETRA type vacuum chamber. The loss parameter of the latter is

$$k'_{pm} = 0.5 \cdot 10^{10} \text{ eV/C} \cdot \text{m}$$

for a bunch length $\sigma_s = 3.7$ cm[34]. The PROPER parameters[35] are $N_p = 8.10^{11}$, $k_b = 8$ and $\sigma_s = 30$ cm.

If k'_{pm} scales with σ^{-2}, we obtain

$$p_{pm} = 1.3 \text{ W/m} \quad ,$$

for $k'_{pm} \sim \sigma^{-1.3}$

$$p_{pm} = 5.5 \text{ W/m}$$

This heat-load at $\sim 4^{\circ}$K is comparable to the heat-load of the magnets expected to be around 5 W/m[36]. Thus, the refrigerator power might have to be increased substantially if a cold bore vacuum system is adopted in combination with bunched proton beams of such high peak intensity.

4. Luminosity

For simplicity, a bunched proton beam is considered colliding head on with the electron beam. The luminosity[37,38] is given by

$$L = \frac{f_o \cdot k_b \cdot N_e \cdot N_p}{2\pi(\sigma_{px}^2 + \sigma_{ex}^2)^{\frac{1}{2}} \cdot (\sigma_{py}^2 + \sigma_{ey}^2)^{\frac{1}{2}}} \tag{19}$$

with f_o the revolution frequency, k_b the number of bunches; N_e and N_p are the number of particles per bunch; σ describes the r.m.s. beam dimensions at the crossing point. The number of particles cannot be chosen at will; it is limited by the condition that the non-linear forces exerted by a bunch on its counter-rotating partner remain within certain bounds. It is generally accepted that the maximum linear tune-shift ΔQ, created by the interaction of the two bunches, is a good measure for this non-linear force, and that the non-linear forces do not become destructive if ΔQ does not exceed a certain value. The linear tune-shift is approximately

$$\Delta Q_{ni} = \frac{r_n}{2\pi} \frac{\beta_{ni}}{\gamma_n} \frac{N_\ell}{\sigma_{\ell i}(\sigma_{\ell i} + \sigma_{\ell j})} \tag{20}$$

where n is the index of the particles (e or p) experiencing the tune-shift, ℓ is the index of the particles (p or e) creating the non-linear forces. The index i (x or y) refers to the direction where the tune-shift is calculated; the index j (y or x) to the orthogonal transverse direction.

Evidence is available from small e^+e^- rings that the electron tune-shift ΔQ_e can be as high as 0.05 to 0.06[39,40]; initial performance of PETRA has indicated lower limits[41]. Some computational studies have been done on the tune-shift sustained by protons interacting with electron bunches[42] but no experimental evidence is available. The only guidance comes from coasting proton beam-beam experiments in the ISR[43], indicating that a tune-shift 0.005 to 0.01 is acceptable. During standard operation (beam lifetime ≥ 1 month) of the ISR, a tune-shift of only $\Delta Q_p = 0.001$ is reached because of current limitations;

at this level, the non-linear beam-beam effect is not noticeable. In order to elucidate this problem, it would be very desirable to perform the ep experiments at DORIS which were proposed a long time ago[44].

Great attention should be paid to all other beam-beam effects[45] and to the non-linear resonances created by misalignment of the two beams in the interaction point[46], because ep machines do not benefit from the automatic alignment so beneficial in e^+e^- machines consisting of a single ring.

At this point it is useful to examine the limitations imposed on some of the individual parameters.

Inspecting (19) shows that the luminosity is proportional to k_b as in e^+e^- rings. In an e^+e^- ring, k_b is usually chosen to be one half of the number of interaction points to avoid crossing of the bunches in the normal lattice. In an ep machine, however, k_b is not limited in this respect because the beams circulate in two rings. Thus, more bunches can be used to the benefit of higher luminosity provided that enough RF power is available in the e ring. If the RF power in the e ring is limited, it is also advantageous to operate with the highest possible number of bunches k_b, because this reduces the peak current and also therefore the direct parasitic mode loss as well as its contribution to the power dissipation in the RF cavities. Hence, a higher average electron current

$$I_e = e\, f_o\, k_b\, N_e \tag{21}$$

is sustained by the RF system with a concomitant gain in luminosity as can be seen from (19)[47]. Unfortunately, the number of bunches cannot be increased beyond certain limits set by multi-bunch instabilities. If the spacing between the bunches becomes too short, these instabilities become very serious[48].

The limitations on the number of particles per bunch and on the transverse cross-sections at the interaction points are the same as in e^+e^- or pp rings; for this reason, they are not treated here though they must also receive careful attention in an ep design.

Examination of all these criteria leads to the conclusion that no trustworthy general scaling law for the luminosity can be given. No fundamental limitations seem to exist and the only real restriction comes finally from the available funds. This is corroborated by the fact that all ep machines so far conceived reach, theoretically at least, within a factor of 2 the "magic" luminosity of 10^{32} $cm^{-2}s^{-1}$ at nominal energy[49].

For a given ep machine the scaling of luminosity with electron and proton energy depends on the detailed boundary conditions, making it very difficult to establish general rules. However, certain optimization techniques exist which can be found in the descriptions of the facilities worked out in detail[20,35,50,51].

5. Design of the insertions

5.1 Longitudinal polarization

Radiative polarization directs the spin parallel to the main magnetic field[5] with the preferred spin direction defined by

$$\frac{\vec{P}}{|\vec{P}|} = - \frac{\vec{v} \times \dot{\vec{v}}}{|\vec{v}| \cdot |\dot{\vec{v}}|} \tag{22}$$

where v is the velocity of the particles. The experiments, however, require a longitudinal polarization of the beam in the interaction point. For this reason, a number of schemes were invented which rotate the spin before the interaction point into the longitudinal direction and turn it back into the transverse direction before the particles again enter the magnetic field of the lattice. This rotation can be performed by a sequence of horizontal dipole fields[52)] or by a combination of horizontal and vertical magnetic fields[53)].

The spin precession depends only on magnetic field times the length of the magnets; however, the orbit in the rotating magnets also depends on the energy of the particles. Thus, if the orbit is kept constant at all energies, the spin rotation will be correct at only one energy, though a judicious lay-out of the magnets may attenuate this effect[53)]. A better solution is to accept a variable orbit geometry in the spin-rotating magnets; this provides a correct spin rotation over a wide energy range[54)]. When designing a spin rotation scheme attention must be paid to the fact that the radial fields have to be rather weak in order to reduce their depolarizing effect.

From the physics point of view[3)] a capability of spin reversal at the interaction point would be very desirable so that both helicities would become available at the collision point. This can be done in various ways:

i) The transverse polarization of the whole beam is reversed by crossing an artificially excited spin resonance[55)]. Since the radiative polarization will restore the spin in the original direction, this scheme is practical only if the natural polarization rate is low.

ii) Strong reverse bending ($\rho_e < 0$) can be used according to (6) to change the sign of the transverse polarization[10)], negative "kinks" being the most efficient way[12)] to accomplish it.

iii) A supervariable geometry can "over-rotate" the spin in the insertion[54)]. This method is likely to work only in a narrow energy interval.

iv) two distinct channels can be foreseen, one for each helicity. This method appears to be rather clumsy and has not received great attention.

5.2 Geometry

Another problem particular to ep is the separation of the electron beam from the proton beam after the crossing region. Various insertion geometries have been proposed. In most of them, the electron orbit is bent away from the proton orbit by bending magnets at or close to the interaction point. This brings about a serious background problem because the photons created by synchrotron radiation in these magnets can hit the protons[56,57)]. A small crossing angle alleviates the problem but is reputed to worsen the beam-beam effect according to experience in DORIS[48)].

Not only the direct synchrotron radiation but also the back-scattered radiation can give rise to substantial background in the detector due to the high primary photon flux. A well-designed system of absorbers must reduce it to a tolerable level[58)].

Since the e-p centre-of-mass frame is moving in the laboratory, the detectors tend to become highly asymmetrical. Many of the interesting events fall into a narrow cone around the proton beam, and the detectors are in competition for space with the focussing elements. It is then essential that the design of the insertion and the detector are fully integrated in an ep machine; all possibilities should be explored for detectors specifically adapted to the asymmetrical e-p requirements.

6. Acknowledgements

B.W. Montague helped with stimulating discussions and encouragement. He, A. Hutton and E. Keil read the manuscript and made useful suggestions. To all thanks are due.

References *)

1) M.H.R. Donald, P.L. Morton and H. Wiedemann, Chromaticity correction in large storage rings, IEEE Trans. Nucl. Sci. NS-24 (1977) 1200.

2) M. Sands, The physics of electron storage rings. An introduction, Proc. Int. School of Physics "Enrico Fermi", Corse XLVI (ed. B. Touschek) New York, 1971, 257.

3) C.H. Llewellyn Smith and B.H. Wiik, Physics with large electron-proton colliding rings, report DESY 77/38 (1977).

4) R.F. Schwitters, Experimental review of beam polarization in high energy e^+e^- storage rings, report SLAC-PUB.2258 (1979), to be published in Proc. IIIrd Int. Symp. on High Energy Physics with Polarized Beams, Argonne (1978).

5) A.A. Sokolov and I.M. Ternov, On polarization and spin effects in the theory of synchrotron radiation, Sov. Phys. Dokl. 8 (1964) 1203.

6) Ya.S. Derbenev, A.M. Kondratenko and E.L. Saldin, Polarization of electrons in storage rings by circularly-polarized electromagnetic waves, Preprint IYaPh (Novosibirsk) 78-64 (1978).

7) Ya.S. Derbenev, A.M. Kondratenko and E.L. Saldin, Polarization of the electron beam in a storage ring by hard, circularly-polarized photons, Preprint IYaPh (Novosibirsk) 78-68 (1978).

8) V.N. Baier and V.M. Katkov, Radiational polarization of electrons in inhomogeneous magnetic field, Phys. Lett. 24A (1967) 327.

9) A. Hutton, Control of the low energy characteristics of the LSR electron ring using wiggler magnets, internal report CERN/ISR-LTD/76-18 (1976).

10) Ya.S. Derbenev, A.M. Kondratenko and A.N. Skrinskij, On obtaining beams of required polarization in storage rings, Preprint IYaPh (Novosibirsk) 76-62 (1976).

11) Ya.S. Derbenev, A.M. Kondratenko, S.I. Serednyakov, A.N. Skrinskij, G.M. Tumaikin and Yu.M. Shatunov, Radiative polarization: obtaining, control, using, Particle Accelerators 8 (1978) 115.

12) A. Hutton, CHEEP - polarization kinks, internal report CERN/ISR-TH/77-48 (1977).

13) D. Möhl and B.W. Montague, Depolarisation in large electron storage rings, Nucl. Instr. Meth. 137 (1976) 423.

14) Ya.S. Derbenev, A.M. Kondratenko and A.N. Skrinskij, Radiative polarization at very high energies, Preprint IYaPh (Novosibirsk) 77-60 (1977).

15) L. Burnod, private communication (1977).

16) Ya.S. Derbenev and A.M. Kondratenko, Longitudinally polarized electrons and positrons from a new mechanism of radiative polarization, Preprint IYaPh (Novosibirsk) 76-84 (1976).

17) B.W. Montague, Polarized $e^{\pm}$ beams in LEP, internal report CERN-ISR-TH/78-25 (1978) to be published in Proc. IIIrd Int. Symp. on High Energy Physics with Polarized Beams and Polarized Targets, Argonne (1978).

18) Ya.S. Derbenev, contribution to Proc. IIIrd Int. Symp. on High Energy Physics with Polarized Beams and Polarized Targets, Argonne (1978).

19) B.W. Montague, Depolarization effects in PETRA, report DESY 77/31 (1977).

20) D. Blöss, J. Dupin, D. Fiander, J. Gervaise, R. Gregoire, O. Gröbner, P. Hannhart, W. Hardt, H. Hoffmann, A. Hofmann, K. Hübner, A. Hutton, K. Johnsen, E. Jones, K.H. Kissler, J.R.M. Maidment, B. Milman, B.W. Montague, J.A. Riche, B.W. Wiik, C. Wyss and C. Zettler, An e-p colliding beam facility with the CERN SPS, in CERN report 78-02 (1978) 113.

21) A.W. Chao, Estimate of spin polarization for the electron storage rings SPEAR and PEP, SLAC-PUB-2245 (1979) to be published in IEEE Trans. Nucl. Sci. (1979).

22) Ya.S. Derbenev and A.M. Kondratenko, Diffusion of particle spins in storage rings, Sov. Phys. JETP 35 (1972) 230.

23) K.W. Robinson, Depolarization in a storage ring, report Cambridge Electron Accelerator CEAL-TM-197 (1972).

24) A.M. Kondratenko, The stability of the polarization of colliding beams, Sov. Phys. JETP 39 (1974) 592.

25) A.W. Chao and R.F. Schwitters, More on beam depolarization at PEP, note PEP-237 (1977).

26) B.W. Montague, Beam-beam depolarization in SPEAR and PEP, note PEP-260 (1979).

27) E. Keil, Perspectives on colliding beams, Proc. IXth Internat. Conf. on High Energy Accelerators, Stanford (1974) 660.

28) C. Hauviller, H. Schönbacher and A. van Steenbergen, Beam dump absorber for the 400 x 400 GeV^2 p-p superconducting large storage rings (LSR), internal report CERN-ISR-GE/79-4 (1979).

29) A. Hofmann, E. Peschardt, F. Sacherer and W. Schnell, Longitudinal bunch dilution due to RF noise, IEEE Trans. Nucl. Sci. 24 (1977) 1452.

30) D. Boussard, L. Evans, J. Gareyte, T. Linnecar, W. Mills and E.J.N. Wilson, Acceleration and storage of a dense single bunch in the CERN SPS, internal report CERN-SPS-DI/79-7 (1979), to be published in IEEE Trans. Nucl. Sci. (1979).

31) S. van der Meer, Stochastic cooling theory and devices, Proc. Workshop on Producing High Luminosity High Energy $p\bar{p}$ Collisions, Berkeley (1978) 73.

32) H. Herr and D. Möhl, Bunched beam stochastic cooling, Invited paper given at Workshop on Phase Space Cooling of High Energy Beams, Madison (1978).

33) M. Sands and J. Rees, A bunch measurement of the energy loss of a stored beam to a cavity, note PEP-95 (1974).

34) M. Bassetti, H. Gerke, K. Hübner and R.D. Kohaupt, First measurement of parasitic mode losses in PETRA, report DESY 79-07 (1979).

35) E. Dasskowski, K. Steffen, G.A. Voss, An e-p facility at PETRA, report DESY 78-02 (1978).

36) SCISR Study Group, Superconducting conversion of the intersecting storage rings, CERN report 77-20 (1977).

37) L. Smith, On the calculation of luminosity for e-p colliding beams, LBL note PEP-20 (1972).

38) T. Suzuki, General formulae of luminosity for various types of colliding beam machines, report KEK-76-3 (1976).

39) I.B. Vasserman, I.A. Koop, V.P. Kutovoj, A.P. Lysenko, S.I. Mishnev, A.N. Skrinskij, G.M. Tumajkin, Yu.M. Shatunov and V.G. Shamovskij, High luminosity operation of the e^+e^- storage ring VEPP-2M, Proc. All-Union Conf. on Charged Particle Accelerators, Dubna (1976) 252.

40) M. Cornacchia, Report on some beam-beam functional dependencies in SPEAR, note PEP-275 (1978).

41) A. Piwinski, Observation of beam-beam effects in PETRA, to be published in IEEE Trans. Nucl. Sci. (1979).

42) E. Keil and A.M. Sessler, Studies of bunched electron beams interacting with coasting proton beams, internal report CERN/ISR-AS/74-60 (1974).

43) B. Zotter, Experimental investigation of the beam-beam limit of proton beams, Proc. Xth Internat. Conf. on High Energy Accelerators, Protvino (1977) 23.

44) H. Wiedemann, e-p machine experiments in DORIS, Proc. Seminar on e-p and e-e storage rings, Hamburg (1973) 603.

45) G. Guignard, Review of the investigations on the beam-beam interactions at the ISR, internal report CERN-ISR-BOM/79-28 (1979), to be published in Proc. on Nonlinear Orbit Dynamics and the Beam-beam Interaction, Brookhaven (1979).

46) J.-P. Gourber, Control of betatron frequencies and of resonance excitation in the ISR, Proc. 4th All-Union Nat. Conf. on Particle Accelerators, Moscow, Vol. II (1974) 73.

47) A. Hutton, Insertion design for e^+e^- storage rings, internal report CERN-ISR-TH/79-6 (1979), to be published in IEEE Trans. Nucl. Sci. (1979).

48) DESY Storage Ring Group, DORIS - a status report, Proc. Xth Internat. Conf. on High Energy Accelerators, Protvino (1977) 458.

49) K. Steffen, Proceedings of this meeting.

50) T. Nishikawa and E. Keil, Note on ep collisions, KEK-Preprint-78-9 (1978), to be published in Proc. ICFA Workshop on Accelerator and Detector Possibilities and Limitations, Fermilab (1978).

51) A. Hutton, Optimization of luminosity for e-p collisions, internal report CERN-ISR-TH/79-13 (1979), to be published in IEEE Trans. Nucl. Sci. (1979).

52) R. Schwitters and B. Richter, A method for producing longitudinal beam polarization at PEP, 1974 PEP Summer Study, Berkeley (1974) 384.

53) B.W. Montague, Longitudinal polarisation of high-energy electrons in colliding-beam storage rings, internal report CERN-ISR-LTD/76-2 (1976).

54) A. Hutton, CHEEP - variable geometry insertion, internal report CERN/ISR-TH/77-51 (1977).

55) B.W. Montague, CHEEP - spin reversal by resonance crossing, internal report CERN/ISR-TH/77-49 (1977).

56) H.F. Hoffmann, Interactions of the synchrotron radiation with the proton beam in the LSR ep interaction regions, in CERN report 76-12 (ed. L. Camilleri) (1976) 209.

57) G. Fischer et al., Some remarks about large storage rings (LSR) ep interaction regions: a preliminary report, ibid, 161.

58) U. Amaldi et al., Physics with e-p colliding beams, in CERN report 78-02 (1978) 59.

*) All papers designated as notes are unpublished.

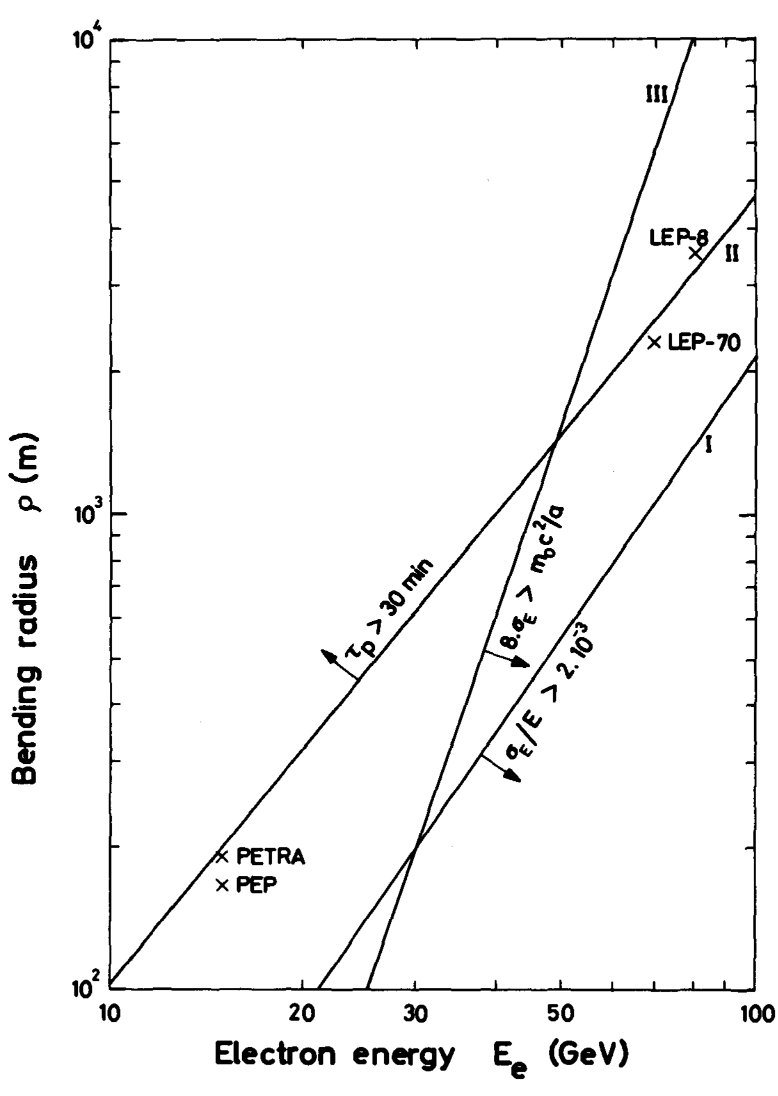

Fig. 1. Limitations on the bending radius of the electron ring versus energy of the electrons.

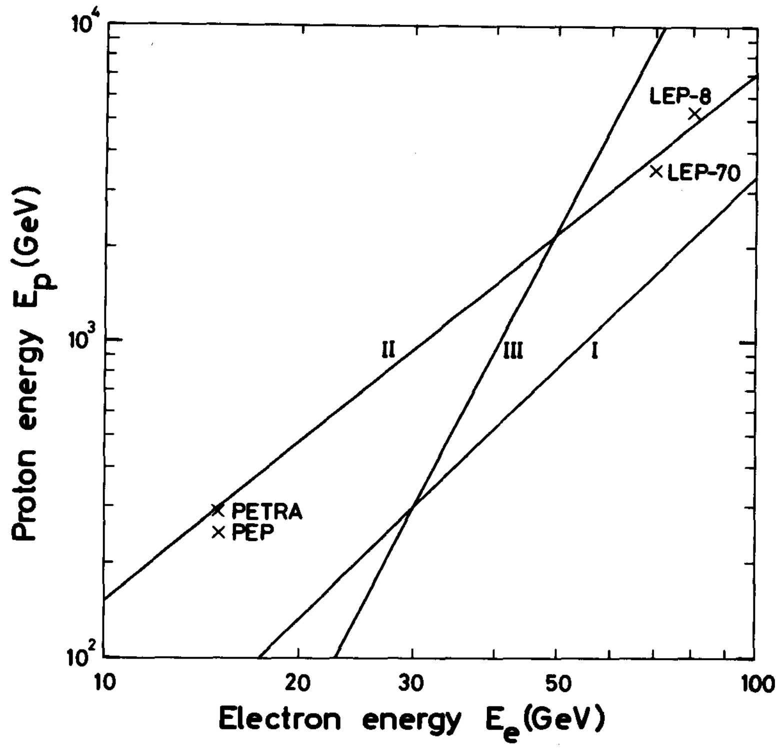

Fig. 2. Maximum proton energy versus electron energy for a proton ring housed in the same tunnel as the electron ring. The magnetic field is 5T in the proton ring.

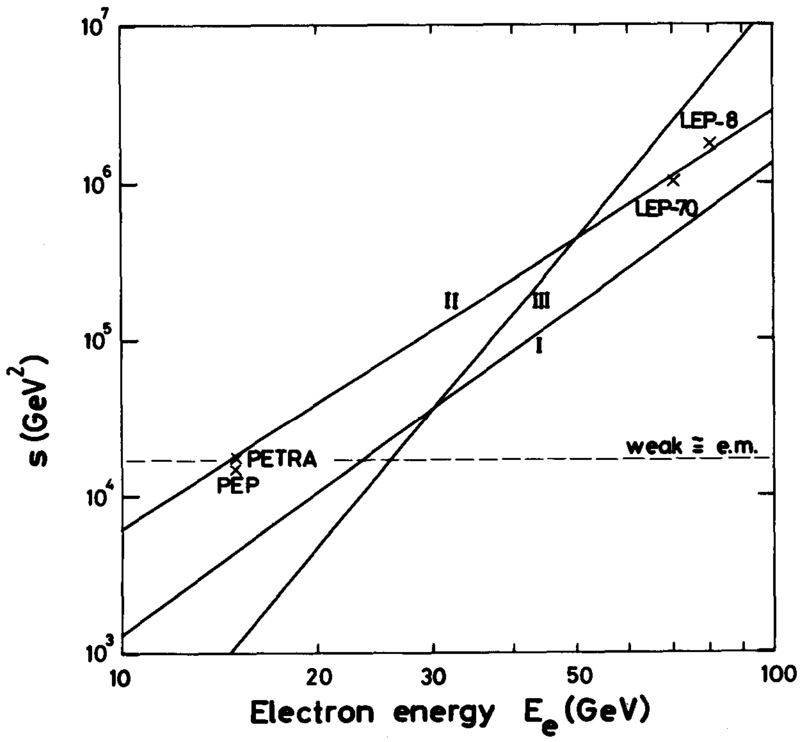

Fig. 3. Maximum centre-of-mass energy squared versus electron energy. Proton ring as for Fig. 2.

SUMMARY OF THE GENERAL DISCUSSION

(G.A. VOSS)

The discussion centered on a number of technical and physical problems: If the transverse polarization angle of the electrons is to be turned to produce a longitudinal polarization at the interaction points vertical bending magnets close to the interaction region are necessary. The background to the experiments due to the synchrotron radiation from these magnets must be avoided by specially designed interaction region vacuum chambers.

The question of collision angle between the two beams was discussed at some length. A collision angle between the two beams would make it easier to separate these two beams but the space charge limits may be considerably lower than that for head-on collisions.

Another topic of discussion was the field quality in the superconducting proton magnets. The discussion was not very conclusive, but it was generally felt that in view of the much strong nonlinearities due to the beam-beam interactions a field homogenuity of $3 \cdot 10^{-4}$ in the bending magnets might be adequate.

Also discussed were the questions of space charge limits for electron and proton beams. As far as the ΔQ in electron storage rings is concerned there seems to be a considerable amount of empirical data with more data soon to be expected from PETRA, PEP and CESAR. There is no such relevant experience with proton storage rings. The experiments in the ISR suggest that ΔQ-shifts for beam-beam interactions of 0.005 may be tolerable.

But since the ISR has an unbunched beam and these ΔQ-shifts were only applied in one plane it may be dangerous to extrapolate these numbers to e-p storage rings as they have been proposed. It was felt that the experience with the p-$\bar{p}$ - experiment in the SPS may yield the most relevant numbers.

A very important aspect of most of the proposed ep projects is that the proton beams are bunched. Since there is no damping mechanism for protons like in electron-positron storage rings long term stability of proton bunches with high density is very important.

T. Wilson from CERN showed a video tape of single bunch motions in the SPS that were observed in experiments to test the feasibility of the p$\bar{p}$ project. At bunch lengths of 1.0 m and about 10^{11} protons per bunch longitudinal instabilities were observed. Also a slow increase in longitudinal emittance developed. In view of the fact that these numbers were not so far from the assumptions made for various ep projects and in view of the fact that the SPS vacuum chambers were not especially designed for low longitudinal impedance there was some degree of optimism that the problems of long term stability of high density proton bunches might be manageable.

SESSION ON SUPERCONDUCTING MAGNETS

Discussion Leader: **H. Schopper**

Scientific Secretary: **S. Wolff**

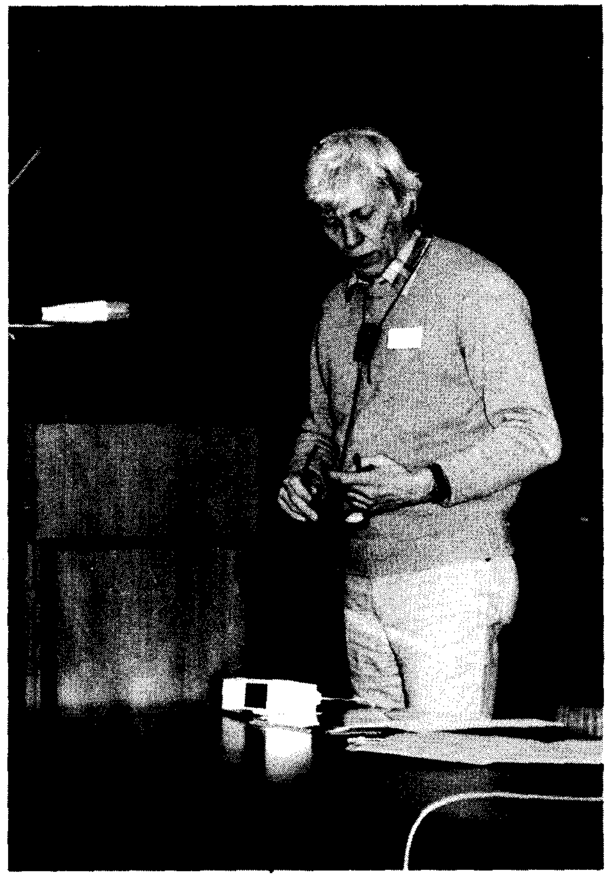

STATUS OF THE FERMILAB TEVATRON PROJECT

A.V.Tollestrup*

Fermi National Accelerator Laboratory†

Batavia, Illinois

SUMMARY

A brief survey of the Fermilab Tevatron is presented, with emphasis on the magnet development. Some operational aspects of strings of up to 24 magnets are presented.

---

*A great many individuals under the direction of R.R.Wilson have contributed enormously to this project. Recognition of some of these contributions is given by means of references -- others are presumably having their deeds recorded by Abou Ben Adhem and will be rewarded at an appropriate time and place.

---

†Operated by Universities Research Association, Inc., under contract with the U.S.Department of Energy.

The Energy Doubler is a proton accelerator that receives its injected beam from the Fermilab Main Ring at 150 GeV and is capable of accelerating the beam to 1000 GeV. Fixed target physics as well as colliding beam experiments are planned and both slow (few seconds) and fast extraction (~1 msec) are planned at intensities of 2×10^{13} protons per pulse.[1]

In the ring there are 760 dipoles and 240 quadrupoles. These elements, consisting of four dipoles and one quadrupole per half cell, are all connected in series and operate at a current of about 4500 A. The field in the dipoles is near 4.5 T and the quads have a gradient of about 20 kG/inch.

The magnets are powered by six 2 kV supplies distributed around the ring that are capable of generating a 75 GeV/sec ramp rate.[2] At flat top a single very well regulated low voltage, low ripple, holding supply will maintain the current during extraction or colliding beam experiments.

Since at full field each magnet stores almost 0.5 MJ, it is obvious that a sophisticated protection system is necessary to protect the magnets during a quench of any one of them. The system planned,[2] uses a micro-processor to monitor the voltage across each half cell and compares it with all the others. In the event of a quench the increasing resistive drop is detected and identified as a quench condition. That half-cell is then shorted and internal heaters fired to drive the four magnets normal as quickly as possible. The energy is absorbed in the cold part of the magnet structure, which increases its temperature to less than 150°K and the energy in the rest of the ring is dumped into resistors.

The refrigeration system[3] consists of a very large Central Helium

Liquefier Plant and 24 satellite stations placed around the ring. The Central Plant is capable of producing up to 5000 ℓ/hr of liquid helium. In normal operation each satellite is supplied with 92 ℓ/hr and acts as an amplifier to produce 966 watts of cooling at 4.2°K. Each satellite feeds a string of about 32 dipoles and 8 quads. The satellites in a stand-alone mode are capable of maintaining the ring superconducting in case of failure of the Central Plant.

PRESENT STATUS

The Tevatron will be the first large high energy accelerator employing superconducting technology. Not only is it planned as an accelerator, but also it will be used as a storage ring. This is an exceedingly ambitious project with no antecedents for guidance and consequently we have concentrated our efforts on answering as many of the new and fundamental problems as possible. So far the following five areas have mainly occupied our attention:

1. Methods to fabricate magnets
2. Measurement of the magnet characteristics
3. Behavior of strings of magnets both from a cryogenic point as well as protection under quench conditions
4. Effect of high energy protons striking the superconducting coils
5. Development of the necessary cryogenic plant.

We address some of these areas here.

1. Magnet Fabrication

The magnet[4] consists of two shells (see Figure 1). The inner subtends a half angle of ~72° and the outer ~36°. The wire is trapezoidal with dimensions of .307" wide, inside height .045" and outside

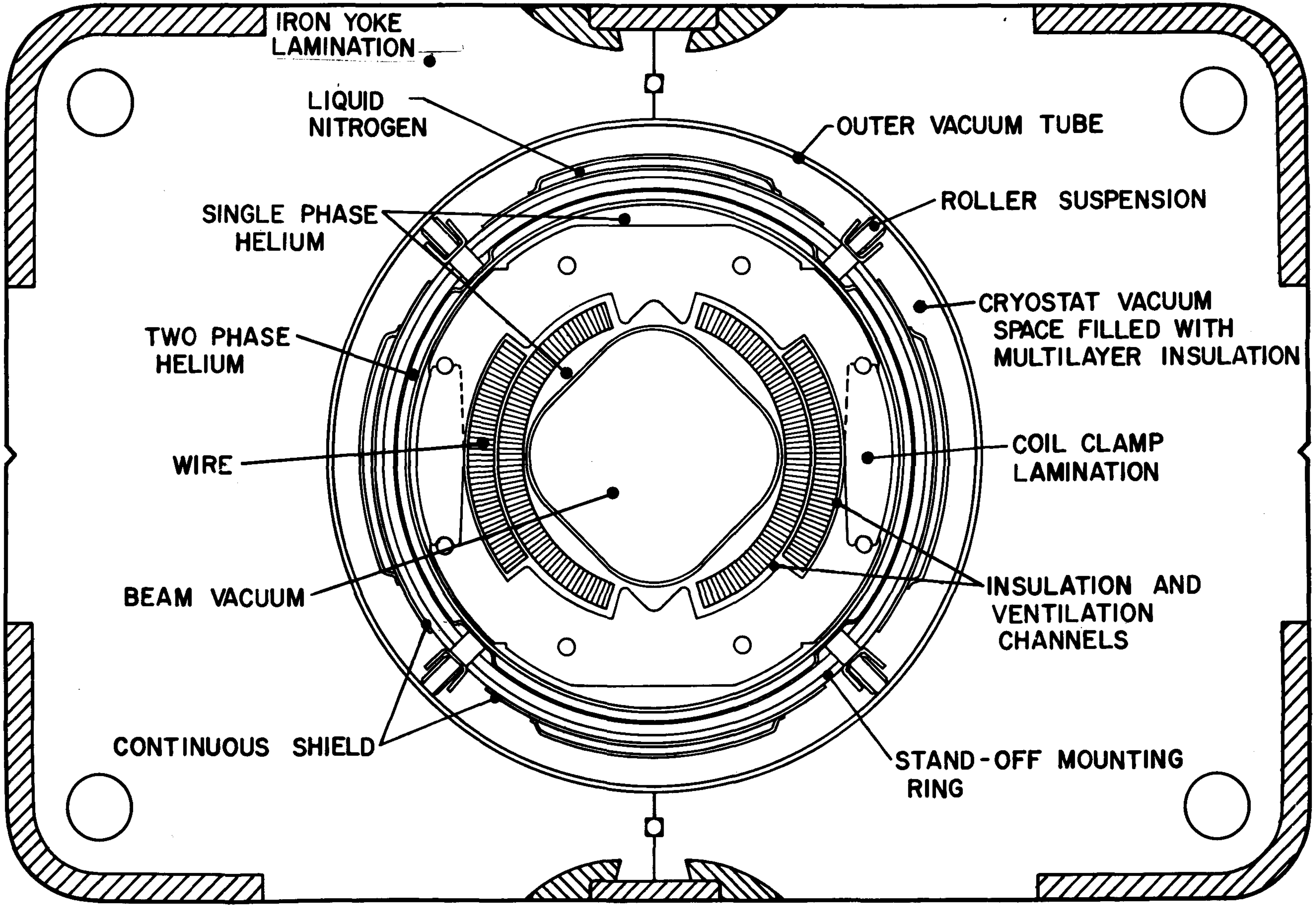

Figure 1. Magnet Cross Section

height .056". It will carry >5300 A of 5 T, and is insulated by a double overlap wrap of 1 mil Kapton and a spiral wrap of B-staged glass tape.

The inner half-coil of 35 turns is wound flat and pressed into shape in a 3000 ton, 24' long precision press. The cross section of the mold is controlled by constructing it from precision stamped laminations.

The outer half-coil of 21 turns is wound over the inner one, using it as a mandrel. This whole structure is again placed in a precision mold, pressed into shape with a second 3000 ton press and cured to its final shape at about 240°F (see Figure 2).

After the half coils are molded, they are measured for circumferential length with a gauge that can apply pressure up to 2000 lb/linear inch on either the inner or outer coil. The size at 1500 lb/linear inch is measured at 10 places along the axis and on each side of the coils. The average of these 10 readings can be controlled to about ±2 mils. Magnet #172 had measurements as given below:

Magnet 172 Coil Sizes

	Inner		Outer	
	Right	Left	Right	Left
Top	2.117±.002	2.117±.002	1.272±.002	1.272±.002
Bottom	2.115±.0015	2.116±.002	1.273±.003	1.2725±.002

The error is the rms fluctuation of the 10 measurements. It is very important to control the size of the coil halves very accurately or when the coil is collared the median plane will not be centered and a quadrupole moment will arise. For instance, a shift of the median plane of .001" of the two coils relative to the fixed corners in the collars will generate a skew quadrupole, a_1, of 2×10^{-4} inches^{-1}.

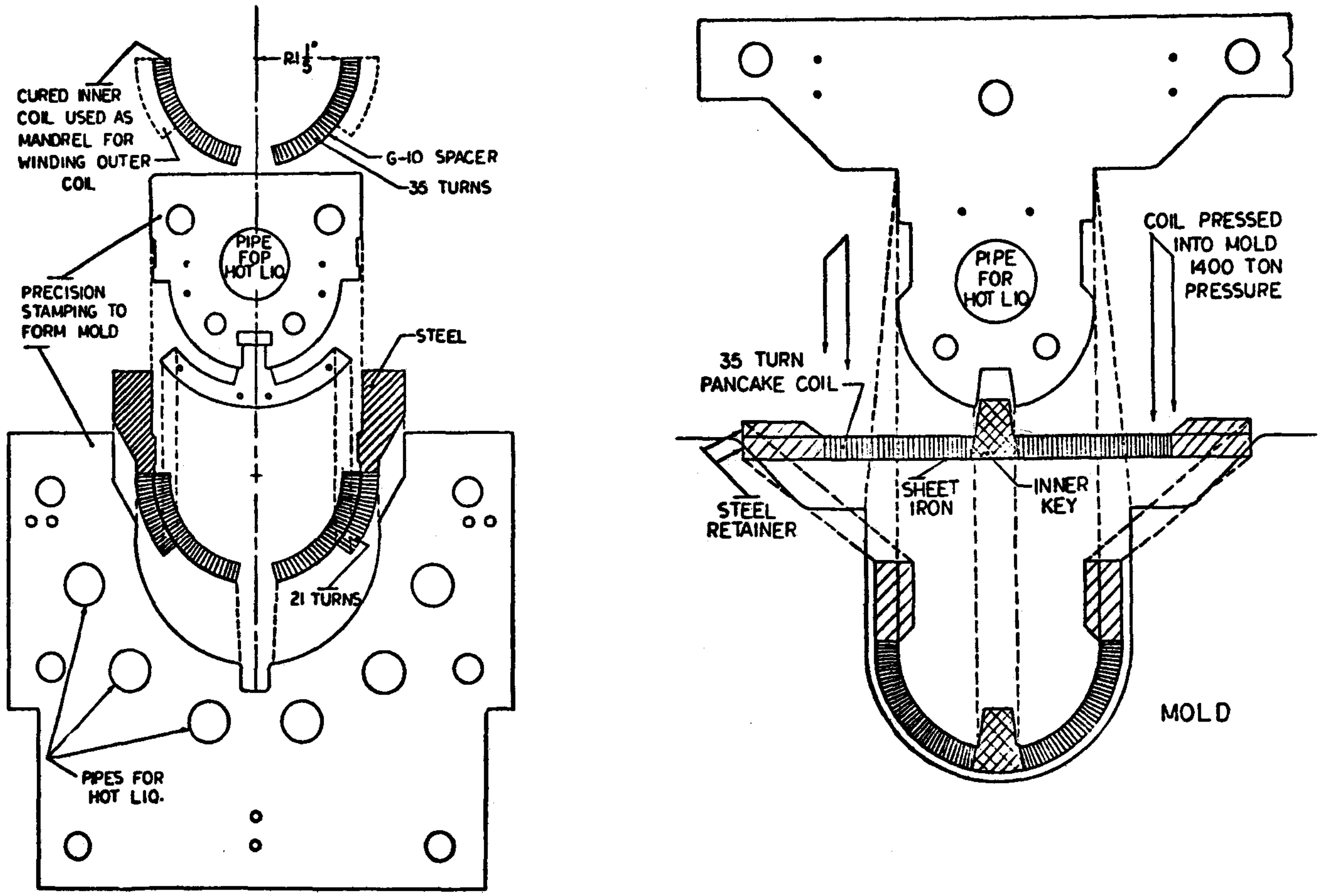

Figure 2. Coil Mold Laminations

A second reason that the coils must be accurately sized is that the "preload" on the coils when collared must be carefully controlled. In order that the coils not move away from the key surfaces in the collar, it is necessary to compress the inner coils with an elastic force of 1300 lb/inch and the outers with 500 lb/inch. However, when the coils are cooled, they shrink more than the collars. The stress-strain curve for the coils, both warm and cold, has been studied[5] and it is found that an initial room temperature compression of the outer coils of 1500 lb/inch and the inners by 4000 lb/inch is necessary in order to achieve the required preload when the coil is cold. These compressions give a differential Young's modulus for the coils of about $10^6(\text{psi})^{-1}$.

The control of coil size is crucial to understand, and additional techniques are still being developed to improve and simplify the accurate fabrication of coils.

After the magnet is collared, the field in the horizontal plane is measured at room temperature.[6] This is done by inserting into the magnet bore a set of 12 long loops 0.195" wide × 24' long, spaced .215" ℄ to ℄. The coils are supported in a stainless steel tray and cast into epoxy for stability. The magnet is then excited at 11 Hz with a current of about 10 A and a lock-in amplifier used to measure the difference of the induced voltages between adjacent loops. This gives a number proportional to the gradient of the field. The coil must be calibrated since differences in area are much greater than the change in B over the aperture ($\delta B/_B \sim 10^{-4}$). We have been able to refine these measurements sufficiently so that we can determine b_1, b_2, b_3, b_4. These parameters as measured at room temperature without an iron yoke can be related to their final value with a yoke and with the coil superconducting.

The block diagram of the factory then can be outlined as in Figure 3.

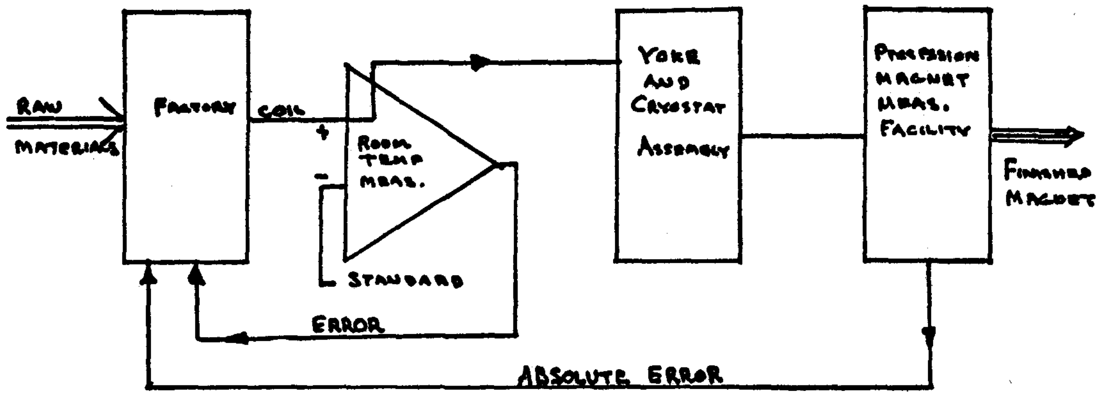

Figure 3. Block Diagram of Factory

The room temperature measurements provide a means for immediately monitoring the quality of the collared coil.

If deviations outside of acceptable limits occur in a coil, it can be set aside for recollaring, and appropriate adjustments made in the next coil to correct the trouble. The long-term stability of the system is controlled by a slow feed-back loop provided by the precision magnet test facility.

Two very important points are implicit in the operation of this scheme. First, the factory must make reproducible coils. Fluctuations from coil to coil cannot be removed by the fast feed-back loop. The reproducibility is controlled by the very precise tooling used in the manufacture. It was necessary to invent the "laminated tooling" in order to achieve the necessary small tolerances.[4]

The second important discovery came when it was realized that absolute dimensional accuracy is not required anymore. Consider a coil of the shape shown below (Figure 4).

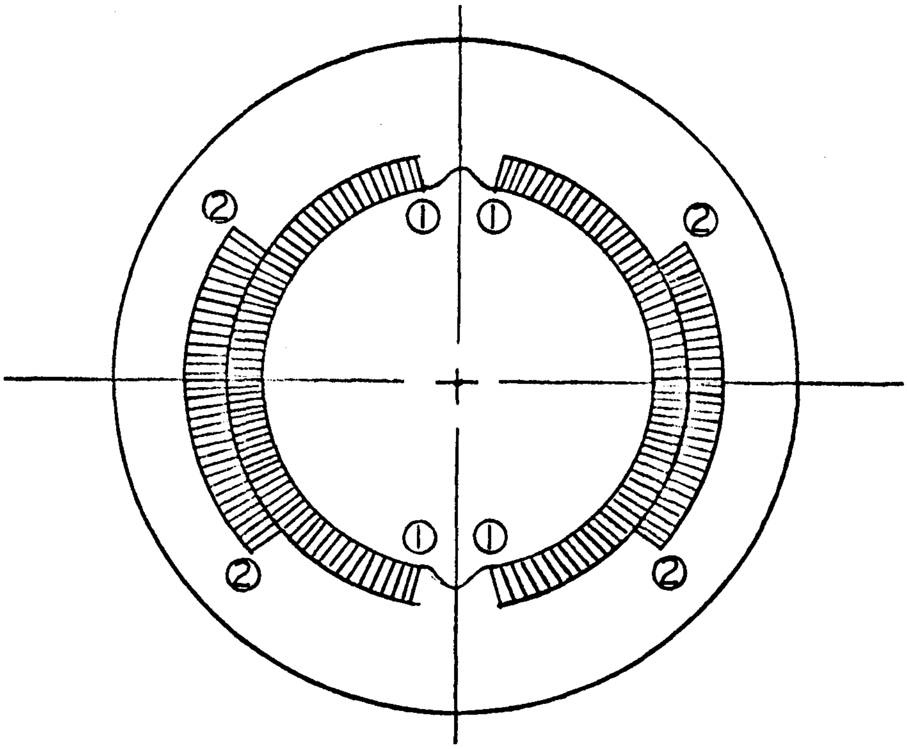

Figure 4. Coil Cross Section

The structure is designed in such a way that the stainless steel shim stock can be inserted before collaring, at the points labeled ① and ② . Thus the angles of the coil blocks can be changed by small amounts at will.

Consider the harmonic structure of such a coil. The calculated movements in $\delta B/B$ at 1" are given below (integrated through the magnet).

$$b_2 = 0$$
$$b_4 = 1.1\times10^{-4}$$
$$b_6 = 4.4\times10^{-4}$$
$$b_8 = -12.1\times10^{-4}$$
$$b_{10} = 3.6\times10^{-4}$$
$$b_{12} = -0.8\times10^{-4}$$
$$b_{14} = .07\times10^{-4}$$

These coefficients give a $B(x)/B_0$ (integrated through magnet) as function of x as shown in Figure 5.

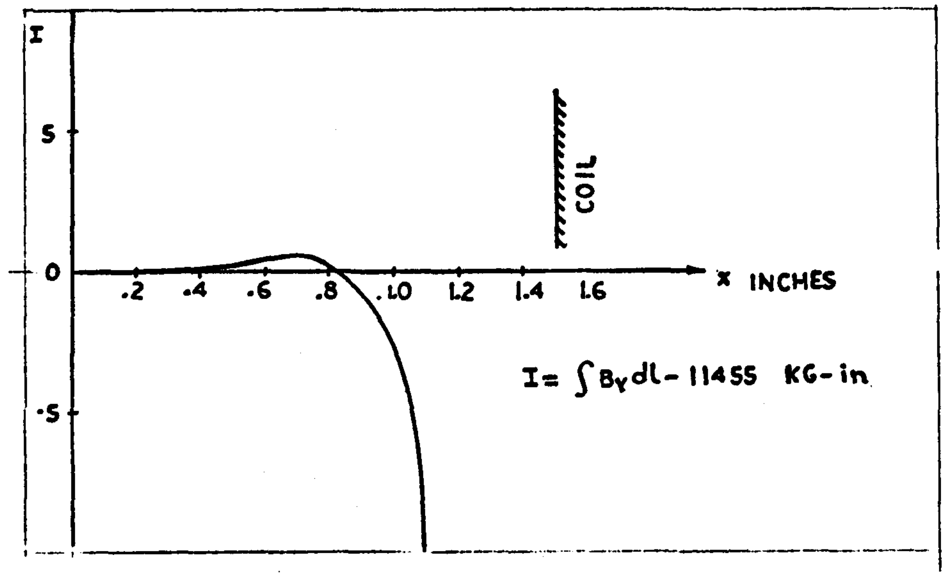

Figure 5. Variation of the Integral of B Through the Magnet as a Function of Radius

With a little work it can be shown that for small changes of the coil shape only the multipoles below the 14-pole will change. Thus, if the coil is not exactly circular, but perhaps a little elliptical or square, or some other shape, the higher multipoles which are determined by the Fourier components of the current block corners will be nearly the same as in the correct coil shape. However, the decapole terms and below will be different and there are eight places shims can be inserted into the coil structure to modify these components.

Thus we arrive at an important point. If the factory is reproducible, a coil can be built, measured, and the next one corrected to have a uniform field without having to produce a coil whose absolute dimensions are known. This process will leave a small random fluctuation in the central field, B_0, but this is very small and the orbit distortions can be corrected by the horizontal correction elements that are necessary in any event.

We now present some data gathered over the last two years. Over 170 coil assemblies have been constructed during the development of the coil fabrication technique. Some of these coils are suitable for accelerator tests after their insertion into a cryostat. Some are being used in rather extensive systems tests to be described later, and many of the rest will be useful for beam transport. To get some idea of the overall quality of these magnets, for use in beam transport systems, it may be said that the random errors have always been small enough so that a single pass through 740 such randomized magnets leaves the phase space inside ±½" essentially an undisturbed ellipse.

The last major hurdle was to close the room temperature feedback loop, which was done in January 1979. In the meantime the magnets have been shortened by one foot in order to accommodate shielding in the quadrupole cryostats which will help protect the dipole coils from stray beam at injection and extraction. Since April 1979 the new series of 21' magnets has been underway. On the basis of what we have learned it is expected that "Accelerator quality" magnets will be produced. The factory has been operated at a level of five magnets per week for short test periods and should be capable of 10/week. The main problems expected are in the quality control area.

MAGNET MEASUREMENTS

We begin by presenting data obtained in vertical dewar tests of the collared coils.[7] The yoke and cryostat are not yet assembled and only measurements of training, peak field, ramp rate dependence, change in radius of the coil, azimuthal motion of the wire, transfer constant, and residual field due to persistent currents are measured.

Figure 6 shows the training history of one of the recent coils, #167, and Figure 7 gives the B dependence of the quench point. A typical load line and maximum quench point are given in Figure 8. With the iron, the peak field point is 1.1 B_0 at the key of the inner coil, and without iron the high field point is at the inner turn at the very end of the coil. The end turns are spaced out slightly to reduce the field at the end.

Now to examine the statistics of a number of coils we show the following three histograms. Figure 9 shows the number of quenches to reach 95% of I_{max}, and Figure 10 shows the percent of expected short sample current that the coil achieves. The short sample curve of each reel of wire is measured after being received from the manufacturer. Finally, Figure 11 shows the distribution of peak quench currents obtained.

The ramp rate dependence of the coils is determined by both the heat generated during ramping as well as by the cooling. The coils initially were wound with Stay-Brite-coated wire. Subsequently it has been determined that eddy current losses in the coil package were too high with such good contact between the strands of wire. Consequently we are now using Ebonol-(copper oxide) coated strands and the losses are essentially all due to hysteresis.

COIL LOSSES

	Ebonol	Stay-Brite
Hysteresis	200J	200 J
Eddy Current	~20J	160-560 J

The above numbers are for the following ramp:

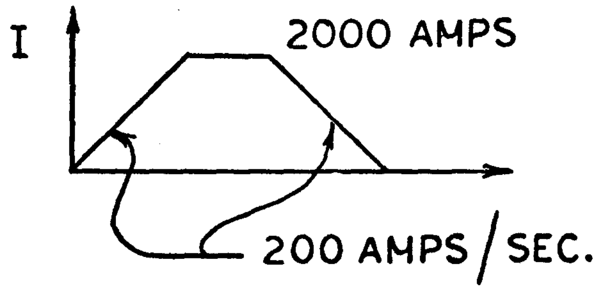

The collars must contain a force in the x direction of 6000 lb/inch, which tends to blow the coil apart. Fatigue studies were made of the collaring system and a lifetime in excess of 10^8 cycles is now expected. Figure 12 shows the radial deflection as a function of coil current. It is accurately parabolic and a histogram of the deflections of 23 magnets is given in Figure 13. There are other elastic motions of the wire. These have been studied and their net effect on the field shape is well within the level of the correction circuits. It is worth noting that the persistent currents generate a rather strong sextupole field (~10 gauss) which must be corrected and in general, in superconducting magnets, there must always be dynamic correction elements which are under program control and with a magnitude of a few $\times 10^{-4}$.

After the magnet coil is assembled in its cryostat[8] it is given a complete set of precision magnetic tests in the Magnet Test Facility.[9] This Facility consists of six test stands where a magnet may be connected to power and refrigeration, and a 1500 watt refrigerator capable of cooling the system. Each magnet is vacuum tested, tested cryogenically, trained, its ramp rate dependence measured as well as the energy loss per cycle at various $\dot{B}$'s. Finally, a complete set of dc and ramped field harmonics is measured at eleven different currents. The $\int B \cdot dl$ is measured by a combination of NMR and Hall probes that are moved through the magnet automatically by the computer. This complete

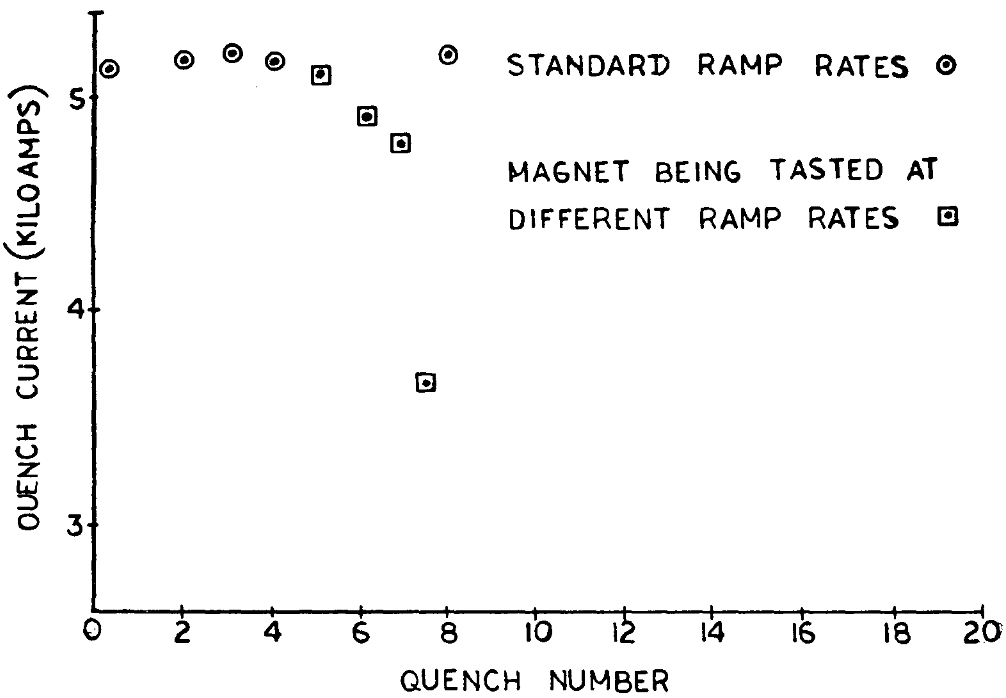

Figure 6. Training - #167

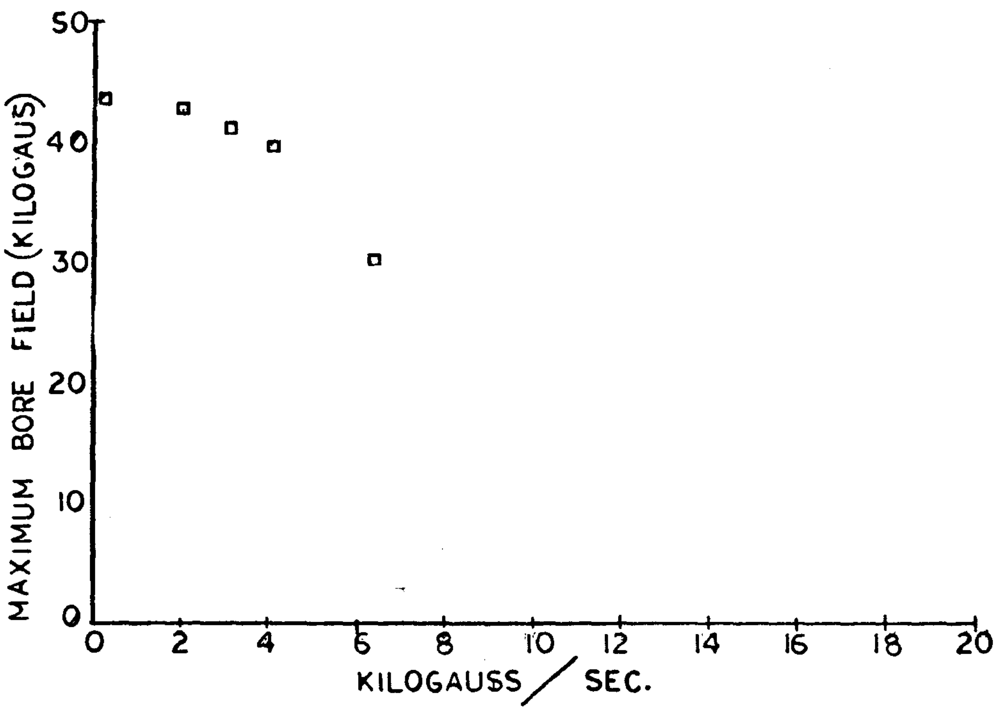

Figure 7. $\dot{B}$ Curve

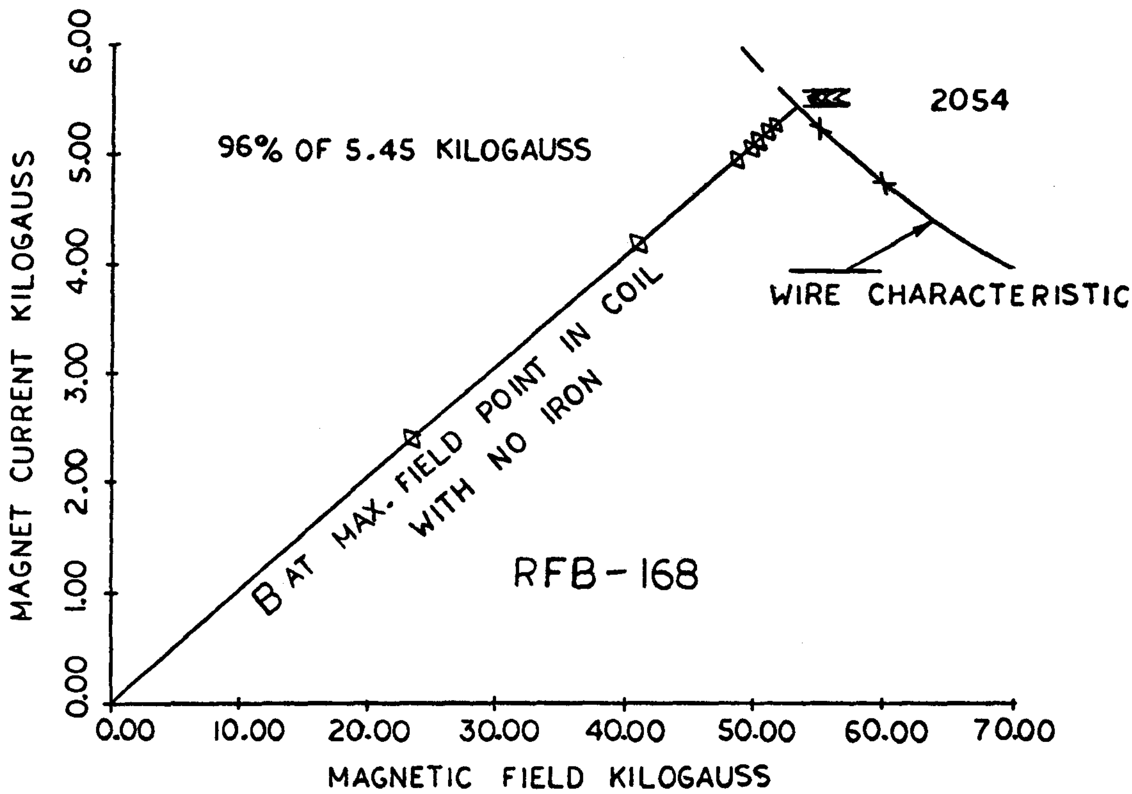

Figure 8. Load Line and Short Sample Limit

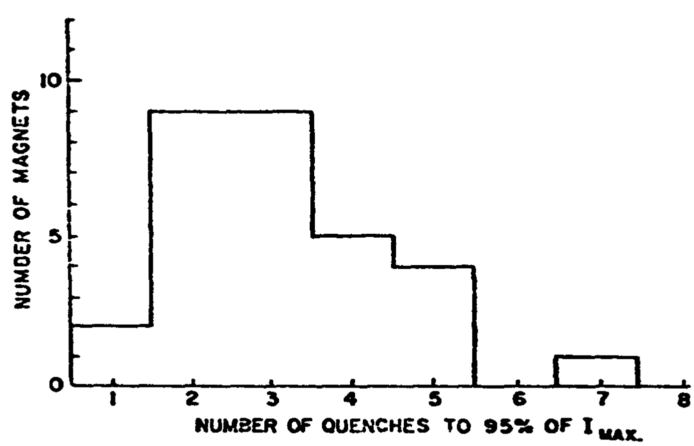

Figure 9. Train Current Distribution

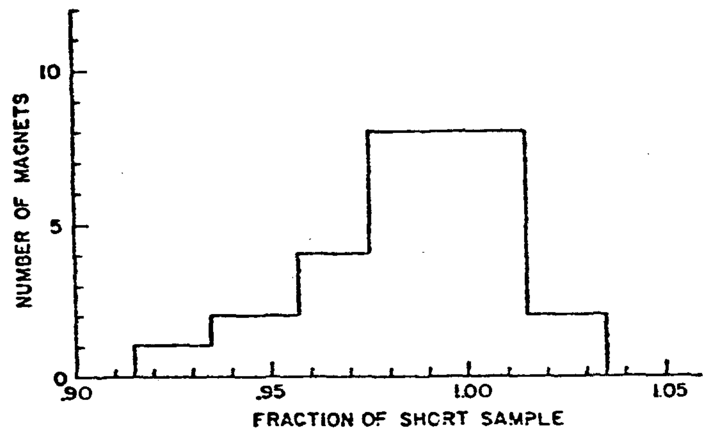

Figure 10. Distribution of Final Training Current as a Fraction of Short Sample Limit

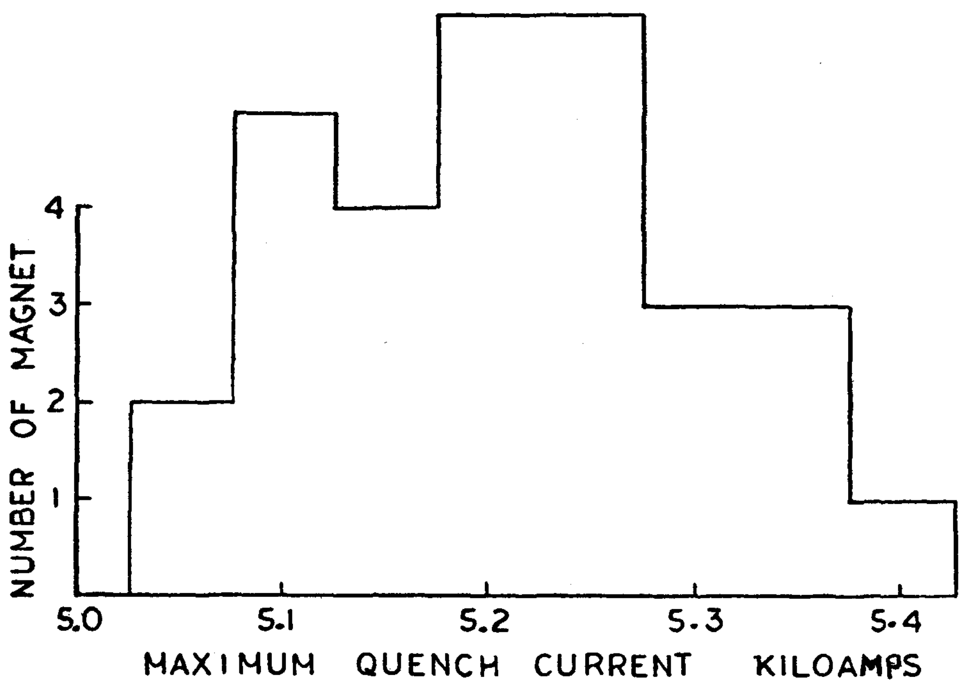

Figure 11. Distribution of Max. Quench Current

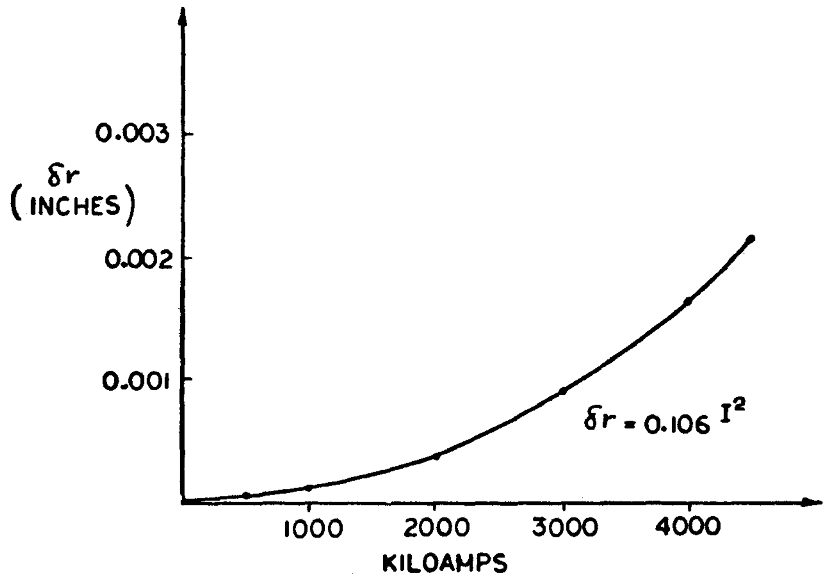

Figure 12. Radial Deflection vs Magnet Current

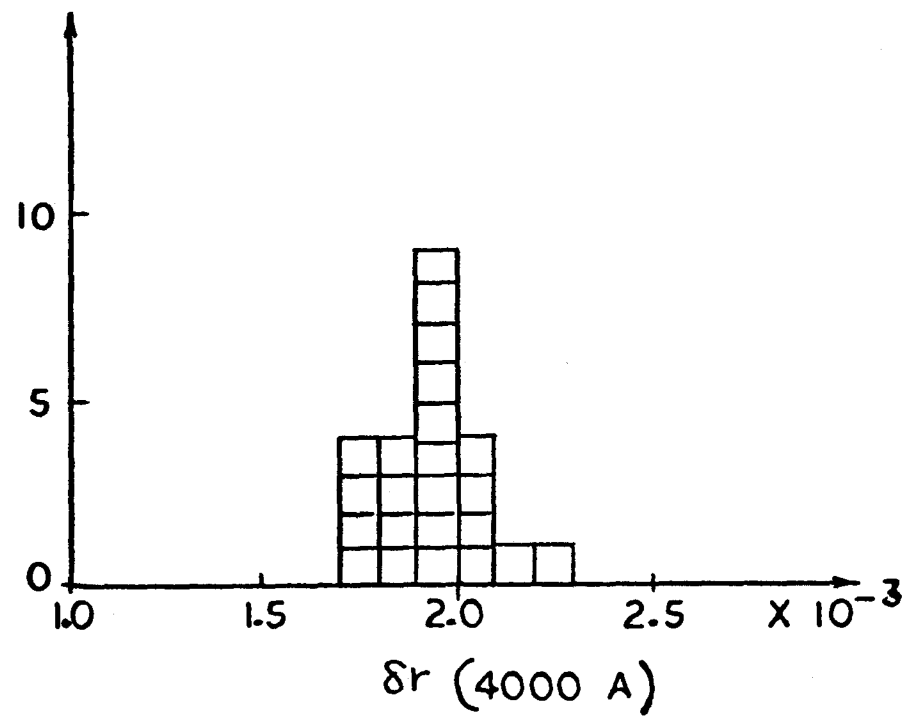

Figure 13. Distribution of δr at 4000 Amps

set of data plus assembly data is stored on a DISC File as permanent data for each magnet. So far about 40 magnets have had a complete set of measurements made, and almost 80 have had partial measurements. We can now examine some of this data.

Figure 14 shows a histogram of the quench current at 200 A/sec. The effects of different types of conductors can be seen in Figure 15a. Figure 15b shows a histogram of the magnet effective length. Some identifiable structure changes took place and account for some of the spread in the histogram.

Both the normal and skew harmonics are measured up to 30-pole. The following Table lists the harmonics averaged over 24 magnets.

TABLE I

		Average		Limits	
K	Pole	A(k)	B(k)	A(k)	B(k)
1	Quadrupole	1.78±3.18	-0.16±1.65	±2.5	±2.5
2	Sextupole	0.58±0.89	-9.20±6.15	±1.6	±6.4
3	Octupole	-0.16±1.72	0.33±0.71	±4	±4
4		0.11±0.62	3.69±1.87		
5		-0.18±0.48	0.33±0.40		
6		-0.26±0.38	3.41±0.49		
7		0.15±0.34	-0.01±0.36		
8		0.21±0.67	-12.96±0.41		
9		0.36±0.45	0.06±0.45		
10		-0.00±0.45	4.42±0.37		
11		-0.16±0.34	0.08±0.37		
12		0.00±0.37	-1.13±0.36		
13		0.06±0.42	-0.04±0.53		
14	30-pole	-0.01±0.40	-0.01±0.33		
		All units $\frac{\delta B}{B}\cdot\times 10^4$ at 1^4			

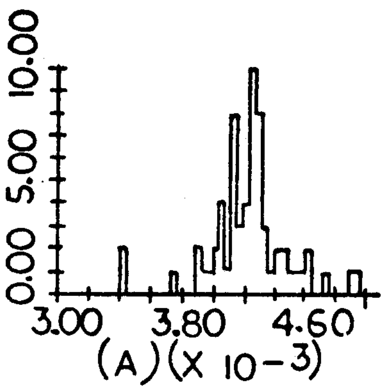

Figure 14. Distribution of I_Q at $\dot{I}$ = 200 A/sec

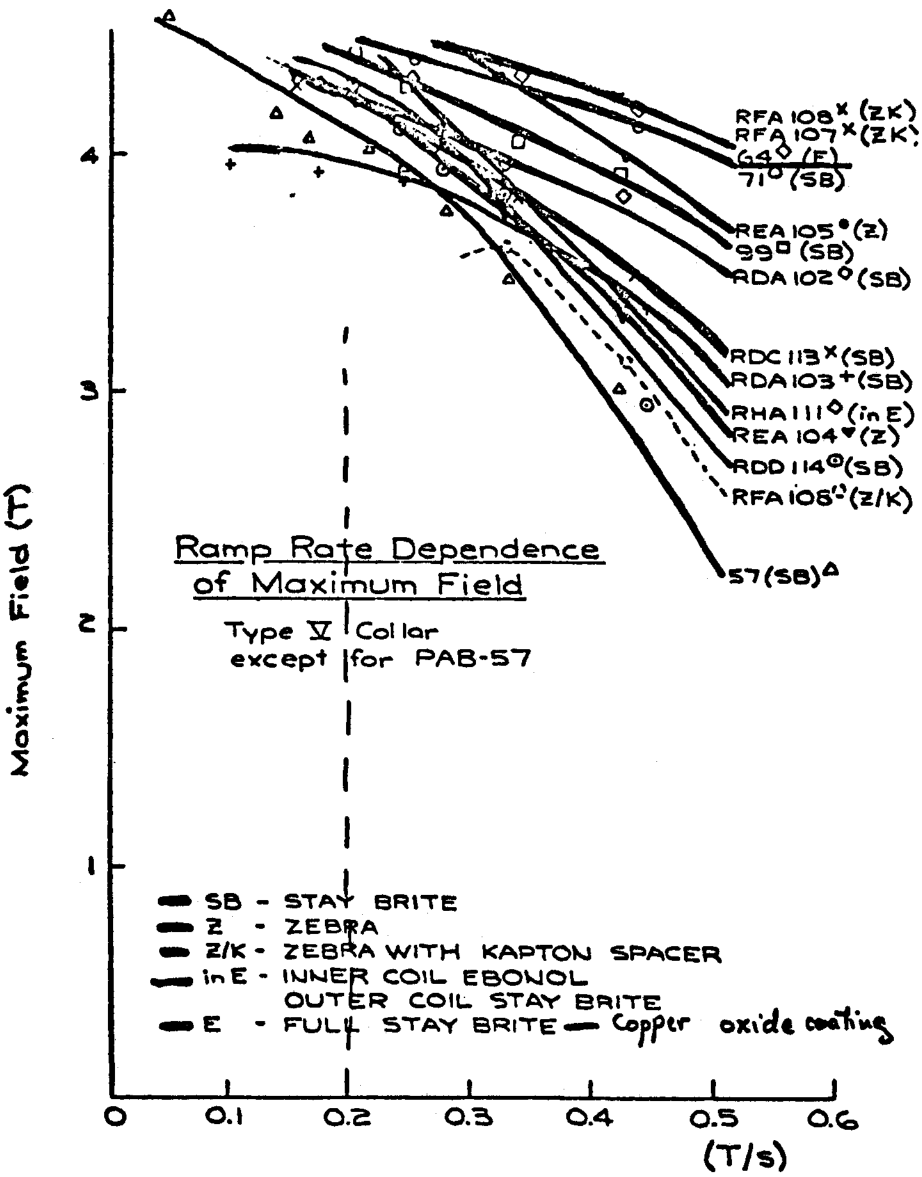

Figure 15a. Ramp Rate Dependence of Magnets in Cryostats

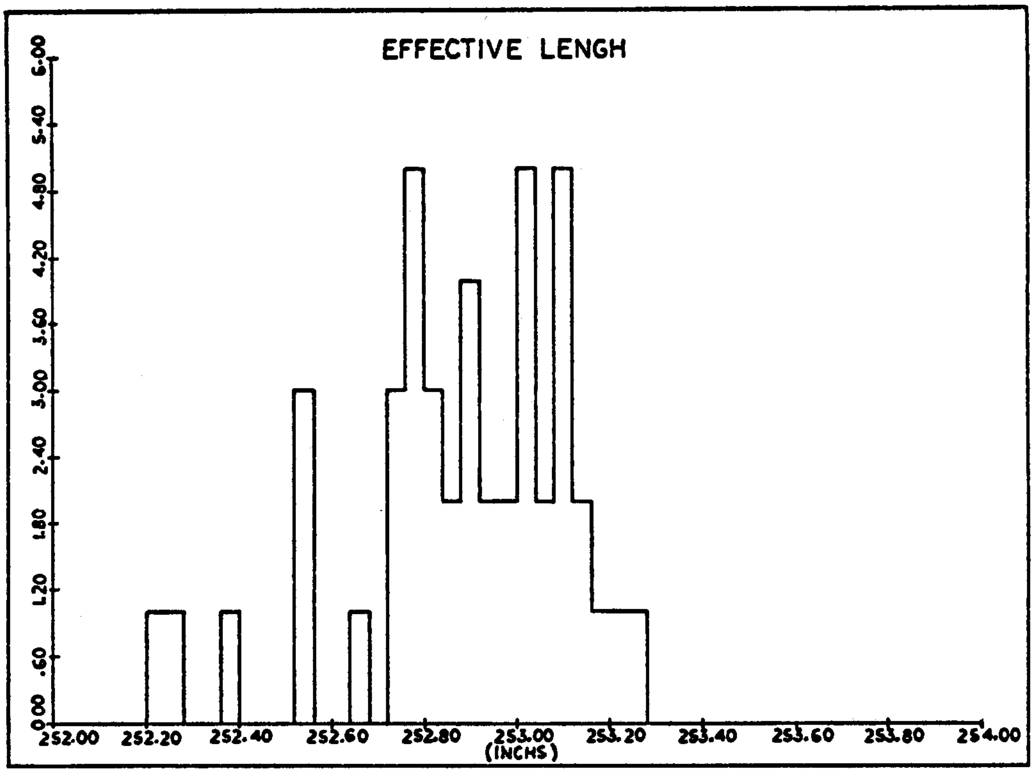

Figure 15b. Effective Length at 2 T

All of the a_n and the odd b_n should be missing in an ideal magnet. These terms therefore give some indication of the random errors generated during coil fabrication. The even b_n are permitted and their values are listed on page 9, along with the design value. It is seen that above the decapole the design values agree well with the desired ones. The sextupole and decapole are not correct. These will be corrected by adjusting the shims at the keys. The line labeled "Limits" indicates the results of theoretical studies on the acceptable limits for various multipoles in the Tevatron. This study is not yet finished and work is still in progress. Limits on multipoles not listed will shortly be specified.

Small effects due to coil motion and persistent currents in the superconductor cause the multipole movements to be current dependent.

Eddy current effects are also present in the cable strands. All of these effects mainly show up in the sextupole moment. Eddy currents in the Ebonol winding are too small to measure, but Figure 16 shows the hysteresis in the sextupole moment b_2. Dynamic corrections are planned to cancel out this variation. The results of many other measurements are given in Reference 9.

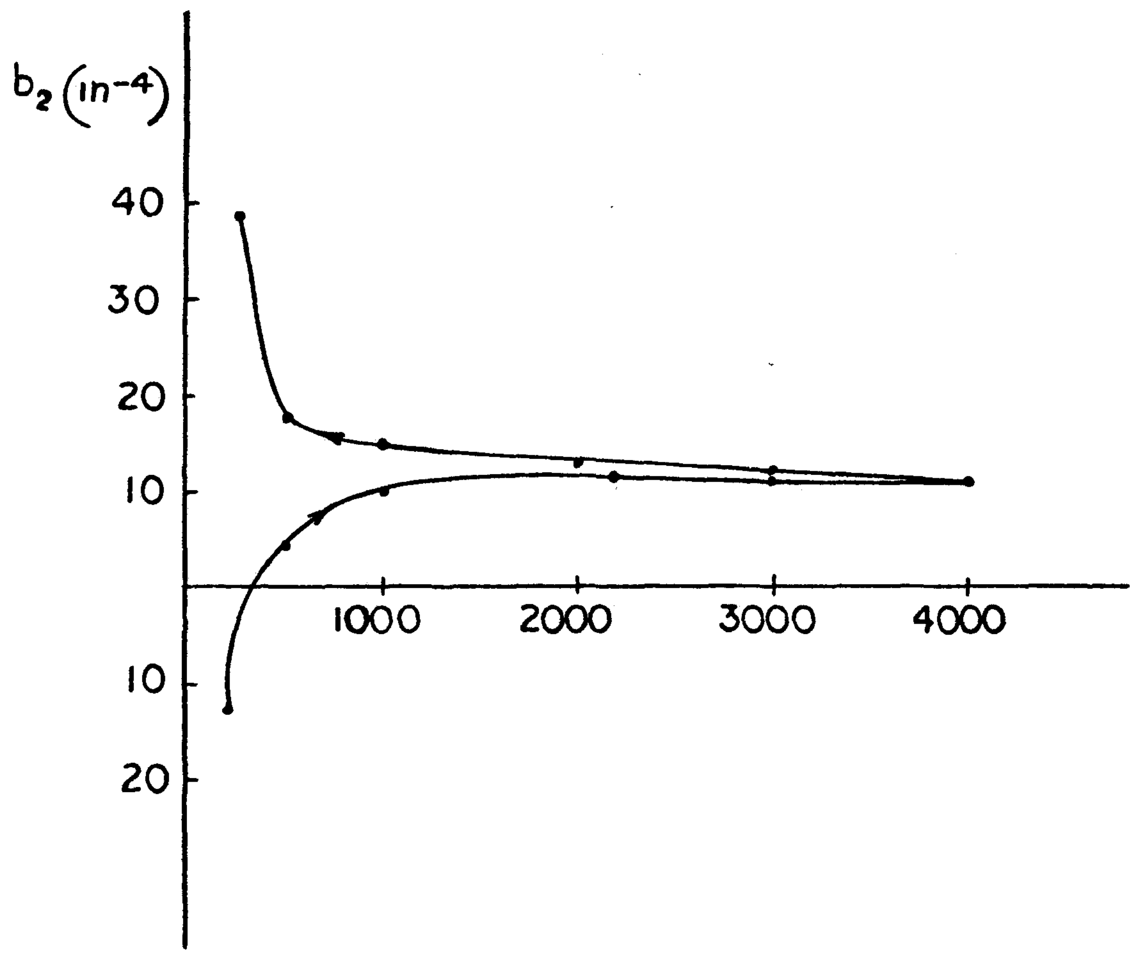

Figure 16. Sextupole Moment vs Magnet Current

BEHAVIOR OF STRING OF MAGNETS

At present tests on strings of magnets are being intensively studied. Three types of tests have been conducted.

First, strings of four to eight magnets have been cooled, pulsed to full field and their behavior under quench conditions studied.[10] These tests were above ground and no beam was involved and their primary option has been to develop the quench protection system and a prototype power supply. Cryogenic tests have also been made, which verify the initial calculations of the static heat load of a magnet being about 6 watts.

Figure 17 shows the enthalpy of the coil itself, the coil plus collars, and the helium. It is seen that the helium serves as an energy "ballast" at operating temperature and that a full energy quench with all of the energy uniformily deposited throughout only the coil would raise the coil temperature to no more than 100°K. The main function of the heaters that are fired when a quench is detected is to bring as much of the coil as possible into active energy absorption. The crosses show the temperature actually recorded in the magnet structure gas at about 2-3 minutes after a quench. It is seen that some fraction of the energy is carried off by the helium. This is not yet quantitatively understood and further work is in progress to study these effects.

Figure 18a, b, shows the $\int I^2 dt$ and the pressure in the cryostat vs the current in the magnets for induced quenches in a string of four magnets.

In the near future the string of four magnets will be increased to eight and then 16 -- which is close to half of a "cryogenic string".

In addition to tests above ground, three series of tests have been carried out with beams of protons passing through the magnets.[11] We reproduce here a curve from the study by Cox which shows the variation of the number of protons at 400 GeV hitting the magnets that will

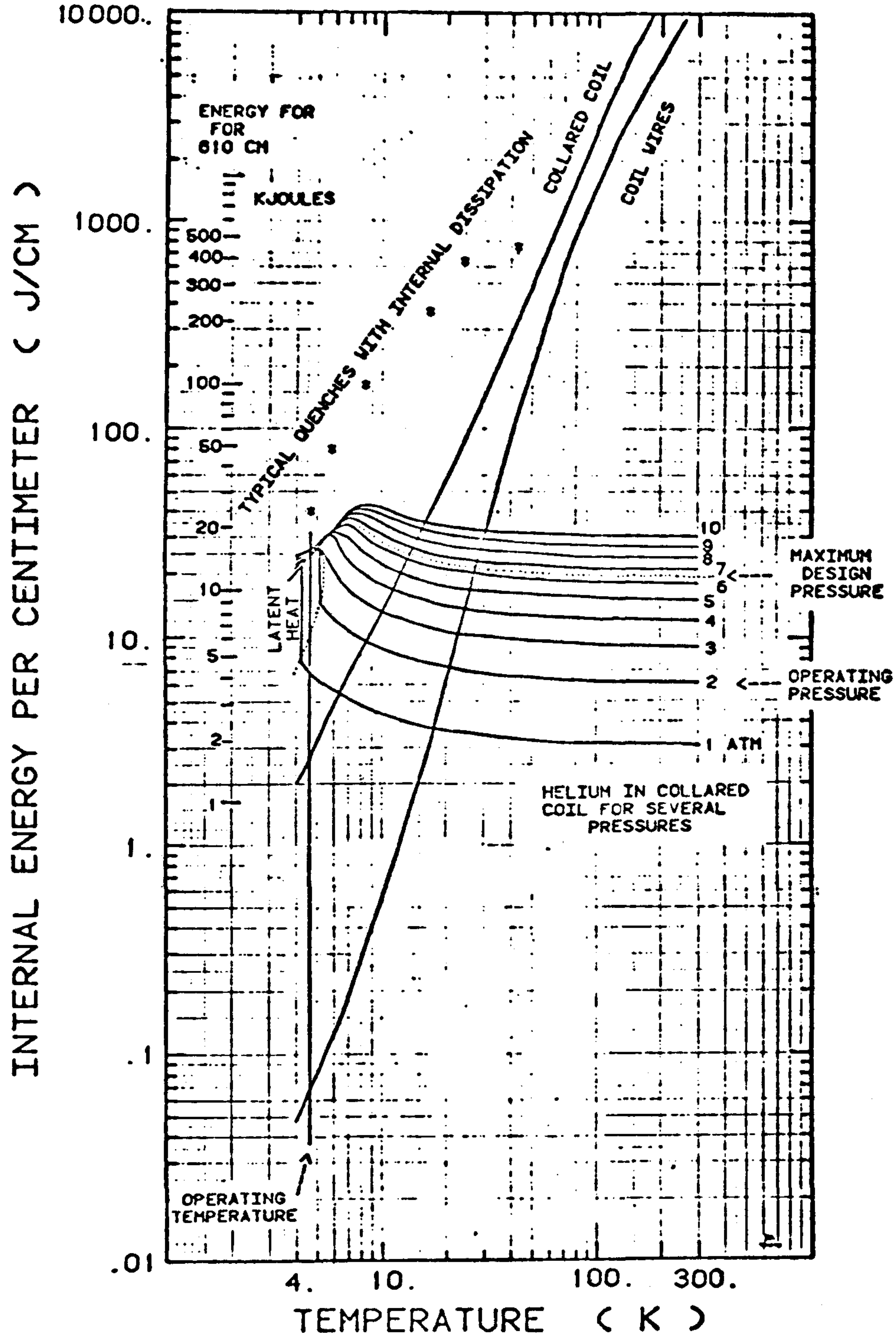

Figure 17. Enthalpy of Coil and Magnet Structures

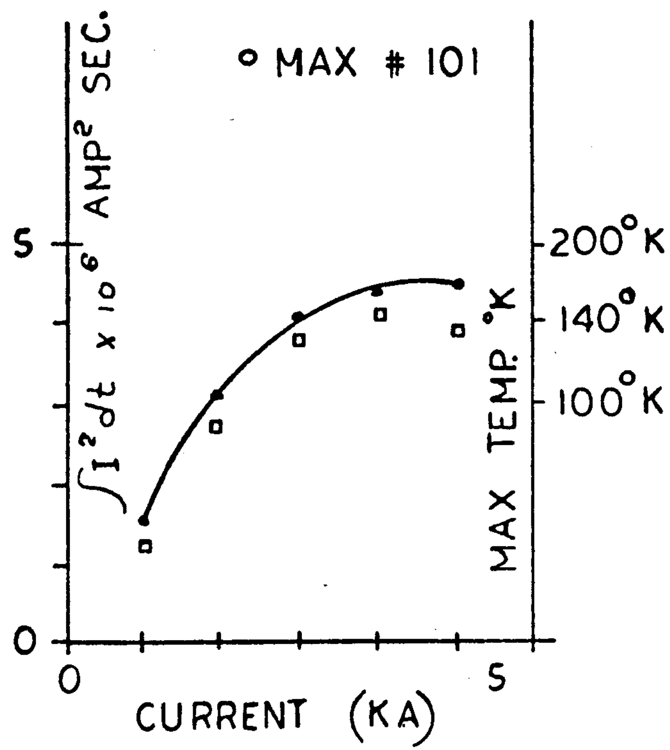

Figure 18a.

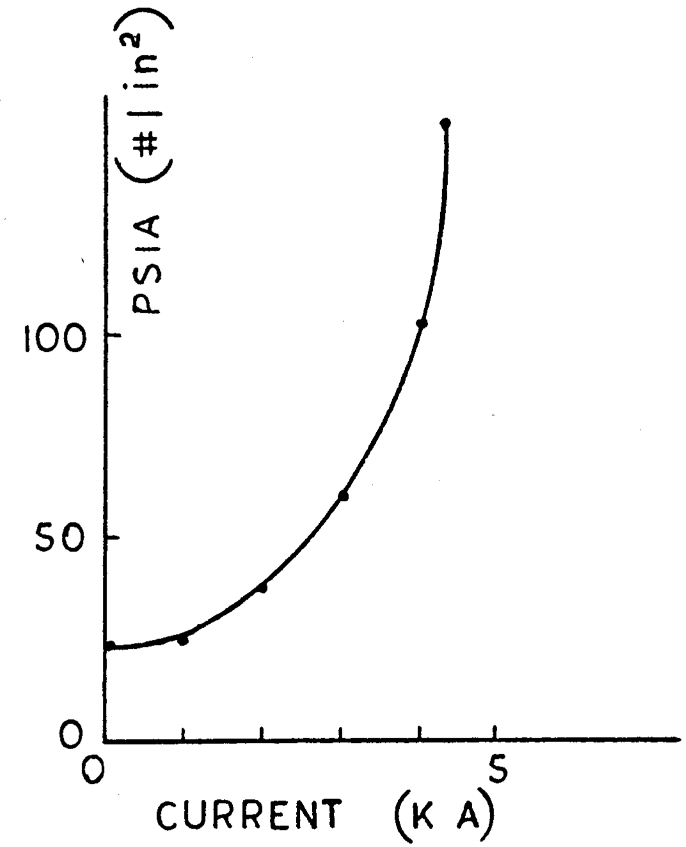

Figure 18b.

$\int I^2 dt$ and the Pressure in the Cryostat vs the Current in the Magnets cause a quench vs the magnet current. The magnet has a no beam quench limit of about 4000 A. Calibration of the beam indicated that at 3500 A in the magnet, 4 mW/g for slow extraction, or about 1 mJ/g per pulse (1 msec) for fast extraction will cause quenching of the magnets. Extensive studies of technique for shielding the magnets during extraction have been carried out,[12] and techniques are being developed so that the Tevatron can provide both slow as well as fast extracted beam.

Finally, a string of 24 magnets and their associated quadrupoles are installed in the Main Ring tunnel and are being cooled by a satellite refrigerator. (See Figure 18.) Beam was first passed through the string at 90 GeV in January 1979. Much experience has been gained in learning how to install and cool Doubler magnets under the actual conditions that must finally be faced. At the low injection energy it was very pleasant to discover that the string of magnets would recover from a beam induced quench in less than 30 sec. These studies are being continued, but full field studies will not be carried out until tests above ground on smaller strings of magnets have been studied in greater detail.

SUMMARY

The program at Fermilab is now about ready to go into production of accelerator-quality magnets suitable for installing in the final Tevatron ring. It is felt that the major problems of producing high quality, rugged, vacuum-tight and cryogenically acceptable magnets have been overcome. It is hoped that a major step toward applying superconductivity to accelerator magnets has been mastered and that the way is opened to applying these techniques to still higher energy machines in the future.

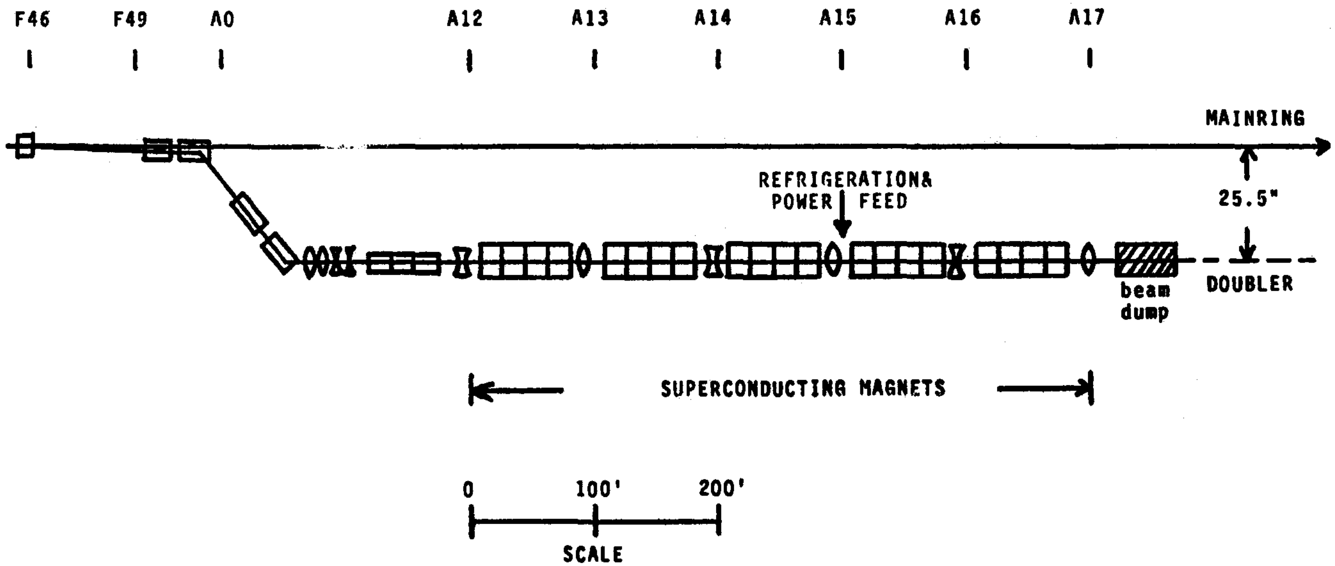

Figure 19. String Magnets

REFERENCES

1. Project Description:

   a. The Energy Doubler - A Progress Report for the Energy Doubler, Saver, Collider Project, Fermilab, June 1976.

   b. R.R.Wilson, The Tevatron, Phys. Today, 23-30 (October 1977).

   c. The Energy Saver, Fermilab Report, January 1978.

   d. H.T.Edwards et al, Report on the Design of the Fermilab Superconducting Accelerator, Fermilab, May 1979.

   e. A.V.Tollestrup, Progress Report -- Fermilab Energy Doubler, IEEE Trans. Magn., MAG-15, No. 1, 647 (January 1979).

2. Magnet Power Supply and Quench Protection System:

   a. R.Stiening et al, A Superconducting Synchrotron Power Supply and Quench Protection Scheme, IEEE Trans. Magn., MAG-15, No. 1, 670 (January 1979).

   b. R.H.Flora and G.S.Tool, Doubler-Tevatron μP Quench Protection System, Paper D-47 presented at the 1979 Particle Accelerator Conference, San Francisco, CA, March 12-14, 1979.

3. Refrigeration System:

   a. R.Rihel et al, Central Liquefier for the Fermilab Tevatron, Paper J-32 presented at the 1979 Particle Accelerator Conference, San Francisco, CA, March 12-14, 1979.

   b. A.Visser et al, Power for the Fermilab Tevatron Helium Liquefier, Paper K-21 presented at the 1979 Particle Accelerator Conference, San Francisco, CA, March 12-14, 1979.

4. Mechanical Structure of Magnet:

   a. G.Biallas et al, The Support and Cryostat System for Doubler Magnets, IEEE Trans. Magn., MAG-15, No. 1, 131 (January 1979).

5. Fabrication of Magnet Coils:

a. K.Koepke et al, Fermilab Doubler Magnet Design and Fabrication Techniques, IEEE Trans. Magn., MAG-15, No. 1, 658 (January 1979).

6. Room Temperature Field Measurements:

a. R.E.Peters et al, Room Temperature Field Measurements of Superconducting Magnets, IEEE Trans. Magn., MAG-15, No. 1, 134 (January 1979).

7. Results of Vertical Dewar Tests:

a. A.V.Tollestrup, Progress Report -- Fermilab Energy Doubler, IEEE Trans. Magn., MAG-15, No. 1, 647 (January 1979).

8. Cryostat Production:

a. B.P.Strauss et al, How to Mass Produce Reliable Cryostats for Large Particle Accelerators, Paper K-22 presented at the 1979 Particle Accelerator Conference, San Francisco, CA, March 12-14, 1979.

9. Magnet Test Facility:

a. D.A.Gross et al, Production Measurement of Energy Doubler Magnets, IEEE Trans. Magn., MAG-15, No. 1, 137 (January 1979).

b. M.Wake et al, AC Loss in Energy Doubler Magnets, IEEE Trans. Magn., MAG-15, No. 1, 141 (January 1979).

c. D.A.Gross et al, Results of Recent Measurements of Energy Doubler/Saver Magnets, Paper K-7 presented at the 1979 Particle Accelerator Conference, San Francisco, CA, March 12-14, 1979.

10. Multiple Magnet Test Program:

a. P.Brindza et al, The Multiple Magnet Test Program, Paper K-5 presented at the 1979 Particle Accelerator Conference, San

Francisco, CA, March 12-14, 1979.

11. Measurements of the Effect of Beam Striking Energy Doubler/Saver Magnets:

    a. B.Cox et al, Sensitivity of an Energy Doubler Dipole to Beam Induced Quenches, Fermilab Technical Memo 828-A, November 1978.

12. Calculations of Effect of Beam Striking Energy Doubler/Saver Magnets:

    a. H.T.Edwards et al, Studies on Radiation Shielding of Energy Doubler Magnets, Fermilab UPC-30, December 27, 1978, UPC-40 (up-date), January 12, 1979.

Discussion

Weber/DESY:

Could you say something about the rumors that the length of the magnet was changed recently?

Tollestrup:

Yes, we changed the length when we changed directors at FERMILAB. The new management thought that there was not enough space left for correction coils and for shielding. The subject will come up more later. So the magnets have now been shortened. I would not be surprised if we end up without empty space, but everybody feels much more comfortable now.

Schopper:

How long are they now?

Tollestrup:

21 feet!

Weber:

Instead of 28?

Tollestrup:

Instead of 22! It is a five percent change. That is why I said the peak field for 1 TeV would have to change by 5 %, up to 44.5 kilogauss.

The ISABELLE Superconducting Magnets*

W.B. Sampson
Brookhaven National Laboratory
Upton, New York 11973

Introduction

The basic design concept for the ISABELLE superconducting magnets can be traced back at least fifteen years. The first magnet of this type was a short quadrupole wound from Nb_3Sn tape conductor.[1] In the intervening years the fundamental features of the design have changed very little but continuous improvements have been made in the conductor and assembly techniques. Dipoles have been constructed with apertures ranging from 5 cm to 25 cm and with lengths up to 475 cm.[2-3] In addition a number of quadrupoles have been fabricated with lengths in the one to two meter range.[4] The magnets consist of a single layer of very wide conductor wound into coils of circular cross section which are enclosed in a tightly fitting cylindrical iron core. In this paper the details of the design are outlined and recent results from commercially produced coils are summarized. Some suggestions are included on how the design might be modified to match the requirements of the proposed proton ring for the PETRA machine.

Conductor

An important feature of the coil design is the fact that only a single layer of conductor is used. This requires a conductor of very high aspect ratio. The ISABELLE conductor is approximately thirty times as wide as it is thick, and is formed by braiding many small wires (0.3 mm diameter). Each of these wires is, of course, a composite containing many very fine filaments of NbTi. The width of the conductor is a function of the number of wires used in the braid and determines the field obtain-

*Work performed under the auspices of the U.S. Department of Energy.

able from the magnet for a given current density. The parameters chosen for the ISABELLE magnet conductor are given in Table I. To date two manufacturers have successfully produced finished conductor and both are now in the process of mass producing this wire for the first one hundred magnets of the machine.

Table I.

Conductor Parameters

Type	Flat Braid
Dimensions	16 mm x 0.6 mm
Critical Current (4.2 K, 5 T)	5000 A
No. of Strands	97
Strand Size	0.3 mm
No. of Filaments	500
Filaments Size	7 μ
Insulation	Spiral Wrapped Fiberglass
Manufacturers	Airco and I.G.C.

The conductor fabrication process was developed at BNL and the technology then transferred to industry. Approximately 10^5 kilos of conductor will be required to wind all the coils of both proton rings.

Magnet Assembly

The magnets consist of coils whose current distribution approximates Cos (n θ), enclosed in cylindrical iron yokes. Dipoles contain two identical saddle coils and quadrupoles four. Both types of windings are made by high pressure molding using "B stage" thermosetting epoxy to bond the conductors together. The winding fixture is shown in Fig. 1. Pneumatically operated clamps are used to position and tension the turns during winding. Pressure is applied hydraulically while the coil is being cured. The winding fixture is internally heated to approximately 140°C to polymerize the epoxy. A central post and wedges, precast from special epoxy, are used to form the circular shape of the coils. The Cosnθ distribution in current is achieved by the incorporation of "inert" or spacer turns which are wound in parallel with the superconducting braid. These spacer turns are also braided but contain no superconductor. A cross section of the turns distribution for the dipole is shown in Fig. 2a and for the quadrupole in Fig. 2b. Coils formed in this way are monolithic, rigid structures which are then assembled into the completed magnet. In the dipole, two of the saddle coils are clamped onto a fiber wrapped stainless steel bore tube which contains the trim windings. The coils are then banded with a fiberglass epoxy wrap and cured at room temperature. When fully cured, the bands are ground to size and the coil assembly is inserted into the iron core. Since the magnetic forces are to be transmitted to the core by the bands the preloading of the coil package must be maintained as the magnet is cooled to operating temperature. This is done by making the bands slightly larger than the bore of the core, cooling the coil assembly in liquid nitrogen and inserting it, cold, into the warm iron shield. The resulting interference fit between the bands and core ensures that the coils are under a compressive mechanical load at all temperatures. Spiral grooves and notches in the bands provide flow passages for the high pressure helium gas which cools the magnet. The iron shield is formed by stacking flat "washer" laminations in a heavy walled stainless steel tube which serves as the pressure vessel. Three functions are performed by the iron core:

1. enhancement of the central magnetic field
2. reduction of the external or stray field
3. containment of the magnetic forces exerted by the windings

The magnet is then installed in its vacuum vessel to complete the assembly. A cross section is shown in Fig. 3 and Fig. 4 is a schematic illustrating two magnets side by side in the tunnel.

Magnet Design

As indicated in Fig. 2a a six block approximation is used to simulate the ideal cos θ distribution. It can easily be shown that such an approximation will allow the elimiation of the first six allowed harmonics in the magnetic field produced by the windings (i.e. one allowed harmonic for each block). The following procedure is used to determine the azimuthal position of the turns:

I. The region to be occupied by the turns is divided into six equal current blocks defined by the Beth[5] angles.

II. Using the computer program MAGFLD[6] the current density required to produce the desire field shape is calculated. It should be noted here that the ISABELLE magnets are designed with a "built-in" sextupole component to minimize the trim current required for chromaticity adjustment in the machine. This can be calculated easily since the program will determine the currents required for any distribution of harmonics. Harmonics other than the sextupole are normally set to zero.

III. The nearest integral number of turns in each block is then calculated by normalization from the mid-plane or highest current density block and the appropriate number of inert turns added to fill the available space.

IV. Next MAGFLD is used to reposition the blocks slightly to compensate for the effect of having integral turns.

The resulting turns distribution produces a very high quality dipole field with a superimposed sextupole field. Six current blocks were chosen as optimal for the dipole, since fewer blocks would compromise the field quality, while the potential provided by a larger number of blocks can not be realized due to positional errors inherent in construction. Experience with a number of magnets indicates that the random error in turns placement that can be expected in mass-production is about 0.05 mm. This random error gives rise to the distribution of harmonics listed in Table II. In this table the coefficients are given in the usual cylindrical expansion with the b's representing the normal and the a's the skew components. The coefficient given for b_2 is, of course, the mean variation expected about the "built-in" value. The design procedure is identical for the quadrupole except that only three blocks are used because of the higher order symmetry, and there are no built-in field components.

Table II

Harmonic Components	Dipole	Quadrupole	Units
a_0, b_0 (dipole 1θ)	1.7	1.4	10^{-4}
a_1, b_1 (quadrupole 2θ)	7	4	10^{-5} cm^{-1}
a_2, b_2 (sextupole 3θ)	7	11	10^{-6} cm^{-2}
a_3, b_3 (octapole 4θ)	12	12	10^{-7} cm^{-3}
a_4, b_4 (decapole 5θ)	20	20	10^{-8} cm^{-4}
a_5, b_5 (duodecapole 6θ)	32	32	10^{-9} cm^{-5}

In addition to the main winding each type of magnet is provided with a set of a auxiliary windings used to control the details of the field shape. The dipoles have the following three "trim" coils:

1. Sextupole; to compensate for the effect of iron saturation at high field and maintain the sextupole component at the correct value.

2. Octupole; for machine "tuning".

3. Decapole; to compensate for iron saturation.

The quadrupoles also contain three windings:

1. Dipole; for closed orbit compensation.

2. Quadrupole; to allow for adjustment of the effective length of the focusing and defocusing magnet.

3. Duodecapole; to compensate for iron saturation.

The main windings in each ring are connected in series. Tracking between the bending and focusing fields is provided by a "by-pass" circuit as illustrated in Fig. 5a. This is required because the saturation effect is more pronounced in the dipoles (See Fig. 5b). The design assumes that the main windings operate in excess of 90% of the short sample current, at 5 Tesla. This requirement is considerably less stringent in the auxiliary windings where the maximum current required never exceeds 30% of the short sample critical current.

Magnet Performance

As originally conceived, ISABELLE was to consist of two intersecting rings operating at a peak field of 4.0 Tesla, equivalent to a proton energy of 200 GeV. More recent designs have been upgraded to 400 GeV at 5 Tesla. Some parameters, of the magnets for the two versions are summarized in Table III.

Table III

	200 GeV x 200 GeV	400 GeV x 400 GeV
Magnetic Field	4 Tesla	5 Tesla
Dipole Length	4.25 m	4.75 m
Dipole Inner Diameter	12 cm	13 cm
Operating Temperature	4.5 K	3.8 K
Allowed Training	1st quench >4 T (i.e. no training)	10 quenchs to 5.2 T

Obviously, the most significant change was increasing the field to 5T. This was to be accomplished by reducing the operating temperature and allowing for a certain amount of "training". In addition improvements in the critical current of the conductor and a small increase in the transfer function at the new larger aperture make the achievement of 5T a reasonable design goal. Immediately after the project was approved, it was decided to have a series of magnets built in cooperation with industry as a pre-production test of the construction technique. Six dipoles and two quadrupoles which would then be assembled into a prototype "first cell" were contracted for with the Westinghouse Corporation.

Since these dipoles were to represent the beginning of production, they were given the serial numbers 001 thru 006. This section will be confined to the performance of this series of magnets, the earlier developmental coils having been adequately covered elsewhere.[7]

At the time that this report was prepared, four of the six dipoles and one quadrupole had been tested. The tests were performed in liquid helium at 4.6 K using vertical test cryostats. Testing in the forced flow configuration at 3.8 K will be attempted as soon as the new cryogenic system is available. All four dipoles exhibited excessive training, the first quench occuring at approximately 4T and subsequent quenches at higher and higher fields. The increase in field with quench number was very gradual indicating that an enormous number of quenches would be required to reach the design field. This is illustrated in Fig. 6 for dipole number 003. Also shown in Fig. 6 are results for an earlier magnet (MkV) which exhibited markedly better training characteristics. The test data for the MkV magnet were obtained using the forced flow gas cooled mode of refrigeration. At the present time the reason for the excessive training in this new series of dipoles is not fully understood and a number of possible explanations are being investigated. Measurements of the overall length of the coil assembly before and after installation in the iron core indicated that considerable axial stress was being applied to the winding when the coil and core reached thermal equilibrium. At one time the relaxation of this stress as the magnet was energized was thought to be responsible for the training but the testing of later coils with reduced amounts of interference fit showed that this was not the case. Another possible source of training is thought to be inadequate bonding of the turns in the low current density regions. A modification in the winding technique used only in the Westinghouse coils has been shown to give insufficient epoxy in the blocks near the central post and little or no bonding between the turns in these regions. This is being corrected in the new series of magnets along with a number of detail changes which are expected to improve the training situation.

The quadrupole, however, did reach its operating level after only five quenches and its performance was acceptable in all respects. A training curve for this quadrupole is shown in Fig. 7.

In addition to the poor training performance of the dipoles, the transitions to the normal state (quenches) were observed to occur much too slowly. This would lead to excessive heating of portions of the coil if some of the energy was not extracted during the quench. Since the electrical system designed for ISABELLE requires that a quenching magnet absorb all its own stored energy[8] this situation is not tolerable. The slow quench propagation is caused by the copper braid used as inert turns in this series of magnets. The high conductivity of this material slows the azimuthal propagation leading to overheating of the ajacent single turns. This problem is exagerated in the third block from the post (See Fig. 2a) where the discontinuity between the turns which incorporate a copper braid and the single turns occurs on both sides of the block. In retrospect the choice of copper as a material for the spacers was a mistake and cupro-nickel will be subsituted in future dipoles in this series.

The magnetic measurements for the first four dipoles are given in Table IV along with the mean and standard deviation for each harmonic. A comparison of this table with Table II shows that, except for the b_2 and b_4 components, the agreement with expected values is excellent.

Table IV

Harmonic Coefficiant	001	002	003	005	Avg.	Std. Dev.
b_1 ($\times 10^{-5}$ cm^{-1})	-5	-6	-5	-3.5	-5	1
b_2 ($\times 10^{-6}$ cm^{-2})	-500	-595	-521	-544	-540	40
b_3 ($\times 10^{-7}$ cm^{-3})	-1.5	-6.4	1	7.5	0	6
b_4 ($\times 10^{-8}$ cm^{-4})	270	420	360	340	350	60
b_5 ($\times 10^{-9}$ cm^{-5})	5	-18	.5	6	-1	12
a_1 ($\times 10^{-5}$ cm^{-1})	-5	14	-10	2	0	10
a_2 ($\times 10^{-6}$ cm^{-2})	3	7	-11	-14	-4	10
a_3 ($\times 10^{-7}$ cm^{-3})	30	50	-8	13	20	25
a_4 ($\times 10^{-8}$ cm^{-4})	-20	10	8	10	2	15
a_5 ($\times 10^{-9}$ cm^{-5})	5	-2	4	-12	-1	8

The sextupole data, however, exhibits considerable scatter and is not in good agreement with the designed in component (approximately 300 x 10^{-6} cm^{-2}). The source of these discrepancies has been traced to errors in the tooling used to mold the coils. Differential expansion between the coils and the steel mold at the curing temperature combined with a certain amount of "spring-back" lead to deviations from the ideal distribution. This will be compensated for by modifications to the molding fixture. The procedure used to clamp the dipole halves on the bore tube for banding has also been modified to eliminate a slight ellipticity observed in this first series of magnets.

Because of the high order symetry these problems are much less apparent in the quadrupole.

The present dipole situation is summarized below;

<u>Training</u>

While the first quench occurs at a reasonable field level (4 T) the rate of trianing is much too slow. Detail changes in the construction and operation in the forced flow condition are expected to lead to a significant improvement in this area.

Quench Propagation

Previous experience indicates that the slow quench propagation observed in these first commercial coils can be corrected by using inert turns of higher resestivity. Cupro-nickel braid will be substituted in the next group of dipoles.

Field Quality

All the harmonics forbidden by symmetry are in good agreement with those expected from the random construction errors. Tighter control over the allowed and built-in harmonics will be achieved by changes in the molding technique.

Quadrupoles

The smaller size and higher symmetry of the quadrupole coils effectively eliminates the above problems so that no significant changes are contemplated before production begins.

Application to PETRA Ring

The principal dificulties in adopting the ISABELLE magnet design for use in an existing tunnel would seem to be the rather large external dimensions of the vacuum vessel and the stray magnetic field which could effect the operation of the existing electron ring. The large size of the vacuum vessel arises from three considerations;

1. Large Magnet Aperture. This requires a considerable iron thickness (approximately three coils radii) to efficiently return the flux.

2. High Design Field. To make maximum use of the field enhancement capabilities of the iron core it must be tightly coupled to the windings, so that relatively little flux can return in the space between the coil and the core. This in turn leads to a thick core to reduce the stray field to an acceptable level.

3. Low Heat Leak. To achieve the very low heat leak (4.6 watt/dipole) large insulation spaces are provided between the magnet and the heat shield and between the shield and the outer vacuum vessel walls.

A much more compact design could be developed if some of these requirements were relaxed. In Fig. 8 a possible modification which might be applicable to the PETRA tunnel is shown. The coils are formed using the same technique as for the ISABELLE magnets but are of smaller aperture (9 cm). A stainless support tube is used to constrain the coils and a larger annular space provided to reduce the coupling between the core and coil. The much thinner iron core could then be used as the intermediate heat shield resulting in an overall outside diameter less than 40 cm.

Calculations indicate that a coil of this type would produce a field of approximately 4.5 T when operating at the current density specified for the ISABELLE dipoles. A similar configuration has been used successfully in smaller Nb_3Sn gas cooled dipoles.[9]

Acknowledgements

The information contained in this report has been produced by the large number of people now working on ISABELLE magnet development and production, and the author is indebted to them for use of their data and illustrations.

References

1. W.B. Sampson, Proc. 2nd Int. Conf. Mag. Tech. Oxford p. 574 (1967)
2. K.E. Robins et al. IEEE Trans. Nuc. Sci. Vol. NS-24 No. 3, p. 1320 (1977)
3. A.D. McInturff et al. " " " " " " " p. 1242 "
4. W.B. Sampson et al. " " " " " " " p. 1296 "
5. R.A. Beth, BNL Accelerator Dept. Report AADD-102 (1966)
6. G.H. Morgan, BNL Accelerator Dept. Report AADD-145B (1970)
7. A.D. McInturff et al. Proc. Part. Acc. Conf. San Francisco (1979) (In Press)
8. R.J. Nawrocky et al. Proc. Part. Acc. Conf San Francisco (1979) (In Press)
9. W. B. Sampson et al. Proc. App. Supercon. Conf. Pittsburg p. 117 (1978)

Figures

1. Winding and pressure molding fixture for ISABELLE coils.

2. Cross section of a) dipole and b) quadrupole showing the distribution of active and inert turn used to approximate the Cosθ and Cos2θ current distributions.

3. Cross section of magnet and cryostat assembly.

4. Drawing of side by side dipoles which form the two intersecting proton rings.

5a. Dipole field and quadrupole gradient as a function of energizing current. The "by-pass" current maintains the relationship between them at high current levels.

5b. Relative saturation effect in dipoles and quadrupoles as a function of current.

6. Training curve for dipole 003. Also shown are data for the MkV magnet cooled by supercritical helium in the forced flow mode.

7. Training curve for quadrupole 3001.

8. A possible modification of the ISABELLE magnet design for use in an existing tunnel of limited space.

COIL WINDING
FIXTURE

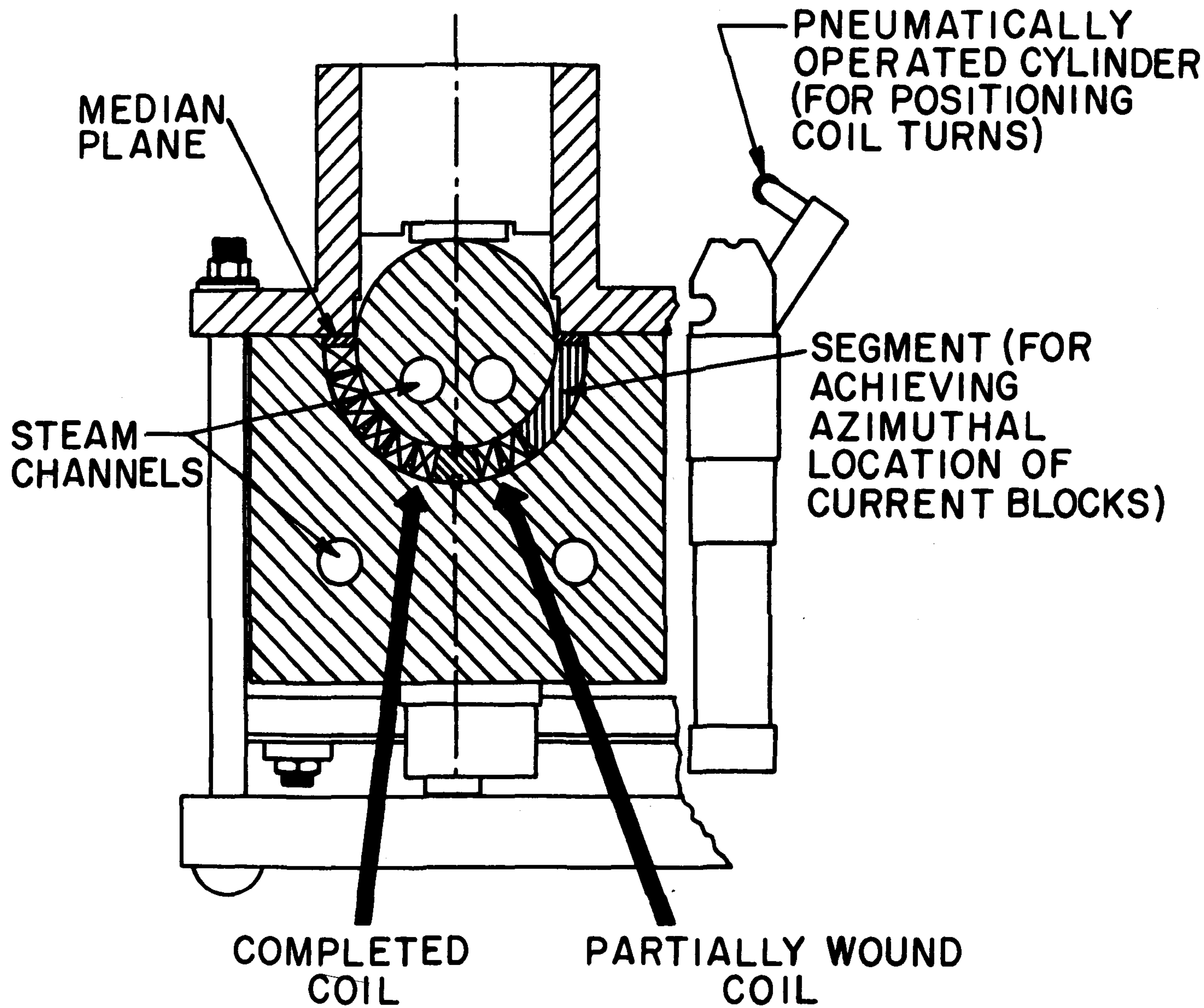

Fig 1

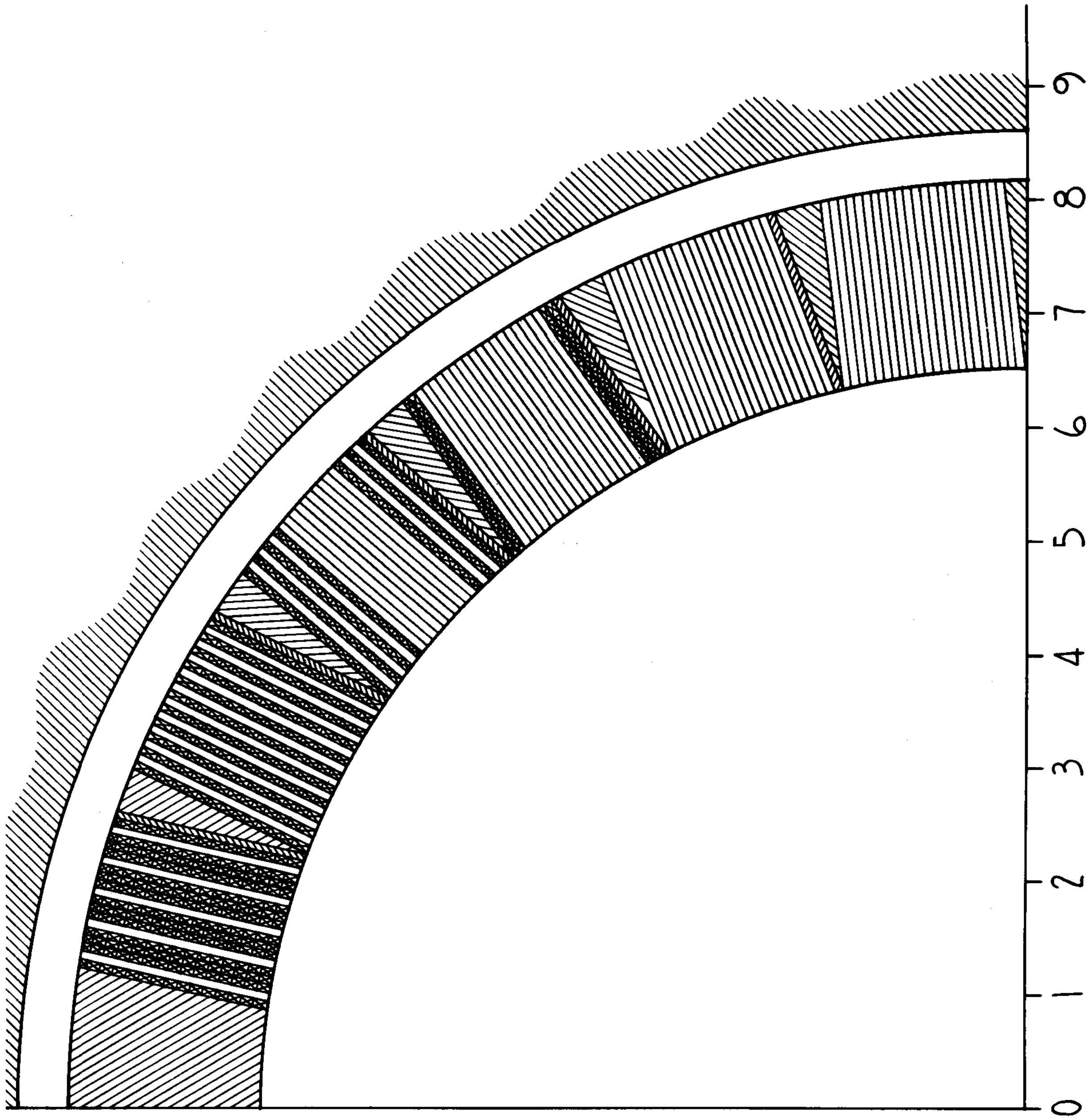

Fig. 2a

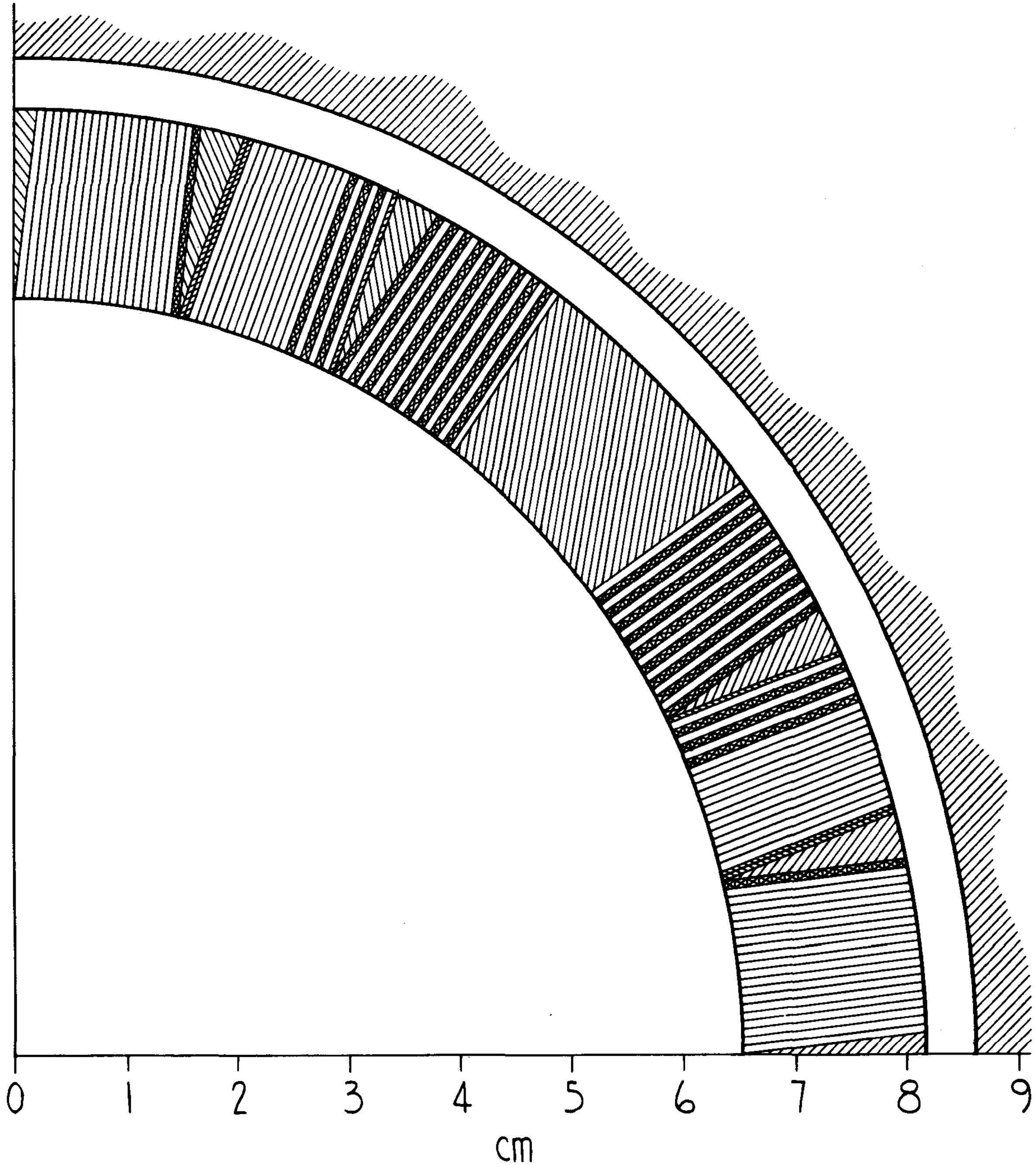

Fig. 2b

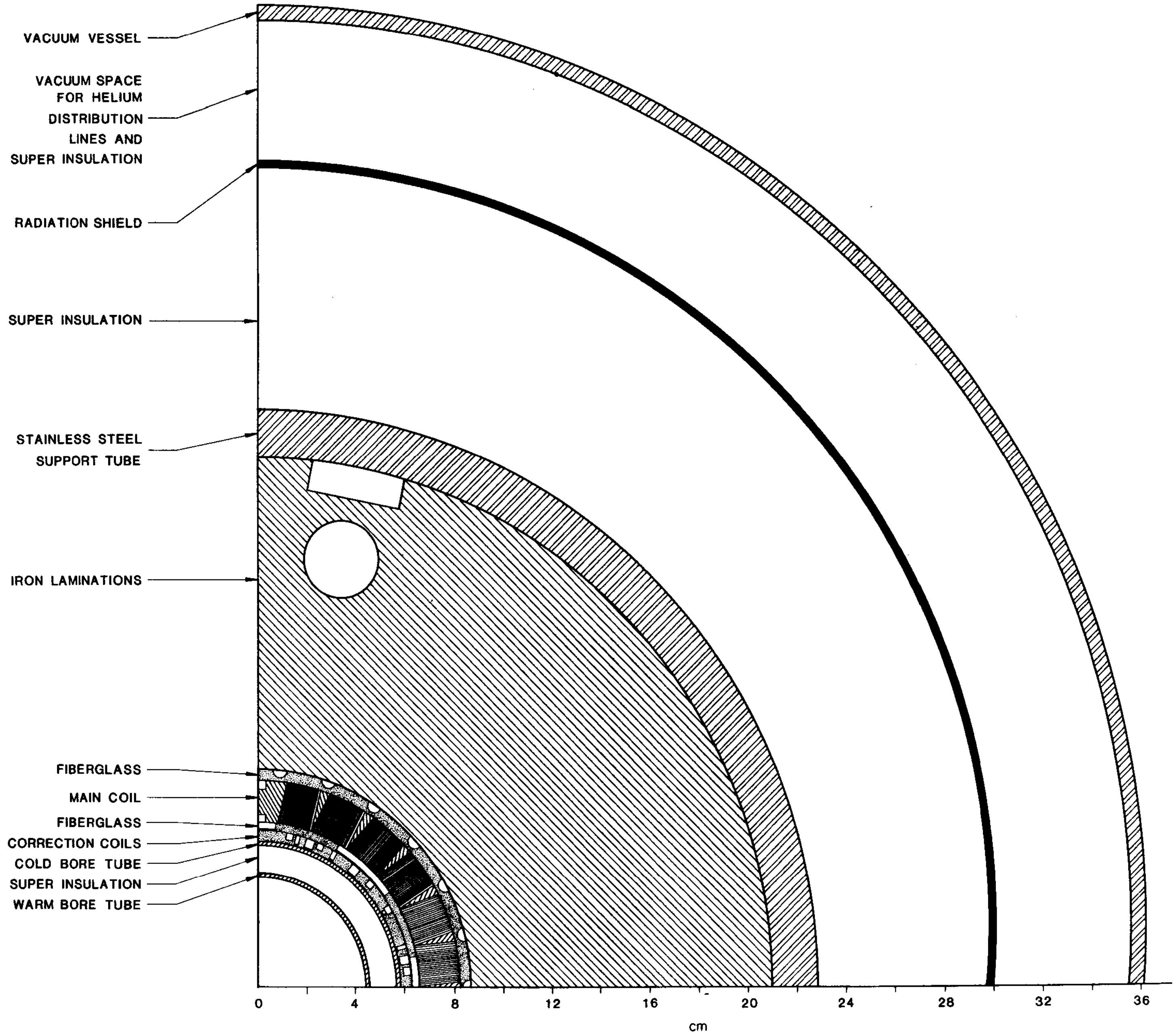
VACUUM VESSEL
VACUUM SPACE FOR HELIUM DISTRIBUTION LINES AND SUPER INSULATION
RADIATION SHIELD
SUPER INSULATION
STAINLESS STEEL SUPPORT TUBE
IRON LAMINATIONS
FIBERGLASS
MAIN COIL
FIBERGLASS
CORRECTION COILS
COLD BORE TUBE
SUPER INSULATION
WARM BORE TUBE
0
4
8
12
16
20
24
28
32
36
cm

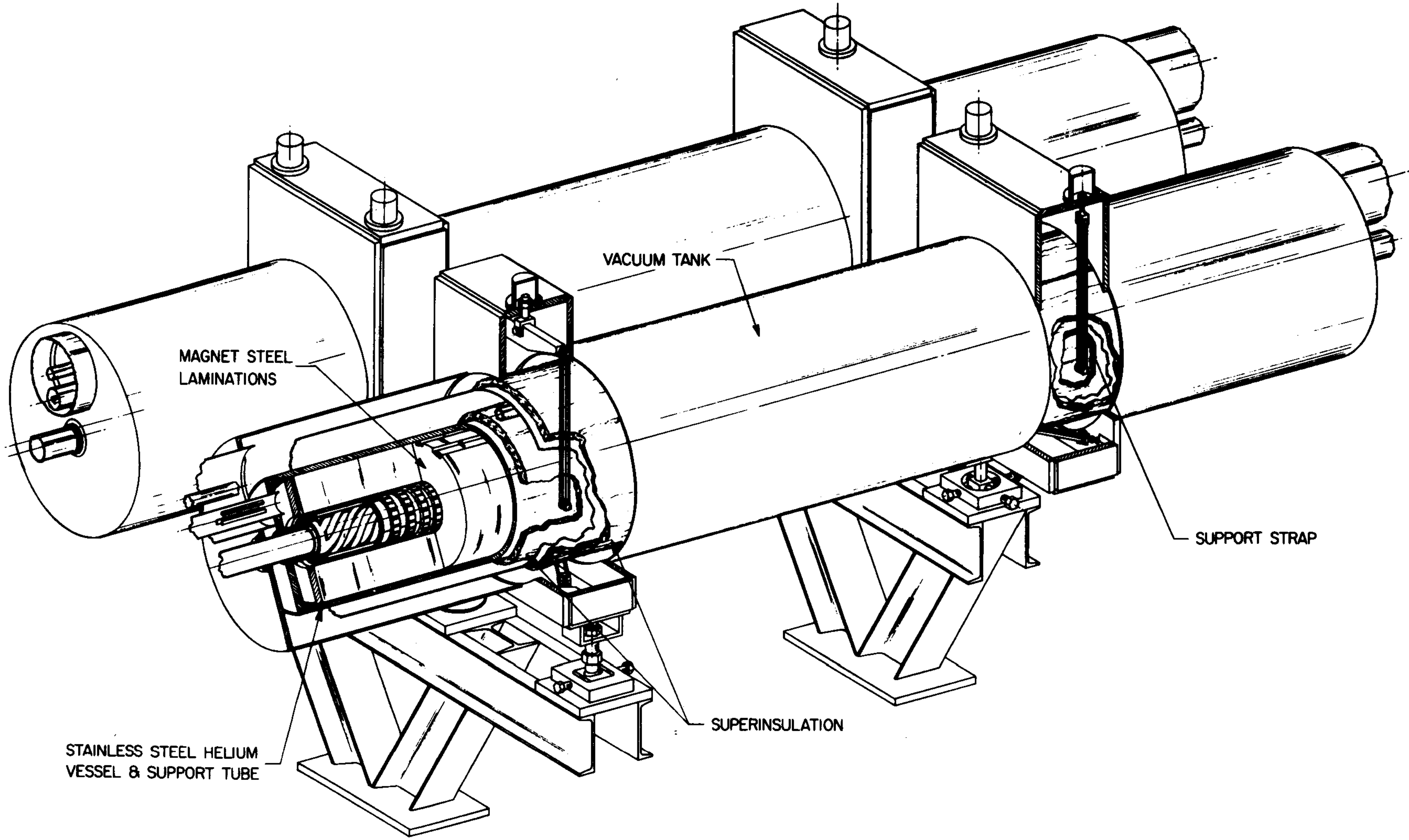
VACUUM TANK
MAGNET STEEL LAMINATIONS
SUPPORT STRAP
SUPERINSULATION
STAINLESS STEEL HELIUM VESSEL & SUPPORT TUBE

Fig. 4

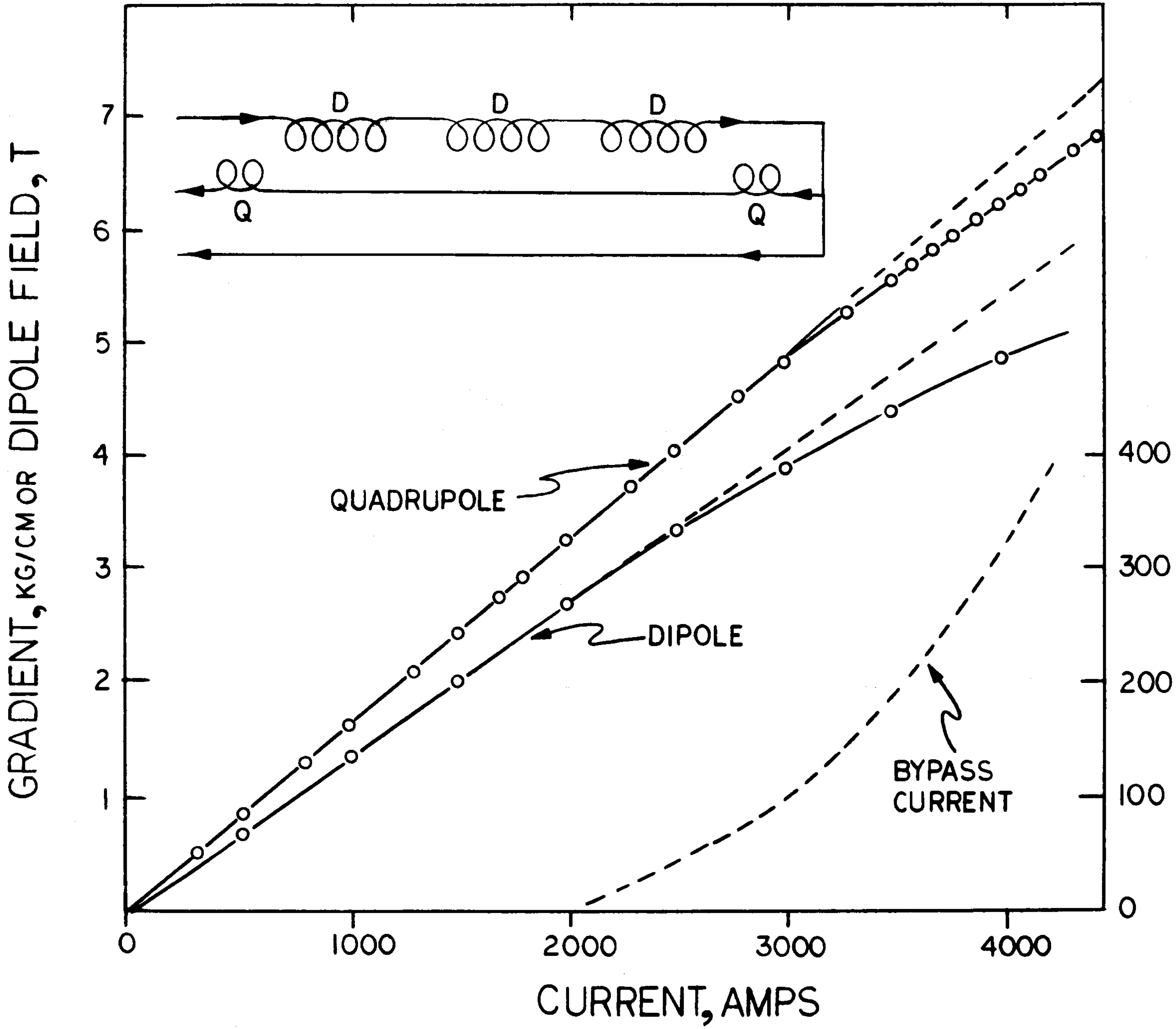
D
D
D
Q
Q
QUADRUPOLE
DIPOLE
BYPASS CURRENT
GRADIENT, KG/CM OR DIPOLE FIELD, T
CURRENT, AMPS
0
1000
2000
3000
4000
1
2
3
4
5
6
7
0
100
200
300
400

Fig.5a

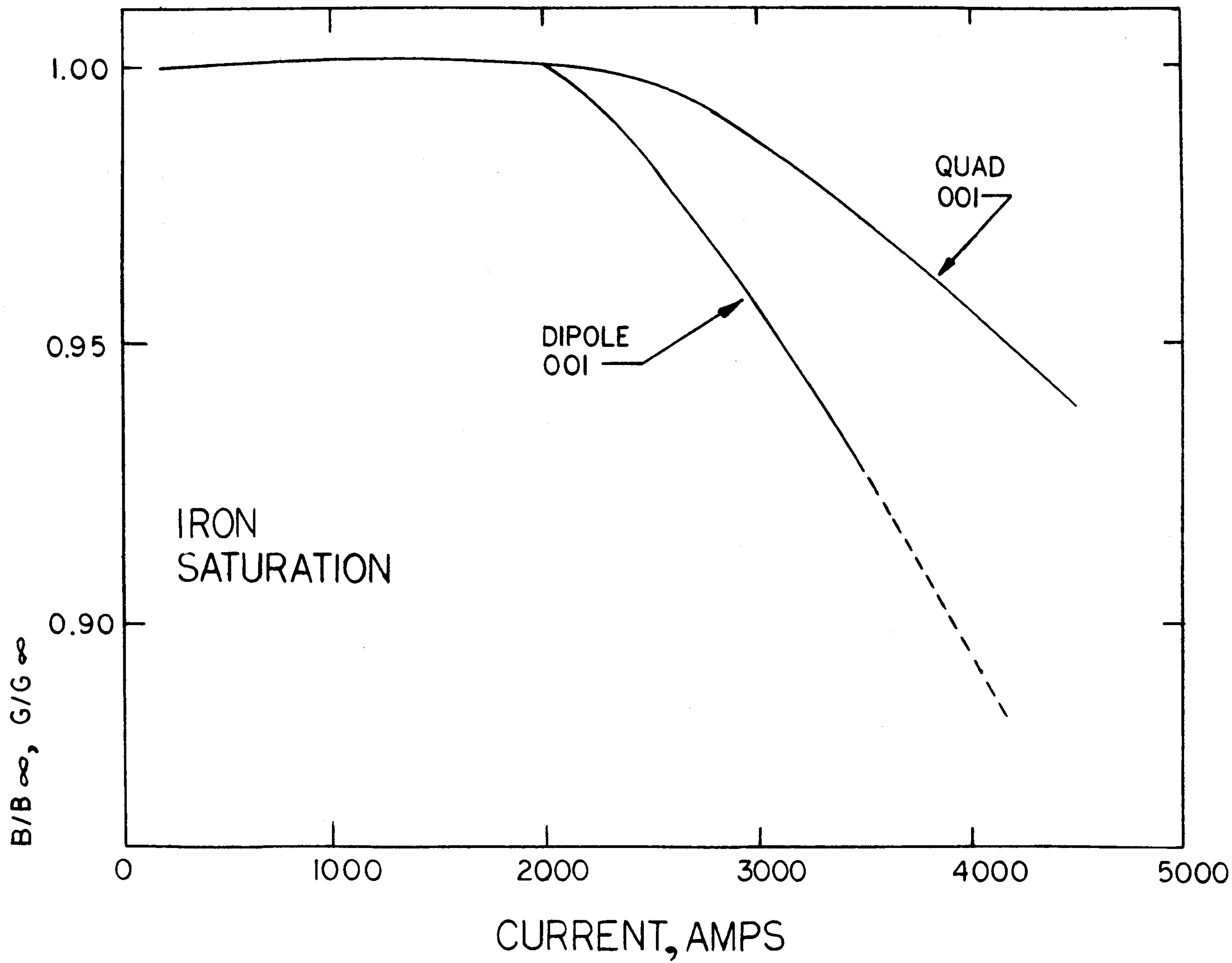
1.00
0.95
0.90
0
1000
2000
3000
4000
5000
CURRENT, AMPS
B/B∞, G/G∞
QUAD
001
DIPOLE
001
IRON
SATURATION

Fig.5b

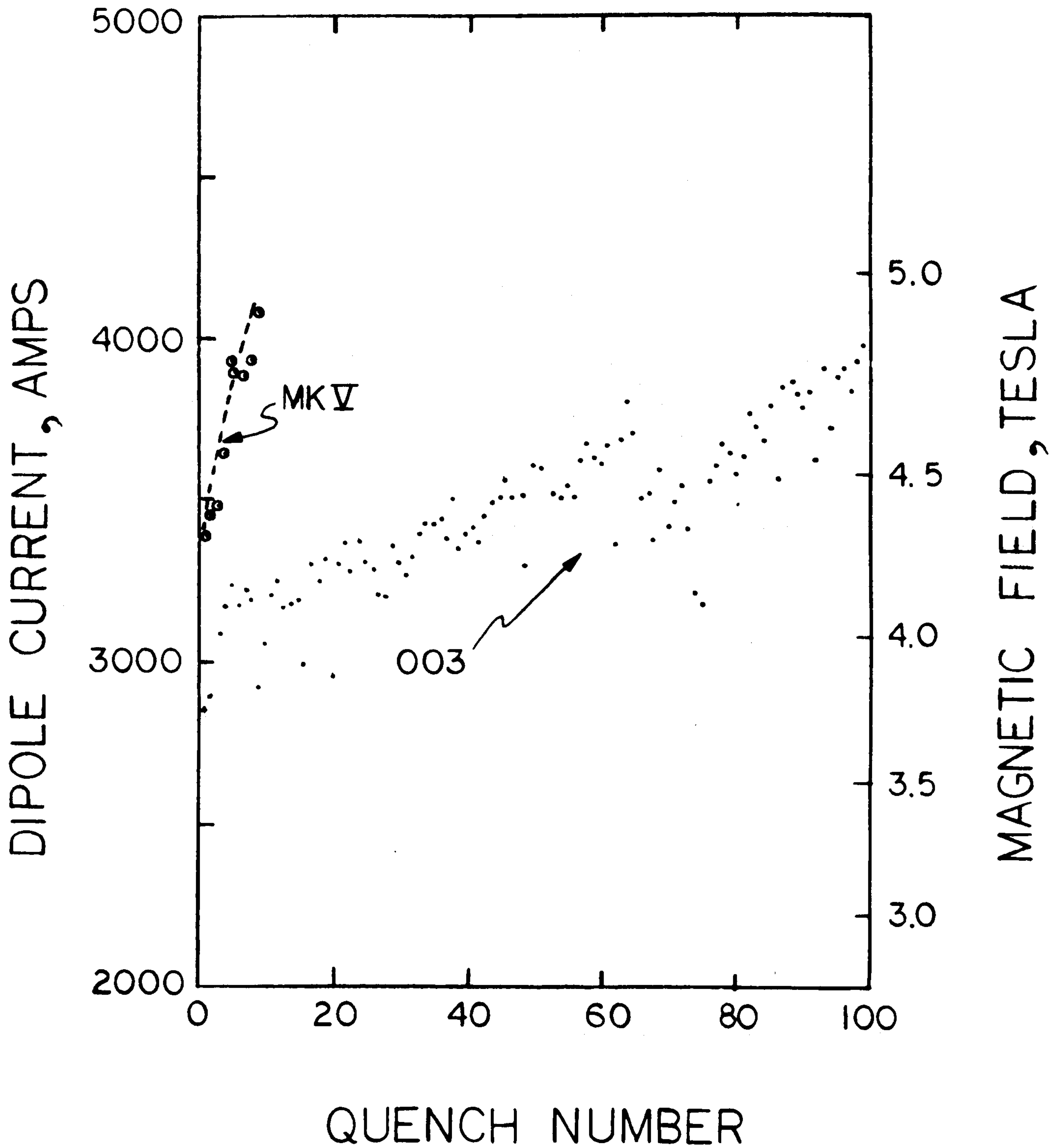
5000
4000
3000
2000
0
20
40
60
80
100
5.0
4.5
4.0
3.5
3.0
DIPOLE CURRENT, AMPS
MAGNETIC FIELD, TESLA
MK V
003
QUENCH NUMBER

Fig. 6

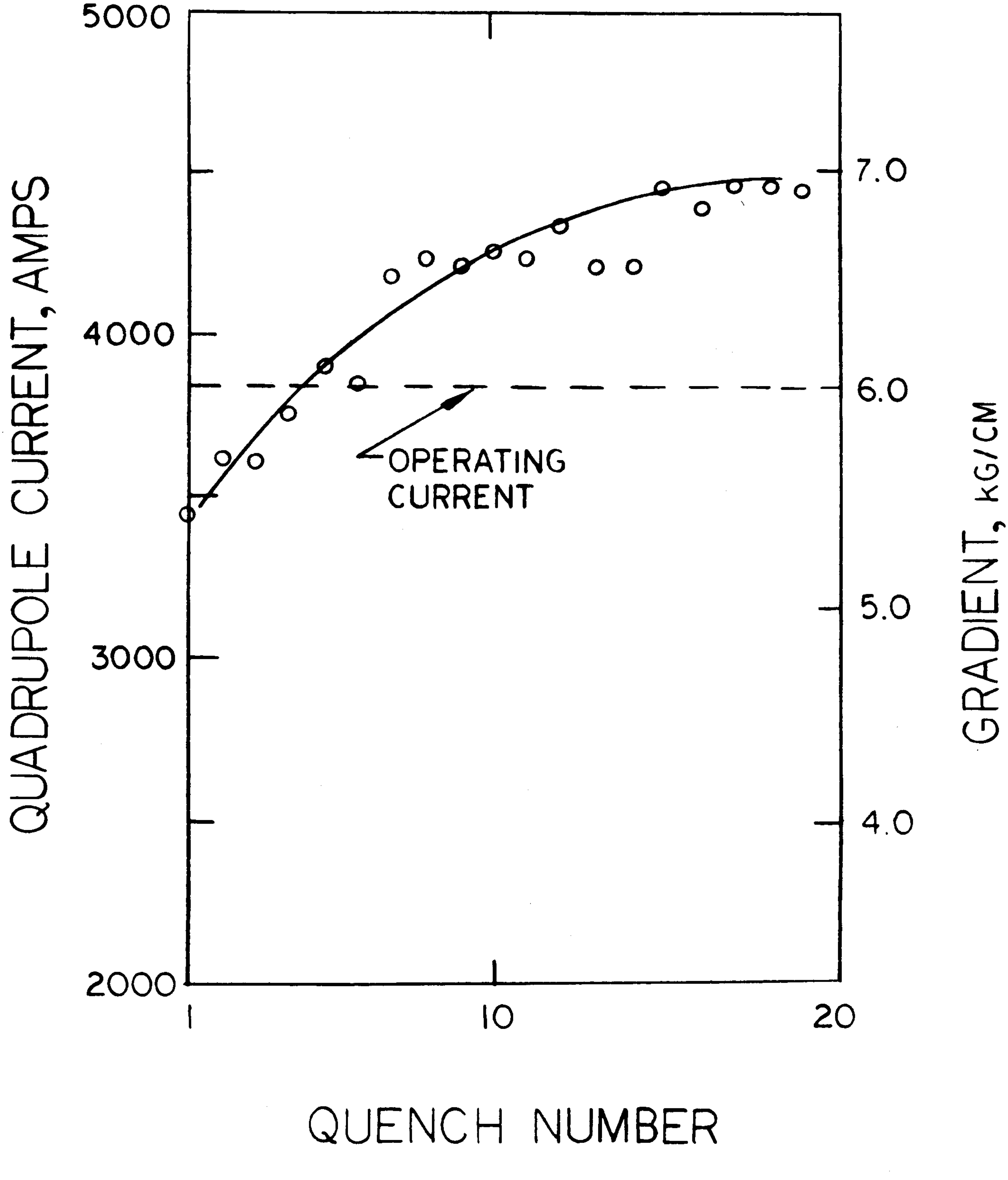
5000
4000
3000
2000
7.0
6.0
5.0
4.0
OPERATING
CURRENT
1
10
20
QUADRUPOLE CURRENT, AMPS
GRADIENT, kG/CM
QUENCH NUMBER

Fig. 7

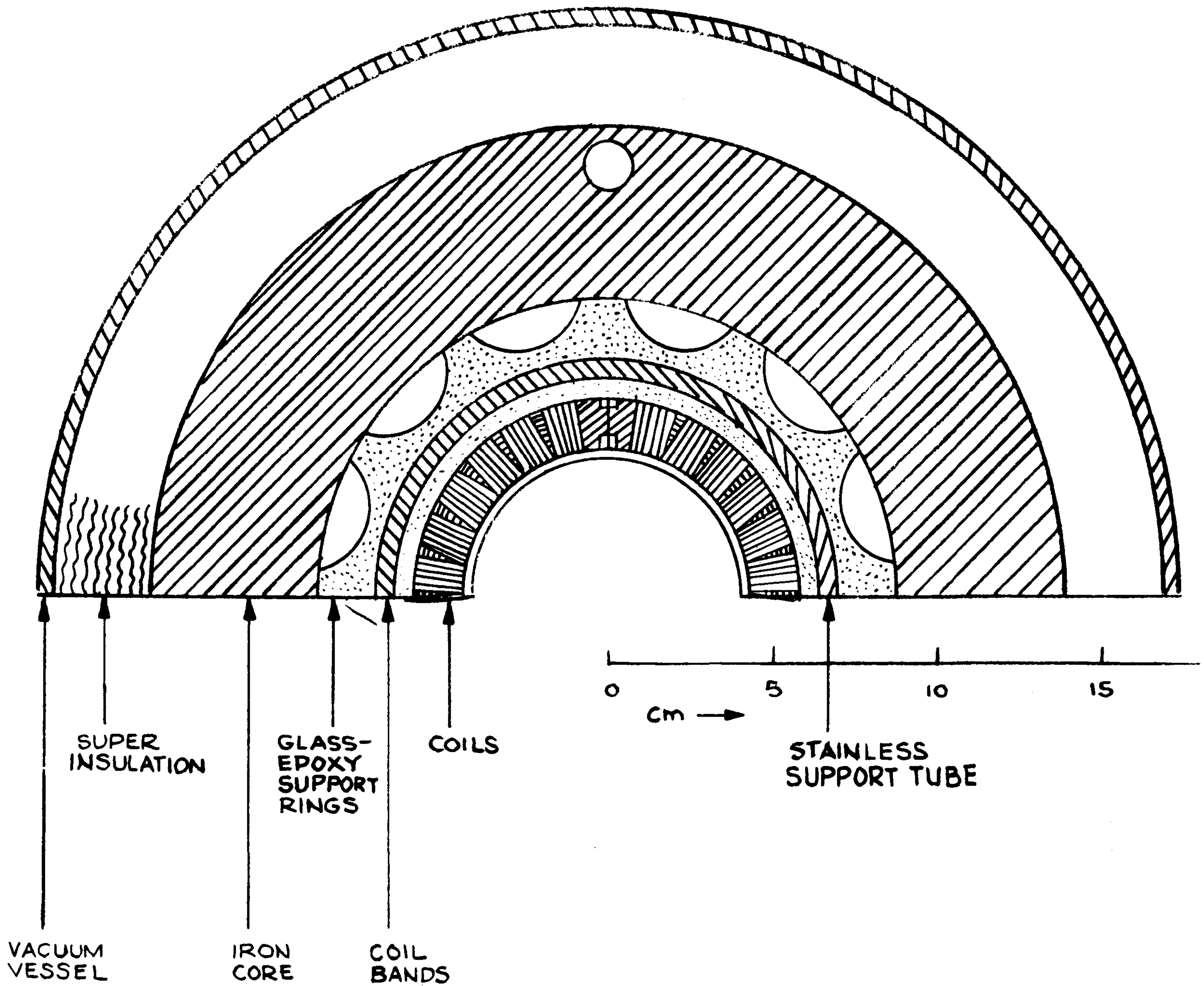
0
5
10
15
cm →
SUPER INSULATION
GLASS-EPOXY SUPPORT RINGS
COILS
STAINLESS SUPPORT TUBE
VACUUM VESSEL
IRON CORE
COIL BANDS

Discussion

Weber/DESY:

Can you quote the price per meter of ring the magnets would cost?

Sampson:

10 000 $ with the cryostat.

Weber:

And how much is it in your case, Alvin?

Tollestrup:

The number that is going now into diary is around 35 000 $ per magnet.

Weber:

Per magnet! That has to be devided by 7, gives you 5 000. You said how much?

Sampson:

10 000. It is about 45 000 $ for a 4 3/4 m magnet.

Hahn:

I think one has to compare also the aperture!

Sampson:

Yes, there is a difference in aperture.

Superconducting proton ring for PETRA

E. Baynham[+], K.P. Jüngst[*], J. Pérot[†]

GESSS Laboratories

[+] Rutherford Laboratory, Chilton, Didcot,
Oxfordshire OX11 OQX, England

[*] Kernforschungszentrum Karlsruhe GmbH
Institut für Technische Physik
7500 Karlsruhe, Postfach 3640
Bundesrepublik Deutschland

[†] Centre d'Études Nucléaires de Saclay
Commissariat a l'Énergie Atomique
Boite Postale No. 2
Gif-sur-Yvette, France

Paper presented at the "Study of an ep facility for Europe", Hamburg, April 2 and 3, 1979 by J. Pérot

1. Introduction

A powerful new facility for colliding beam physics could be provided by adding a proton storage ring in the range of several hundred GeV to the electron-positron storage ring PETRA at DESY[(1)]. This can be achieved in an economic way utilizing the PETRA tunnel and taking advantage of the higher magnetic fields of superconducting magnets which would be placed above or below the PETRA magnets. A central field of 4 Tesla in the bending magnets corresponds to a proton energy of 225 GeV.

Production of magnets of this field level can be considered available technology. There are already large accelerators and storage rings based on superconducting magnets under construction at Fermilab and BNL, respectively. These two designs represent the most advanced technology and must be considered carefully in any new machine proposal.

Development work on superconducting accelerator magnets has been performed at LBL and the GESSS collaboration Karlsruhe, Rutherford and Saclay. The aim at LBL was the construction of an experimental superconducting accelerator, while the GESSS laboratories undertook an extensive collaboration to design and construct magnets suitable for the SPS at CERN. Prototype magnets produced fields in the 4-5 Tesla range. With the decision to build a conventional SPS the emphasis in Europe turned to other areas of applied superconductivity. Only recently Saclay has resumed work on accelerator magnets in a collaboration with Serpukhov and is building short model dipoles which are designed very similar to Fermilab magnets.

When GESSS was asked by DESY to contribute to the design of the superconducting proton ring this study has been prepared as a first step. It should evaluate the available technology and assess the feasibility of a construction schedule to provide an ep machine at DESY by the end of 1984.

While a more thorough study could take into account also the experience with design and construction of superconducting beam line magnets at different places, e.g. CERN, this paper concentrates on accelerator magnet designs from BNL and Fermilab for a 4 Tesla option scheduled for 1984 or an improved 5 Tesla option for 1986. First results from calculations on a 8 Tesla option based on Nb_3Sn conductor are also included. This study emphasizes the designs of dipole magnets compared to quadrupole magnets, since dipole magnets need more intense investigation.

2. Preliminary Design Parameters

For the superconducting proton ring for PETRA one will adopt the PETRA lattice. Therefore the ring will consist of 232 dipole magnets, about 300 quadrupole magnets and 152 sextupole magnets. Preliminary parameters of the dipole magnets are listed in Table I.

Table I.: Dipole magnet parameters

length	5.5 m
warm aperture diam.	60 mm
cold aperture diam.	90 mm
winding aperture diam.	100 mm
central field	4 ... 8 T
field homogeneity $\Delta B/B$ within warm aperture	$\lesssim 3 \cdot 10^{-4}$
reproducibility, standard deviation of $\int Bdl$	$1 \cdot 10^{-3}$
rise time	300 s
outer dimensions	
height	0.6 m
width	0.6 m
stray field at yoke of PETRA magnets	< 0.01 T

The magnetic length of the magnet should not be too much different from the geometric length.

The question of cold or warm bore is still open, although a warm bore is preferred at present. A warm bore e.g. shields the magnets and the cryogenic system from the heat input produced by higher mode losses and permits easy access to the vacuum tube. However, it has to be investigated whether for vacuum reasons baking of the tube would be necessary. The decision between warm and cold bore should be made as soon as possible because it can significantly influence the interior design of the magnets.

The rise time of 300 s is not yet fixed and could be increased by some 50%, if e.g. conductor losses would be lowered considerably.

The field homogeneity requirements are not easy to meet for superconducting magnets as they depend on highly exact positioning of the conductors. The only economic way is to allow higher field errors produced by the main coils and to provide correction. The correction can be achieved by correction coils in the dipoles or by correction elements in the succeeding quadrupole magnets.

The most severe constraint, however, is to have the ring ready for operation in 1984.

3. <u>4 Tesla option</u>

For first ring operation in 1984 only one solution is considered feasible and that is to adapt one of the two most advanced designs from BNL and Fermilab to PETRA requirements.

3.1 BNL dipole magnet

The Brookhaven dipole design is based on a current block

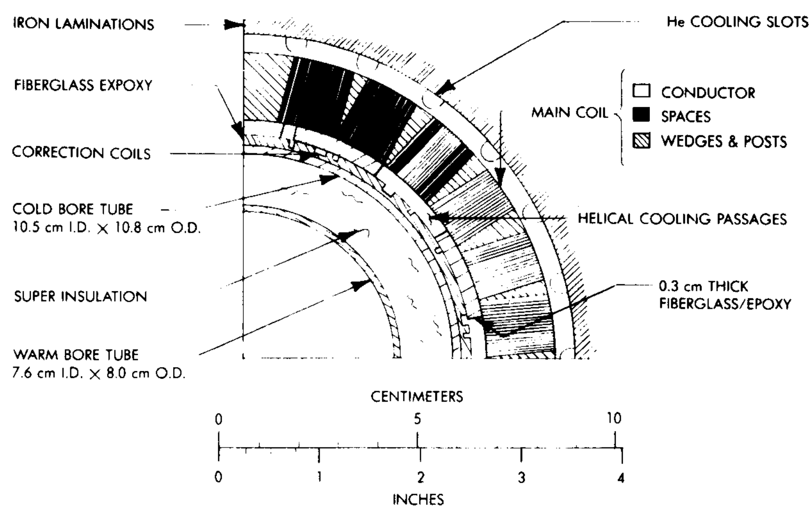

Quadrant of dipole magnet, showing conductor arrangement, coil support structure, and bore tube arrangement.

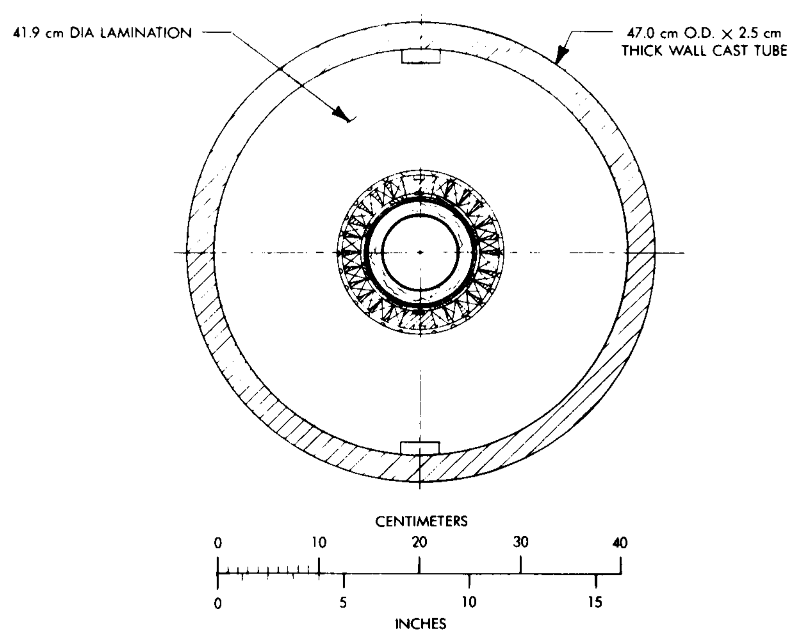

<u>Fig. 1:</u> BNL dipole magnet

approximation to the ideal cosΘ current density distribution (Fig. 1). Appropriate adjustment of the six current blocks theoretically allows a highly homogeneous field. Through a full set of correction coils within the magnets field errors due to fabrication tolerances can be minimized. Main field errors to be corrected are generated by saturation of the cold iron yoke above $\sim$3.5 T. The coil is clamped in the iron yoke by interference fit giving a rigid and well clamped coil structure.

The magnet is cooled by high pressure gas with coolant channels at the inner and outer coil boundaries and percolation through the coil.

The design field is 5 Tesla at 3.8 K. However, this field is not always achieved and a significant amount of training has been observed in recent magnets.

In the production of series magnets, coils, yokes and cryostats will be manufactured in industry and the final assembly and testing will be undertaken by BNL. The production schedule requires $\sim$100 magnets for FY80 and this will give valuable information on reproducibility of magnets and on production capability.

A summary of magnet parameters is presented in Table II.

3.2 Fermilab dipole magnet

The Fermilab design is based on a two layer winding (Fig. 2). This coil geometry allows cancellation of the first two field harmonic terms only. A sufficiently uniform field can be obtained, however, over a fractional aperture by adjustment of the layer angles. This adjustment is made by a laminated stainless steel clamp which can be manufactured with high

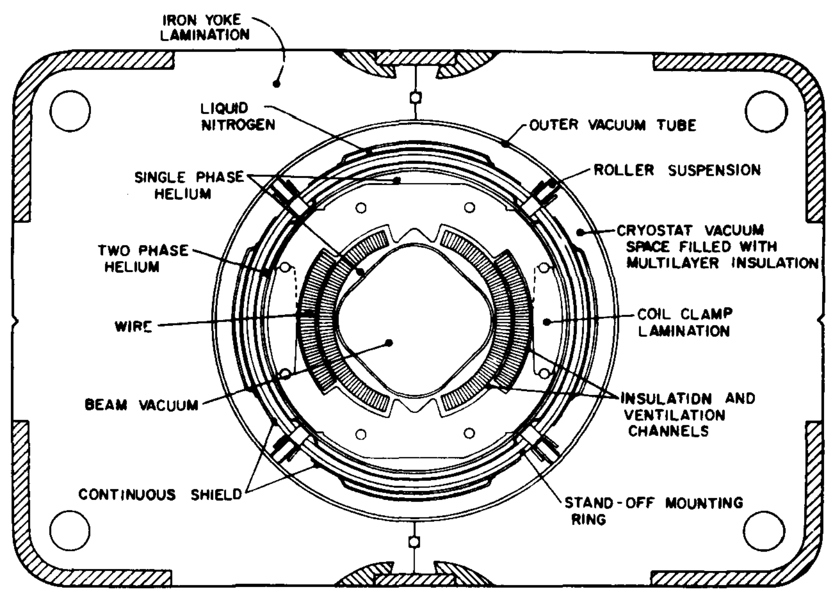

Fig. 2: Fermilab dipole magnet in cross section

accuracy. Central fields up to 4.5 Tesla are attainable.

The iron yoke is at room temperature and stray fields are at low level. The alignment of coil and iron yoke is difficult through the cryostat shells. Misalignment generates quadrupole errors which have to be studied carefully.

Random field errors may be of importance. As series magnet production has started the question of reproducibility will probably be answered in 1979.

The design allows application of production line techniques and routinely 5 magnets/week can be produced. Magnets are currently being installed in the accelerator ring in order to undergo a sextant test where beam will be passed through the superconducting magnets. An extensive magnet test facility is in operation.

3.3 Suitability for PETRA

The two discussed designs are so different in concept that it is essential to compare the individual designs with PETRA requirements rather than with each other. In Table II the main parameters of PETRA proton ring magnets are listed together with data of BNL and Fermilab magnets. Sufficient data are not available on key issues to select a design at this stage. Field measurements on series magnets are expected for 1979.

As the listed central fields are maximum values and not obtained in all magnets the two US designs are considered 4 Tesla designs for PETRA application. The warm aperture of BNL dipole is well within PETRA specification. The Fermilab magnet originally has a cold aperture but an estimation for a warm bore is given. For PETRA a copy of Fermilab magnets would have to be significantly enlarged in aperture. The aperture can be expanded without increasing training as recent experimental results from

Table II: Magnet parameters

	PETRA	BNL	Fermilab
length	5.5 m	4.75	6.7
warm ap. diameter	60 mm	88	(47)
cold ap. diameter	90 mm	113	72
winding ap. diam. correction ap. diam.	100 mm	130 120	76
central field	4 T	5 T	4.3 T
field homogeneity $\Delta B/B$ within ap.	$\leq 3 \cdot 10^{-4}$		
reproducibility, standard deviation of $\int Bdl$	$1 \cdot 10^{-3}$	$3 \cdot 10^{-4}$	
rise time	300 s	240 s	20 s
outer dimensions			
height	0.6 m	0.94	0.26
width	0.6 m	0.94	0.385
stray field at yoke of PETRA normal magnets	<0.01 T	~0.01 T (for 4 T)	~0.001 T

a small model magnet of Fermilab type have shown which has been constructed at Saclay. The influence on field homogeneity will also be studied.

The authors believe that there has to be provision of correction in order to meet the field quality requirements in magnets produced in series and at reasonable cost. It has to be investigated whether correction coils inside dipole magnets are necessary or separate correction elements could be sufficient. The latter case will ease the construction of the dipoles.

As the iron yoke is not saturated in the Fermilab design the stray fields are fairly low while those of BNL magnets are marginal for PETRA application at 4 T. The cold iron of BNL magnets heavily saturates and the stray fields increase rapidly above 4 T. Further increase of yoke thickness of BNL magnets results in a still larger cryostat.

The BNL magnets need much more space of the tunnel than is available without lifting the existing magnet ring. Therefore at least a modification of the cryostat would be required. The Fermilab magnets fit well above or below the PETRA ring, even with scaled aperture.

3.4 Time schedule

Having assessed the status of magnet technology it is appropriate to analyse the feasibility of achieving an operational proton ring at PETRA by the end of 1984. This short period does not allow significant modification of the existing magnet designs. Although neither magnet meets fully the initial PETRA magnet specification, there will be no time to wait for successful construction and operation of prototype magnets before selecting a manufacturer and the design for the series. However, in order to minimize the risk for both the manufacturer and DESY following procedure is proposed. A preliminary order could be given to at least two manufacturers who would get the full order only after successful construction and operation of 3 or 4 magnets. The manufacturers will be paid for tooling designed by DESY and magnet fabrication. In case one manufacturer fails that set of tooling may be transferred to another firm.

An appropriate time schedule is developed in figure 3. Close contact to the US laboratories is required to get more information about construction details and field measurement results. In parallel with the dipole programme the quadrupole magnets have to be designed and constructed, and a concentrated effort has to be made to specify, select and acquire the refrigeration and ancillary cryogenics as well as magnet power supplies,

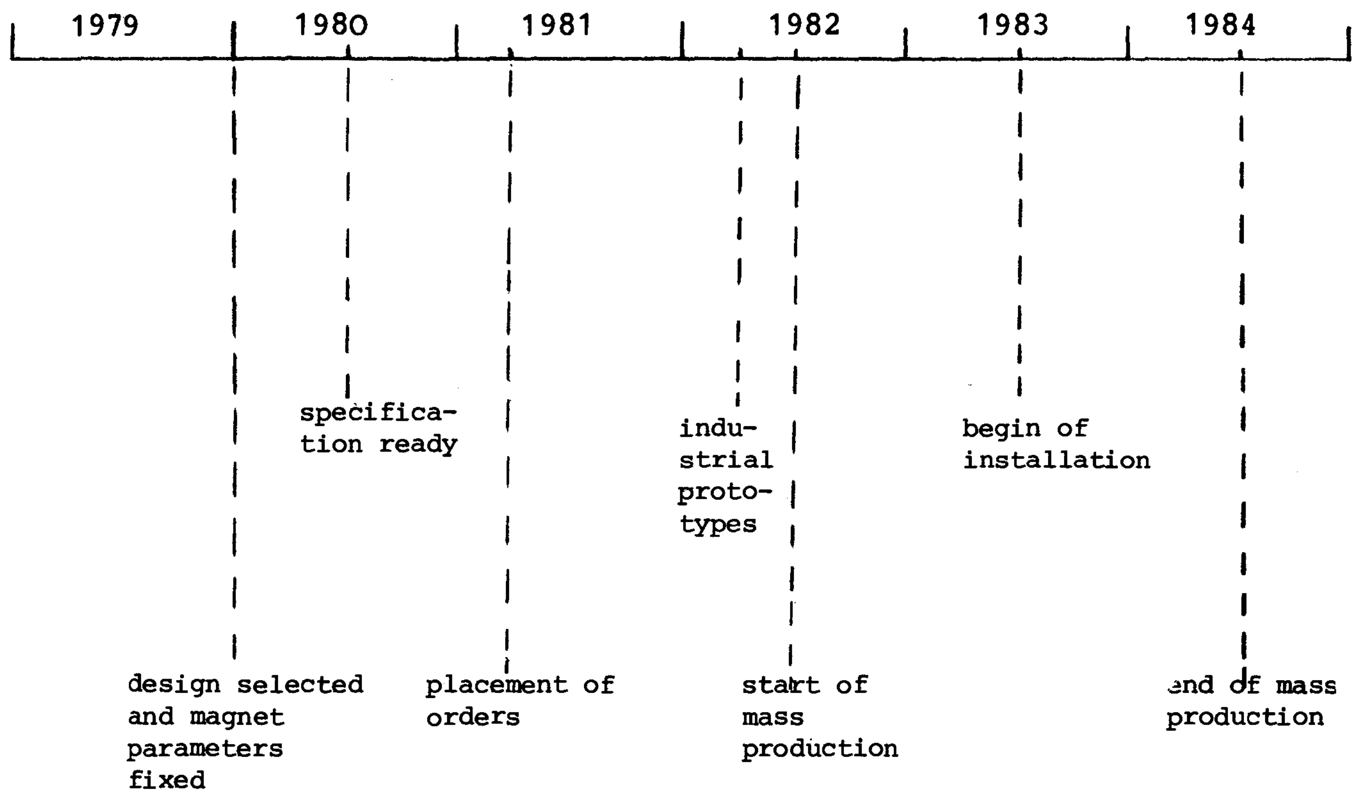

Fig. 3: Time schedule, 4 T option

quench protection system and instrumentation. An extensive magnet test facility is required by midst of 1982.

3.5 Cost Estimate

A rough cost estimate is given below for magnets, refrigeration and power supply. Costs for testing and test equipment including refrigerator and buildings have to be added. These figures are more difficult to be estimated.

Table III: Cost estimate(in $ 1000)

	BNL	FNAL	DESY	total
Dipoles	50/unit	35/unit	50/unit	11.600
Quadrupoles	25/unit	25/unit	25/unit	7.100
Sextupoles			8	1.200
Refrigeration				10.000
Power supply				2.500
Miscellaneous				2.500
			Total	~35.000

4. 5 Tesla option

Accelerator magnets with reliable operation up to 5 Tesla could be developed based on the existing designs. The required increase of ampere turns may be achieved by adding another shell of windings or by enlargement of the current carrying capability of the conductor. Corresponding investigations would have to be made including design and construction of short models.

This development work needs about two years time so that the ep machine can be in operation at proton energies up to 280 GeV by 1986. Industry should be involved from the beginning and should take over the development at the latest when prototypes have to be designed and constructed.

This development work needs about two years time so that the ep machine can be in operation at proton energies up to 280 GeV by 1986. Industry should be involved from the beginning and should take over the development at the latest when prototypes have to be designed and constructed.

5. 8 Tesla option

5.1 Magnet design

In principle, NbTi is applicable for 8 Tesla magnets, too. However, as its current density is significantly decreasing above 6 Tesla a very large number of turns would be required. Consequently the construction would become rather complicated and the overall size would grow to dimensions unacceptable for PETRA.

For high magnetic fields Nb_3Sn superconductor is better suited. In recent years significant progress has been made in the development of filamentary Nb_3Sn superconductor. This development has reached the stage where it is now feasible to consider the construction of dipole magnets in the 8 Tesla field range.

Solenoidal magnets are already being produced on a commercial basis and conductor development is underway for fusion applications. Future high energy accelerators will probably be based on Nb_3Sn superconductor and it is appropriate to consider the status of Nb_3Sn technology in relation to a proton ring for PETRA.

A preliminary design study has been made at Rutherford of a Nb_3Sn dipole magnet to operate at 8 Tesla central field which corresponds to a PETRA proton energy of 450 GeV. The aim has been to establish the scale of magnet, identify the important design features and assess possible time scales for development. Some consideration has also been given to the construction of a hybrid magnet of NbTi-Nb_3Sn but this magnet would not fit into the PETRA tunnel.

The preliminary magnet design is shown in Fig. 4. The coil geometry is based on a four layer system in which the current density is graded. The block current density required for the inner layers is 250 A/mm^2 at 8 Tesla. Preliminary calculations indicate that a force support structure of ~50 mm of stainless steel is required with an annular space of ~30 mm for the cryostat. The low carbon steel yoke is at room temperature.

A first conductor design results in a 23 strand flat cable enclosed in a pure copper jacket of 2.2 x 9 mm outer dimensions. The protected copper in the strands and the outer shell is required for quench protection and stability which is still increased by liquid helium filling the free space within the cable.

For a dipole magnet the use of prereacted Nb_3Sn superconductor is not considered feasible because of detrimental stresses in the conductor imposed by the small radii in the coil ends. The alternative procedure of winding followed by reaction to form the Nb_3Sn layer requires that all magnet components withstand temperatures in the range 650-720°C. While the basic technology for wind & react construction is available from small magnets development work is required on insulation methods, impregnation and scaling up in magnet size. Further progress is e.g. expected from short Nb_3Sn dipole models which will be built at Saclay. The first model is scheduled for 1979.

Several factors affect field homogeneity of Nb_3Sn magnets in addition to those present in NbTi magnets. As the quantity of superconductor is increased and the current density of this superconductor is high the effects of superconductor magnetization may be more significant. Coil movements under magnetic forces will be greater at 8 Tesla and the problem of maintaining manufacturing tolerances through

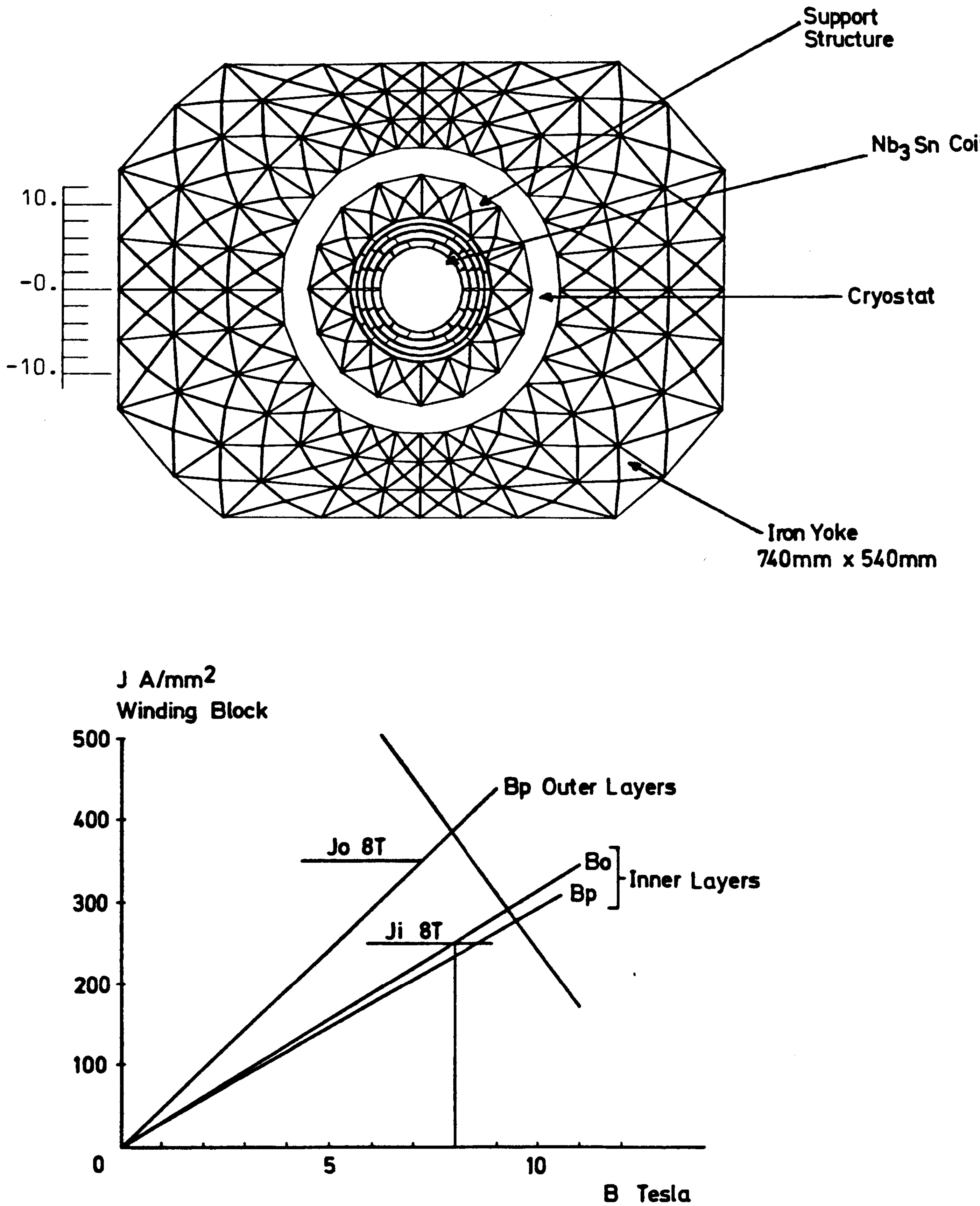

Fig. 4: 8T Nb_3Sn Dipole

the winding and reaction phases will increase random error amplitudes. Predicted iron saturation effects are small but the problem of out of balance forces between the coil and warm iron is accentuated at the higher field level. Because of stray field requirements a relatively massive yoke structure is necessary, the overall magnet dimensions, however, stay close to PETRA specifications.

5.2 Time schedule

The later stages in the development programme require a time scale similar to the NbTi magnet system. A significant extension, however, is required in order to develop prototypes. Basic development work on conductors and test coils has to be done leading to a short dipole model in 1980/81. In the period 1981-84 full scale prototypes would be developed both in the laboratory and in industry. The number of prototypes should be at least ten magnets leading to project approval in mid-1984. Similar to NbTi schedules about another four years are required until operation of the ring. Accurate costing of such a system is difficult because present conductor prices are related to development rather than mass production.

6. Conclusion

Three options for realization of a superconducting proton ring at PETRA are presented. Although no existing design fits directly the quickest solution is to adapt one of the most advanced american designs to PETRA requirements. This would lead to a 225 GeV machine operated at 4 Tesla. It should be mentioned that the reported time scale for operation by 1984 is hard to get along with as it is assumed that everything proceeds smoothly and the results from series fabrication of the US magnets prove the magnets to be reliable and reproducible. In addition it is questionable whether a special long shut down of PETRA will be provided for installation of magnets and cryogenic equipment or regular shut downs can be used only. In the latter case there will be a corresponding shift of first operation of the proton ring.

Increase of proton energy up to 450 GeV can be expected by development of Nb_3Sn magnets with a central field of 8 Tesla. However, extensive development work is required in order to start operation of the ring in 1988.

All time scales depend on the assumption that the project would be approved or work can start by mid-1979. A delay in the beginning cannot be compensated and will delay the end.

The authors wish to thank G. Horlitz and S. Wolff for valuable discussions.

The cited work of Brookhaven and Fermilab is presented in detail in further contributions to this study meeting.

Discussion

G. Wolf:

A question to the rise time of the magnets. You mentioned that the Isabelle magnets have a rise time of about 200 seconds while the NAL magnets have a rise time of 20. What sort of compromise does one have to make to get the short rise time?

Pérot:

I think Alvin Tollestrup can answer this question, but it is mainly because the doublermagnet has to be used at a synchrotron and the Isabelle magnet has to be used at the storage ring.

G. Wolf:

So what are you saying, at no costs you can get a rise time of 20 seconds.

Pérot:

Yes. It is not needed because for a storage ring the rise time is not important. The beam is stored for hours, so that if we rise the field in 300 seconds it is not significant.

G. Wolf:

Is that all true with respect to the field homogeneity?

Pérot:

Yes.

Hahn:

I have a minor correction to your numbers. I think, for our magnets they must have referred to the old design because the cold bore aperture is 13 cm instead of 12 and the physical length is four and three quarters of

PRESENT ACTIVITIES ON SUPERCONDUCTING ACCELERATOR MAGNETS AT CERN

L. Resegotti and D. Leroy

CERN

Geneva, Switzerland

presented by L. Resegotti at the

ep Study Meeting

Session on technology of superconducting magnets

2 April 1979

PRESENT ACTIVITIES ON SUPERCONDUCTING ACCELERATOR MAGNETS AT CERN

L. Resegotti and D. Leroy*

1. Introduction

As many other laboratories, CERN has produced a number of superconducting magnets for beam handling purposes, some of which are presently in use in secondary beams of the SPS experimental areas. They are of different designs, according to the different aims and preferences of their designers. It would not be possible, and probably not very useful, to list them here in a short review. It seems preferable to give some details of two main lines of activity which are being followed at present.

The first line is oriented towards the design and construction of large aperture, high precision magnets, which are suitable either for magnetic spectrometry in beams or for proton storage rings. After the successful construction of prototype quadrupoles at CERN and of two beam spectrometer dipoles at Saclay by a CEA-CERN collaboration, the project of a superconducting low-beta insertion in the ISR is being implemented. Design studies for a superconducting conversion of the ISR (SCISR) and of new superconducting storage rings for 400 GeV protons (LSR) have been published a year ago.

The second line of activity is concerned with the design and construction of long, small aperture magnets for transport systems of low-emitttance, high-energy beams. A prototype 5 m long dipole with a central field of 4.5 T is being built, in view of a possible specific application at the SPS, namely a 500 GeV primary beam (called PO beam), requiring five such dipoles in series.

---

* CERN, Geneva, Switzerland

2. The storage ring magnets

The basic concepts of the proton storage ring magnet design are:

a) The field quality must be good over a relatively large fraction of the aperture, corresponding to the momentum bite between the injection orbit and the top of the stored proton stack, over the whole range of operating energies.

b) The positions of the magnetic axes and planes must be precisely determined with respect to geometric references outside the cryostats by means of magnetic measurements in the laboratory.

c) No tensile stresses should occur in the coil insulation under the action of the electromagnetic forces during normal operation.

d) The magnets must be able to absorb their own stored energy without damage in case of quench.

In the case of the low-beta insertion for the ISR, a further requirement is that the vacuum system of the machine must be independent from that of the magnet cryostats and independently bakeable.

These requirements can best be satisfied by a cylindrical assembly of sector coils, externally precompressed by a cold iron yoke. If the coils have an inner diameter about 1.7 times the beam width, there is enough space inside them for a separate thick pipe, carrying the auxiliary windings, which are necessary to adjust the machine tune and its derivatives. Some of theses windings can also compensate the saturation effects due to the proximity of the iron.

The features of such a system can be distinguished by a closer inspection of the proposed magnets for the ISR conversion. The structure and the conductor are the same for dipoles and quadrupoles, the only difference being their specific symmetries, as shown by Figs. 1 and 2.

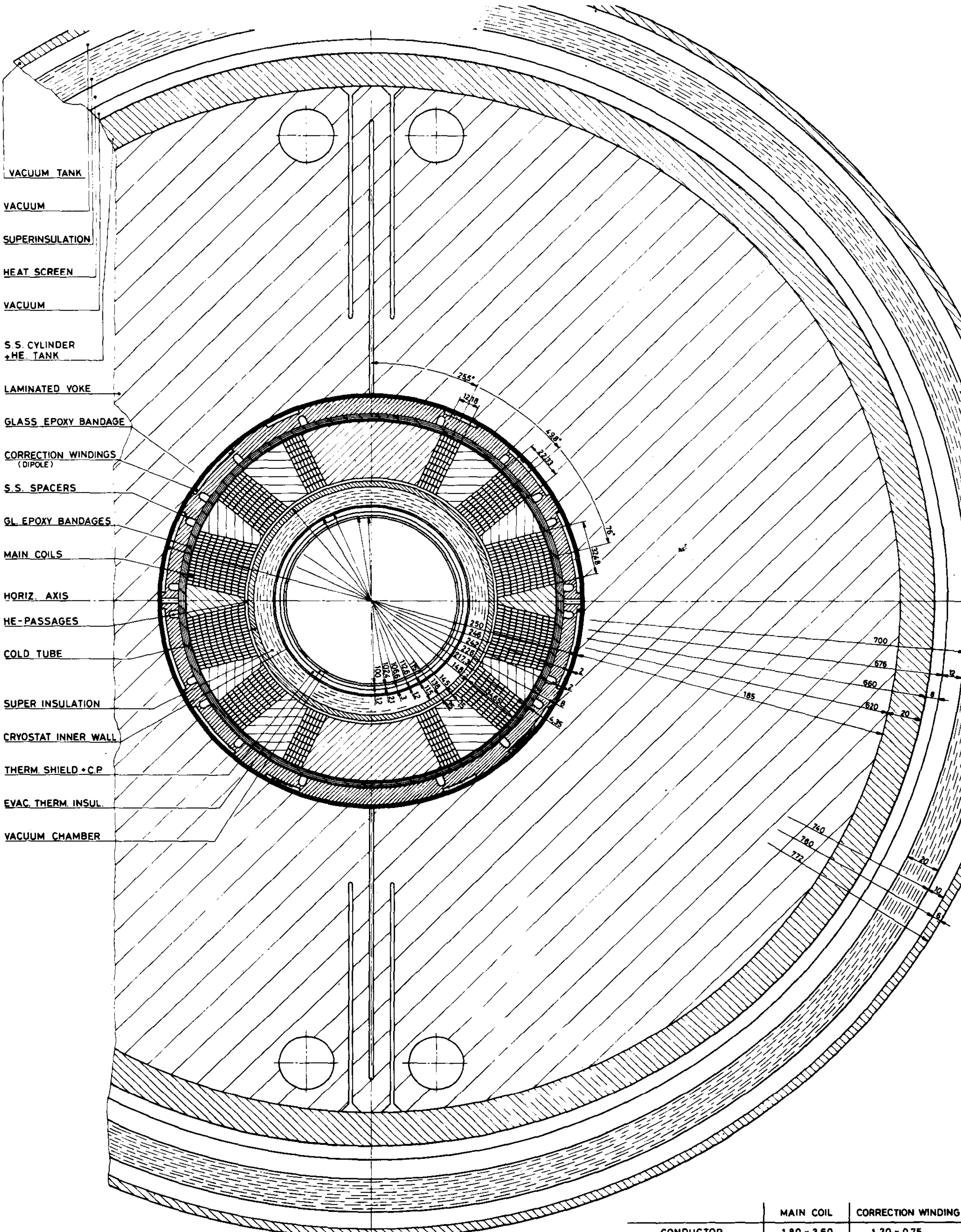

	MAIN COIL	CORRECTION WINDING
CONDUCTOR	1,80 x 3,60	1,20 x 0,75
CONDUCTOR INSULATED & TOLERANCES	2,03 x 3,85	1,28 x 0,83
TURNS OF WIRE :		
BLOCK 1	6 x 9	25
" 2	11 x 9	42
" 3	16 x 9	60
TOTAL	297	127

Fig. 1 Cross-section of a SCISR dipole

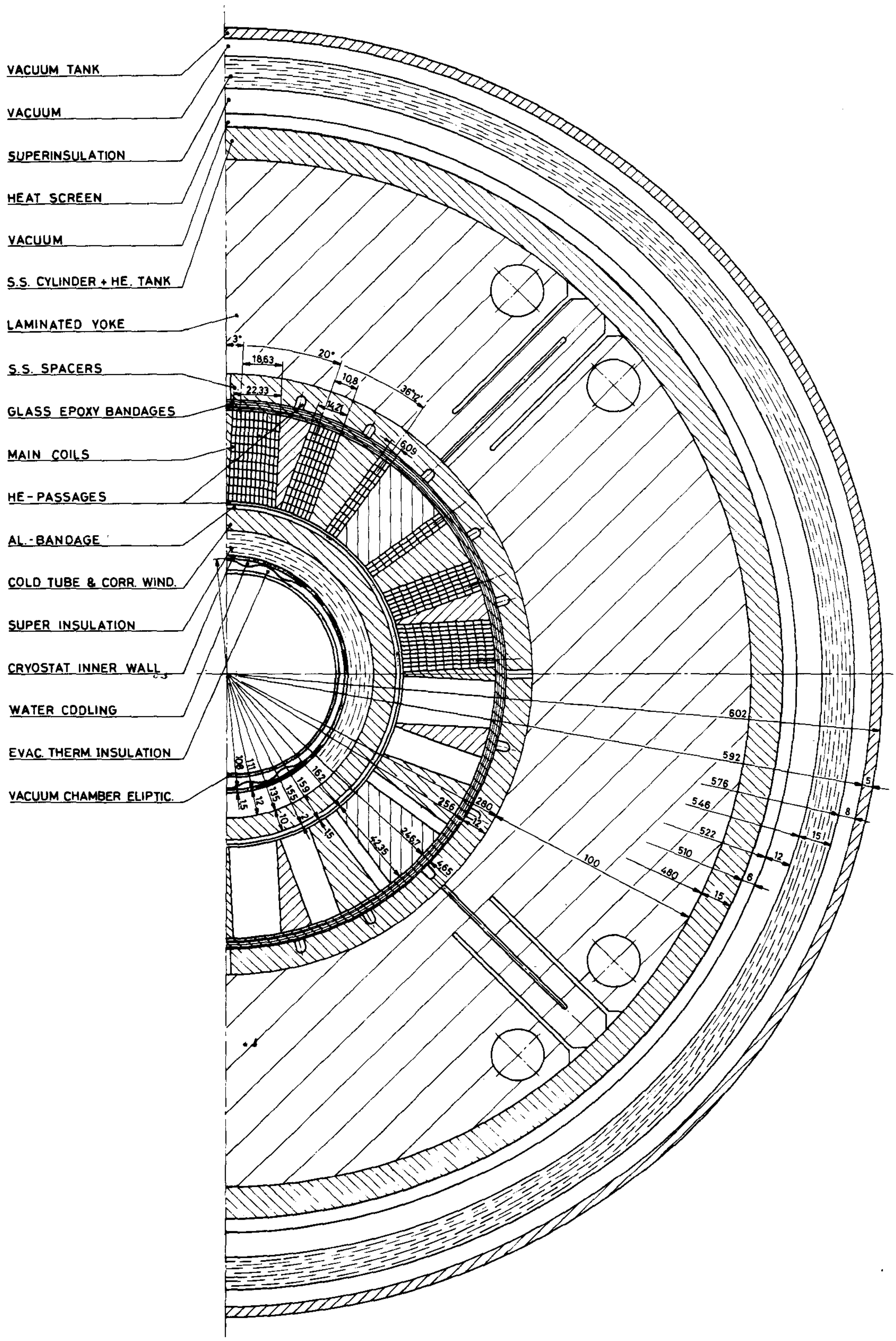

Fig. 2 Cross-section of a SCISR quadrupole

The main windings are assemblies of two and four coils, respectively. Each coil is made of three blocks of conductors. These are wound tightly, under tension on a central stainless steel post and copper spacers, with constant perimeter end shape (Fig. 3). They are then vacuum impregnated with epoxy resin. The coil assembly is held together by glass-fiber bandages which transmit the prestress from the yoke to the windings. Stainless steel spacers are inserted between the yoke and the bandages.

The conductor is a twisted multifilamentary composite, with a rectangular cross-section of 3.6 × 1.8 mm. The filament diameter is about 50 μm. The relatively large sizes of filaments and conductor and the block structure of the coils favour electromagnetic and thermal propagations of the quenches, so that the stored energy of the magnet is absorbed by the whole winding, without undue local overheating. This feature has been thoroughly tested experimentally on the prototype quadrupoles for the ISR, shown in Fig. 4. A stored energy of 700 kJ has been repetitively absorbed by a 1.25 m long prototype with maximum temperature rises between 80 and 100 K.

The coolant is in contact with the coil assembly over the whole inner cylindrical surface, which is completely free, and over about half of the outer cylindrical surface, where channels are left between the glass-fiber bandages. The cooling is adequate to permit a field rate of rise of 300 G s^{-1}. This means that full excitation is reached in about three minutes, which is short with respect to the setting up time and to the duration of phase displacement acceleration in the ISR.

As can be seen in Fig. 5, in the ISR low-beta quadrupoles the steel yoke is made of four monolithic sectors, held together by aluminium

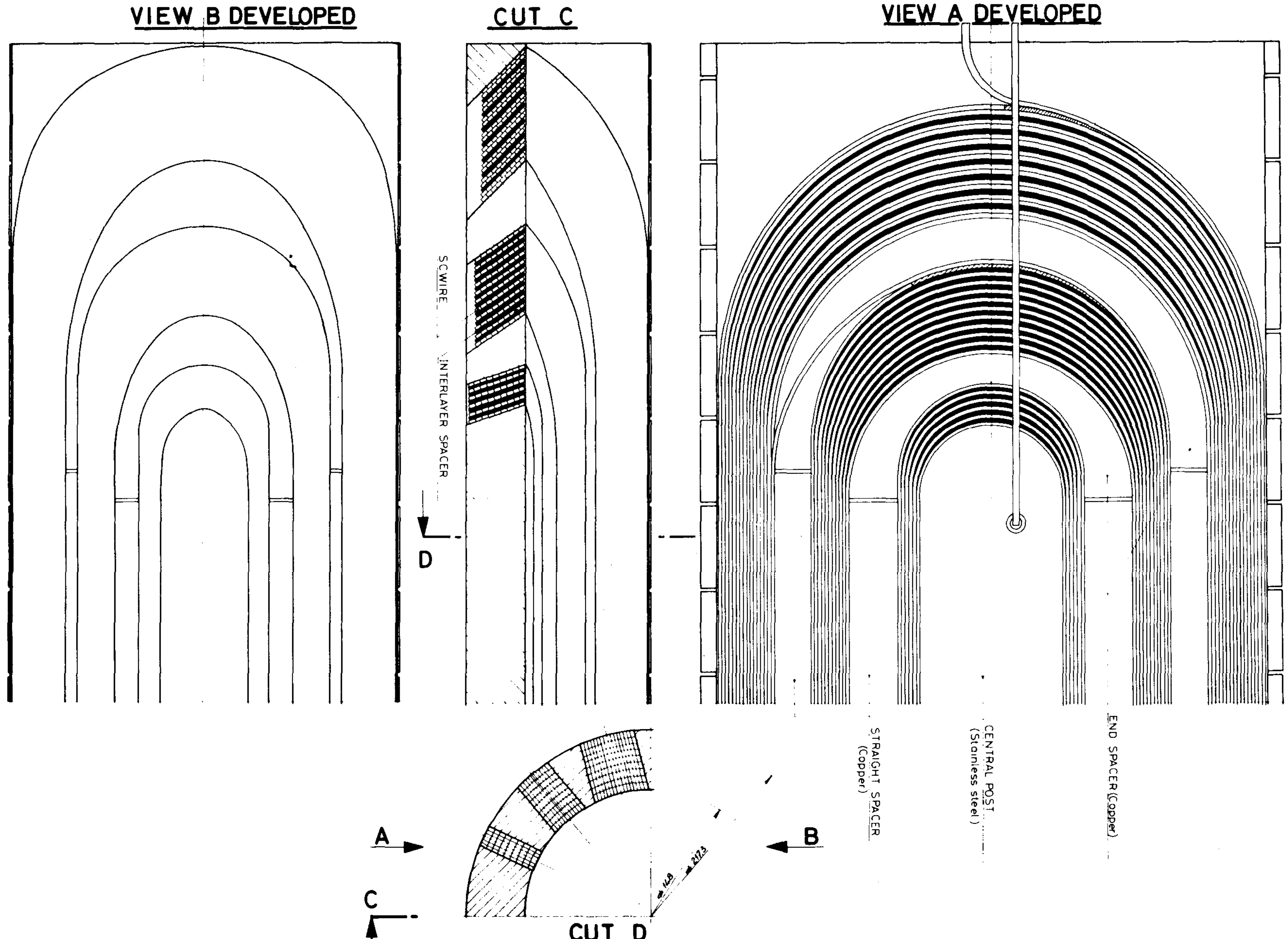

Fig. 3 Coil end shape of a SCISR dipole

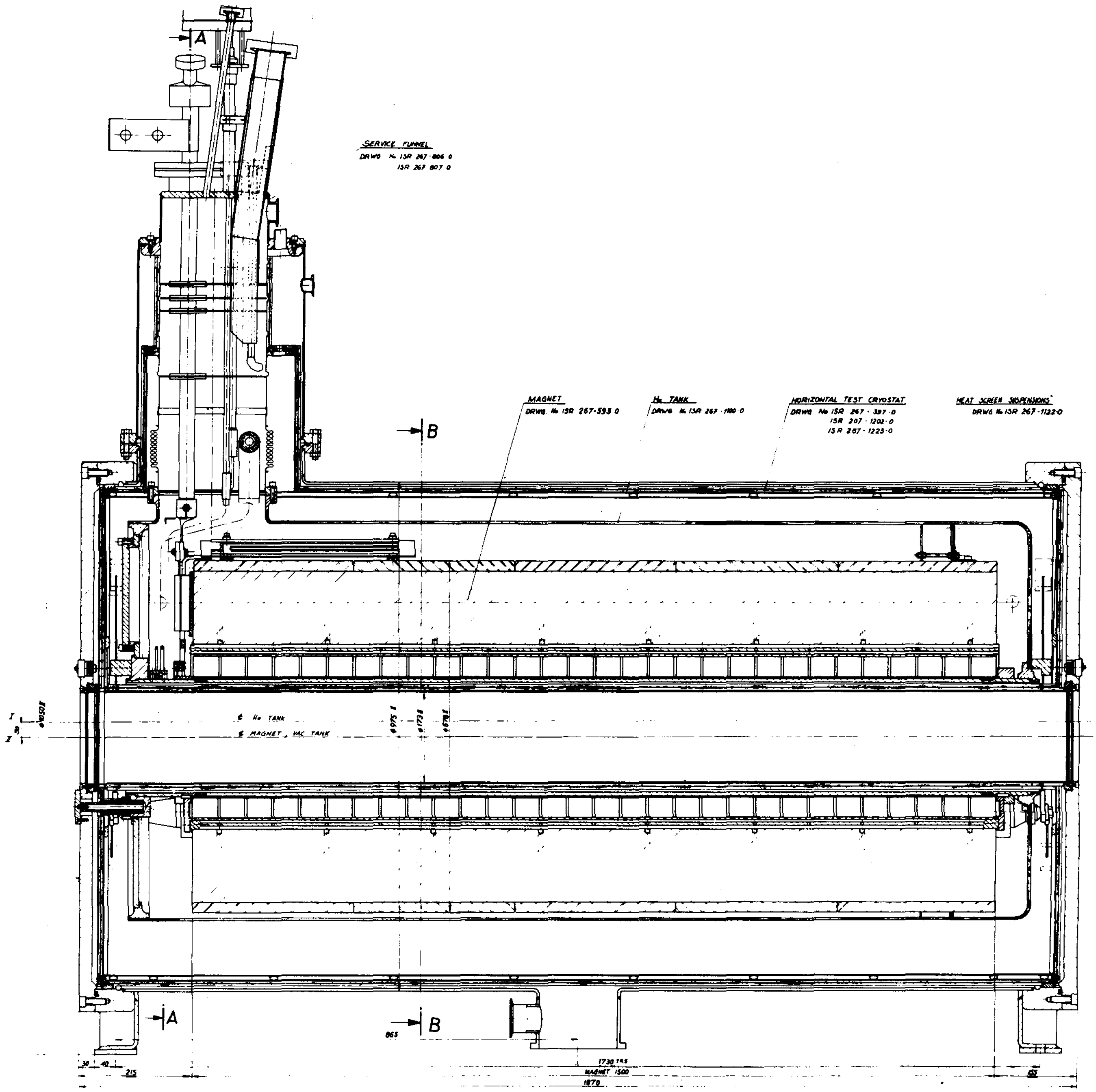

Fig. 4 Longitudinal section of the prototype ISR quadrupole

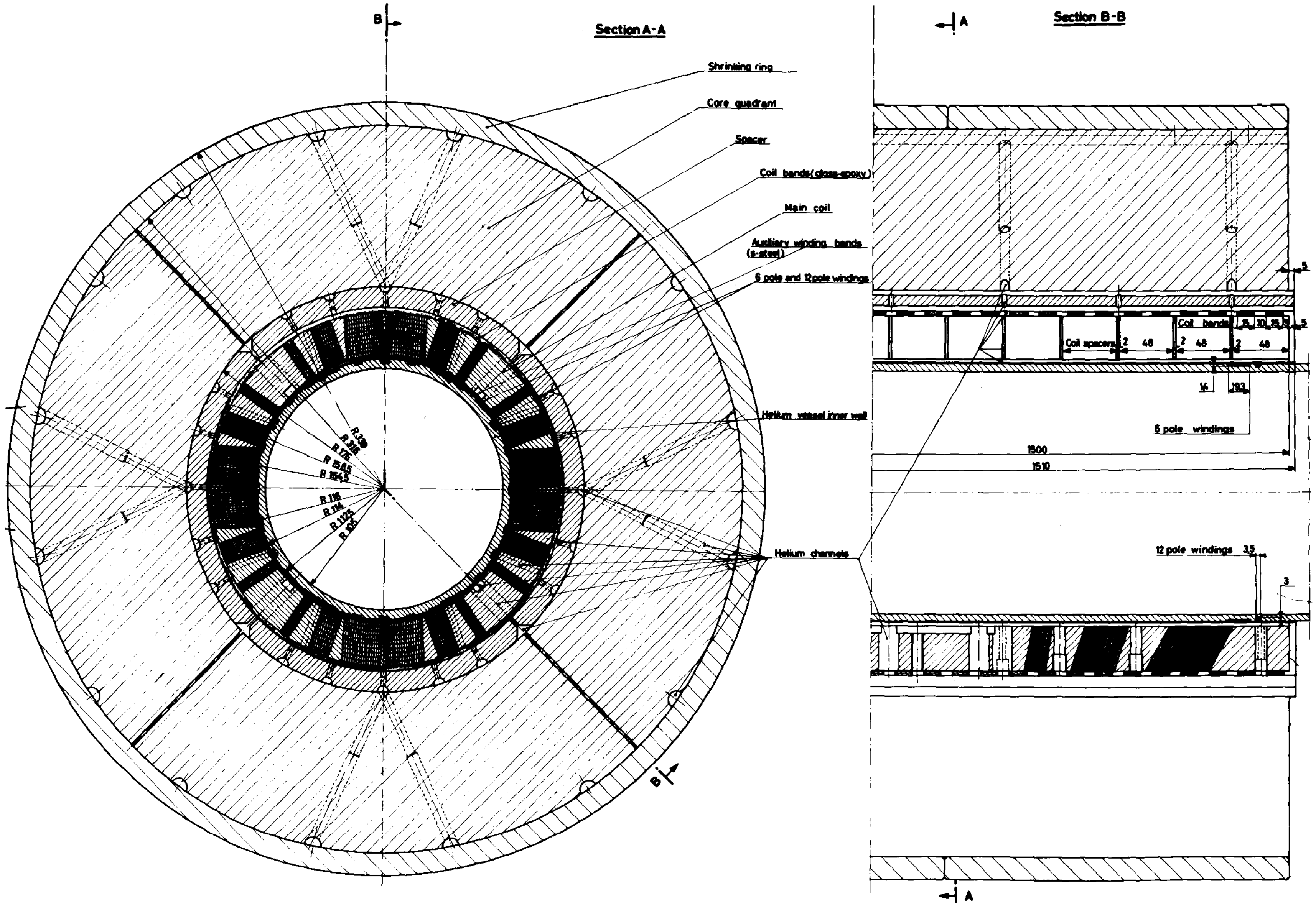

Fig. 5 Cross-section of an ISR low-beta quadrupole

rings, since the small numer of magnets and their short lengths would have made a laminated structure unnecessarily expensive. In the SCISR and LSR designs (Figs. 1 and 2), as in the magnets for ISABELLE, the yoke is a stack of ring-shaped steel laminations inside a stainless steel cylinder, but the laminations are locally slotted at the positions of the poles, so that they should behave like springs. At magnet assembly, the stack, temporarily held together by longitudinal bolts, would be slightly opened by means of hydraulic cushions, to receive the windings at room temperature. The pre-heated cylinder would then be fitted onto both. Thus, the prestress on the coils would be low at room temperature, at which flow of the organic insulation might be feared, and would be increased during cooldown by the radial shrinkage of the stainless steel cylinder. The longitudinal contraction of the yoke, as determined by the stainless steel, is about the same as that of the coils.

The precompressed "cold-iron" structure, which is very compact and rigid, ensures good mechanical stability and tight positional tolerances. It has the disadvantage that the whole mass of iron has to be cooled inside the cryostat, but the advantage that the suspensions are simple and their heat intake low. It is, therefore, quite suitable for a storage ring, which has long periods of steady operation.

In our superconductive storage ring conversion studies, the magnets have a warm bore. That choice does not imply loss of useful aperture, because the warm pipe wall and its superinsulation occupy only that peripheral region where the field quality is not adequate for the beam. However, a cold bore aperture permits to maintain a larger clearance between beam and wall and, therefore, it might be advantageous for applications requiring smaller beam apertures. We know now that such a solution can be safe from the point of view of vacuum even in a high-intensity proton storage ring. Recent experiments at the ISR have shown that beams above 30 A can be circulated inside a glow discharge cleaned, unbaked vacuum chamber at liquid helium temperature, without inducing pressure rises.

The ISR low-beta insertion, shown in Fig. 6, requires eight superconducting quadrupoles, with gradients from 38 to 43 T m^{-1} in warm apertures of 173 mm. The tolerance on the integrated gradients is 10^{-3} over a beam width of 130 mm.

The prototype quadrupole, built at the ISR to demonstrate the feasibility of the superconducting low-beta insertion, confirmed the expectations concerning maximum gradient, rise time, field quality and ability to absorb its own energy in case of quench. This prototype built in 1976, has since been cooled down and warmed up many times and repeatedly quenched for testing purposes, without any deteriorations.

The methods and techniques used in the construction of the prototype were described in detail in the specifications, addressed to industrial firms, which were invited to tender for the production of the eight quadrupoles required by the low-beta insertion. All tools and equipment, such as, for example, the instrument which continuously monitors interturn and ground insulation, were demonstrated to prospective tenderers and their drawings were made available on request. Efforts were directed to make every operation simple and reproducible, so that the firms could expect the transfer of technology to be possible without development work in the factories. Separate tenders were invited for the supply of the superconducting wire, the construction of the quadrupoles themselves and for the cryostats. The response was positive and really competitive offers were obtained.

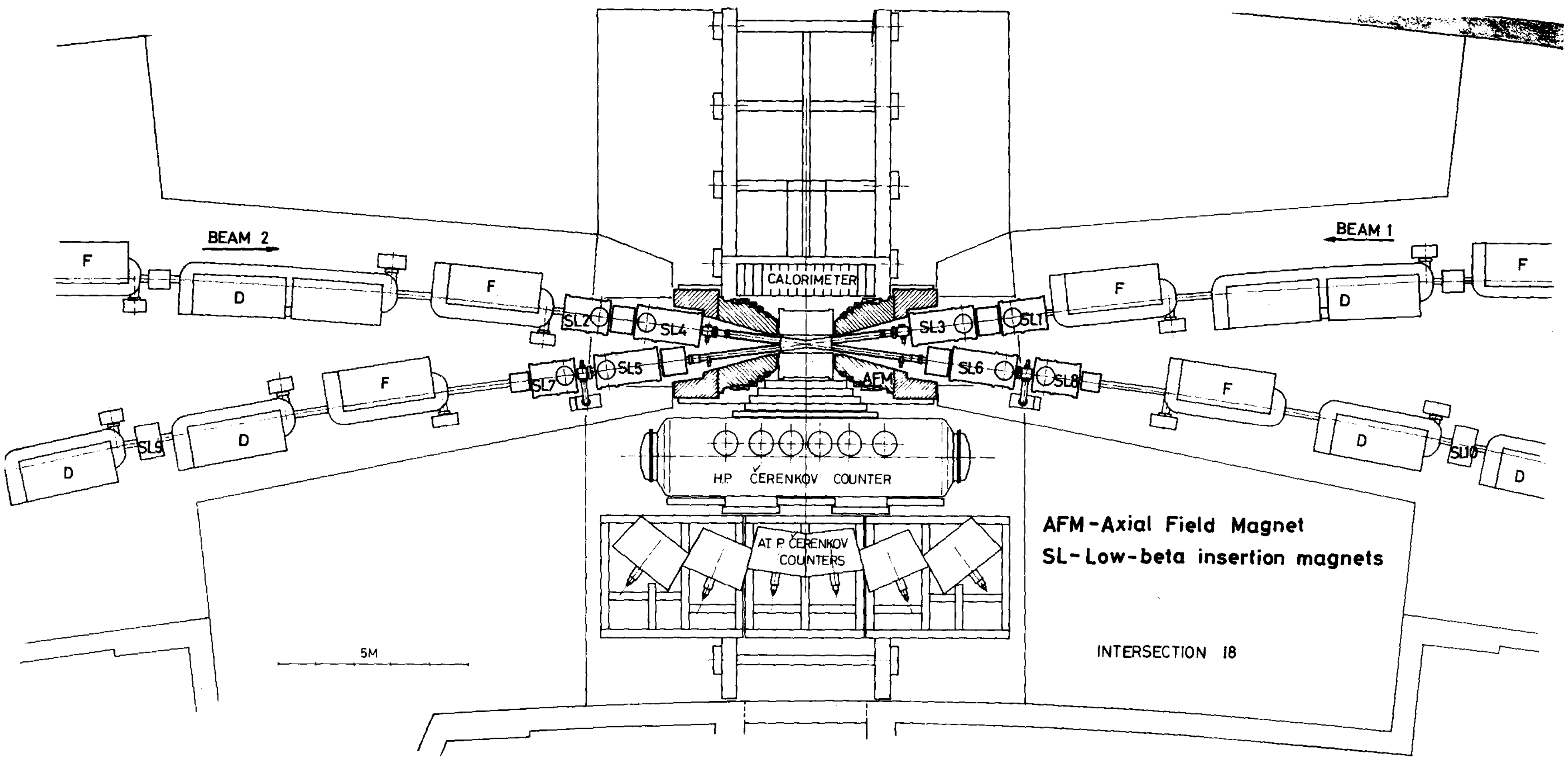

Fig. 6 Layout of the superconducting low-beta insertion in the ISR

The initial apprenticeship and the setting up of series production at the factory making the magnets proper required about a year. By now, more than half of all coils have been wound, other components are being regularly produced, and the first two quadrupoles have been delivered. Figure 7 sh.ws the winding installation at the factory and Fig. 8 the first quadrupole as delivered. In Fig. 9, one can see, inside the quadrupole proper, the stainless steel pipe which carries the auxiliary windings, namely a sextupole winding, which is necessary to produce the required chromaticity in the low-beta insertion, and a dodecapole windings, for the correction of the integrated gradient pattern. This pipe constitutes the inner tube of the liquid helium vessel. The auxiliary windings are wound on it at CERN.

All quadrupoles will first be tested in a vertical cryostat for the purpose of provisional acceptance and then assembled and measured in their own cryostats. The first quadrupole of the industrial production reached its maximum operating current of 1500 A, which, as can be seen in Fig. 10, corresponds to a gradient of 41 T m^{-1} and to a maximum field of 5.2 T in the windings, after two quenches. The magnet was further trained to 1800 A to check its ability to withstand quenches without energy extraction, which is part of the contractual conditions.

Figure 11 shows a phase of the subsequent assembly of the quadrupole into its own horizontal cryostat and Fig. 12 shows the finished quadrupole during magnetic measurements. Before the measurements, the quadrupole was excited directly at 1680 A for a 24-hour endurance test, without quenching. Figure 13 shows the integrated gradient pattern in the quadrupole, measured at its maximum operating current.

We must still wait to see what level of reproducibility will be achieved in the series production; but for the moment it looks as if this industrial production of superconducting quadrupoles has had a good start.

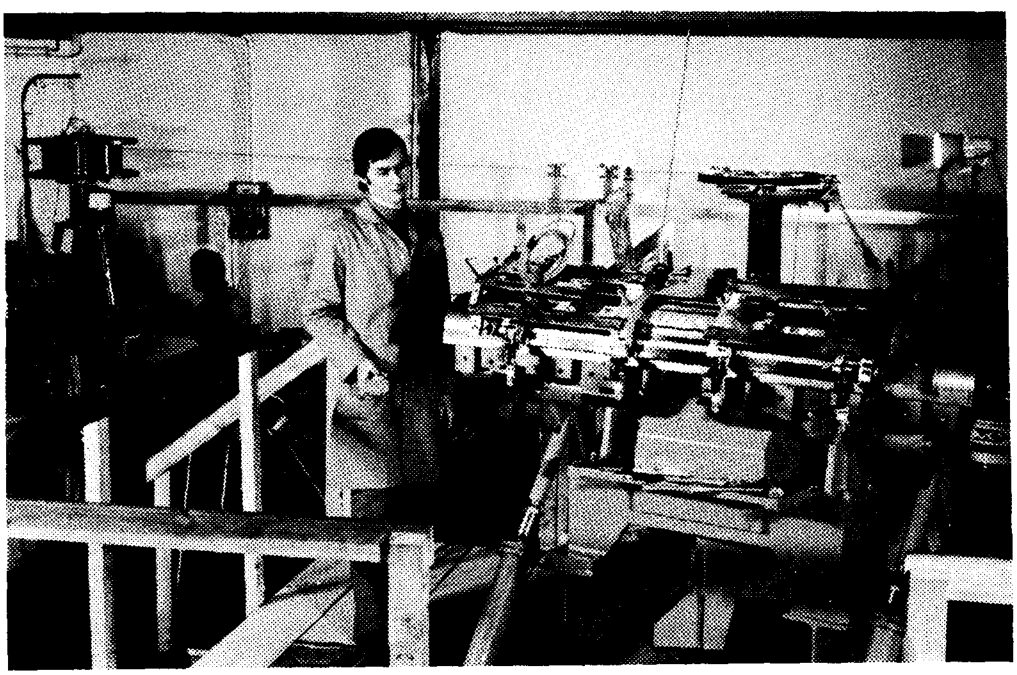

Fig. 7 A quadrupole coil being wound at the Alsthom factory

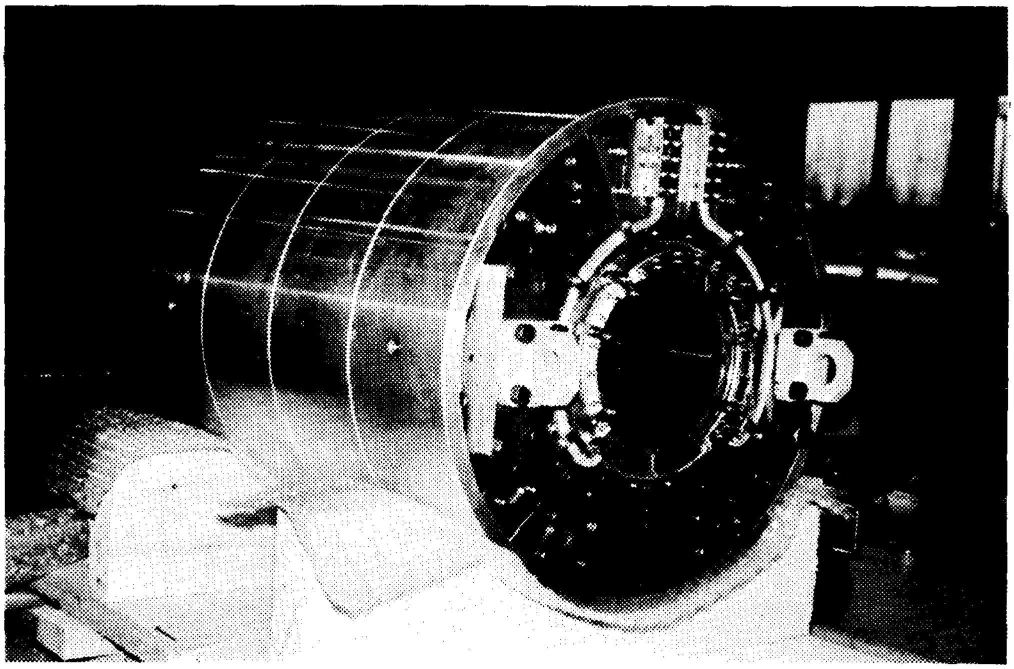

Fig. 8 The first finished quadrupole as delivered

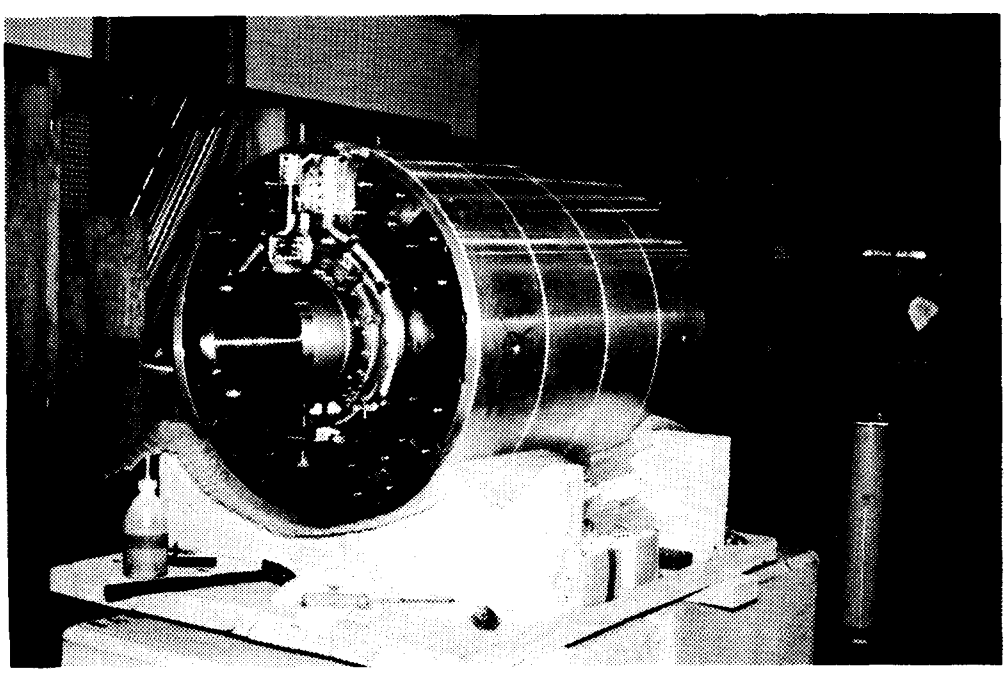

Fig. 9 The auxiliary windings have been mounted inside the quadrupole proper

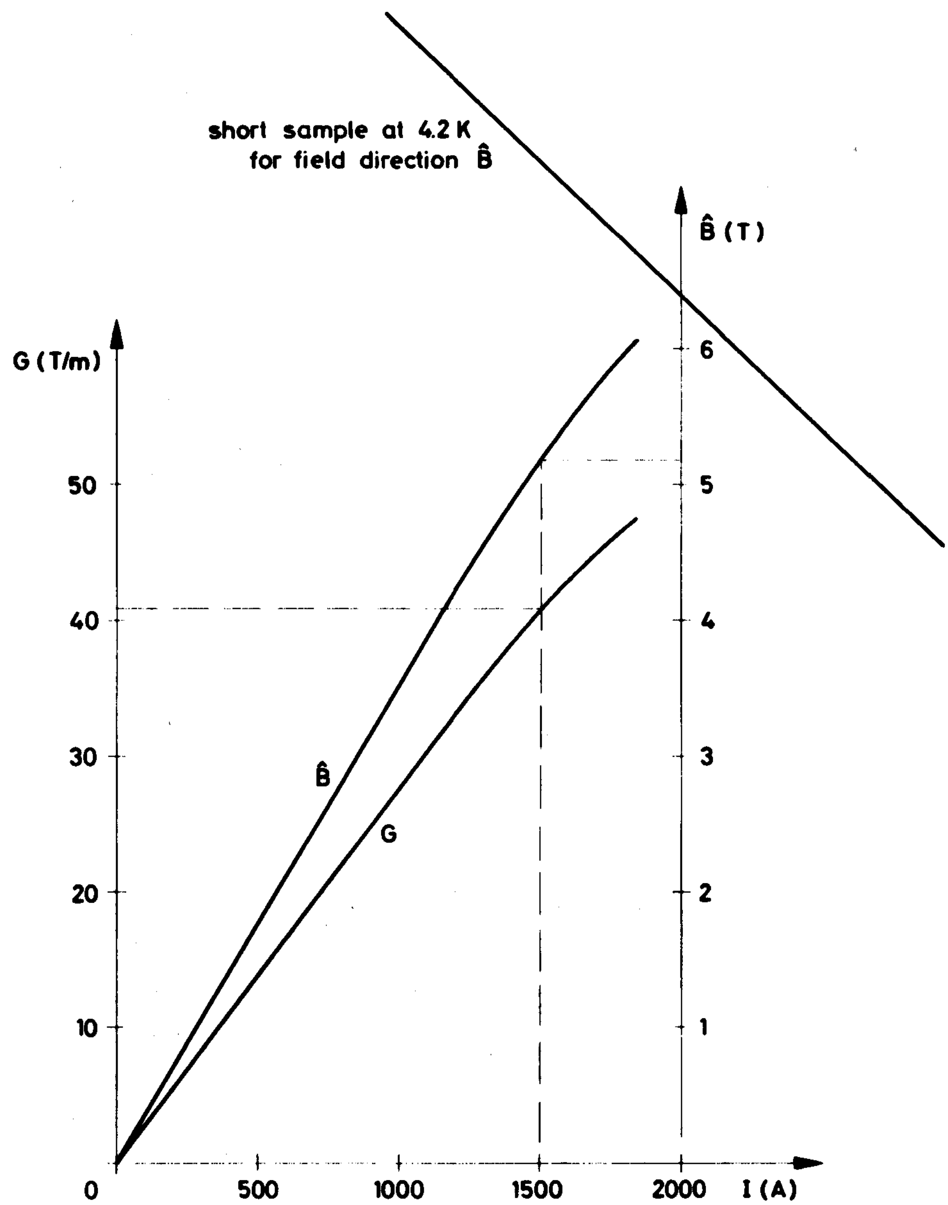

Fig. 10 Operating characteristic of the first low-beta quadrupole

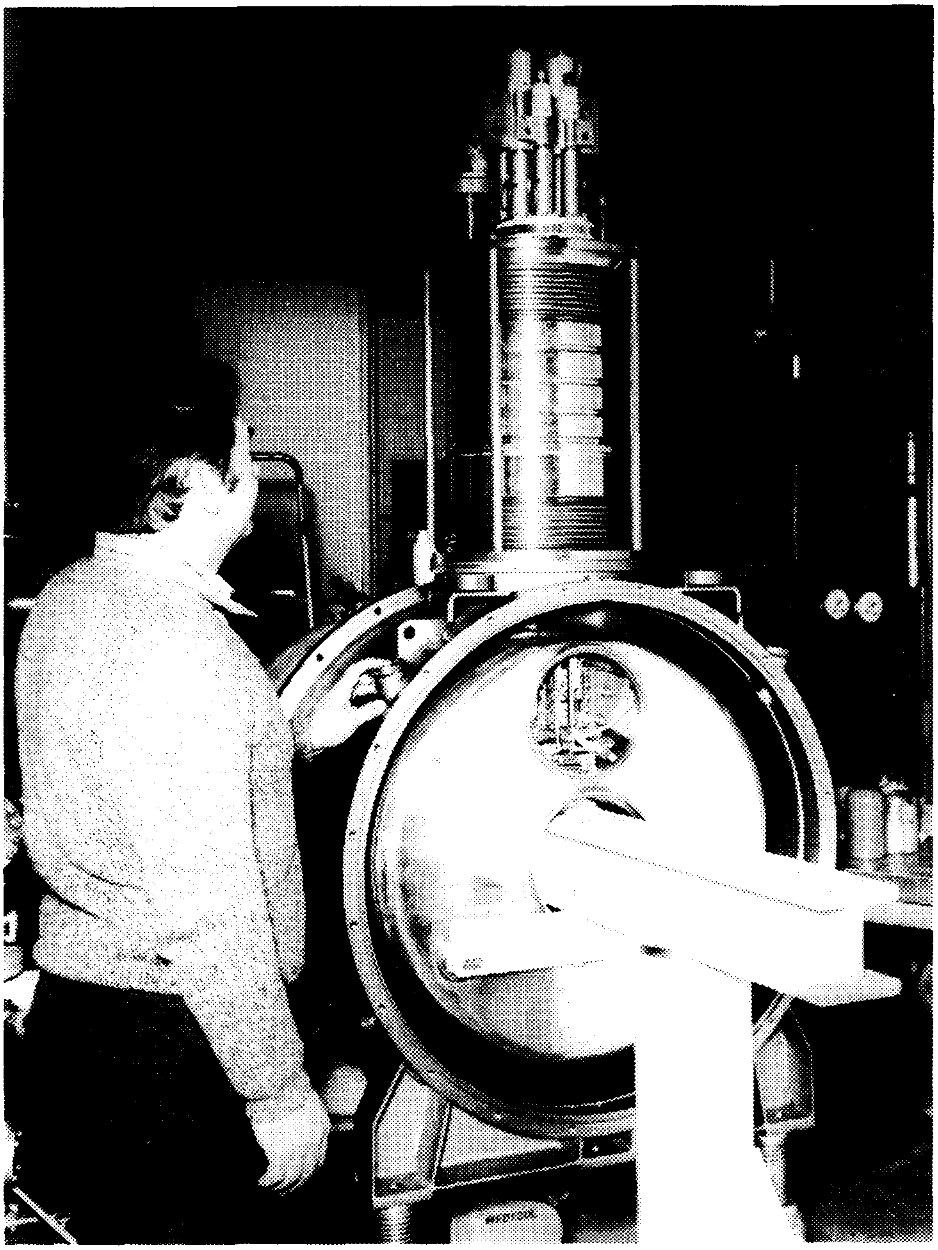

Fig. 11 Assembly of the first quadrupole into its cryostat

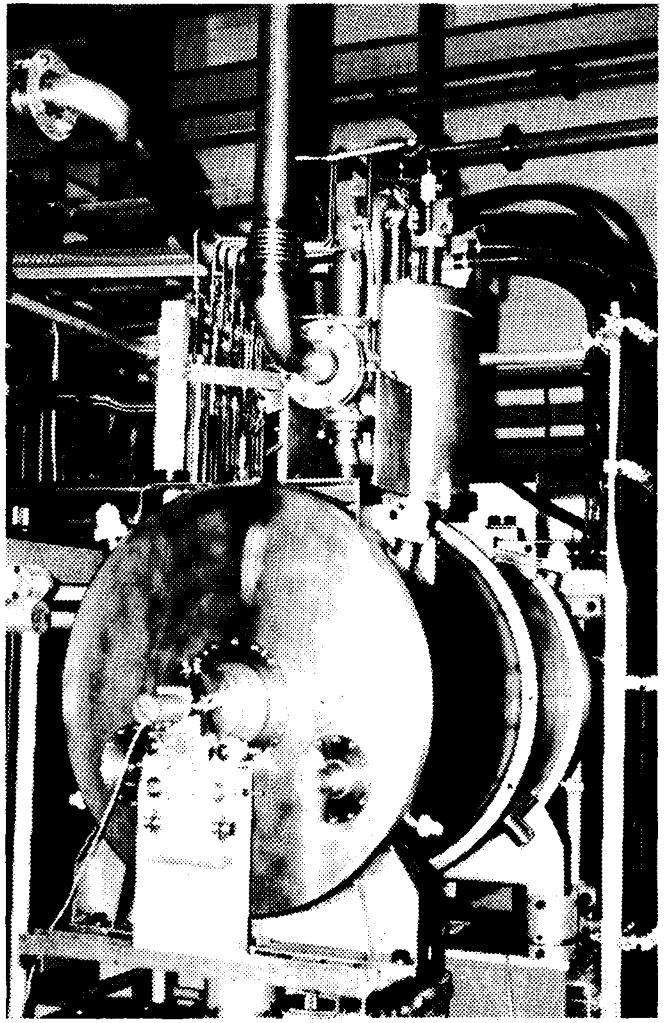

Fig. 12 The first complete unit during magnetic measurement

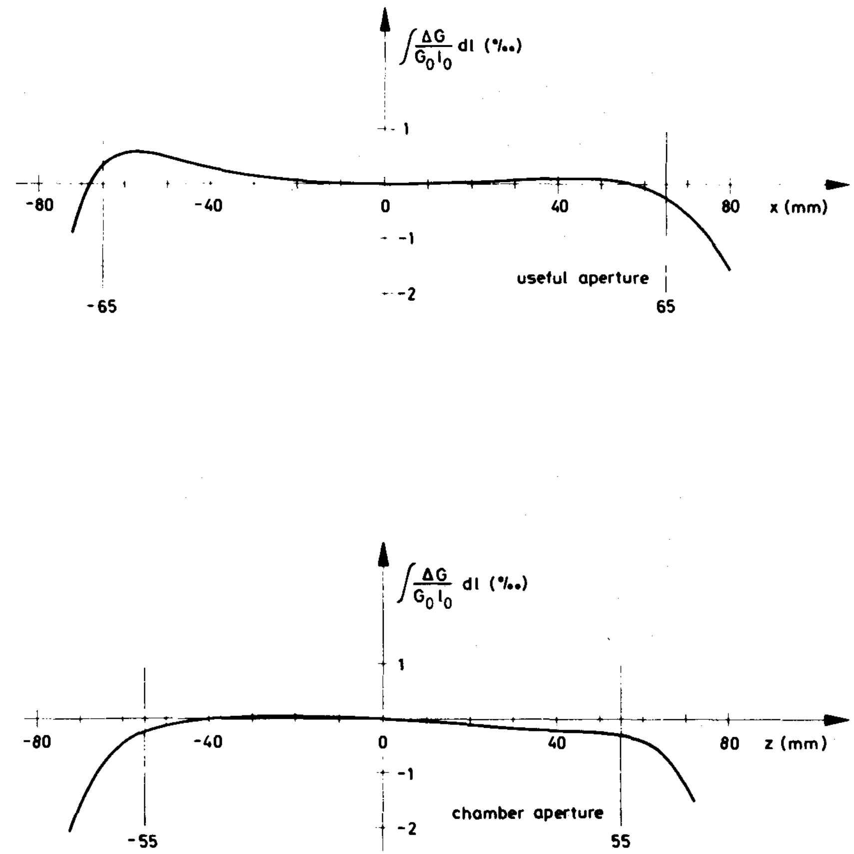

Fig. 13 Integrated gradient errors in the aperture of the first quadrupole

3. The PO beam dipoles

The interest in small aperture dipoles for high-energy, low-emittance beams arose at CERN two years ago, when the primary proton beam PO for the North Area extension of the SPS was designed. This beam has a concentrated bend of 54 mrad at its branch-off, which requires a bending strength of 90 Tm at 500 GeV/c. Five 4 T dipoles, each about 5 m long, would meet this requirement. The horizontal emittance of the beam is 0.4 π mm mrad, which corresponds to a maximum amplitude of 8.8 mm at 2 σ. The orbit sagitta in a 5 m long, 4 T bending magnet is 6 mm. Thus, a good-field region (field spread $\Delta B/B \leq 2 \times 10^{-4}$) about 30 mm wide is adequate, whereas a free aperture of about 60 mm is desirable, to limit particle losses from the tails of the distribution. The energy dissipation due to such losses is expected to remain lower than 0.75 mJ cm^{-3} per pulse.

An appropriate solution in this case is offered by magnets with a cold aperture coinciding with the beam pipe and with an inner coil radius of 35 mm. This radius is adequate to provide the required good-field region over the whole range of the proton beam energies, if iron saturation effects are kept low by placing the iron yoke far enough from the coils. Such a string of cold bore, warm iron dipoles is similar to the FNAL doubler structure. The same type of solutions as adopted at FNAL can also be used for powering, cooling and protecting them.

During the past two years, the work of the group concerned has been directed to the design and construction of a suitable prototype for the dipoles of the beam line, with a view to their possible industrial production in future.

Figure 14 shows the basic structure of the prototype. The coils consist of a two-layer winding encased into a system of stainless steel combes, which take the mechanical stresses resulting from the electromagnetic forces. The single-phase pressurized helium vessel, in which the coils and the combes are contained, is surrounded by a coaxial cylinder, through which two-phase helium circulates, and this, in turn, by a screen, cooled by helium vapour. The whole cold ensemble is centred in the warm steel yoke by radial spacers. The main characteristics of the magnet are given in Table 1.

Table 1

Main characteristics of PO prototype dipole

Cold bore radius	32	mm
Coil inner radius	35	mm
Coil outer radius	56.4	mm
Comb outer radius	82.5	mm
1 ϕ cryostat outer radius	85	mm
2 ϕ cryostat outer radius	86.5	mm
Iron inner radius	120	mm
B_0 (with iron) at 5250 A	4.5	T
B_0 (without iron) at 5250 A	3.95	T
Length of straight part	5	m
Overall length	6	m

A number of detailed studies, technical developments and experimental tests have been performed in view of the construction of the prototype. The main results can be described as follows:

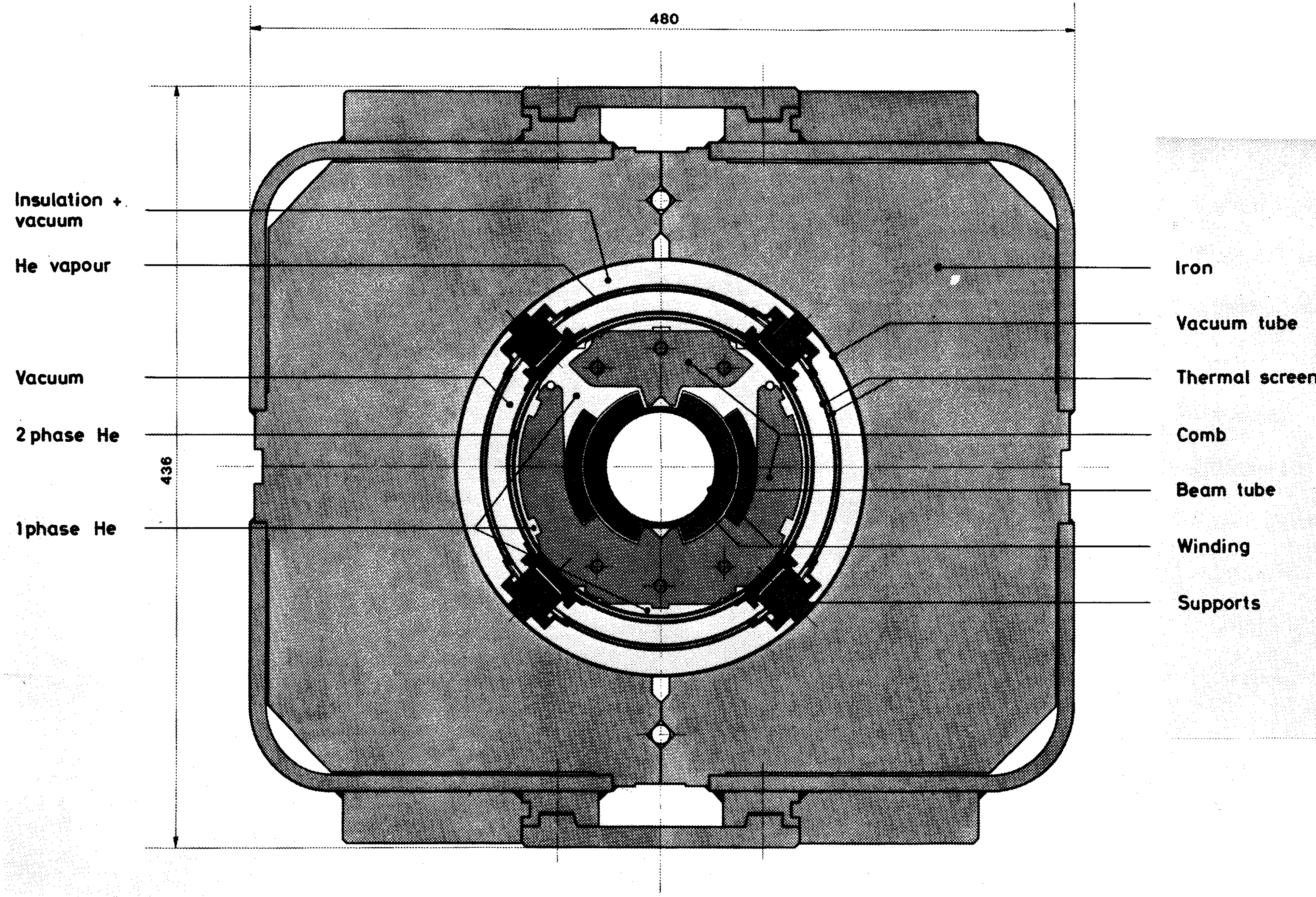

Fig. 14 Cross-section of the prototype dipole for the PO beam of the SPS

3.1 Cable production

Industrial production of Rutherford-type cables of up to 40 elementary conductors has been obtained. Some of them also include a central trapezoidal wedge, which should improve the mechanical behaviour of the coils and reduce the losses under pulsed operation. Typical cross-sections are shown in Fig. 15. The characteristics of the cable adopted for the prototype are shown in Table 2.

Table 2

Cable characteristics for the PO prototype dipole

Strand:		
Diameter	0.7	mm
Filament diameter	≤ 18	μm
Twist pitch	12	mm
I_c (5 T, 4.7 K)	≥ 270	A
Cable:		
Trapezoidal dimensions	1.2/1.35 × 9.4	mm^2
Number	≥ 26	
Transposition pitch	≤ 100	mm
I_c (5 T, 4.7 K)	≥ 7000	A
Insulation:		
Kapton ribbon (45 % overlapping)	2 × 25	μm
Triangular Kapton spacer	0.2 mm × 8	mm
B stage fiberglass ribbon	80	μm
Dimensions of the insulated conductor	1.46/1.81 × 9.7	mm^2

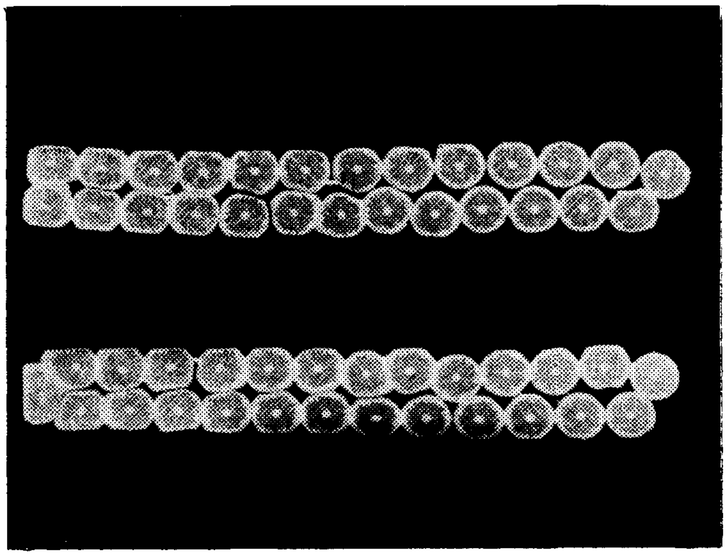

BBC conductor; 26 strands of 0.7 mm diameter;

$1.2/1.35 \times 9.4\ mm^2$; I_c (5 T, 4.7 K) = 8260 A.

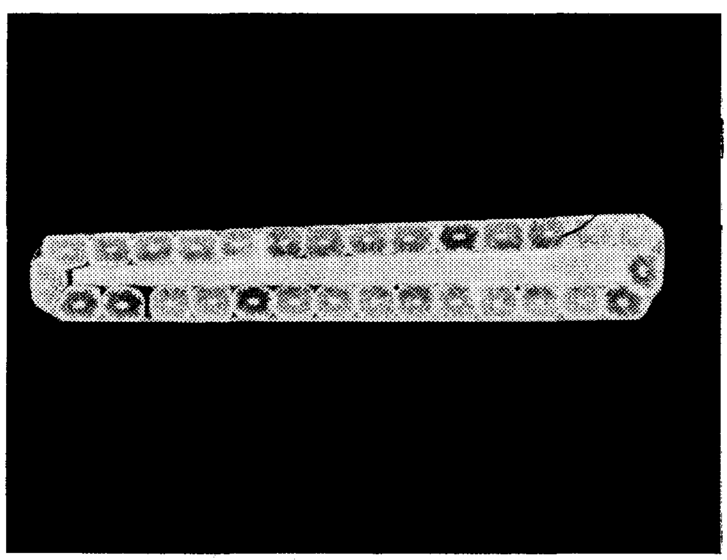

BBC conductor; 30 strands of 0.6 mm diameter;

$1.2/1.55 \times 9.4\ mm^2$; I_c (5 T, 4.7 K) = 8460 A.

Fig. 15 Cross-sections of industrially made prototype cables

3.2 Tests of coil winding and coil compaction

The conductors are wound in two layers. After polymerization of the first layer, small disc spacers are glued onto it, to create cooling channels between the layers. The second layer is then wound and polymerized. Experimental work has been carried out on a model of a winding machine, to study the mechanical characteristics of such coils. The azimuthal compaction before polymerization narrows the conductor package by about 13 %, when the conductors are compressed up to 15 kg mm^{-2}. Under these conditions, equivalent elastic moduli of more than 1500 kg mm^{-2} have been reached after polymerization, as shown in Fig. 16. Different mechanical treatments, such as vibration and cycling, are being tested, to improve the uniformity of the compaction in the coils.

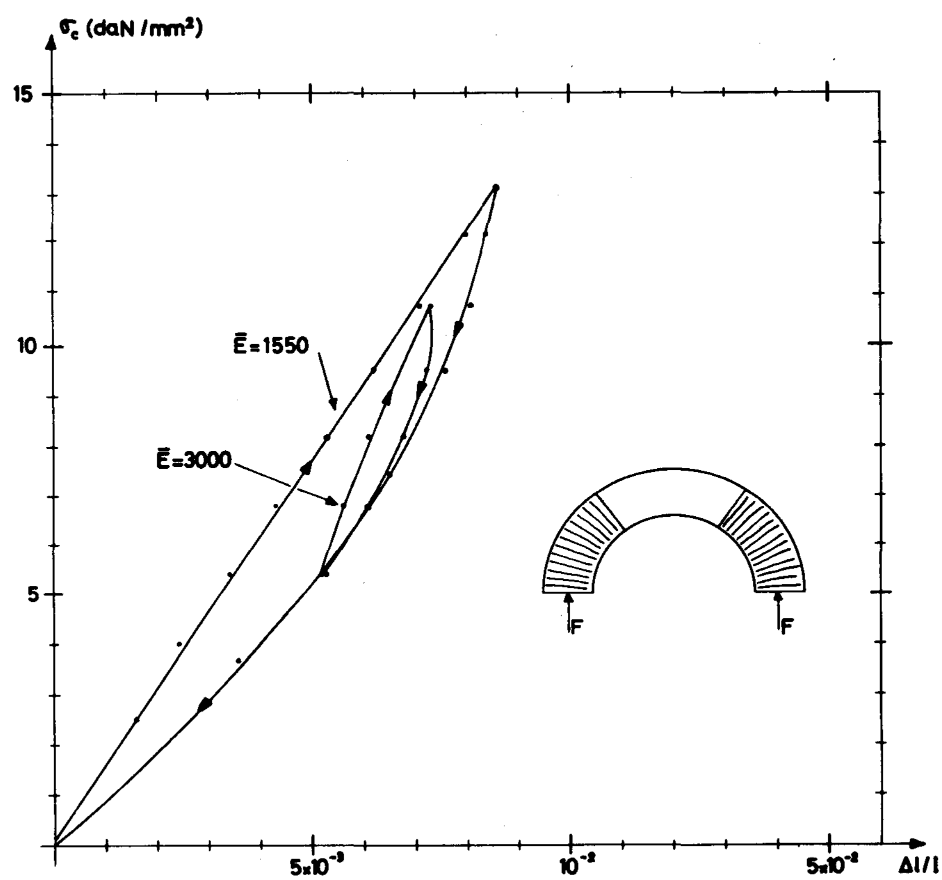

Fig. 16 Coil characteristics from azimuthal compression tests

3.3 Coil retaining structure

The combes are interleaved stacks of 2 mm thick laminations, made of 316LN stainless steel. A pair of laminations is shown in Fig. 17. Each comb is 140 mm long. The combes are tightened with a force of 200 kg mm^{-1}, before being welded and locked together. Figure 18 shows the distribution of the electromagnetic forces in the coils. Deflection measurements on a number of laminations, having a width of 23.4 mm in the median plane, have shown a deflection of 0.07 mm under a force of 100 kg mm^{-1}. In the prototype, the laminations will be 26 mm wide. No difference in performance has been found between structures with welded or glued locking keys.

3.4 Suspensions

The weight of the active part of the magnet is 800 kg. An off-centring of 0.1 mm with respect to the yoke would produce a force of 100 kg in its direction. The thermal contraction of the active part reduces its diameter by 0.52 mm at cooldown. Therefore, prestressed supports with a high spring constant must be used.

Cylindrical supports, in which heat conduction occurs along a coaxial labyrinth, have been tested. Figure 19 shows the cross-section of one of them. The compressed cylinders are made of a glassfiber epoxy composite, which offers a low ratio K/E of thermal conductivity to elastic modulus whereas the members in tension are of stainless steel. It is planned to use six sets of four supports, which will be precompressed by 0.8 mm under a force of 4 ton. The tests have shown that, with this structure, a force of 150 kg would not off-centre the magnet with respect to the yoke by more than 0.03 mm.

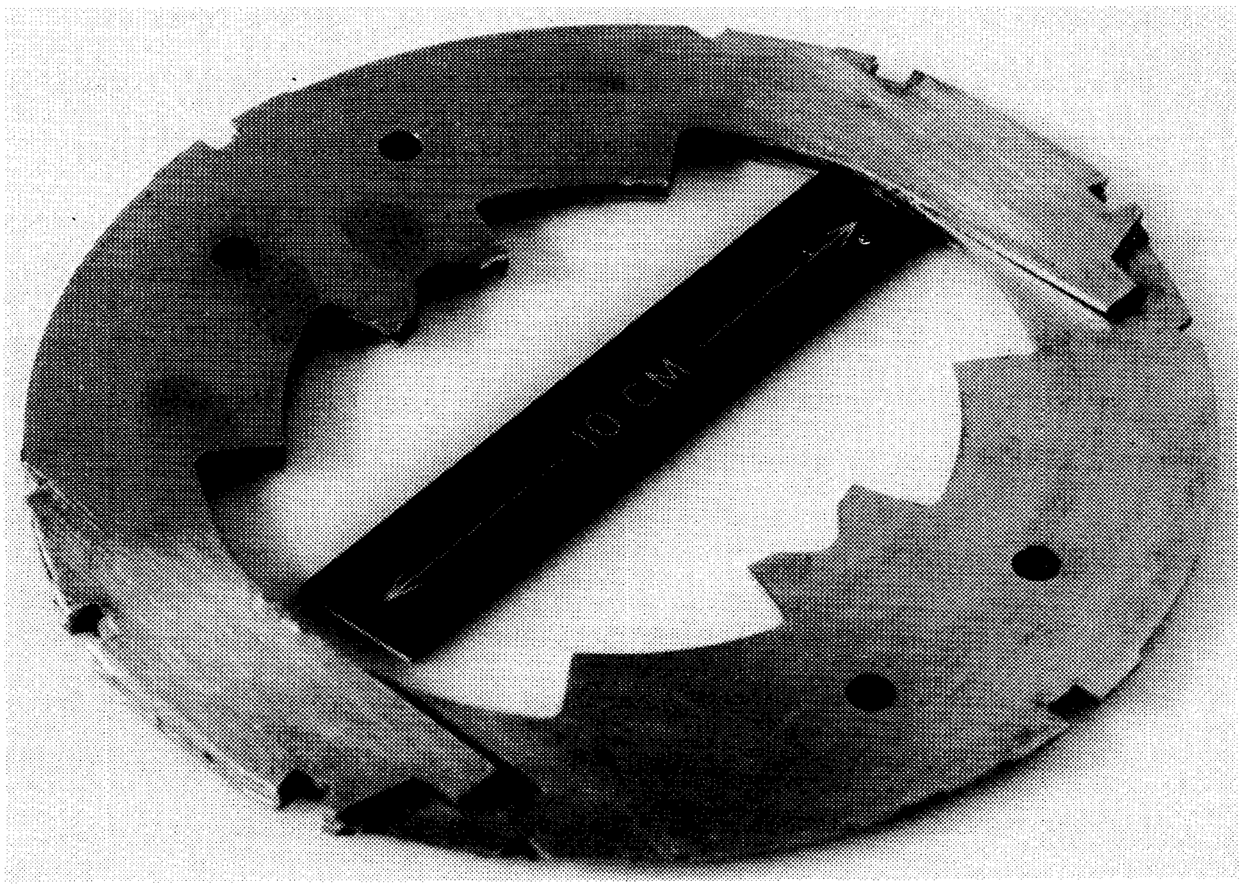

Fig. 17 Pair of comb laminations

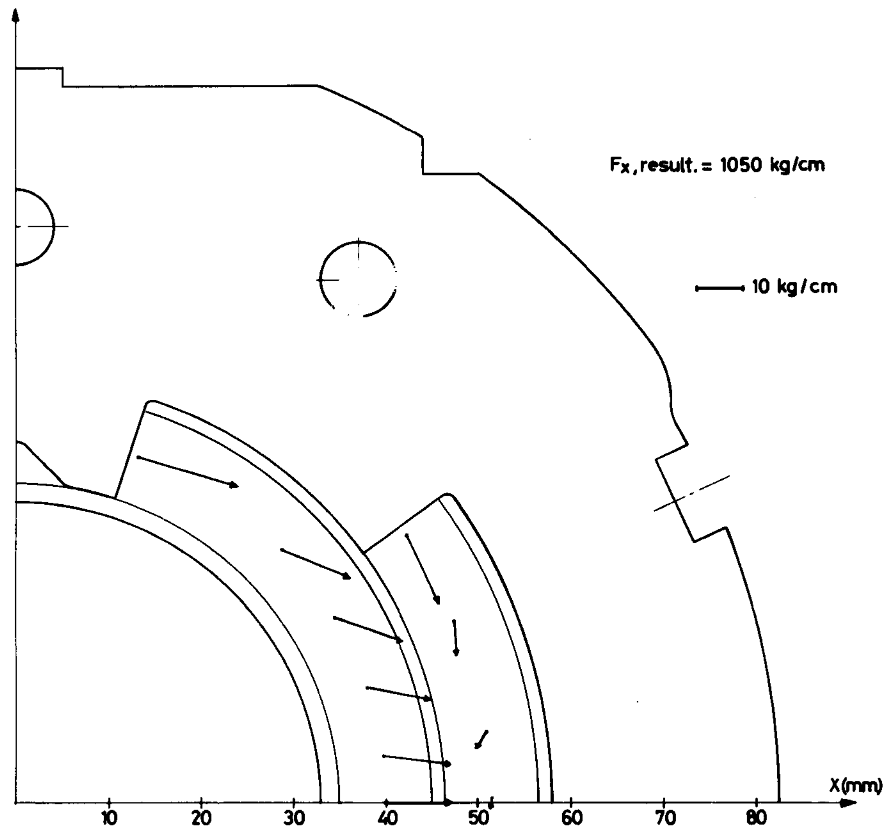

Fig. 18 Distribution of the electromagnetic forces in a PO dipole coil

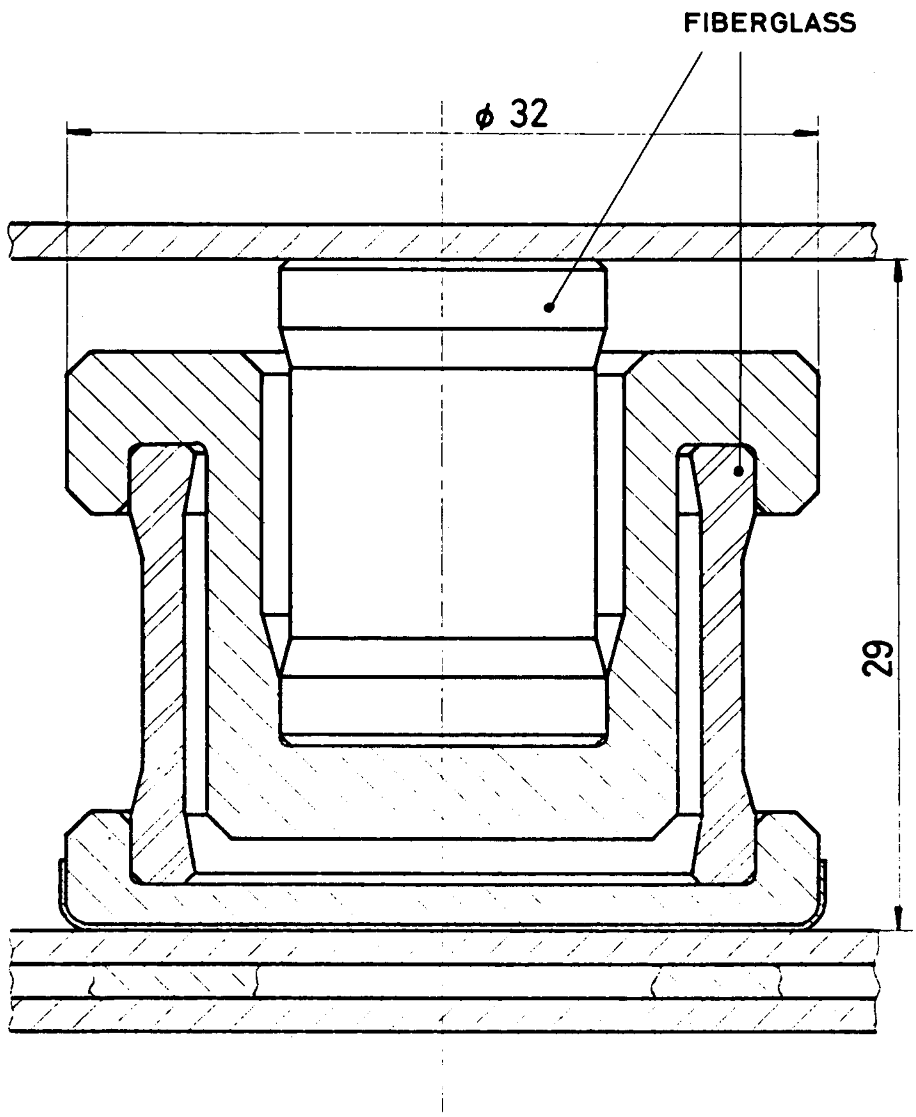

Fig. 19 Longitudinal section of a "cylindrical labyrinth" support

3.5 Cryostat and cooling

The cooling scheme is shown in Fig. 20. The single-phase helium flows through the coils at a pressure of about 1.8 bar and is expanded in two J-T valves at the end of the line of magnets, from which it comes back as a two-phase fluid at 4.2 K in the outer envelope and as vapour in the screen. Heat is removed from the single-phase helium by thermal exchange with the two-phase helium. It has been computed that, under pulsed conditions with a 40 s cycling period, the coil temperature would not rise by more than 0.2 K.

3.6 Protection

At the appearance of a quench, resistive transitions would be induced in the whole magnet by discharging electric capacitors into eight heating resistors placed along the coils. Experiments have shown that a dissipation of 1.25 J per resistor is enough to induce a quench within a delay of 15 ms. The pressure would then rise rapidly in the magnet until the opening of release valves at its ends.

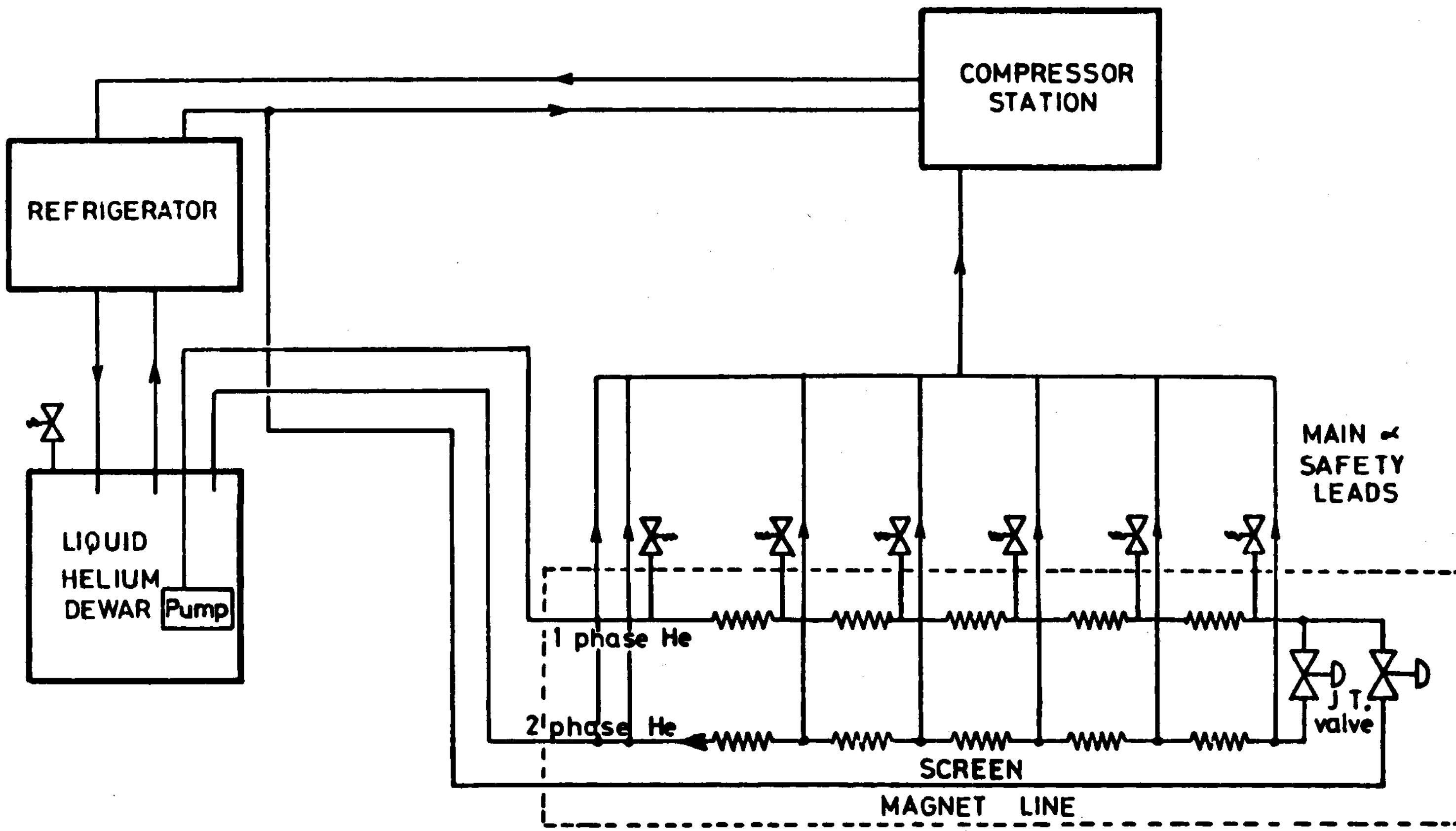

Fig. 20 Cooling scheme for the PO beam line

4. Conclusion

This short summary gives only an idea of the detailed investigations through which the construction of the prototype has been prepared. It is hoped that this approach will provide CERN with a good insight into the technology of small aperture, cold bore, warm iron magnets for beam transport and accelerators.

From the point of view of technical choices they are, in many respects, the opposite of the spectrometer dipoles and storage ring magnets, which have been described in Chapter 2. Each of these two types of magnets has its own internal coherence and its specific field of application. The two large projects of ISABELLE and Energy Doubler provide good evidence to the above statement.

Discussion

Hübner:

On the GESSS List for the comparison between magnets which will be suitable for PETRA, I have seen the Brookhaven design, I have seen the NAL design but I wonder whether there could not be a third list; we have heard now there are European designs of quadrupoles and I wondered why this is missing! I ask that very innocently. I am a layman in this question.

Resegotti:

Well, perhaps I have not been very clear, but this design, the conversion of the ISR is not very different basically from the Brookhaven concept, except perhaps for this idea of having the slotted laminations which would be precompressed. Of course the conductor is also different, but the reason why the conductor is different is very historically. At the moment when we started the conversion we had no experience with any other conductor whereas Brookhaven has been developing their conductor for many years.

Kleinknecht:

Which of these two desings requires more cooling power? The warm iron or the cold iron?

Resegotti:

There is not really much difference, because there are elements which compensate each other. In the cold iron system one has - of course the dimensions are so large - a certain amount of heat intake from the warm bore and in the other case intake does not exist. In the case of the warm iron there is a certain amount of heat intake from the supports, which are relatively short and connect the warm region with the cold region. Wherever they are, part of the losses can be absorbed either by liquid nitrogen as in the case of Fermilab, or by gas, helium vapour. So, I would really be in difficulty with trying to give a sharp answer.

Schopper:

The cooling down times must be different, and this might be important.

Resegotti:

Oh, certain! The cooldown time is much longer for the cold iron.

Schopper:

We come back to that comparison in the panel discussion.

Dalpiaz:

What is the risetime of these magnets?

Resegotti:

These are all magnets which are intended for d.c. operation. The risetime for the magnets of the low β insertion to maximum field is less than two minutes, about 100 seconds. From the point of view of field quality I can only say that when looking at the superconducting ISR conversion we were looking at the time for phase displacement acceleration which was of the order of 10 minutes, a quarter of an hour.

Dalpiaz:

What is the price per meter if you consider the production in the laboratory scale?

Resegotti:

This is something you know only after havin gone really to tender for a large production. It is clear that a price we have for 8 quadupoles cannot be considered representative.

PANEL DISCUSSION ON TECHNICAL PROBLEMS

Participants: H. Hahn, BNL
B. Montague, CERN
D. Thomas, Rutherford Lab.
A. Tollestrup, FNAL
G. A. Voss, DESY

Chairman: H. Schopper

Scientific Secretary: S. Wolff

P a n e l D i s c u s s i o n on Technical Problems:

1. Field Quantitites and Tolerances of Magnets

G. V o s s

I think one will have to distinguish between higher field harmonies in bending magnets and quadrupoles which are systematic effects - and there I think one should perhaps mostly talk about octupole fields and higher order fields because the sextupoles are anyway part of the system and one will have sextupoles for chromatic corrections. I think this morning there was no conclusive argument given what the tolerances on those higher harmonic fields really have to be. All the designs which we had seen have numbers of the order of $3x10^{-4}$ in terms of $\Delta B/B$ over the useful aperture but I don't think there has been a very conclusive theoretical argument whether this is perhaps a too tight tolerance or not quite sufficient. Clearly, I would think, the tolerance will depend on the value of β-functions and it will be much more stringent in quadrupoles near the interaction points which have high β values and probably can be at least one order of magnitude less in the normal bending fields.

I think the general conclusion of feeling seems to be that these magnets which we have seen are certainly better than the nonlinearities which are introduced by beam-beam effects and I think there is a real problem in talking about electron proton storage rings of this kind, and the problem is really actually specifically mentioned here. So I think I allow me just to put in one word: I think this is the real most important question here: what is the beam-beam limit in electron-proton rings? And I would remind everybody there is no theory about to space charge limitations which has given accurate predictions. There are not even tracking programs which allow to simulate such effects and give the right predictions and which have worked. Anyway, there is dispute whether any tracking program really has simulated what goes on in reality. In case of electrons, it was more an empirial approach. One had built storage rings and had seen what happened. In case of electron proton, these rings do not exist and the comparison with the ISR is a little bit difficult because we talk about quite a different machine. So, perhaps I might say, the fields seem to be better than the non linearities from beam beam interactions, but the distructive effects from those interactions are not really well known yet. Another thing is how does the field have to be from one magnet to the other. 10^{-3} as the $\Delta B/B$ in comparison between magnets seem to be some kind of a standard number. Really that question is not so critical because it just depends on the number of steering elements which you provide. When PETRA was built I think we have said that 10^{-3} should be quite adequate for the number of steering elements we had provided. It turned out that we were about a factor of five better and I still think that 10^{-3} should also be a number which might be sufficient for such a ring as it has been discussed today.

2. Maximum Obtainable Field

H. H a h n

I think it's quite obvious that this particular question is the most difficult question to answer. I am to make projections over the range of one to two years. This is very difficult and I would say that I do hope for objections to what I am going to say now. Certainly there will be objections. There was one basic assumption and that is a project where you have to make the decision, let us say, in one to two years. I think, that's how I interpret it, your three to four years. That would be the first stage, the 1984 in terms of the GESSS expertise. My premise is, there is not going to be a break through in the period of the next two years. I would like to consider the next two years as a phase of consolidation. We have started projects and we have to get the magnets which are on the way really into a good production stage. No break through, that means in any view that we will have to use NbTi as the material for these magnets. The use of Nb_3Sn for accelerator magnets personally I am a little bit sceptically even beyond the range of one to two years and my view is that the next application of Nb_3Sn will not be so much in terms of higher field like 8T but rather than higher temperatures which would help tremendously in terms of operating costs of refrigeration and similar items. My personal reason is that the forces are so overriding at 8T and in this range that if it's one material or the other I don't really see how you will be able to handle it in these small accelerator type magnets. I was reminded by Alvin Tollestrup that there was clearly a substantial progress reported at the Applied Superconductivity Conference in terms of Nb_3Sn, but it did refer mostly to the magnets for fusion, these large magnets where some of the problems of the accelerator type magnets do not exist. Dave Thomas made the very fine and necessary distinction between the design and the defined field level. The design is where the short sample current would be reached. For example to have a defined magnet of 50 K-Gauß you will have to design the magnet for 60 K-Gauß, correspondingly for 65 K-Gauß defined you would need something like 80 K-Gauß, and for 80 K-Gauß you need essentially 100 K-Gauß. These numbers are my own numbers. There is another boundary condition and I think that is an important one, that is, if you want to build the most economical magnet you will arrive - if you don't have the constraint of a particular site or a particular tunnel - at a different magnet than if you have the problem of putting the biggest energy magnet into a tunnel. To come to some numbers, I feel that a comfortable level is around 45 to 50 K-Gauß with obvious examples of Fermilab and Brookhaven. I did try to go through some exercises about cost, but I have the feeling that the consideration of price at around this level is not clear cut and if you run at 45 or at 50 K-Gauß it probably is the same. They are relatively economical and you have not started paying the price for going to very higher fields. The reason for going with Isabelle to the 50 K-Gauß was that we did start to be constrained in terms of sites. Of course the site in itself is much larger but we wanted to be north of Isabelle and then we had to reserve 300 and more meters of space between the boundaries. At the time when we switched from the 200 GeV to the 400 GeV we had site selected and 50 K-Gauß was established, if you want, not only the optimum on cost but also the availability of space.We could have perhaps gone to higher fields but then we were constrained by the particular concept of our single layer coil and I think our 50 K-Gauß is about the limit of what you can achieve in a single layer coil and we did not want to go to a double layer because that would have been research and development. Although I would like to mention that we have built a double layer magnet where two full layers were put over each other and we did reach 62 K-Gauß without any difficulty on this magnet. In the case where you are limited by a given tunnel, I myself would recommend a value between 60 K-Gauß and 70 K-Gauß as a reasonable number even in the next one to two years. Depending on the aperture - I think that is important - I probably would more tend to 60 K-Gauß than to 70, but I think that is the range where you could go. In this context I have mentioned that we have tried a double layer magnet which worked very well and we are in the moment building two beam transport magnets of a different type, of the windowframe type, and that is going to be installed in the external beam providing 20^{o} bends. The design is for 60 K-Gauß and the magnets have to run at that field or otherwise we don't get the beam out. The magnets are 3 m long and have an 8 cm coil inner diameter and as I said, the design is 60 K-Gauß. I don't say you should build one design or the other, that is the decision of a particular person, I just wanted to say that we at Brookhaven had two magnets running at 60 K-Gauß.

Cold / Warm Bore and Iron

H. H a h n

Brookhaven, as you know, is using warm bore and Fermilab is using a cold bore. There has been a long discussion of what is better and every time and every meeting it comes up again.
The Brookhaven decision was reached at a time when there were scientific questions as to the feasability or usability of a cold bore. The problem is desorption of condensed gases on the

surfaces and when we did make the decision this information was not available. Recently - this morning there was a report by Resegotti - CERN has made an experiment which proved that a cold bore would work. So, the scientific aspect of this question is clearly settled and a cold bore will work. In fact, we do consider to use a cold bore at places in what we call the first quadrupoles left and right of the ejection region where we do perhaps need a bigger aperture to get the beam out and one of the possibility would be to use there a cold bore quadrupole.

But that is limited to two or three quadrupoles. Inspite of the change as to the scientific background we do not have any regret. The argument used against a warm bore centers mostly around the question of the heat load. In our magnet we have a contribution of 2 Watt coming from the warm bore out of 4 W per magnet. In the total system that includes everything, transmission lines, leads etc., we have 2 kW coming from the warm bore. The total heat load is 16 kW. The fraction of the warm bore, if you look at it from a system point of view, is very small. Even this number could be effectively eliminated by using a heat shield around the warm bore.
The space required is about 6 mm in diameter to accomodate an intermediate 50 K heat shield. I don't consider the question of heat leak as a decisive argument against the warm bore. The other point is the aperture loss. As we heard, because of the various types of tolerances only 2/3 of the aperture of magnets is really usable for storage rings at least.We have a coil aperture of 13 cm, 2/3 of it is essentially 8-9 cm and our warm bore is 8.8 cm. So, we have not lost aperture in our magnets. I really feel that the decision between cold or warm is a question of convenience, is a question of engineering difficulties or simplicity. Questions like positron electrodes, how often do you need them, how do you go through the vacuum envelope into the cold area and make your position measurements are important. Perhaps you don't need clearing electrodes if you are in a cold bore, the vacuum is very much better. 20-30 % of the circumference is warm anyhow, I mean the insertions definitely would be warm. Therefore

you will have a large number of transitions. To make the transitions between the cold bore and the warm bore is a feasable problem, but definitely it is a problem. If you have leaks from the helium system into the vacuum system the cold bore does not help you in terms of pumps, so you must be truly leakfree. In the warm bore the leakes only would come from normal ambience but not from the helium part. A minor point is the fact that we would like to measure the magnets after they have been assembled, and it is more difficult to make precise measurements, NMR measurements, in a liquid helium ambience compared to a room temperature ambience after the complete assembly of the magnets. For Isabelle we do want to retain the option using bunched beams. We don't plan on it, but we would like to retain the option of being able to collide bunched beams. Using a stainless steel vacuum tube is prohibited because simply the heat load induced by the image current would be too big. One could go to copper but I was informed by our vacuum people that they do not like copper as a vacuum material. Finally, for a machine like DESY, where you would have very short proton bunches, you have questions of the higher mode losses - Huebner gave a nice summary this morning - and if I hear of 2 Watt/m, which potentially would go into the heat load, this is prohibitive. And then I mean arguments like scattering of synchrotron radiation which would again impact on magnets at least in the vicinity of the crossing point and increase the heat load. I think this would go again against the use of a cold bore.

In summary, the cold bore will work but I think convenience and engeneering arguments still support the use of a warm bore.

D. Thomas

To design a magnet you need windings. Then around these windings you need mechanical support to take the bursting forces. In fact that should be enough on its own. I would concentrate a little on the question of support.

Here we have a two-dimensional cross section and certainly the bursting forces can be taken. But in an accelerator magnet, which might be 6 or 7 m long - here you have effectively a tube

of 30 cm diameter - I have to think about how that is going to twist or bend and the whole way I am going to support it. This is very important on this argument between warm iron and cold iron. May be - this is a provocative statement - may be 30 cm is not enough to get the rigidity you need to get to the field quality, may be under pulsing conditions if it is a synchrotron. Why do we need the iron at all?
The main reason to need the iron is to protect equipment that's near it from strong fields . If you are going to high fields like anything four to eight Tesla you would really got to have massive bit of iron. A considerable increase on amount of material to what appeared to me to withstand bursting stresses! What do you get from the iron since you now have to put it in to minimize stray field? The first thing you get: you get a little extra field. If you use the iron as a force restraining as well - that is equivalent to the Brookhaven design - and you are aiming for 40 K-Gauß then you get until 13 K-Gauß because of the iron. The iron produces this high field which is imposed on the superconductor. Therefore it lowers the current capacity of the superconductor. If the iron were not there you are able to put more current in the superconductor and raise the central field just by virtue of the current. What the iron is giving you in effect is something like a 6 K-Gauß enhancement which you could not get with that quantity of superconductor alone. When you go to high fields this 6 K-Gauß stays more or less constant. You can't get very much more depending on the dimensions of the coil etc. When you get to 80 K-Gauß or whatever the proportional benefit you get from having iron adjacent to the coil drops off.

Let us talk about the warm iron option. What obviously you get here is a very neat small cryostat. When you are talking about capital costs the cryostat in the cold iron solution is considerably greater, more expensive and will have slightly greater heat losses. To me the argument goes really between two aspects:
One is, can you design a mechanically rigid system, bearing in mind you can probably only support the magnet at a limited number of positions along its length if you are going to keep the

heat transfer between room temperature and helium temperature adequate? Can you design an acceptable mechanical structure within the dimension of something like 30 cm? If you can't do that you then have to use cold iron for additional structure support and live with the additional capital cost, a larger cryostat and also slightly higher losses.

4. Operational Experiences

A. T o l l e s t r u p

I would like to pull together few subjects here that may be seem disconnected but they all have to do with how you operate these magnets. Calculations by Helen Edwards show how much energy a magnet can absorb before it quenches. It is just straight thermodynamics. You assume there is no instantaneous cooling to the magnet. All energy you put in goes into heating up the coil and as you operate at various values of I/I_{max} you can put more Joules in instantaneously before you raise the temperature and the critical current takes over and quenches the magnet. On the other hand when you are putting a slow beam into you get cooling active and the various limits on how effective our cooling is can place you down. The thing to note is that if you want to operate up near the limit there is something like 1/2 millijoule/g you can deposit in the conductor.

There was a test setup with a 400 GeV beam being run into one of the magnets. The beam can be deflected to hit the magnet at various places. There is a loss monitor situated by the magnet which allows you to get the intensity of the protons. The results show some differences between the slow spill and the fast spill.

All experimental results have been fed into what we feel is the necessary shielding in the magnets.

There is a second setup in Fermilab which is a string of four dipoles that have had extensive string tests. There are four magnets running now that will shortly be changed to a string of 16. These magnets have been studied as a system as the quench protection system goes. When we detect a quench on a magnet, we short the half cell across its ends. There is a safety lead at each quadrupole. Wher a quench is detected SCR's are fired, that bypass the current. We also fire heater on that magnet in order to drive as much of the magnet normal as quickly as possible. When we do this the maximum temperature in the magnet goes up to something like 40 or 50 K. The rest of the energy of the string is taken out and dumped into a resistor. You can't go into inversion with your power supply because the power may not be there. You have to assume that may be the power company was involved in the whole difficulty.

There is a unit I need to define in order to describe the behaviour of magnets during a quench. We use it in Fermilab. It is called a 'mite'. For heating of a little piece of cable, if there is no cooling, I^2R dt is equal to the heat capacity times dT. R is a function of temperature, so you can put R and c together and you have only a temperature integral on one side and only an $I^2 \cdot t$ on the other. The units are A^2xt and we can have $10^6 \cdot A^2 \cdot t$ that we call a mite. The units that I will be using are in mite and the temperature goes exponentially with mite as you get up near room temperatures. Our wire gets up to a point where it fuses the insulation which is about 200^oC for 7 mites in it. That is a constant of the cable. If the magnets go normal very fast then the current decays fast and the number of mites going into the wire becomes smaller. If you don't fire any heaters at all the mites go into a very little quench point and the wire will fuse.
It can be shown that as we go up in current the number of mites goes up to around $4^1/2$ and this is the point where we operate actually. This corresponds to something like 150 K for the peak temperature. We have done that string test with four magnets and we shall go up shortly to 16.
If one looks at the energy in the system versus temperature one finds another interesting thing: The wire has less than 1/10 of the energy stored in at the collars and helium has an available heat of vaporisation that is perhaps a factor of 10 times what is

in the collars.

Let us look at the energy that is stored in the magnet. Namely at full field the energy stored is 1/2 megajoule. That has to be absorbed by the magnet and when it goes completely into the magnet structure uniformly the temperature goes up to 50 or 60 K. When you measure the temperature of the gas in the cryostat during a quench an interesting thing comes out. The matter is that energy stored in a magnet is much more than the temperature actually observed. The difference apparently came out in kinetic energy with a big swish. There is a roar when these things quench and that energy is apparently being moved kinematically from the magnet chain.

Finally we had some experience with a chain of 25 magnets in the tunnel with a 95 GeV extracted beam. We use a normal extraction channel. We get the beam down to a chain of 25 magnets that we have tested. This chain is operated at a 95 GeV beam. That is a long way from the peak field. On the other hand there have been some exiting things here that we have learned. We had all thought that we could not tune this machine in a way amateurs are accustomed to. You turn them on 'right away' and run the beam into one side then turn them up right away and run the beam into the other side. We actually found you can do that just when it quenchs in a string of magnets. The magnets have a safety system on them, that looks out the current for 30 seconds after you fit the beam and essentially they have recovered within that 30 seconds from this type of operation. But the currents are in the order of 10^{11}-10^{12} protons. It is very easy to establish a first pass beam. There is no problem with that type of sloppy operation. The recovery is in a few seconds.

That is basically what we have learned in the operation: we have limits of how much energy these things can absorb. In that little sector test we passed 10^{13} protons through without trouble. In the single magnet switchyard test we passed similar kinds of intensity through without trouble. It is true, when you measure the energy loss that these things can absorb it is down in a region of a few millijoules per cm^3 or a few milliwatts per cm^3 depending on slow spill or fast spill.

5. Cryogenics

H. Hahn

I can say that we at Brookhaven do prefer a single refrigerator to a collection of refrigerators. Our first proposal as a matter of fact did contain, I think, 6 refrigerators which were designed so that five could work with one broken down. We have given up this scheme mostly because of the operational requirements which we would expect with 6 refrigerators. It seems at least at our place a fact that once you have a refrigerator, you need one or two persons serving it.
If you have only one refrigerator then you don't need 12 people times the shifts etc. for the servicing crew of the refrigerator. We also believe that the costs of a single refrigerator is adventageous. There is this famous power to the 0.7 law that indicates that you should go to the largest refrigerator which you can technically build. It is true that our refrigerator would be the biggest refrigerator built. But we have gone through estimates and through independent consultant studies and the advices that one can build a refrigerator of this type. Our single refrigerator has all the important items at the higher temperatures in parallel. We can switch over from one heat exchanger to the other without interruption of the operation of the refrigerator. Only the lower temperature devices where under normal conditions we don't expect that they accumulate contamination are single.

A. Tollestrup

I am not sure of the history of the refrigeration system at Fermilab. Those decisions were taken before I got there. About the time I arrived, there became available a plant on surplus from a test station of NASA which was a big nitrogen-liquid oxygene actually - refrigerator. Two of the compressors have been converted to helium compressors and one to nitroger That plants will be tested this spring. It makes 5000 liquid liters of helium and about 2000 of nitrogen. In additic there are 24 individual satellite stations that are fed about 90 l/h helium from the central plant. The capacity of those small satellites located at each of the service buildings is about 1 kW. So the total capacity of the cooling ring on its supply of helium from the central plant is about 24 kW. The technology that has gone into the satellite refrigerators is low level technology. The satellites are not terribly expensive. I think that problem is only control.

6. Experiment Related Problems

B. M o n t a g u e

I should draw attention to a few important features. I think we can expect transversely polarized beams in the electron rings up to an energy of 25 to 30 GeV by more or less conventional methods. Above 30 GeV it seems rather questionable for reasons that K. Huebner explained this morning, where essentially the energy spread overlap the in situ resonances. The Siberian Snake still offers some hope of getting out of this but at the moment there are certain problems which are specific to electrons or positrons which make it difficult to implement, essentially due to the quantum fluctuactions and the stochastic motion. The Sibirian Snake looks very promising for proton machines for accelerating orver large ranges of energies without crossing resonances: The depolarising resonances where the main ones are the integer resonances with number k and those associated with betatron motion. The Betatron resonances you can to some extent keep clear of because with a separate function machine at least you can change the tune according to the energy you want to cover so that you are working away from the Betatron resonances.The strength of the integer resonances is determined essentially by the amplitude of the k-th harmonic of closed orbit and over this sort of energy range up to 20 or 30 GeV this k is in this region which would require all the correction methods which are perhaps a little more sophisticated than we normally use. It would need care and it probably needs a fairly fast polarimeter to be able to adjust the correction in a reasonable time. Having got the transverse polarization you want to rotate it into the longitudinal direction. This can be done by a system of alternating vertical and horizontal bending magnets which bend the orbit of course and you have to take this into account. It gives the rise to a certain loss of polarization because the normal radiative mechanism works in an unfavourable direction in some of these magnets. In fact this goes with the cube of the bending radius essentially and over part of the trajectory the radiative polarization is trying to fight in a different direction from the one you want. You loose overall around the machine. How much you loose depends on how strong the special magnets are. The weaker you make them, the less you loose. If you want to do these sorts of gymnastics over a wide energy range you have to use some kind of very good geometry.

An example is described in the CHEEP report in detail. This leeds into the subject of how you design the ep interaction regions. There are some basic problems we have to handle. You have essentially three problems which lead to need for beam separation. The first is the geometry. Unlike e^+e^- machines you have two rings and the geometry is different. You have separate electron and proton beams. Whenever I mean electrons I mean positrons as well. So there is a geometrical problem. There is also the need to reduce the long range beam-beam interaction that is the electromagnetic interaction in the regions where the bunches are actually colliding or are rather near to each other. This is important in ep because the proton bunches tend to be much longer than the electron bunches and so the long range interaction extends to a substantial distance. To achieve this you may need a small crossing angle to help you. This can be of the order of a few milliradians, perhaps less than five milliradians. One way doing this is to use common dipole magnets. You can benefit from the fact that the momentum of electrons and protons is considerably different. So you can bend the electrons at a fair angle and hardly affect the protons. There are various configurations you can consider for this. If you have a solenoid field detector you have a compensation problem in the interaction region. In e^+e^- machines of course you compensate both beams and you can do this with local solenoids or with skew quadrupoles. You have to compensate the coupling to this purpose. If you use skew quadrupoles you can compensate the coupling outside the interaction region. Skew quadrupoles don't compensate spin rotation. If you want transverse polarization in the interaction region which some people do, you have to compensate the rotation effect of the solenoid. That probably requires another solenoid or solenoids or maybe a system of bends. Another feature of the ep interaction region is that there is a basic asymmetry arising from the energy difference between the electrons and the protons. I am raising that instead of having symmetrical solenoid compensators always out of the detector whether you can have a single one on one side and then use the asymmetry to some adventage in the design of the detector. This brings me to one of my favoured topics.

There are two horizontal dipoles needed to bring the electron beam into approximately zero angle to the proton beam. The question is can these separating magnets be incorporated into the detector design. It is not fashionable, people prefer solenoid detectors, but it has the following adventages: If these dipole fields can be used as part of the detector and incroach into the space normally dedicated to the detector, we can get the low β quadrupoles near the interaction points and that can be beneficial. This can give you an improvement in luminosity or can give you the same luminosity at a lower current. That is a question that I put firmly to discussion: is anyone interested in detectors using dipole fields rather than solenoid fields, where these fields can be used also to suit to the geometry of the machine?
As soon as you bring up fields so close to the detector you get into the synchrotron radiation problem. There are essentially three sources of this: The direct synchrotron radiation going straight into the

detector. There is the situation you can have when the synchrotron radiation interacts with the residual gas and produces electrons which mill around and also get into the detector. So you clearly need a very good vacuum in this region. Then there is the direct interaction between the synchrotron radiation and the incident protons. You can get a range of interactions from this, give you γp going to γp, have compton scattering, pair production or $\pi^0\pi^+$ production . A study of ep interaction regions for the large some hundred GeV storage rings has been made. It contains two examples. One is with a one milliradian crossing angle and 0.05 Tesla separating field. This is a field actually around the interaction point itself. There you get typically 6 compton scatterings per second. With a zero crossing angle and .3 Tesla which is a more dramatic case you get 40. So this ranges from 6 to 40. For the pair production it ranges from $2x10^4$ to $4x10^5$ per second for these two cases and then for the π-production it is from 0.05 to 10 per second. The problem here depends very critically on how you distribute the dipole field around the interaction region. These figures are just there to give an example. I think this problem is managable but it involves very careful design of the interaction region. I think ep is a case where you need a fully integrated design of the detector and the interaction region components, more than in any other kind of machine. It is worth devoting quite a lot ot thoughts how one is going to lay this out and how one is going to choose the detectors and their configuration in conjunction with the design of the low β section of the machine. A rather asymmetric example is contained in the ISR ep option. There are several possible ways of changing the polarization from positive to negative. You can have different channels for + or - helicity and this is very clumsy and probably very difficult in this small machine. You can use a brute force method of reversed wigglers but this costs you a lot in r.f. power. You can use in principle a spin flip method where you run the particles throguh one of the spin resonances. You have to exite one of those integer resonances strongly enough that when you change the energy of the beam slightly there is an adiabative crossing of the spin resonance and the more adiabaticly you do it the higher the degree of spin reversal.

This would be very beautiful on proton machines, because you could really take your time, but in electron machines you are up against a coherence problem because of the synchrotron radiation. You really need a machine which has a long energy damping time and a very slow synchrotron oscillation frequency.
Typical machines just seem to be in the grey region where it is not quite clear whether you can meet the adiabaticity conditions or not.

Summary of the Panel Discussion by H. Schopper

1. Field Qualities and Tolerances of Magnets
The results of FNAL and BNL show that superconducting magnets can be built which meet the requirements necessary for storage ring operation. This applies to the field quality inside each magnet as well as to the differences in field length from magnet to magnet. There was no argument for closer tolerances given by beam theoreticians.

2. Maximum Obtainable Field
With NbTi as the material to be used at presence and in near future 5 Tesla seem to be a reasonable number for the maximum central field although even somewhat higher fields may be reached. The technique of Nb_3Sn needs several years of further investigations.

3. Cold / Warm Bore and Iron
There is no general conclusion whether cold or warm bore or cold or warm iron would be the best. The decision for one or the other solution must be based on detailed technical and financial considerations, and is dependent on several other boundaries like necessary aperture and available space for the magnets.

4. Operational Experience

The operational experience with single magnets and magnet chains at Fermilab is positive and gives confidence to the whole concept. Beam induced quenches behave as theoretically foreseen. There were no problems in tuning a magnet chain operated with a 95 GeV extracted proton beam.

5. Cryogenics

There is no general conclusion whether one single central refrigerator or a refrigerator with a lot of satellites would be the best. The decision depends on several boundary conditions at the special site of the storage ring. For economic reasons one central refrigerator may be desirable if provision can be made to achieve a fail safe operation.

6. Experimental Related Problems

Electron polarization with conventional methods is possible at energies up to 30 GeV. At higher energies much more complicated methods have to be used. New criteria are necessary for designing the interaction regions and the detectors. It is desirable to incorporate dipole magnets into the detectors and to have quadrupoles as near as possible to the interaction points.

Parallel Session on Superconductive Magnets

A Summary by G. Horlitz (DESY)

Parallel Discussion on Superconductive Magnets

Some selected topics of superconductive magnet problems have been discussed in a separate session:

1. Field Tolerances, Field Measurements

There was a long discussion on the best way of use and presentation of field measurements. Both Brookhaven (Sampson, Hahn) and FNAL (Tollestrup) measure the field harmonics using rotating coils. Hahn defines a mean value of error in a field as

$$\left\langle \frac{\Delta B}{B} \right\rangle = \sqrt{\frac{1}{2a} \int_{-a}^{+a} \left(\frac{\Delta B}{B}\right)^2 dx}$$

where "a" is the radius of the aperture. For two Isabelle Magnets at about 4 T he gave the number of

$$\left\langle \frac{\Delta B}{B} \right\rangle = 2.3 \times 10^{-4}$$

This value includes a dipol term of 1.4×10^{-4}. With this error they expect a closed orbit deviation of 1 mm rms. (a = full width of the vacuum tube)

If one calculates the field error in the two medium planes, using the measured field harmonics (n = 0 to 5) one gets

$\frac{\Delta B}{B} < 2 \times 10^{-4}$ in horizontal direction

$\frac{\Delta B}{B} < 2 \times 10^{-4}$ in vertical direction (sextupole excluded)

Sextupol is 4 times the tolerances. The total error in the magnet (including sextupole) is 4×10^{-4}.

NAL preferes to presentate completely the random variations of harmonics. A mean value only does not give information on the gradient of the error in the outer regions.

All magnets have a variable sextupole at low fields due to induced currents in the filaments. For mean fields the sextupole is constant and will be given a finite value in the BNL-magnet for correction of chromaticity. At high fields $B > 1.8$ T the BNL iron saturates and causes a field dependent variation of the sextupole which has to be compensated by a correction winding. The correction current is the same for all magnets, one does not expect variations of the saturation properties in the iron from magnet to magnet.

At low fields BNL found a temperature dependence of the sextupol of about $8 \times 10^{-6}/\mathrm{cm}^{-2}$ per Kelvin.

2. Cold iron - warm iron

There seems to be no basic physical argument whether cold or warm iron is to be prefered. Cold iron contributes a little bit more to the magnetic field because it is located closer to coil and aperture. The higher saturation errors mentioned above could be handled by correction coils. The position of the coils in respect to the iron is easier to maintain.

Cooling down of cold iron magnets takes more time. This might be no problem for ideal magnets which are at helium temperature for months, but if magnets have to be changed frequently one looses time for experiments. (BNL expects a cooling down period of 2 - 3 weeks for the total magnet.)

Another problem is the fact that the thermal contraction of magnetical steel is only 2/3 of that of the coils. This causes axial stresses in the case of a magnet where the magnetic steel is used as mechanical support for the coil. The contraction factor of stainless steel mechanical structures is more adapted to that of the coils.

3. Dynamic effects in the conductors

FNAL reported on investigations on the influence of strand insulation on dynamic losses and magnetic field. With Ebobol insulation (copper oxyde) the dynamic losses disappeared almost completely (with exception of hysterese losses) compared to Staybrite insulation (silver-tin cover). Difficulties at the beginning of Ebonol application (bad current sharing, abrasive sensitive to mistreatment) led to the use of a "zebra-cable" (alternately Staybrite and Ebonol). Now Ebonol insulated conductors are used for the inner shells, Staybrite in the outer.

The absolute contribution of eddy currents to the field was only a few gauss even with full Staybrite insulation.

4. End effects

The contribution of the end fields to the total integrated field is not so important because the aperture is small compared to the total magnet length. BNL has calculated the positions of the wire blocks in the ends and FNAL has matched the peak field in the ends using the end of the iron in respect to the coil end as parameter. The sensitivity of endfields to fabrication tolerances is negligible.

5. Miscallaneous

Perot (Saclay) reported on a 0.6 m dipol model which was an upscal (9 cm coil diameter) of the FNAL design. It was powered within 2 s to a field of 2 T and within 8 s to 4 T without training and quench (the maximum field was limited by the power supply). He also measured the same order of magnitude for dynamic losses as have been obtained in FNAL.

Between a two (or more) layer shell structure or a one layer cos Θ approximation as in the case of Isabelle there seems to be no basic difference. It is a question of conductor type, current density and other more technical reasons, which type is chosen.

BNL gives a price of \$ 15.000 per coil including material, \$ 12.000 are material, \$ 3.000 labor.

FNAL requires 250 man hours per magnet. With two shifts a day they estimate a fabrication rate of 5/day. This might be doubled.

BNL estimates about two weeks per coil set, but with about 10 tooling sets working in parallel they hope to achieve also a production rate of about 1 magnet per day.

List of Participants

Name	Institute
Alvin Tollestrup	FNAL
Harald Hahn	BNL
Bill Sampson	BNL
K.P. Jüngst	KfK
H. Wümpelmann	DESY
S. Wolff	DESY
H. Kaiser	DESY
H. Desportes	Saclay
C. Lesmond	Saclay
D. Leroy	CERN
E. Baynham	Rutherford
W. Hassenzahl	Saclay
	+ Los Alamos Scientifi Laboratory
P. Limon	Fermilab Paris VI
G. Horlitz	DESY

SESSION ON NEW CURRENTS AND NEW PARTICLES

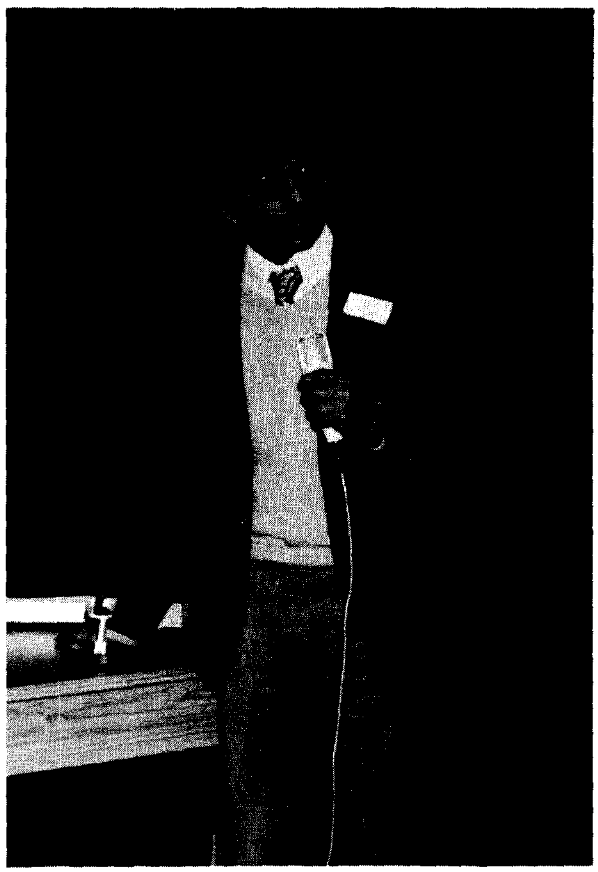

Discussion Leader: L.M. Sehgal

Scientific Secretary: H. Krasemann

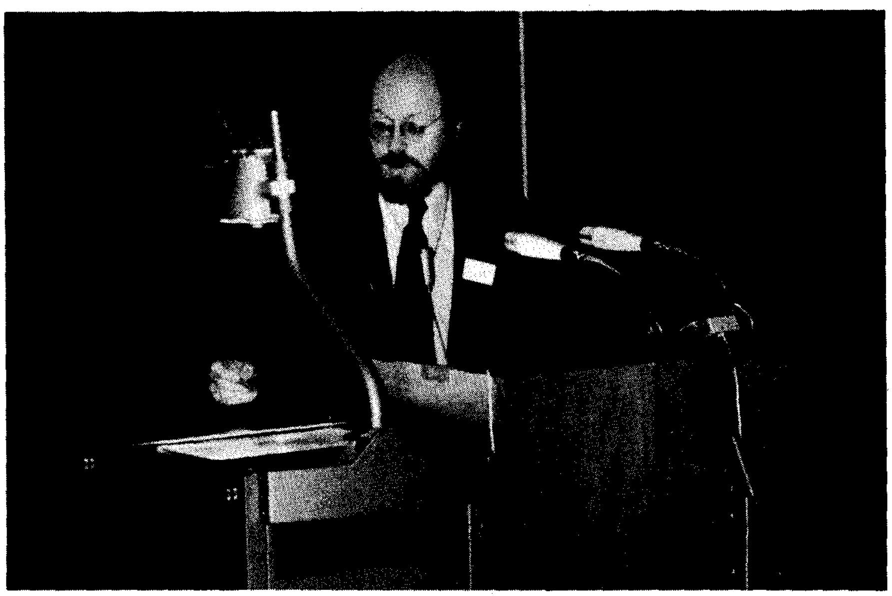

NEW PARTICLES AND NEW CURRENTS

R.J. Cashmore

Department of Nuclear Physics
Oxford University,
Oxford.

Review talk at the ECFA study of an ep facility for Europe held at DESY, Hamburg, 29.4.79.

NEW PARTICLES AND NEW CURRENTS

1. Introduction

2. Quarks

3. The Production of Weak Quanta, W, Z.

4. Higgs Mesons in ep.

5. Neutral Currents

6. Charged Currents

7. New Currents and Associated New Particles

8. Summary and Conclusions.

1. INTRODUCTION

In this report I want to review the impact of an ep machine on our present ideas and then speculate in what ways such an accelerator could investigate physics beyond our present framework. This speculation will lead to some criteria for the major parameters of such an accelerator, in particular the luminosity, energy and polarization of the electron beams. We will conclude that its principal advantages are:

(i) the investigation of charged currents to mass scales beyond those accessible at LEP,[1]

(ii) the observation of new currents (charged or neutral) of either chirality coupling to leptons and quarks,

(iii) the observation of new particles associated with such currents.

Some of these views have been emphasized in earlier reports[2,3] so that I will concentrate on the new points and emphasis generated by the group* of physicists who have been studying this topic over the last few months. Clearly part of this discussion involves a comparison with the other facilities that should be available in the mid to late 1980's, i.e. $\bar{p}p$ collider[4], pp (Isabelle)[5] and e^+e^- (LEP)[1]. I will not present a detailed comparison but rather allude to these other accelerators when relevant.

In order to begin this review I have summarised briefly in Table 1 the present theoretical framework of particle physics, which we all assume.

* R.J. Barlow, D. Binnie, R.J. Cashmore, R. Cleymans, R. Jaffe, G. Ross, B. Saitta, L. Sehgal, P. Zerwas, J. Benecke.

TABLE 1

PRESENT FRAMEWORK

Particles	Gauge Group of Current	Interaction
u,d,c,s,t(?),b		
$e,\nu_e,\mu,\nu_\mu,\tau,\nu_\tau$		
gluons (8)	$SU(3)_c$	Strong
$W^\pm, Z^\circ, \gamma$	$SU(2)_L \times U(1)$	Electro-weak
Higgs		

In the discussion I will concentrate on the following topics:

(i) Production of free quarks

(ii) Production of weak quanta $W^\pm$, Z° and Higgs.

(iii) Neutral currents.

(iv) Charged currents.

(v) New neutral and charged currents and associated particles.

The emphasis in items (iii) and (iv) will be on the extent to which the ideas of Table 1 can be substantiated. Not because this will be the most important contribution at that time ($\bar{p}p$, pp will already exist and LEP will be soon available) but as a background in which departures from conventional wisdom might be indicative of the existence of further interactions.

Finally, detailed calculations have been made for two possible options:

(i) 20 GeV e^- x 280 GeV p (PROPER[6])

(ii) 100 GeV e^- x 400 GeV p (LEP/SPS collider[7]) with a peak luminosity of 10^{32} cm^{-2}/sec which corresponds (in a 'theoreticians day') to an integrated luminosity of 8.6 x 10^{36} cm^{-2}. (A more realistic estimate would correspond to reducing this number by a factor of 4 and even this may still be rather optimistic.) However, these calculations should be regarded as guides as to what is possible and interpolations made for other possible accelerators. In particular polarization of the beams might be available in (i) whereas it is very difficult, perhaps impossible, to obtain in (ii).

2. QUARKS

The concept of confinement has not been proved within QCD and hence the possibility of liberating quarks exists. Thus at any new accelerator one should always be prepared for this eventuality and be aware of the properties such objects might have[8,9] and the effects which might result from their liberation. In this context I want to mention quarks which possess any combination of the following extreme properties:

(i) integer or fractional charges

(ii) point-like or large extended objects.

(a) Point-like Integer Charge Quarks

This could correspond to a model in which colour was liberated.[10] In this case one might expect changes in the inclusive cross-section corresponding to the charges of the 'true' quarks being exposed, e.g. there would be a 67% change in F_2 (in the valence parton approximation)

$\sum_i Q_i^2 q_i$	$2 \times (\frac{2}{3})^2 + (\frac{1}{3})^2$	$\rightarrow$	$2(\frac{2}{3}) + \frac{1}{3}$
F_2	1	$\rightarrow$	$^5/_3$

In such models the possibility exists of interaction with other constituents, e.g. charged coloured gluons leading to further changes in F_2 and the inclusive electroproduction cross-section. Of course the mass scale on which such effects occur is unknown.

(b) Point-like Fractional Charge Quarks

In this situation there would be no dramatic change in the cross-section, since we already assume these quarks are free within the proton. However they would be identified by their characteristic signatures of:

(i) $\frac{dE}{dx}$ corresponding to charges of $^1/3$ and $^2/3$,

(ii) supermomentum, i.e. the fact that they are bent less in a magnetic field and hence appear to have a high momentum (when interpreted as having integer charge).

(c) Large Extended Quarks of Integer or Fractional Charge

The large extended nature of such objects would probably imply that their production is reduced by form factor effects and hence we would not expect dramatic changes in the electroproduction cross-sections except perhaps near a threshold. However such quarks might have rather peculiar properties[9] leading to large mass objects with high charge (due to their large appetite for absorbing nucleons and their large interaction cross-sections) which would have rather characteristic signatures in detectors.

I can conclude this short discussion by remarking that any dramatic change in the structure functions would be indicative of new physics - new quarks, quark liberation, quark substructure - and hence would be very exciting. In particular the liberation of point-like quarks would be comparitively easy to detect whereas the observation of quarks with an extended structure would probably be very difficult. Moreover to observe such objects experimentalists must remain alert and not design apparatus with integer charges solely in mind.

3. THE PRODUCTION OF WEAK QUANTA, $W^{\pm}$, $Z°$

The production of $W^{\pm}$ and $Z°$ is very small at an ep machine as concluded in earlier studies.[3] The major diagrams responsible are shown in Fig. 1 and the cross-sections can be calculated using the

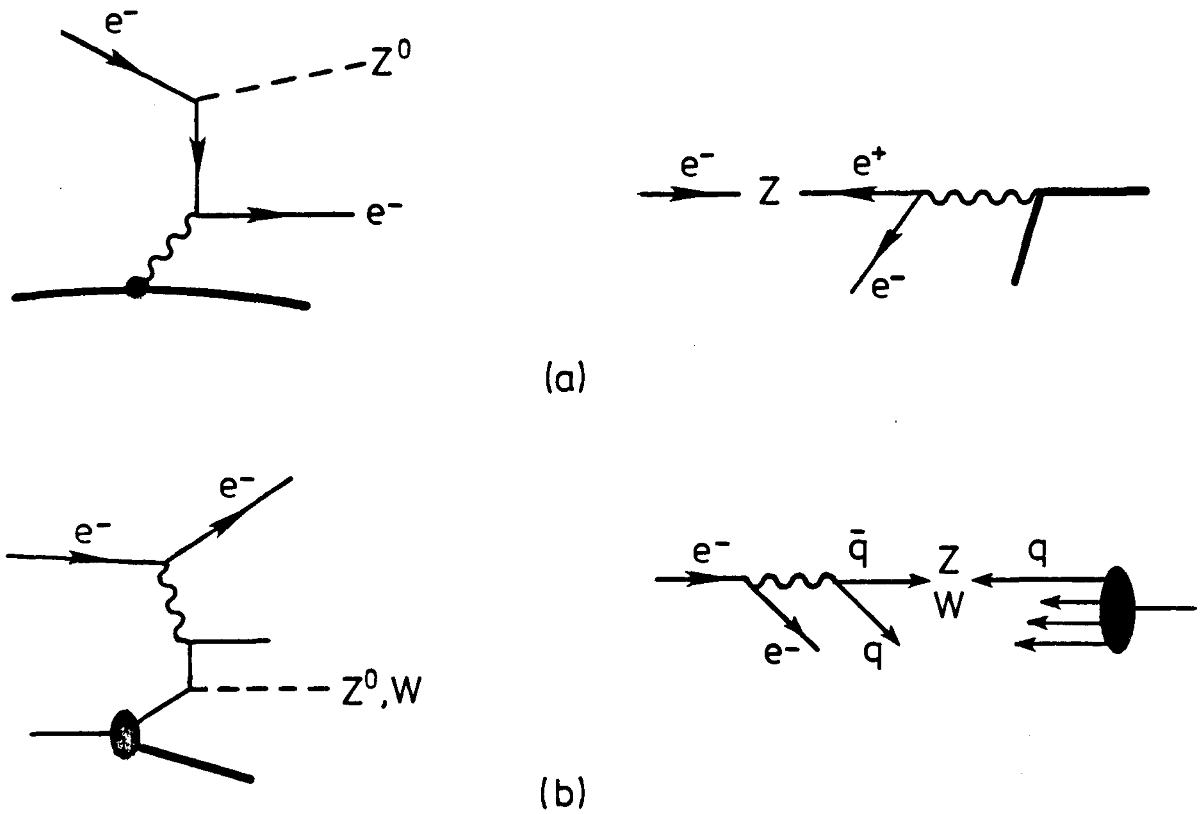

FIG. 1 The major mechanisms for W and Z production.

'equivalent particle spectra'.[11] The results are in excellent agreement with earlier calculations[2,3] and one example is given in Fig. 2.

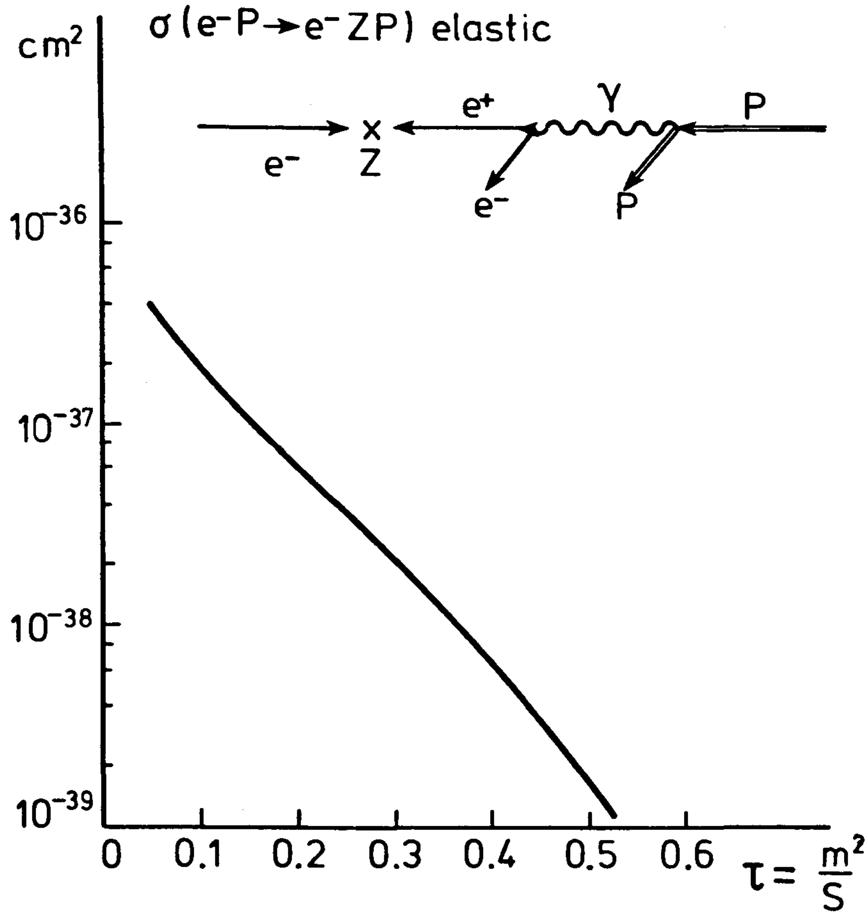

FIG. 2 The cross-section for the process $e^-p \rightarrow e^- + Z^\circ + p$.

The cross-sections are given approximately by

$$\sigma \sim 0.6\ e^{-11\tau} \times 10^{-36}\ \text{cm}^2 \qquad 3.1$$

where $\tau = \frac{m^2}{s}$

This means that the cross-sections are $\sim 10^{-38}$ cm^2 for a 20 x 280 machine and $\sim 3 \times 10^{-37}$ cm^2 for a 100 x 400 machine leading to very small event rates ($\lesssim 1$ per day). These numbers have to be compared with the Z° cross-section at LEP of $\sim 10^{-31}$ cm^2 and Z and W production cross-sections in pp and $\bar{p}$p storage rings of $\sim 10^{-33}$ cm^2. One immediately concludes that this is not an ideal method of producing W's and Z's and moreover if they exist they will almost certainly have been found in $\bar{p}$p and pp collisions.

4. HIGGS MESONS IN ep

Higgs mesons are an essential ingredient of current gauge theories but unfortunately their properties are not well specified. In general hypotheses may be made about their couplings but the mass is unknown. In what follows I will consider a variety of Higgs systems.

(i) Standard Higgs

In the standard model of spontaneous symmetry breaking in gauge theories[12] one scalar Higgs remains with prescribed couplings to the fermions and gauge bosons

$$g_{f\bar{f}H} = \frac{m_f}{v}$$
$$g_{w\bar{w}H} = \frac{gm_W^2}{v} \qquad 4.1$$

where v is the vacuum expectation value of the Higgs fields, i.e. the Higgs will couple to the heaviest particle possible and thus decays to e^+e^- and $\mu^+\mu^-$ will have small branching fractions.

(ii) 'Supersymmetric' Higgs

In this case the Higgs couplings are proposed to be

$$g_{f\bar{f}H} \sim g \qquad 4.2$$

i.e. the couplings are the same to all particles. This immediately implies that more than one Higgs doublet is necessary to achieve the different fermion and boson masses and hence we expect the existence of charged Higgs, $H^{\pm}$. Furthermore the preference for decay to the heaviest particle is removed and we expect all decays to be approximately the same. However to ensure that low energy phenomena, e.g. $(g-2)_{\mu}$ are unaffected, it is probably necessary for $m_H > 100$ GeV.

(iii) Coloured Higgs

These scalars are expected in models[10] where colour may be liberated. However, except for a few parenthetical remarks I will not consider them in detail.

In what follows I will consider how Higgs mesons might manifest themselves either through propagator effects or direct production.

(a) Exchange of Higgs Mesons

In Fig. 3 the process occurs via the exchange of a Higgs rather than a photon, Z° or $W^\pm$. In the case of charged Higgs exchange the

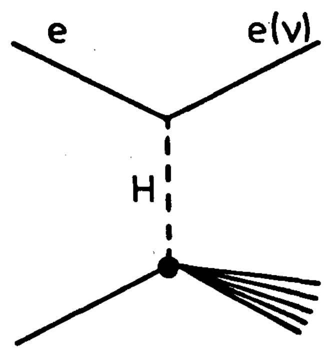

FIG. 3 Higgs Exchange in ep collisions

reaction would only be induced by right hand electrons

i.e.
$$e^-_R + p \to \nu + X$$
$$e^-_L + p \to \nu + X \qquad 4.3$$

due to the scalar exchange flipping the helicity. The cross-section is then given by

$$\frac{d^2\sigma}{dxdy} = \frac{g^2_{eLH}\, g^2_{q\bar{q}H}}{(q^2+m^2_H)^2}\; 2y^2(2xF_1)\frac{S}{2\pi} \qquad 4.4$$

and this would contribute to violations of the Callan-Gross relation.[13] This cross-section may be compared with that due to W exchange

$$\frac{d^2\sigma^H}{d^2\sigma^W} = \frac{g^2_{e\nu H}\, g^2_{q\bar{q}H}}{g^4} \left[\frac{8(q^2 + m_W^2)}{q^2 + m_H^2}\right]^2 \qquad 4.5$$

with

$$\frac{g^2}{8m_W^2} = \frac{G_F}{\sqrt{2}} \qquad 4.6$$

Standard model: The ratio (4.5) is $\lesssim 10^{-8}$ and the effects are negligible.

Supersymmetric: Here

$$\frac{d^2\sigma^H}{d^2\sigma^W} \sim \left[\frac{q^2 + m_W^2}{q^2 + m_H^2}\right]^2 \qquad 4.7$$

and there is no particular advantage of achieving high s (and hence big q^2) unless either

(i) $m_H \gg m_W$ (rates small)

or (ii) the Higgs couples the electron to a new massive lepton (and probably an 'old' quark to a new quark) so that it is necessary to cross an energy threshold.

Coloured Higgs: Clearly the exchange of coloured Higgs will result in colour being liberated at a vertex and hence high s may be required to cross such a threshold. Furthermore the coupling at the lepton vertex would produce some new lepton, presumably of high mass.

(b) Production of Higgs Mesons

A variety of mechanisms can be considered for the production of Higgs.

(i) Bremsstrahlung

In this case the Higgs is produced either at the lepton or hadronic vertex by a 'bremsstrahlung' type process as indicated in Fig. 4. (Coloured

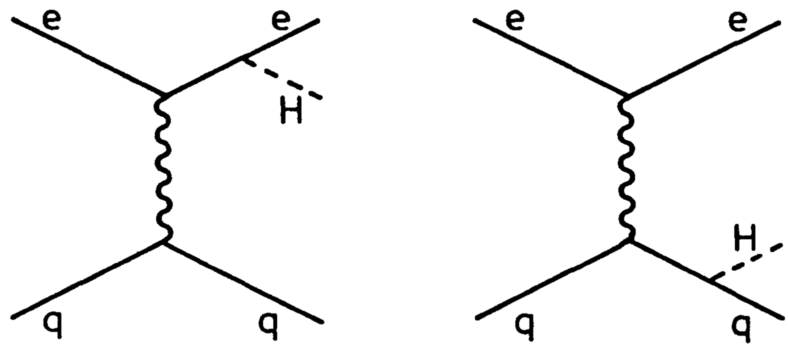

FIG. 4 Bremsstrahlung production of Higgs Mesons.

Higgs would not couple at the electron vertex to give an electron in the final state.) For a massive Higgs particle the bremsstrahlung cross-section is given by[14,15]

$$d\sigma^H(p,k,\theta) \sim (G_H)^2 \frac{k^2 dk\ d(\cos\theta)}{2\pi^2\ k_o(2p.k + m_H^2)} d\sigma(p) \qquad 4.8$$

where $d\sigma(p)$ is the cross-section without bremsstrahlung

k 4-momentum of Higgs

p 4-momentum of particle emitting Higgs

θ angle between $\underline{k}$ and $\underline{p}$

Standard Model: Due to the small coupling of the Higgs to fermions the cross-section will be small

$$\frac{\sigma(eN \to eXH)}{\sigma(eN \to ex)} \lesssim 10^{-7} \qquad 4.9$$

Supersymmetric: Equation 4.8 gives a cross-section

$$d\sigma^H(p,k,\theta) \sim \alpha \frac{2}{\pi} \frac{k^2 dk d\cos\theta}{k_o m_H^2} d\sigma(p) \qquad 4.10$$

i.e. Higgs production could be as much as $O(10^{-2})$ of the total cross-section (providing we ignore mass effects.)

Coloured Higgs: If the couplings is similar to that in the standard model bremsstrahlung will be negligible. However, if the couplings are of the supersymmetric type, then the cross-section will be large and the Higgs accompanied by coloured hadronic states. Thus the centre-of-mass energy must be large to exceed any thresholds.

(ii) Production via Intermediate Vector Bosons

The mechanism for production is given in Fig. 5 and the cross-section has been calculated(14)

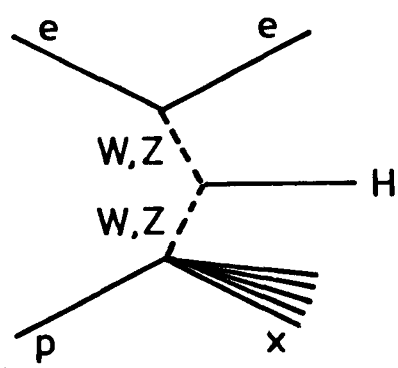

FIG.5 Production of Higgs Mesons by W, Z exchange.

Standard:

$$\frac{\sigma(e^-p \to \nu Hx)}{\sigma(e^-p \to \nu x)} \sim \frac{G_F\langle x\rangle s}{12\sqrt{2}\,\pi^2} \sim 10^{-8}s \qquad 4.11$$

This implies that for $s \sim 22400\ \mathrm{GeV}^2$

$$\frac{\sigma(e^-p \to \nu Hx)}{\sigma(e^-p \to \nu x)} \sim 10^{-4} \to 10^{-3} \qquad 4.12$$

which is a rather small cross-section.

Supersymmetric: In this case the preference for coupling to W's is no longer valid and the cross-sections will be even smaller.

(iii) Production via 2 Photon Processes

In this case the coupling of the Higgs to two protons is exploited as a production mechanism as indicated in Fig. 6. The cross-sections depend

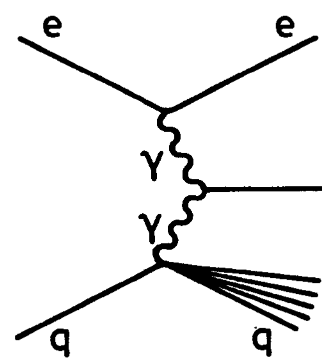

FIG. 6 Production of Higgs Mesons by 2 photon exchange.

on the width of the Higgs to $\gamma\gamma$ (19,16,3)

$$\sigma \sim \frac{8\pi\alpha}{m} \; \frac{\Gamma_{\gamma\gamma}}{m} \; \ln\left(\frac{t_{max}}{t_{min}}\right) \tag{4.13}$$

and once again result in an unappetizingly small cross-section of $\sim 10^{-40}$ cm^2. for standard Higgs.

Since the major contribution to the $\gamma\gamma$ width in the standard Higgs model is from graphs containing virtual heavy particles this width will be suppressed for supersymmetric Higgs because there is no longer the preference for heavy states.

(iv) Production of Coloured Higgs from Gluons

In this case the production mechanism is shown in Fig. 7. The cross-section will be enhanced over the two photon process by factors $\sim \frac{\alpha_s}{\alpha}$ which could lead to cross-sections of $\sim 10^{-38} - 10^{-39}$ cm^2.

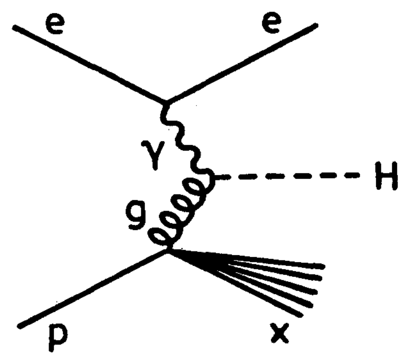

FIG.7 Coloured Higgs production from a γ and coloured gluon.

From the discussion the possibilities of observing these Higgs or their effects can be summarised as follows:

Standard: There is no attractive mechanism in ep collisions.

Supersymmetric ($m_H > 100$): In this case the Higgs might be seen either by the propagator effects or through bremsstrahlung production. However, it is difficult to see why such a particle would not have been observed in $\bar{p}p$ or pp collisions. Its production would be copious although the backgrounds may be high.

Coloured Higgs: To produce such states the colour threshold must be exceeded but once again $\bar{p}p$ and pp should be copious sources of colour gluons which might naturally lead to coloured Higgs.

In general the observation of Higgs would be difficult at an ep machine and for many of the mechanisms a $\bar{p}p$ or pp machine would appear at least as attractive.

5. NEUTRAL CURRENTS

In this section I want to discuss the measurements that could be made at an ep machine which might reveal the structure of neutral currents, beginning with the Weinberg Salam model for this structure.

(a) The Neutral Current Cross-Sections

Within conventional wisdom there are two contributions to the neutral current cross-section as shown in Fig. 8. The first of these

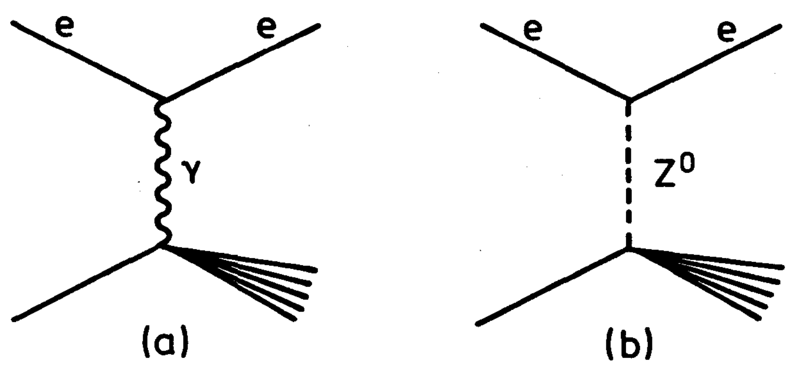

FIG. 8 Photon and Z° contributions to the neutral current cross-section.

contributions, photon exchange, follows from QED while a model is required for the mass of the Z° and its couplings. The most popular and successful model is the $SU(2)_L \times U(1)$ model of Weinberg and Salam.[12] In this the masses of the weak gauge bosons and all the couplings to the elementary fermions are specified in terms of the Weinberg Angle, θ,

$$m_W = \frac{37.4}{\sin\theta}$$

$$m_Z = \frac{37.4}{\sin\theta\cos\theta} \qquad 5.1$$

$$J = J_{weak} - \sin^2\theta J_{em}$$

Since right handed fermons belong to singlets in this model the couplings of right and left handed particles are different and parity violation ensured, e.g. the weak neutral current couplings of the electron are:

$$e_L \; \alpha \; -\frac{1}{2} + \sin^2\theta$$
$$e_R \; \alpha \; \sin^2\theta \qquad 5.2$$

The cross-section then has three contributions:

$$\sigma = \sigma_\gamma + \sigma_{int} + \sigma_{weak} \qquad 5.3$$

where

$$\sigma_\gamma \; \alpha \; \frac{1}{Q^4} \qquad 5.4$$

$$\sigma_{int} \; \alpha \; G_F \frac{m_Z^2}{m_Z^2 + Q^2} \frac{1}{Q^2} \qquad 5.5$$

$$\sigma_{weak} \; \alpha \; G_F^2 \left[\frac{m_Z^2}{m_Z^2 + Q^2}\right]^2 \qquad 5.6$$

Thus as Q^2 increases the importance of the weak terms increases and the structure can be studied in detail. In this discussion only high Q^2 will be considered, the region of $Q^2 < 1000$ GeV^2 being the QCD domain of other speakers.(17) However, in order to calculate the cross-sections structure functions are required and the parameterization of Buras and Gaemers(18) is used.

(b) The Measurable Quantities

In Fig. 9 I present the rates for the process

$$e^- p \rightarrow e^{-\prime} + x \qquad 5.7$$

at high Q^2. There are clearly healthy event rates at these large values of Q^2 so that meaningful measurements can be made. In Fig. 10 the individual contributions are compared to the purely electromagnetic cross-section (σ_{em}). Pronounced effects occur in regions where the event rate is still large.

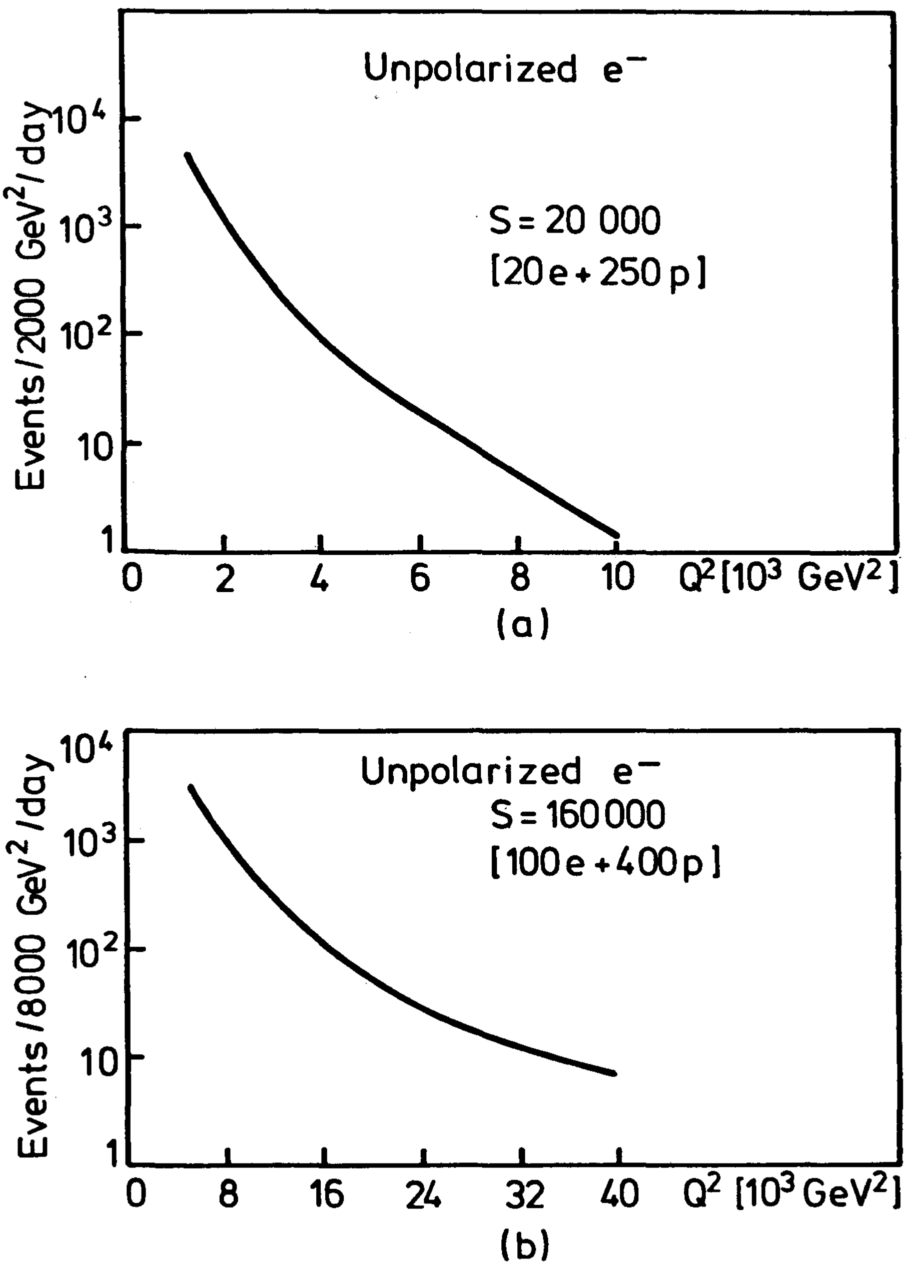

FIG. 9 Event rates for the neutral current cross-section at (a) 20 x 250 GeV and (b) 100 x 400 GeV.

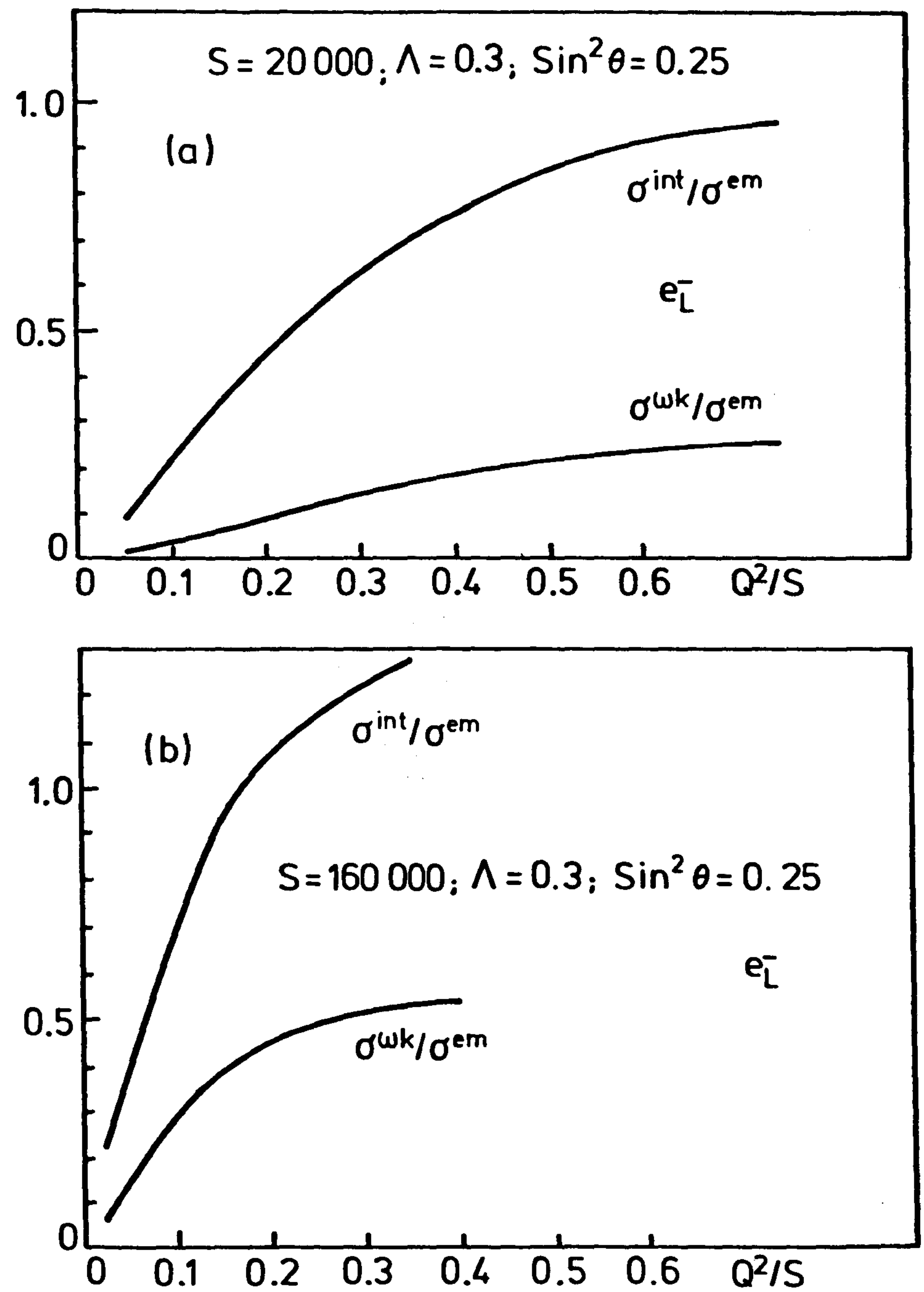

FIG. 10 Comparison of $^{\sigma}/\sigma_{em}$ for different helicity lepton beams at 20 x 250 GeV.

However, the real nature of the weak current is revealed by the different cross-sections for e^-_L, e^-_R, e^+_L and e^+_R as indicated in Fig. 11.

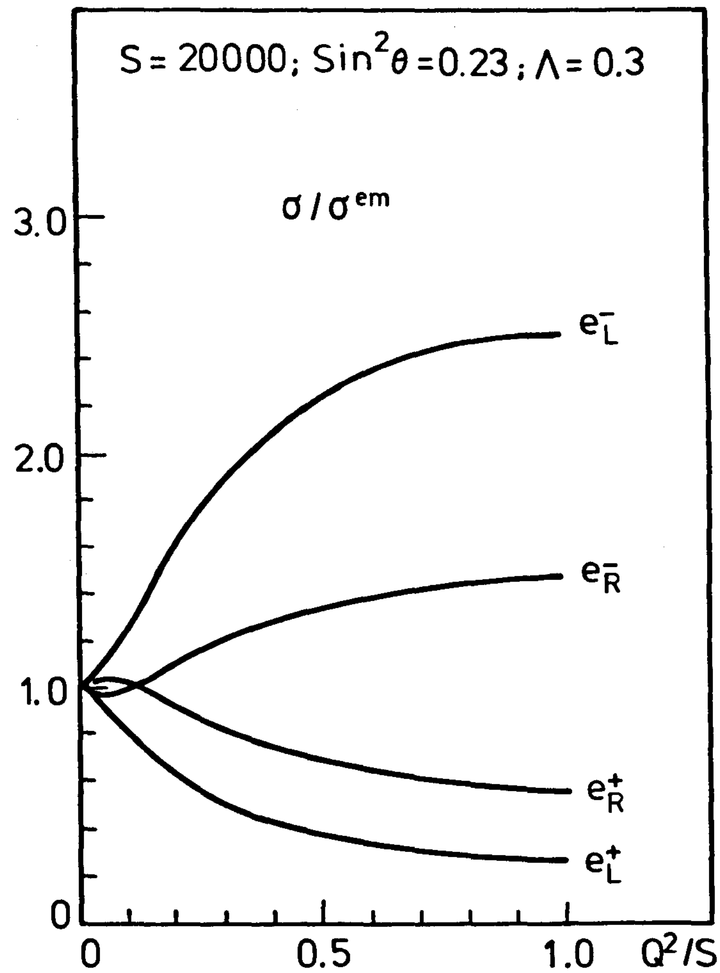

FIG. 11 Comparison of σ/σ_{em} for different helicity lepton beams at 20 x 250 GeV.

These differences can be presented in terms of an asymmetry between the scattering of left handed and right handed leptons

$$A = \frac{\sigma_L - \sigma_R}{\sigma_L + \sigma_R} \qquad 5.8$$

as demonstrated in Fig. 12 or as the asymmetry in the scattering of electrons and positrons (see Fig. 15)

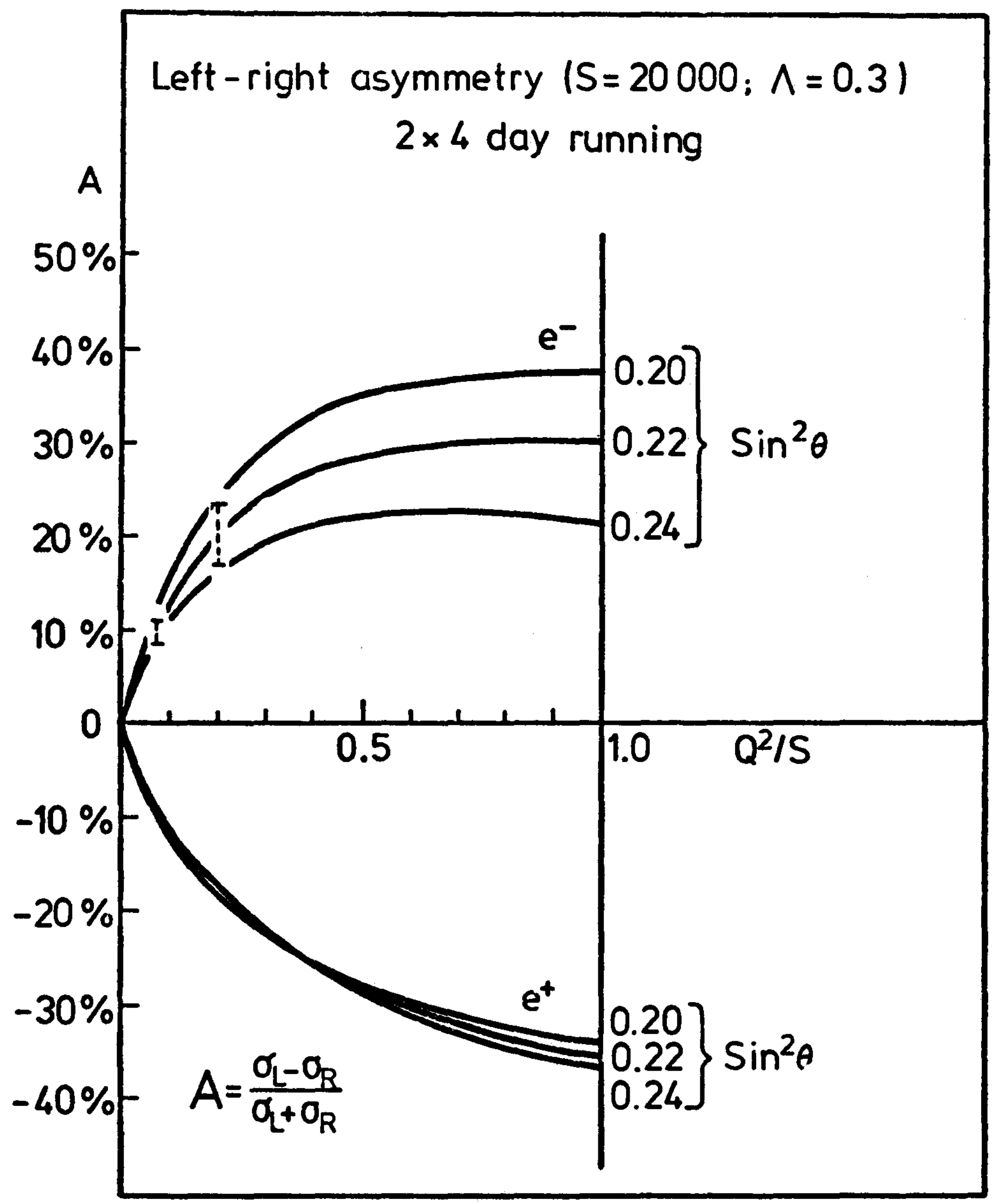

FIG. 12 The variation of $A = \frac{\sigma_L - \sigma_R}{\sigma_L + \sigma_R}$ with Q^2 as a function of $\sin^2\theta$ for e^- and e^+ beams. Hypothetical data points are included from 2 x 4 day experiments.

$$A = \frac{\sigma(e^-) - \sigma(e^+)}{\sigma(e^+) + \sigma(e^+)} \qquad 5.9$$

(c) Sensitivity to $SU(2)_L \times U(1)$ Parameters

In this section in discussing asymmetries I will assume that two experiments are performed, each of 4 days (theoretician variety) duration. This will then allow some estimation of the errors that might be achieved in measuring these quantities and hence the sensitivity to the $SU(2)_L \times U(1)$ parameters.

(i) $\sin^2\theta$ from polarization asymmetries

In Fig. 12 the variation of the asymmetry as a function of $\sin^2\theta$ is shown together with the results of the above 'experiment'. It is clear from this that $\sin^2\theta$ should be measured to an accuracy of

$$\Delta(\sin^2\theta) \lesssim 0.01 \qquad 5.10$$

(ii) m_Z from polarization asymmetries

In an experiment with the order of accuracy shown in Fig. 12 the variation of A in terms of m_Z as shown in Fig. 13 would lead to a measurement of m_Z with an accuracy

$$\Delta(m_Z) \sim 5\text{-}10 \text{ GeV} \qquad 5.11$$

(iii) $\sin^2\theta$ and m_Z from charge asymmetries

Figs. 14 and 15 demonstrate the charge asymmetry as a function of m_Z and $\sin^2\theta$. It is clear that m_Z would be measured to an accuracy

$$\Delta(m_Z) \sim 10 \text{ GeV} \qquad 5.12$$

but there is essentially no sensitivity to the Weinberg angle (at the level required 6-8 years from now).

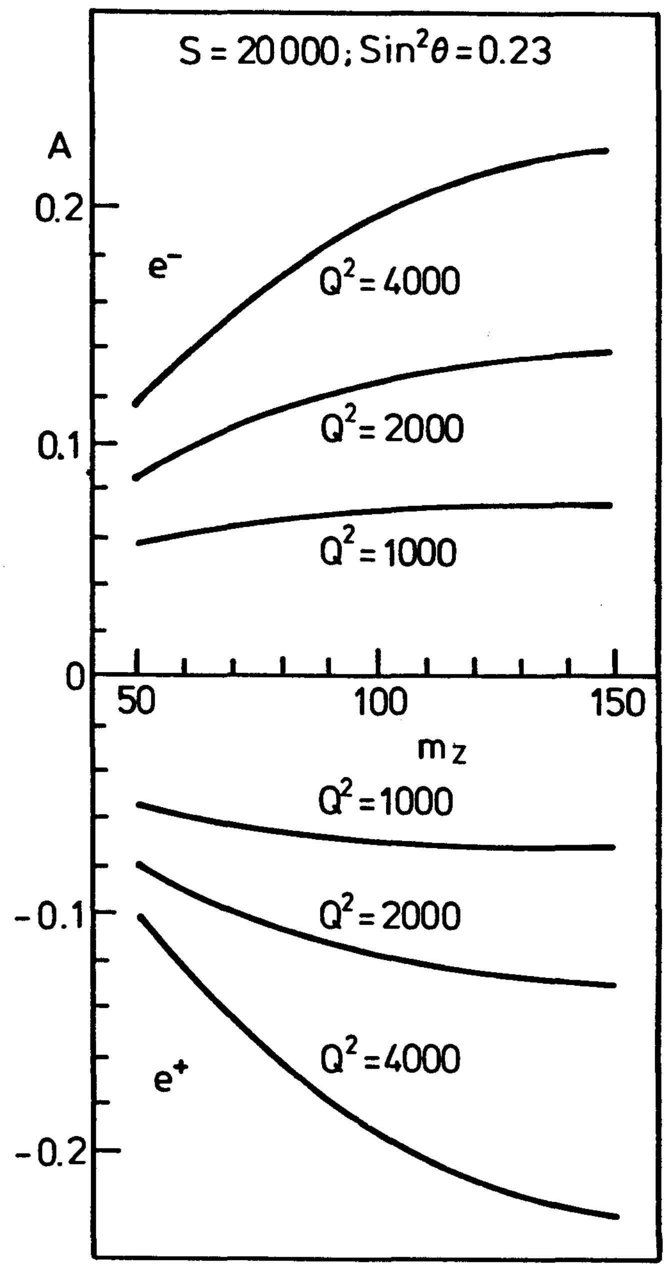

FIG. 13 Variation of A at different Q^2 as a function of the mass of the Z° (m_Z).

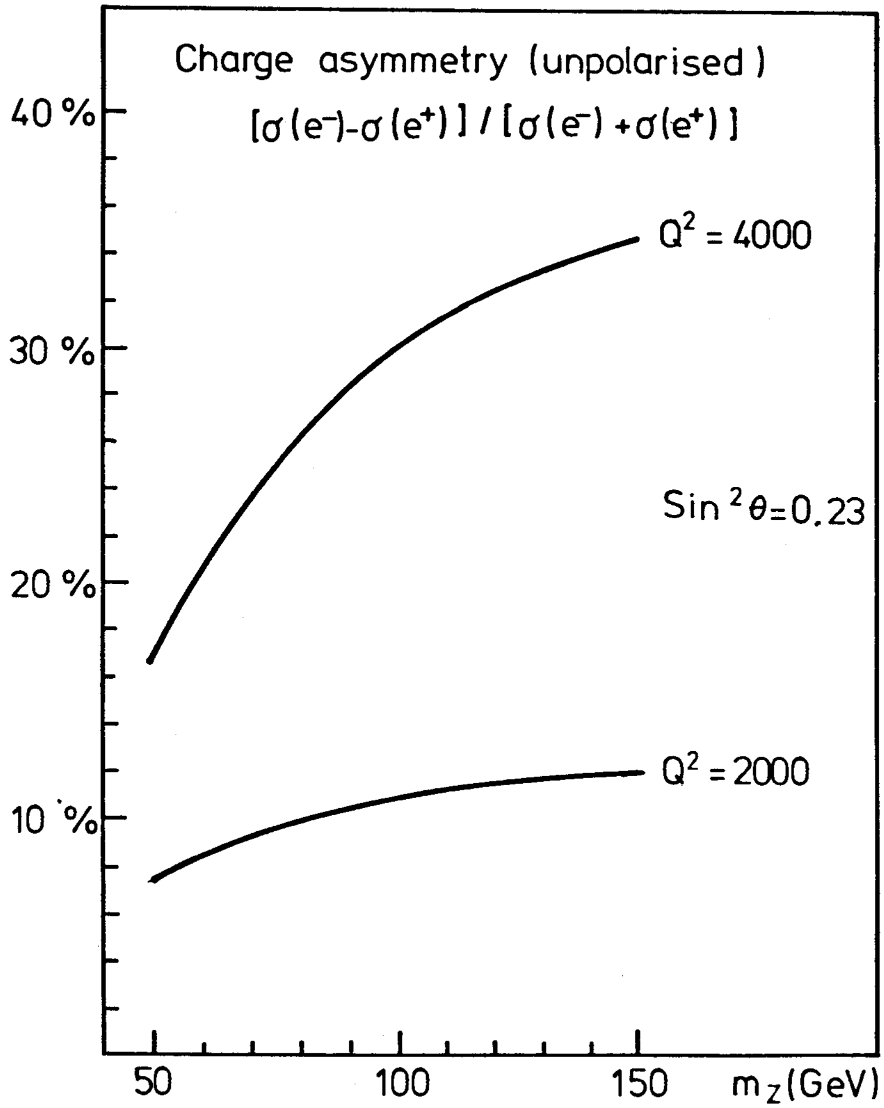

FIG. 14 The charge asymmetry $\frac{\sigma(e^-) - \sigma(e^+)}{\sigma(e^-) + \sigma(e^+)}$, at different Q^2 as a function of m_Z.

Charge asymmetries are also confused by the presence of 2 effects. However these have a very different Q^2 behaviour(3,19)

$$\frac{\sigma^{2\gamma}}{\sigma^{1\gamma}} \sim - \frac{3}{2}\frac{\alpha}{2\pi} \ln \frac{Q^2}{m^2} \qquad 5.13$$

which should allow the separation of the Z° contributions.

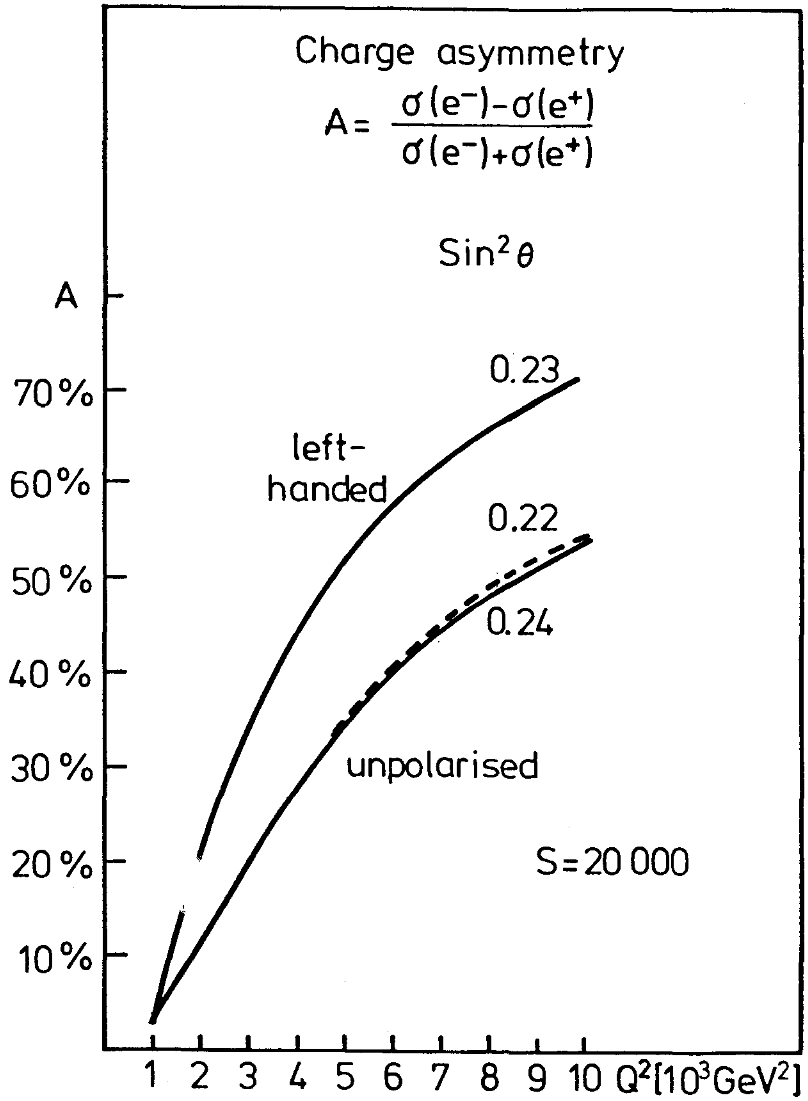

FIG. 15 The charge asymmetry as a function of Q^2 indicating the insensitivity to $\sin^2\theta_W$ for unpolarized beams.

This discussion demonstrates that polarization of the lepton beams is vital in unravelling the structure of the neutral current and will have an essential role in experiments at an ep machine. (The high energies in LEP essentially rule out this possibility.) Charge asymmetries alone, although valuable, are not enough.

(d) Production of Charmed Quarks

Charm quarks (and others) are produced via the mechanism in Fig. 16. The rates of production of c quarks are quite large, $\gtrsim$200/day

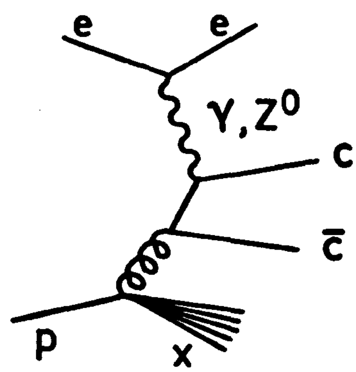

FIG. 16 The production of charm quarks from the sea

at $Q^2 > 1000$ GeV^2, and can be identified via their semileptonic decays leading to final states containing $e^-\mu^\pm$. Fig. 17 shows the variation of

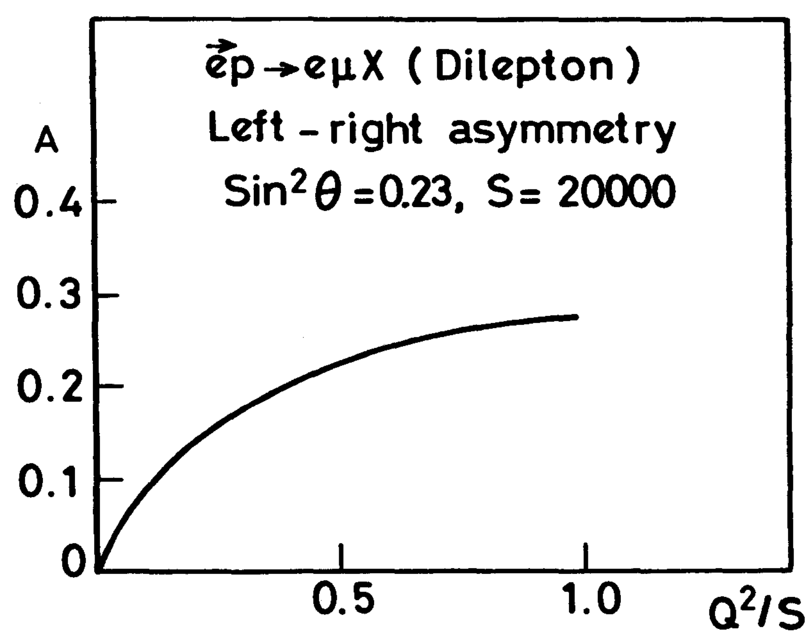

FIG. 17 The variation of the dilepton asymmetry,

$$A = \frac{\sigma_L(e^-\mu) - \sigma_R(e^-\mu)}{\sigma_L(e^-\mu) + \sigma_R(e^-\mu)}$$

with Q^2.

polarization asymmetry as a function of Q^2 while in Fig. 18 the sensitivity to m_Z is demonstrated.

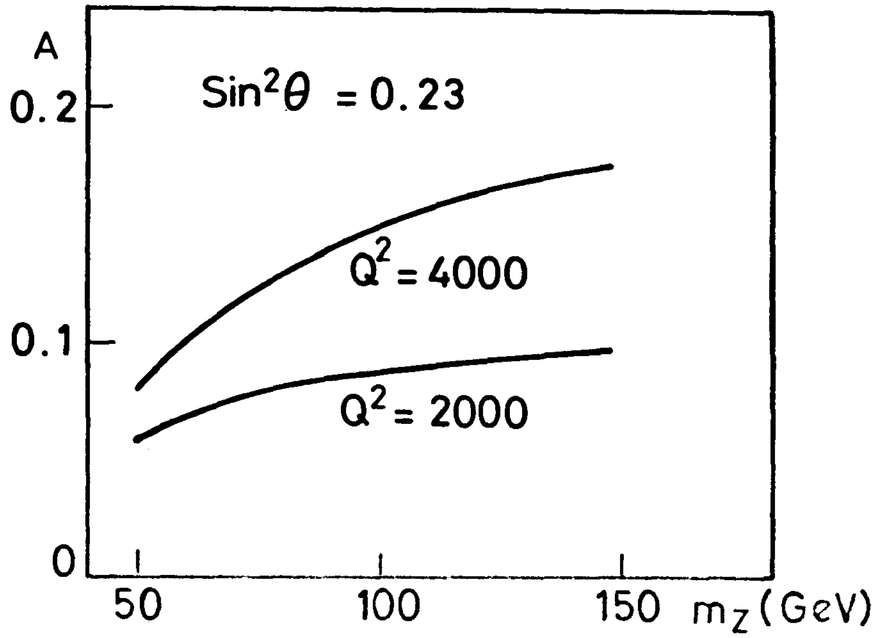

FIG. 18 The variation of the dilepton asymmetry as a function of m_Z.

The rates, after introducing a semi leptonic branching fraction, probably preclude any detailed studies. However, the observation of an asymmetry would demonstrate that the c quark (and higher mass states) couple to the Z°.

(e) Production of New Quarks

The production rates of new quarks are difficult to estimate as this requires a reliable model of the quark sea. In Table 2 the rates for heavy quarks (of charge $^2/3$) at s = 22400 GeV are summarized.

TABLE 2

Heavy Quark Production at s = 22400

M	Rate/Day
5	15000
10	∿1500
25	∿30
50	-

In these events only one quark is 'seen', the other being lost down the beam pipe with the other target fragments. This compares poorly with e^+e^- annihilation in which both jets are seen in an environment where the signal/background is much better (and the rate at least comparable if not much higher). Only heroic efforts would reveal the existence of such a new quark in ep collisions.

(f) Conclusions

(1) It is clear that it would be possible to consolidate our knowledge of the weak neutral current to accuracies

$$\Delta(\sin^2\theta) \sim .01$$
$$\Delta(m_Z) \sim 5 \text{ GeV} \qquad 5.14$$

(2) If m_Z is known and hence $\sin^2\theta$ (within $SU(2)_L \times U(1)$) then asymmetries and propagator effects in these ep reactions will reveal any further structure in the neutral currents. This implies that it will be possible to study coupling to mass scales well above m_Z.

To conduct these investigations requires two things:

- High s and hence high Q^2 (σ_{weak} also increases with s)
- polarized beams

i.e., the highest s possible should be achieved consistent with polarization of the beams.

6. CHARGED CURRENTS

One of the major contributions an ep machine could make would be to study the properties of the charged weak current. In this context it is worth remembering that W studies will only be made at LEP when the centre of mass energy exceeds $2m_W$ and then the rates will still be very low (∿10's per day with maximum luminosity). Moreover this threshold might not be passed until a second phase of LEP, i.e. the 1990's.

(a) Charged Current Cross-Sections and Event Rates

The reaction occurs via the process in Fig. 19 where the exchanged W strikes a parton leading to two jets of particles, one associated with

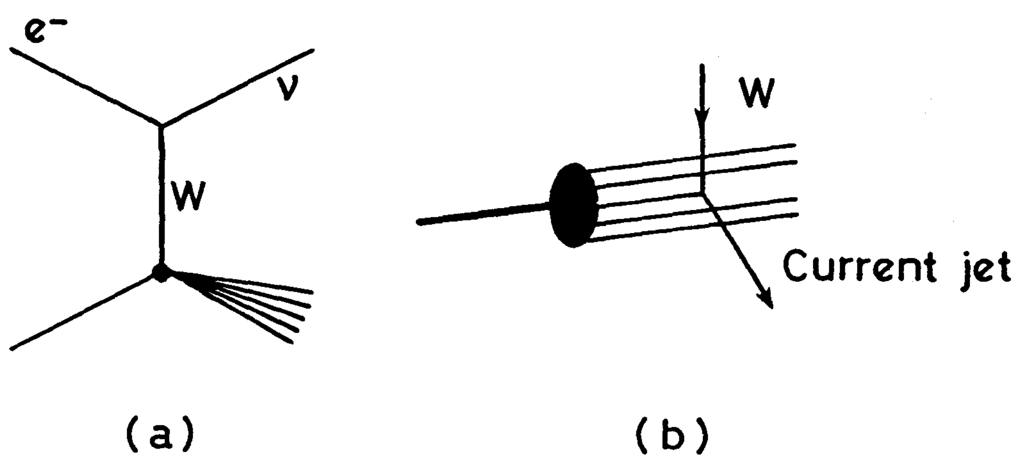

FIG. 19 The charged current process in ep collisions.

the target fragments (lost in the beam pipe) and the other associated with the struck parton - the current jet.

The cross-section for this process is

$$\frac{d^2\sigma}{dxdy} = \frac{G^2 s}{2\pi} P \times [f_q(x,Q^2) + (1 - y)^2 f_{\bar{q}}(x,Q^2)] \qquad 6.1$$

where P is a propagator factor

$$P = \left(\frac{m_W^2}{m_W^2 + Q^2}\right)^2 \qquad 6.2$$

and $f_q(x,Q^2)$, $f_{\bar{q}}(x,Q^2)$ are quark distribution functions.

In order to estimate rates, the following have been used:

(1) Buras and Gaemer's parametrization[18] of the quark distributions.

(2) $m_W = \infty$ i.e. point like Fermi interaction

(3) $p_T > 10$ GeV in order to ensure the possibility of measuring the current jet.

The event rates are summarized in Fig. 20 and Fig. 21 for an unpolarized beam and one day (theoretician's) of running. In both

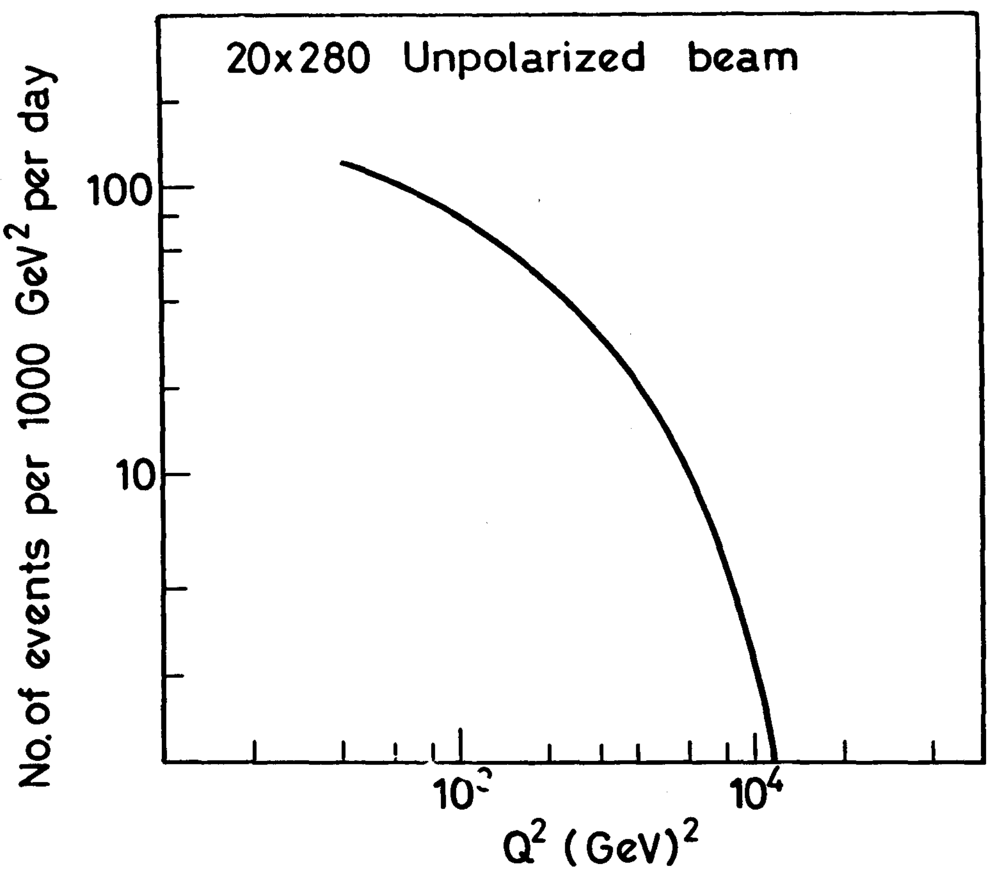

FIG. 20 Event rate/1000 GeV^2/day for charged current reactions as a function of Q^2 for 20 x 280 GeV^2 collisions with unpolarized beams.

cases the rates are appreciable

20 x 280: ~250 events/day

100 x 400: ~2000 events/day

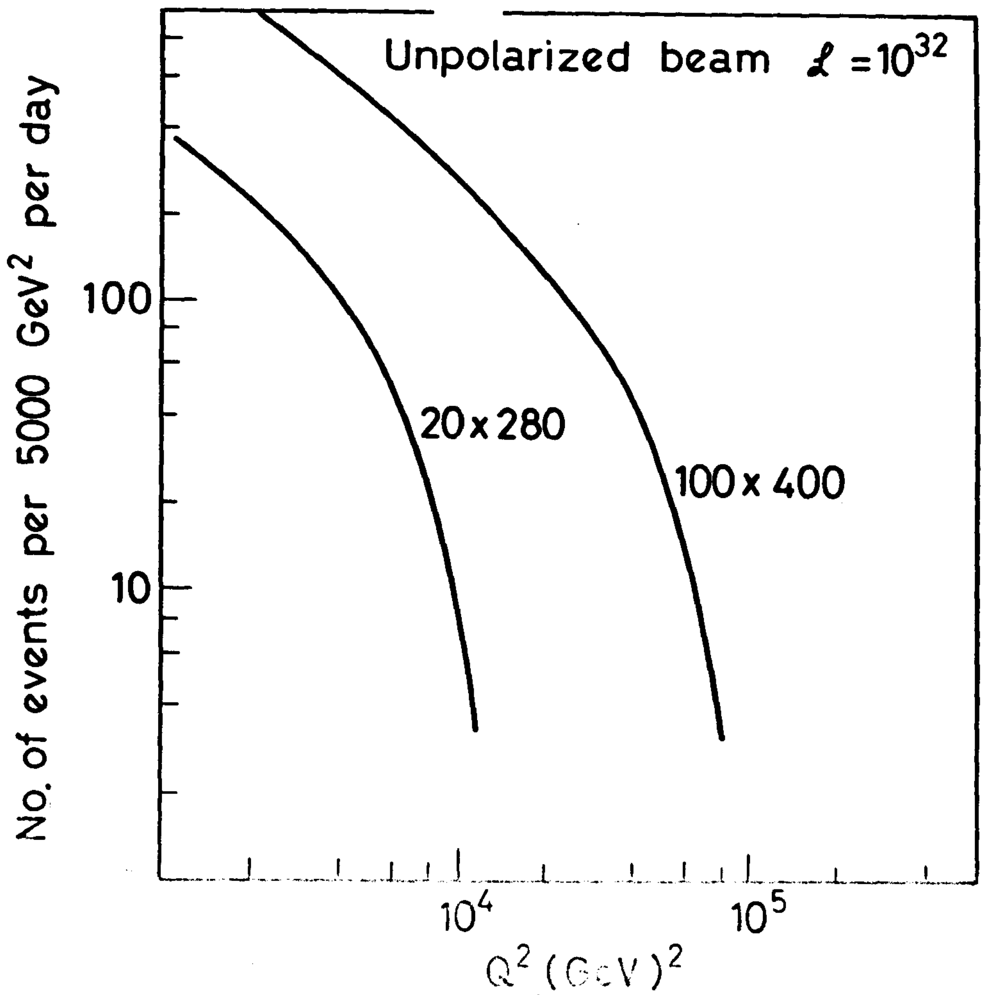

FIG. 21 Event rate/5000 GeV^2/day for charged current reactions for both 20 x 280 GeV^2 and 100 x 400 GeV^2 collisions with unpolarized beams.

This increase is due basically to the increase in s, the weak cross-section rising accordingly. I should also remark that these cross-sections would increase by a factor of 2 if left handed polarized electrons were used.

In the following discussion I will compare all changes due to propagator effects, etc. with this point cross-section rather than in terms of absolute rates.

(b) Measurement of the Current Jet

The presence of a charged current event is basically inferred from the absence of transverse momentum (i.e. the neutrino) compensating the transverse momentum of the current jet.[3] Thus it is essential in discussing this type of event to make some assumptions about the accuracy of measurement of the current jet. I have assumed

(i) $$\frac{\Delta E}{E} = \frac{.5}{\sqrt{E}} \tag{6.3}$$

(E measured in GeV)

(ii) $$\Delta\theta_{jet} = 50 \text{ mrads} \tag{6.4}$$

In Fig. 22 the effect of this resolution on the measurement of the point cross-section is indicated for the 20 x 280 GeV machine. The sharp rise near Q^2_{max} is due to the fact that there are very few 'true' events in this region and hence the migration of events from more populated areas, due to inaccurate estimation of Q^2, leads to large values

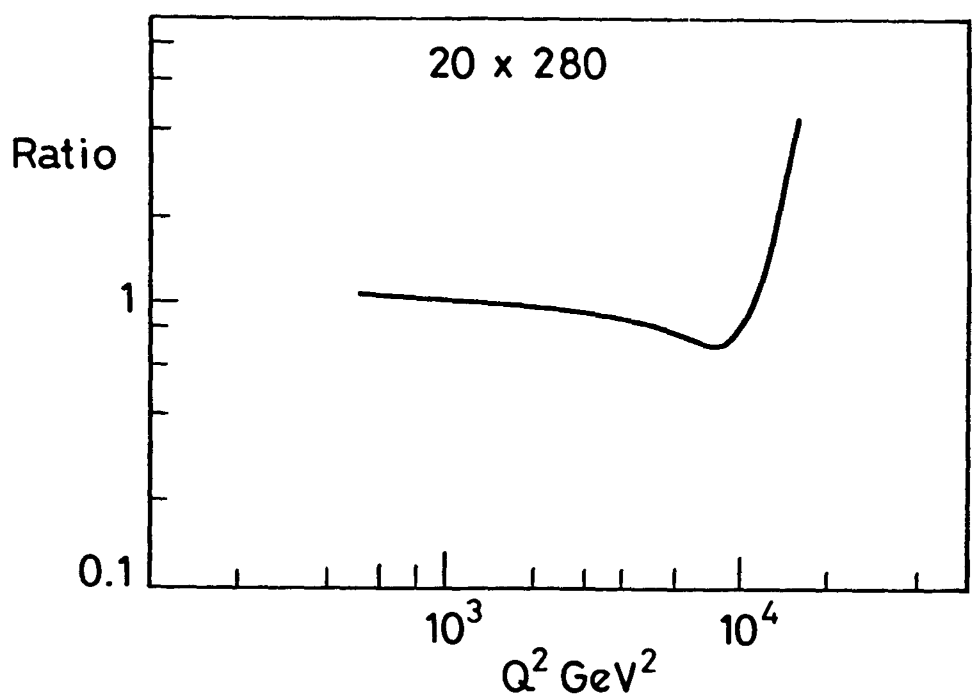

FIG. 22 The effect of resolution in the measurement of charged current cross-sections as a function of Q^2. Comparison is made using a point like ($m_W = \infty$) cross-section.

for the ratio of observed to expected events. A similar effect can be observed in Fig. 24. In all subsequent discussion of propagator effects these consequences of resolution have been introduced into the calculations.

A study of rates and resolutions (Figs. 20, 21, 22 and 24) indicate that the effective maximum Q^2 for experiments is given approximately by

$$(Q^2_{max})_{effective} \sim \frac{1}{4} Q^2_{max} = \frac{1}{4} S \qquad 6.5$$

(c) Sensitivity to m_W

In order to study this the effects of different m_W are shown in Fig. 23 and Fig. 24 together with the hypothetical results of a 4 day experiment. The first remark is that the resolution effects mimic

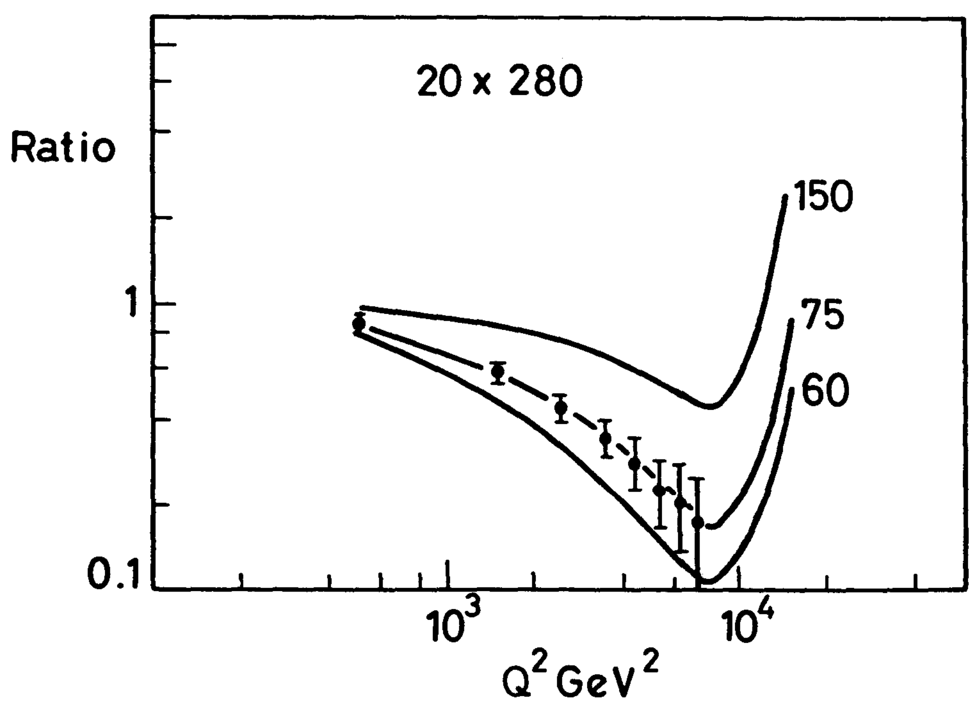

FIG. 23 The effect of different W masses as a function of Q^2 for 20 x 280 GeV^2 collisions. (The cross-section is compared with that obtained when $m_W = \infty$.) Hypothetical data points are included from a 4-day experiment.

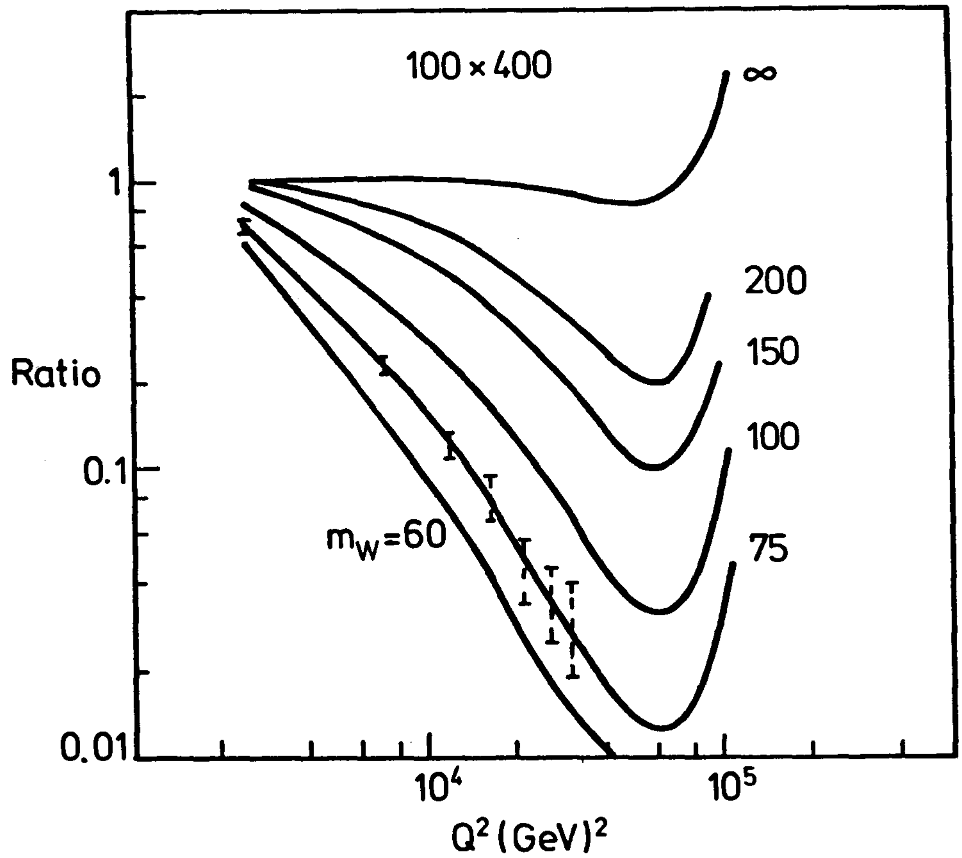

FIG. 24 The effect of different W masses as a function of Q^2 for 100 x 400 GeV^2 collisions. Hypothetical data points are included from a 4-day experiment.

the presence of a W propagator and at a 20 x 280 GeV machine experiments would be insensitive to $m_W \gtrsim 200$ GeV. The accuracy obtained in such experiments would be

$$\begin{aligned} &\Delta(m_W) \sim 5\text{-}10 \text{ GeV} &&\text{at } 20 \times 280 \\ &\Delta(m_W) \lesssim 5 \text{ GeV} &&\text{at } 100 \times 400 \end{aligned} \qquad 6.6$$

A better resolution is obtained at the higher energy machine and a sensitivity to a greater variety of W masses. The reason for this is clear. At a 20 x 280 GeV^2 machine, the useful Q^2 region is less than m_W^2, whereas at the higher energy, it is greater than m_W^2 and the propagator effects are more pronounced.

(d) Charged Current Couplings

In the standard model the charged current transitions between quarks are summarised in the Kobayashi and Maskawa[20] mixing matrix. The hadronic charged weak current is

$$J_\mu = (\bar{u},\bar{c},\bar{t})\gamma_\mu(1 - \gamma_5)M\begin{pmatrix} d \\ s \\ b \end{pmatrix} \qquad 6.7$$

where M is this 3 x 3 unitary mixing matrix. This can be written in terms of four parameters

$$M = \begin{pmatrix} c_1 & -s_1c_3 & -s_1s_3 \\ s_1c_2 & c_1c_2c_3-s_2s_3D & c_1c_2s_3+s_2c_3D \\ s_1s_2 & c_1s_2c_3-c_2s_3D & c_1s_2s_3-c_2c_1D \end{pmatrix} \qquad 6.8$$

with $c_i = \cos\theta_i$, $s_i = \sin\theta_i$, $D = e^{i\delta}$

The measurement of these parameters is clearly important for our understanding of the weak interactions of the quarks. However, information can only be obtained from:

(i) weak decays of charm, bottom or top particles. In this case the signal will be hard to identify and interpret.

(ii) charged current interactions where the $W^\pm$ strike the u and d quarks, as in Fig. 25, exciting the new flavours. To estimate the rates for these processes the assumption is made that

$$\theta_2 = \theta_3 = \theta_{Cabibbo} \qquad 6.9$$

Unfortunately, the resulting number of interesting events is rather small

$$\begin{aligned} e_L^- &\to b \qquad \sim 1 \text{ event/day} \\ e_R^+ &\to t \qquad \sim 0.4 \text{ event/day} \end{aligned} \qquad 6.10$$

even before event identification is included.

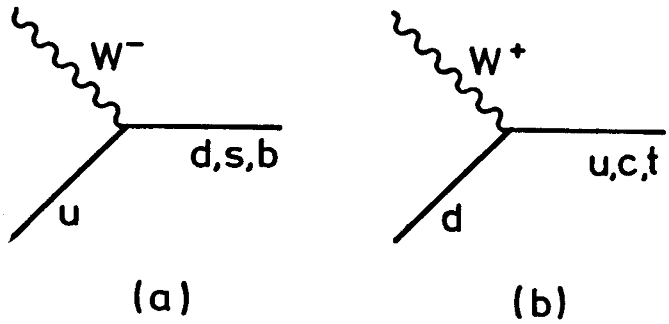

FIG. 25 Charged current transitions from the valence partons within a proton producing both new and old quarks.

Thus we must conclude that the measurement of this matrix, M, will be very difficult and certainly at an ep machine this will not be an easy measurement to make.

(e) Conclusions

(i) It is clear that the rates are large and resolution effects do not grossly impair the experiments.

(ii) The error on the W mass will be

$$\Delta(m_W) \sim 5 \text{ GeV}$$

This sort of accuracy will allow consistency checks with the $SU(2)_L \times U(1)$ model and implies that there will be sensitivity to higher mass structure in the charged current (see section (7)). However, this sensitivity will be enhanced by the higher energy because both the effective Q^2 range will be larger and the event rates higher.

(iii) The mixing matrix for the flavour changing transitions will be exceedingly difficult to measure.

From points (i) and (ii) it is clear that the higher the machine energy the better. However, the presence of polarization is important (Section 7) since the chirality of the couplings can be investigated. e.g.

$$\sigma(e_R^- P \to \nu X) = 0 \qquad 6.11$$

for the weak charged current.

7. NEW CURRENTS AND ASSOCIATED NEW PARTICLES

The orthodox view is that the weak and electromagnetic interactions are governed by an $SU(2)_L \times U(1)$ gauge group [12] and at present this is remarkably successful in describing the data that exist.[21,22] Any new machine should be able to penetrate to kinematical regions where discrepancies from this might be identified. To obtain an idea of the sorts of effects that might be expected, I will consider three different models. I would like to emphasize that these are not models which would necessarily survive a close scrutiny or detailed comparison with data but are intended more as guides. They will however be consistent with the Weinberg-Salam model (as much as possible).

A	$SU(2)_L \times SU(2)_{L'} \times U(1)$	7.1
B	$SU(3)_L \times U(1)$	7.2
C	$SU(2)_L \times SU(2)_R \times U(1)$	7.3

Models A and B[23] contain only left handed currents, whereas in C[24] there are new right handed currents. In general the simplest way to ensure agreement with Weinberg Salam is for the new currents to couple old leptons and quarks to new leptons and quarks of high mass. This mass threshold (which is above the centre-of-mass energy of present experiments) ensures the non-participation of these currents in present experiments. Hence the observation of new currents probably implies the existence of new particles.

(a) New Left Handed Currents Coupling to eν

It is possible to construct models in which there is a new current, mediated by a heavy W', which couples the electron to the neutrino as indicated in Fig. 26. Such models almost certainly predict the existence

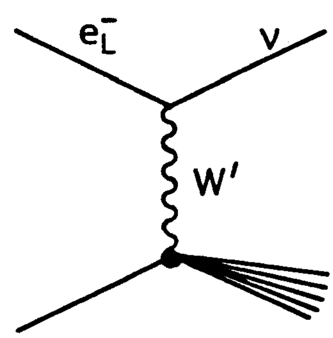

Fig. 26 The contribution of a new left handed current in $e^-p \rightarrow \nu + x$

of new lepton doublets (and probably new quark doublets also). It is instructive to know whether the existence of such a W could be detected and to investigate the possibility the following model was made.

In equation 6.2 the single W propagator was replaced by two propagators

i.e.

$$\frac{m_1^2}{m_1^2+Q^2} \rightarrow \frac{gm_1^2}{m_1^2+Q^2} + (1-g)\frac{m_2^2}{m_2^2+Q^2} \qquad 7.4$$

with $m_1 = 75$ GeV, $m_2 = 200$ GeV

The cross-sections (including resolution effects) were then calculated and are compared with the single W cross-section in Fig. 27 and Fig. 28 From these figures it is clear that a deviation from $m_W = 75$ GeV $g = 1$ can be detected, but the simplest interpretation would be to give the W a higher mass rather than identify the existence of a second W'. However,

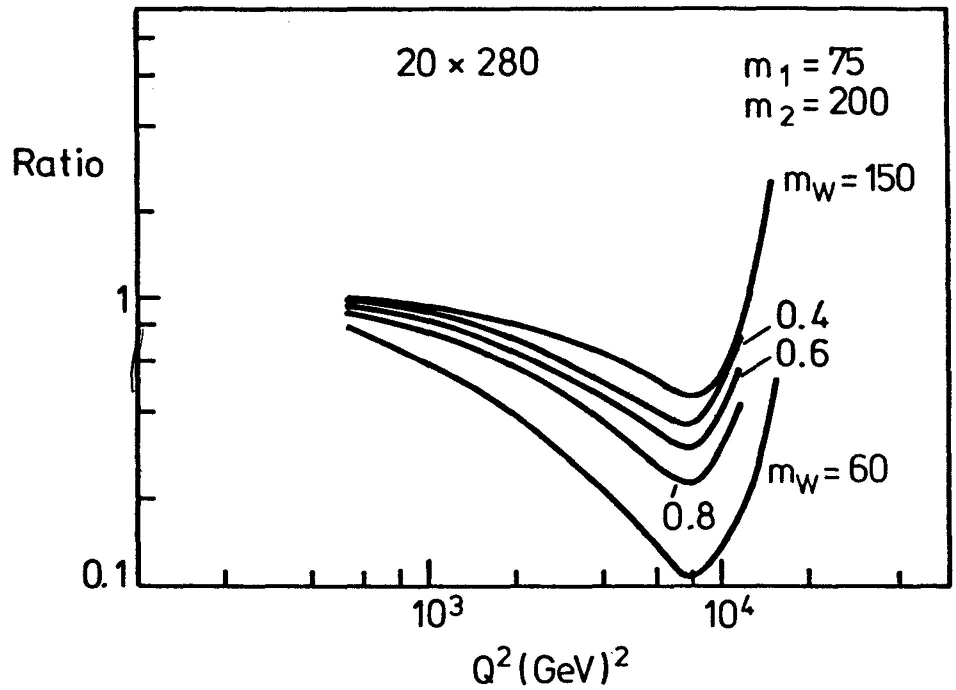

FIG. 27 The effect of 2 W bosons (m_1 = 75, m_2 = 200) on the charged current cross-section at 20 x 280 GeV^2 collisions. The various curves correspond to different relative coupling strengths. Comparison is made with the point like cross-section.

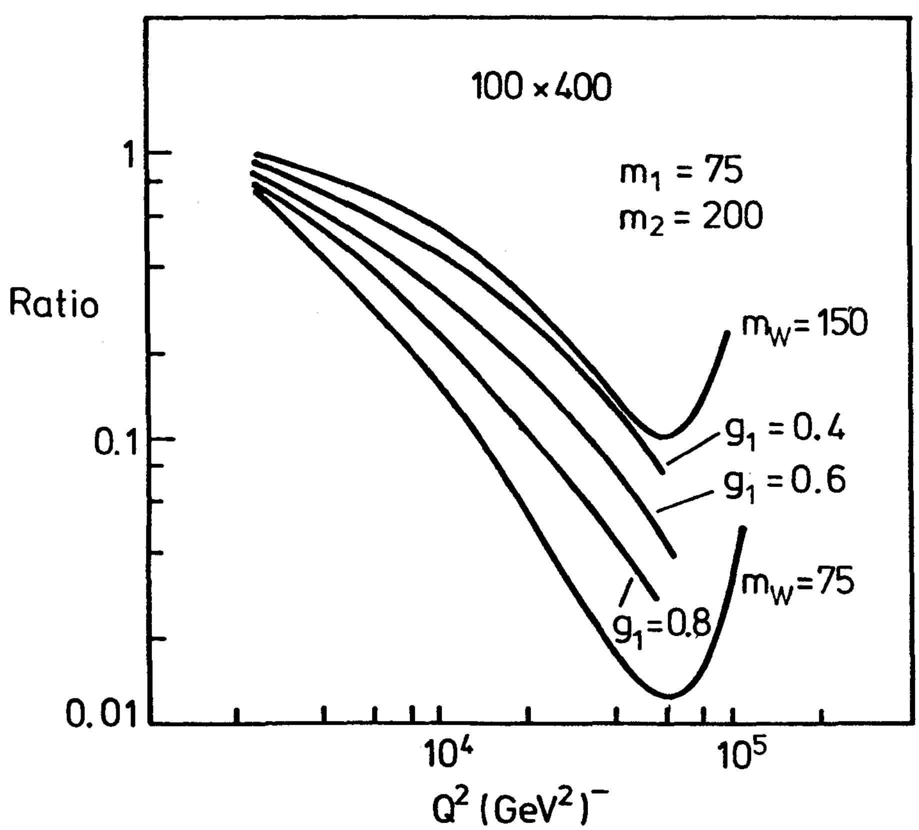

FIG. 28 The effect of 2 W bosons on the charged current cross-sections at 100 x 400 GeV^2 collisions.

if the mass, m_1, is known, e.g. from $\bar{p}p$ or pp experiments, these deviations would demonstrate the presence of a second higher mass contribution to the chraged current. This would then be a sensitive test of whether charged currents are 'understood' and consistent with $SU(2)_L \times U(1)$.

Study of Figs. 27 and 28 indicate that the higher the energy the greater the sensitivity to high mass effects. Clearly $Q^2 > M_1^2$ will reveal better this high mass character and unfortunately in the 20 x 280 GeV machine the useful Q^2 region is less than m_1^2.

Thus one concludes that this is probably the only way of investigating high mass (Q) charged current effects, since LEP will be limited to charged currents with $m_W \lesssim 100$ GeV. To make this search as good as possible it is necessary to push the Q^2 range (and hence S) as far as possible.

(b) New Leptons and Quarks Associated with Left Handed Currents

Cross-sections and Rates:

In Fig. 29 the mechanisms for producing these new quarks and leptons are shown. All three diagrams are applicable to models of type A

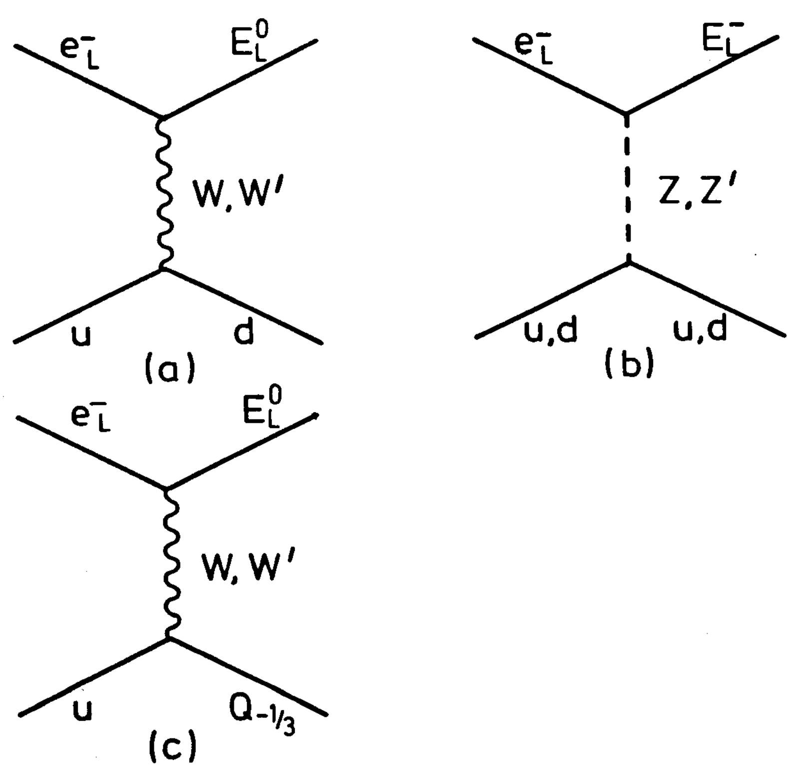

FIG. 29 Production mechanisms of new quarks and leptons by left handed currents.

whereas only Fig. 29(c) corresponds to Model B (with only w's operating). In general we must cross a threshold to see these new currents. In order to calculate the production rates it is necessary to make some model and in these cases the following choices were made:

(i) m_W = 75 GeV with a coupling equivalent to G_F

(ii) Buras and Gaemers parameterizations of the quark distribution functions

(iii) suppression factors(25) associated with m_L, $m_Q \neq 0$.

The results are shown in Fig. 30 and Fig. 31. The rates are clearly very healthy (with these assumptions) and would allow searches for new heavy leptons up to the masses indicated in Table 3 (for the

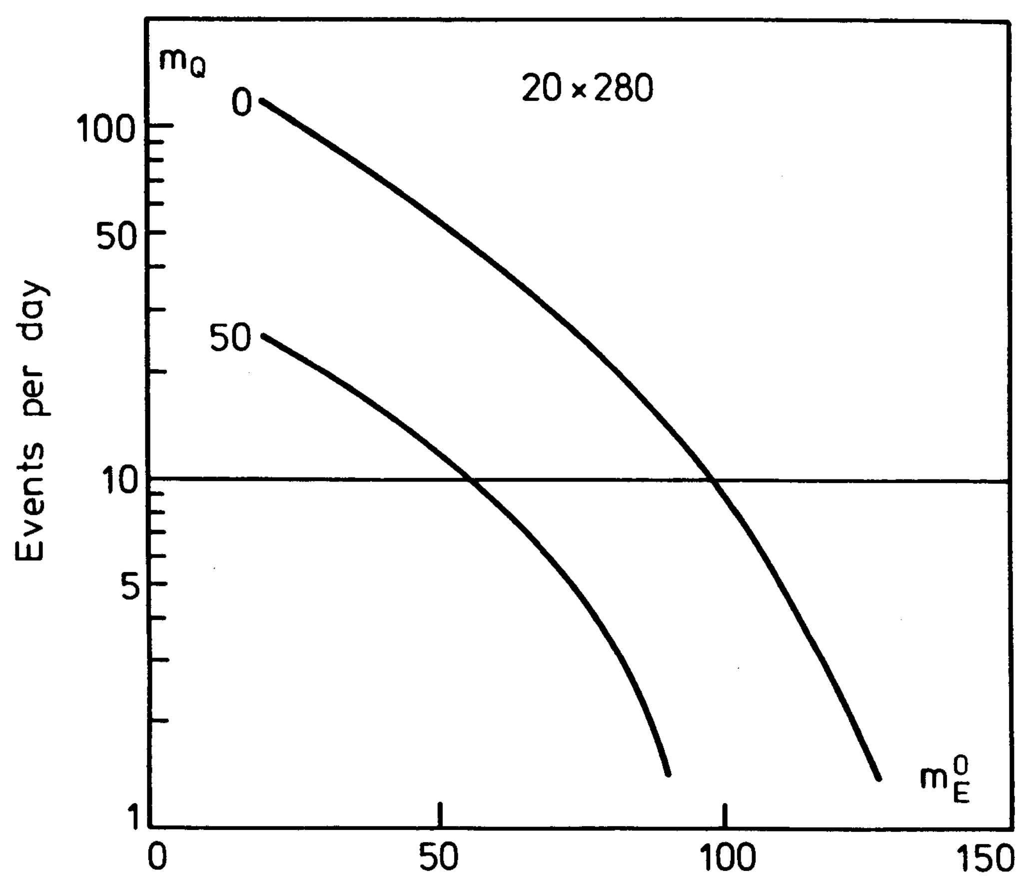

FIG. 30 Event rates for heavy lepton production with and without a new massive (50 GeV) quark in 20 x 280 GeV^2 collisions.

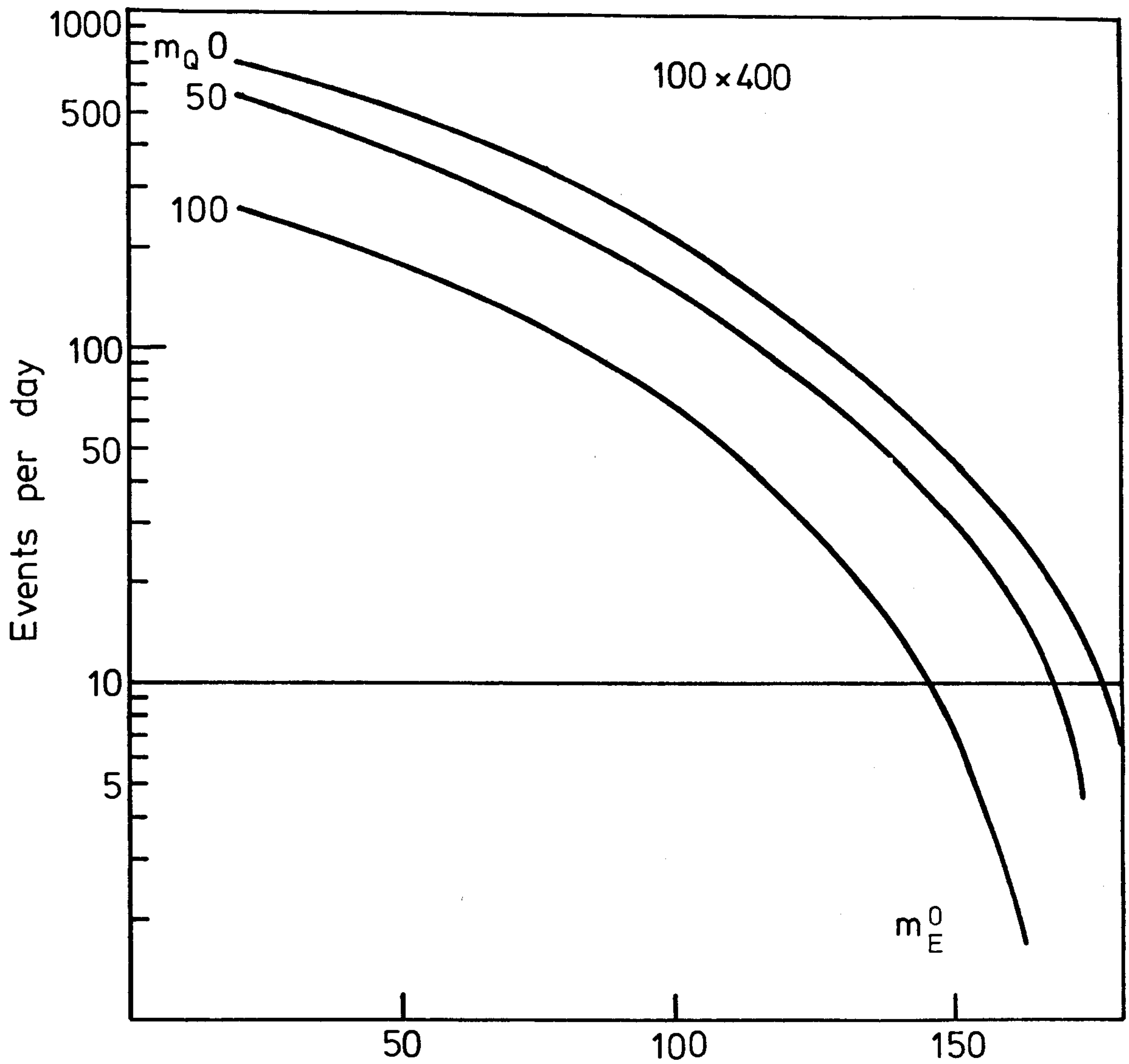

FIG. 31 Event rates for heavy lepton production with 0, 50 and 100 GeV quarks in 100 x 400 GeV^2 collisions.

assumed associated quark masses) if $\gtrsim$10 events/day are required.

TABLE 3

MASS LIMITS FOR HEAVY LEPTONS

Machine	m_L	m_Q
20 x 280	∿100 ∿50	∿0 ∿50
100 x 400	∿190 ∿170 ∿140	∿0 ∿50 ∿100

Thus this machine would be excellent for studying leptons coupling to the electron.

Production Mechanisms: The possibility of polarized beams provides a unique opportunity of testing the chirality of the coupling at the lepton vertex and the production mechanism at the hadronic vertex. For left handed currents

$$\sigma(e^-_R) = \sigma(e^+_L) = 0 \qquad 7.5$$

while Table 4 indicates the sort of variation in cross-section one might expect in different models (the calculation is made in the parton model approximation).

TABLE 4

VARIATION IN PRODUCTION CROSS-SECTION (left handed currents)

Model	$\sigma(e^+_R)\ \sigma(e^-_L)$
$\begin{pmatrix} u \\ d \end{pmatrix}_L$	$\frac{1}{6}$
$\begin{pmatrix} u \\ Q_{-\frac{1}{3}} \end{pmatrix}_L$	<<1

Other models can be expected to give equally varied results.

Signatures: The mechanisms by which new leptons of Model A decay are indicated in Fig. 32. Furthermore if $m_{E^-} > m_{E^\circ}$ the decay

$$E^- \rightarrow E^\circ + \ldots \qquad 7.6$$

may also exist (if $m_{E^\circ} > m_{E^-}$ then $E^\circ \rightarrow E^- + \ldots$).

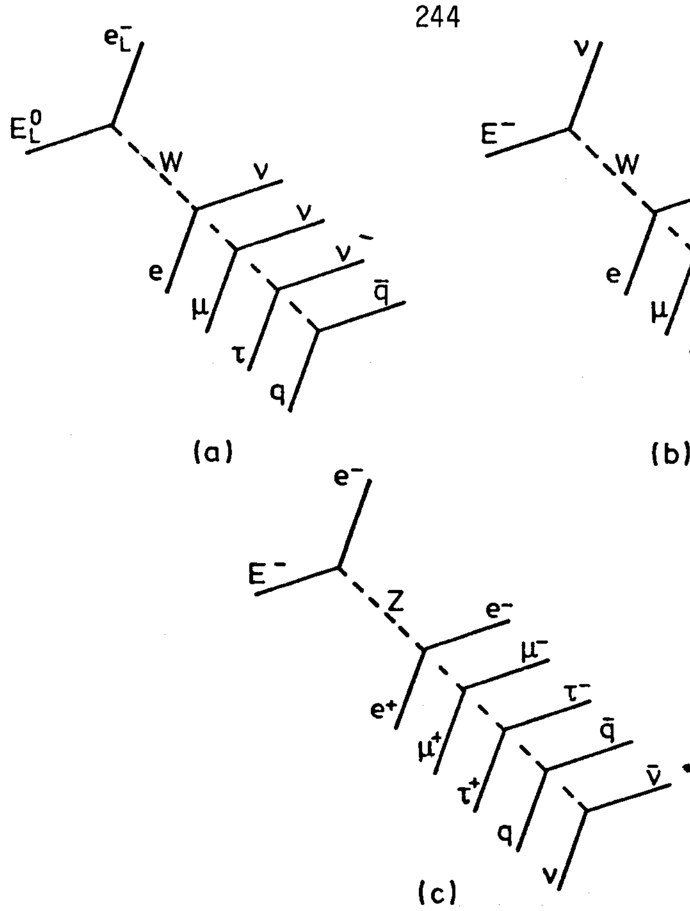

FIG. 32 Decay mechanisms for new heavy leptons with couplings to both new and old weak currents.

Thus these decay chains may lead to rather spectacular events in which the current jet (from the hadron vertex) is accompanied by multileptons or jets containing leptons (see Fig. 32). If the branching fraction is $\sim$5-10% there remains $\gtrsim$1 event/day in individual channels which can provide vital parameters of this new lepton (e.g. the mass of E^- could be obtained from $E^- \to e^- + e^+ + e^-$).

The decays associated with the particles of model B might be even more intriguing as indicated in Fig. 33. If the new current (W') only couples an old lepton (quark) to a new lepton (quark) then:

(i) if $m_Q > m_L$ a stable lepton will exist

(ii) if $m_L > m_Q$ a stable quark (i.e. meson) will exist.

and thus experiments should be capable of identifying long lived particles.

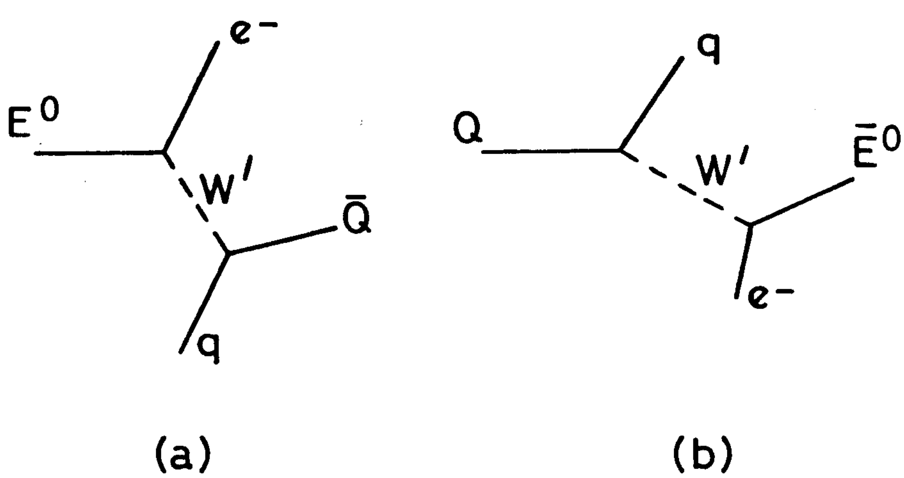

Fig. 33 Decay mechanism for a new lepton (a) and a new quark (b) solely coupled to anew charged current.

For leptons and quarks which couple to new currents such a machine is highly competitive with LEP, the mass rnge possible with 100 x 400 machine certainly exceeding that of LEP, i.e. the greatest advantage is obtained by pushing S as high as possible. Furthermore, the special properties (i.e. beam polarization at lower electron energies) provide a unique facility for studying the chirality of the current and production mechanisms at the hadron vertex.

(c) <u>New Leptons and Quarks Associated with Right Handed Currents</u>

In this context I will discuss model C i.e. $SU(2)_L \times SU(2)_R \times U(1)$ with the following possible multiplets of particles

Leptons:

$$\begin{pmatrix} L^\circ \\ e^- \\ E^{--} \end{pmatrix}_R \qquad 7.7$$

Quarks:

$$\begin{pmatrix} u \\ d \end{pmatrix}_R , \begin{pmatrix} u \\ Q_{-\frac{1}{3}} \end{pmatrix}_R , \begin{pmatrix} Q \\ u_{-\frac{5}{3}} \end{pmatrix}_R \begin{pmatrix} d \\ Q_{-\frac{4}{3}} \end{pmatrix}_R \qquad 7.8$$

The variations on this theme are enormous but choices should be made which are consistent with $SU(2)_L \times U(1)$. This particularly constrains the assignment of the electron[22] whereas it is still possible to put the u and d quarks in a right handed doublet since the only constraints would come from non-leptonic weak decays which are poorly understood. Note that in this case a doubly charged lepton is possible.

Cross-sections and Rates: The production mechanisms are shown in Fig. 34. The event rates, calculated under the assumptions of section 7(b), are as shown in Fig. 30 and Fig. 31 except that the reaction is now induced by the right handed electron,

$$\text{i.e.} \qquad \sigma(e_R^- \to L^\circ) \sim \sigma(e_L^- \to \nu) \qquad 7.9$$

(ignoring mass factors).

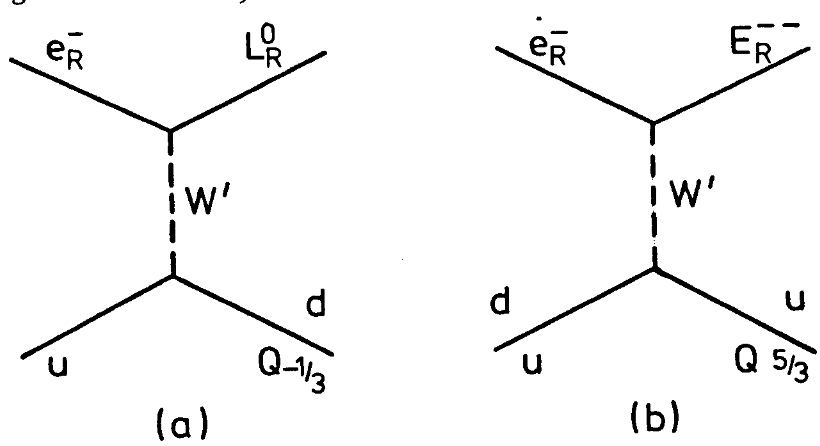

FIG. 34 Production mechanisms of new quarks and leptons coupled to right handed currents.

Production Mechanisms: In this case the exact opposite of (7.5) is true, i.e. the cross-section from left handed electrons must be zero

$$\sigma(e_L^-) = \sigma(e_R^+) = 0 \qquad 7.10$$

Furthermore the variety of models (7.8) lead to very different predictions of $\sigma(e_L^+)/\sigma(e_R^-)$ as calculated in the valence parton model approximation. These are summarised in Tables 5 and 6.

TABLE 5

VARIATION IN PRODUCTION CROSS-SECTION FOR $e^- \rightarrow E^\circ$ $(e^+ \rightarrow \bar{E}^\circ)$ WITH MULTIPLET MODEL

Model	$\sigma(e^+_L)/\sigma(e^-_R)$
$\begin{pmatrix} u \\ d \end{pmatrix}_R$	$\frac{1}{6}$
$\begin{pmatrix} u \\ Q_{-\frac{1}{3}} \end{pmatrix}_R$	$\frac{1}{6}$
$\begin{pmatrix} d \\ Q_{-\frac{4}{3}} \end{pmatrix}_R$	<<1
$\begin{pmatrix} Q_{\frac{5}{3}} \\ u \end{pmatrix}_R$	>>1

TABLE 6

VARIATION IN PRODUCTION CROSS-SECTION FOR $e^- \rightarrow E^{--}$ $(e^+ \rightarrow E^{++})$ WITH MULTIPLET MODEL

Model	$\sigma(e^+_L)/\sigma(e^-_R)$
$\begin{pmatrix} u \\ d \end{pmatrix}_R$	$\frac{2}{3}$
$\begin{pmatrix} Q_{\frac{5}{3}} \\ u \end{pmatrix}_R$	<<1

Thus again the polarization is invaluable in revealing the production mechanisms involved.

Signature: There is nothing to add to the discussion of section 7(b). The possibility of stable leptons or quarks again exists as well as a potential for very spectacular events.

Given the assumptions the rates are large and certainly an ep machine is competitive with LEP in the production of new leptons and quarks coupling to a right handed current. The higher the machine energy the greater the mass range probed and thus one should push to as high an energy as possible.

(d) General Comments

Clearly with an ep machine which contains polarized beams the chirality of any new charged current is revealed. Furthermore, information is obtained on the weak couplings of new objects which might only be obtained at LEP through studying decay mechanisms (a difficult activity).

If gauge theories are not correct then there might well be dramatic changes in cross-sections, e.g. in some models[26] the present weak current is due to the exchange of scalar (pseudoscalar) objects as indicated in Fig. 35. When the threshold for production of

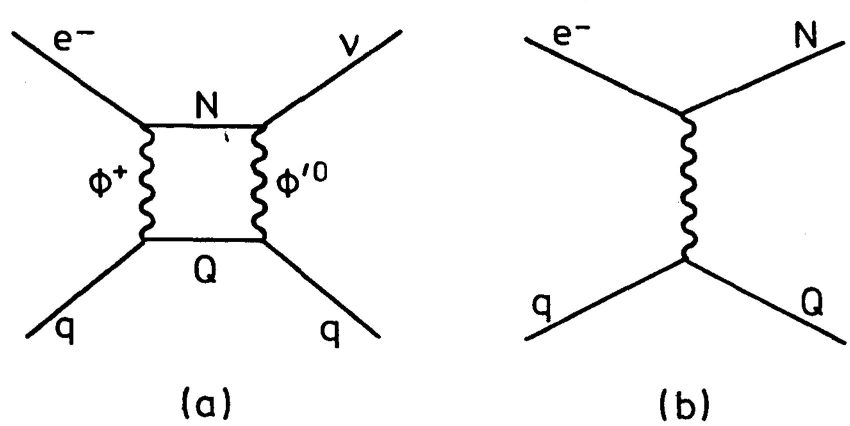

FIG. 35 (a) The conventional weak interaction as mediated by the exchange of scalar and pseudoscalar objects.

(b) The mechanism for production of new leptons and quarks above threshold.

the intermediate leptons is crosssed the cross-section will change and there will be a dramatic variation in the y distributions (associated with spin 0 exchange).

8. SUMMARY AND CONCLUSIONS

An ep machine is clearly not a device for producing copious quantities of the weak quanta, the Z, W and Higgs. Its great importance lies in being able to penetrate to high masses the character of the weak interaction, indeed on a mass scale that will not be reached at LEP. This is obtained by:

(i) studying propagator effects

and (ii) searching for new particles associated with new currents.

Furthermore it is especially powerful for the study of right handed currents.

To achieve these sorts of results requires:

1. As high Q^2 as possible which implies as high an energy as possible.
2. Polarized beams to as high an energy as feasible.

In this talk I have not dealt with the variety of options that might exist for quark substructure, e.g. gluinos, scalar quarks etc. Perhaps the most exciting prospects for an ep machine would be the observation of such objects or even more bizarre possibilities.

REFERENCES

1. Proceedings of the LEP Summer Study, 1978, CERN 79-01.

2. C.H. Llewellyn-Smith and B.H. Wiik, DESY, 77/38.

3. CHEEP, An ep facility in the SPS, CERN 78-02.

4. Antiprotons in the SPS, CERN/DG-2, 1977.

5. Proceedings of the Isabelle Summer Study, BNL 20550 (1975).

6. An ep facility at PETRA, E. Dasskowski et al, DESY 78/02.

7. A. Hutton, CERN/ISR-TH/78-7.

8. L.W. Jones, RMP 49 (1977), 717.

9. A. De Rujula, R. Giles, R.L. Jaffe, PRD17 (1978), 285.

10. J.C. Pati and A. Salam, PRD8 (1973), 1240, and PR D10, (1974), 275.

11. M.S. Chen and P. Zerwas, PR D12 (1975) 187.

12. S. Weinberg, PRL 19 (1967) 1264.
A. Salam, Proc. 8th Nobel Symposium, Stockholm, 1968 (ed. N. Soartholm) (Almquist and Wiksells, Stockholm 1968) p.367.

13. C.G. Callan and D.G. Gross, PRL 21 (1968) 211.

14. J. Ellis, M.K. Gaillard and D.V. Nanopoulos, NP B106 (1976) 292.

15. G. Ross, Private Communication.

16. L. Resnick, M. Sudareson, P. Watson, PR D8, 172 (1973).

17. C. Sachrajda, Proceedings of this Meeting.

18. A. Buras, K.J.F. Gaemers, NP B132 (1978) 249.

19. V.G. Gorslikov et al, Soviet J. Nuclear Physics 6 (1967) 361; J. Bartels, NP B82 (1974) 172.

20. M. Kobayashi and K. Maskawa, Prog. Th. Physics 49, 652 (1973).

21. L.M. Sehgal, Conference Proceedings, Neutrino '78. Ed. Fowler (Purdue University, p.253)

22. C.Y. Prescott et al, PL 77B (1978) 347.

23. B.W. Lee and R.E. Schrock, FNAL preprint PUB-77/48-THY (1977).

24. A. De Rujula, H. Georgi and S. Glashow, AP 109 (1977) 258.

25. J.D. Bjorken and C.H. Llewellyn-Smith, PR D7 (1973) 887.

26. W. Kummer and G. Segre, NP64 (1965) 585.

New Currents and New Particles

prepared by L. M. Sehgal

The report on "New Currents and New Particles" prepared and presented by R. Cashmore was based on the work of a study group that involved the following people: R. Barlow, J. Benecke, D. Binnie, R. Cashmore, J. Cleymans, R. Jaffe, G. Ross, B. Saitta, L. Sehgal and P. Zerwas. Three meetings were held (two at Aachen and the last at DESY) in the course of which the objectives of the study were defined, reports prepared by members discussed, and conclusions reached.

It was agreed that the main interest of an e p colliding beam project, insofar as "new currents and new particles" are concerned centres on two themes: (i) An e p machine would make possible the study of neutral and charged current interactions at momentum transfers of many thousands of GeV^2. In such conditions, the effects of the intermediate boson propagators would be discernible, revealing the range of the weak force and allowing an important test of our ideas concerning the electroweak interactions. (ii) Because of the large centre-of-mass energy, an e p machine would permit a search for currents involving the coupling of electrons to heavy leptons and of quarks to heavy quarks, with the ability to reach masses as high as 100 GeV. The availability of polarized beams would be a special advantage since it would allow a specific search for charged currents involving right-handed fermions.

As is evident from Cashmore's report, the above two themes dominated the discussions within the study group. At the same time it was recognised that an e p machine would be exploring a large new kinematical territory, and, as always, the greatest interest of such exploration lies in the possibility of uncovering totally new phenomena.

In the discussion following Cashmore's talk, attention was drawn to the importance of two-photon exchange contributions to e^+-e^- asymmetries. While these are not very well estimated, they do have a Q^2 dependence $\sim \log Q^2$ which is quite different from that due to Z-γ interference, which may help to separate them out. It was also noted that by the time e p physics becomes operational, there might be interest in looking for radiative corrections to the lowest-order electro-weak amplitudes, since these corrections are interesting tests of the gauge theory framework.

Perhaps one ought to stress the simple fact that physics with an e p collider would be, first and foremost, a continuation of the kind of work that has been done in the past with electron, muon and neutrino beams (with extraordinary rewards), and that it would extend the kinematical domain of such investigations by nearly two orders of magnitude in Q^2 and s. It should also be stressed that such physics is complementary to that which will be delivered by e^+e^-, pp and $\bar{p}p$ projects in the future, and that a study of lepton-hadron interactions in the domain of both space-like and time-like momentum transfers is essential for any proper understanding of the physics of elementary particles.

SESSION ON LARGE q^2 PHYSICS AND HADRON STRUCTURE

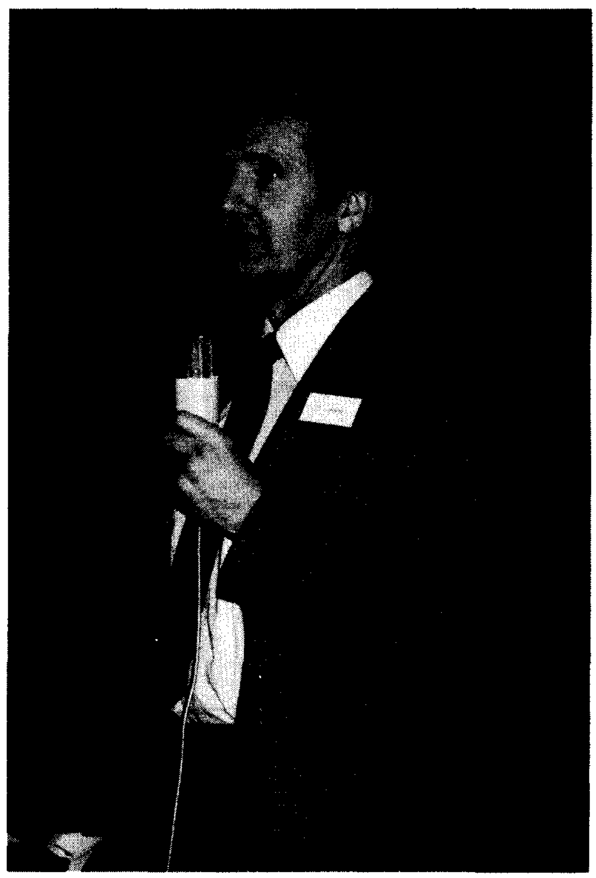

Discussion Leader: D. H. Perkins

Scientific Secretary: H. Ackermann

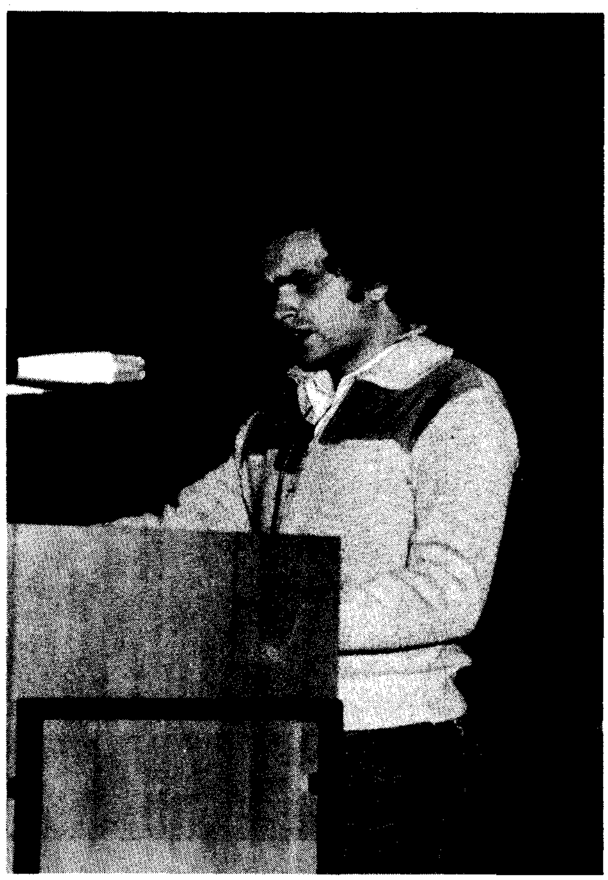

FOREWORD BY D. H. PERKINS

The working group on large q^2 and hadron structure consisted of the following:-

A. Clegg	University of Lancaster
D. Cundy	CERN
J. Dainton	University of Glasgow
J. Morfin	University of Aachen
R. Mount	University of Oxford
D. H. Perkins	University of Oxford
C. Sachrajda	CERN

The main results obtained from these studies are discussed in the following report by Sachrajda. In addition, contributions were received from physicists in other working groups. In particular, a report by Coignet on acceleration of deuterons in reproduced after the main report by Sachrajda. Following this is an edited version of the discussion session and a summary by me of the main points arising in the discussion as well as some of the open problems in this subject.

A STUDY OF PROTON STRUCTURE AT LARGE Q^2

C. Sachrajda

Report of a working group consisting of

A. Clegg, University of Lancaster
D. Cundy, CERN
J. Dainton, University of Glasgow
J. Morfin, Aachen
R. Mount, University of Oxford
D. Perkins, University of Oxford
C. Sachrajda, CERN

1. INTRODUCTION

In order to put the material of this talk in context, it instructive to consider how few of the major discoveries of experimental high-energy physics over the past 30 years or so would have been predicted in a talk such as this, many years before the machine which made the discoveries was built. Although I trust that the contents of this lecture, together with the other lectures in this session, will demonstrate convincingly that a high-energy electron proton colliding beam machine has a crucial rôle to play in our efforts to understand the interactions between elementary particles, it would be disappointing and surprising if such a machine did not find new and unexpected effects which would make us revise some of our ideas.

Two years ago two studies were published on the subject of physics at a high energy ep collider, "Physics with Large Electron-Proton Colliding Rings"[1)] by C. Llewellyn Smith and B. Wiik, and "CHEEP - An e-p facility in the SPS"[2)] edited by J. Ellis, K. Hübner and B. Wiik. We have used these two reports extensively. Since then there have been two major areas of progress:

1) We have learnt to calculate Quantum Chromodynamics (QCD) predictions for hard scattering processes; in particular we can make qualitative and quantative predictions about the final state jets. Since QCD is the only candidate for the theory of strong interactions it is imperative to test it wherever possible.

2) There has been substantial evidence for the Weinberg-Salam[3)] model of weak and electromagnetic interactions (especially the SLAC parity violation experiment) and evidence against its major competitors. As has already been discussed in Refs. 1) and 2) a high energy e-p collider will provide critical tests of our ideas about weak interactions (particularly with polarized electron and positron beams). These important tests are discussed in detail in the report of R. Cashmore in these proceedings.

In our working group we concentrated on the studies of strong interaction physics at large Q^2. As a guide we considered a 20 Gev electron beam colliding with a 270 Gev proton ring at a luminosity of $10^{32}cm^{-2}sec^{-1}$. What value of Q^2 will we be able to reach? For $Q^2 = 5000\ Gev^2$ we estimate that there will be ~ 30 electromagnetic events per day if the structure functions scale, and ~ 10 events/day if they violate Bjorken scaling in the way predicted from QCD [these rates are in agreement with those in Refs. 1) and 2)]. Thus we take $Q^2 \sim 5000\ Gev^2$ to be the largest one attainable in practice. This enables us to study proton structure down to distances of the order of $3 \cdot 10^{-16}$ cm. Similar rates are predicted for charged current reactions (the rates are a factor ~ 1.2 larger if $M_W = 63$ Gev and a factor 5 larger if $M_W = \infty$).

What about other existing or planned machines. The obvious one to compare with is the Tevatron at Fermilab. There we will have comparable rates (for both μ and ν scattering on a target of 1 ton of Hydrogen)*) for $Q^2 \sim 400$ Gev^2, assuming that there will be 10^{12} protons/second. Such a comparison indicates that with an e-p collider we will have for the study of proton structure, an order of magnitude more in Q^2.

The quantitative tests of QCD which I will present are those which are calculable in perturbation theory. It is new and exciting to be able to make quantitative predictions in strong interaction physics. A few years ago we were unable even to make these predictions, so that the field is new and we certainly do not expect to have found the best possible tests of QCD yet. In particular we are only beginning to understand to expected structure of individual jets.

At present we have no theoretical understanding of the mechanism of the confinement of quarks. Hopefully some progress will be made in this direction and then an e-p machine (with precisely one hadron involved in the collision) should be ideal for testing any new ideas, or for providing clues for their further development.

We have divided the material into two sections. Section 2 contains details of what can be learnt from studying structure functions, and Section 3 discusses studies of the final state in deep inelastic electroproduction.

2. DO STRUCTURE FUNCTIONS SCALE ?

The experimental discovery that deep inelastic structure functions approximately scale with q^2 [4)], as had been earlier predicted theoretically by Bjorken[5)], suggest that the electromagnetic and weak currents at wavelengths $\sim 10^{-14}$ cm. couple to point like constituents inside the proton, and on a time scale shorter than the characteristic one of the interactions between the constituents. This "impulse approximation" picture has since been generalized to other "deep" processes (for example massive lepton pair production in hadronic reactions, the production of particles with large transverse momenta in hadronic collisions, etc; see, for example, the reviews[6)]). Moreover the experimental observation that

---

*) From the point of view of the physics discussed later we considered this to be the fairest comparison.

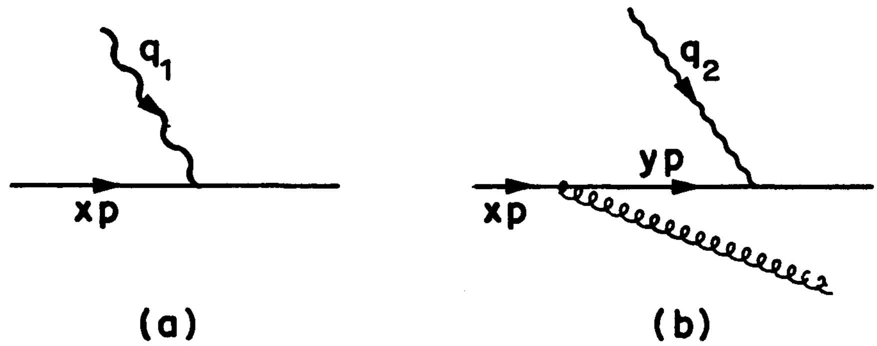

Fig. 1 : As q^2 increases a quark (a) is resolved into a quark and a gluon (b).

$\sigma_L << \sigma_T$ implies that the constituents to which the electromagnetic and weak currents couple have spin ½. I think it is fair to say that during the time when these sim-simple scaling parton ideas were being formulated, it was hoped that the partons interact by means of some quantum field theory, and that if we could find the theory and calculate its predictions for these deep processes we would find that the parton model results are approximately satisfied. We now have a candidate theory of the strong interactions (QCD), in which the impulse approximation does not hold, nevertheless in which the behaviour of the structure functions with q^2 is calculable and is found to be only logarithmic. QCD is an asymptotically free theory*) $[g(\mu^2) \to 0$ as $\mu^2 \to -\infty$, where μ is the renormalization point$]$, whereas theories which are not asymptotically free have structure functions which violate scaling by powers of q^2. Thus the study of the behaviour of structure functions with q^2 provides vital information about strong interaction dynamics.

Let us see what we would expect to happen qualitatively as q^2 increases. Imagine that with a current of momentum q_1^2 we probe the proton and find a quark with a fraction x of the proton's momentum p [Fig. 1 a)]. If we now increase q^2 (to q_2^2 say) we have a finer resolution probe and may discover that the "quark" is in fact a quark of momentum $yp (y < x)$ and a gluon with momentum $(x - y)p$ [Fig. 1 b)]. Thus we expect to find that $F(x,q^2)$ decreases with q^2 at large x and increases at small x. This phenomenon has indeed been seen in ep, μp and νp[8] experiments, and is predicted to continue. Quantitatively the predictions of QCD are particularly simple when expressed in terms of the moments of structure functions defined by

---

*) In fact the only asymptotically free theories are non-Abelian gauge theories such as QCD [7].

$$M^N(q^2) \equiv \int_0^1 dx\, x^{N-1} F(x, q^2) \tag{1}$$

and the predictions are that

$$M^N(q^2) = A^N_{NS} \left(\ln q^2/\Lambda^2\right)^{-\gamma^N_{NS}} + A^N_+ \left(\ln q^2/\Lambda^2\right)^{-\gamma^N_+} + A^N_- \left(\ln q^2/\Lambda^2\right)^{-\gamma^N_-} \tag{2}$$

where γ^N_+, γ^N_- and γ^N_{NS} are calculable positive numbers[9)], whereas Λ, A^N_{NS}, A^N_+ and A^N_- have to be determined from the data[*)]. They can be determined from existing deep inelastic scattering data, enabling us to predict the moments and hence the structure functions at higher values of q^2.

Figure 2 shows the predicted behaviour of the structure function F_2^{ep} [**)] as a function of x at four different values of q^2 [10)]. We see very clearly the expected feature of the decrease with q^2 at large x and the increase at small x. The curves of Fig. 3 show the predictions for the evolution of the structure function F_2 with q^2 at four different values of x. They are taken from Ref. 11) which is an independent analysis (from that of Martin which produces Fig. 2), the two analyses agree. The curves of Fig. 3 show a very slow variation with q^2. The normalization conditions (required to determine the A^NS' of Eq. 2) are chosen such that at $q^2 = 4$ Gev^2 the quark and gluon distributions used in the analysis of Martin[10)] (Glück and Reya[11)]) are:

$$x\left[u_v(x) + d_v(x)\right] = \frac{3}{B(\alpha_3, \alpha_4+1)}\, x^{\alpha_3} (1-x)^{\alpha_4} \tag{3a}$$

where $\alpha_3 = 0.65$ (0.624) and $\alpha_4 = 3$ (2.657)

$$x\, d_v(x) = \frac{1}{B(\alpha_1, \alpha_2+1)}\, x^{\alpha_1} (1-x)^{\alpha_2} \tag{3b}$$

---

*) The A's depend on which structure function is being measured whereas the γ's do not. The A's for different structure functions are related in a calculable way.

**) Here we give the results for electromagnetic structure functions. Similar predictions exist for the charged current structure functions (see the talks of R. Cashmore and P. Innocenti).

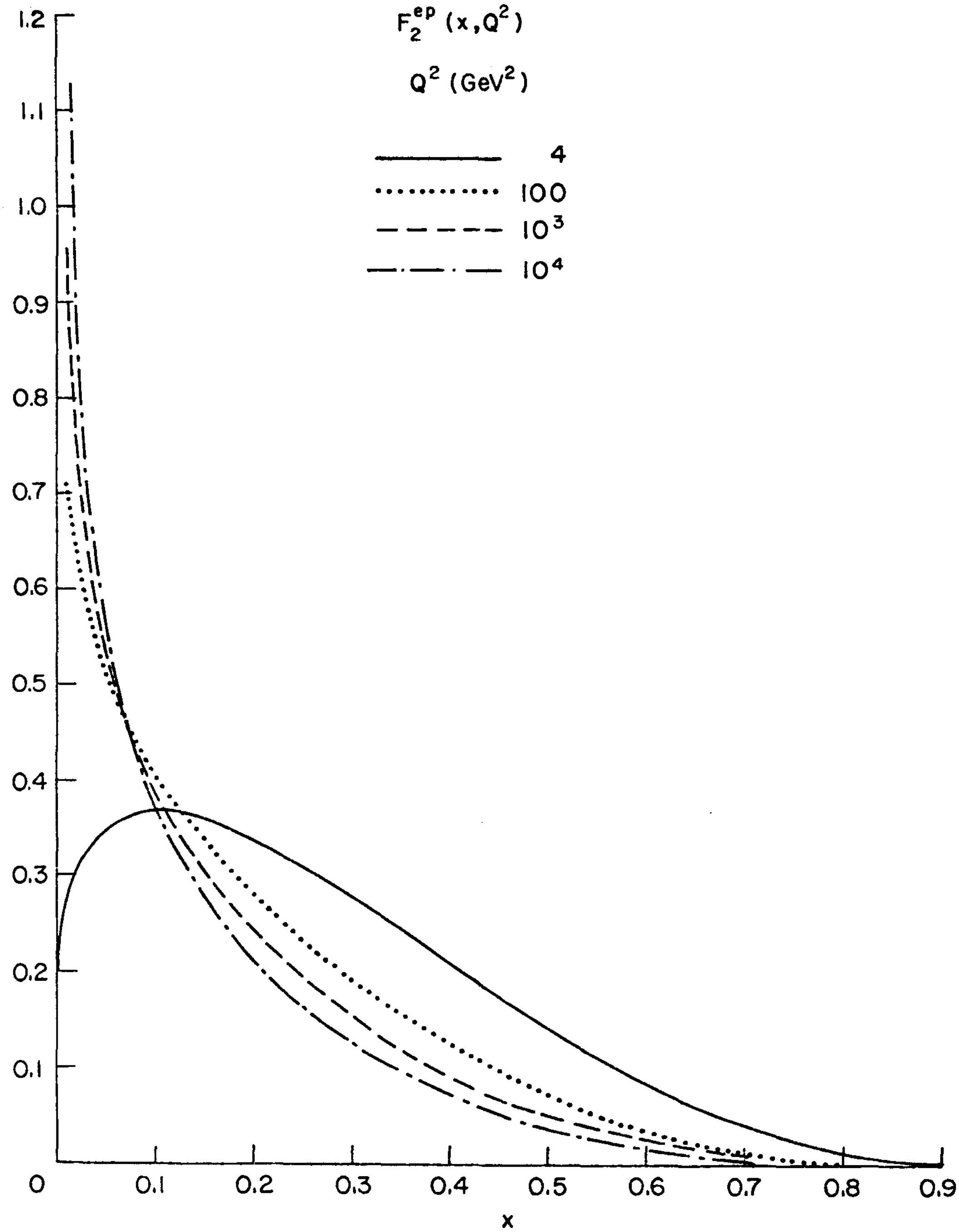

Fig. 2 : The predicted behaviour of $F_2^{ep}(x,Q^2)$ as a function of x for four different values of Q^2.

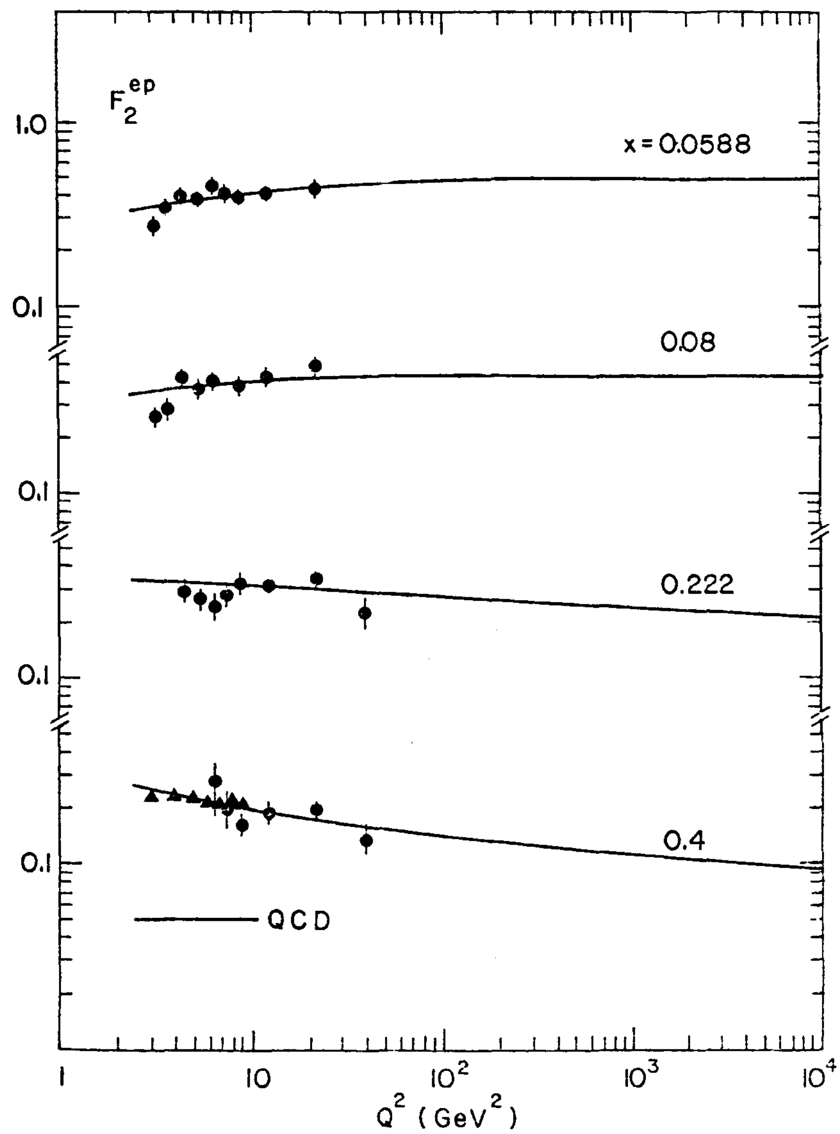

Fig. 3 : The predicted behaviour of $F_2^{ep}(x,Q^2)$ as a function of Q^2 for four different values of x. The data are from Refs 12) and 13).

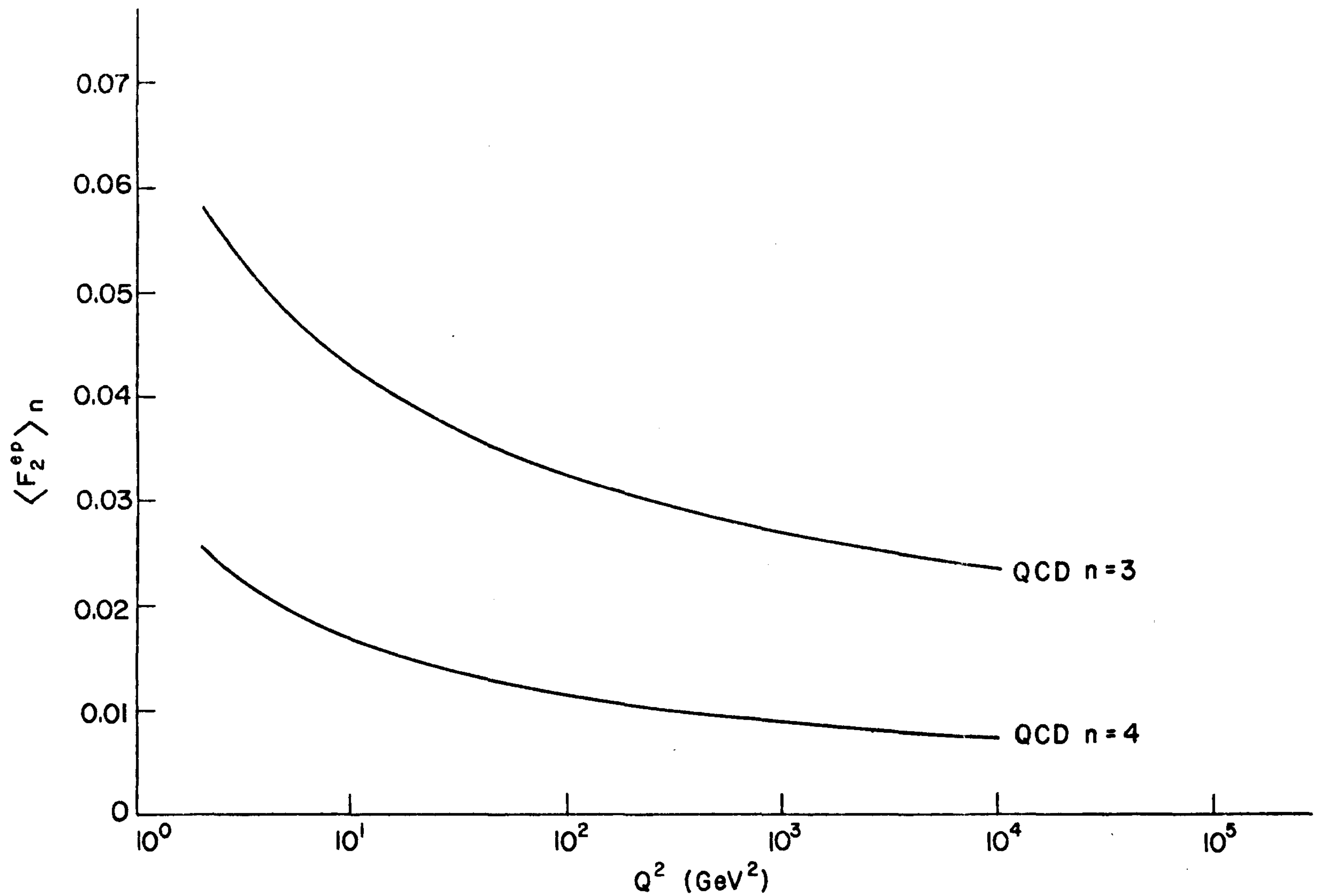

Fig. 4 : QCD predictions for the third and fourth moments of F_2 as a function of q^2.

where $\alpha_1 = 0.89\ (0.773)$ and $\alpha_2 = 3.78\ (3.7)$

$$xG(x) = 2.425\,(1-x)^4 \quad \left(2.6\,(1-x)^5\right) \tag{3c}$$

$$x\bar{u}(x) = x\bar{d}(x) = 0.15\,(1-x)^7 \quad \left(0.17\,(1-x)^7\right) \tag{3d}$$

$$xs(x) = 0.06\,(1-x)^7 \quad \left(0.17\,(1-x)^7\right) \tag{3e}$$

and

$$xc(x) = 0.02\,(1-x)^7 \quad \left(0.05\,(1-x)^{30}\right) \tag{3f}$$

where u, d, s, c stand for up, down strange and charmed quark distributions, and G stands for the gluon distribution. The parameter Λ was taken to be 500 Mev. Fig. 4 shows the QCD prediction[14)] for the third and fourth moments of F_2 as a function of q^2, the moments fall logarithmically with q^2.

When F_2^{ep} will be measured either:

i) the data will agree with the predicted curves [Figs 2)-4)] or

ii) it will not.

Both cases will be very interesting. If (1) would be true we would have the striking feature that quarks look like point-like elementary objects from Q^2 of 10 Gev^2 to $5\cdot10^3$ Gev^2 (or higher). Would this mean an unambiguous triumph for QCD ? To answer this question we would have to be able to calculate predictions for scaling violations in other theories, in particular, in fixed point theories [$g(\mu^2) \to g^*$ as $\mu^2 \to -\infty$, $g^* \neq 0$ or ∞]. For fixed point theories we can only proceed if for some unknown reason g^* is small. In this case the moments of the structure functions fall with q^2 like a small power of q^2, and not logarithmically as in QCD. Glück and Reya[*)] have carried out a systematic study of possible fixed point theories and find no candidates which survive comparison with existing data. It may be of course that the true theory of strong interactions is different from any of those considered so far. The fixed point theories have the feature that $\int_0^1 F_2(x,q^2)dx$ should increase with q^2 (up to a predicted asymptotic value), whereas resent measurements[8),13)] show that it decreases. We see thus that studies of the violations of Bjorken scaling provide important tests of theories of strong interactions and QCD in particular.

---

*) Revised version of Ref. 11) (Feb. 1979). The original version had a different conclusion.

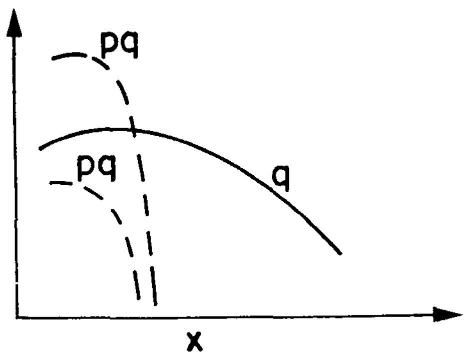

Fig. 5 : If quarks have substructure, the distribution of pre-quark (pq) is expected to be prominent at smaller X than that of quarks (q).

If the data did not reproduce the QCD predictions of Figs 2)-4) the situation would be more interesting. Here obviously we can only speculate*) as to the possible sources of derivations from the QCD predictions. We could of course just have the wrong theory of strong interactions, in which case we want experimental evidence of this and scaling violations provide a good test of our theory.

It is also possible that at the very small distances studied in these machines quarks will no longer look point-like, but will turn out to be composite. We would then expect the usual situation of a resonance region of excited quark states (q^*) for W^2 not too much above threshold, merging into a continuum region for large W^2. It is doubtful whether the resonance peaks will be observable (due to "fermi-motion" of the quarks inside the nucleon), but the q^* may appear as a high mass, very wide jet. Since each subquark carries only a fraction of the quarks longitudinal momentum, the structure functions should be peaked at small x (see Fig. 5). The normalisation of the structure function depends on (among other things) the charges of the subquarks, e.g.,

$$\text{a)} \quad u \to 3u_s\left(Q=\tfrac{2}{9}\right) \Rightarrow Q_u^2 = \tfrac{4}{9} \to \Sigma\, Q_{u_s}^2 = \tfrac{4}{27} \tag{4}$$

$$\text{b)} \quad u \to u_s\left(Q=\tfrac{4}{3}\right) + 2u_s\left(Q=-\tfrac{1}{3}\right) \Rightarrow Q_u^2 = \tfrac{4}{9} \to \Sigma\, Q_{u_s}^2 = 2$$

*) See also the talk of R. Cashmore in these Proceedings.

Although this is very speculative, it would be extremely exciting and unexpected to discover quark structure. Present attempts to unify strong, weak, and electromagnetic interactions assume that quarks and leptons are elementary up to scales of the order of the Plank mass.

Another property which is often attributed to the strong interactions which may not be true is that colour is our exact symmetry. It is possible that at sufficiently short distances the colour degrees of freedom are excited and that fractionally charged quarks are resolved into averages over integrally charged quarks of different colours. For example the u and d quarks are resolved as follows

$$\begin{aligned} u\left(Q=\tfrac{2}{3}\right) &\rightarrow u_R(Q=1),\ u_Y(Q=1),\ u_B(Q=0) \\ d\left(Q=-\tfrac{1}{3}\right) &\rightarrow d_R(Q=0),\ d_Y(Q=0),\ d_B(Q=-1) \end{aligned} \tag{5}$$

so that the electroproduction cross-section would rise substantially above colour threshold, e.g., for the u and d quark distributions

$$\begin{aligned} \left(\tfrac{2}{3}\right)^2 u(x) &\rightarrow \tfrac{1}{3}\left(1^2+1^2+0^2\right) u(x) = \tfrac{2}{3} u(x) \\ \left(-\tfrac{1}{3}\right)^2 d(x) &\rightarrow \tfrac{1}{3}\left(0^2+0^2+1^2\right) d(x) = \tfrac{1}{3} d(x) \end{aligned} \tag{6}$$

In the simple valence quark approximation $u(x) = 2d(x)$ the electroproduction cross-section would rise by $\sim$ 67% as the colour threshold was crossed.

The longitudinal Structure Function F_L:

Once we have determined A^N_{NS}, A^N_+ and A^N_- [see Eq. (2)] from the measurements of νW_2 for example, we can predict cleanly any other structure function, including the longitudinal one F_L. This is expected to be very small (in QCD it is down by a factor of $\log Q^2$ relative to νW_2) so that if our ideas are correct, the experimental measurements will only be able to set an upper bound on F_L. This of course has to be checked, especially since the theoretical predictions[15)] at presently accessible values of q^2 tend to lie below the data[16)] (which, it should be pointed out, has enormous error bars).

Structure Function of a Pion[17)]

The e-p colliding beam facility would give us the possibility to measure the structure function of a (slightly virtual) pion[18)], by means of the reaction

$$e + p \rightarrow e' + n + X$$

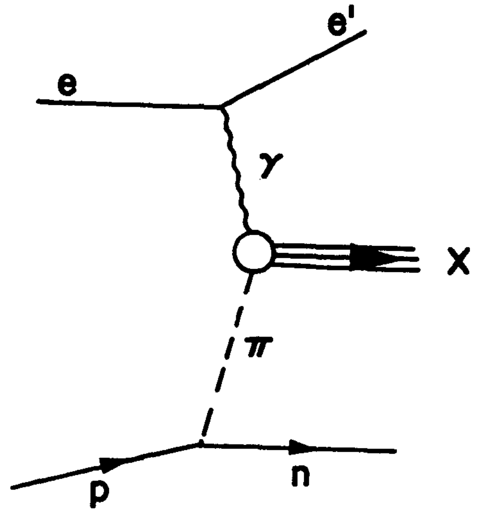

Fig. 6 : The reaction $e + p \to e' + n + X$

where the momentum transfer between the proton and the neutron is small (see Fig. 6). The experiment can be performed detecting the highly energetic, nearly forward neutrons with a calorimeter placed far away from the interaction region, in coincidence with the electron detector. For the 20 GeV electron on 270 GeV proton case, for $|t| < 0{\cdot}5$ one has θ_n (where θ_n is the angle at which the neutron emerges, relative to the beam direction at the interaction point) $< 3{\cdot}10^{-3}$ and E_n (the energy of the neutron) $\gtrsim 130$ GeV. The scaling variable for the photon-"pion" inclusive deep inelastic scattering $x_\pi \equiv -q^2/2q\cdot(p_p - p_n)$ lies in the range $2x \lesssim x_\pi \leq 1$. Figure 7 show the p_n versus θ_n distribution for typical values of q^2 and x obtained by a Monte Carlo generation, bands corresponding to constant x_π and constant $|t|$ are also shown. In obtaining these curves, a triple-Regge parametrization for the hadronic vertex and a model for the pion structure function[19)] were used. The estimate for the counting rates indicates that this process should be measurable at least for $Q^2 \lesssim 100$ GeV^2.

A hadronic calorimeter with a radius of one metre, placed at a distance of $\sim$ 300 m from the interaction region, covers all the solid angle corresponding to small ($\lesssim 0.6$ GeV^2) $|t|$. Moreover a vertex reconstruction of the hadronic shower with an error of $\sim$ 5 cm entails a very good accuracy in the angular determination (comparable with the divergence of the beam).

From the figures we see that the pion structure function should be determined fairly well in the small x_π region, and somewhat less accurately in the large x_π region. It will be interesting to compare the results of this determination with the implicit one using the reaction[20)]:

$$\bar{\pi}p \to \text{Massive Lepton Pair} + X$$

which assumes the Drell-Yan mechanism as being responsible for the production of the massive lepton pair.

The measurement of this process is much more difficult using a fixed target machine, because in this case one should detect recoiling neutrons of low momentum ($\lesssim$ 700 MeV) spread over a large solid angle.

Measuring the Structure Function of Deuterium[21)]

An interesting possibility to bear in mind is the possibility of accelerating deuterons in the proton ring, thus doubling the luminosity. This gives us access to en physics in a cleaner way than a in fixed liquid deuterium target, since the detection of the spectator proton allows for a clean signature of the process. Knowledge of both the proton and neutron structure functions provides us with substantial information about the u and d quark distributions seperately, perhaps giving us some insight into the confinement mechanism.

If we know both the proton and neutron structure functions, we can check perhaps the simplest QCD predictions, those for the difference $F_2^p - F_2^n$. The sea gluon contributions to this difference cancel, which simplifies the theory $[A_+^N = A_-^N = 0$ in Eq. (2)$]$.

In QCD from the combination $F_2^p + F_2^n$ we can extract the gluon distribution[22)], and this is important to make predictions for other hard scattering processes (such as massive lepton-pair production, or the production of particles at large transverse momentum in hadronic collisions). To a good approximation the gluon distribution (G) is obtained from the relation

$$Q^N(Q^2) = Q^N(Q_0^2)\left[\alpha_N e^{-\gamma_-^N s} + (1-\alpha_N) e^{-\gamma_+^N s}\right] + G^N(Q_0^2)\left[\beta_N e^{-\gamma_-^N s} - \beta_N e^{-\gamma_+^N s}\right] \qquad (7)$$

where α_N, β_N are calculable numbers, $s = \ell n\,[\alpha(q_0^2)/\alpha(q^2)]$ and $Q^N(G^N)$ are the N^{th} moment of $F_2{}^p + F_2{}^n(G)$. Measurement of Q^N at two different values of Q^2 enables us to determine $G^N(Q_0^2)$.

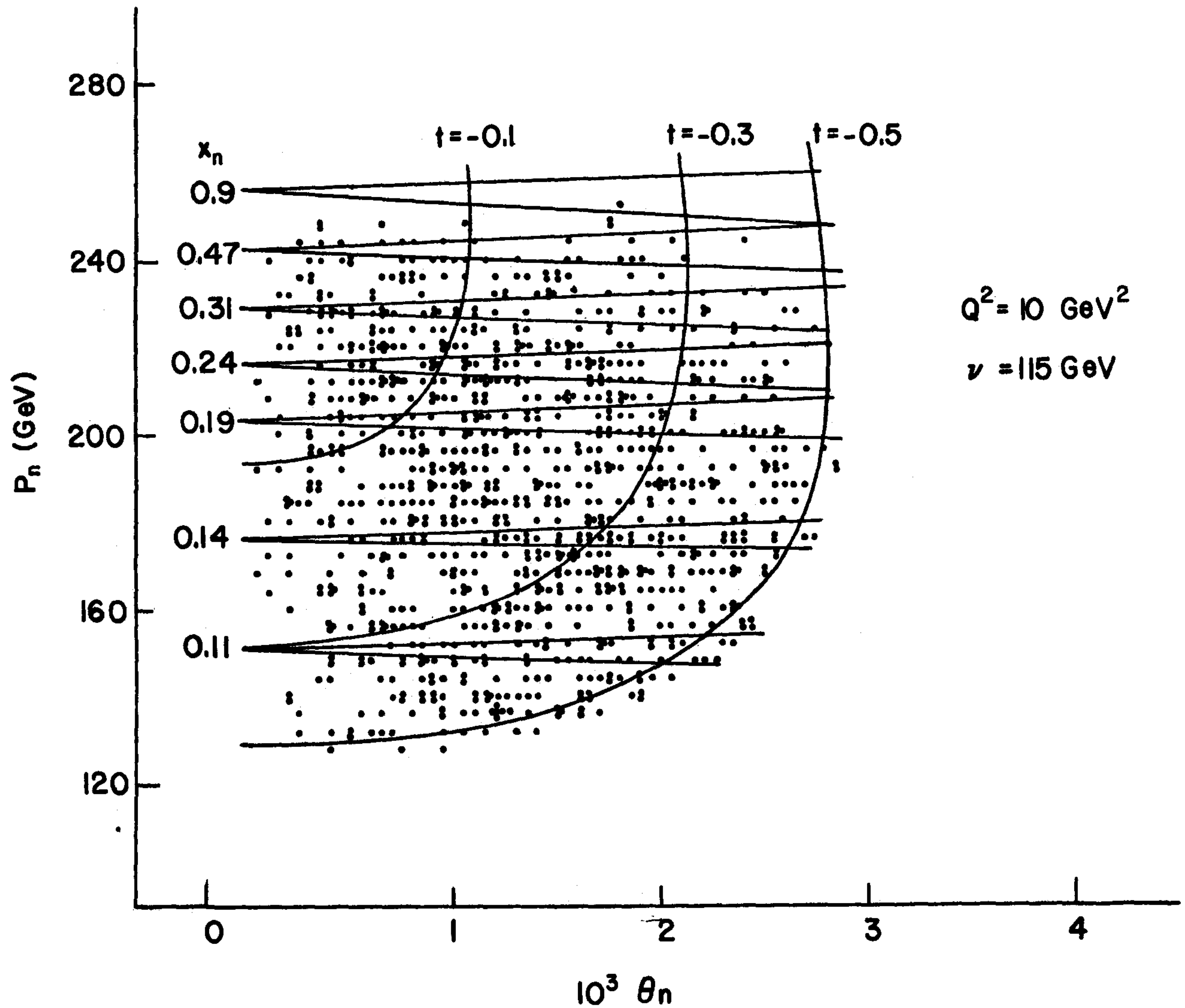

Fig. 7a : Distributions of p_N vs θ_N for typical values of q^2 and X.

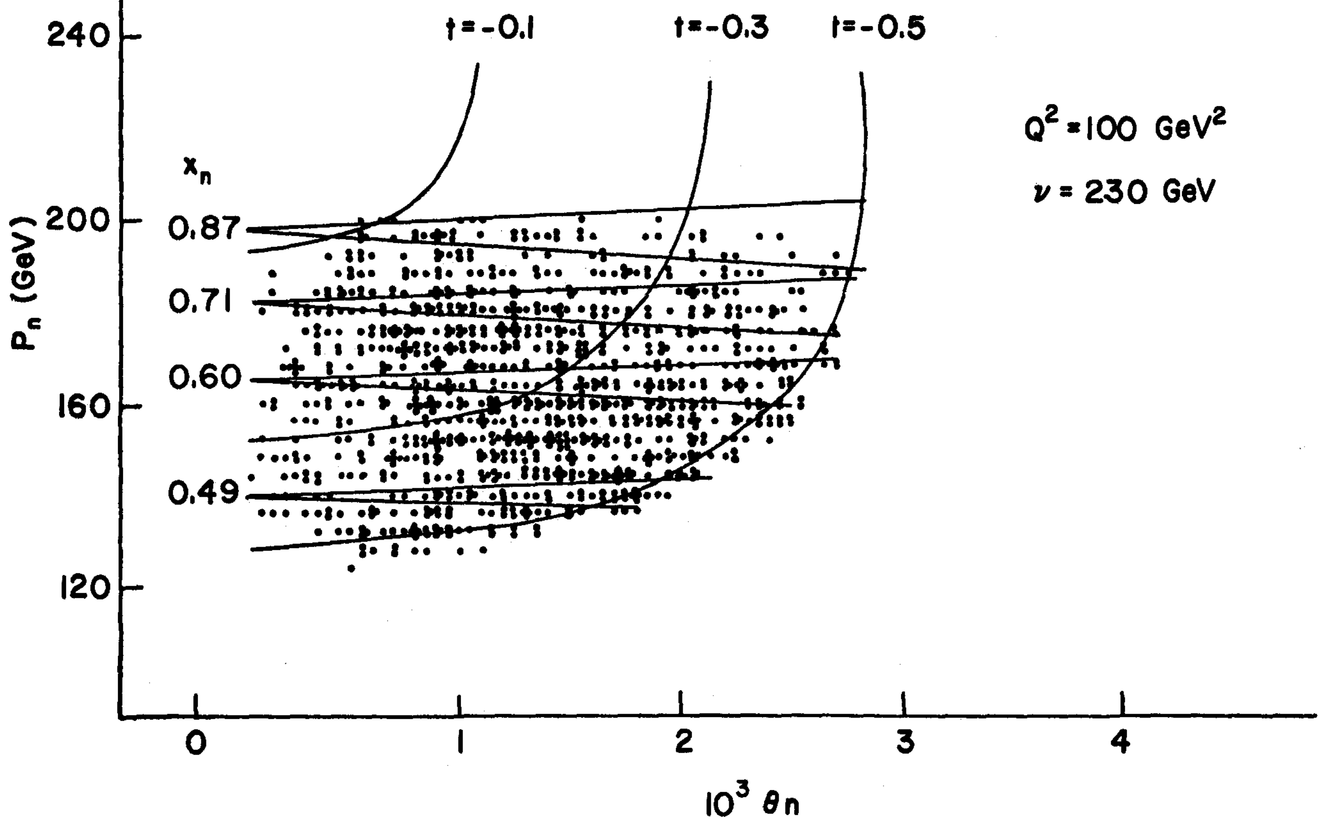

Fig. 7b : Distributions of p_N vs θ_N for typical values of q^2 and X.

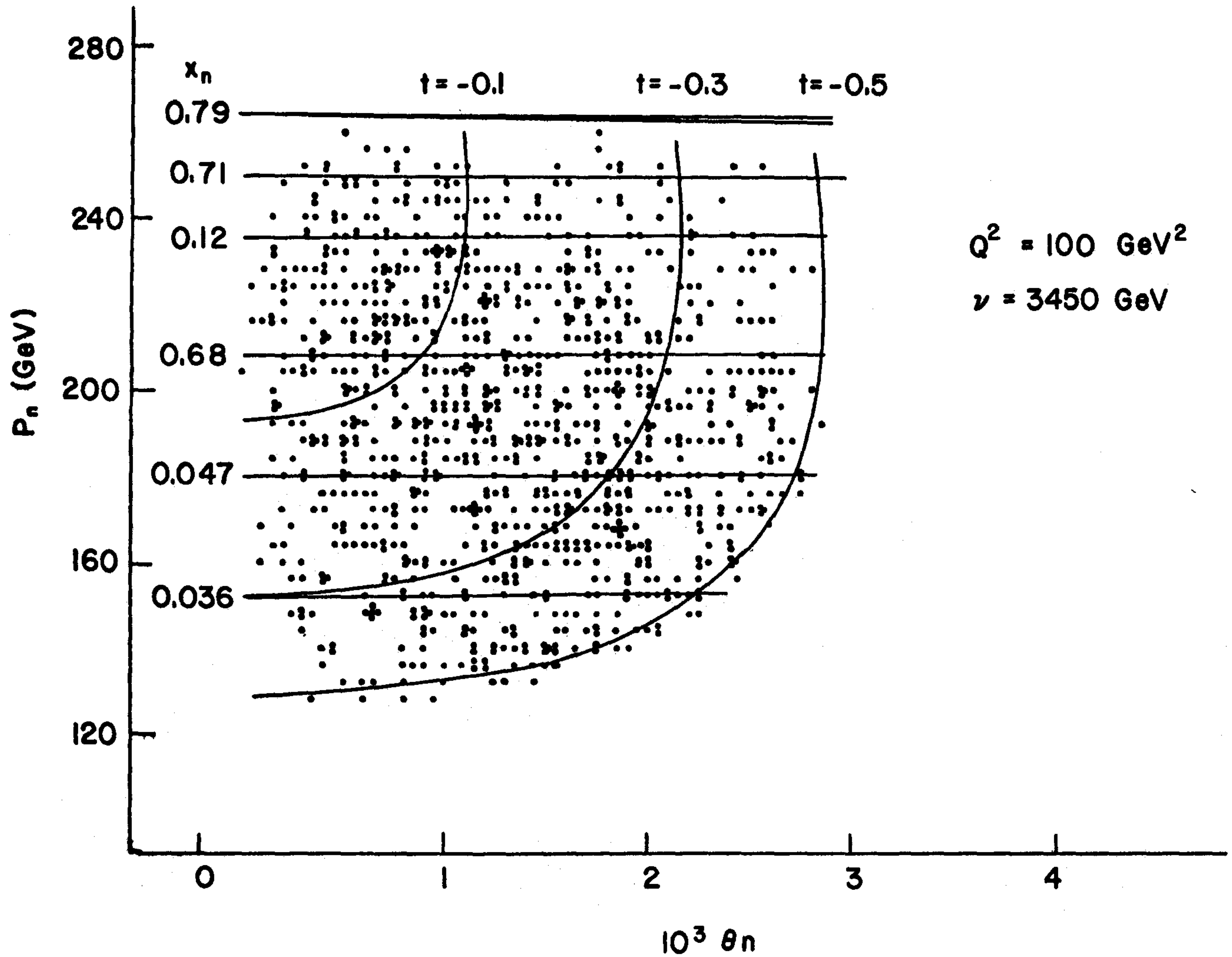

Fig. 7c : Distributions of p_N vs θ_N for typical values of q^2 and X.

3. STRUCTURE OF THE FINAL STATES IN DEEP INELASTIC ELECTROPRODUCTION

In hadronic physics transverse momenta are typically much smaller that longitudinal ones, indeed it was long thought that

$$\langle p_\perp \rangle \sim 300 \text{ MeV} \tag{8}$$

independently of the longitudinal momenta. As an example consider the process $e^+e^- \to$ hadrons. What we would naively expect (Fig. 7) is that we should observe two jets of hadrons with a $1 + \cos^2\theta$ distribution relative to the incident lepton direction, and that the average transverse momentum of the particles within a jet should be $\sim$ 300 MeV. This is exactly what is observed, using a sphericity analysis, at SPEAR[23)]. Such a transverse momentum cut-off is characteristic of "soft" field theories, i.e., ones in which the coupling constant has dimensions of mass, and in the parton model this phenomenon was put in by hand. QCD (like any other renormalizable quantum field theory) is not a soft field theory, and indeed we expect that the average p_T^2 of particles in a jet should grow with Q^2 like

$$\langle p_\perp^2 \rangle \sim \alpha(Q^2) \cdot Q^2 \tag{9}$$

In addition we expect a smearing in transverse momentum due to the hadronization process, this smearing is not calculable in perturbation theory, and by itself is expected to be responsible for (8). When the right-hand side of (9) (together with the constant of proportionality) is evaluated at SPEAR energies we find it is less than the 300 MeV, so that here the transverse momentum distribution of hadrons in a jet is still dominated by non-perturbative effects. As Q^2 increases however the perturbative contribution becomes relatively more important until at least the large p_T tail of the transverse momentum distribution is dominated by calculable perturbative contributions.

This broadening in p_T is an important consistency condition for QCD to satisfy. It should already be observed (?) at PETRA-PEP, but there the standard jet analyses [24)] will be complicated by new thresholds (perhaps) and decays of heavy mesons (D's, B's, etc.).

In spite of the fact that I will present only a few quantitative predictions here, it will become clear that a high energy electron-proton collider will be an excellent machine for detailed studies of the predictions of QCD (or any other theory) concerning the nature of jets. Both in the parton model and in QCD the

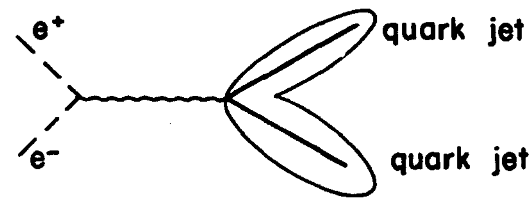

Fig. 8 : Expected two jet structure, observed at SPEAR.

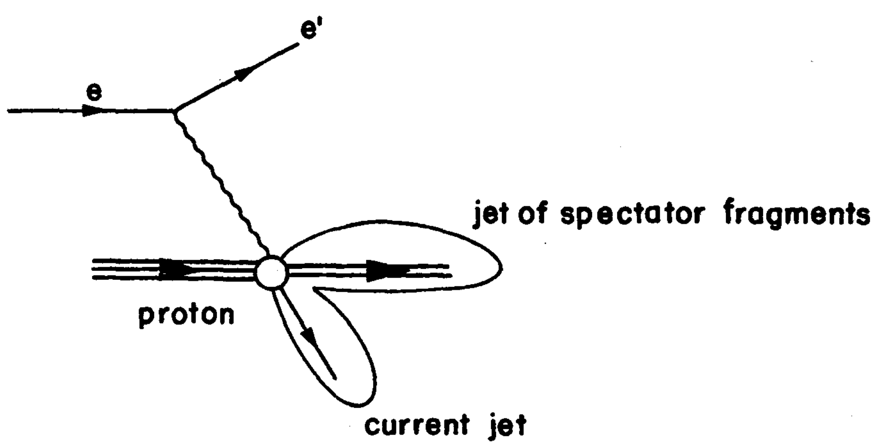

Fig. 9 : Two Hadronic Jet Structure expected to be dominant in deep inelastic scattering.

hadrons are predominantly expected to emerge in two jets, the current jet and the jet of proton spectator fragments (Fig. 9). In spite of the fact that the electron energy is so much smaller than the proton energy the kinematics is such that the two jets can be distinguished throughout most of phase space. This has been discussed in detail in the CHEEP report[2)] and we will not repeat the discussion here. The salient features can be seen in Fig. 10, from which we can read off the angle at which the current jet would emerge for various values of x and q^2.

Perhaps the first thing we would like to know is whether the current jet at such high energies is a "fixed p_T" jet as whether the expected "p_T broadening" discussed above occurs. The effect should be very striking. In Fig. 11 we show the expected distribution of the hadronic energy of the current jet per unit angle[*)] in a limited transverse momentum model and in a QCD motivated model for a typical event at the 20 GeV on 270 GeV machine. The current jet in the two models looks completely different and so there should not be any difficulty in distinguishing between them. We are only beginning to understand the QCD predictions concerning the nature of quark and gluon jets [see e.g. Ref. 25)] by the time we have a high energy electron-proton machine, more sophisticated predictions than the one in Fig. 11 will be available.

Many interesting studies can be made in the small cross-section region, where more that two hadronic jets emerge. Before QCD we would have expected such processes to be heavily suppressed (like an exponential or a power of q^2) relative to the two jets ones, in QCD however they are only suppressed by a factor of $\alpha(q^2) \sim 1/(\log q^2/\Lambda^2)$. Here we will present a few examples.

Let us work in the rest system of the final state hadrons and define

$$W^2 \equiv (p+q)^2 \tag{10}$$

and

$$x_i = \frac{2E_i}{W} \tag{11}$$

where E_i is the energy of the i^{th} hadron. The variable Thrust[26)] is defined by

---

*) Not per unit solid angle. This accounts for the dip at small angle.

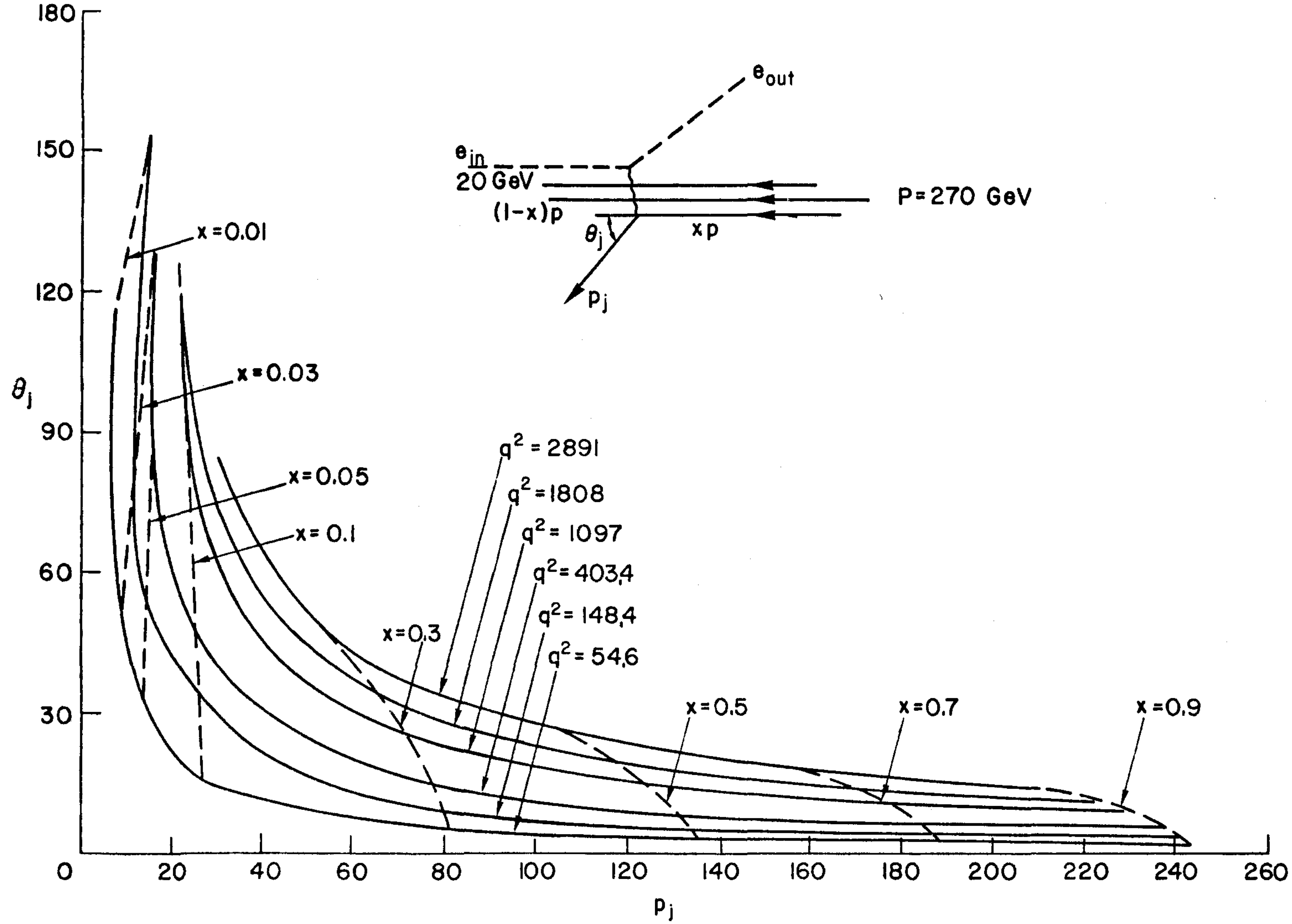

Fig. 10 : The angle at which the current jet emerges, plotted as a function of its momentum.

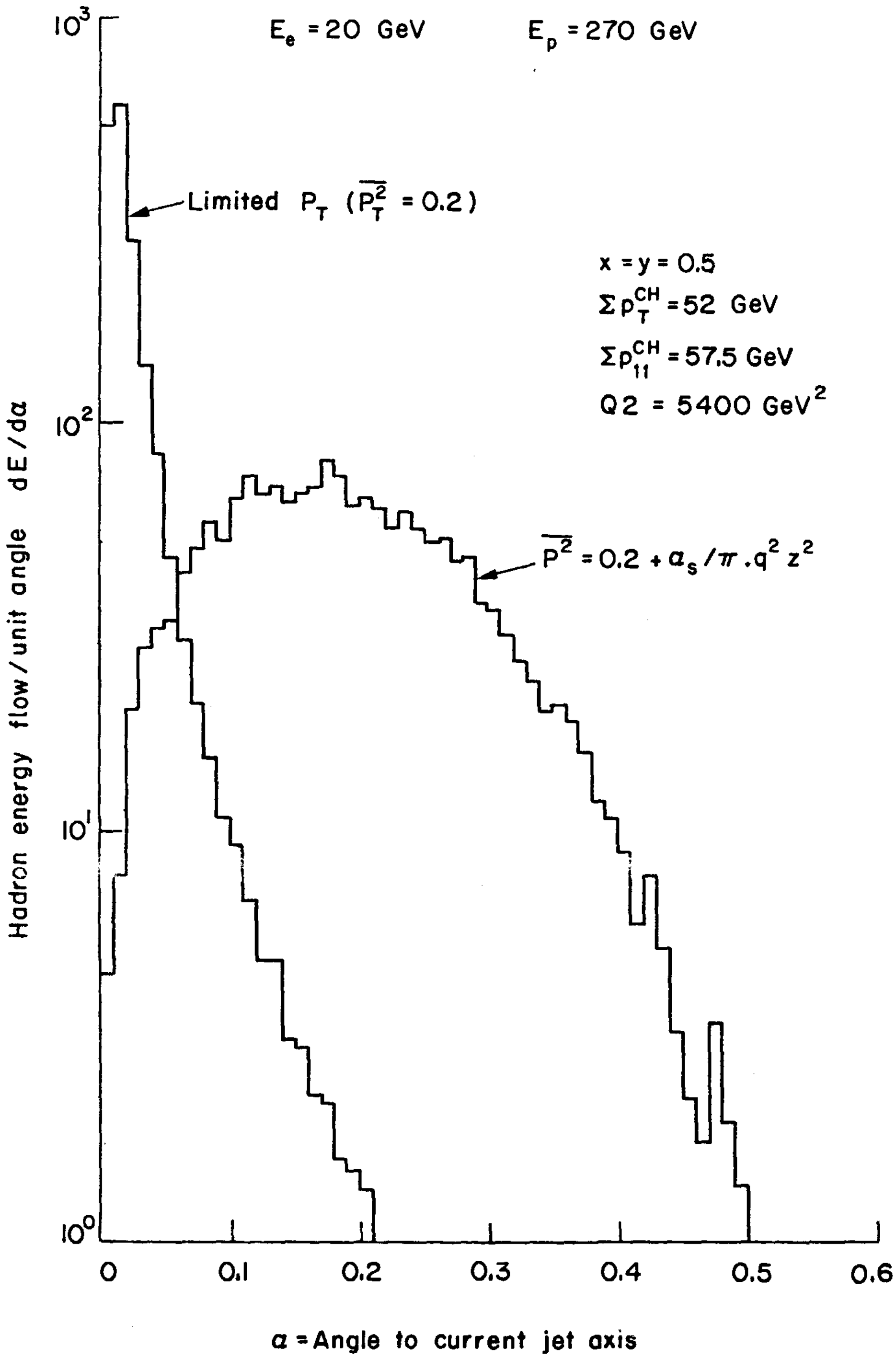

Fig. 11 : Energy flow/unit angle for a limited p_T and a QCD motivated model.

$$T = 2 \max \frac{\sum_i^{\sim} p_\parallel^i}{\sum_i |p_i|} \tag{12}$$

where the sum in the denominator runs over all final state hadrons. The $p_\parallel$'s are the components of p_i along the jet axis , the jet axis defines two hemispheres and the sum in the numerator runs over all particles in one hemisphere. The maximization is over all jet axes. If we have only two particles (or two jets with zero spread in transverse momentum) in the final state then the thrust distribution will be a δ-function at $T = 1$. If we have three particles (or three jets with zero spread in transverse momentum) then

$$T = \max (x_1, x_2, x_3) \tag{13}$$

and is restricted by kinematics to lie in the range

$$\frac{2}{3} \leq T \leq 1 \tag{14}$$

Naively therefore we would expect that if we want to study three (or more) jet events, we should look at events which have $T < 1$. However we have also to include the non-perturbative effects due to the hadronization process, and although these give only a finite p_T spread, nevertheless they smear out the δ-function at $T = 1$ for two jet events. Thus we can obtain $T < 1$ events for two reasons:

i) gluon bremsstrahlung which is present in QCD and is calculable, which gives a transverse momentum spread which increases with W^2;

ii) the hadronization process by which quarks and gluons materialize as hadrons, which is not calculable in perturbation theory but in which the transverse momentum spread is expected to remain constant with W^2.

When we look at the thrust distributions (for $T < 1$) from existing neutrino data[27] (Fig. 12) we find that they lie considerably above the predictions from QCD (effect (i) above)[28]. Moreover with a simple reasonable model for hadronization (effect (ii) above) the data can be fairly well understood. This indicates that for presently accessible values of W^2 we have no real test of QCD predictions.

As we increase W^2 however the QCD contribution to the thrust distribution (for $T < 1$) becomes relatively more important until finally a significant part of the thrust distribution becomes completely predictable. This is extremely exciting,

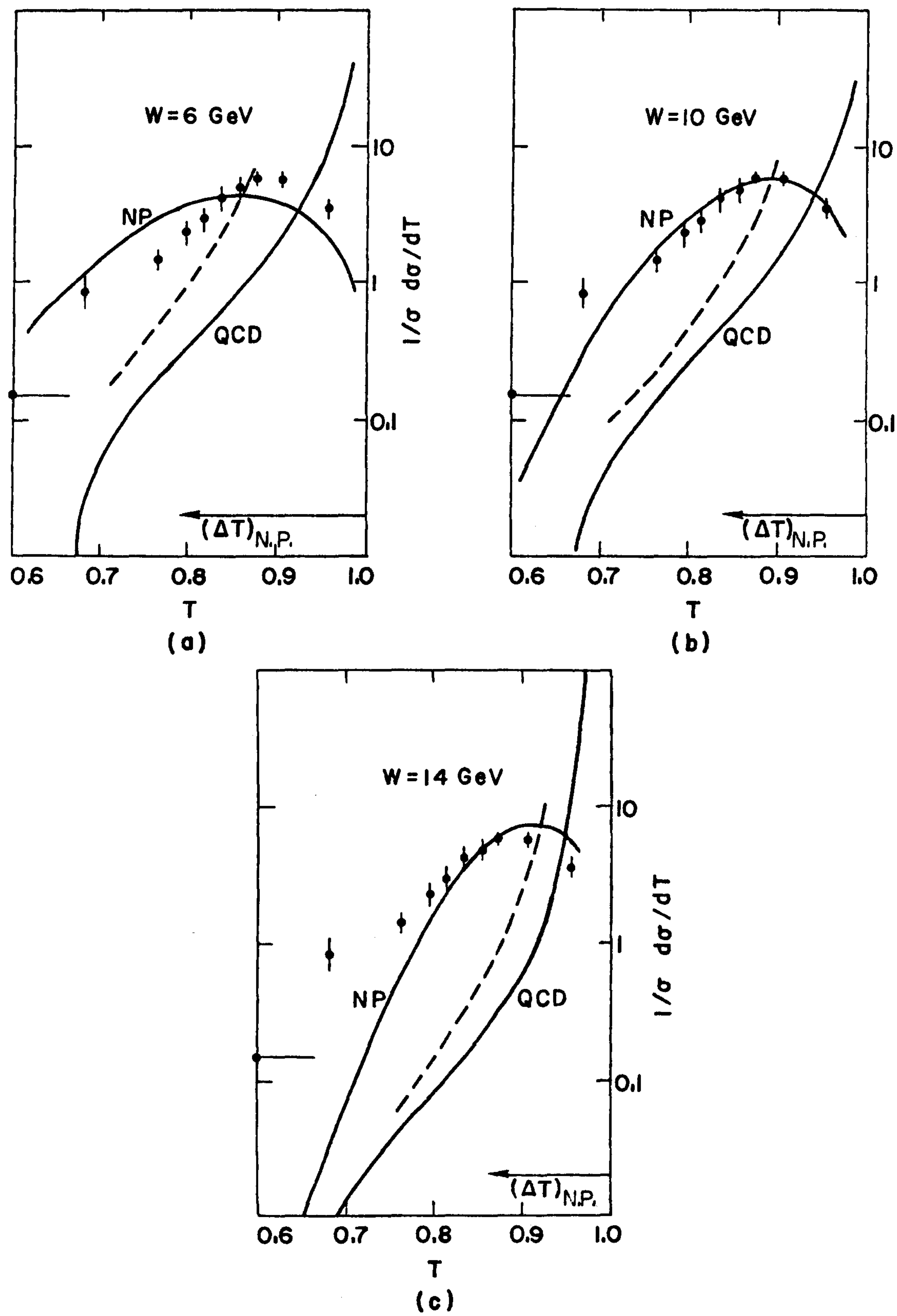

Fig. 12 : $(1/\sigma)$ $(d\sigma/dT)$ for various values of W integrated over $Q^2 \geq 1$ GeV^2. The Data are form Ref. 26). NP stands for the non-perturbative two jet contribution. The dashed curves correspond to the QCD contributions smeared over T bins of width $(\Delta T)_{NP}$ indicated at the bottom of the figure.

it is only relatively recently that we have learnt how to make quantitative predictions for measurable quantities in strong interaction physics. In Fig. 13 we show the predictions[29)] for a machine with 25 GeV electrons colliding with 400 GeV protons. We see that very important and stringent tests of QCD will be possible, particularly at small x where there are more events.

These sorts of tests of QCD will be easier to perform in an electron-proton machine than in an electron-positron machine due to the presence of thresholds and heavy resonances in the e^+e^- case. Resonances which are produced just above threshold decay in a way which leads to a more isotropic distribution of hadronic energy than expected from the calculable quark and gluon subprocesses. As an example we show in Fig. 14, which is taken from Ref. 30), the expected thrust distribution in e^+e^- annhialation at a centre of mass energy of 20 GeV. We see that at this energy the (expected) presence of B mesons (i.e., those which contain a b quark) and their decays make it impossible to study pure QCD effects. The study of QCD jets in e^+e^- annihilation is complicated be the presence of heavy resonances and quarks, a complication which we will not have in ep machines.

Another way to study three jet events is by means of the Pointing (not Poynting) vector[24)]. This is defined as follows:

i) Find the thrust axis $\underline{e}$, i.e., the jet axis which maximizes $\tilde{\sum}_i (p^i_\parallel)/\sum_i (\underline{p}_i)$ in Eq. (12).

ii) The plane normal to the thrust axis divides phase space into two hemispheres, one of which contains the smaller amount of $\sum_i |p^i_T|$. Define as $\theta = 0$ the $\underline{e}$ direction in that hemisphere.

iii) Find the plane containing $\underline{e}$ with respect to which the perpendicular momentum is minimized. The angle θ is to be measured in this "event-plane".

iv) Finally, to choose with which sense (clockwise or anticlockwise) θ should increase, proceed as follows: the $90^0 < \theta < 180^0$ quadrant is distinguished from the $180^0 < \theta < 270^0$ quadrant by choosing the former to be that which has the greater $\sum_i |\underline{p}^i_p|$, where $\underline{p}^i_p$ is the projection of the three momentum of the i^{th} particle onto the event plane.

Thus each event must be rotated so that its $+\underline{e}$ direction is at $\theta = 0^0$. The simple particle Pointing vector is then defined by

$$P_i = \frac{1}{\sigma} |\underline{p}_i| \frac{d\sigma}{dT\, d\cos\theta} \tag{15}$$

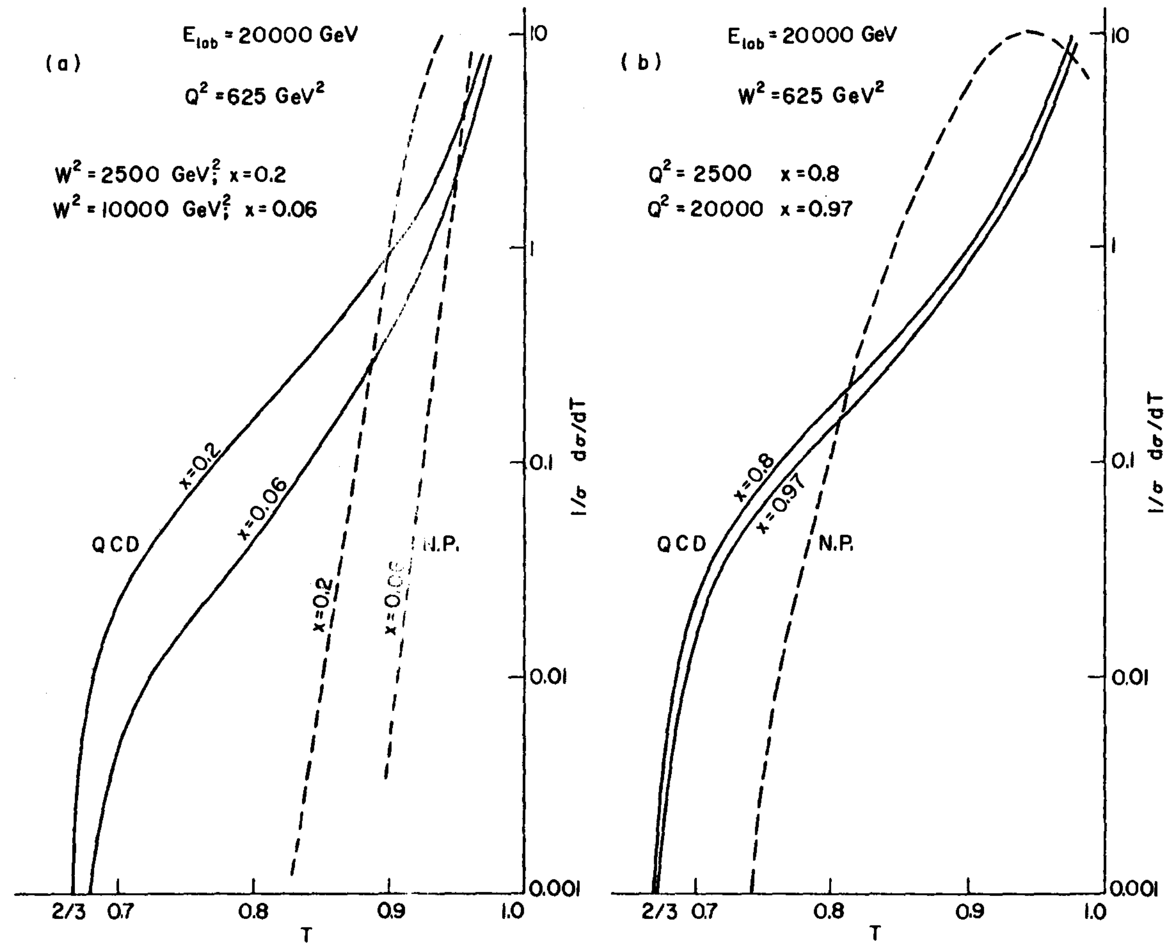

Fig. 13 : Predictions for thrust distributions at a high energy ep collider.

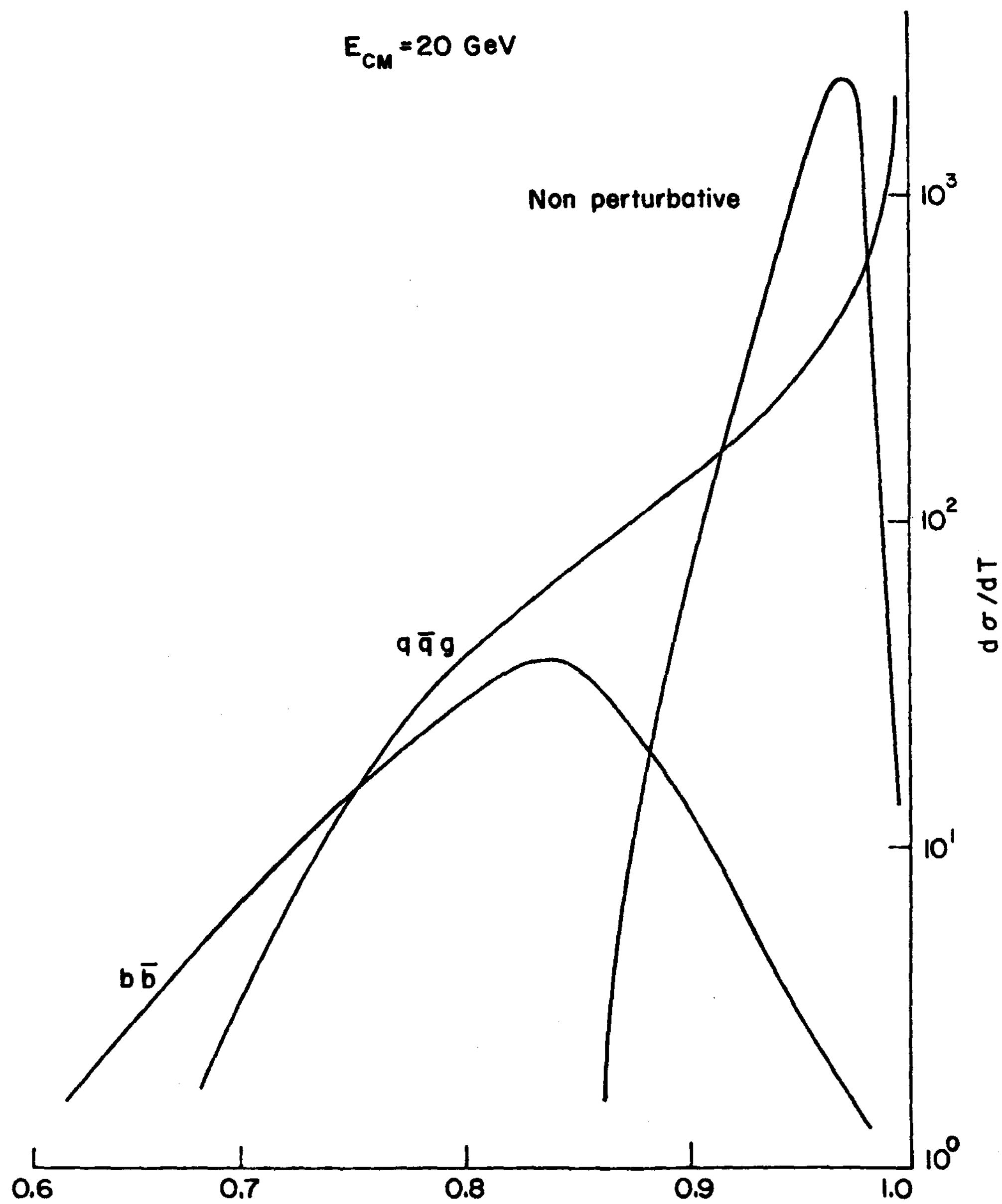

Fig. 14 : Thrust distribution for e^+e^- annihilation at E_{cm} = = 20 GeV, from $e^+e^- \rightarrow q\bar{q}g$, $e^+e^- \rightarrow b\bar{b} \rightarrow 6$ jets and non-perturbative effects.

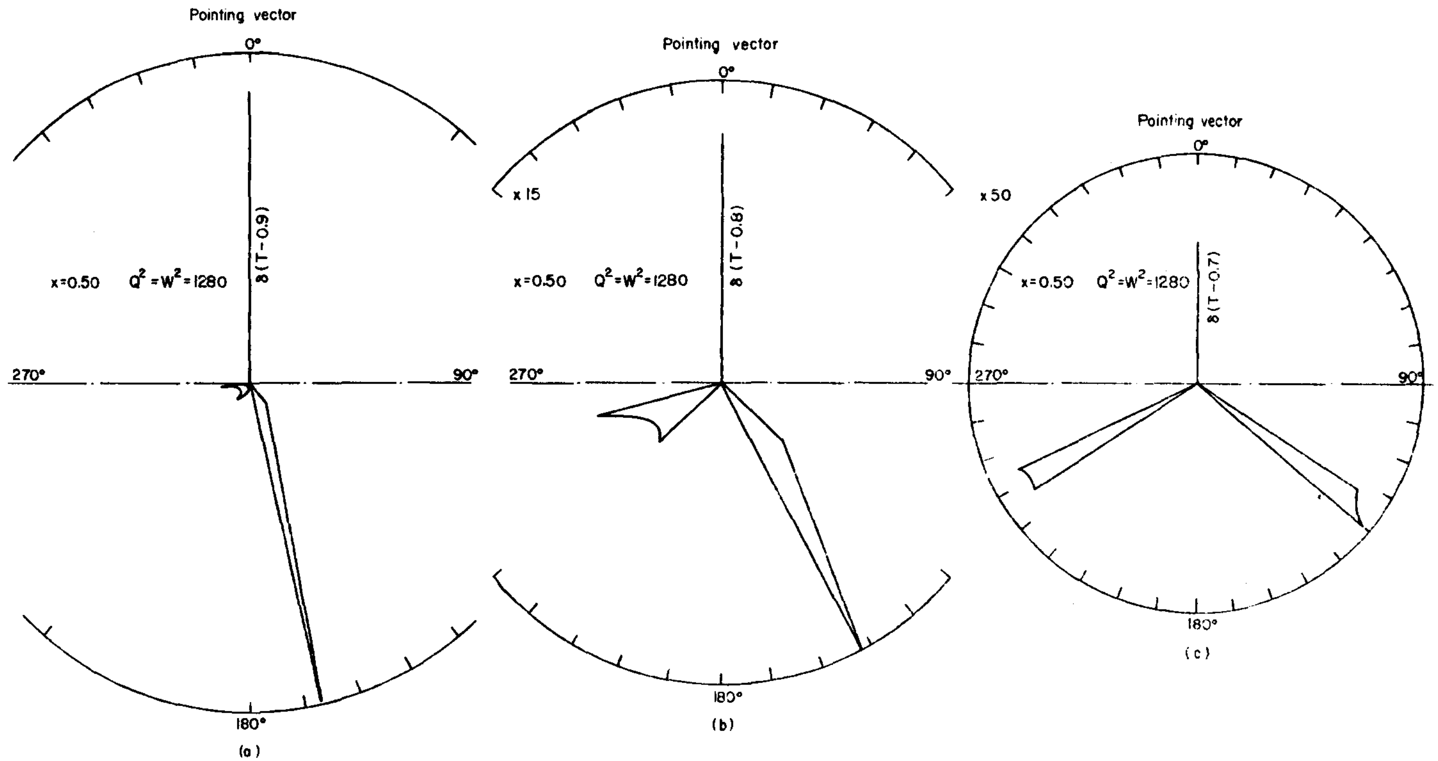

Fig. 15 : Pointing vector cross-sections from QCD effects. Smoothing from infra-red effect has not been included, see text.

and is a measure of where the energy goes in the final state. In Fig. (15) we show the QCD predictions[29] for p_i at the 25 GeV electron on 400 GeV proton machine. Non-perturbative effects have not been included yet and therefore must be added, they will round off the edges in Fig. 15*). Thus we have another quantitative test of QCD.

There are currently appearing many theoretical papers studying the properties of QCD jets in various collisions and I have outlined only a handful of approaches**). The game is still new, and it is to be expected that in the next few years better ideas than the ones described above will be invented. What is certain is that when the exact parameters of a new electron-proton machine and the possibilities of the future detectors are known, quantitative, very stringent predictions for measurable distributions will be calculated by theorists before the experiments are done. If these predictions turn out to be wrong, QCD (in spite of its theoretical appeal) is not the correct theory of strong interactions.

There is an interesting consistency check on our understanding of deep inelastic phenomena. In the parton model the cross-section for the three jet events and the longitudinal structure function F_L, are both zero (up to terms which fall like powers of q^2). In QCD on the other hand they are both only suppressed by a logarithm of q^2, and the same mechanism (gluon bremsstrahlung Fig. 16) is responsible for both being non-zero. Thus if we look at the contribution to F_L from, for example, low thrust events we should find an anomalously large contribution. This last statement can be made more quantitatively although this has not been done yet.

So far we have discussed jets, but from studying single particle inclusive distributions we can obtain interesting information about the fragmentation functions of the light quarks (as opposed to e^+e^- annihilation where there is an abundance of heavy quarks). QCD predicts that the fragmentation functions have a similar behaviour to the distribution functions, asymptotically falling at large z and using at small z. The prediction for the single particle inclusive cross-section is

$$\frac{d\sigma}{dx\,dy\,dz\,dQ^2} = \sum_{\substack{\text{partons}\\ i}} F_i(x,Q^2)\, D_i(z,W^2)\left[1+(1-y)^2\right] \tag{16}$$

---

*) For how this happens in e^+e^- annihilation at lower energy (where the non-perturbative effects are more important) see Ref. 1).

**) See also the interesting calorimetric tests suggested by Bigi[31].

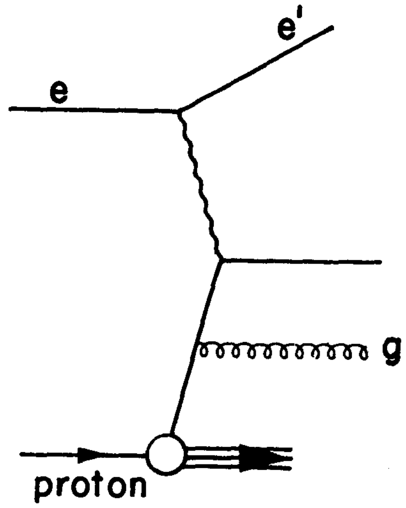

Fig. 16 : Gluon bremsstrahlung, which leads to a non-zero F and also to three-jet events.

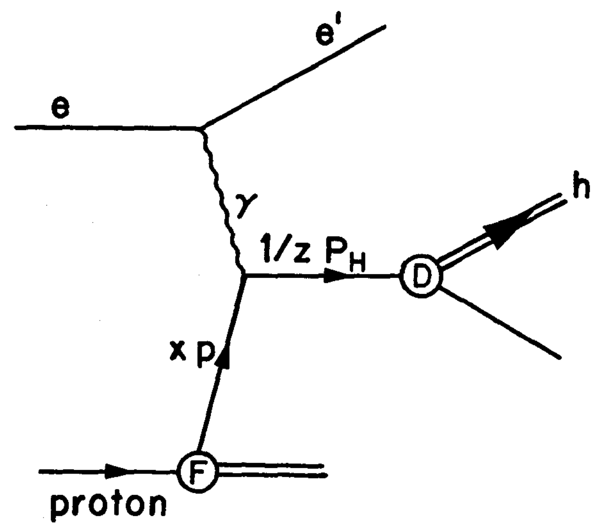

Fig. 17 : Schematic representation of Eq. (16).

where F_i is the distribution function of the i^{th} parton in the proton and D_i is the appropriate fragmentation function (see Fig. 17). In QCD there are logarithmic corrections to Eq. 16) which break the simple F.D factorization, these corrections have recently been calculated[32)]. Again we have definite predictions to compare to the data.

CONCLUSION

An e-p collider will be an excellent machine for testing and developing our ideas concerning strong interactions*), proton structure and

?

ACKNOWLEDGEMENT

During the course of this study we received several extremely interesting and useful contributions from colleagues not directly involved in the working group (see list of references); we are extremely grateful for these contributions.

---

*) For studies of weak interactions see the report of R. Cashmore.

REFERENCES

1) C.H. Llewellyn-Smith and B.H. Wiik, DESY Report 77/38 (1977).

2) J. Ellis. B.H. Wiik and K. Hübner (Eds), CERN Yellow Report 78-02 (1978).

3) S. Weinberg, Phys. Rev. Letters 19 (1967) 1264;
A. Salam, Proc. 8th Nobel Symposium, Stockholm, 1968 (Ed. N. Svartholm) (Almquist and Wiksells, Stockholm, 1968) p. 367.

4) W.K.H. Panofsky, Proc. 14th Internat. Conf. on High Energy Physics, Vienna, 1968 (Eds J. Prentki and J. Steinberger) (CERN, Geneva, 1968) p.23;
M. Breidenbach et al. Phys. Rev. Letters 23 (1969) 935.

5) J.D. Bjorken, Phys. Rev. 179 (1969) 1547.

6) J. Ellis, in Weak and Electromagnetic Interactions at High Energy (R. Balian and C. Llewellyn-Smith Eds) (North Holland 1977);
D. Sivers, R. Blankenbecler and S. Brodsky, Phys. Rep. 23C (1976) 1.

7) S. Coleman and D.J. Gross, Phys. Rev. Letters 31 (1973) 851.

8) E.M. Riordan et al. SLAC-PUB 1634 (1975);
H.L. Anderson et al. Phys. Rev. Letters 36 (1976) 1422;
P.C. Bosetti et al. Nucl. Phys. B142 (1978) 1;
J.G.H. de Groot et al. Z. Physik C. Particle and Fields 1 (1979) 143.

9) H.D. Politzer, Phys. Reports 14C (1974) 129.

10) F. Martin, Contribution to this Study.

11) M. Glück and E. Reya, DESY preprint 79/13 (1979).

12) H. Anderson, "Muon Scattering at 219 GeV" University of Chicago report (1978).

13) B.A. Gordon et al., Phys. Rev. Letters 41 (1978) 615;
H.L. Anderson et al., Phys. Rev. Letters 40 (1978) 1061.

14) E. Reya, contribution to this study.

15) A. De Rujula, H. Georgi and H. Politzer, Ann, Phys. 103 (1977) 315.

16) A.J. Buras, E.G. Floratos, D.A. Ross and C.T. Sachrajda, Nucl. Phys. B131 (1977) 308.

17) U. Amaldi, M. Lusignoli, P. Pistilli, F. Rapuano and Y. Srivastava, Contribution to this study.

18) J.D. Sullivan, Phys. Rev. D5 (1972) 1732.

19) G. Altarelli, N. Cabibbo, L. Maiani and R. Petronzio, Nucl. Phys. B92 (1975) 413;
M. Lusignoli, P. Pistilli and F. Rapuano, Rome University Preprint n 125 (1979).

20) J. Lefrançois, Moriond Conference (1979) (to be published in the Proceedings):
L. Lederman, Rapporteurs Talk at the Tokyo Conference 1978.

21) G. Coignet, Contribution to this Study.

22) P.C. Bosetti et al., Nucl Phys. B142 (1978) 1.

23) G. Hanson, Proceedings of the XVIIIth International Conference on High Energy Physics, Tbilisi 1976 (JINR Dubna 1977).

24) A. De Rujula, J. Ellis, E. Floratos and M.K. Gaillard, Nucl. Phys. B138 (1978) 387

25) R. Ellis and R. Petronzio, Phys. Lett. 80B (1979) 249;
W. Furmanski and S. Pokorski, CERN Preprint (1979).

26) E. Farhi, Phys. Rev. Letters 39 (1977) 1587.

27) A. Vayaki, Aachen,Bonn, CERN, London, Oxford Saclay Collaboration, CERN/EP/PHYS/78-28 (1978).

28) P. Binétruy and G. Girardi, CERN-TH.2611 (1978).

29) P. Binétruy and G. Girardi, Contribution to this Study.

30) A. Ali, J.G. Körner, G. Kramer and J. Willrodt, DESY Preprint 78/47 (1978).

31) I. Bigi, Physics Letters 79B (1978) 262.

32) N. Sakai, CERN-TH.2641 (1979).

WHY A DEUTERON OPTION FOR AN ep MACHINE ?

Guy Coignet

(LAPP-Annecy-le-Vieux-France)

In this note, we consider the use of a deuteron beam accelerated in the proton ring of a future ep machine.

Assuming that the number of stocked deuterons were as high as that of the protons[(1)], the gain in luminosity would apply for all the processes with small cross-section[(2)]:

$ed \to e + X$ at large q^2 and large y

$\to$ new flavours (toponium, bottonium, ...)

$\to$ heavy lepton (E°, E^+, E^-)

$\to$ intermediate boson (Z°, W^+, W^- ...)

$\to$ Higgs boson H°

$\to$ .....

The better statistical precision may be important in some specific cases: for instance, the manifestation of any propagator effect in both charged or neutral current interactions would be cleaner than ep scattering. Another difficult experiment is the $R = \frac{\sigma_L}{\sigma_T}$ measurement of the electromagnetic interaction: it is expected to be small and R_d would probably be easier to measure than R_p.

A deuteron option would be useful even with a lower luminosity, i.e. $L^{ed} \simeq \frac{L^{ep}}{4}$.

The first important point is that the deuteron is an ISOSCALAR allowing a complementary study to the proton case: the singlet moments and then the moments of the gluons can be deduced in a similar way as that performed with a neon filled bubble chamber in neutrino physics[(3)].

The second important use of a deuteron beam would be the access to en physics: this can be done by the classical subtraction method en = ed - ep and in a cleanest way by the detection of the spectator proton. The price to be paid in the latter case is on the maximum available values of ν, W , q^2, ... which are a factor of two lower than in ep scattering. Switching from a proton to a neutron target allows to change the relative content of u and d valence quarks.

It is then possible to measure the ratio $\frac{\text{neutral current ep}}{\text{neutral current en}}$ and study the $Z^\circ u$ and $Z^\circ d$ coupling at high s values[4].

In the electromagnetic interaction it provides, when measuring the neutron structure function, direct access to the valence d quark distribution $d_v(x,q^2)$; the sea and gluonic contributions can, in principle, be eliminated by looking at the structure function difference $F_2^p - F_2^n \propto x(u_v(x,q^2) - d_v(x,q^2))$. In the simple quark parton models one expects also the sum rule $S = \int_0^1 [F_2^p(x) - F_2^n(x)]\frac{dx}{x} = \frac{1}{3}$ to be valid, when available experimental data are far from saturating this rule[5]. QCD and other field theories have specific predictions for other moments of the structure functions. It is then important to test this rule at the highest q^2, since the AFGT models predict a large increase of the sea with q^2 and a more similar variation of F_2^p and F_2^n as shown in Fig. 1 and 2 extracted from reference 6.

It is also important to have a rough estimate of R_n, since the extraction of $F_2^n(x,q^2)$ depends on R_n: SLAC data[7] are roughly consistent with $R_p \simeq R_d$; it is then assumed that $R_n = R_p$. Now, in QCD model, R is expected to be small, decreasing logarithmically with q^2 and such that $R_n = R_p$; it has to be tested at fixed q^2 and ν by varying the electron or the deuteron momentum.

One can also mention that, still in deep inelastic scattering, the ratio[8] of the two photon contribution $\sigma(2\gamma)$ to the one photon contribution $\sigma(1\gamma)$

$$\frac{\sigma(2\gamma)}{\sigma(1\gamma)} \simeq -\frac{3}{2}\frac{\alpha}{2\pi} e_q \ln^2 \frac{Q^2}{M^2}$$

is proportional to e_q, the charge of the interacting quark so that this contribution is expected to be less important for a neutron than for a proton target.

The jets and the hadroproduction also present a certain interest since the presence of an excess of d quarks has to reveal itself in the fragmentation functions in the π^+/π^-, K^+/K^- ratios and in the quark charge retention in the jet.

As a final remark, it seems worthwhile to mention the possibility of polarization of the deuterons; due to the lowest gyromagnetic ratio, by more than one order of magnitude, it is, in principle, easier to maintain the polarization during the acceleration cycle for deuterons than for protons. In PS type machines, a large polarization of deuterons seems reachable[9] but precise calculations of depolarization effects have still to be performed for a 270-400 GeV synchrotron. Assuming that the final polarization is still sizeable, a long straight section has to be envisaged to align the spin of the deuteron parallel or antiparallel to its momentum. Combined with an electron beam of variable helicity, two new structure functions $G_1^p(x,Q^2)$ and $G_1^n(x,Q^2)$ are measurable:

with $$G_1^{n,p}(x,Q^2) = \frac{1}{2}\sum_i e_{q_i}^2 \left(f_i^{\uparrow}(x,Q^2) - f_i^{\downarrow}(x,Q^2)\right)$$

where $f_i^{\uparrow}(f_i^{\downarrow})$ represents the distribution of quarks with spin parallel (antiparallel) to the proton spin. G_i^n is expected to be small but has never been measured until now.

REFERENCES

1. A luminosity $L^{ed} \simeq \frac{L^{ep}}{4}$ seems easily accessible, $L^{ed} \simeq L^{ep}$ can in principle be reached with a special machine design: from K Hüber (private communication).

2. See for instance: CHEEP, an ep facility in the SPS, CERN yellow report CERN 78-02, Chapter I and II or Physics with large electron-proton colliding rings C.H. Llewellyn-Smith and B.H. Wiick, DESY 77/38.

3. P. Bosetti et al (ABCLOS Collaboration) Nucl. Phys. B.142 (1978) 1.

4. The ratio $\frac{NC\ \nu p}{NC\ \nu n}$ has been measured only for E lab less than 10 GeV: M. Pohl et al, Phys. Lett. 79B (1978) 501.

5. S. Stein et al, Phys. Rev. D12 (1975), 1884 measured at SLAC: $\int_{0.02}^{0.82} [F_1^p(x) - F_2^n(x)] \frac{dx}{x} = 0.20 \pm 0.04$

6. A.J. Buras and K.J. Gaemers, CERN TH 2322 and Nucl. Phys. B132 (1978), 249.

7. R.E. Taylor, Rapporteur talk at Int. Symp. on Lepton and Photon Interactions at High Energies, SLAC, Stanford, 1975, p.679.

8. V.G. Gorslikov et al, Soviet J. Nuclear Phys. 6 (1967) 361: J. Bartels, Nuclear Phys. B82 (1974) 172.

9. R. Beurtey CERN Int. Report. NP/Int 67.21.

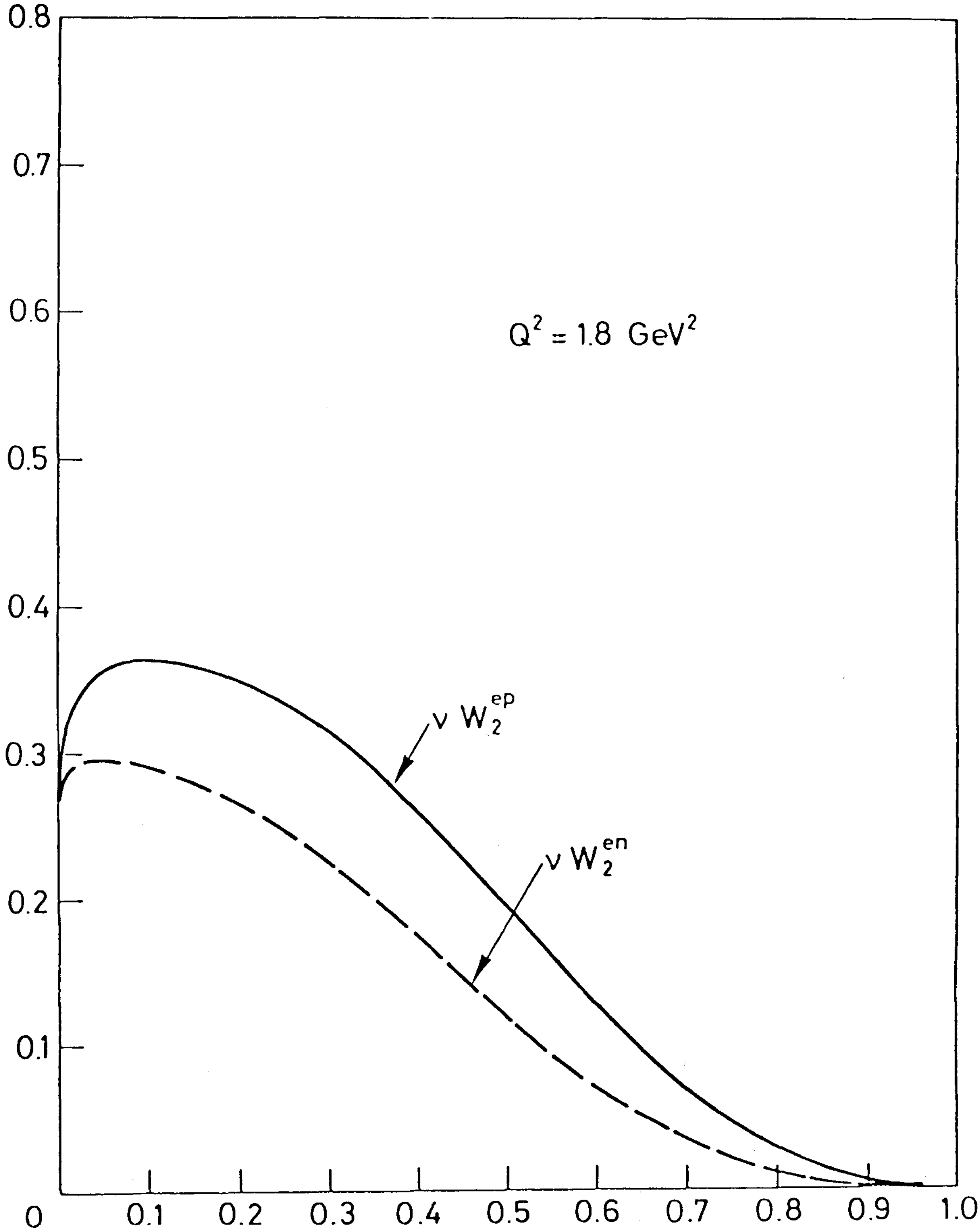
0.8
0.7
0.6
0.5
0.4
0.3
0.2
0.1
0
0.1
0.2
0.3
0.4
0.5
0.6
0.7
0.8
0.9
1.0
x
$Q^2 = 1.8\ GeV^2$
νW_2^{ep}
νW_2^{en}

FIG. 1

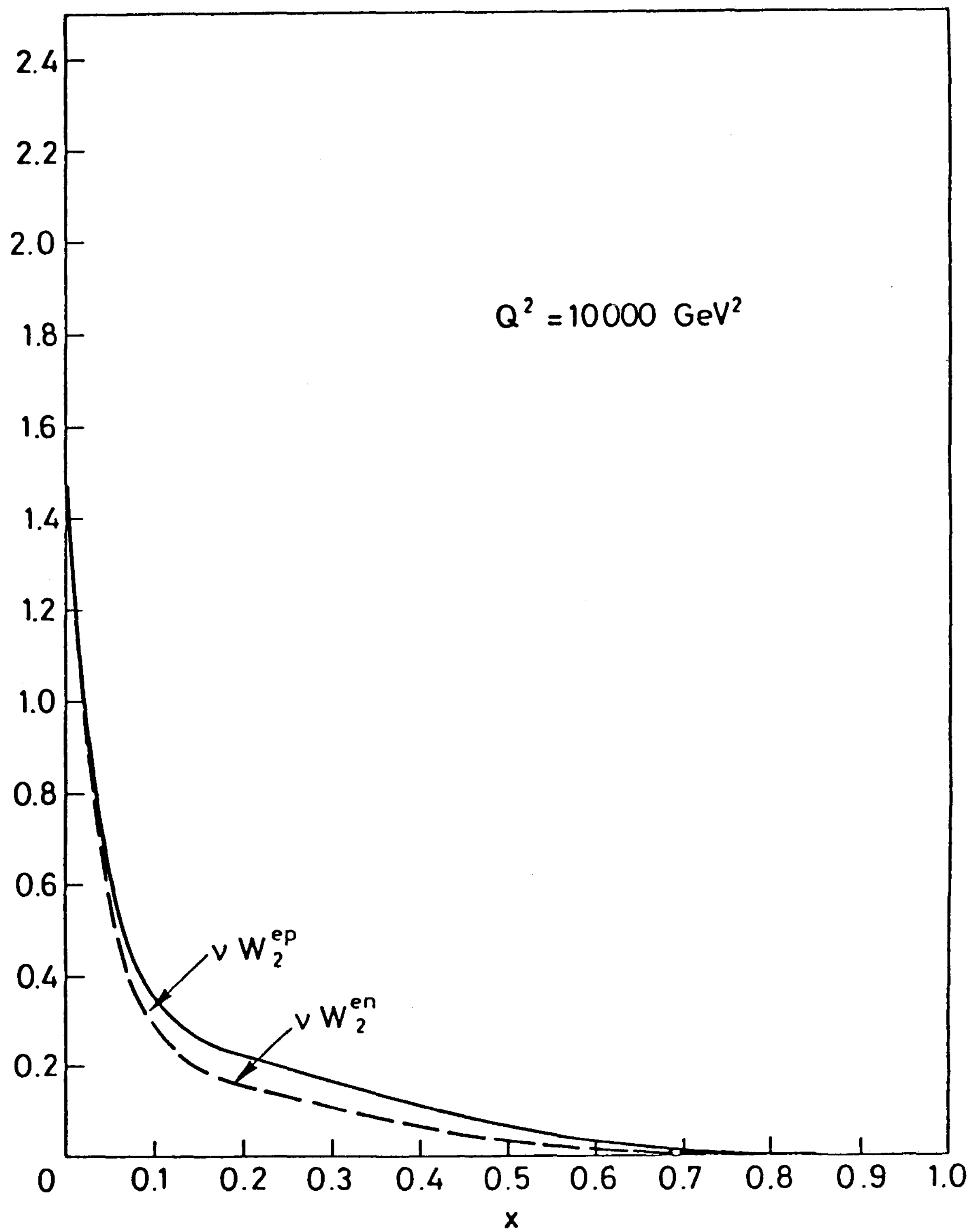
2.4
2.2
2.0
1.8
1.6
1.4
1.2
1.0
0.8
0.6
0.4
0.2
0
0.1
0.2
0.3
0.4
0.5
0.6
0.7
0.8
0.9
1.0
x
$Q^2 = 10000\ GeV^2$
νW_2^{ep}
νW_2^{en}

FIG. 2

DISCUSSION SESSION ON LARGE Q^2 AND HADRON STRUCTURE

(edited by D. H. Perkins)

This account of the discussion is based on a transcript of the tapes prepared by the DESY staff. It has been rather radically edited by me, in the interests of intelligibility and continuity. I hope I have not destroyed the sense of anyone's remarks or left out statements of importance. If this hope is misplaced, I sincerely apologise to those concerned.

S.C.C. Ting (DESY-MIT):-

I have a question to the first speaker. In one of your first slides you mentioned correctly that for a 20 GeV electron on a 300 GeV proton you have a luminosity of 10^{32} and a useful maximum q^2 of 5000. This enables you to probe into a distance of 3.10^{-16} cm and that is, of course, very, very important because this distance goes into protons where new phenomena will be found. That corresponds also to your first slide of unexpected results. The thing on which I would like a comment from you is the following. You mentioned that for the TEVATRON the effective useful maximum q^2 is about 400, therefore the distance you can probe (which is not q^2 but q) is about three times less; but, the intensity, of course, may be somewhat higher or at least comparable. It depends on how you do this. So I was wondering, how does this strike you?

C.T. Sachrajda (CERN):-

I really find it very hard to answer that question.

S.C. Ting (DESY-MIT):-

OK

D.H. Perkins (Oxford University):-

If you are comparing ep with μp or νp you should do it for a fixed target machine using a hydrogen target for the lepton beam. We took the rates/day from the EMC experiment at the SPS; and we scaled these up for the TEVATRON. Assuming 10^{12} protons per second we claim that the rates in events per day, for $q^2 \gtrsim 400$ from the TEVATRON (be it for μ-scattering experiments or a ν-scattering experiment on a hydrogen target) are the same as at $q^2 \gtrsim 5000$ on the ep machine, assuming a luminosity of 10^{32}.

S.C.C. Ting (DESY-MIT):-

There was another thing on one of your slides. This is a very interesting idea by, I think Ugo Amaldi, of measuring the pion form factor.

C.T. Sachrajda (CERN):-

I think that Sullivan, originally, was the first person to have this idea.

S.C.C. Ting (DESY-MIT):-

But I think a quite interesting idea. What puzzles me a bit is: how can you make sure if it is only one-pion, rather than multi-pion exchange?

C.T. Sachrajda (CERN):-

I guess I should leave that to the people who did the work.

U. Amaldi (CERN):-

The idea is not very new. The advantage here with respect to previous proposals is that one gains from the fact that the neutron goes forward at small angles (with a big energy spread) and it is much easier to detect than in an experiment with a fixed target proton where you have the production of neutrons of very low energy. The exchange of the pion Regge trajectory is expected to dominate, but I would like to stress that the background has not been computed. Of course one should not only look at the lepton shower, but also at the current and the proton jets, and this would allow the kinematics to be reconstructed and events in which some Δ's or higher resonances are produced to be disentangled. Incidentally, the neutron will go at very small forward angle so one can think of having a detector of one metre diameter put at 300 m from the target, and one can measure energies with resolutions of 1-2%.

Th. F. Walsh (DESY):-

About the pion exchange and looking at the pion-structure function. Maybe it is just my ignorance; I was a little puzzled there because I was under the impression that to isolate pion exchange you have to go down to t of the order of $m_{\pi}2$. Is that true or false, can someone answer that question?

E. Gabathuler (CERN):-

Can I refer to the question of the pion form factor? I would like to know how this compares with measuring the pion-structure functions directly using Drell-Yan? We now know that there are very nice data coming out giving a distribution $(1-x)^{1\pm.1 \text{ or } .2}$. I would like to know how does this technique of measuring the pion-structure function compare; you go up in ν and, therefore you start to see the effect of things like A_2 exchange coming in, as well as single pion exchange, and therefore, presumably you have to go to very, very small t to make sure you are only measuring the form-factor of the pion. Therefore, I would like first of all to know how it is done, because we know that these other effects are going to be there.

C.T. Sachrajda (CERN):-

Isn't it a question of faith? You go down to as low a t as you can and see when you increase t whether it is the same or not. John has some comments, I think, on that.

J. Ellis (CERN):-

I am just going to remark that actually an experiment on which Perkins is a collaborator is actually trying this pion-structure function measurement already, in neutrino scattering. I mean they have a handful

J. Ellis (CERN):- (cont.)

of events or something like that! But as I understand it, it works. Now, one way which they can check to see whether pion exchange is actually relevant is by looking at things like a Δ in the final state and by looking at the polarization matrix element of the Δ. And there you can check explicitly, if the thing does work out to t of the order of .5 or something like that. I don't know whether it is possible to observe a Δ with this sort of ep colliding ring, but that would certainly give you a handle on it, and you would already have some experimental information. With regard to this point about Drell-Yan: I think the whole point is to check whether the pion-structure function is the same as Drell-Yan or not. And this is highly nontrivial and totally demonstrating the exciting test of a theory.

E. Gabathuler (CERN):-

Can I just make one comment in connection with Prof. Ting's question: if you take 6 m of hydrogen and a beam of 10^7 muons per pulse and say, 6 or 7 pulses per minute, that corresponds to an effective luminosity of about $1.5 \cdot 10^{31}$ cm^{-2} s^{-1}. So that would be equivalent to the same figure I suspect you will get from the FERMI-lab DOUBLER if one worked with 3/4 of the energy of the protons.

Can I, when I have the floor, make another comment? If I may, Mr. Chairman, you told me not to bounce up and down.

Can I have your first slide, please, your first transparency which shows the q^2, ν plot? I think it is interesting to put on there perhaps with your pen, the triangle that corresponds to the present SPS/FERMI-lab neutrino or muon experiments because I think this illustrates something that was raised yesterday by Prof. Fubini: that one really can cover a tremendous range in the q^2 plot, and people should be aware of this. Thank you. So this brings me to my question; let me say, in fact, we do measure both the incident and scattered electron: we are measuring, therefore a sum of the one photon exchange plus the weak part. Then in principle, if you do a plot as a function of q^2 for various x values, can the theories exactly predict the whole spectrum as a sum? In other words: will the effects of the mass of the W or other effects at large x, will these tend to come in? Or will it be possible to do an experiment where you can actually measure the total rate for the scattered electrons andthen use that to just basically give essentially a total cross-section where one can then make a prediction against QCD?

C.T. Sachrajda (CERN):-

You said, you want a cross-section at fixed s at some x and y?

E. Gabathuler (CERN):-

Yes, at some s for various values of q^2 plotted versus x or whatever you like; I am just asking: can you take the whole electron rate and do a calculation as a QCD prediction rather than have to do the separation between weak and electromagnetic effect?

C.T. Sachrajda (CERN):-

I see, you want just what you are going to measure essentially.

E. Gabathuler (CERN):-

Yes.

C.T. Sachrajda (CERN):-

Well, if the Weinberg-Salam model is right, and prejudices about all the parameters are right, we can certainly give you those curves. On the other hand we would like to have some check on whether those things are correct or not.

(... a drink for the speaker ... applause...)

I think we can answer now. It is going to take a while, clearly to disentangle exactly all effects, for example we expect strong interaction scaling violation to be more important at smaller q^2 and weak interactions to be important at larger q^2. If you have both electron and positron beams and polarizations you expect effects to go various different ways. So I hope with a good study you will be able to untangle the effects. And if the theory is right, I mean, if both QCD and the Weinberg-Salam model are right, then we can tell you what your curves ought to look like.

Th. F. Walsh (DESY):-

I have a couple of questions following up on Ting's:

1. The comparison with the TEVATRON was for a hydrogen target, but, of course the CERN EMC is also used with a stack target, and in principle one can imagine doing μ-scattering experiments on the TEVATRON perhaps with a fairly massive stack target. I wonder if that changes things?

Th. F. Walsh (DESY):-

2. The reaction ... (electron + proton) goes to (neutrino + anything). In principle one can compare that with the TEVATRON with, say, a 1000 ton iron calorimeter and how do the rates compare there?

C. Geweniger (Universität Heidelberg):-

For the rates at the TEVATRON narrow-band beam which is due to 800 GeV neutrino energy, you get for q^2 above 800 GeV^2 more than roughly 1000 events ... for 10^{19} protons on the target and a 600 ton detector.

Y. Eisenberg (DESY-Weizmann Institute):-

It is just a comment regarding the question that was raised before about the purity of the pion propagator for small t's. We have done an NAL experiment in which neutrons were bombarded by protons (these are hadron experiments, of course, and one may not perhaps mention that here) and indeed we find that for t smaller than .5 there is perfect agreement with the pure single pion exchange.

J. Ellis (CERN):-

I had 3 random comments which I will arrange in increasing order of the excitement. The most boring remark which I can think of is that in addition to doing scattering off a pion you can also do scattering off a pomeron, if anybody remembers what the pomeron was! Instead of measuring a low momentum transfer neutron coming out to measure a low momentum transfer proton coming out and then as long as the momentum transfer is small you probably struck a pomeron which, maybe, is made out of glue and that may or may not be an interesting thing to look for.

The second remark which is more exciting even than that is, if you come to your triangle plot in q^2 and ν, the region of that triangle which is not accessible to perturbative QCD is presumably somewhat thinner than the black line along the bottom. Since you believe that you can calculated anything with $q^2 > 1$ GeV^2, certainly it gives everybody plenty of opportunity to prove if the theory is totally wrong.

J. Ellis (CERN):- (cont.)

The third comment was that actually the theory might turn out to be right, but still nothing at all looks like any of the distributions which Chris Sachrajda has shown, because you talk about SU(3) x SU(2) x U(1) as being the group of the world. Well, that may well be true. But maybe, there are just more particles in the world than we like to think. As a totally stupid example which I thought of last night or this morning you can imagine that everything was supersymmetrised. If everything is supersymmetrised, then you get particles which look just like the ones that we now have except they differ by spin of 1/2, so for example you have spin 1/2 gluons, called gluinos and all that we know at the moment is that the gluino has a mass bigger than 0, but you could have a mass anywhere. Let me tell you what the gluino would do. You show that picture for the momentum fraction carried by quarks which were supposed to be constant from here to q^2 of the mass of universe. If there were gluinos at some point we suddenly stop and go down to some totally different value, because suddenly you would find that half of the momentum of the proton was being carried by gluinos.

L.M. Sehgal (TH Aachen):-

I have a question as to whether one can learn something about QCD by studying the weak-electromagnetic interference carefully. And I think the answer to that is that the asymmetries that you will see at the level of weak-electromagnetic interference are extremely insensitive to the parameters of the QCD theory. The parameter Λ for example. So the best place to test QCD would really be in the domain of q^2 smaller than 1000 GeV^2 where the weak interference effects are unimportant.

S.C.C. Ting (DESY-MIT):-

Can I take a look at your first or second slide, the one where you showed that most of the important discoveries really have nothing to do with the purpose for which the accelerator was built.

I have two remarks with regard to this: the first is with regard to form factors and scaling. As you know the form factor is discovered not only at SLAC but also at DESY. But what is important is that, since the discovery of scaling in 1968 there has been a large amount of work done to study various final states. But so far we are not really able to have a very clear understanding of the implications of those experiments.

My second remark consists of what you would expect from let's say, a 20 GeV on 200 GeV machine or a 20 GeV electron on a 300 GeV proton. In this case, I mean, the thing you compare with would be like, for example, a SUPERSPEAR or PEP or whatever that is. In this case you are somewhat hindered in looking for new particles, because you are down somehow by the proton form factor. This is something you cannot avoid. With an e^+e^- collider, of course, you are also down by a form factor, but on the other hand the cross-section is quite big.

K. Winter (CERN):-

I would like to contribute something to the discussion comparing the possibilities of the TEVATRON and an ep ring. And that is: what you always do in your discussion is as if these beams were 100% polarized, and that is, of course, not the case. Already electron beams can at most be polarized to about 90%, if there are not other depolarizing effects. And for muon beams you should not forget that the most standard and the most intense muon beams always have the wrong handedness, for instance you get μ^- right handed and μ^+ left handed. And if you want the natural component you have to take those particles which are emitted backwards in the system of the decaying parent and as a matter of fact you go down first by a factor of, well, I would guess at least 10 in rate; but also the degree of polarization is smaller, because of the angular acceptance. I have not done any calculations, but I have the impression, if you go up with energy this is going to spoil the polarization degree of this beam; so I think in doing these comparisons one should be a little more accurate in doing it. Because I think we all agree that the value of these ep rings rests very solidly on the possibility of having polarized beams with both helicities. And in that context also I would like to make a comment on what has been called here the 100 + 400 option. I mean that is not a real option. That is a possibility if LEP is built next to the SPS there will be one crossing and if you want to use this for ep physics and you have to switch off the e^+e^- physics. And I guess that will not be done for the first 10 years of LEP!

T. Ekelof (CERN-Uppsala):-

Coming back to the question, asked already yesterday about comparing ep collisions with e$\bar{p}$ collisions which again implies, of course, the SPS at CERN. But who would be interested? I mean when we are discussing deuterons then what about e$\bar{p}$? And the second question: I would imagine that comparing with hadron-hadron collisions and lepton-lepton collisions that the lepton-hadron collisions could have some unique information on confinement in the sense that you probe an already confined system with the pointlike probe. Could you make your comments on that.

C.T. Sachrajda (CERN):-

Well, I think the p$\bar{p}$ and ep tend to show two different things. First of all this is obviously a pretty bad new particle factory, but this is really an instrument to study the structure of the proton. Now in p$\bar{p}$ collisions you have both the structure of both hadrons plus whatever the interaction mechanism between them is. And you hope that you understand sufficient of each that you can still learn something from them. Here you hope that you understand at least the weak and electromagnetism structure better so that you really just measure the structure of the proton. So I think this is a proton structure measuring machine. As you say, it should provide information about the mechanism of confinement. But here we are stuck theoretically. However, we hope that you can get some hints - for example, the various different schemes which predict different ratios of up quark to down quark distributions as $x \to 1$ and all things like that. With these things we hope one day to understand theoretically and to get some hints from machines like that. But theoretically, those ideas are not as clear - so I didn't concentrate on them.

Th. F. Walsh (DESY):-

I have one last comment. Of course, if QCD is right then presumably the q^2 variations over the range of this machine of a structure function is going to be very small. The largest variation is the lowest q^2, of course. So if one is really looking as far as testing QCD is concerned, nothing much happens.

Th. F. Walsh (DESY):- (cont.)

Second point; looking at final states. As far as the large event rates are concerned it appears to me that what you have with an ep machine where the proton has, let us say, 5 or 10 times the energy of the electron beam is basically an electron-quark machine, an electron-quark colliding machine. But the electron and the quark have roughly equal energies (which means 20 GeV electrons, say, on 300 GeV protons). The ep machine is basically PETRA with a positron replaced by a quark. I don't think that the studies of final states with such a machine are going to be much more conclusive than they can be in PETRA with the exception, of course, that new thresholds can mess things up at PETRA and they are, of course, very disagreeable from that point of view.

G. Knies (DESY):-

You show that determining the Weinberg angle and the Z mass done at this large q^2 is possible at about the same accuracy as has been done with the polarized electron beam scattering at SLAC so far already, so that the main thing then is not a better determination of the Weinberg angle but comparing the Weinberg angle as determined from large q^2 processes and low q^2 processes. What is the physics behind this comparison, could you comment on that?

C.T. Sachrajda (CERN):-

We have a lot: we have a theory which gives us various relations between things, and we know that if $\sin\theta_W$ is measured in our experiment we know exactly what it should be in other experiments, and it had better be that. The usual thing that is taken is a particular mechanism for giving the W's their masses. It is a particularly simple thing: you take the lowest representation you can, take a complex doublet, so it is just one real Higgs particle. Life could be more complicated and things could go wrong. So clearly you want to check this in as many places as you can. That is true. If you just take $\sin\theta_W$ as the parameter and you look at all existing data you get very small error bars. But things could go wrong.

D.C. Cundy (CERN):-

I think the conclusion was that the optimum was not far from 20 on 270, but it would be better to have the electron at 30 GeV or something. But already for most of x range you are quite a long way out in angle. I think that was the conclusion - 30 on 270.

D.H. Perkins (Oxford University):-

That was our conclusion. I mean, obviously you want to go up to q^2 on the order of $(1/4)q^2(\max)$. After all you are looking at the high q^2 region and then I think a ratio of the electron to proton energy of the order of $1/10^{th}$ to $1/5^{th}$ brings the current jet out at 90° in the laboratory - that's where you want to have it to measure it easily and to stop too many fragments going down the beam pipe.

S. Fubini (CERN):-

The Chairman said that interest in this kind of physics is related to the number of questions. So let me add one more. It is not really a question but a statement. Looking at the situation I feel one should look at things a little bit in perspective. In other words: a sentence which I don't like to say is "well, we test chromodynamics and then what?" Now, if you think that we are all discussing the physics which will be done, say for 8 years from now, one might think; what would have been the talks of rapporteurs, say 8 years ago? Now very likely the conclusion of people then could have been that we have no theory of strong interactions, they only can think that we can do consistency tests. On one thing we are sure. We understand very well what happens at long distances. We will never be able to understand what happens at small distance and large p_T are forbidden.

Now from what I hear from the speaker the situation is exactly the opposite. We have a theory, a very good candidate for a theory; we understand well what happens at small distance, and the big mystery is confinement which is the large distance phenomena. Now large p_T (if the theory should work) seems to be different from what people thought.

S. Fubini (CERN):- (cont.)

So, in my opinion the problem of testing chromodynamics would not be something you can say, well, let's use LEP which by the way I like and forget about anything else at least in order to test the theory. You need a source for experimentation in many different conditions. I like to think about the grandfather of the thing which was Regge theory or dispersion theory. Our opinion about that was due to very thorough experimentation in many conditions. So I don't think it is very reasonable to say, what it is better to do; ISABEL, or the DOUBLER, to do this or to do LEP. I really think we need all possible information about all tests of chromodynamics. It won't be easy. After all, now the logs come out well. And it is an amazing fact from one of my friends who was making a comparison with strong interaction physics over a long time. He was saying, well, you know when you look at multiplicitiy we are two clubs, one who wants a power law, one who wants a log. (By the way, I wanted a log at the time and I also like log now.) And the log people won because they shouted louder!

So I feel it will be extremely important - this fact that we have a logarithmic effect that you can compute is an amazing fact which I would not have predicted. So in my opinion it is very important to make experimentation on many different topics and compare.

D.H. Perkins (Oxfurd University):-

Thank you very much; that seems a very good point at which to close the session. Thank you all.

SUMMARY OF DISCUSSION SESSION AND OPEN QUESTIONS

(D.H. Perkins)

Here I want to try to summarize the main points of the discussion and reply to those questions which were perhaps not fully answered, and also mention the open problems in the subject.

1. RESOLUTION

One point made by Ting was that the (20 + 270) ep design gives only a factor 10 in q^2 or 3 in spatial resolution, as compared with lepton beams from the TEVATRON: how useful is this?

This is clearly a matter for judgement, but personally I believe that when you increase the resolution by a factor 3, you will be almost bound to find new phenomena. If you don't for example, if QCD is right and variations are gentle and logarithmic - then that's also very important. Recall that the improvement in resolution between the SLAC electron plus PS (Gargamelle) neutrino experiments of the late 60's/early 70's, on the one hand and the muon/neutrino experiments at SPS/FNAL over the last few years on the other, was indeed just that same factor of 3. Those SPS/FNAL lepton experiments have, I think, started to add a new dimension to our understanding of hadron structure; their importance may be judged from the fact that 65% of all SPS protons have been poured into them.

Having said this, it is equally clear that the highest available collision energies are desirable, and that a (45 + 500) ep collider would give a further factor 2 in resolution as compared with (20 + 270).

At the same time, it is important to realise that experimentation gets more difficult at the higher energies. While, for the (20 + 270) ep collider, one is thinking to get by with PETRA-type detectors (with some modifications around the forward direction to cope with target fragments), much more powerful solenoids etc. would be necessary for the (45 + 500) machine. Transverse momenta of >10 GeV/c for particles in the current jet would be common. These are some of the open questions on which further study is required by the "detector" working groups.

2. COMPARISON WITH HYDROGEN OR HEAVY TARGETS AT THE TEVATRON?

The working group made comparison between ep and TEVATRON μ, ν beams on hydrogen targets. In the discussion Walsh and Geweniger mentioned iron or other heavy element targets for both muon and neutrino beams. Obviously, you can go up a bit in q^2 by using greater effective luminosity - but not very much. However, my main point is that I hope that by 1986 or whenever the ep collider could be operational, we shall be a bit more sophisticated than that. If QCD is still alive by then, it will be important to tie together the (quark/gluon) substructure of the proton in the initial state, with the fragmentation (of those quarks and gluons) to hadrons in the final state, and for this you do need elementary targets. For example, crucial tests of QCD relate to the non-factorization, at finite q^2, of the x and z distribution, observation of gluon jets, etc. Nuclear complications are the last thing you want, so I think it is completely fair and correct to compare proton targets in both cases.

3. ELECTRON-QUARK VERSUS ELECTRON-POSITRON

In the course of discussion, it was remarked that the (20 + 270) ep collider was, effectively, a machine colliding 20 GeV electrons with, typically, 50 GeV quarks - and therefore not so different from PETRA or PEP colliding 20 GeV e^- on 20 GeV e^+. I would argue very strongly that this superficial resemblance of numbers conceals very profound differences of physics and principle. PETRA and PEP are basically quark-antiquark factories; their very excellence in generating new flavours carries with it the very grave disadvantage that there is little possibility of relating the hadrons observed to fragmentation of particular types of quark/antiquark. On the other hand, especially for charged current reactions, $e^{\pm}p \to \nu, \bar{\nu}X$, all flavours apart from u and d are strongly suppressed. $e^-p \to \nu X$ looks at the fragmentation of the d-quark only (with a little $\bar{u}$ at small x and large y), $e^+p \to \bar{\nu}X$ at u-quark fragmentation. So, one has a much better-defined situation.

In the context of QCD which is at present the only game in town and to which I therefore have to appeal as a basis for comparison - there are other very significant differences expected in the two cases.

$e^+e^- \rightarrow Q\bar{Q}$ involves only flavour singlet quark-antiquark combinations, while a proton target provides both singlet and non-singlet combinations which can be selected for example by comparing $e^+p \rightarrow \bar{\nu}X$ with $e^-p \rightarrow \nu X$ or by analysing different combinations of hadrons in the current jet. The difference is crucial to QCD, since the predictions for the non-singlet functions are much more straightforward than for the singlet case.

The very difficulty of exciting new quark flavours at an ep machine is compensated (as pointed out in the discussion) by the fact that the corresponding threshold effects at an e^+e^- machine are largely absent in the ep case - again making easier the comparison of cross-sections with theory.

Finally, as pointed out in the discussion, our understanding of quark confinement is more likely to be advanced by studying an already confined B = 1 system like a proton, than the 1^- vacuum state. And if quarks are ever to be liberated, at some level, of course it is important to study that too, in as many experimental situations as possible.

4. THE RATIO OF ELECTRON TO PROTON ENERGY

This ratio was mentioned by Cundy and others in the discussion session. Although it is not very critical, it is a very nice feature of the shape of the proton structure function, on the one hand, and of the relative energies attainable for electrons and protons on the other, that the preferred solutions (20 + 270; 45 + 500) are nearly the ideal ones. Effectively one is looking at electron-quark collisions, with $E_{quark} = xE_{proton}$ At high q^2, the current jet will therefore come out at a large angle to the beam-pipe if the electron-quark CMS is at rest in the laboratory, i.e. if $E_e \sim (0.1 - 0.2)\ E_p$.

Perhaps it was implied in the discussion that large departures from the optimum ratio, <x>, could send many current fragments down the beam-pipe. Actually this could only happen in the extreme case of very small x and low q^2. The working group did not pursue this matter in depth, and further study is certainly desirable. Over most of the x range, however, it appears that at most only 1% or so of current fragments could end up near the beam-pipe. One of the difficulties in making estimates is that the answers you get depend on the model assumed for "hadronisation" of the current (struck) quark and of the target (spectator) quarks. We used Monte Carlos based on lepton scattering data in the q^2 = 1-100 GeV region, and we do not know what will happen to the rapidity distribution, for example, when you increase q^2 by 2-3 orders of magnitude. Clearly however, further calculations would be worthwhile, comparing the predictions for different models of hadronisation.

5. SUMMARY

Let me in a few sentences try to summarise the case, as I see it, for the ep collider.

The (20 + 270) collider would give a useful counting rate (10-20 events/day for $L = 10^{32}$) for both neutral and charged-current events, at values of q^2 which are 10-20 times larger than those attainable with lepton beams at the SPS or FNAL for the same counting rates. For the (45 + 500) collider, the useful range of q^2 would be 50-100 times those at SPS/FNAL. This will, without question, open a whole new range of physics. Either one can be optimistic and dream of sub-quarks, colour brightening etc., or one can take a very conservative view and regard such a machine as the instrument which will finally underpin our theory of strong interactions between the fundamental fermions (quarks).

As Fubini said in the discussion, we want to have many experimental possibilities; $p\bar{p}$, pp, e^+e^- and $e^{\pm}p$. Each machine has its own peculiar advantages and disadvantages, and each can give us a unique window on the sub-nuclear world. What will come out of these machines will almost certainly be quite different and much more exciting than any of us can think now.

SESSION ON SMALL Q^2 PHYSICS AND PHOTOPRODUCTION

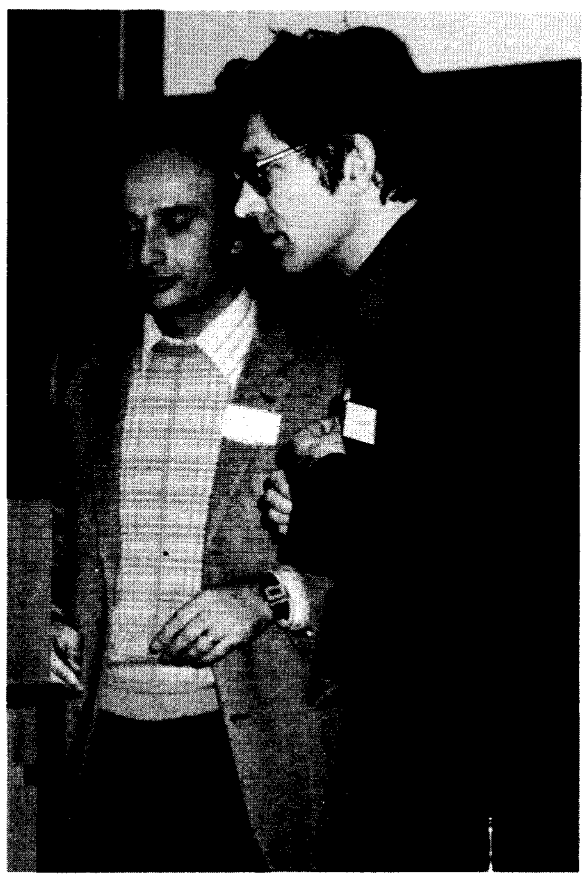

Discussion Leader: M. Greco

Scientific Secretary: D. Lueke

Report of the ep study group on SMALL Q^2-PHYSICS AND PHOTO PRODUCTION

by

W. Hoogland

NIKHEF-H, Amsterdam

Contents

I INTRODUCTION

In this report electroproduction is considered for Q^2-values below $Q^2 \approx 5$ GeV^2. In particular in the limit of $Q^2 \to 0$ the process can be interpreted as the scattering of an (almost) real photon off the proton. The interest of using an ep collider for studying low Q^2 processes lies obviously in the large c.m. energies that can be obtained for the γp system. In Table I the relevant parameters are listed for two possible ep facilities, one (PROPER) associated with PETRA[1)], another with LEP[2)].

Table I

E_e[GeV]	E_p[GeV]	s[GeV^2]	ν max[GeV]	L[cm^{-2}s^{-1}]
20	270	21600	11510	10^{32}
100	270	108000	57550	10^{32}

Even for a PROPER type ep collider ν_{max} is almost two orders of magnitude larger than the values that can be obtained with other sources of either real or virtual photons. A possible 3000 GeV proton accelarator (UNK) would still be off by one order of magnitude.

The interest of photonphysics lies in the unique property of the photon to have both a hadronic (meson-like) and a point-like component - both a rich source of heavy flavour quarks. If we consider the photon as a superposition of vectormeson states, an ep facility allows us to study meson-proton interactions up to s-values of about 20000 GeV^2 (PROPER) or 100000 GeV^2 (LEP). On the other hand, if we allow for the point-like component of the photon, point-like interactions of the photon may be studied in a clean way by looking for large p_T γp processes. Apart from photon physics an ep collider can be used to extend conventional lepton-proton inelastic scattering experiments to large ν (small x) and make it possible to control the transition from the VMD region at very small Q^2 to the approximate scaling region, assuming that scaling sets in at $Q^2 \simeq 1\text{-}2$ GeV^2 independent of ν.

II Kinematics, photon energy spectrum and luminosities

The kinematics of the process is indicated in fig. 1.

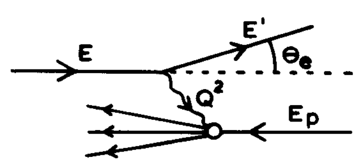

Fig. 1 Event kinematics for small Q^2 electroproduction reactions

$$E_\gamma = E - E' \simeq yE \qquad \text{II.1}$$

$$Q^2 \simeq E^2(1-y)\theta_e^2 + \frac{m_e^2 y^2}{1-y} \simeq EE'\theta_e^2 \qquad \text{II.2}$$

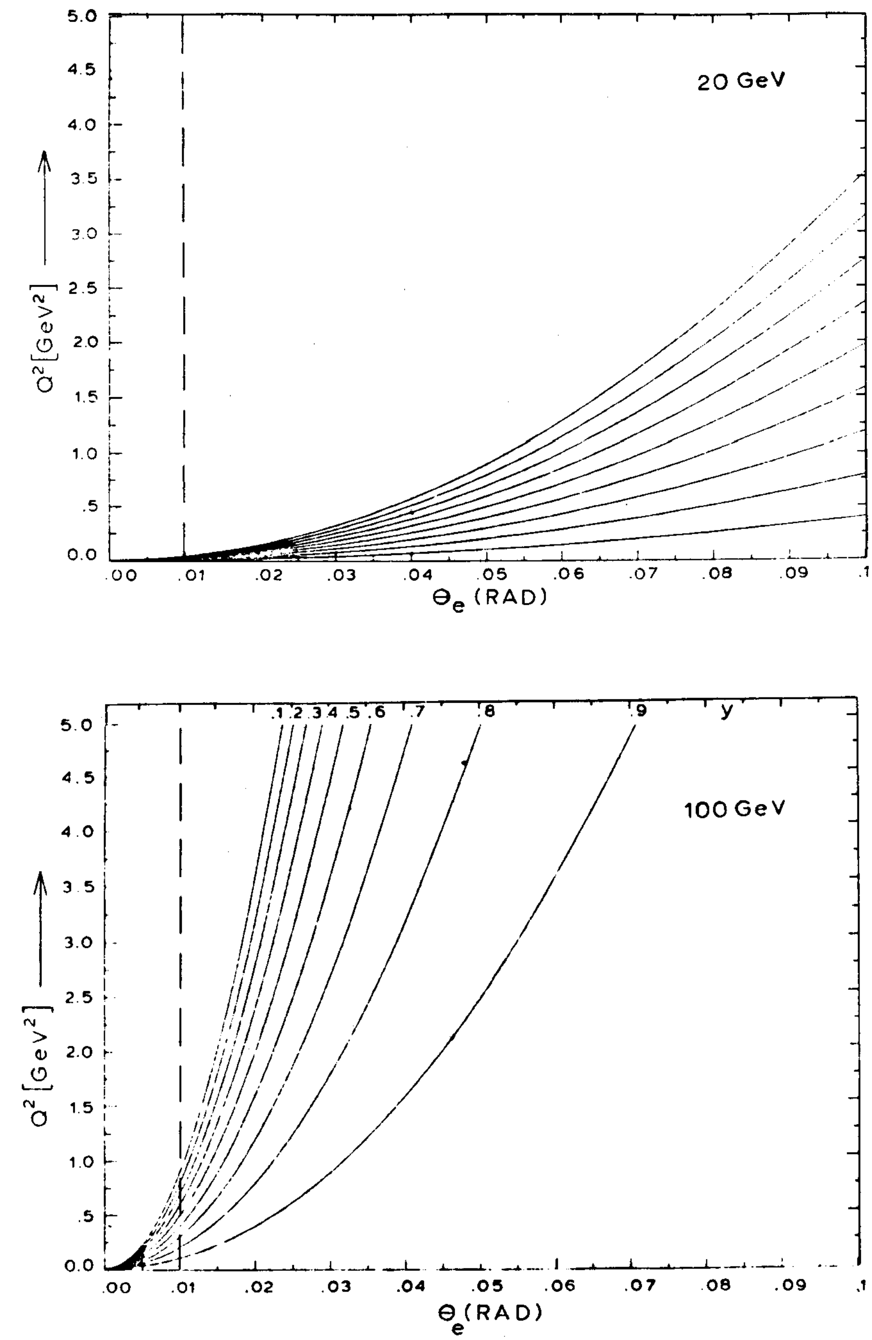

Fig. 2 Q^2 as a function of tagging angle Θ_e for fixed values of y; $E_\gamma \simeq yE_e$. A possible minimum tagging angle of 10 mrad is indicated (a) 20 GeV electrons on 270 GeV protons (b) 100 GeV electrons on 270 GeV protons.

Small Q^2 is equivalent to small values of θ_e. The scattered electron should therefore be tagged, down to the smallest possible angles. In fig. 2 Q^2 is plotted vs θ_e for fixed values of y both for a possible 20 x 270 and a 100 x 270 GeV ep collider. A realistic minimum tagging angle of 10 mrad, as indicated in the figure imposes a severe restriction on the accessible small Q^2 values for the 100 x 270 GeV option. If tagging below 10 mrad cannot be achieved, physics with very small Q^2 would be impossible with such a machine.

The standard expression for the one photon exchange cross section in terms of the transverse and longitudinal γp cross sections σ_T and σ_L is

$$\frac{d^2\sigma}{dxdy} = \frac{\alpha}{\pi}\,\frac{1-x}{xy}\,[(1-y+y^2/2)\ \sigma_T(Q^2,\nu) + (1-y)\sigma_L(Q^2,\nu)] \qquad \text{II:3}$$

where x and y are the usual dimensionless parameters.

$$x = Q^2/2M\nu$$

$$y = \nu/\nu_{max}$$

$$\nu = q.p/M;\ \nu_{max} = s/2M$$

In the limit of $Q^2 \to 0$ σ_T and σ_L behave as

$$\lim_{Q^2\to 0} \sigma_T(Q^2,\nu) = \sigma_{\gamma p}(\nu) \qquad \text{II.4}$$

$$\lim_{Q^2\to 0} \sigma_L(Q^2,\nu) = 0 \qquad \text{II.5}$$

with $\sigma_{\gamma p}(\nu)$ the real photon-proton cross section at an incident photon-energy ν.

In the equivalent photon approximation the limiting values (II.4) and (II.5) are assumed to hold also for $Q^2 \neq 0$ but small, so that (II.3) reduces to

$$\frac{d^2\sigma}{dxdy} = \frac{\alpha}{2\pi}\,\frac{1+(1-y)^2}{y}\,\sigma_{\gamma p}(\nu)\,\frac{1-x}{x} \qquad \text{II.6}$$

This equation integrated over x, may be approximated for $y \gtrsim .1$ by the well known Weiszacker-Williams formula

$$\frac{d\sigma}{dy} \approx \frac{\alpha}{2\pi}\,\frac{1+(1-y)^2}{y}\,\sigma_{\gamma p}(\nu)\,\ln\frac{Q^2_{max}}{Q^2_{min}} \qquad \text{II.7}$$

or for a tagging detector, which covers the angular range $\theta_e^{min} < \theta < \theta_e^{max}$

$$\frac{d\sigma}{dy} \approx \frac{\alpha}{\pi}\,\frac{1+(1-y)^2}{y}\,\bar{\sigma}_{\gamma p}(\nu)\,\ln\frac{\theta_e^{max}}{\theta_e^{min}} \qquad \text{II.8}$$

When using (II.7) and (II.8) to estimate cross sections for small Q^2 ep interactions one should keep in mind that we assume

i. $\sigma_T(Q^2,\nu) = \sigma_T(0,\nu) \equiv \sigma_{\gamma p}(\nu)$, and

ii. $\sigma_L(Q^2,\nu) = 0$

We know however, that for typical hadronic processes where VMD is assumed to hold, this can only be true for very small Q^2, since assuming ρ-pole dominance.

$$\sigma_T(Q^2,\nu) \simeq (1+Q^2/m_\rho^2)^{-2}\sigma_T(o,\nu), \text{ and} \qquad \text{II.9}$$

$$\sigma_L(Q^2,\nu) \simeq Q^2/m_\rho^2 \quad (1+Q^2/m_\rho^2)^{-2}\,\sigma_T(o,\nu) \qquad \text{II.10}$$

The Williams-Weiszacker formula is nevertheless useful for a rough estimate of the cross section for small Q^2 processes and thus of the effective luminosities for γp interactions. For this we integrate (II.7) with respect to y over the interval $.1 < y < .9$.

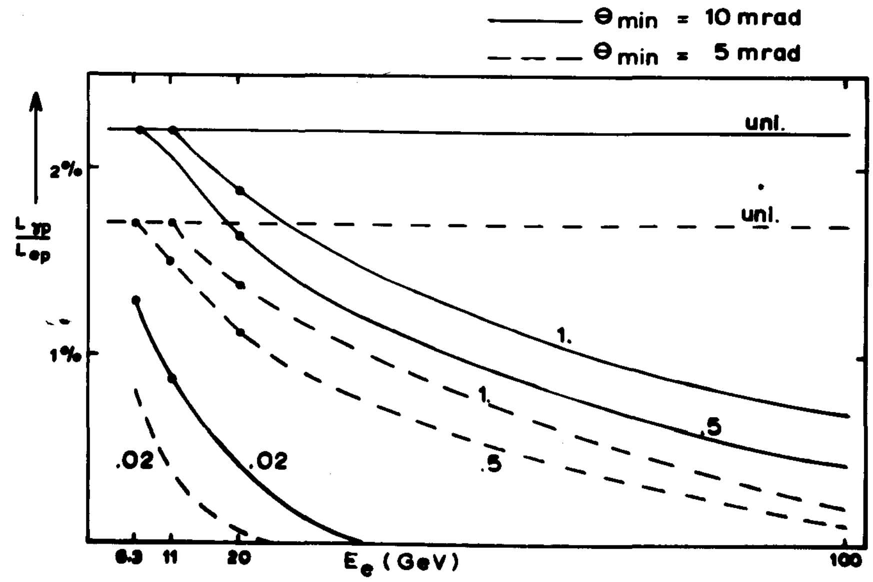

Fig. 3 Effective photon luminosity relative to ep luminosity for minimum tagging angles of 5 and 10 mrad respectively and for various limiting values of Q^2, Q^2_{max}= .02, .5, 1., unlimited

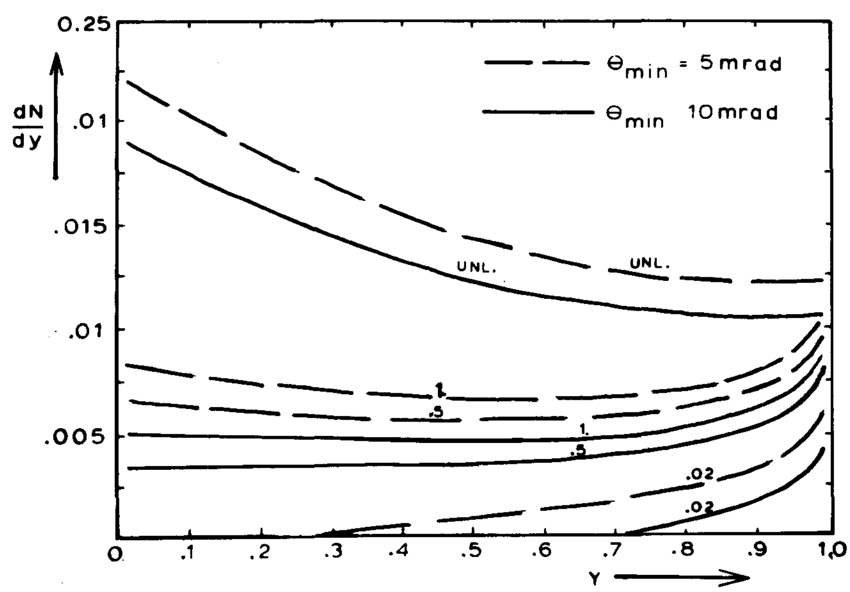

Fig. 4 Intensity of the virtual photon spectrum per electron versus photon energy for a tagged 20 GeV electron beam with Q^2_{max}= .2, .5, 1., unlimited and θ_e^{min} = 5 and 10 mrad respectively.

The result is shown in fig.3 as a function of the electron energy for two values of θ_e^{min} (5 and 10 mrad) and for different values of Q^2_{max}(.02, .05, 1., and unlimited).

In fig. 4 the photon energy spectrum is plotted as a function of y for a 20 x 270 GeV machine with θ_e^{min} = 5 and 10 mrad and for different values of Q^2_{max}.

Fig. 3 is another illustration of the fact that a 100 GeV electron beam would be a poor source of 'real' photons unless θ_e^{min} could be reduced by at least an order of magnitude.

At 20 GeV however, the effective luminosity is quite large, of the order of $10^{30}cm^{-2}s^{-1}$, assuming an ep luminositiy of 10^{32} and a Q^2_{max} of about .5.

Table 2

Luminosities of some existing or proposed photonbeams.

A 1 meter hydrogen target is assumed

		photon-luminosity (E_γ > 100 GeV)
a) γ-beams	γ-flux	
BEG 500 GeV(CERN-SPS)	$5x10^7$	$2.3x10^{31}$
BEG 400 GeV(CERN-SPS)	$2x10^7$	$.9x10^{31}$
FNAL wide band neutr.	$5x10^6$	$2.3x10^{30}$
E4 (CERN-SPS)	$8x10^5$	$3.6x10^{29}$
b) μ-beam	μ-flux	
CERN 200 GeV	$2.4x10^5$	$1.1x10^{29}$
280 GeV	$6.4x10^4$	$3x10^{28}$

The effective luminosity at lower electron energies would be even larger. An additional increase will come from the larger ep luminosity when the energy of the electron beam is reduced below its maximum value. In Table 2 we compare these luminosities with luminosities of either existing or proposed beams, both real and virtual, assuming the target to be a 1 meter liquid hydrogen target.

We conclude that with a PROPER type ep collider γp luminosities can be achieved that are competitive even with the highest. intensity γ beams, while the γp center of mass energies are up to two orders of magnitude larger.

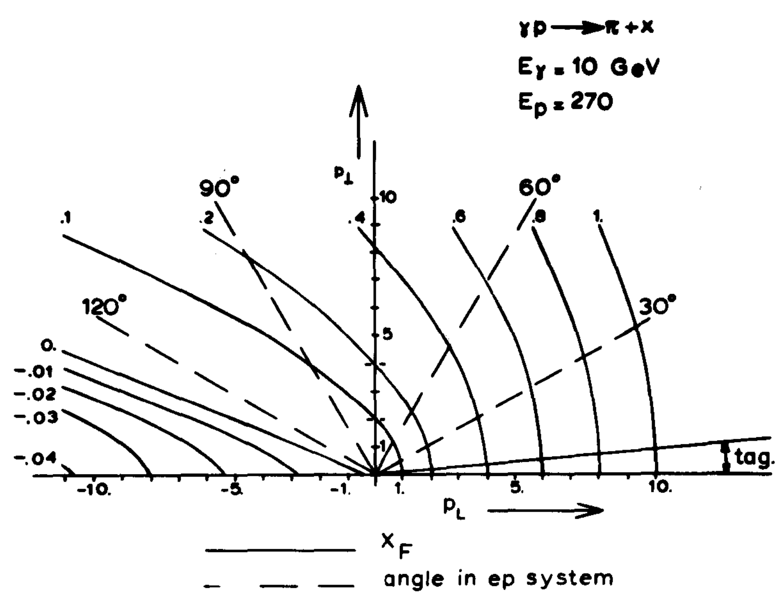

Fig. 5 Longitudinal vs transverse momentum in the lab. system of inclusively produced π-mesons in the reaction $\gamma+p \rightarrow \pi+x$ for fixed values of Feynman x_F. The incident photon energy is 10 GeV, the proton energy is 270 GeV.

The kinematics of the ep collisions in the proposed colliders is rather peculiar, with a center of mass that is moving rapidly along the incident proton direction. This asymmetry is even more accentuated if we consider the small Q^2 reactions as being γp interactions.

In fig. 5 we show for a limited range of p_L and p_T values, contours of fixed x_F for π mesons, produced in the inclusive reaction

$$\gamma + p \rightarrow \pi + x$$

The photon energy is 10 GeV, the proton energy 270GeV. The figure shows that particles in the proton fragmentation region have small angles and large energies and will therefore be difficult to measure. The photon beam fragmentation region, however, is easily accessible. In this respect an ep collider will be superior to fixed target accelerators, where beam fragmentation products will have large momenta, will be produced at small angles and therefore may be obscured by the large electromagnetic background. An ep collider will thus be an excellent tool to study the γ-beam fragmentation products in γp interactions.

III Electron tagging

To determine Q^2 and ν, E' and θ_e of the scattered electron have to be measured (fig. 10; eq. II.1 and II.2). For fixed E', the Q^2 range is determined by the angular range of the tagging detector.

For a conventional tagging system, consisting of an e.m. shower detector downstream of the intersection, the minimum tagging angle θ_e^{min} will depend on the detailed design of the intersection region i.e. the length of the straight section, requirements concerning radiation shielding and the cross section of the vacuum pipe.
If we assume a straight section of 7.5 m and a cross section of the vacuum pipe similar to that of PETRA i.e. 7 x 12 cm^2, θ_e^{min} = 10 mrad will be about the best that can be achieved. Smaller values of θ_e^{min} would be desirable, not to gain in over-all luminosity, which goes proportional to $\ln(\theta_e^{max}/\theta_e^{min})$ but to gain luminosity at small Q^2. However, problems with background, associated with the electron beam will increase rapidly for decreasing tagging angles.

The maximum tagging angle is a rather arbitrary value. The tagging detector has to fill the gap left over by the central detector, which generally covers electron angles down to about 100 mrad. Accordingly in our studies the tagging range has been set to 10 mrad < θ_e < 100 mrad

The resolution in Q^2 and ν is given by

$$\frac{\Delta Q^2}{Q^2} = \left\{ \left(\frac{\Delta E'}{E'}\right)^2 + \left(\frac{2\Delta\theta}{\theta}\right)^2 \right\}^{\frac{1}{2}}$$

$$\frac{\Delta\nu}{\nu} \simeq \frac{\Delta E'}{E-E'} = \frac{1-y}{y}\,\frac{\Delta E'}{E'}$$

The requirements of a tagging detector for γp physics will be different from those for $\gamma\gamma$ physics with an e^+e^- machine. In $\gamma\gamma$ physics one aims for the best energy resolution. In γp physics, where cross sections vary only slowly as a function of ν the energy resolution $\Delta\nu/\nu$ can be relatively poor. However, since cross sections very rapidly with Q^2, $\Delta Q^2/Q^2$ has to be quite good.

In Table 3 and 4 we give values for $\Delta Q^2/Q^2$ and $\Delta\nu/\nu$ for three possible detectors types (NaI, Liquid Argon, and Pb Scintillator) with energy resolutions of respectively $.02/E'^{\frac{1}{4}}$; $.05/E'^{\frac{1}{2}}$; $.15/E'^{\frac{1}{2}}$. We have further assumed that θ_e is measured with drift chambers giving an absolute error $\Delta\theta$ of .5 mrad.

Table 3

E_e GeV	y	Θ_e mrad	Q^2 GeV^2	$\frac{\Delta Q^2}{Q^2}$(Pb-Sc)	$\frac{\Delta Q^2}{Q^2}$(L.A.)	$\frac{\Delta Q^2}{Q^2}$(NaI)
20	.1	10	.004	.15	.11	.10
20	.1	50	.1	.10	.04	.025
20	.1	100	.4	.10	.035	.015
20	.5	10	.02	.11	.11	.11
20	.5	50	.05	.05	.025	.025
20	.5	100	2.	.045	.015	.01

Table 4

E_e GeV	y	$\frac{\Delta\nu}{\nu}$(Pb-Sc)	$\frac{\Delta\nu}{\nu}$(L.A.)	$\frac{\Delta\nu}{\nu}$(NaI)
20	.1	.31	.11	.09
10	.1	.45	.14	.10
6	.1	.59	.18	.11
20	.5	.05	.02	.015
10	.5	.65	.02	.015
6	.5	.09	.03	.015

Tables 3 and 4 show that both $\Delta Q^2/Q^2$ and $\Delta\nu/\nu$ are acceptable for a Pb-Sc detector, apart from y $\lesssim$ .2 where $\Delta\nu/\nu$ would become very poor. However, to reach small ν it might be preferable, to use a lower momentum electron beam instead of measuring at very small y. This would result in a better $\Delta\nu/\nu$, while at the same time Q^2_{min} would be reduced. We conclude that even a cheap and relatively simple Pb-Sc shower detector might be satisfactory for electron tagging in small Q^2 physics with an ep collider.

IV Small Q^2 physics

A 20 x270 GeV ep collider has been shown to be a rich source of photons with small Q^2. The large center of mass energy of the γp system allows the study of γp interactions in an energy range which is inaccessisble to other γ sources. The very special kinematics favours experiments where the reaction products are studied in the beam fragmentation region of the photon.

Extensive reviews of photoproduction experiments can be found in references [3]. The use of an ep facility for doing photon physics has been previously -but not very extensively- discussed by Llewelyn Smith and Wiik[4)] and the CHEEP study group[5)]. In this report we will consider in more detail the interest and feasibility of a few possible experiments, which we think are representative for the small Q^2 physics of an ep collider. These are:

A. the measurement of the total cross section for very small values of x, allowing in the limit of $Q^2 \to o$ a determination of $\sigma_{\gamma p}^{tot}$;

B. the study of large cross section exclusive processes In particular elastic Compton scattering; the diffractive production of vector meson states and Primakoff production;

C. the study of jets and single particles at large p_t in photon interactions

A. Total cross section

A measurement of the total inclusive ep cross section $\frac{d^2\sigma}{dE' d\Theta_e}$ (i.e $\frac{d^2\sigma}{dxdy}$) is certainly one of the first experiments to be done.

For small Q^2 the standard expression for the electroproduction cross section is given by (II.3). Because of (II.4) and (II.5) $\sigma_{\gamma p}$ can be determined by extrapolating the measured cross section to $Q^2 = o$.

This is true for any γp cross section, and consequently for $\sigma_{\gamma p}^{tot}$.

$\frac{d^2\sigma}{dxdy}$ can also be written in terms of the proton form factors νW_2 and MW_1

$$\frac{d^2\sigma}{dxdy} \simeq \frac{4\pi^2\alpha}{sx^2y^2}\,\nu W_2(Q^2,\nu)\,\left[1-y+\frac{y^2}{2(1+R)}\right] \qquad \text{IV.1}$$

$$\text{where } R = \frac{\sigma_L}{\sigma_T} \simeq \frac{W_2}{W_1}\frac{\nu^2}{Q^2} - 1 \qquad \text{IV.2}$$

Therefore, provided R is small, the total cross section measures essentially νW_2.

R can in principle be determined, but requires the cross section to be measured for at least two values of the c.m. energy.

(1) $\sigma_{\gamma p}^{tot}$

The total γp cross section has been measured on hydrogen for incident photon energies E_γ up to ~200 GeV[6]. The data are shown in fig. 6. Also shown are the predictions from simple VMD and the additive quark model.

These relate $\sigma_{\gamma p}^{tot}$ to the (measured) πp and Kp total cross sections i.e.

$$\sigma_{\gamma p}^{tot} \propto \sum_{\rho,\omega,\varphi} \alpha\frac{4\pi}{f_V^2}\,\sigma_{Vp}^{tot} \qquad \text{IV.3}$$

and

$$\sigma_{\rho p}^{tot} = \sigma_{\omega p}^{tot} = \tfrac{1}{2}(\sigma_{\pi^+p}^{tot} + \sigma_{\pi^-p}^{tot}) \qquad \text{IV.4}$$

$$\sigma_{\varphi p}^{tot} = \sigma_{K^+p}^{tot} + \sigma_{K^-p}^{tot} - \sigma_{\pi^-p}^{tot}$$

For E_γ > 200 GeV the VMD predictions are extrapolated assuming a $\ln^2 s$ rise of the total meson-proton cross sections. The equivalent E_γ for a 20 x270 GeV ep collider goes up to

10.000 GeV i.e. two orders of magnitude up the energy scale. An ep collider therefore provides a large lever arm to establish the s-dependence of the rising meson-proton total cross section.

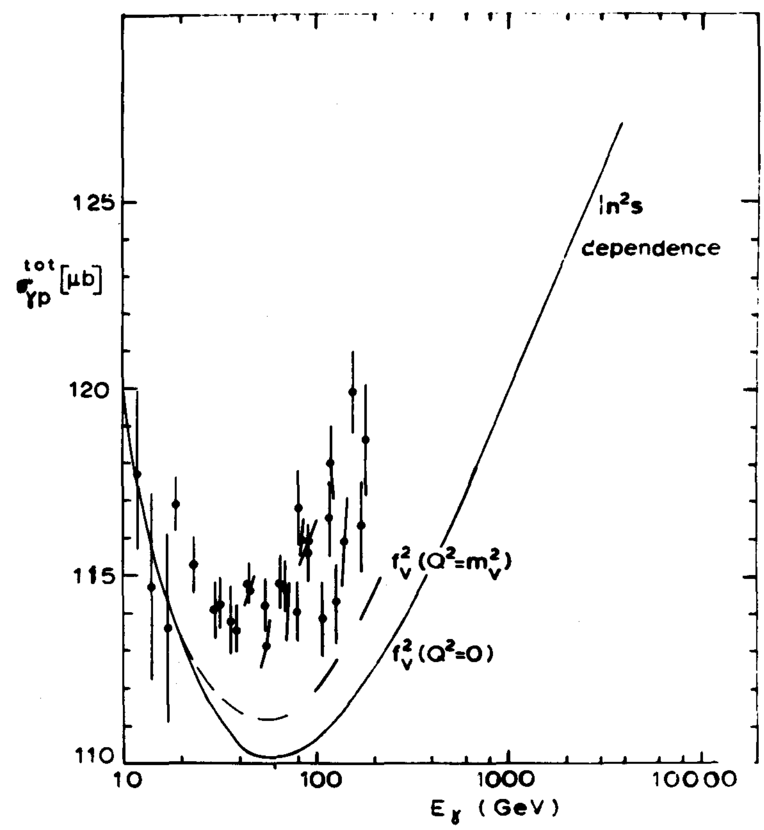

Fig. 6 Total γp cross section as a function of E_γ (proton at rest). The curves are predictions based on simple VMD and the additive quark model[6], using two different determinations of $f^2{}_V$, the γV coupling constant. The extrapolation assumes a $\ln^2 s$ rise of $\sigma_{\gamma p}^{tot}$

There has been some discussion about the apparent discrepancy of 2-5 μb between the data and the predicted values. If not simply due to a normalization problem -in particular the fact that the contribution of the continuum to (IV.3) is accounted for by the normalization of the data- it might indicate

i. the opening of the charm threshhold[7], in which case the effect appears to be quite large however, or

ii. the onset of an important contribution due to point-like γ-interactions[8].

The measurements of $\sigma^{tot}_{\gamma p}$ over a large s-range, if accompanied by similar data for elastic vector meson production may help to understand this point.

In ep interactions $\sigma^{tot}_{\gamma p}$ is determined indirectly from an extrapolation to $Q^2 = 0$ i.e.

$$\sigma^{tot}_{\gamma p}(ys) = \lim_{Q^2 \to 0} \underbrace{\frac{\pi}{\alpha} Q^2 \frac{x}{(1-y)(1+R)+y^2/2} \frac{d^2\sigma}{dQ^2 dy}}_{\sigma_{\gamma p}(Q^2, ys)} \qquad \text{IV.6}$$

To find out how reasonable such an extrapolation would be, we show in fig. 7 the estimated behaviour of $\sigma_{\gamma p}(Q^2,y)$. For this, we have used the following parametrizations of νW_2 and R at small Q^2 [9]

$$\nu W_2(Q^2,\nu) = \{\sum_{i=3,4,5} C_i (1-x)^i\}\{1-W_{el}\} \qquad \text{IV.7}$$

$$W_{el} = \frac{G_E^2 + \frac{Q^2}{4M^2} G_M^2}{1+\frac{Q^2}{4M^2}}$$

$$R = \frac{.2Q^2}{Q^2+.5} \qquad \text{IV.8}$$

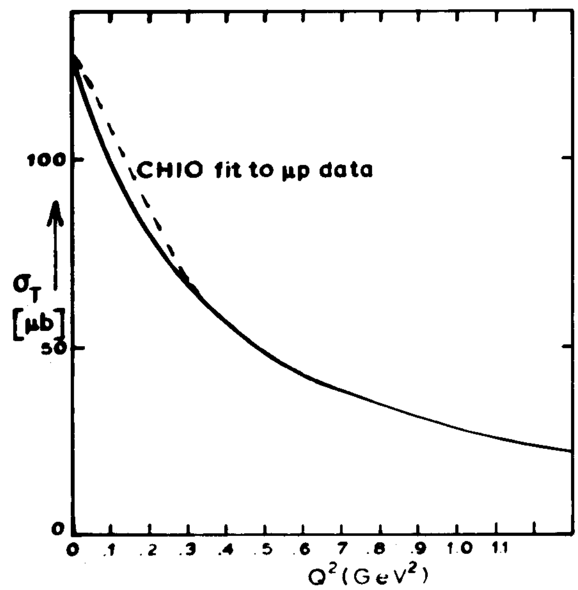

Fig. 7 $\sigma_{\gamma p}^{tot}$ as a function of Q^2, using parametrizations of νW_2 and R, described in the text. The dotted line is a fit to data from the CHIO μ-experiment in the ν-range 170-200 GeV as presented by Gabathuler [7].

This seems to be quite acceptable comparing the estimated curve with a (scaled) fit to μp data from the CHIO collaboration[10]. Near $Q^2 = 0$, $\frac{d\sigma}{dQ^2} \simeq 250$ μb GeV^{-2}, while $\Delta Q^2/Q^2 \simeq 10\%$.

Since data are obtained down to very small Q^2 (see fig. 2) the resulting error in $\sigma_{\gamma p}^{tot}$ should be small.

(2) νW_2

In fig. 8 lines of constant θ_e and constant x are shown in a Q^2 vs ν plot for a 20 x 270 ep collider

With a minimum tagging angle of 10 mrad x is measured in the range $10^{-3} < x < 10^{-5}$.

μp scattering data exist, which measure νW_2 down to $x \simeq .001$, however, with $Q^2 < 2$ GeV^2 for the low x data and with poor statistics[11].

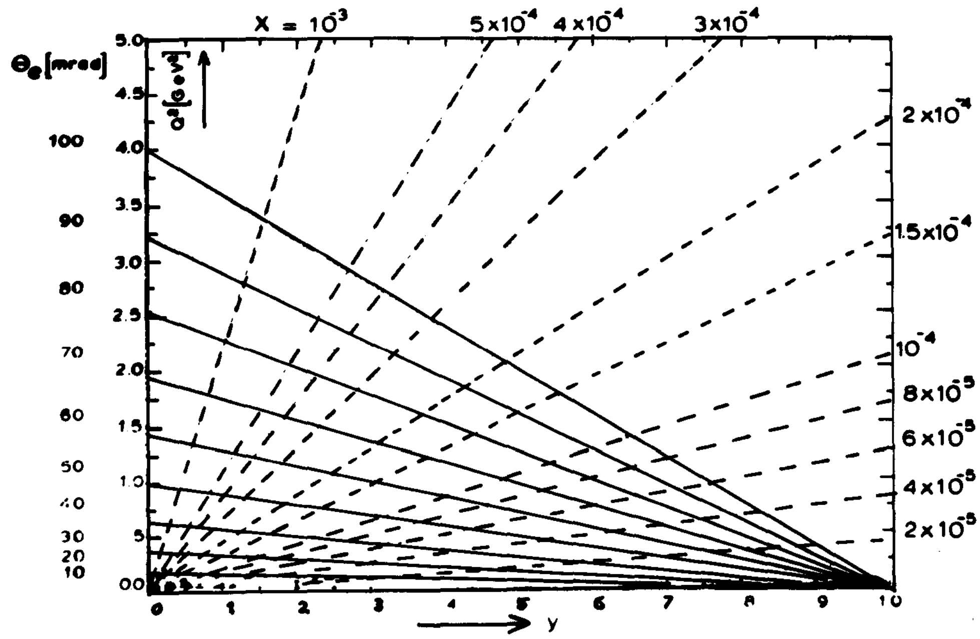

Fig. 8 Lines of constant x and Θ_e in the Q^2, y plane for 20 GeV electrons on 270 GeV protons, at small Q^2.

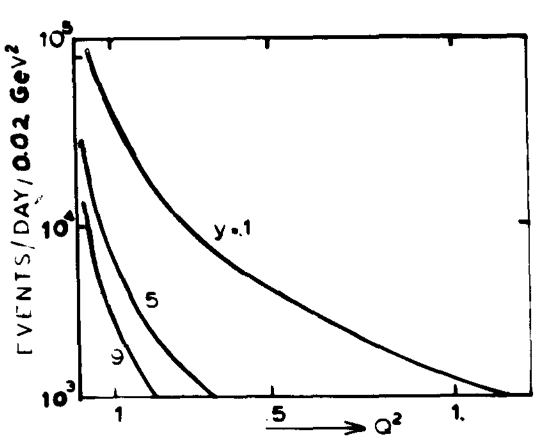

Fig. 9 Expected rates/day/.02 GeV^2 for small Q^2 reactions of 20 GeV electrons on 270 GeV protons, as function of Q^2, for y = .1, .5, .9

An ep collider would extend these limits considerably and with better statistics. Compare for instance the total integrated luminosity of 2 x $10^{35}cm^{-2}$ of the quoted μp scattering experiment with the integrated luminosity of $10^{37}cm^{-2}$ for one running day of the ep machine. Some rates estimated as a function of Q^2 and for different values of y are shown in fig. 9; the same parametrization for νW_2 and R (IV.7 and IV.8) has been used as in the previous paragraph.

(3) R

Equation (IV.1) can be written as

$$\frac{\pi}{\alpha}\frac{d^2\sigma}{dxdy}\frac{xy}{1-y+y^2/2} = \sigma_T(ys,x)\left[1+R(ys,x)\frac{1-y}{1-y+y^2/2}\right] \qquad \text{IV.9}$$

If the LHS of (IV.9) is plotted for fixed ys as a function of $(1-y)/(1-y+y^2/2)$ we obtain a straight line the slope of which determines R(ys,x). This is illustrated in fig. 10. The determination of R requires the measurements of $\frac{d^2\sigma}{dxdy}$ for at least two values of s such that $s_1\ y_1 = s_2\ y_2$ and obviously with $x_1 = x_2$. The two measuring points should be wide apart in order to get the best resolution in R. With an ep machine this can be readily achieved by varying the momenta of the colliding beams. In fact, since both electron and proton momentum are varied, the range of the kinematic variables is much larger than with a fixed target machine. In fig. 10 we show as an example two possible measuring points for machine energies of 20 x270 and 13 x 175 respectively. The error in R will be mainly determined by the relative normalization of the luminosities, the statistical error being negligible at these small Q^2, and provided other systematic effects can be kept under control. If we assume that the relative normalization is known to within a few procent R may be determined down to values of about .1.

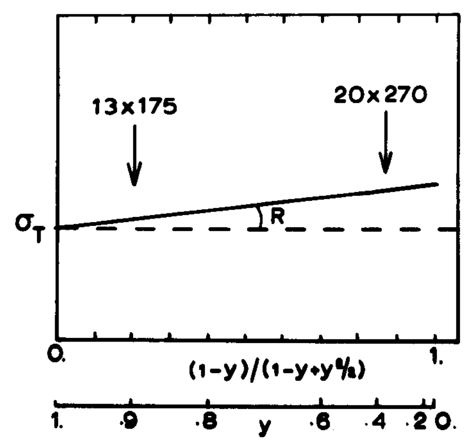

Fig. 10 $\frac{\pi}{\alpha}\frac{d^2\sigma}{dxdy}\frac{xy}{1-y+y^2/2}$ plotted as a function of $(1-y)(1-y+y^2/2)$, for fixed values of sy should give a straight line, the slope of which is R. Indicated are the two possible measuring points with ep momenta of 20x270 GeV and 13x175 GeV respectively.

B. Exclusive photoproduction processes.

Because of the very high c.m. energies we may expect only diffractive γp collisions to occur with measurable cross sections.

In this section we restrict ourselves to elastic processes i.e.

1) $\gamma_V(Q^2) + p \to \gamma + p$ elastic compton scattering, and

2) $\gamma_V(Q^2) + p \to V + p$ elastic vector meson production

In addition we will discuss

3) $\gamma_V(Q^2) + p \to X + p$ Primakoff production

In principle these processes are rather clean, the γ, V or X in reactions (1), (2), (3) carry almost all the incident photon energy, while the recoil proton is almost undisturbed in the ep system. Thus

$$E_\gamma/E_V/E_X \simeq E-E'$$
$$E'_p \simeq E_p$$
$$\theta_p \simeq \sqrt{t}/E_p$$

However because of the large proton energy, the elastic processes may be difficult to separate from interactions where the proton is diffractively excited. From ISR data we know that single diffractive excitation i.e. p+p → N*+p occurs with a comparable cross section as the purely elastic process [12].

The invariant mass of the N* is peaked at low masses and falls approximately as $1/M^2$. A similar situation may occur in ep scattering. The high momentum of the (excited) proton will make it difficult to distinguish the elastic from the inelastic diffractive process, unless the proton is detected and its momentum and direction are measured.

Since the proton angles are small -a four- momentum transfer t = .1 corresponds with $\theta_p \simeq 1$ mrad if E_p = 270 GeV- this requires proton tagging down to very small angles with respect to the incident proton beam.

Taking into account the beam divergence (~ 1/3 mrad) θ_p^{min} will be of the order of 2 mrad, with the angular resolution limited by the beam divergence.

A momentum resolution of a few procent would be sufficient to reduce a possible background from inelastic diffractive processes to an acceptable level (fig. 11). The above conditions i.e. $\theta_p^{min} \simeq 2$ mrad; $\Delta\theta_p \simeq .3$; $\Delta p/p \simeq \mathcal{O}(1\%)$ might be fulfilled by a tagging detector located far downstream the intersection point, using bending elements of the proton ring itself to provide for the necessary bending power. The feasibility of this has to be discussed. A serious problem might be the background from beam gas interactions, which could be important because of the large source length and the large hadronic pp cross section (see CHEEP report[5] p.65).

A θ_p^{min} of 2 mrad would correspond to a t_{min} of .3, .12, .04 GeV^2 for proton momenta 270, 175, 100 GeV respectively. Therefore, in order to reach small t the machine has to run at relatively low momentum.

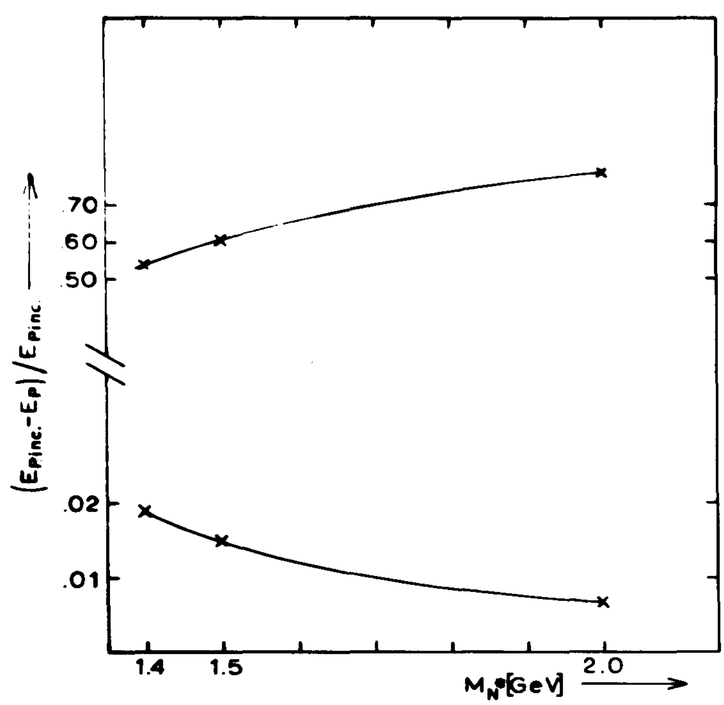

Fig.11 Lower and Upper limit of the ratio $(E_p-E_{p_{inc}})E_{p_{inc}}$ for a proton from the decay $N^*\to p\pi$, as a function of N*invariant mass, the N* is produced in an inelastic diffractive process of the type $\gamma+p\to V+N^*$.

(1) Elastic Compton scattering

Published data on elastic Compton scattering exist for E_γ up to 17 GeV[13].

Moreover, the process has been observed for energies $75 \text{ GeV} < E_\gamma < 140 \text{ GeV}$ at FNAL[14].

From the optical theorem

$$\left.\frac{d\sigma}{dt}\right|_{t=o} = \frac{{\sigma_\gamma^{tot}}^2}{16\pi} \quad (1 + \alpha_\gamma)$$

we may estimate $\sigma^{tot}_{\gamma p \to \gamma p} \simeq .1 \ \mu b$, assuming

- $\sigma^{tot}_\gamma \simeq 100 \ \mu b$
- $\alpha_\gamma \simeq 0$
- $d\sigma/dt \simeq e^{8t}$

A slope parameter of ~ 8 GeV^{-2} follows under the assumption of VMD with ρ-pole dominance. The slope appears to be rather independent of energy. Photoproduction of the J/ψ indicates a much flatter t-dependence with a slope $b \simeq 2$[15]. Accordingly we may expect the J/ψ to dominate elastic Compton scattering at large t resulting in a break in the slope of the differential cross section near $t \simeq .8$. This break should shift towards smaller t-values when Q^2 increases, the ρ-propagator falling off much faster than that of the J/ψ. It would be interesting to see this effect by measuring the elastic Compton scattering cross section as a function of t and Q^2.

It has been suggested that point-like diagrams may dominate at large t in Compton scattering, resulting in an almost real amplitude described by a fixed pole at J=0[16].

This point-like behaviour might be demonstrated by comparing the s-dependence of the elastic cross section $\gamma + p \rightarrow \gamma + p$ and $\gamma + p \rightarrow V + p$ for fixed t/s. If a point-like coupling of the proton is present the counting rules predict a different s-dependence for these two processes resulting in a rising value for the ratio $\sigma_{\gamma\gamma}/\sigma_{\gamma V}$.

Although the study of elastic Compton scattering at large t appears to be most interesting, the rates unfortunately are rather disappointing. With a cross section of .1 μb, a slope parameter b = 8 GeV^{-2}, and an effective luminosity $L_{\gamma p} = 10^{30} cm^{-2} s^{-1}$ the total elastic Compton rate is of the order of 10^4 events/day, while for $t \gtrsim 1$ GeV^2 only 3 events/day may be expected. In fig. 12 t is plotted versus the production angle of the scattered photon for different values of y. Assuming the incident γ_V to be parallel to the incident electron direction the scattered photon may only be detected if its angle is larger than θ_e^{min}. Moreover, if we also require tagging of the scattered proton in order to discriminate against inelastic processes, we have t > .3 GeV^2. It may be possible to relax the tagging condition by requiring only the proton to be measured, but not the electron, getting the energy information from the single, low momentum, scattered photon. This would increase the rate for t > .3 GeV^2 by a factor of 10.

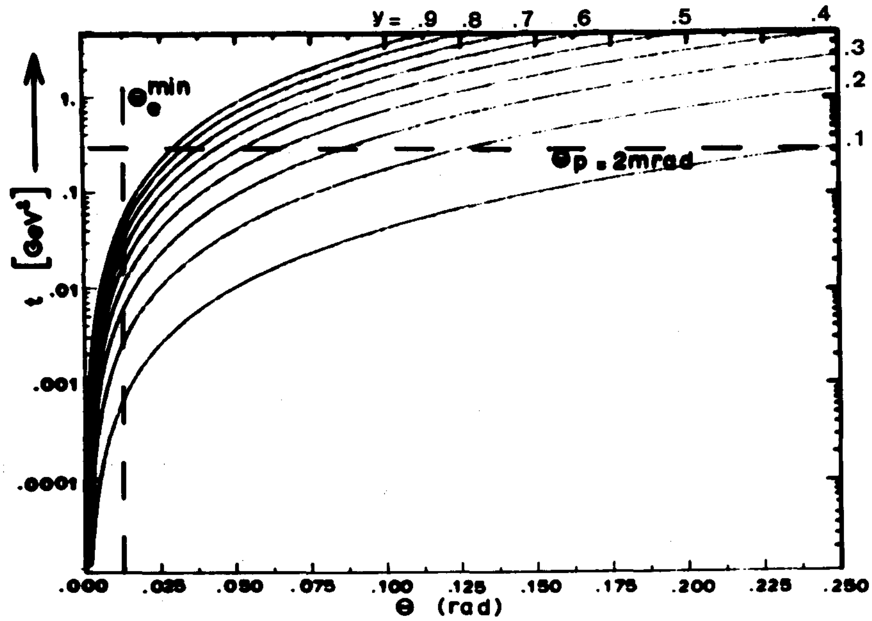

Fig. 12 t vs $\Theta\gamma$ for elastic Compton production for different values of $E\gamma = yE_e$ (E_e = 20 GeV; E_p = 270 GeV). Indicated are a possible lower limit in the angle for γ-detection of 10 mrad and a lower limit on t if proton tagging is required.

(2) Diffractive production of vector mesons

VMD and the optical model link the photoproduction of vectormesons to the total vectormeson-nucleon cross section

$$\frac{d\sigma}{dt}\ (\gamma N\to VN)\ =\ \alpha\frac{4\pi}{f_v^2}\ \frac{d\sigma}{dt}\ (VN\to VN)$$

$$\frac{d\sigma}{dt}\ (\gamma N\to VN)\Big|_{t=o} = \frac{\alpha}{16\pi}\ \frac{4\pi}{f_v^2}\ (1+\alpha)\ \sigma_T^2(VN)$$

Phenomenologically σ_T (VN) appears to satisfy a universal scaling function[17)].

$$\sigma_T(VN)\ \sim\ \frac{1}{m_v^2}\ F\ (\frac{s}{m_v^2})$$

further

$$\frac{1}{f_{V^2}} \simeq \frac{\Gamma_V^{e\bar{e}}}{m_V}, \text{ and}$$

$$\Gamma_i^{e\bar{e}} \sim Q_i^2$$

so that

$$\frac{d\sigma^V}{dt}(s)\Big|_{t=o} \sim \frac{1}{A}\,\frac{1}{m_V^5}\,\Gamma_V^{e\bar{e}}\ \tilde{F}\left(\frac{s}{m_{V^2}}\right)$$

$$\text{with } A \simeq 1.7 \times 10^{-8}$$

Cross sections for vectormeson production are estimated, assuming that for $s/m_{V^2} \gtrsim 50$ the universal scaling function approaches a constant $F(s/m^2_V) \simeq 50$ (nb GeV^2). Experimental data on the photoproduction of the ϕ-meson actually show an increase of the cross section by about a factor 2 from $E_\gamma \sim 20$ GeV to $E_\gamma \sim 200$ GeV[10], so that the above value of $F(s/m^2_V)$ has to be considered as a lower limit. The rates estimated are given in Table 5 below

Table 5

	$\frac{d\sigma}{dt}\Big\vert_{t=o}$	$\sigma^{tot}_{(\gamma p \to Vp)}$	slope	Events /day ($L_{\gamma p}=10^{30}cm^{-2}s^{-1}$)
ρ	~70μb GeV^{-2}	~ 9μb	~8 GeV^{-2}	9×10^5
ω	~ 8 "	~ 1μb	~8 "	1×10^5
ϕ	~3.5 "	~.5μb	~8 "	5×10^4
J/ψ	~50nb GeV^{-2}	~25nb	~2 "	2.5×10^3
Υ	~50pb GeV^{-2}	~25pb	~2 "	2.5

For the J/ψ, folding in a branching ratio of 7% for the decay into $e^+e^-/\mu^+\mu^-$ we obtain an estimated 150-200 tagged events a day. The rate for Υ production, taking into account its decay into an observable decay channel, will certainly be too small. The measurement of the cross section for vector meson production may be related by the additive quark model to the cross sections for πp, Kp and Dp interactions.

$$\sigma_{\rho p} = \sigma_{\omega p} = \tfrac{1}{2}(\sigma_{\pi^+ p} + \sigma_{\pi^- p})$$

$$\sigma_{\phi p} \propto \sigma_{K^+ p} + \sigma_{K^- p} - \sigma_{\pi^- p}$$

$$\sigma_{\psi p} \propto \sigma_{D^+ p} + \sigma_{D^- p} - \sigma_{\pi^- p}$$

It thus will provide information on meson proton total cross sections up to very high energies. In particular photoproduction of the J/ψ may demonstrate a possible rise of the Dp total cross section.

In fig. 13 we show for ρ, ϕ and J/ψ the lab. angles of the two decay particles (for ep energies 20 x 270 GeV).

In all cases the vectormeson is produced with $P_\perp = 0$. The lines correspond to different values of $\cos\theta$, with θ the Gottfried-Jackson angle; the points indicate increasing values of y, starting with y=.1. The energies of the decay products will always be less than the incident electron energy of 20 GeV. For the low mass vectormesons (ρ and even more so the ϕ-meson) the production angles are small. It therefore may experimentally be preferable to go to lower ep momenta. The momenta of the decay products of the vectormeson will be lower, which

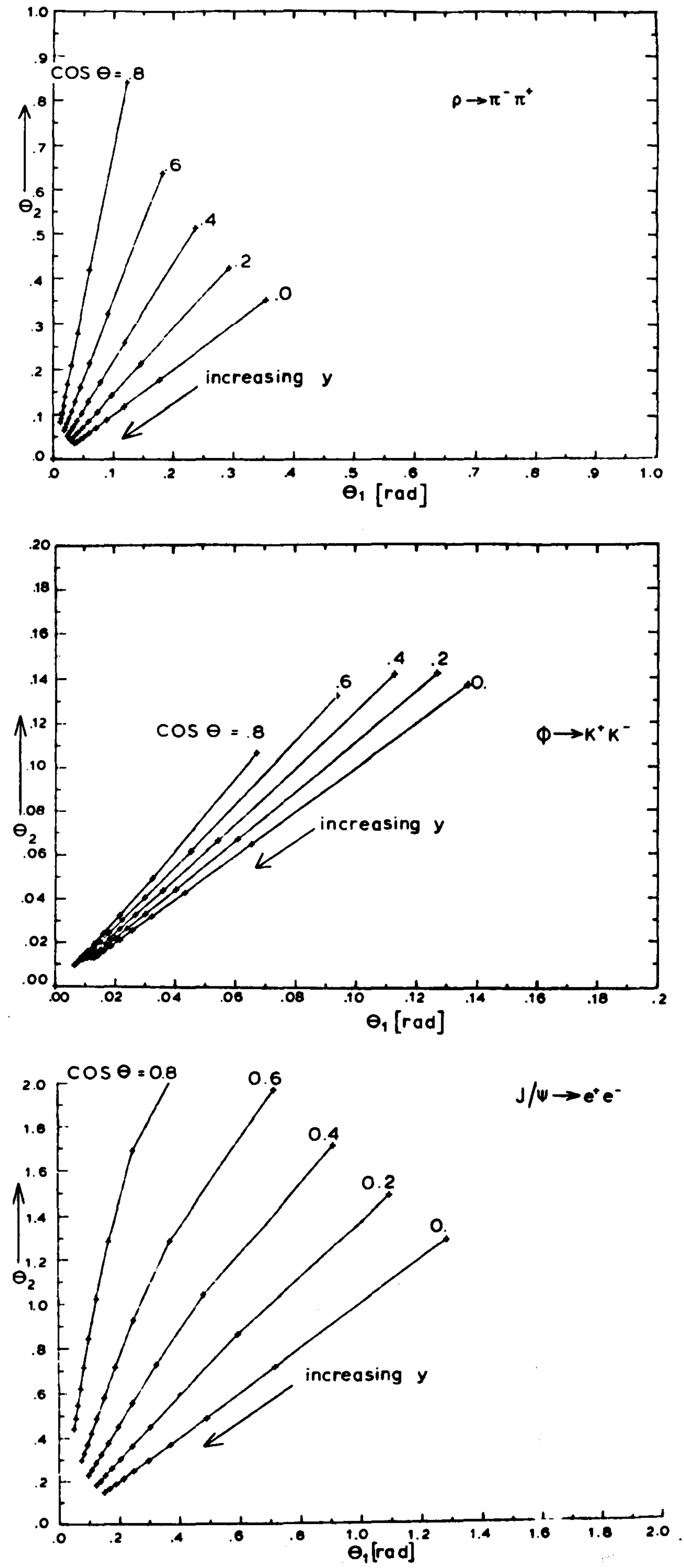

Fig. 13

Production angles Θ_1 and Θ_2 of the decay products of
(a) $\rho \rightarrow \pi^+\pi^-$
(b) $\phi \rightarrow K^+K^-$
(c) $\psi \rightarrow e^+e^-$
produced in the reactions $\gamma + p \rightarrow V + p$ for different decay angle $\cos\Theta_{GJ}$ and y, and with $p_\perp^V = 0$

will improve the momentum resolution and possibly facilitate the particle identification. Also the recoil proton has a larger angle for the same t. so that proton tagging does not impose a too severe cut on the four momentum transfer.
For the J/ψ the angles of the decay particles (e^+e^- or $\mu^+\mu^-$) are relatively large. They should be easily measurable with a good momentum resolution when a central-magnetic detector is used.

(3) Primakoff production

The cross section for the Primakoff production of a particle X is given by

$$\frac{d\sigma}{dt} = \frac{8\pi\alpha}{M_x^3}\,\Gamma_{\gamma\gamma}\,\frac{t-t_{min}}{t^2}\,\left|F(t)\right|^2$$

The cross section is steeply peaked at low t, in the first place because of the 1/t dependence and ~~secondly~~ due to the strongly damping proton form factor ($F(t) \sim (1+t/.71)^{-2}$).
The only significant contribution to the cross section therefore comes from small t. The integrated cross section, setting F(t) for small t equal to 1 becomes

$$\sigma = \int_{t_{min}}^{t_{max}} \frac{d\sigma}{dt} \simeq \frac{8\pi\alpha}{M_x^3}\,\Gamma_{\gamma\gamma}\left\{\ln\left(\frac{t_{max}}{t_{min}}\right) - 1\right\}$$

With $t_{min} \simeq \frac{M_x^4\, m_p^2}{s^2}$ and $t_{max} \simeq .1$ we obtain the cross section and rates estimates given in Table 6 below.
The effective luminosity is assumed to be $10^{30}\ cm^{-2}s^{-1}$.

Table 6

	$\Gamma_{\gamma\gamma}$ (GeV)	σ (nb)	events/day
π^0	$8\text{x}10^{-9}$	5	5000
η	$3.2\text{x}10^{-7}$	2	2000
η	$6\text{x}10^{-6}$	6.5	6500
η_c	$\simeq 1\text{x}10^{-6}$	$\simeq .025$	$\simeq$ 25
η_b	$\simeq 1\text{x}10^{-6}$	$\simeq .0005$	$\simeq .5$

The partial width of η_c and η_b is expected to be of the order of a few KeV . We have used 1 KeV to get an estimate of the order of magnitude of η_c,η_b production. Only, η_c and η_b production seem to be of any interest, but will occur with very low rates. If we take into account the branching ratio into some observable decay channel -we assume BR($\gamma\gamma$)/BR(Hadrons) $\simeq$ $(\alpha/\alpha_s)^2 \simeq \mathcal{O}(10^{-3})$; also branching rates for typical hadronic decay channels will be of the order of 1%- then the rates even for η_c production are prohibitively small.

Moreover, since all events are concentrated at t $\lesssim$ .1 proton tagging will not be feasible. Accordingly it will be impossible to demonstrate the occurrence of Primakoff production by its characteristic steep t-distribution.

C. Production of jets and single particles in large $p_\perp$ γp interactions

A very interesting subject in photon physics is the study of interactions in which the point-like component of the photon is probed. Generally the interaction of a low Q^2

photon in electron proton scattering is thought to proceed through its hadronic component, in contrast to large Q^2 photons which are assumed to couple point-like to the partons.

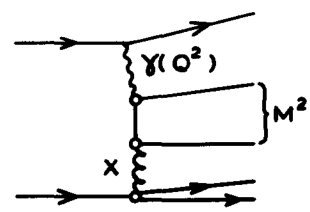

Fig. 14 Parton diagram for production of a quark pair with invariant mass M by a small Q^2 virtual photon off a gluon with momentum fraction x of the proton

However, parton diagrams as shown in fig. 14 may be valid for low Q^2 photons provided M^2 is large, thus setting the scale at which lowest order pertubation theory in QCD is assumed to be applicable. We take as a lower limit $M^2 = 10\ \mathrm{GeV}^2$.
Neglecting parton masses it follows from fig. 14 that

$$x = (Q^2 + M^2)/2M_p\nu$$

i.e for small Q^2 and large M^2 $\quad x = M^2/2M_p\nu$

In this section we will discuss the lowest order point-like diagrams shown in fig. 15.

They are associated with the following processes:

a. deep inelastic Compton scattering[18)]

b. the QCD analogue of Compton scattering[19)]

c. the QCD analogue of the Bethe Heitler process[20)]

d. Drell-Yan di-muon production

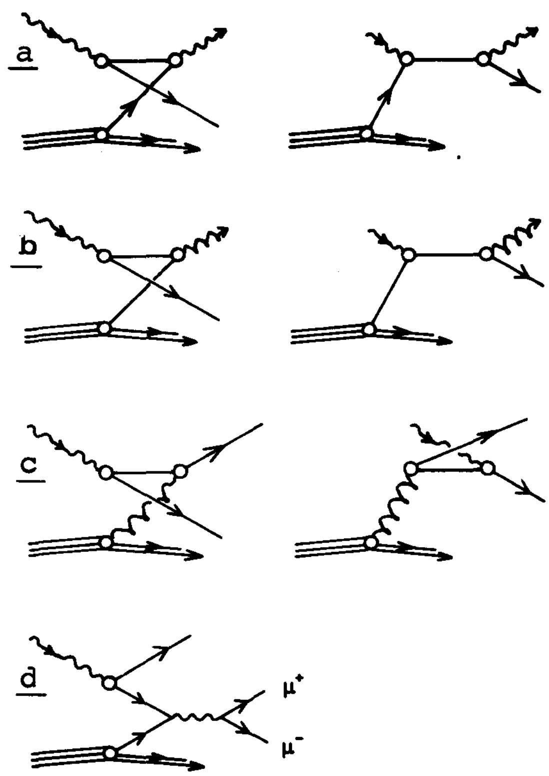

Fig. 15 Parton diagram corresponding to
(a) deep inelastic Compton scattering
(b) the QCD analogue of Compton scattering
(c) the QCD analogue of the Bethe Heitler process
(d) dilepton production through the Drell-Yan process.

All reactions are hard scattering processes, in which the proton transmits all its energy to the final partons. The relevant kinematic variables are given in fig. 16. At the large energies of an ep facility two jets of particles will emerge in the photon fragmentation region as long as $\hat{s} \ll s$ (i.e. for small x). This is demonstrated by fig. 17 in which the angles of the two parton jets in the ep reference frame are plotted for a fixed ratio $R = x/y$. x and y are the momentum fraction of the photon and electron carried by respectively the parton and the photon.

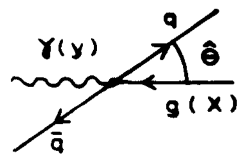

$$\hat{s} = xys$$
$$\hat{t} = -\tfrac{1}{2}\, xys\ (1 - \cos\hat{\Theta})$$
$$\hat{u} = -\tfrac{1}{2}\, xys\ (1 + \cos\hat{\Theta})$$
$$\text{for}\ \ m_q = 0$$

Fig. 16 Kinematics of the hard scattering process of a photon with momentum yE_e and a parton with momentum xE_p.

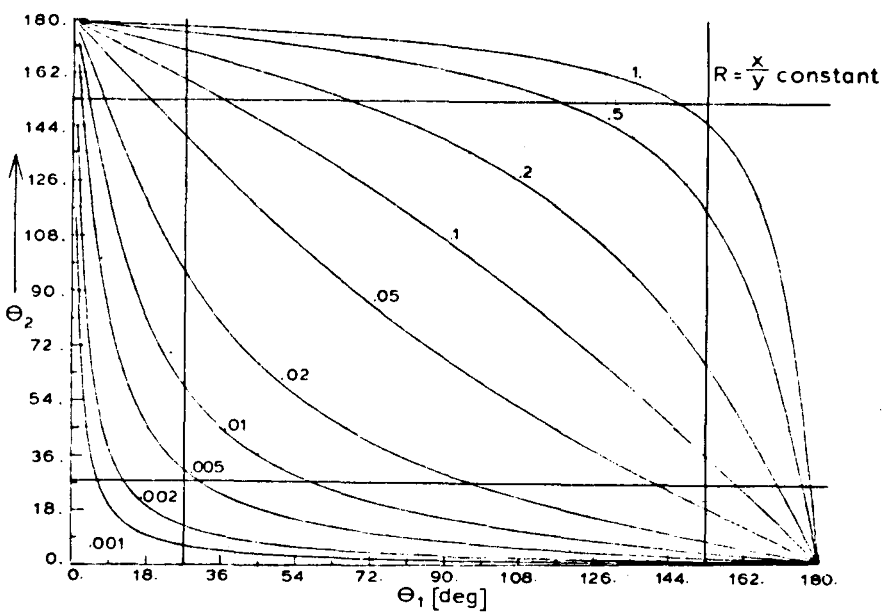

Fig. 17 Angles Θ_1 and Θ_2 of the two final state particles (jets) in the ep lab system for fixed values of the ratio $R = y/x$, for a 20×270 GeV ep collider. The drawn lines indicate the possible solid angle covered by a central detector.

Experimentally these point-like photon interactions will be selected by looking for collisions in which large momentum transfers are involved. The condition on M^2 will certainly be satisfied in that case, while competing background processes will be suppressed.

We first consider reactions (a), (b) and (c). The cross sections are given by the following expressions, using the notation of fig. 16 [28].

$$(a) \quad \frac{d^2\sigma}{d\hat{s}d\hat{t}} = R^{e_q}(x) \frac{2\pi\alpha^2}{\hat{s}^3} F_2(x) \left\{ -\left[\frac{\hat{s}-m_q^2}{\hat{u}-m_q^2} + \frac{\hat{u}-m_q^2}{\hat{s}-m_q^2}\right] + \right.$$

$$\left. + 4m_q^2 \left[\frac{1}{\hat{s}-m_q^2} + \frac{1}{\hat{u}-m_q^2}\right] + 4m_q^4 \left[\frac{1}{\hat{s}-m_q^2} + \frac{1}{\hat{u}-m_q^2}\right]^2 \right\}$$

$$(b) \quad \frac{d^2\sigma}{d\hat{s}d\hat{t}} = \frac{8\pi\alpha\alpha_s}{3\hat{s}^3} F_2(x) \left\{ -\left[\frac{\hat{s}-m_q^2}{\hat{u}-m_q^2} + \frac{\hat{u}-m_q^2}{\hat{s}-m_q^2}\right] + \right.$$

$$\left. + 4m_q^2 \left[\frac{1}{\hat{s}-m_q^2} + \frac{1}{\hat{u}-m_q^2}\right] + 4m_q^4 \left[\frac{1}{\hat{s}-m_q^2} + \frac{1}{\hat{u}-m_q^2}\right]^2 \right\}$$

$$(c) \quad \frac{d^2\sigma}{d\hat{s}d\hat{t}} = \frac{\pi\alpha\alpha_s}{\hat{s}^3} e_q^2 \, G(x) \left\{ \left[\frac{\hat{t}-m_q^2}{\hat{u}-m_q^2} + \frac{\hat{u}-m_q^2}{\hat{t}-m_q^2}\right] - \right.$$

$$\left. - 4m_q^2 \left[\frac{1}{\hat{t}-m_q^2} + \frac{1}{\hat{u}-m_q^2}\right] - 4m_q^4 \left[\frac{1}{\hat{t}-m_q^2} + \frac{1}{\hat{u}-m_q^2}\right]^2 \right\}$$

with $R^{e_q}(x) = \dfrac{e^4_q q(x)}{e^2_q q(x)}$

R^{e_q} is only slightly dependent on x. Assuming the quark distribution q (x) of the nucleon to be exclusively determined by either valence or sea quarks gives the following limits $3/9 \lesssim R^{e_q} \lesssim 4/9$.

A constant value R = 3/9 has been accordingly used.
Both scaling and scale breaking structure functions have been used to evaluate the above expressions. We first discuss the results for scaling structure functions. A suitable parametrization for $F_2(x)$ which represents well the FNAL muon scattering data is provided by [28]

$$F_2(x) = \begin{cases} 0.25(1-x)^6 + 1.13x^{\frac{1}{2}}(1-x)^3, & x \lesssim 0.2 \\ 0.25(1-x)^6 + 3.93x\,(1-x)^5, & x \gtrsim 0.2 \end{cases}$$

The form of the gluon dustribution functions is uncertain.
We take

$$G(x) = \frac{3}{x}\,(1-x)^5$$

The normalization is such that the gluons carry half of the momentum of the proton.
The QCD running coupling constant α_s is approximated by a constant value $\alpha_s = .3$. With these assumptions the cross section from processes (a) (fig. 18), (b) and (c) (fig. 19 and 20) have been calculated both for a 20 x 270 and a 100 x 270 ep collider. The results are shown in figures 18-20. In fig. 18 and 19 $p_\perp$ is plotted versus p_L, for fixed values of the expected daily rates for events with a $p_\perp$ larger than the indicated value in an angular range $\Delta\theta = 10^0$. An effective integrated ep luminosity of $10^{37}cm^{-2}$ is assumed. The same results are shown in fig. 20 as $dN/dp_\perp$ for lab. angles in the interval $45^0 < \Theta < 135^0$.
Obviously, these results should be considered as rough estimates, they give however some idea about the order of magnitude of these processes and allow us to draw the following general conclusions.

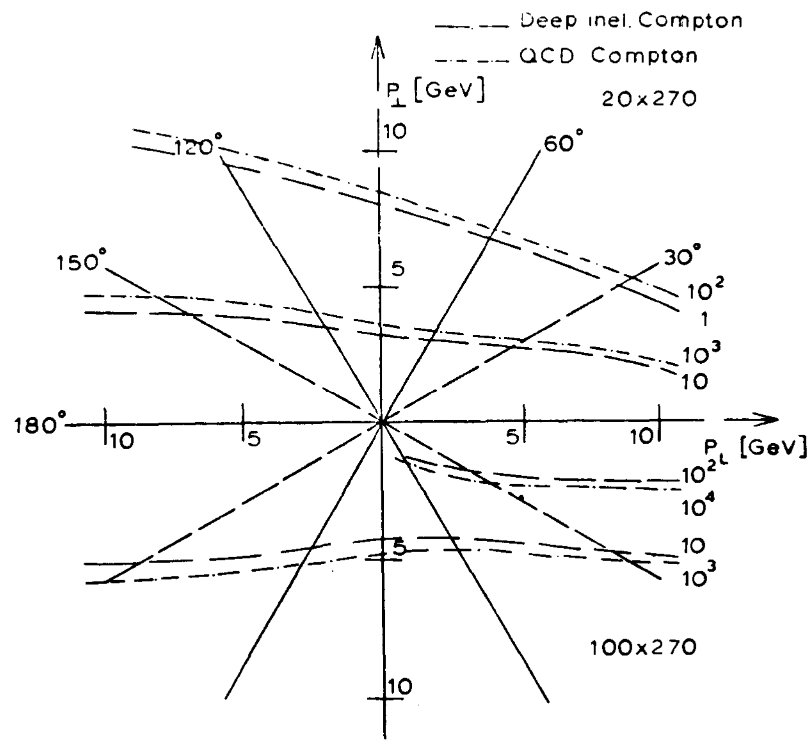

Fig. 18 $p_\perp, p_L$ plane showing lines of constant daily rates for inelastic Compton and QCD Compton in an angular interval $\Delta\Theta = 10^0$, with $p_\perp > p_\perp^{\text{indicated}}$; upper half for a 20 x 270 GeV, the lower half for a 100 x 270 GeVep collider. Rates are calculated under the assumption of scaling structure functions

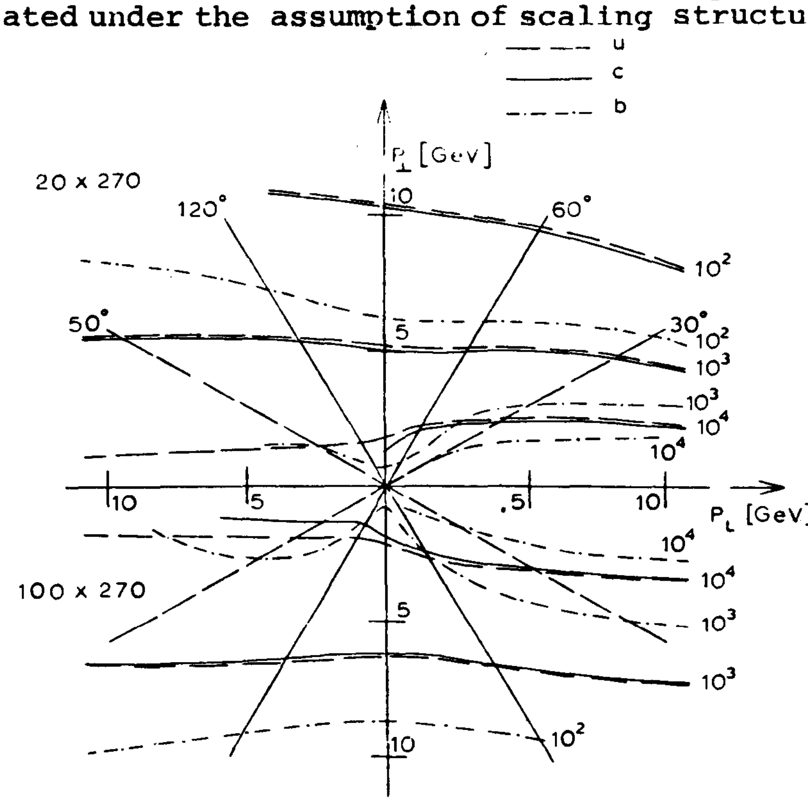

Fig. 19 $p_\perp$, p_L plane showing lines of constant daily rates for pair production of u, c, b quarks in an angular interval $\Delta\Theta = 10^0$, with $p_\perp > p_\perp^{\text{indicated}}$; the upper half for a 20 x 270 GeV, the lower half for a 100 x 270 GeV collider, and assuming a scaling gluon structure function.

i The rates for hard scattering γ-parton processes are confortably large. They should allow to study in detail the dependence of jet production on angle, $p_\perp$ and s and thus establish the existence of the above QCD processes.

ii The rates for gluon jet production are much smaller than those for quark jet production. It will therefore be difficult to establish the existence of gluon jets in these experiments.

iii Process (c) is a copious source of quarks with new flavours. Apart from threshhold effects the rates are proportional to e^2_q. We may thus expect large e, μ/π ratios for large $p_\perp$ jet events and might possibly use these processes for the observation of heavy flavour states.

iv Threshhold effects in the production of heavy flavour are reduced for 100 x 270 ep collisions, thus leading to considerably larger rates for b-quark jets in the later case.

The fraction of events for which both jets are contained within the angular range $30^0 < \Theta < 150^0$ of a possible central detector is found to be larger than 60%. The processes might therefore be easily detectable, showing up as two jets (or a jet and a single γ) in opposite halves of an azimuthally symmetric central detector.Energy and momentum conservation then allows to check whether there was a $2\rightarrow 2$ collison involving the initial photon. In that way we may hope to distinguish the lowest order processes from higher order diagrams as for instance the one shown in fig. 21, which have a spectator jet

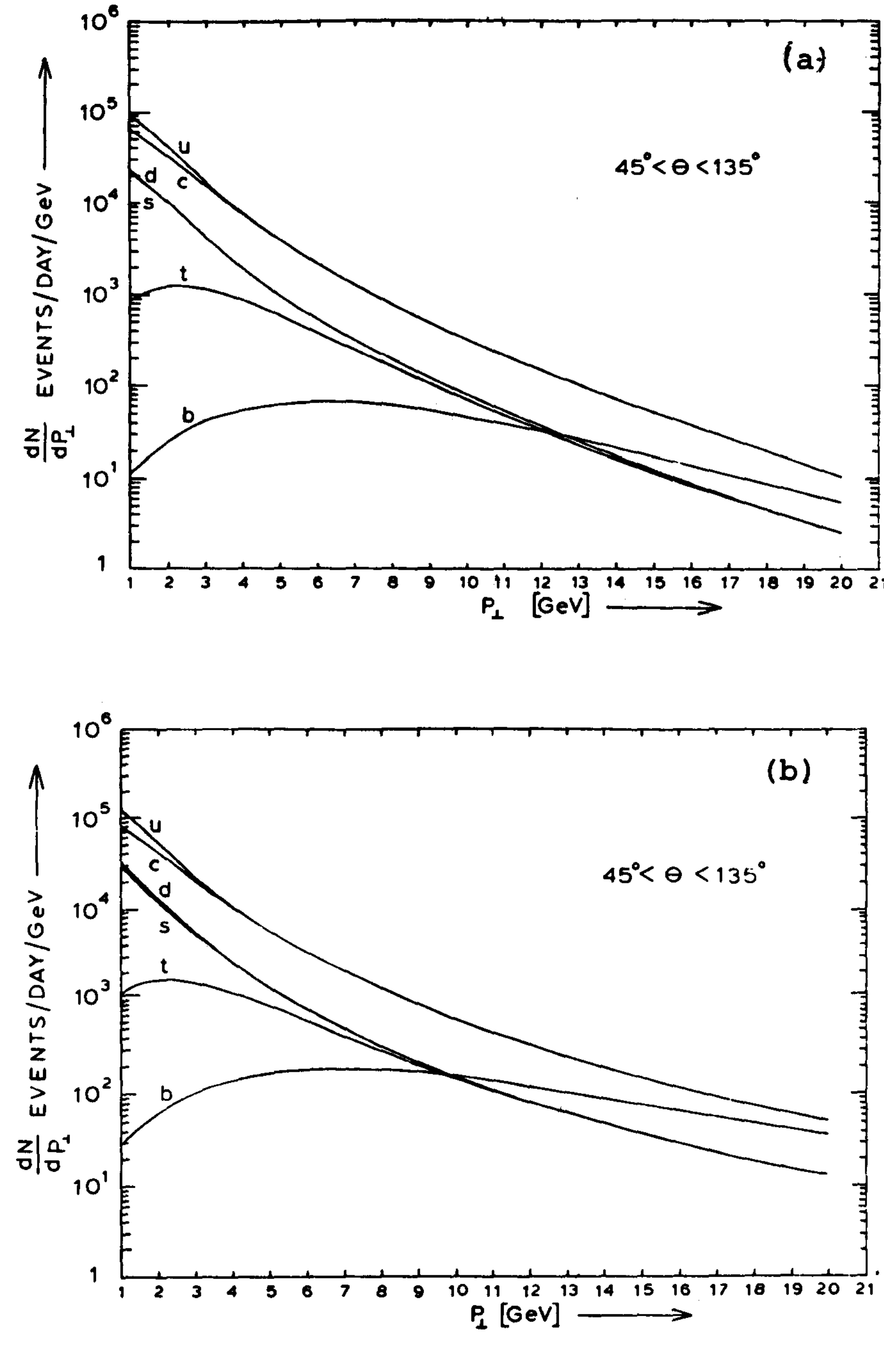

Fig. 20 Daily rates as a function of $p_\perp$ for pair production of u, c, b quarks integrated over the angular interval $45^0 < \Theta < 135^0$. A scaling structure function is used.
(a) 20 x 270 GeV (b) 100 x 270 GeV.

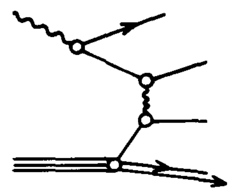

Fig. 21 One of the possible higher order diagrams contributing to large $p_\perp$ jets in γp interactions.

along the photon direction. The $d\sigma/dp_\perp$ distributions shown in fig. 20 gives the $p_\perp^{-3}$ dependence expected from dimensional counting. The exact $p_\perp$ behaviour, however, will be more complicated due to scale breaking and possible smearing effects of the proton[21]. The effect of the intrinsic transverse momentum of the parton should be small at the large $p_\perp$ where these processes are studied.

The effect of scale violating structure function is shown in fig. 22. The Buras-Gaemers parametrization for the scale breaking effects is used [22]. As expected it leads to an increase of the slope of the $p_\perp$ distribution.

- Single photon and π^0 production

The feasibility to distinguish the single photon of deep inelastic Compton scattering from QCD Compton and Bethe Heitler processes depends on the rate and the energy of π^0 and γ fragmentation products in the jets produced in the latter two processes.

A 10 GeV π^0 has a 2γ opening angle of about 30 mrad. In a central detector with a 1 meter radius these two photons are

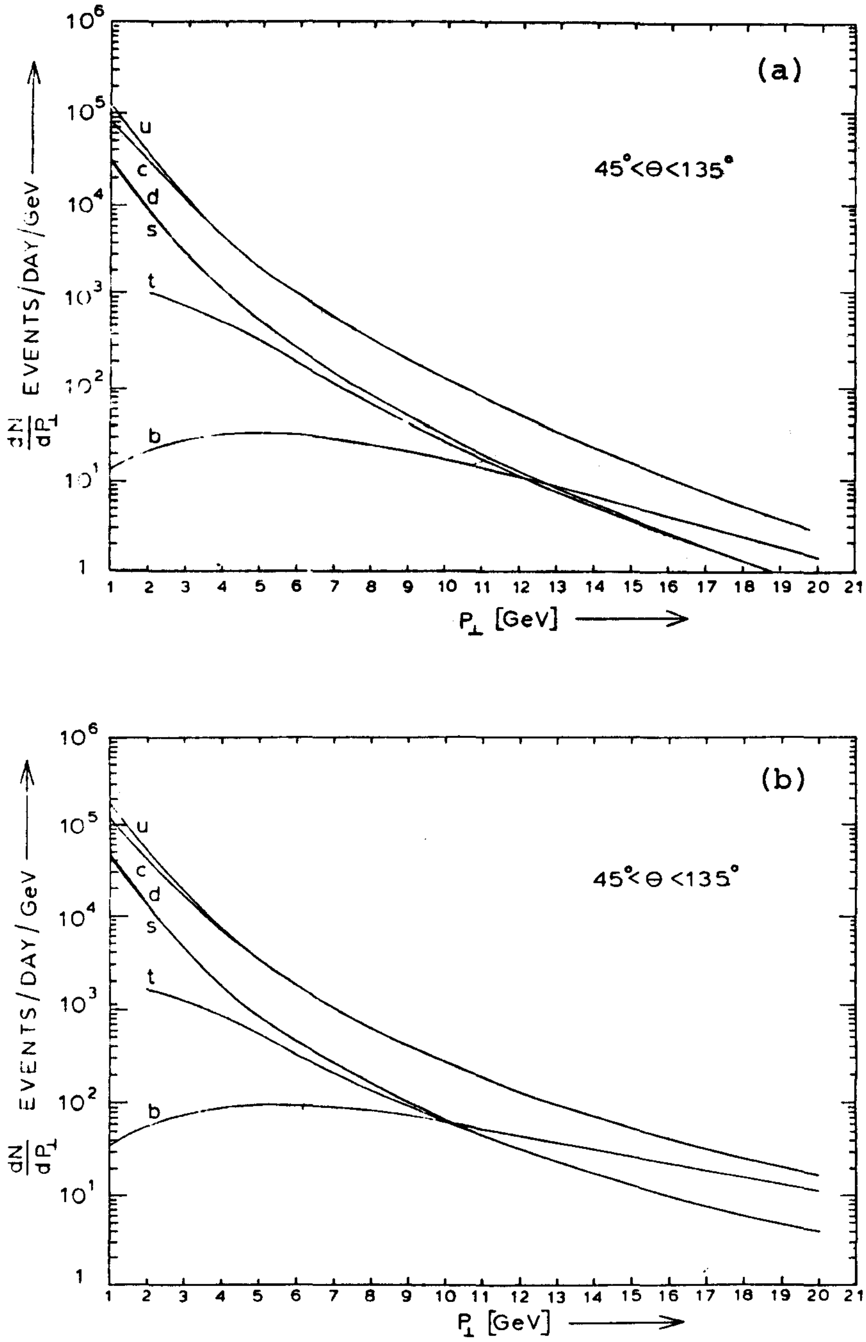

Fig. 22 Daily rates as a function of $p_\perp$ for pair production of u, c, b quarks integrated over the angular interval $45^0 < \Theta < 135^0$, using a scale violating gluon structure function.
(a) 20 x 270 GeV (b) 100 x 270 GeV

only 3 cm apart and therefore require a corresponding two photon resolution of the e.m. shower detector in order to distinguish the π^0 from a single γ. It might be that for large $p_\perp$ the single photon and the opposite quark jet are well separated, thus allowing the identification of the inelastic Compton process. In that case the problem of distinguishing the inelastic Compton process will be overestimated.

π^0 rates are estimated using both scaling and scale breaking fragmentation functions for quark and gluon jets.

As scaling fragmentation functions we used

$$D_{\pi^0/q}(z) = \tfrac{1}{2}(1-z)/z$$

$$D_{\pi^0/q}(z) = \tfrac{3}{4}(1-z)^2/z$$

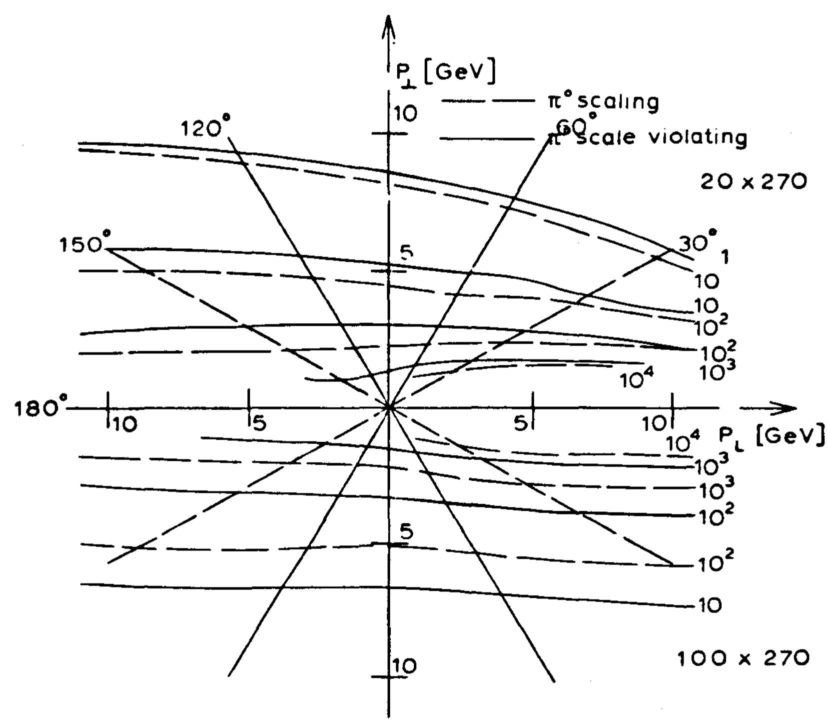

Fig. 23 p_L, $p_\perp$ plane showing lines of constant daily rates for large $p_\perp$ π^0 production from QCD γp processes, with $p_\perp > p$ indicated and $\theta = 10^0$. The drawn lines correspond to scale violating structure and fragmentation functions. The dashed lines to the scaling functions.

The resulting π^0 rates are shown in figure 23. We also plot in fig. 24 the ratio of γ's produced in the inelastic Compton process relative to this π^0 rate to have some idea of the difficulties in identifying the inelastic Compton process. The scale breaking fragmentation functions are given by

$$D_{\pi/q}(z) = \tfrac{1}{2}A(1-z)^B, \text{ with}$$

$$A = e^{.69C}(-\log z)^{4C}; \quad C = .16\bar{s}; \quad B = 1/(1+2C)$$

$$\bar{s} = \ln\{\ln(p_\perp^2/\Lambda^2)/\ln(1.8/\Lambda^2)\}; \quad \Lambda = .5$$

They lead to a softer π^0 spectrum and therefore to a larger γ/π^0 ratio. The results are shown in fig. 24.

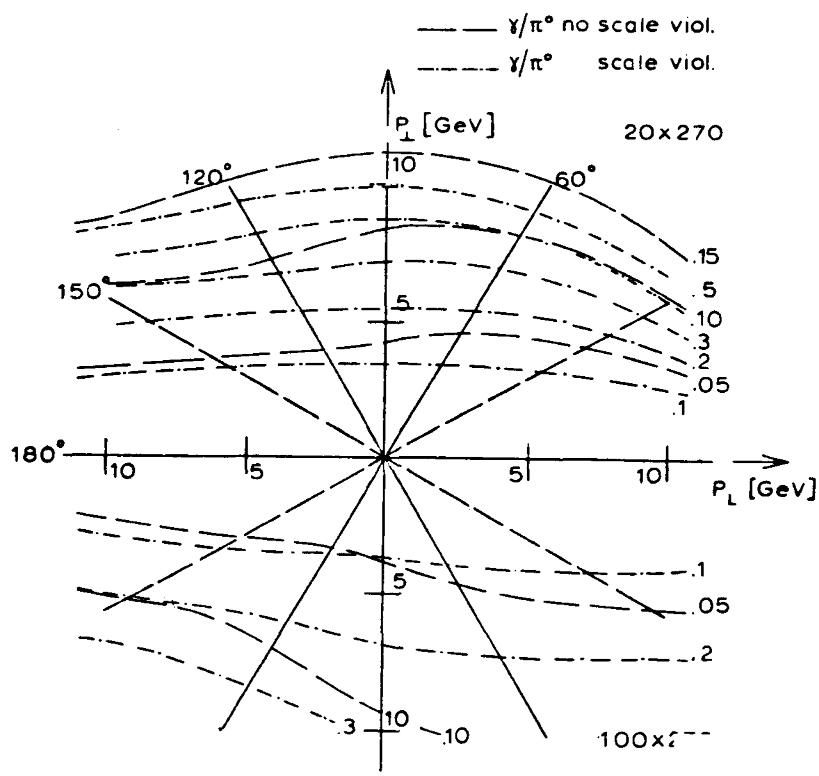

Fig. 24 The ratio of γ's produced by inelastic Compton scattering over π^0's produced in QCD γp processes. The dashed lines correspond to scaling structure and fragmentation function. The dotted lines to scale violating.

-Production of new flavours (from process (C)).

Far above threshhold the rates for heavy quark pair production are comparable to those for light quarks as demonstrated by figures 19 and 20. Accordingly we may expect the ratio e, μ/π to be much larger than the value 10^{-4} found in purely hadronic collisions due to the semi-leptonic decays of c, b, ... quarks. Fig. 25 gives the μ/π ratio as a function of $p_{\perp}$. The observation of such a large lepton rate should be striking evidence for the occurrence of the QCD Bethe Heitler process.
Double lepton events will also be relatively abundant and may indicate the production of quarks heavier than the c-quark.

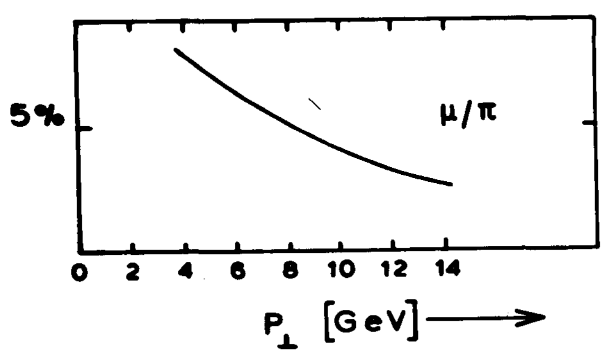

Fig. 25 Ratio of μ/π in QCD jets as a function of $p_{\perp}$. Scale violating structure and fragmentation functions are used.

In particular the cross section for charm production could be quite large. It might even be possible to distinguish between various assumptions of the gluon structure G(x). This is shown in fig. 26. For scaling structure functions the charm photon-production cross section approaches an asymptotic value, the height of which depends on the shape of the gluon structure function. If a scale violating G(x) is assumed such a plateau is not reached. The size of the cross section however varies considerably depending on which prescriptions for the scale violation are used. For the low energy behaviour two different assumptions are made and indicated in the figure.

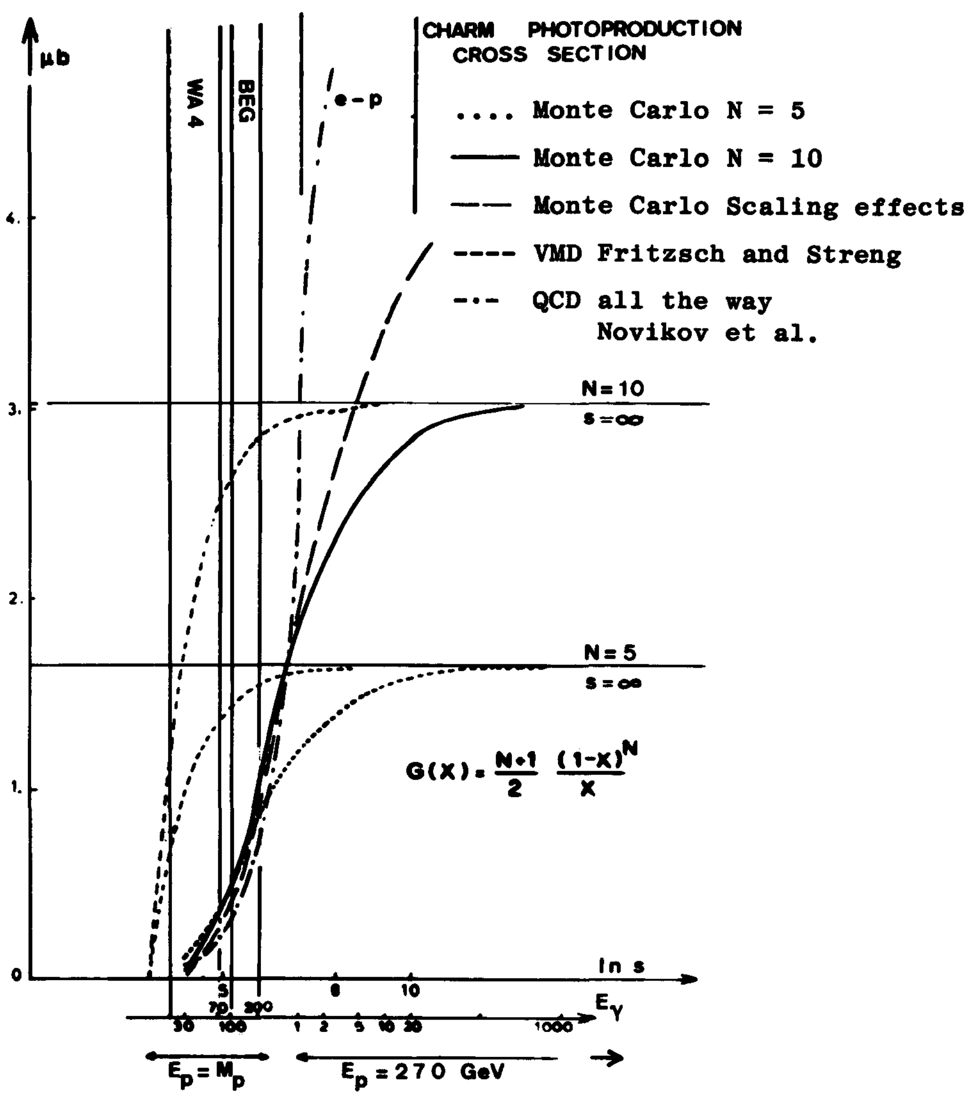

Fig. 26 Total cross section for charm production as a function of Eγ for different assumptions of the gluon structure function.

i From VMD and the optical theorem the total cross section for charm is linked to the photoproduction of the J/ψ [20] the cross section of which can be approximated by $(s-s_{th}/s)^2$, thus:

$$\sigma(\gamma N \to c\bar{c}x) \simeq (s-s_{th})/s \quad \sigma(s=\infty)$$

with $s_{th} = 21.7\ GeV^2$ and $\sigma(s=\infty)$ assumed to be given by QCD.

ii Pure QCD behaviour is assumed all the way down to threshhold[23], this might be correct, since it is mass of the heavy charmed quark that sets the scale of the process.

Recent results from the WA4 experiment at CERN indicate a charm photoproduction cross section of the order of 1 μb and thus favour the first assumption.

The feasibility to observe heavy flavour states depends apart from the kinematics of the photoproduction process in the ep collider (fig.19) on the behaviour of the fragmentation function for heavy quarks.

Theoretical models[24] and experimental data[25] indicate that a flat distribution D(z) = constant, is acceptable. For charmed events such a fragmentation function has been used to calculate the longitudinal momentum distribution of D's fragmenting from the two charmed quarks in the process. The results are shown in fig. 27. We conclude that the observation of heavy flavour states requires a detector which is able to detect and measure very low momentum particles over a large solid angle. To select events, tagging of the promt lepton should of course be considered.

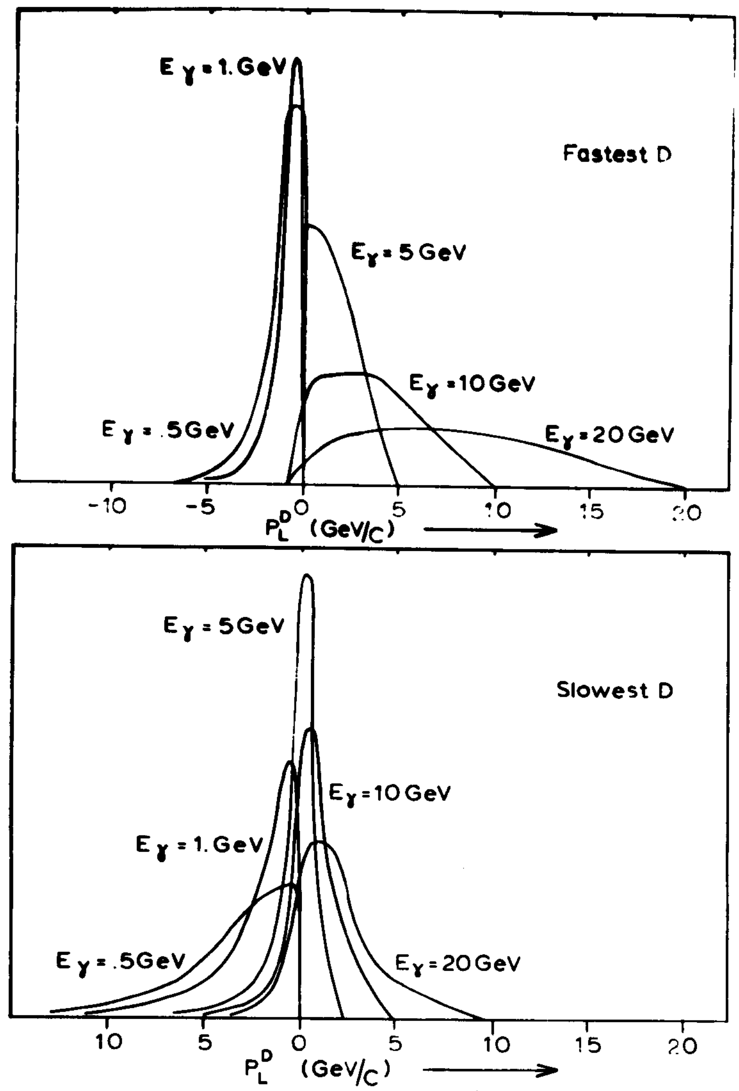

Fig. 27 Longitudinal momentum of (a) the fastest and (b) the slowest D meson produced from a pair of c-quarks.

For the detection of heavy flavour states the merits of a high intensity photon beam (like BEG), compared with those of an ep collider as photon source can be summarized in the following points:

i the BEG intensity is a factor 10 higher

ii however, E_γ(BEG) << E_γ (ep) and therefore a factor 3-4 may be gained because of the higher cross section

iii the kinematics of the ep machine is more favourable. The particles have low momenta, so that a better mass resolution can be obtained.

iv in the ep case there is a better separation between the proton and the photon fragmentation regions.

v the electromagnetic background for the ep machine might be a less serious problem.

We conclude that apart from a marginally smaller event rate an ep collider would be a better tool for studying heavy flavour production than a high intensity fixed target photon beam.

So far we have only considered the lowest order diagrams, shown in fig. 15. Apart from these there may be large $p_\perp$ contributions from CIM processes [29]. Also higher order diagrams like the one shown in fig. 21 may be non-negligible. Calculations have been done to estimate the CIM cross section for π^0 production in $ep \to \pi^0 + x$. The relevant graph is shown in fig. 28.

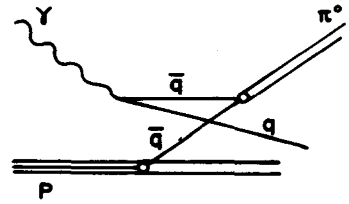

Fig. 28 CIM graph for π^0 production in γp interactions.

The $p_\perp$ and the $x_\perp$ dependence of the CIM cross section is given by

$$\frac{d\sigma}{dp_\perp d\cos\Theta} \sim \frac{A(1-x_\perp)^6}{p_\perp^5}$$

which should be compared with the cross section for the QCD processes which behave as

$$\frac{d\sigma}{dp_\perp d\cos\Theta} \sim \frac{A'(1-x_\perp)^{F(p_\perp/\Lambda)}}{p^{N(p_\perp/\Lambda)}}$$

If scale violation is taken into account $N(p_\perp/\Lambda) \simeq 5$ (instead of about 3 for scaling), while $F(p_\perp/\Lambda)$ may be as much as 6. Consequently CIM and QCD would not easily be distinguishable in that case. However, the position of CIM with respect to scale violations is in general not very clear. The above conclusion should therefore be considered as an extreme possibility. The QCD jet cross section however will always be less steep than the CIM jet cross section, since no fragmentation function has to be included in this case, while for CIM there was no fragmentation anyway.

Calculations of higher order diagram contributions to large $p_\perp$ photons have recently been done for a fixed target experiment with E_γ = 150 GeV[26).]

The conclusion of the authors was that the background from such processes was not serious. These calculations have recently been repeated for the ep case [26)].

-Dimuon production (process (d)).

Contributions to the dimuon continuum come from Drell-Yan and Bethe Heitler processes (fig. 29). The calculation of the Drell-Yan cross section requires the photon structure function as input. The measurement of the Drell-Yan cross section would

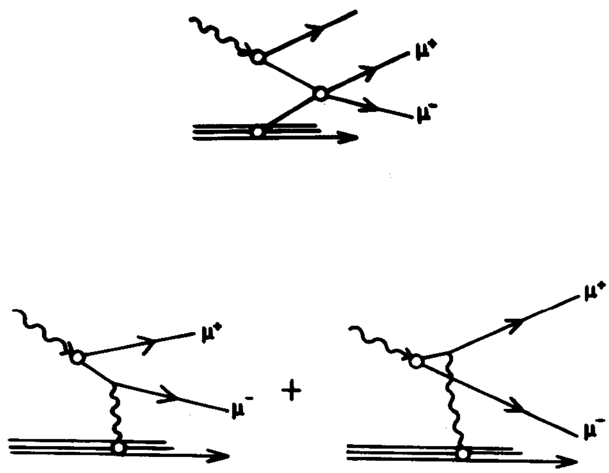

Fig. 29 Drell-Yan and Bethe Heitler diagrams for dilepton production in γp interactions.

therefore allow an experimental determination of this structure function and accordingly would check theoretical calculations which have been done in the context of QCD[27].

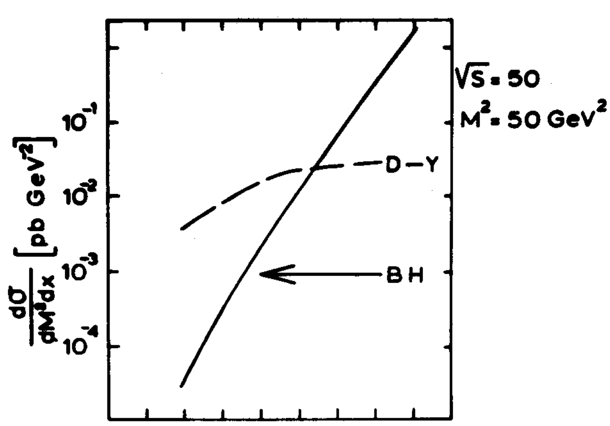

Fig. 30 Cross section estimates for Drell-Yan and Bethe Heitler dimuon production in γp interactions

Both the Drell-Yan and the large M^2 QCD contribution to the dimuon continuum have been calculated[28)]. The result is shown in fig. 30 for s=2500 GeV^2 and $M^2_{\mu^+\mu^-}$ = 50 GeV^2.
With an effective γp luminosity of $10^{30}cm^{-2}$, ΔM=10 GeV^2,Δx=.1, we should have about .001 event/day, thus negligibly small.

Conclusions

In this report the possible use of electron-proton colliders has been discussed as source of small Q^2 photons.
Two configurations have been considered; a 20 x 270 GeV machine proposed at DESY and a 100 x 270 GeV machine suggested as an extension to LEP. It was shown that these colliders, in particular the 20 x 270 GeV option, will provide small Q^2 photons with energies (ν) about two orders of magnitude larger than are presently avaible, while the luminosities are comparable to photon beams from fixed target machines.
The use of a 100 x 270 GeV ep machine for photon physics, however, requires electron tagging at very low angles (of the order of 1 mrad), the feasibility of which has still to be demonstrated.
The energy unbalance of the ep system makes these machines extremely well suited for studying the photon fragmentation region. Several possible experiments are discussed, in which the emphasis is either on the hadronic properties of the photon,or on its point like behaviour.
In the first category fall the measurement of the total cross section and the study of some exclusive reactions like Compton scattering, the diffractive production of vectormesons and Primakoff production.

The total cross section measurement should be a rather straight forward experiment and is certainly one of the first experiments to be done. For the exclusive reactions it might be necessary to tag the final state proton.

Even in that case the study of Primakoff production processes, however, seems to be impossible.

The study of the point-like component of the photon is one of the most interesting and promising subjects. By measuring large $p_{\perp}$ processes hard scattering processes of photons and partons may be studied, like deep inelastic Compton and the QCD analogues of Compton and Bethe Heitler processes. The event rates are confortably large, the possible background of second order and CIM diagrams , however, may complicate the interpretation. The equivalent of the Drell-Yan diagram in photon interactions gives rise to a negligibly small cross section.

REFERENCES

1. E. Dasskowski, D. Kohaupt, K. Steffen, DESY PET-
2. LEP Study Group, CERN/ISR-LEP/78-17
3. Proc. Internat. Symposium on Electron and Photon Interactions at High Energies, Cornell, 1971
   Proc. Internat. Symposium on Electron and Photon Interactions at High Energies, Bonn, 1973
   Proc. Internat. Symposium on Lepton and Photon Interactions at High Energies, Stanford, 1975
   Proc. Internat. Symposium on Lepton and Photon Interactions at High Energies, Hamburg, 1977
   T.H. Bauer, R.D. Spital, D.R. Yennie, and F.M. Pipkin, Revs of Mod. Phys. 50 (1978) 261
4. C.H. Llewelyn Smith and B.H. Wiik, DESY 77/38 (1977)
5. CHEEP, An e-p facility in the SPS, CERN 78-02
6. D.O. Caldwell, J.P. Cumalat, A.M. Eisner, A.Lu, R.J. Morrison, F.V. Murphy, S.J. Yellin, P.J. Davis, R.M. Egloff, M.E.B. Franklin, J.D. Prentice and T. Nash, Phys. Rev. Lett. 40 (1978) 1222
7. F. Close, D.M. Scotland and D. Sivers, Nucl. Phys. B117(1976)134
8. E. Gotsman, D. Siverman, and A. Soni, UC Irvine Techn. Report 79-1
9. R.E. Taylor, in Proceedings of the Internat. Symposium on Lepton and Photon Interactions at High Energies, Stanford, 1975
10. E. Gabathuler, in Proceedings of the 19th Int. Conference on High Energy Physics, Tokyo, 1978
11. H.L. Anderson, V.K. Bharadwaj, N.E. Booth, R.M. Fine, W.R. Francis, B.A. Gordon, R.H. Heisterberg, R.G. Hicks,

T.B.W. Kirk, G.I. Kirkbride, W.A. Loomis, H.S. Matis, L.W. Mo, L.C. Myrianthopoulos, F.N. Pipkin, S.H. Pordes T.W. Quirk, W.D. Shambroom, A. Skuja, L.J. Verhey, W.S.C; Williams, R. Wilson, and S.C. Wright, Phys. Rev. Lett. 37 (1976) 4

12. M.G. Albrow, A. Bagchus, D.P. Barber, P. Benz, A. Bogaerts, B. Bosnjaković, J.R. Brooks, C.Y. Chang, A.B. Clegg,F.C. Erné, C.N.P. Gee, P. Kooyman, D.H. Locke, F.K. Loebinger, N.A. McGubbin, P.G. Murphy, D. Radojicić, A. Rudge, J.C. Sens, A.L. Sessoms, J. Singh, D. Stork and J. Timmer Nucl. Phys. B108 (1976) 1

13. G. Buschhorn, L. Criegee, G. Franke, P. Heide, R. Kotthaus, G. Poelz, U. Timm, G. Vogel, K. Wegener, H. Werner, and W. Zimmermann, Phys. Lett. 37B (1971) 207
R.L. Anderson, D. Gustavson, J. Johnson, I. Overman, D. Ritson, B.H. Wiik, R. Talman, J.K. Walker, and D. Worcester, Phys. Rev. Lett. 25 (1970) 1218
A.M. Boyarski, D.H. Coward, S.Ecklund, B. Richter, D. Sherden, R.H. Siemann and C. Sinclair, Phys. Rev. Lett. 26 (1971) 1600 and 30 (1973) 1098
L. Criegee, G. Franke, A. Giese, Th. Kahl, G. Poelz, U. Timm, H. Werner, and W. Zimmermann, Nucl. Phys. B121 (1977) 31

14. C. Heusch, UCSC 78-077

15. T. Nash, A. Belousov, B. Govorkov, D.O. Caldwell, J.P. Cumulat, A.M. Eisner, R.J. Morrison, F.V. Murphy, S.J. Yellin, P.J. Davis, R.M. Egloff, G. Luste, and J.D. Prentice, Phys. Rev. Lett. 36 (1976) 1233

16. S.J. Brodsky, F.E. Close and J.E. Gunion, Phys. Rev. D6 (1972) 177

17. M. Greco, Phys. Lett. 77B (1978) 84

18. J.D. Bjorken and E.A. Paschos, Phys. Rev. 185 (1969) 1975

19. H. Fritzsch and P. Minkowski, CERN TH 2320

20. H. Fritzsch and K.H. Streng, Phys. Lett. 78B (1978) 447

21. R.D. Field in Proc. of the 19th Int. Confernece on High Energy Physics, Tokyo, 1978

22. A.J. Buras and K.J. Gaemers, Nucl. Phys. B132 (1978) 249

23. V.A. Novikov, L.B. Okun, M.A. Shifman, A.I. Vainshtein, M.B. Voloskin, V.I. Zakharaov, Phys. Reports 41C, no 1, May 1978

24. P. Lichard and J. Pisut. CERN TH 2608
    M. Suzuki, CERN TH 2369

25. R. Odorico and V. Roberto, Nucl. Phys. B136 (1978) 333

26. Tu Tung-Sheng and Wu Chi Min CERN TH 2646 and CERN TH

27. E. Witten, Nucl Phys. B120 (1977) 189
    C.H. Llewelyn Smith, Phys. Lett. 79B (1978) 83

28. A. Donnachie , Private Communication

29. J.F. Gunion, S.J. Brodsky, and R. Blankenbeckler, Phys. Rev. D8 (1973) 287.

CONVENOR'S REMARKS

M. Greco
INFN - Laboratori Nazionali di Frascati (Italy).

1. Informations on the working group.

The report on "Small q^2 physics and photoproduction", presented by W. Hoogland, is based on the work of a study group, in which the following people were involved: F. Close (Rutherford), K. Daum (CERN), B. Diddens (NIKHEF), A. Donnachie (Manchester), J. Gallivan (CERN), M. Greco (Frascati), W. Hoogland (NIKHEF), R. Horgan (CERN), W. Ochs (Max Planck), G. Parisi (Frascati), G. Penso (Rome), P. Pistilli (Rome), F. Richard (Orsay), P. Roudau (Orsay) and P. Weilhammer (CERN).

2. Discussion session.

In the following a taperecording of the discussion is presented. Only minor modifications have been made.

Clegg (Univ. of Lancester)
I want to make one brief correction to your statement that the CERN experiment WA4 has seen 3-4 μb of charm production. That is not true. At the Tokyo Conference upper limits for D production of 0.5 to 1 μb were reported and they have not been changed. The work is continuing.

Ting (DESY, MIT)
You gave a very nice review on photoproduction of vector mesons. As you know photoproduction of vector mesons has been measured above 3 GeV at Daresbury and DESY and up to 20 GeV at SLAC. In this whole energy range no significant change has been observed in the features of vector meson production. Similarly from the SPS and Fermilab there are no concrete changes on photoproduction of vector mesons up to now. You mentioned that you gain a factor of 3 in energy with this ep machine.

But you would expect changes to go like log s, and log s is very small. That is my remark. I do have a question. Did you study vector mesons with masses between 1 and 2 GeV ?

Hoogland

Concerning your remark that ep machine does not extend the energy range very far : you always go as far as you can go. Concerning your second point : the study group did some estimates on vector meson production between 1 and 2 GeV.

Ting

Unfortunately the region between 1 and 2 GeV has not been covered yet by experiments. There is a plan at ADONE to do this.

My last point : You mentioned to study single photons from ep collisions. That must be very difficult. At the ISR there is a big effort to study single photons and as far as I know it has not been settled yet. With an ep machine it will be much more difficult because in electron machines you always have a lot of photons around.

Hoogland

I agree, it will be difficult.

Amaldi (CERN)

One of your figures showed that production of $c\bar{c}$ depends on the gluon distribution $g(x)$. Could you tell us how sensitive the predicted cross section depends on $g(x)$?

Hoogland

The production rate is rather sensitive. A parton with a very small x is colliding with the virtual photon. The gluon distribution $g(x)$ strongly affects the cross section. If you can cleanly separate the process of interest, its rate should provide a rather sensitive test of the gluon structure function.

Montgomery (CERN)

Recently at an SPSC meeting at CERN there was a report from the EMC experiment.

It gave preliminary indication that the q^2 dependence of J/ψ production behaves like vector meson dominance but with a q^2 dependence defined by a mass scale of 9 GeV^2. In your talk you define your transition region between q^2 of 0 and 4 GeV^2. This may be too pessimistic. You should redefine the transition region as a function of ν, and at the energies we are talking about this transition region may extend to high q^2 of the order of 10 or 20 GeV^2. There is a long held idea that the various flavour productions may be enhanced by the mass scale that is controlling the q^2 dependence. So, if you move away from $q^2 = 0$ your signal to noise ratio for the various flavour productions may in fact be enhanced.

Weilhammer (CERN)

I want to make a remark on Prof. Ting's comment on the high p_T single photon measurement. I do not think the background situation on an ep machine is much different from a proton machine. The basic backgrounds are from π^o and η, and there should not be quite a difference. Yet, it may be more difficult to measure low p_T.

Greco (Frascati)

Let me comment Prof. Ting's remark on heavy vector mesons in the range between 1 and 2 GeV. We did some estimates. If you take a leptonic width of 1/10 or 1/20 of those of ϱ, ω, and φ, as suggested by experiments, you can easily calculate the total cross section, using the simple scaling formula discussed by Hoogland. But if you want to measure the vector mesons via electromagnetic decays, they will be hard to see because their leptonic branching ratios will be very very small.

3. Comments and conclusions.

I present here my personal comments on the session "Small q^2 physics and photoproduction", which in light of the limited discussion following Hoogland's talk, can also be considered as general conclusions for this session.

It's certainly clear that the interest for this kind of physics cannot be taken as the primary justification for an e-p machine. However, in a general presentation of the physics arguments in favour of such a pro-

ject, it is important to stress some adjoining physics problems in the realm of small q^2's, which can be uniquely studied with this facility. As emphasized by the various rapporteurs, the kinematical range of e-p collisions covered in both the options under study allows for photon energies (ν) of tens of TeV, with luminosities comparable to those obtained in ordinary fixed target experiments. In the realm of the small q^2 physics this corresponds to extend our investigation on the interaction of a real photon for more than two orders of magnitude.
The measurement of the real photon total cross section $\sigma_{\gamma p}(\nu)$ is clearly the most important experiment in this framework. Whereas the hadron-like behaviour of the photon has been longtime evidentiated, including the recently observed increase of $\sigma_{\gamma p}$ of a few μb at present energies, its pointlike component should reveal itself at very large ν, contributing to the expected rise of $\sigma_{\gamma p}(\nu)$. In addition, the non applicability of the Froissart bound to $\sigma_{\gamma p}$ and a relativity large fraction of new quark flavours expected in the final state, make the measurement of $\sigma_{\gamma p}$ one of the most promising musts for any ep facility. As discussed in detail in Hoogland's report, the very high counting rate (various thousand of events/day) is however balanced by a quite good resolution which is needed to perform an accurate extrapolation of data to $q^2 = 0$.
The detailed study of a real photon fragmentation region can be almost uniquely performed with an e-p facility, the target fragmentation region being completely separated out in the laboratory, unlike any fixed target machine. This allows to investigate the pointlike behaviour of a photon by looking at jets or single particles produced at large transverse momenta. The information obtainable from these deep inelastic photon reactions, which are complementary to those normally provided by large Q^2 processes, are of great importance for our understanding of strong interactions. In particular they will be used to test various predictions of QCD, specifically made for processes involving real photons, and which are hardly testable otherwise.
Finally, an interesting problem which could be easily investigated in the small q^2 region concerns the question of the continuation of $\sigma(q^2)$ from the deep inelastic region to $q^2 = 0$. Any simple connection bet-

ween these two regions, as given for example in GVMD, could be particularly interesting at very high energies for the possible presence of a pointlike component in a real photon interaction, as mentioned above.

SESSION ON DETECTORS FOR CHARGED CURRENT EVENTS

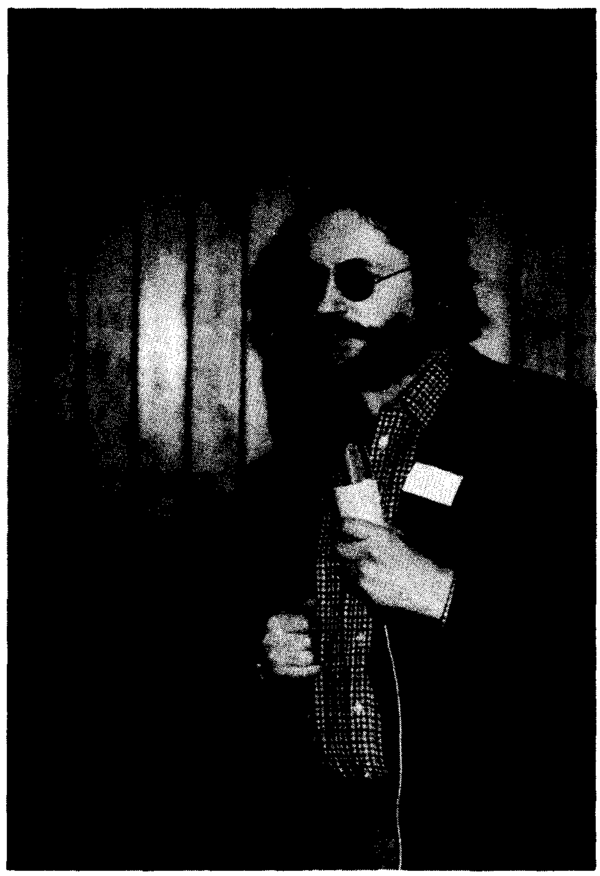

Discussion Leader: K. Tittel

Scientific Secretary: P. Steffen

Report from the Study Group* on

DETECTORS FOR CHARGED CURRENT EVENTS

R. TURLAY

* The members of this study group are :

U. AMALDI, T. BARONCELLI, PH. BLOCH, A. BLONDEL, D. CRENNELL, F. DYDAK, F. EISELE, C. GEWENIGER, V. HEPP, F. JACQUET, G. JARLSKOG, B. JEAN-MARIE, G. KALMUS, K.H. MESS, H. PAAR, E. RADERMACHER, P. STEFFEN, J. RANDER, R. TURLAY, K. TITTEL, T.G. WALKER.

I - INTRODUCTION

A general study of an e-p facility for the SPS has already been presented (ref. the CHEEP* Report). It is in this earlier report that one can find the best summary available on e-p physics and on an e-p machine facility. That report was strongly influenced by the possibilities offered by the 400 GeV proton ring of the present SPS. In December 1978 the ECFA and DESY organised working groups to continue the "Study of an e-p facility for Europe" along lines somewhat independent of the CHEEP study. Among the different proposed working groups an arbitrary choice separated the study of neutral current from charged current. In this report we shall present the results of the charged current group's effort, although as we shall see, it is not clear that the apparatus needed for the detection of either of these interactions is very different. We have concentrated our study on the detection of charged current events, i.e. events

* CHEEP Report - CERN 78-02 - Intersection storage rings division - 27.2.78 GENEVA.

characterised by the following graph :

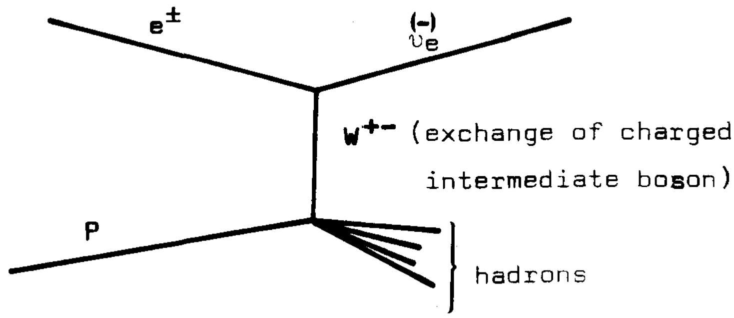

where the exchange of a $W^{\pm}$ in this processes is the same as the one in the neutrino physics in fixed target interaction ($\nu + p \rightarrow e^- + \ldots$ or $\bar{\nu} + p \rightarrow e^+ + \ldots$). Thus this physics can be seen as the continuation of the present neutrino physics programs (SPS or FNAL) but at a value of q^2 tremendously larger. One should keep in mind, however, that with an e-p machine we are dealing with ν_e or $\bar{\nu}_e$ and that all the main knowledge of the neutrino physics up to now is obtained with $\bar{\nu}_\mu$ – but then if universality holds... At a glance the detection difficulty of such events appears due to the evanescent neutrino, it was the purpose of the working group to understand and verify that the detection of such events is possible and furthermore that the physics of this interaction can be worked out. We have emphasized this goal much more than the details of construction of a detector. Concerning the detector we have imagined a reasonable device feasible with present technology and have kept in mind that within 5 or 6 years further technical development could be used to improve such a detector.

All the present calculations were performed assuming an e–p machine with electron energy of 20 GeV and proton energy of 270 GeV, a luminosity of 10^{32} cm^{-2} sec^{-1} and no spatial limitations in the experimental area. It is obvious that detailed characteristics of the machine and experimental area are needed to continue this work, but discussions of this type were not possible from lack of time. We are perfectly aware that serious problems might be posed by a realistic study of machine construction details but we feel that none of the essential aspects of the proposed experimental apparatus will be drastically changed.

II - PHYSICS MOTIVATION

The physics interests for an e-p machine have been previously discussed in general (B.H. WICK, J. ELLIS, CHEEP report). We would like to review here those aspects specific to charged currents.

A) STRUCTURE OF WEAK CHARGED CURRENT INTERACTION.

- The deviation from the four-fermion interaction is expected to be mainly due to the W propagator for $q^2 \geqslant 1000$ GeV^2, assuming the mass of the W is $\simeq 76$ GeV. This damping effect $P_W = m^2_W / (m^2_W + q^2)$ is shown in Fig. 1.

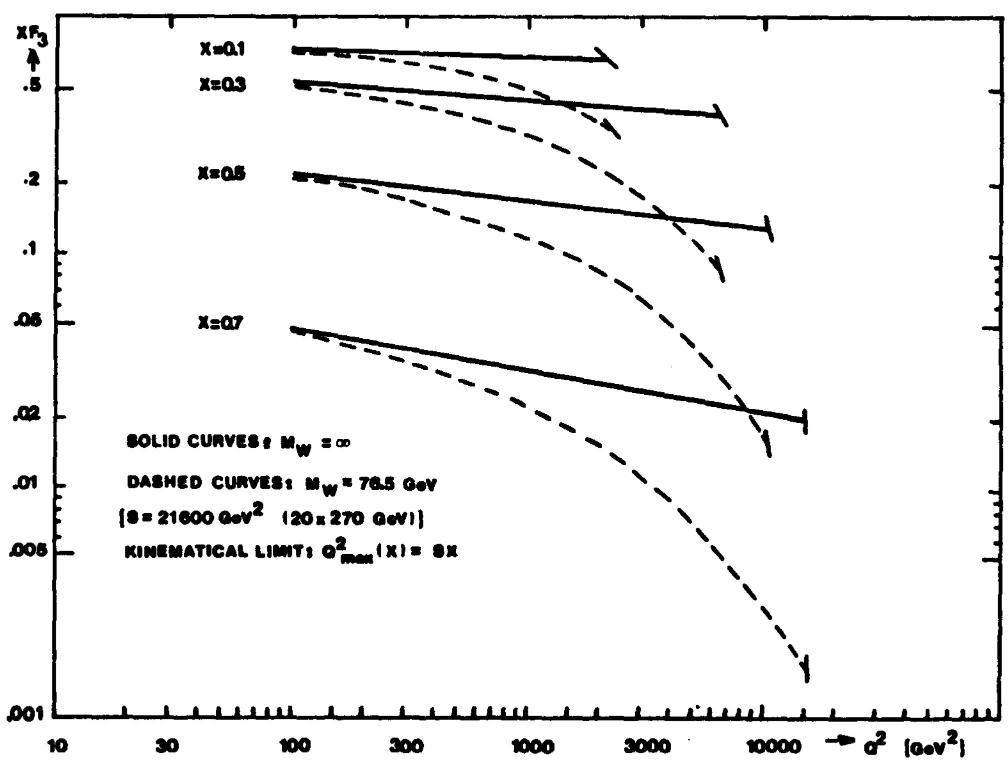

FIG. 1 - BURAS-GAEMERS PREDICTIONS[1] FOR $xF_3(x,Q^2)$
USING CDHS[2] DATA FOR EXTRAPOLATION OF THE FIT.

Such an effect, which can reach an order of magnitude, in the q^2 range available will allow a determination of the mass of the W or at least a limit on this mass, if it is larger than that expected by the Weinberg-Salam model.

- More specific to the form of the charged current is the test on the pure V–A component of the space-time structure of weak interaction. The search for reaction

$$e^-_R + u \rightarrow \nu_e + d$$

$$e^+_L + d \rightarrow \bar{\nu}_e + u$$

which require V+A coupling will be of great interest. The difficulty of such an experiment is clear : one expects to find a small or zero effect within a large background. One such background source is the inefficiency of electron detection for neutral current events.

B) STRUCTURE OF NUCLEON AND FRAGMENTATION FUNCTIONS.

It is precisely on this topic that an e–p machine is far superior to e^+e^- or $p\text{-}\bar{p}$ machine. It offers a point like probe which accesses a very interesting (q^2, x) region and can thus extend the study of nucleon structure functions.

- The sea region at low x, and q^2 as large as 100 GeV^2.
- The large q^2 region for QCD tests (especially in the region before the propagator effect becomes too large).

Structure functions.

Assuming that we can detect events and measure q^2, ν (or x, y) (it is a large part of this report to demonstrate that) we should notice that the study of the structure function is not completely the same as for the neutrino interactions on isoscalar target. In e–p interaction one has two types of processes :

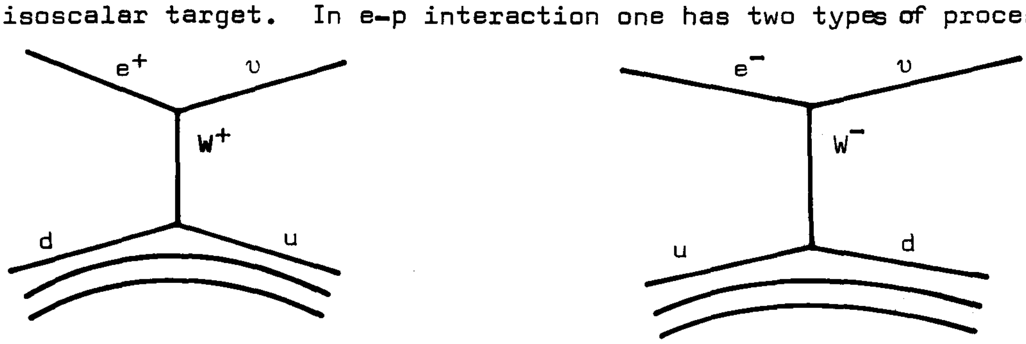

where one measures separately u(x) and d(x). A priori these distributions are not equal and one should write the differential cross sections dependent upon 6 structure functions.

$$\frac{d^2\sigma}{dxdy}(e^- p) \,\alpha\, (1-y)\, F_2(x,q^2) + y^2\, x\, F_1(x,q^2) + (y - \frac{y^2}{2})\, x\, F_3(x,q^2)$$

$$\frac{d^2\sigma}{dxdy}(e^+ p) \,\alpha\, (1-y)\, F_2'(x,q^2) + y^2\, x\, F_1'(x,q^2) - (y - \frac{y^2}{2})\, x\, F_3'(x,q^2)$$

The main difference between a proton and an isoscalar target is clear : the sum of the two differential cross sections does not give $x\,F_3(x,q^2)$. Solving these equations and measuring the F_i and F_i' requires that one runs at least 3 different energies for e^-p and e^+p. This can best be illustrated if we consider an x,q^2 point (for either e^-p or e^+p), it corresponds to a specific value of υ(or y), however the same point for different energies of electron and proton (i.e. different values of υ_{max}) will correspond to different values of y thus yielding a set of solvable equations. Since the energy of the electron and the proton cannot change independently (Refer DESY report 78.02) one can propose respectively 17.5/280, 11/176, 6.3/100 GeV which would give a good lever arm for υ and an order of magnitude larger for q^2 than we can expect to obtain for neutrinos at FNAL with the doubler. (These different running energies should be optimized after discussion with machine design group). Isoscalar target physics, however could be done if we accelerate deuterons (with an expected luminosity loss of a factor of 4). The development

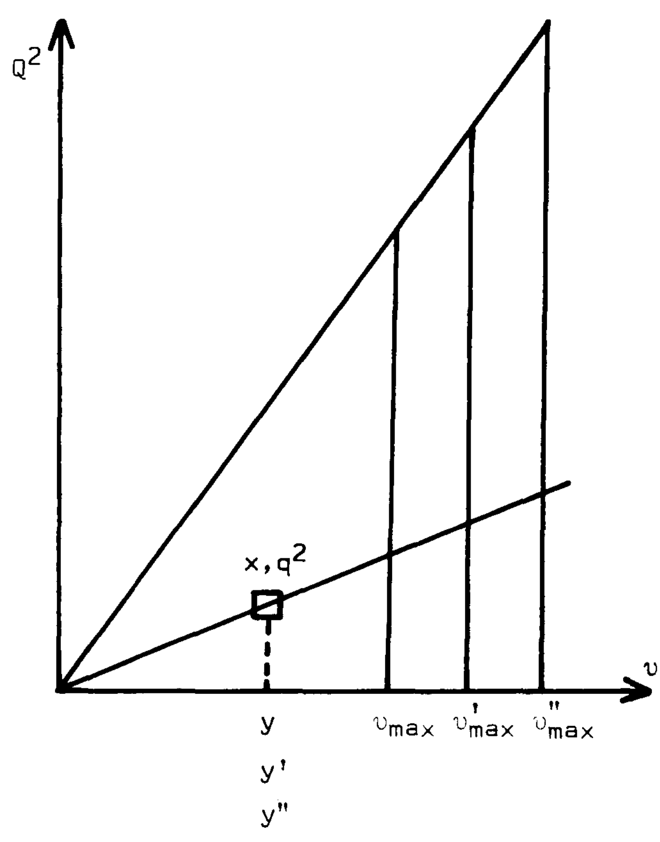

of this possibility will allow tests of charge symmetry $F_i^+(e^+n) = F_i^-(e^-p)$.

Fragmentation function.

The final hadronic state is kinematically more visible in e-p machine than in fixed target physics where both the target and current fragments are mixed together. If the identification of particles is possible, one can study the current jet and test the factorisation hypothesis at large q^2 over a large W range : $\frac{d\sigma}{dxdZ} \propto F(x,z,q^2) \overset{?}{=} q(x,q^2)\, D_q^h(z,q^2)$. With the charged current we have the unique feature of knowing the flavor of the current quark, and thus we should have the possibility of separating the fragmentation functions coming from the valence and the sea together $(D_u^{\pi^+} = D_{\bar{d}}^{\pi^+} = D_d^{\pi^-} = D_{\bar{u}}^{\pi^-})$ from those of the sea only $(D_u^{\pi^-} = D_{\bar{d}}^{\pi^-} = D_d^{\pi^+} = D_{\bar{u}}^{\pi^+})$ which means a possible separation of non singlet and singlet contributions in fragmentation functions.

C) SEARCH FOR NEW QUARK OR LEPTONS.

The available total energy $W \simeq 130$ GeV is surely large enough to be interesting for the search for new heavy objects and the charged current has the advantage of producing single flavors of the presumed new quark rather than quark - antiquark pairs as in e^+e^-. The production of possibly new neutral leptons would also have a very good signature. Nothing new needs to be added here to the CHEEP report on this type of speculation. However, we will come back to this subject for the muon detection chapter.

III - KINEMATICS

The detailed kinematics of the e-p interaction is presented on page 68 of the CHEEP Report. We do not want to repeat here all of this material, but we would rather like to stress some of the main characteristics of the kinematics which help to clarify the detection problems for the charged current events. We define the variables of the following Feymann graph :

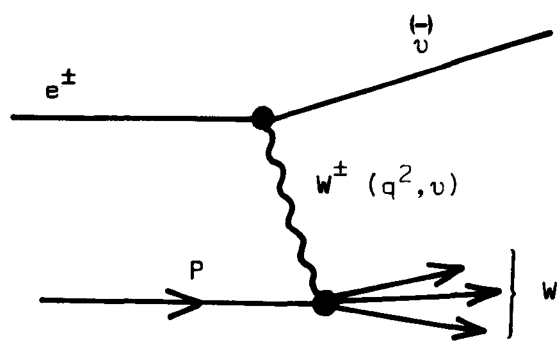

E_e energy of the electron

E_p energy of the proton

E_L energy of the lepton

s (total energy)^2 $\quad s = 4\ E_e\ E_p + m_p^2$

Q^2 four momentum of the current $\quad Q^2 = -q^2 = 4\ E_e\ E_L\ \sin^2 \frac{\theta}{2}$

W effective mass of the final hadronic system $\quad W^2 = 2\ m_p\ \nu + m_p^2 - Q^2$

$$\nu = \frac{p.q}{m_p} = \frac{E_p}{2\ E_e} \left\{Q^2 + 2\ E_p\ (E_e - E_L)\right\} \frac{1}{m_p}$$

$$\nu_{max} = 2\ E_e\ E_p\ /\ m_p$$

Scaling variables :

$$x = \frac{Q^2}{2\ m_p\ \nu} \qquad y = \frac{\nu}{\nu_{max.}}$$

A 20 GeV electron and 270 GeV proton machine gives the following parameters :

$s = 21601\ GeV^2$	$Q^2\ max = 21600\ GeV^2/c^2$
$W_{max} = 147\ GeV$	$\nu\ max = 10800\ GeV$

Although the very large q^2 values at large x do not represent much of the cross-section, this machine allows one to work with reasonable event numbers, with $x \simeq 0.2$, for instance, around a q^2 value of $\simeq$ 2000 GeV^2/c. This is a tremendous step forward. Figure 2 shows in the x, y plane the two variables q^2 and W.

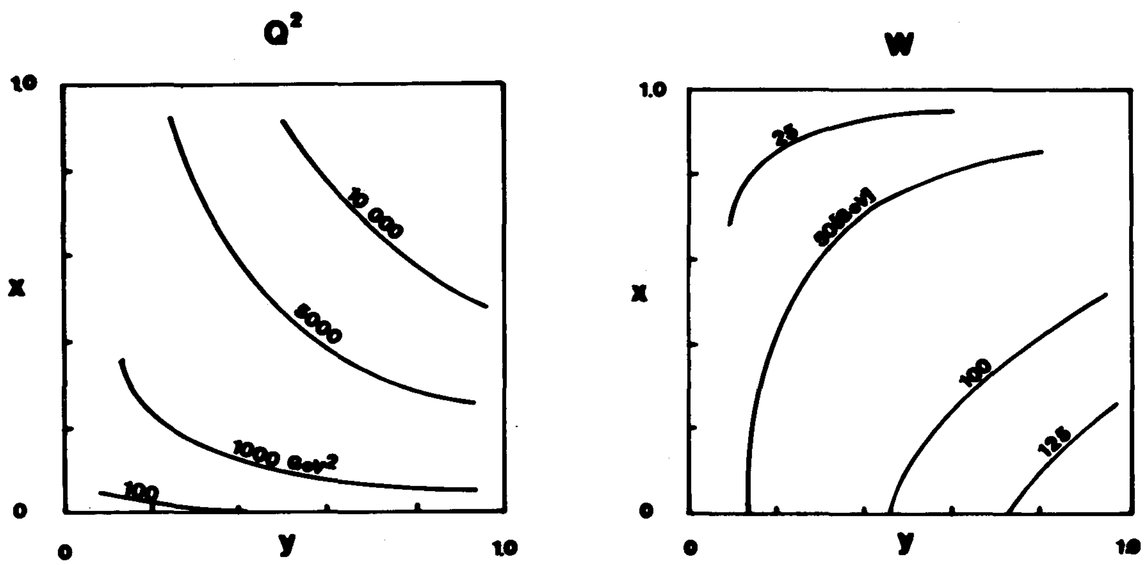

FIG. 2 : Q^2 and W curves for E_e = 20 GeV, E_p = 270 GeV.

Lepton kinematics

In order to calculate the out going neutrino kinematics one needs only momentum and energy conservation. Although the neutrino is not detected it is interesting to calculate its angle and energy. The kinematics are the same as for the electron in the neutral current case and thus we need to know the lepton direction to test if an electron is detected or not.

Hadron kinematics

The calculation of W and ν for hadrons is straight forward, but if we want to know more details about the hadrons' directions, and momenta we need a model. The most commonly used is the quark-parton model.

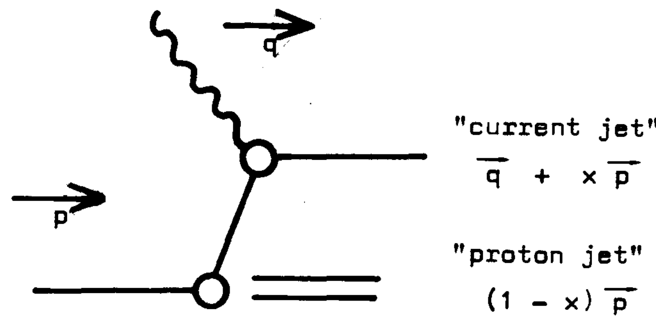

With this model the kinematics only give the angle of the current jet θ_j and assume that the angle of the proton jet is equal to zero. Thus the proton jet follows the direction of the incident proton. This gives us a kind of "3 particle" direction system which shows a priori that in principle the detection of charged current events should not be too difficult.

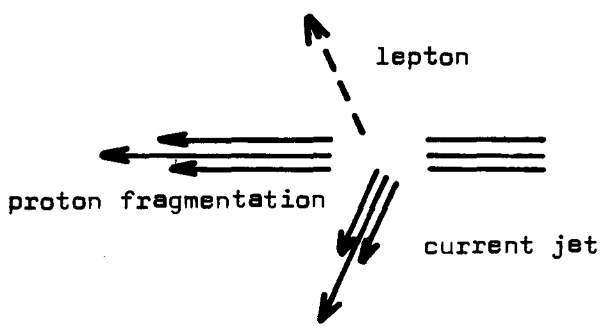

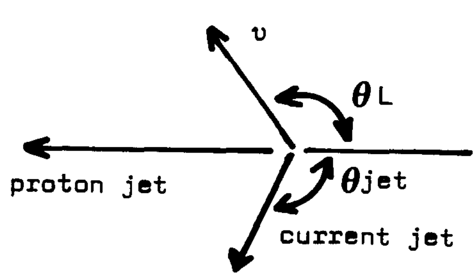

The angles and momenta for each part of this reaction are shown in figure 3 :

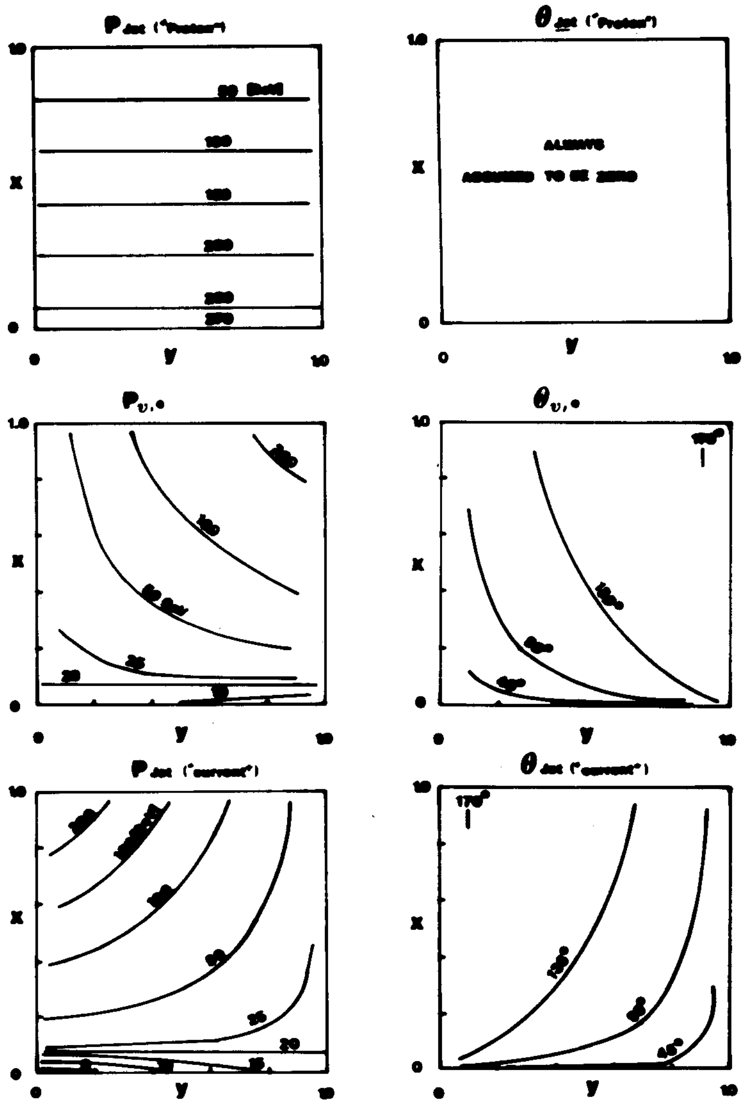

FIG. 3 : Angle and momentum of the lepton, the hadron jet, and the proton jet (E_e = 20 GeV, E_p = 270 GeV).

How to dress the quark

The average direction of the hadron jet is not sufficient if we want to understand in more detail how to detect the hadrons emitted. For this purpose one needs to know how to generate hadrons in a Monte-Carlo simulation. We had at our disposal three Monte-Carlos which were based upon the quark parton model and generated hadrons in the jet.

- The inclusive hadron distribution $f(x_F,p^2) = e^{-4P_\perp^2 - 0.75\langle n\rangle x_F}$ proposed in the CHEEP Report (p.71).
- A program built in this working group "à la Susskind" [3]
- A program constructed by A.L. GRANT [4] using neutrino data for x_F. This program has been used by many people from all the working groups and all details are given in GRANT's article in these proceedings.

However the final "dressing", the overall angles θ_j and θ_p stay the same, only the population density of hadrons will change according to the different recipes. These angles θ_j or θ_p can be changed however by physical processes beyond the simple quark parton picture as for example gluon radiation in any process which will give additional P_T to the proton jet or to the hadron jet. Reciprocally, if we want to learn more about these jets then we will need to detect and identify all of the particles in order to test the simple kinematics involved in the quark parton model.

IV - RATES

We have not calculated new rates, but rather have relied upon the calculated rates of the CHEEP Report for E_e = 25 and E_p = 270 GeV.

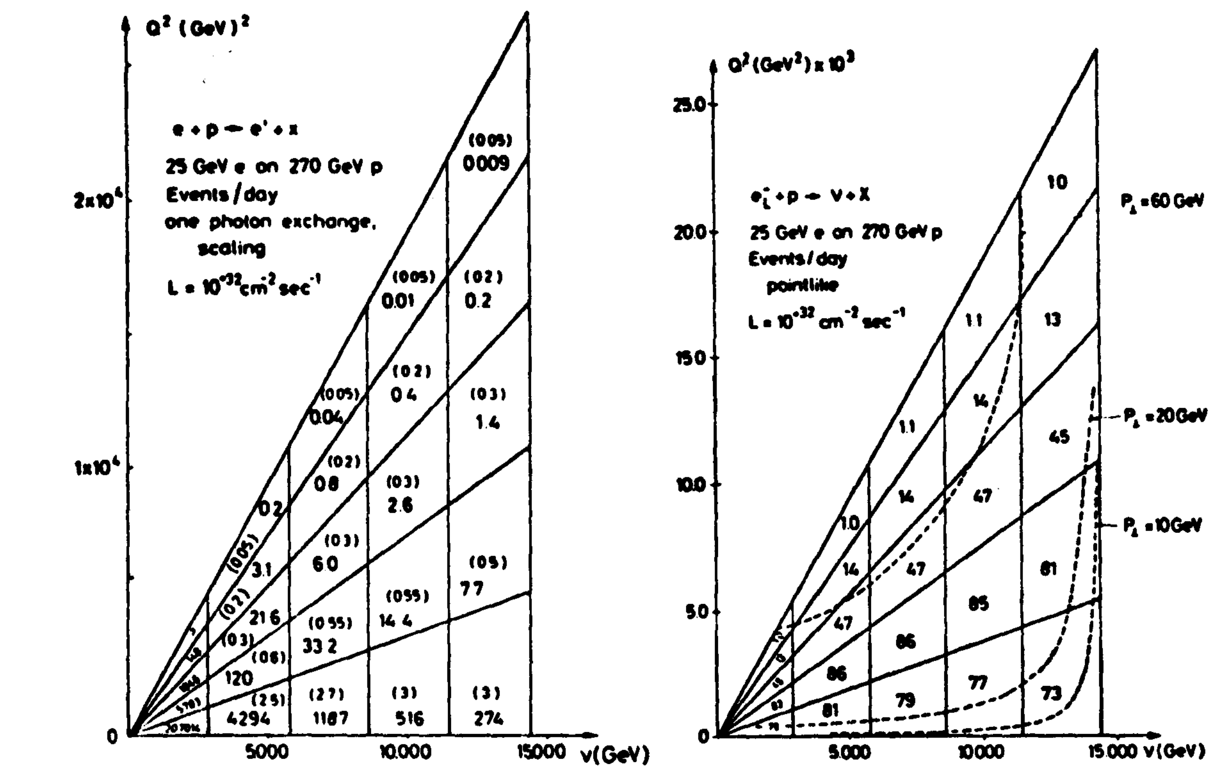

FIG. 4 : Calculated rates for charged and neutral currents from the CHEEP Report (p. 104 and p. 101).

The number of events are in bins of dx dy = 0.04. For the charged current one assumes scaling and a point-like coupling. For the neutral current the rates are evaluated for one photon exchange assuming scaling.

For a luminosity of 10^{32} cm^{-2} sec^{-1} one sees that we can expect $\simeq$ 1000 events a day. We know that the propagator effect with a mass M_W of 63 GeV could decrease this rate by an order of magnitude. It is interesting to note the large number of neutral current events produced at low q^2 (207014 in the smallest q^2 bin). This implies that very good electron identification is necessary to avoid contamination of the charged current event sample by misidentified electrons from neutral current events.

Proton beam

This is the source of background which can be the most severe. The note added at the end of this report and written by H.F. HOFFMANN [5] is the best study presently available. The main conclusion is quite serious and demands a vacuum of 5.10^{-11} Torr.

We feel that more work is obviously needed to clear up this background question, and it is only when its rate is understood that we can worry about the physics consequences for the data.

V - BACKGROUNDS

We are aware that the background can pose severe problems in an e-p collider. We have not studied this question in great detail because of lack of time (and also because our working group had no connection with the machine physicists). This background study however is very important for the charged current experiment for two reasons :

- it can give an overly abundant trigger rate,
- it can contaminate the physics sample of events.

To answer these questions we need to know the amount and the type of background we can expect.

Electron beam

The information we used in this case came from calculated or experimental results from PETRA.

- For background due to *Synchrotron radiation* one expects 10 accidental hits per bunch crossing for an intensity of 20 + 20 mAmps. We can assume that in an e-p machine we will have 10/2 = 5 accidental hits per bunch (20 mA). This can be further reduced by improved schielding in the e-p machine because only one electron beam is circulating.

- For the *beam-gas and beam pipe interactions* only accidental tracks in real event need to be considered. (We expect that a $P_{\perp}$ threshold in the central calorimeter will reduce beam-gas and beam-pipe background to a negligible amount). In this case, the accidental rate at PETRA for an experimental set-up (TASSO) with 2+2 bunches of 2 mA and a vacuum of 10^{-9} Torr is 0.5 % per bunch crossing. In e-p if the total rate scales with the beam current, one expect 2.5 % per bunch (20 mA), which can be < 0.25 % if the vacuum is pushed down to 10^{-10} Torr.

- *The cosmic ray background* within a good event will be < 1 % and will be easily reduced by software.

VI - DETECTION AND STUDY OF THE CHARGED CURRENT EVENT

The selection of charged current candidates relies on the large $P_\perp$ unbalance which characterizes these events. The fact that the lepton is missing and that the "hadron jet" should balance its transverse momentum is a clear signature. However this implies that we detect and measure all of the hadrons produced - charged and neutral - and one must be sure that there is no electron in the direction where one expects the lepton i.e. the neutrino. A selection with a $P_\perp$ cut off larger than 10 GeV for example is efficient and does not reduce the available q^2, υ region as it can be seen in fig. 4. These two criteria - $P_\perp$ cut off and no electron - are sufficient to obtain and select a sample of charged current events.

A METHOD TO STUDY THE STRUCTURE FUNCTIONS

From this sample of charged current events one would like to extract q^2, υ or the scaling variables x and y. What are the available equations ? From pure kinematical consideration one can work out 3 independent equations

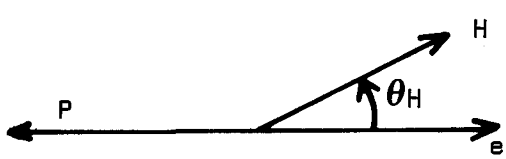

(1) $\sum_i E_H^i = E_e\, Y + E_p\,(1 - XY)$

(2) $\sum_i P_L^i = E_e\, Y - E_p\,(1 - XY)$

(3) $\sum_i P_\perp^{i2} = 4.\, E_e . E_p\, XY\,(1 - Y)$

where momenta are positive in the direction of the electron and the index i is summed over all hadrons produced.

One still assumes that we measure the total energy E_H, the longitudinal momentum P_L and the transverse momentum $P_\perp$ for all the particles. In this condition there is no problem to extract x and y. Proposing a method to measure x and y means trying to determine what is sufficient to measure and what are the consequences in the determination of x and y. In other words we have assumed a 4π detector but in reality there are particle losses in the forward or backward directions which clearly affect the determination of x and y.

It has been the task of this working group to try to discover what are the best variables that we can measure to minimize the effects of these losses.

In the following discussion we outline two different "methods" to extract x and y.

METHOD I (Ref. CHEEP Report p. 81).

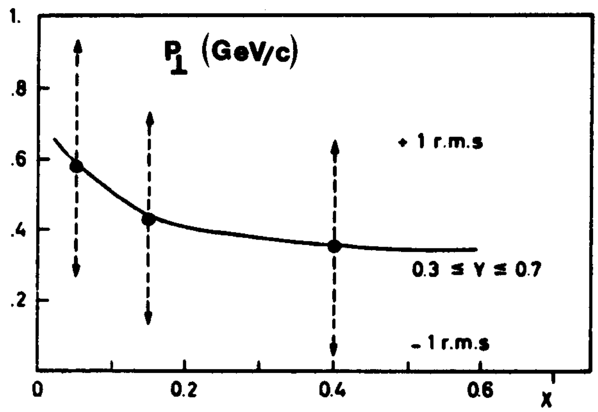

FIG. 5 - from CHEEP Report p.105.
TRANSVERSE MOMENTUM
OF PARTICLE IN FRAGCAL.

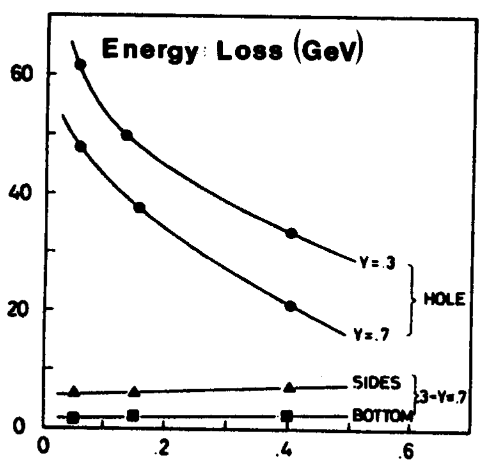

FIG. 6 - from CHEEP Report p.105.
ENERGY LOSS IN FRAGCAL.

- The identification of charged current is based on the missing transverse momentum of all hadrons. Fig.5 shows that the missing transverse momentum due to particle escaping in forward (proton direction) (40×40 cm^2) is negligible compared to a cut off of 10 GeV. In order to separate the charged current from the neutral current events, the direction of the lepton is needed to check that it is not an electron. Kinematically this direction is determined from the total hadron energy. This total hadron energy is however not well determined for some x and y values, e.g. leakage through the forward hole. The conclusion is that one needs good large angle electron detection efficiency.

- Determination of x and y

The proposed calculation considers two of the equations, (2) and (3) :

$$(2) \qquad \sum_i P_L^i = E_e Y - E_p (1 - XY)$$

$$(3) \qquad \sum_i P_\perp^{i2} = 4 E_e E_p XY (1 - Y)$$

It is obvious from equation (2) that because of leakage in the forward direction (shown in Fig. 6) this method is valid for x > 0.4 only.

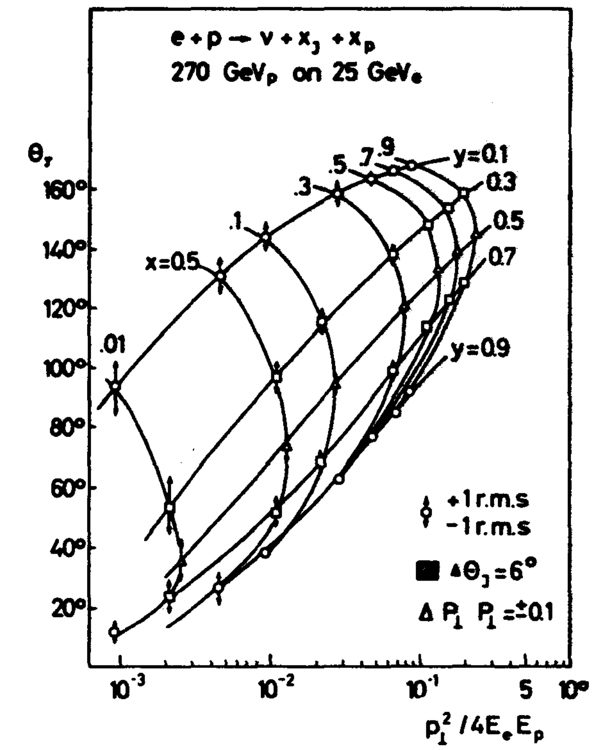

FIG. 7 – from CHEEP Report p.108. LINES OF CONSTANT x AND y IN θ_j, $P_\perp^2$ PLANE.

For $x < 0.4$ one considers the angle θ_j of the hadron "current jet" and the equation (3)

$$(4) \qquad tg^2 \frac{\theta j}{L} = \frac{E_p}{E_e} \times \frac{(1-Y)}{Y}$$

$$(3) \qquad \sum_i P_\perp^{i2} = 4\, XY\, E_e\, E_p\, (1-Y)$$

The resultant error for x and y are presented in Fig. 7. The conclusion is that one can determine x and y with an error less than 0.1 for $x \leqq 0.5$, $y \leqq 0.7$.

Remarks :

This method is limited in that we need two different ways to calculate x and y corresponding to two different regions in the x, y plane, which implies two different types of experimental errors. Furthermore the definition of the jet angle θ_j requires that one disentangles particles of the hadron jet from particles of the proton jet, which could be difficult if the two jets are not well separated. Finally it is required thatthe forward detector have high performance.

METHOD II (Proposed in this Working Group – JACQUET – BLONDEL)

This method relies on the following simple observation : if we add equation (1) and (2) and keep equation (3) on has the following set :

$$(3) \qquad \sum_i P_\perp^{i2} = 4\, E_e\, E_p\, .\, XY\, (1-Y)$$

$$(5) \qquad \sum_i E_H^i + \sum_i P_L^i = 2\, E_e\, Y$$

where one can make the following remarks :

- The problems for equation (3) are the same as before and the error due to the loss of particles going in the forward direction (proton jet) is still small as in the previous method.

- A significant improvement follows from equation (5).

This can be easily seen if we neglect the masses of the particles; then one can write : $E_H + P_{//} \simeq P + P \cos \theta_H$

- If we detect all particles the solution for x and y is trivial.
- The hadrons created with $\theta_H \simeq 0$ incident (electron direction) gives

$$E_H + P_{//} \simeq P \, (1 + \cos \theta_H) \simeq 2 \, P$$

- The hadrons created with $\theta_H \simeq 180°$ incident (proton direction) gives

$$E_H + P_{//} \simeq P \, (1 - \cos \theta_H) \simeq P\theta * \frac{\theta}{2} \simeq P_\perp \, . \, \frac{\theta}{2}$$

In this condition we see that the particles leaving the apparatus (and thus not detected) in the proton direction which previously contributed very much to the method using equations (1) or (2) have much less effect when using equation (5) since this loss is proportional to $P_\perp * \frac{\theta}{2}$ and here the $P_\perp$ lost is multiplied by a small angle. On the other hand particles leaving the apparatus in the electron direction contribute much more to the equation (5) but we profit from the kinematics in that few hadrons are produced at $\theta_H = 0$ (cf. figure 3) and so this effect is small.

The two aspects are perfectly visible in Figure 8 where we have plotted the difference between the $\underline{x}$ and $\underline{y}$ of events generated by Monte-Carlo, and the $\underline{x}$ and $\underline{y}$ reconstructed via Method II, where we assumed particles were lost in both a 15 mrad forward hole (proton direction) and a 100 mrad aft hole (electron direction). We see that in the case of the forward cut the effect on y is very small (proportional to $P_\perp * \frac{\theta}{2}$) and the effect in x is small (proportional to $P_\perp$). In the case of the aft cut the smearing is large in y (proportional to $\simeq 2 \, P_L$) and also in x. Therefore we have conclude that we must also decrease the aft hole cut to 30 mrad. In this condition the method gives the result shown in Figure 9.

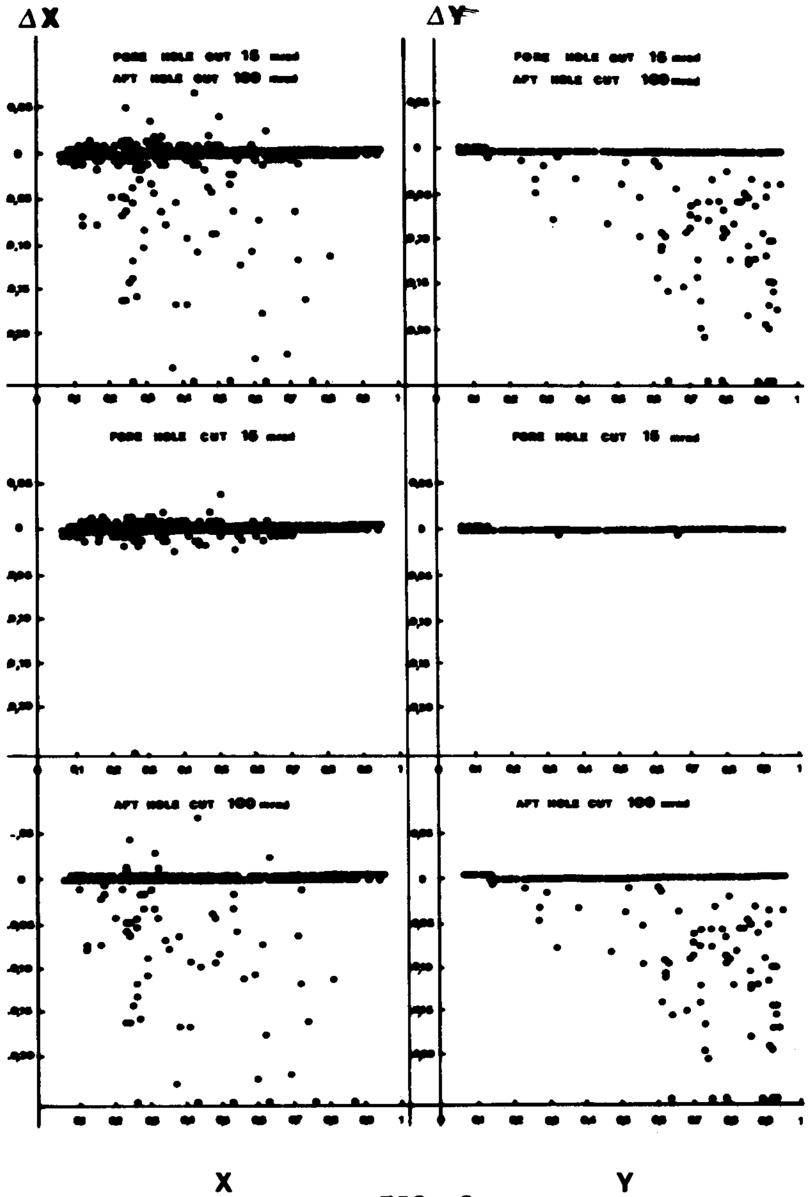
ΔX
ΔY
FORE HOLE CUT 15 mrad
AFT HOLE CUT 100 mrad
FORE HOLE CUT 15 mrad
AFT HOLE CUT 100 mrad
X
Y

FIG. 8.

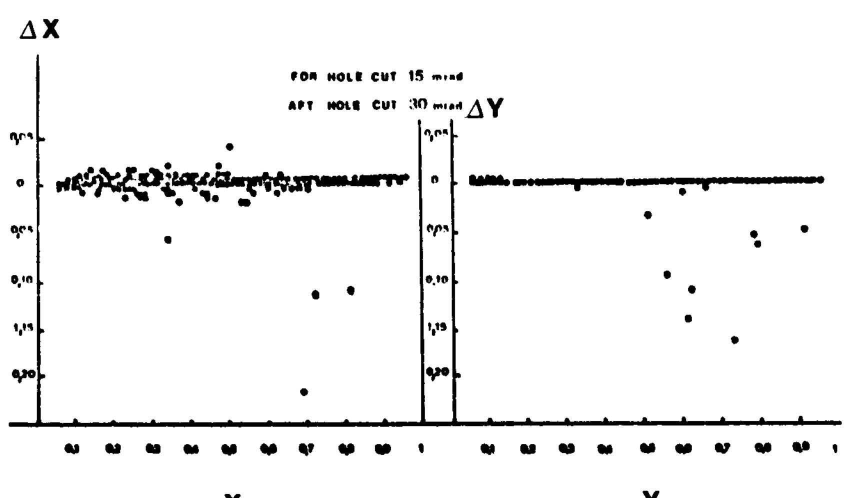
ΔX
ΔY
FOR HOLE CUT 15 mrad
AFT HOLE CUT 30 mrad
X
Y

FIG. 9.

In conclusion, if we can detect all of the hadrons, measure the momentum and the angle in a 4π detector except in two holes of 15 mrad and 30 mrad then we can calculate the <u>x</u> and <u>y</u> scaling variable for each charged current event with reasonably small errors.

We should note here that the hole of 30 mrad in the electron direction will not allow us to distinguish between a neutral current with an electron going in the hole (and thus not detected) and a charged current event. The region in the x, y plane where this occurs is very populated for neutral current events and corresponds to $x < 0.01$ and $y < 0.1$. It is clear for this very small area of the x, y plane that it will probably be impossible to determine the structure functions of the charged current.

VII - DETECTORS

We have primarily tried to optimize the characteristics of the detector for the study of the structure functions of charged currents. However we feel that this is not completely sufficient since we are convinced that the study of the hadron jet (fragmentation functions) is also a very important program. One might say that measuring all of the hadrons for the structure function is, in this respect, also useful for the study of the hadron jet; however for the hadron jet one also needs complete particle identification. This latter problem has not been investigated, neither have we studied in detail the hadron jet physics and the requirements that this study might imply for the detectors.

What are the detector requirements ?

(1) - We need to measure the angle and the momentum (or total energy) of all hadrons.

(2) - We would like to identify an electron, however not necessarily measure it with high precision. Note that this latter requirement could be necessary if one wants to do normalization with neutral current events or for test purposes for example.

(3) - Neutral particles need to be detected.

- The π^0 could be detected in the same detector as that used for electron identification.
- Neutrons and K_L^0's can be measured in the cells of a hadron calorimeter.

(4) - A priori we are not asking for especially high performance in the precision of this detector.

We will confirm this particular point after the discussion of the error-measurement study in the next chapter.

Following the philosophy of the CHEEP Report one group started to study a non magnetic detector and another group a magnetic detector. With time we realized that particles in the hadron jet are not very energetic (see figure 3) for the region $x < 0.2$ where most of the events are expected, and thus the non magnetic detector group found it desireable to add a small magnetic field and the two detectors tended to approach each other in concept.

DETECTOR 1

no magnetic field
↓
high precision calorimeter (U)
↓
angle measurement : small cells in calorimeter
↓
add weak field
And central drift chamber →

DETECTOR 2

strong magnetic field
↓
Precise measurement of momentum and angle
↓
calorimeter normal precision (Fe)
↓

These two detectors begin to converge.

DETECTOR DETAILS

Detector 1

- Aluminium coil $\vec{B}$ = 4 Kgauss
  ≤1/2 radiation length thick Ø= 1.4m
  small return yoke
- Multilayer cylindrical drift chambers

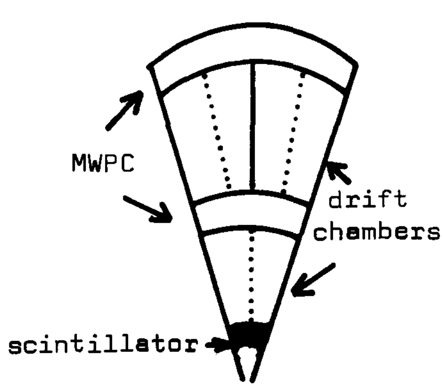

two crowns
$\Delta\varphi$ 4° and 2°

drift chambers
$\theta, \varphi, \frac{dE}{dx}$, V°

Detector 2

- Superconducting coil
  $\vec{B}$ = 15 Kgauss
  return yoke
- Cylindrical inner chambers could be TPC for example if it works for large volumes (or JADE Type chambers)

. Planar drift chamber

Improved precision in the wire direction

. Calorimeter

Uranium and scintillators

radiation length 0.32 cm

interaction length 6.2 cm

Sampling 0.5 radiation length

3 parts (1) 3 R.L. : 90% of electromagnetic particle interact

(2) 15 R.L.: total absorption of electromagnetic shower

(3) 7 Interaction lengths : hadronic component

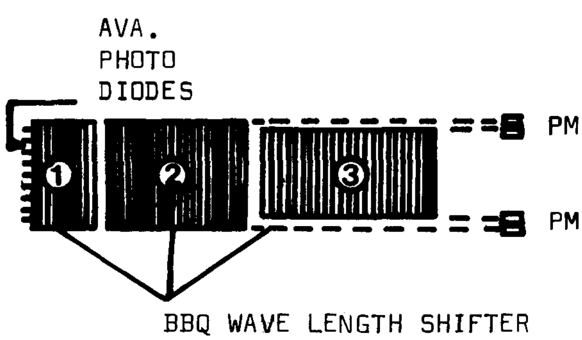

. Light Collection

Section (1) can be serviced by segmented BBQ wave length shifters (1 cm) observed by avalanche photodiodes or by proportional tubes.
Sections (2) and (3) can be handled by BBQ wave length shifter with a precision of 2-10 cm.

$(\frac{\Delta E}{E})_{e.m.} = 0.1/\sqrt{E}$ $(\frac{\Delta E}{E})_{hadron} = 0.3/\sqrt{E}$

. MWPC

Used for triggering purpose and to improve precision in the wire longitudinal direction

. e, γ shower detector

lead and scintillator

3 R.L. one set of drift chamber and then 10 R.L.

$(\frac{\Delta E}{E})_{e.m.} = 0.15 / \sqrt{E}$

. Calorimeter

Sampling of 5 cm in the iron of the return yoke

(Problems of implantation in the return yoke somewhat difficult, but assume it can be solved)

$$(\frac{\Delta E}{E})_{hadron} = 0.6 / \sqrt{E}$$

In summary this requires :
228 T.of Uranium, 24 T.of scintillator, ~30 K.phototubes.
These numbers can be reduced if we accept reduced angular precision.

Details of this detector were not worked out.
There are no specified performances required. Such a detector can surely be done.

FIG. 10

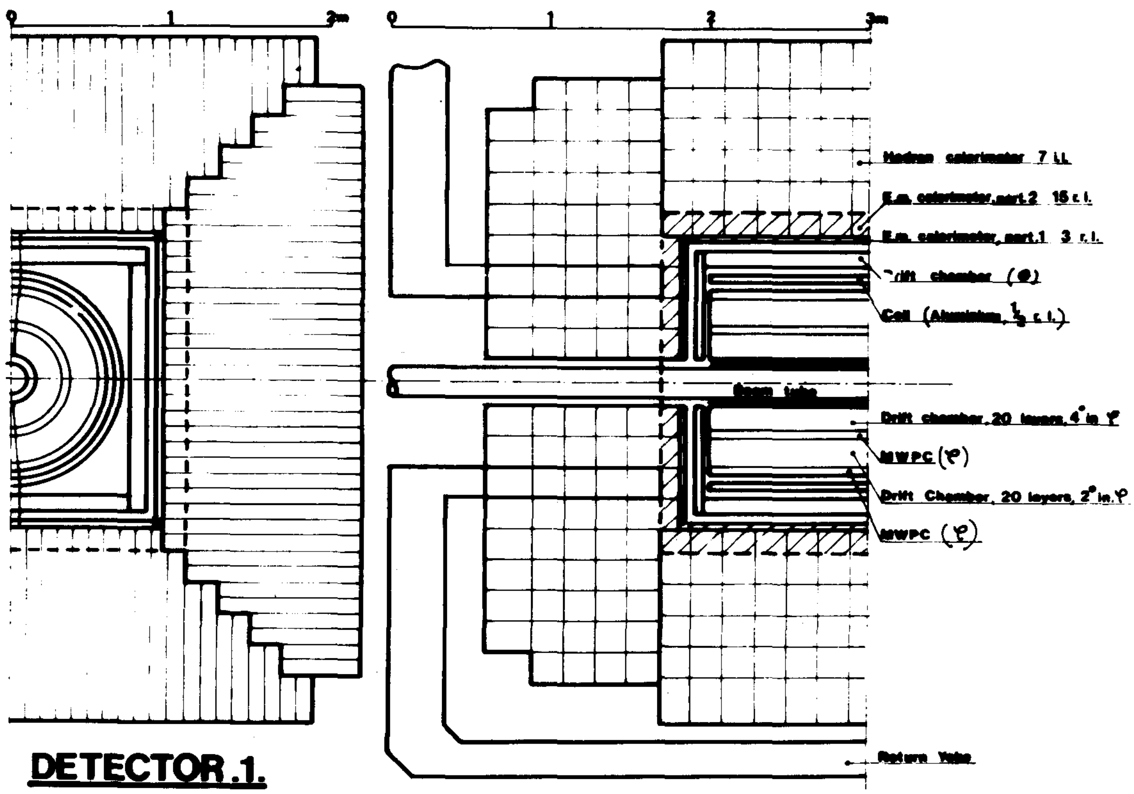

DETECTOR.1.

FIG. 11

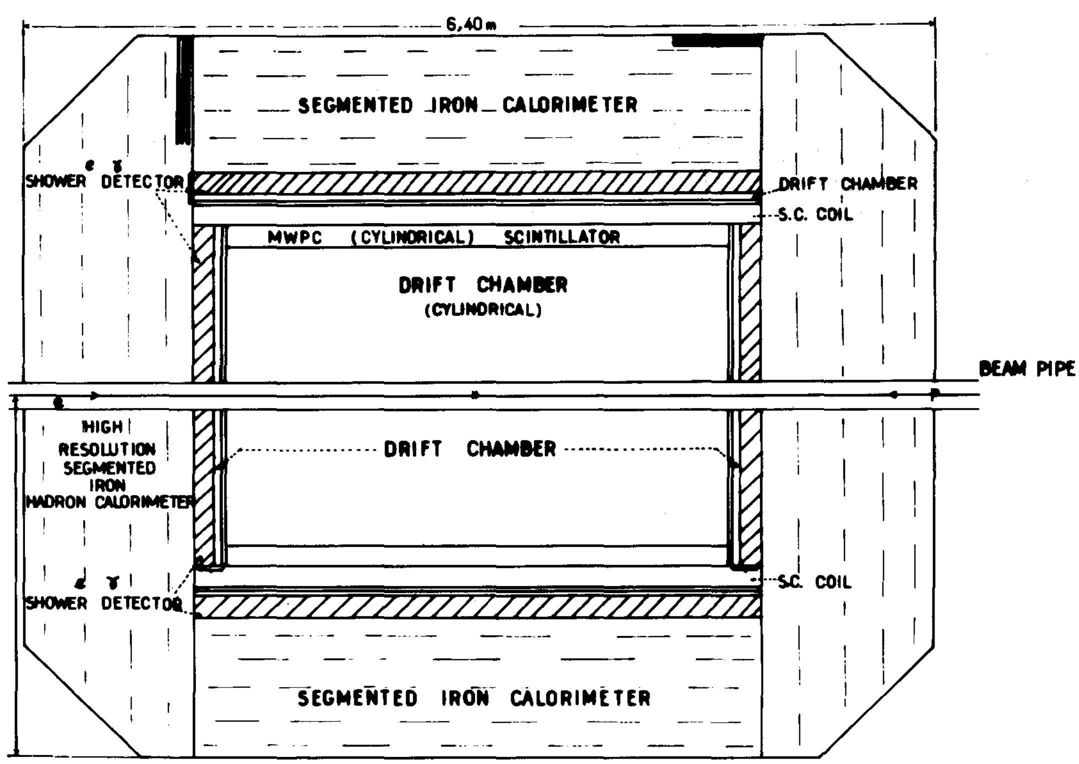

DETECTOR.2.

VIII - FORWARD SPECTROMETER

The forward direction (incident proton direction) presents a special problem because whatever the production model is, a lot of particles are produced in the proton fragmentation region and these are at very high energy in the laboratory.

- On one hand we have seen that if we keep a reasonable aperture (hole of 15 mrad) these escaping particles will not seriously damage the structure function measurement.
- However for jet studies this forward spectrometer is important if we want to examine the details of the proton jet.

Altogether a lot of energy will be lost in the forward direction and we would like to minimize this loss.

To resolve this problem we have studied a separate forward detector which can be added to either of the two central detectors already described.

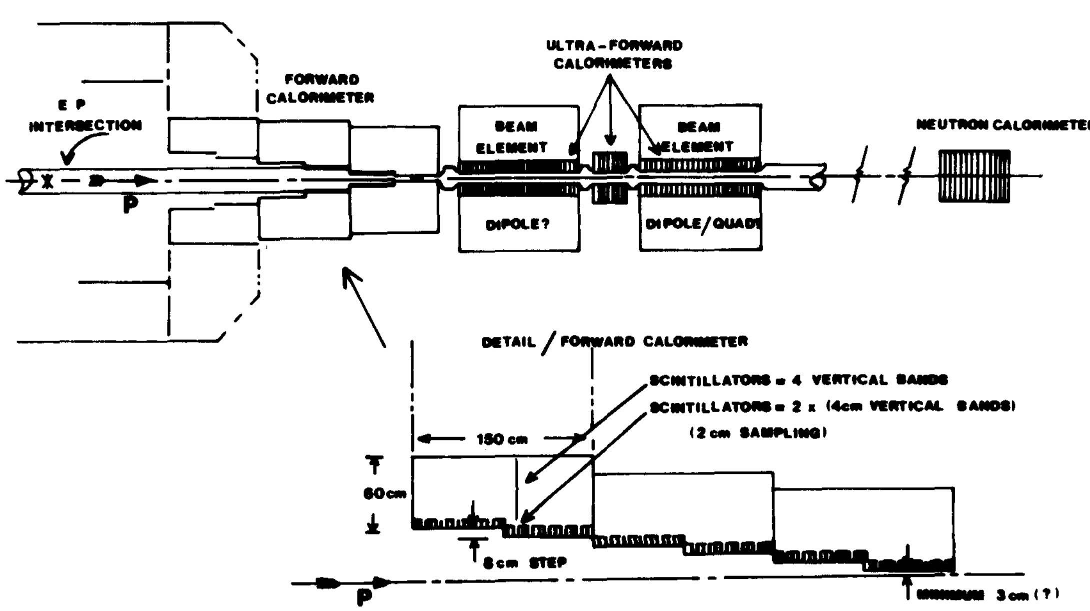

FIG. 12 - FORWARD DETECTOR

This detector has essentially two parts :

- First part, a calorimeter placed upstream of any momentum analysis of particles by magnetic elements of the machine. This calorimeter aperture decreases by steps of 8 cm to the smallest hole that we can obtain (6x10 cm^2). These minimum aperture dimensions can certainly be a problem for the machine study group and should be discussed seriously. The steps of 8 cm allow the $P_\perp$ measurement of particles down to a very small forward angles. (The iron sampling can be of 2 cm and the scintillator lattice of 4 cm).
- Second part, downstream of the first calorimeter, we could envisage a second calorimeter segments in and between the beam elements and finally further downstream a neutron detector in the forward direction. With these we expect to catch as much as possible of the energy leaking through the hole of the first calorimeter.

A Monte-Carlo calculation has been performed using A.L.GRANT generated events to follow the shower development of p, $\pi^\pm$, γ's and π^0s. We have examined the measurement of $P_\perp$ and Y scaling : one considers for each event the pulse heights PH_{xj} and PH_{yi} of the m scintillators and the angle θ_{xj} and θ_{yi} of each scintillator with respect to the z axis. One then calculates the two quantities used to measure the scaling variables x and y

$$P_\perp^2 = \left(2k \sum_{j=1}^{m} \sin\theta_{xj} \; PH_{xj} \right)^2$$

$$Y_{scaling} = \frac{k}{2E_e} \sum_{j=1}^{m} \sin^2\theta_{xj} \; PH_{xj}$$

FORMULAS FOR
The <u>x</u> component.
The same can be written for <u>y</u> direction.

where k is a calibration constant of the calorimeter.

The results are presented Figures 13 and 14. Figure 13 shows the energy lost through the hole as well as the side and end leakage. One should notice that some of the energy lost in the hole can be caught by the second part of the calorimeter which was not included in the Monte-Carlo due to lack of information on possible beam element geometry. Figure 14 shows with what precision one can reconstruct $P_\perp$ and $Y_{scaling}$. These results are very good and quite promising.

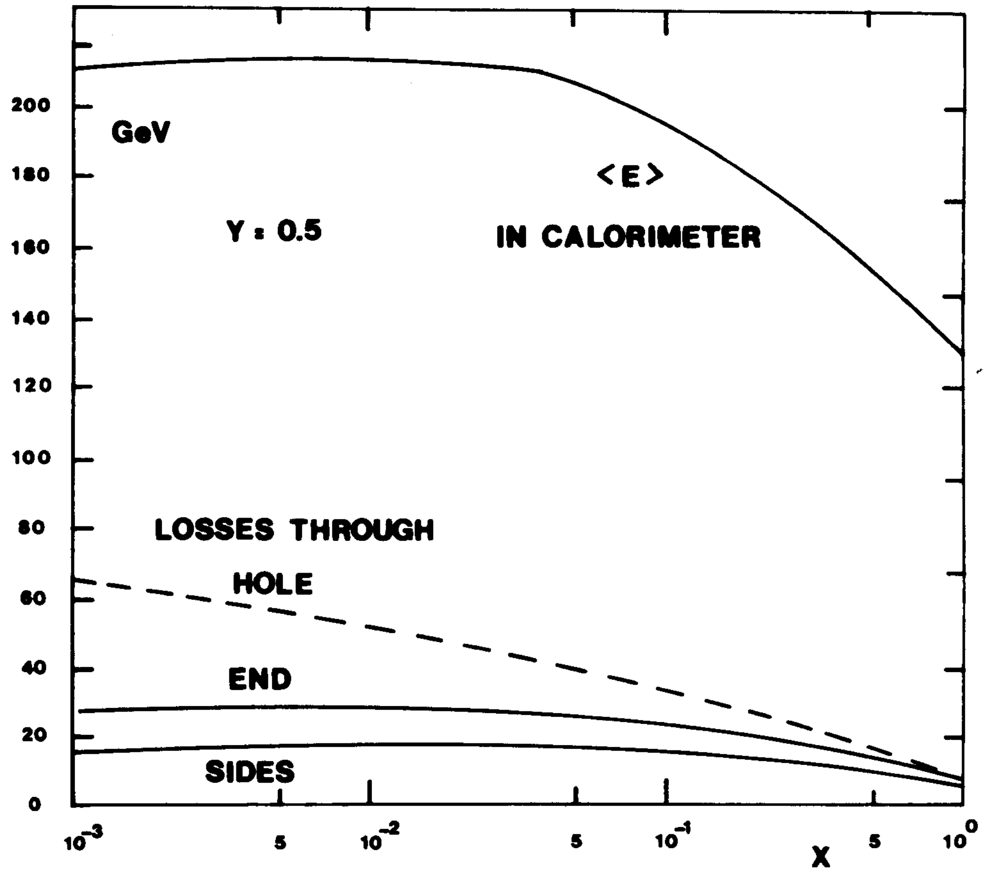

FIG. 13 - ENERGY LOST IN THE FORWARD DETECTOR.

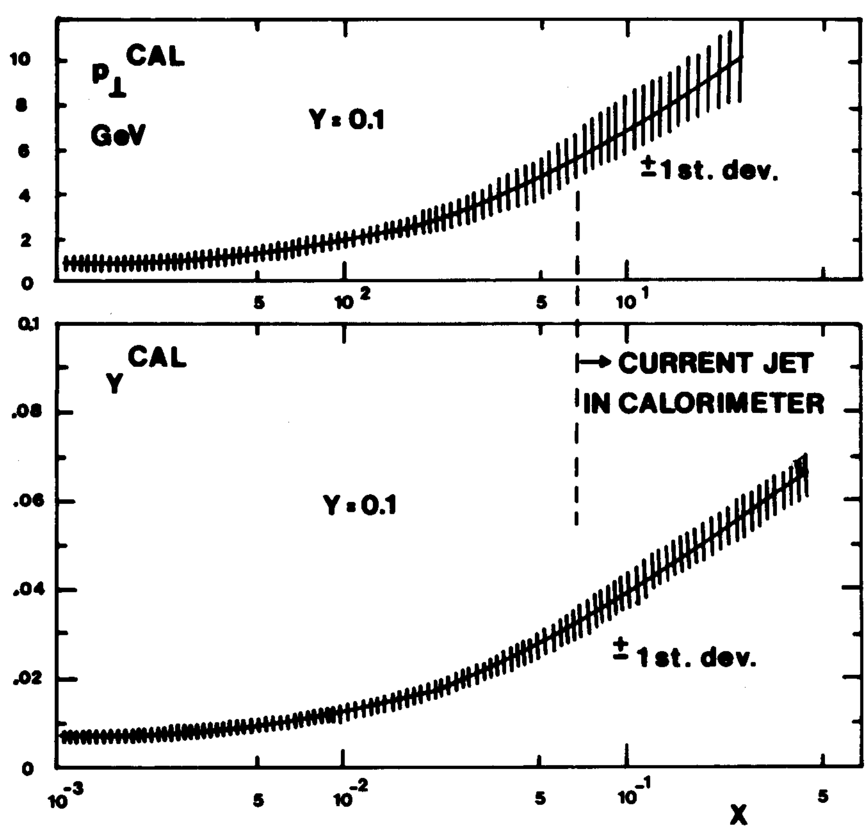

FIG. 14 - ERROR MEASUREMENT TO RECONSTRUCT

$P_\perp$ and Y WITH THE FORWARD DETECTOR ONLY.

IX - BACKWARD SPECTROMETER

We did not study in detail this backward spectrometer (electron direction). We have seen that for structure function analysis we should measure well particles down to 30 mrad, this can be done with the central detector. On the other hand this hole is important for the escaping electrons of neutral current events as these events will appear as charged current events. We have seen that for $x = 0.01$, $y = 0.1$, the angle of the electron is 14°. A 30 mrad hole ($\simeq 2°$) is in this way very conservative, but for triggering purpose this hole can be a problem. So this backward detector should identify the small angle electrons. In this respect our backward detector will be very similar to the one used for the neutral current study, and thus we have left its study to that working group.

X - EXPERIMENTAL ERRORS FOR X, Y SCALING VARIABLES

With an idea of possible detectors one can calculate the expected errors in the measurement of the scaling variables x and y, in particular using the second method described earlier in this report (ref. section VI).

We have calculated these errors with the following resolutions and under the following conditions :

	No field Uranium cal.	Low field Uranium cal.	High field Iron cal.
Charged part. ΔP $\Delta \Phi$	$0.3\sqrt{E}$ GeV/c $2 + 3/P$ mrad	$0.3\sqrt{E}$ or $0.05\ P^2$ $2 + 3/P$	$0.6\sqrt{E}$ or $0.005\ P^2$ $2 + 3/P$
Neutral hadrons ΔP $\Delta \Phi$	$0.3\sqrt{E}$ GeV/c 30 mrad	$0.3\sqrt{E}$ 30 mrad	$0.6\sqrt{E}$ 30 mrad
π^0 ΔP $\Delta \Phi$	$0.15\sqrt{E}$ 15 mrad	$0.15\sqrt{E}$ 15 mrad	$0.15\sqrt{E}$ 15 mrad

The results are presented in Figures 15 and 16.

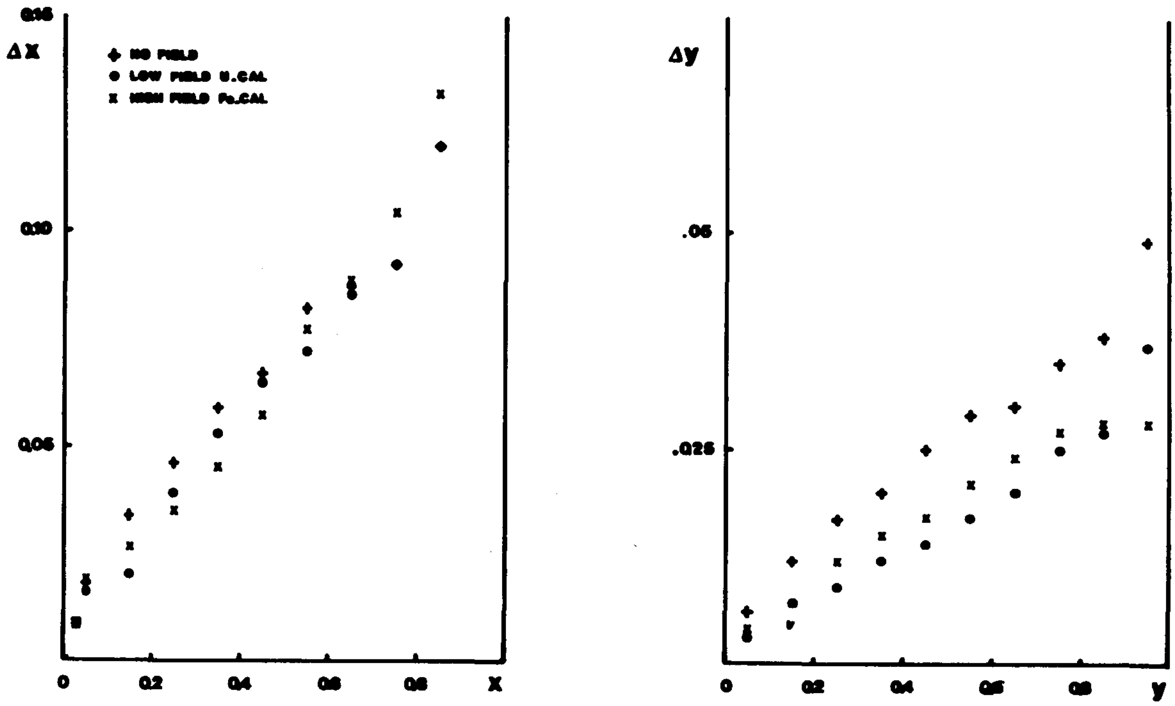

FIG. 15 – MEASUREMENT ERRORS ΔX AND ΔY

FOR THREE POSSIBLE DETECTORS.

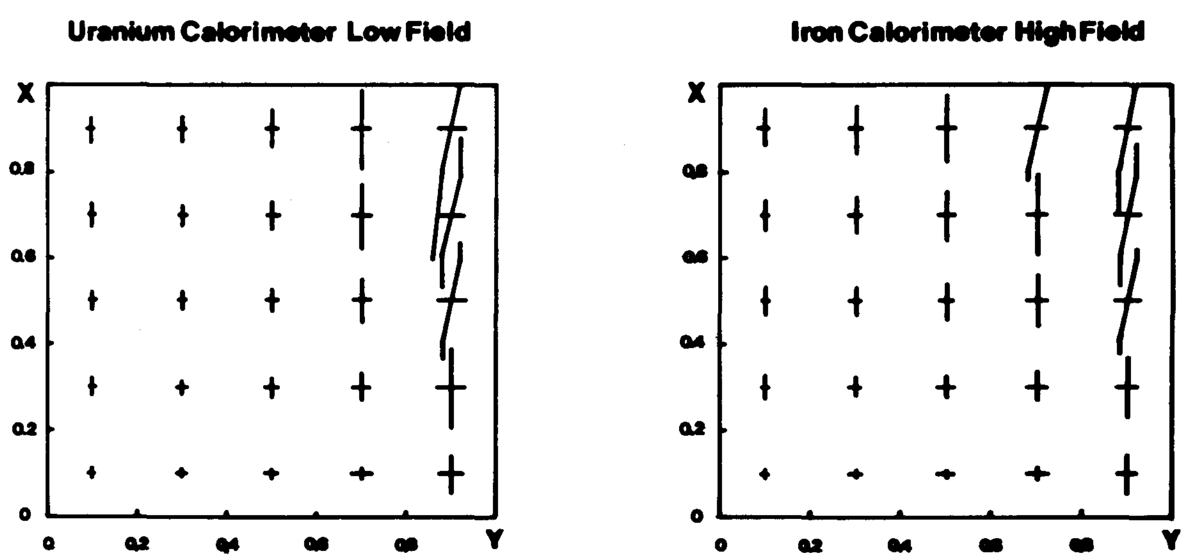

FIG. 16 – MEASUREMENT ERRORS ΔX AND ΔY PRESENTED

OVER THE X–Y PLANE FOR DETECTOR (1) AND (2).

One can see that there is little difference in the performance of the two detectors. We can understand this if we consider the respective contribution to the errors from the momentum and angle measurements as shown in Figure 17 : the largest contribution to the error is coming from the errors on momentum. One thus concludes that the detector should be optimized to obtain the best possible momentum measurement.

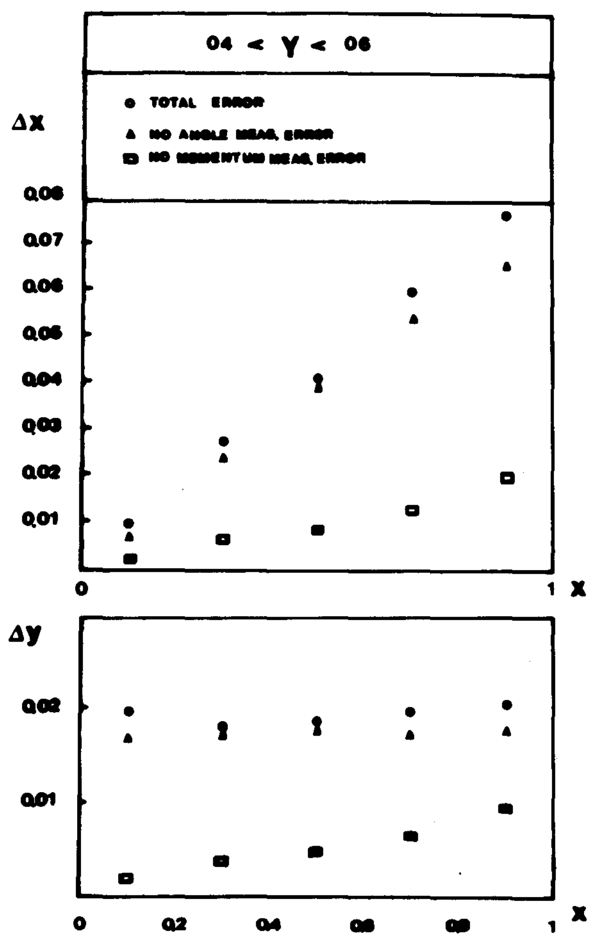

FIG. 17 - SEPARATED CONTRIBUTION ON ΔX AND ΔY OF ANGLE AND MOMENTUM MEASUREMENT.

XI - MUON DETECTION

Muon detection is not specific to the problem of charged currents but we have considered two specific research interests : new heavy lepton and new quark production which might be detected through final state muons. Technically the best way to identify the muon is to use the iron of the return yoke and detect the muon by a minimum ionisation in the calorimeter and a hit in large planar drift chambers outside the return yoke. This type of detector is "classical" and used in almost all the experimental set-ups at present storage ring machines. One has to face two problems in such a scheme :

- Punch through of secondary particles from hadron shower. At 30 GeV one expects still one particle after 1 meter of iron. One can decrease this effect if the track is extrapolated from the central detector. Such a method will decrease the punch through probability to 10^{-6}, if one has a angular resolution for track finding of 5 to 10 mrad.
- The π, K decay. Considering the density of the central detector this is unavoidable ; the averaged one meter of decay possible in the central detector gives a probability of the order of 10^{-3} for π, K decay.

One can use the muon detector to examine two physics questions :

A) NEW HEAVY LEPTON PRODUCTION.

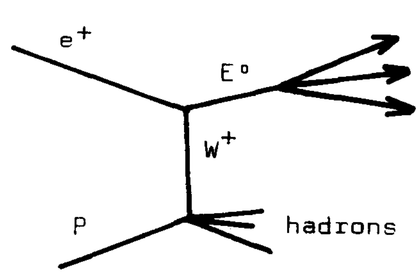

The E° can decay as follows :

$E^\circ - e^- \mu^+ \nu_\mu$

$E^\circ - \nu_e \mu^+ \mu^-$

$E^\circ - E^- \mu^+ \nu_\mu$

The rate as calculated in the CHEEP Report could be 10 a day. The nice thing is that the signature of such events is clean : the E° is produced as we have seen in the opposite direction to the current jet. It means that the "μ" of the decay will be not inside the "hadron jet" cone and so the π, K decay is no longer a problem.

B) NEW QUARK SEARCH.

If one assumes the series of quarks continues

$$\begin{matrix} u & c & t & G & \dots \\ d & s & b & H & \dots \end{matrix}$$

with a W_{max} avaible of 160 GeV , a good way to look for new quark production is via the charged current since we produce one single new flavor thus gaining an advantage in kinematics over processes which require quark-antiquark pair production. On the other hand we loose because of the weak coupling (compared for example to the electromagnetic one for neutral current) and the mixing angle will surely be small. Nevertheless to illustrate the possibilities let's consider the "H" (the lighter) quark of a new set $\binom{G}{H}$, coupled to the present quarks, it might be produced as follows :

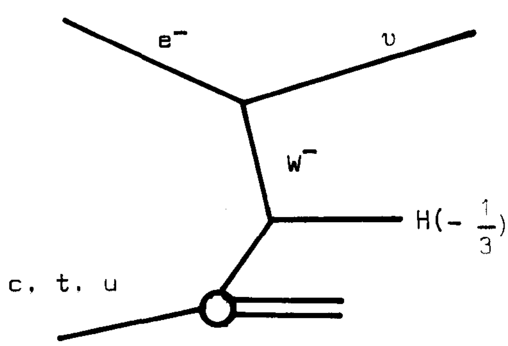

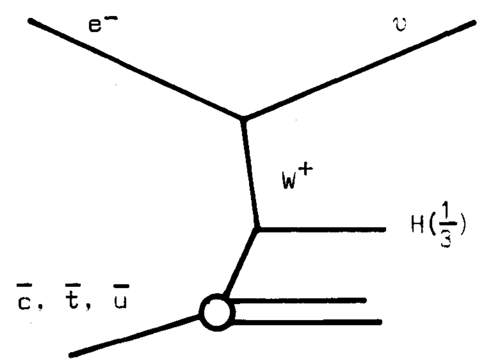

Two features of such a new quark with very large mass will appear :

1. Jet of fragments will have a largely displaced angle (Figure 18). If we measure x, and y for large mass quark then the θ_j will be pushed forward. The scale of this effect is $\dfrac{M_q{}^2}{4\, E_e\, E_p\, y}$ and is very large for masses of 50 GeV.
2. In a semi-leptonic decay of such quark one can expect to see large $P_\perp$ muons : If we assume it is coupled to the top quark for example :

$$\underset{50\ \text{GeV}}{H\left(-\tfrac{1}{3}\right)} \;—\; \underset{15\ \text{GeV}}{T^{+}\left(\tfrac{2}{3}\right)} + \mu^- + \upsilon$$

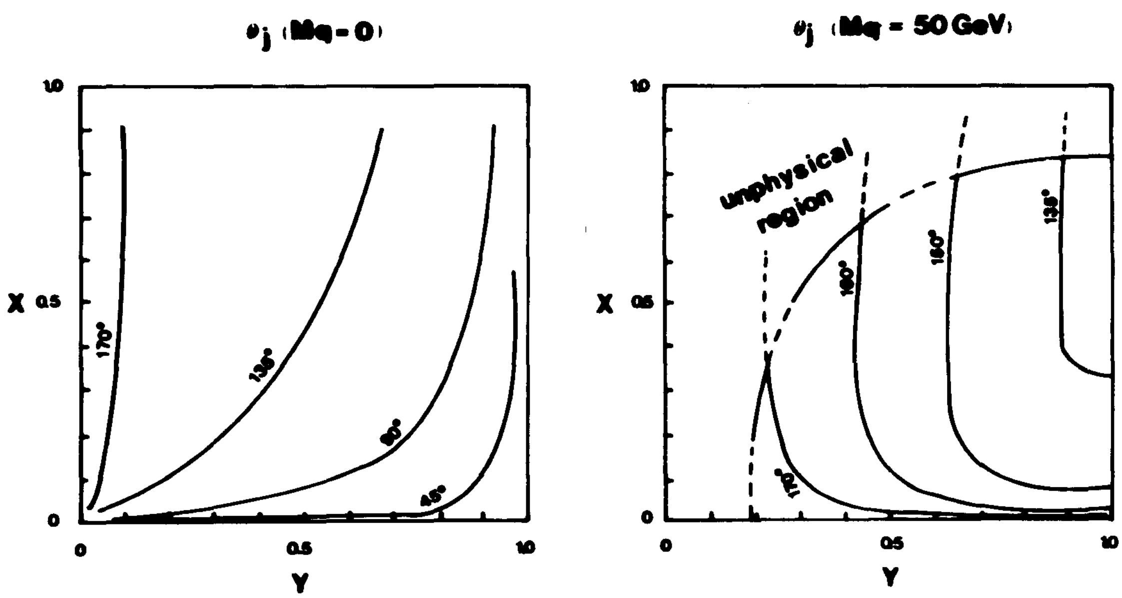

FIG. 18 – Jet angle for a 50 GeV quark production.

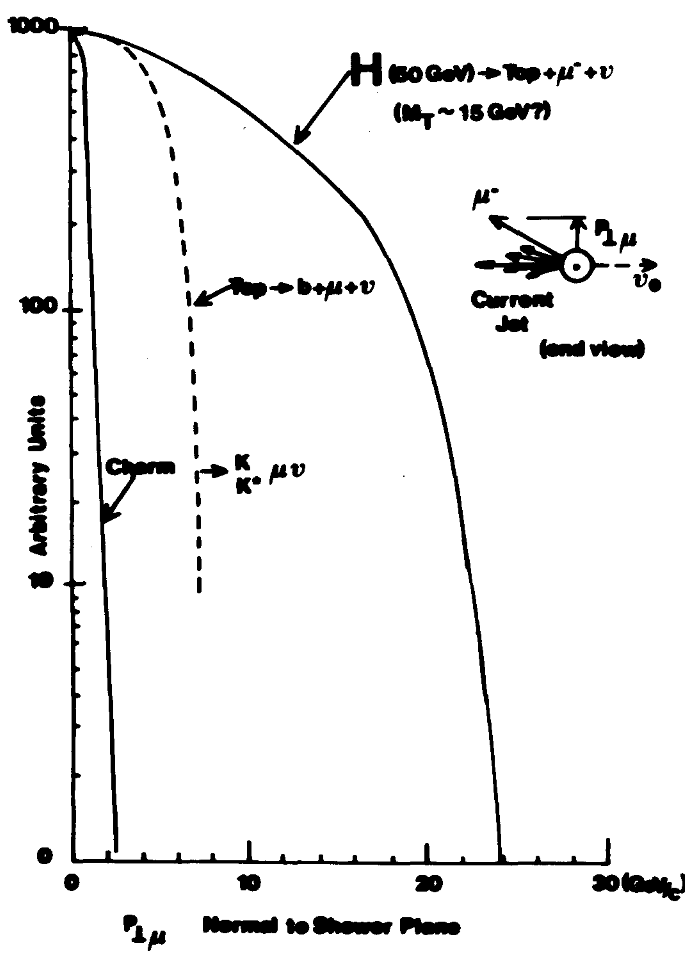

The $P_\perp$ normal to the jet – ν_e plane is <7 GeV> . Figure 19 shows what is expected from charm and top decays for comparison. The muon $P_\perp$'s are quite large. Further more this $P_\perp$ distribution can be compared to the $P_\perp$ distribution for μ from e^+ and e^- running since electromagnetic μ's at large $P_\perp$ will be similar for $e^\pm$.

FIG. 19 – $P_\perp$ of muon decay of H quark.

XII - CONCLUSION

We have clearly demonstrated that the study of structure functions is possible. Detectors for such study can be built using present technology and a fortiori with any improvements that we can hope for in the next years.

In the frame of this working group, or at the level of a proposal, the study of the details of the final hadronic state should be pursued and developed.

This Report is the result of the work of all the members of this working group. Every one has contributed and the ensueing long and open discussions have improved the consistancy of our work. I would like to thank very much particularly J. RANDER who has helped me in the preparation of this written report.

REFERENCES

1. A.J. BURAS and K.J.F. GAEMERS, – N.P., B132, 249 (1978).

2. J.G.M. de GROOT et al, – P.L. 82B (1979) 456.

3. J. KOGUT and L. SUSSKIND, – Phys. Rev. D9, 3501 (1974).

4. A.L. GRANT – Event generation for e–p collidor, note published in this proceedings.

5. H.F. HOFFMANN – Background problems, this proceedings.

Discussion after the talk of R. Turlay

S. Ting:
I have no doubt that one can build such a detector, which is probably very good for high q^2 physics. But have you also thought, how well you can detect new phenomena, like neutral leptons, which would decay into a muon pair with a neutrino?

How well do you have to know the missing neutrino energy in order to identify these events?

R. Turlay:
I can't tell you. The only contribution is the one I mentioned. We did not study the details, how the detector might serve in this and other fields of physics.

U. Amaldi:
New phenomena might happen at very large q^2, like non-conservation of lepton number e.g. the conversion of an electron into a muon or a muonic object. These phenomena could be easily seen.

K. Tittel:
With a detector of this kind we can identify muons and electrons, and we have almost complete calorimetry. So I think it could be a very powerful tool in order to observe these kind of new events, which contain heavy leptons or heavy muons.

H. Wahl:
There is a large background from neutral events with an undetected electron or an electron in the wrong direction. To what extent will you be misled in your conclusions on the charged current events?

R. Turlay:
This background is most severe at small q^2, and for those events the electron goes into the backward direction in a small cone, where we cannot measure. This corresponds to a very small region in the x-y plane.

G. Kalmus:
I would like to point out that this detector is self calibrating. Indeed one detects both neutral current and charged current events. If you reconstruct x and y in neutral current events from the parameters of the hadrons alone you can compare it to x and y calculated from the electron momentum and angle. In this way you obtain a measure of the precision in x and y for the charged current events.

Discussion after the talk of H.F. Hoffmann

G. Kalmus:
You stated that you need a pressure of $5 \cdot 10^{-11}$ torr in order to get o.1 beam gas interactions per bunch. This pressure is considerably lower than the present pressure in PETRA which is $3 \cdot 10^{-9}$ torr.

H.F. Hoffmann:
Here we have a proton on one side and an electron on the other side. And I think in this case you can arrange yourself with good pumps.

G. Kalmus:
Do you believe, you can get a factor of 2oo on the two sides of the interaction region?

H.F. Hoffmann:
Yes, you can.

H. Hoffmann: Background Problems in ep Interaction Areas

Some possible sources of background are described. Numbers given are based on "PROPER" parameters and measurements performed at the SPS (CERN 78-o2, 27.Feb. 1978 "Cheep" report).

Proton beam

The transverse size of the proton beam will slowly increase because of multiple scattering on the residual gas, because of higher order resonances, beam-beam tune shift etc. Eventually the tails of the transverse distribution will drift against the inner most limiting aperture which will probably be near the low- beta quadrupoles. Protons scattered there will create a high energy shower of 1o to 2o particles of which 1 will be a muon. If somewhat arbitraryly the acceptable rate is set to one such event per 1o proton bunches passing and if we assume that all losses occur only near the interaction areas we get a rate of 1oo KHz per area or a loss rate of 1o ppm/min. At the ISR the decay rate is near 1 ppm/min but there are no very high intensity bunches and operation is far from the tune shift limit. Therefore scraper targets or/and collimator systems will be required if possible far away from the interaction areas (and the superconducting magnets !!). The pressure permitted near (+- 5o m) the interaction area for the above requirements is a maximum of 5 x 1o**-11 Torr for a bunch of 8 x 1o**11 protons.

Electron beam

For colliding the electron and the proton beam and for adjusting the polarization vector of the electron longitudinally vertical bending magnets of considerable strength are required near the interaction area giving rise to intense synchrotron radiation in the bending plane. This may result in a vacuum chamber of a funny shape which lets the synchrotron radiation fan coming from the last bending magnet pass freely. The synchrotron radiation may also produce a bad vacuum near the crossing point.

Electrons loose energy through beam gas bremsstrahlung. The production rate at 3 x 1oo**-9 Torr CO-pressure and 125 mA current is about 5o KHz/m for an energy loss exceeding 5 %. Taking a length of up to 3o m upstream of the interaction area from where such degraded electrons might be bent into the interaction area by quadrupoles and bending magnets, then again 1 - 2 electrons appear per 1o bunches passing in the forward detectors (electrons beam), if the pressure given above is obtained.

Conclusion

Background problems are severe in an ep machine and require a careful study beginning at an early design stage. Very good vacuum is required in both the electron and proton ring near the interaction area.

Discussion leader's report (K. Tittel)

Let me start with some remarks on the organization of the work of the study group for a charged current (CC) detector at an ep-machine. All the names have been given already in the heading of R. Turlay's report. We started our task with a meeting in January 79 where in several short reviews the ideas developed already earlier and published in the CHEEP-report were reviewed. The main point then was to define a list of items to be worked on and to attach names to it. Local clusters of interested people have been formed and this turned out to be very effective in getting coherent work done. Two more meetings then were needed to clear up open questions and to deliver the necessary information to the speaker who still had to carry the heaviest load of all of us.

Right from the beginning we have restricted ourselves to the study of the possibilities of a machine with lower energy like PROPER. The CHEEP-solution (1oo + 4oo GeV) was not considered, partly because of lack of time. We felt that in particular the structure function physics could well be performed at the lower energy and it is more important to have the machine early rather than big or if you express it in german: *Lieber den Spatz in der Hand als die Taube auf dem Dach.* Besides that,polarization is of great importance and a PROPER-type machine will have better chances in this respect.

I may state now the main outcome of our studies: The investigation of CC is an interesting and important task, the kinematics of this process can be solved and finally a reasonable detector can be built. The study of structure functions in neutral current (NC) events is complicated by the presence of both weak and electromagnetic effects. The CC offer a simpler access to the structure functions even if the experimental technique is slightly more difficult. CC furthermore see flavour dependent effects, whereas NC are flavour blind. To separate the different structure functions one needs to run at different energies. Reasonably fine steps in energy should therefore be possible at the ep-machine. An alternative way presents the use of deuteron-beams instead of protons. Although lower by a factur of four in luminosity this option should be provided in any case.

The extraction of the kinematical variables is complicated by the fact, that the lepton in the final state is a neutrino, and cannot be measured. It has been found, however, that we get these variables from the hadrons alone with sufficient precision, even if the largest part of the proton jet disappears in the beam pipe. This was the crucial point to be well understood.

To design an appropriate detector seems not to be particularly difficult. However,we came soon to the conclusion that a purely nonmagnetic device is not really adequate. An at least weak magnetic field should be added. It became clear as well that the separation of NC and CC detectors is rather unnatural. The techniques are quite the same and it is almost unavoidable to measure both processes in the same detector.

There are of course still some problems left open. Apart from the problems connected with the use of a machine of higher energy I like to mention two more. The background problem has not been treated in much detail. Here we may encounter still some suprises. The other problem, where only superficial ideas have been presented is the proton fragment detector. It might be interesting to study the proton fragments in detail, but unfortunately almost all of them disappear down the beam pipe. For both cases, only a close collaboration with the machine builders may provide a reasonable solution. In any case physicists and machine builders should collaborate at all stages of the machine design and construction.

Let me conclude with the remark that during our work we have gained the conviction, that the ep-machine is an interesting project, where important and good physics can be done. This machine is complementary to LEP and ISABELLE and has its own domain of interest. This machine should be built. Moreover, it should be built in the near future.

SESSION ON DETECTORS FOR NEUTRAL CURRENT EVENTS

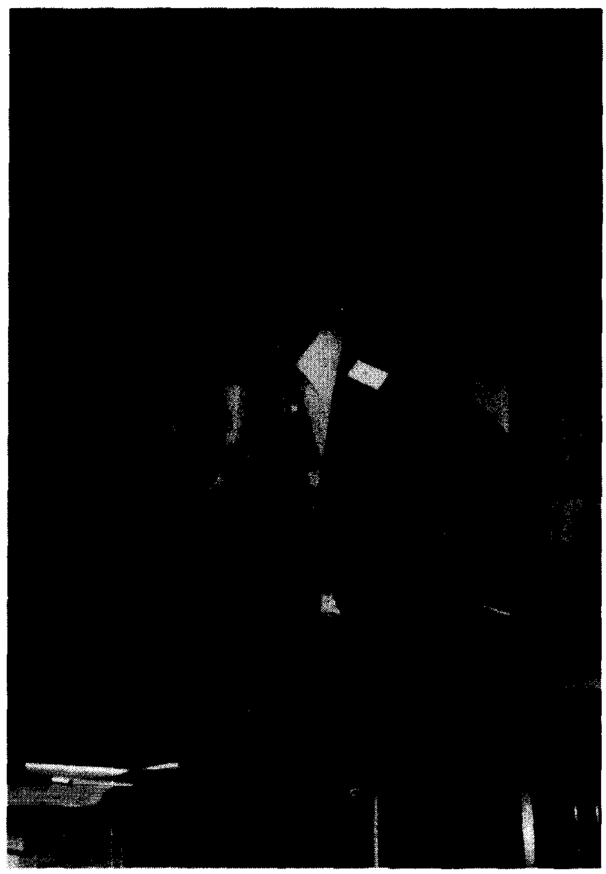

Discussion Leader: M. Holder

Scientific Secretary: H. Schröder

DETECTION OF NEUTRAL CURRENT EVENTS

by

P.G. Innocenti, CERN

May 1979

1. INTRODUCTION

The topics investigated in the course of the study can be broadly divided into three classes:

i) Inclusive measurements of the scattered electron for the determination of structure functions, scaling violations, σ_L/σ_T and weak interaction effects.

ii) Exclusive measurements of the current jet (momentum, energy, particle composition) for the study of fragmentation functions, for search of new particles, new quarks and QCD effects in the jet.

iii) Search for heavy leptons by detection and identification of their decay products.

Most of the calculations have assumed an electron of 20 (25) GeV colliding with a proton of 280 (270) GeV. Specific topics have received attention also in the higher energy range of 100 GeV electrons colliding with 400 GeV protons.

PGI/tj

2. INCLUSIVE MEASUREMENTS OF THE SCATTERED ELECTRON

2.1 Structure function determination under the assumption of scaling.

The determination of structure functions under the assumption of scaling is limited by event rate and the precision of the measurements of the scattered electron, both on angle and energy.

With the notation of reference 1, the double differential cross section for one photon exchange processes is written as:

$$\frac{d\sigma}{dxdy} = \frac{4M\alpha^2}{sx^2y^2}\left\{(1-y)\ F_2(x,Q^2) + y^2xF_1(x,Q^2)\right\} \qquad (2.1)$$

Assuming scaling and the Callan- Gross relation to hold:

$$\frac{d\sigma}{dxdy} = \frac{4M\alpha^2}{sx^2y^2}\ F_2(x)\left\{(1-y) + \frac{y^2}{2}\right\} \qquad (2.2)$$

x and y are determined as functions of the electron scattering angle and energy.

The expected rate is given in fig.1 (taken from reference 2) as a function of x, y and Q^2. (The factors in parenthesis are relevant to the discussion of sec. 2.2.)

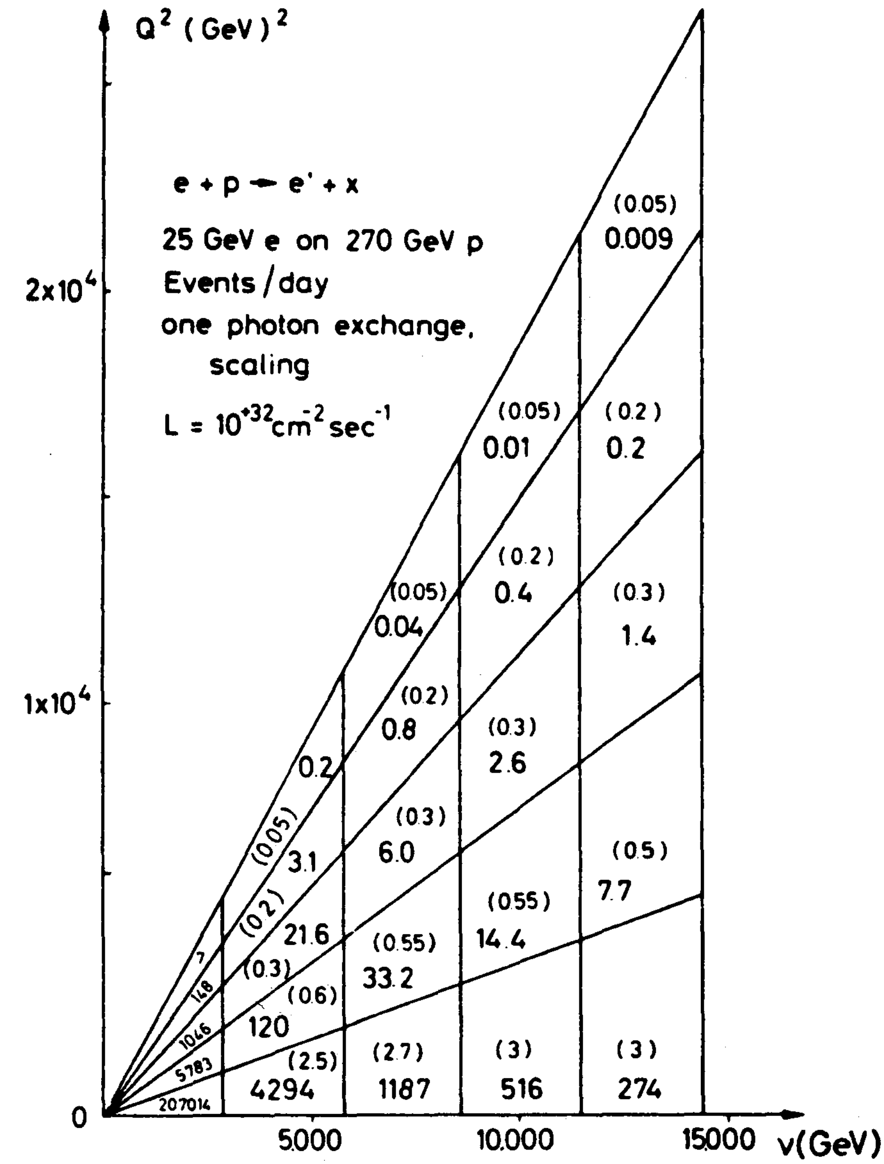

FIG.1

The influence of electron scattering angle and energy measurement error separately on x and y is given in figs 2 to 4, under the assumption that angle θ and energy E are measured to a precision of $\sigma_\theta = 10$ mrad, and $\sigma_E = 0.1\sqrt{E}$ (E in GeV), which seems achievable with current techniques.

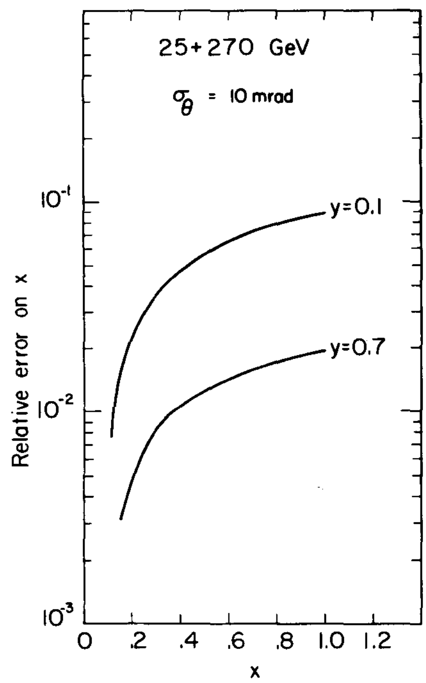

FIG.2

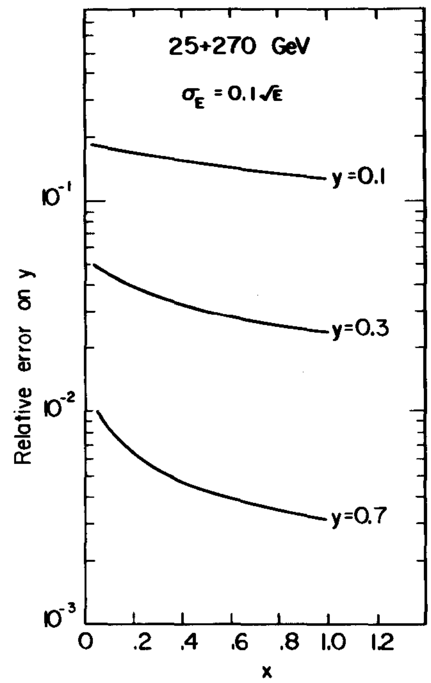

FIG.3

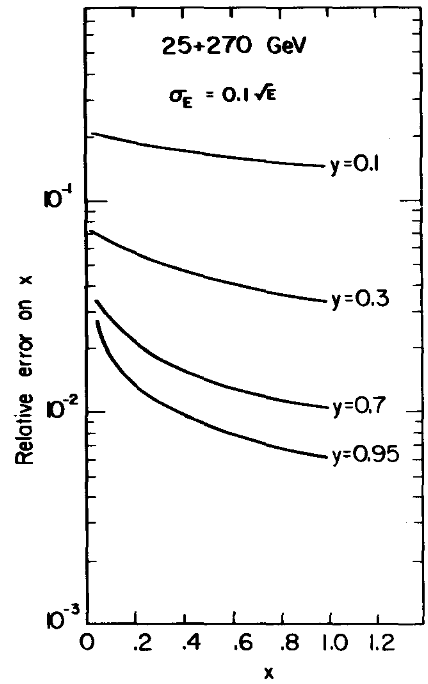

FIG.4

The relative error on x and y becomes larger than 10^{-1} at low y, except for $\sigma_{y/y}$ due to σ_θ (not shown) which is always below 10^{-2}.

The angular and energy measurement errors separately influence the cross section as shown in fig. 5 and 6.

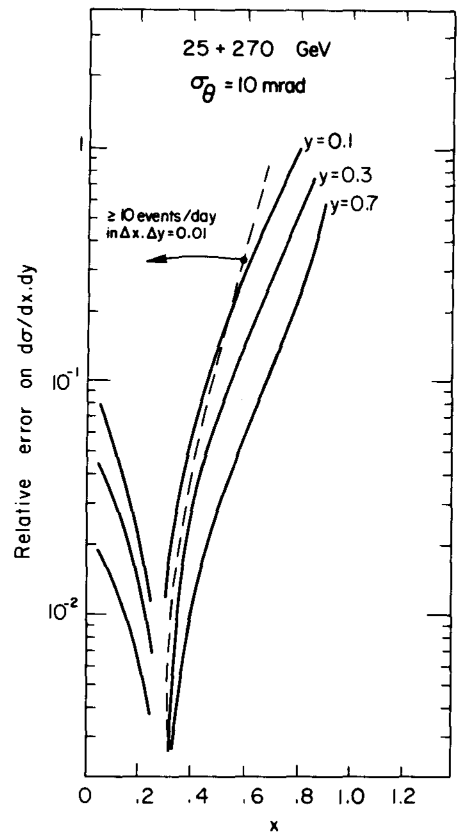

FIG.5

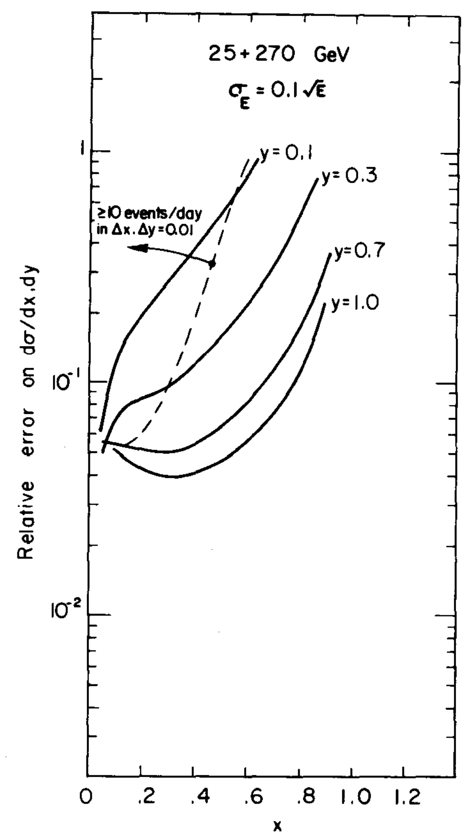

FIG.6

A line connecting (x,y) pairs corresponding to 10 events/day in $\Delta x \Delta y = 0.01$ at a luminosity of $L = 10^{32}\ cm^{-2}\ s^{-1}$ is also shown on fig. 5 and 6.

It can be concluded that the angular error on the scattered electron permits adequate measurements of the cross section in all the range accessible with adequate rate. The error on the energy of the scattered electron is sizable and prevents adequate measurements for large x, small y.

At higher energy (100 + 400 GeV) the relative errors on x and y become smaller, hence cross section measurements become more favourable, subject, however, to rate limitations.

2.2 Measurements of scaling violation effects.

The effects of scaling violation, under the assumption of an asymptotically free theory, are shown in fig.1 as a multiplicative factor to the rate (in parenthesis). Rates are enhanced up to a factor 3 for $x < 0.2$ and depressed elsewhere. This has the effect of moving the 10 events/day line of fig.5 and 6 to the left and further reduce the access to high x. Precision remains adequate in the regions where the rate is acceptable.

2.3 Neutral weak current effects.

From fig.18 to 21 of ref.1 and fig. I.22 to I.28 of ref.2 it appears that neutral weak current effects modify the one photon cross section by factors up to ~ 1.5 for $x = 0.25 \quad y = 0.5$. It seems therefore possible to single out a region where the resolution is sufficient to detect neutral weak current effects with manageable counting rate, provided beam polarization is not far from unity and both electrons and positrons can be collided with protons.

2.4 Measurement of σ_L/σ_T

Define

$$A = 2xF_1(x,Q^2)/F_2(x,Q^2) \tag{2.3}$$

related to R by

$$R = \frac{\sigma_L}{\sigma_T} = \frac{1}{A} \left(4 \frac{M_p^2 x^2}{Q^2} + 1\right) - 1 \tag{2.4}$$

The differential cross section can be rewritten in terms of A:

$$\frac{d\sigma}{dxdy} = \frac{4\pi\alpha^2}{sx^2} F_2 \left(\frac{1-y}{y^2} + \frac{A}{2}\right) \tag{2.5}$$

A measurement of R (or A) as a function of x and Q^2 probes the nature of partons in the nucleon. On the other hand, a value of A has to be assumed when extracting F_2 from cross section measurements.

By taking data at two different beam energies one can keep x and Q^2 fixed and measure the cross section for two different values of y: F_2 then drops out in the measurement of A.

The statistical accuracy on $\frac{dA}{A}$ for a measurement at beam energy

1. 17.5 + 280 GeV
2. 11.0 + 176 GeV

for an integrated luminosity of $5 \cdot 10^{37}$ cm^{-2} is given in fig.7, for various bin sizes in x and Q^2, y_2 referring to the low energy beam settings.

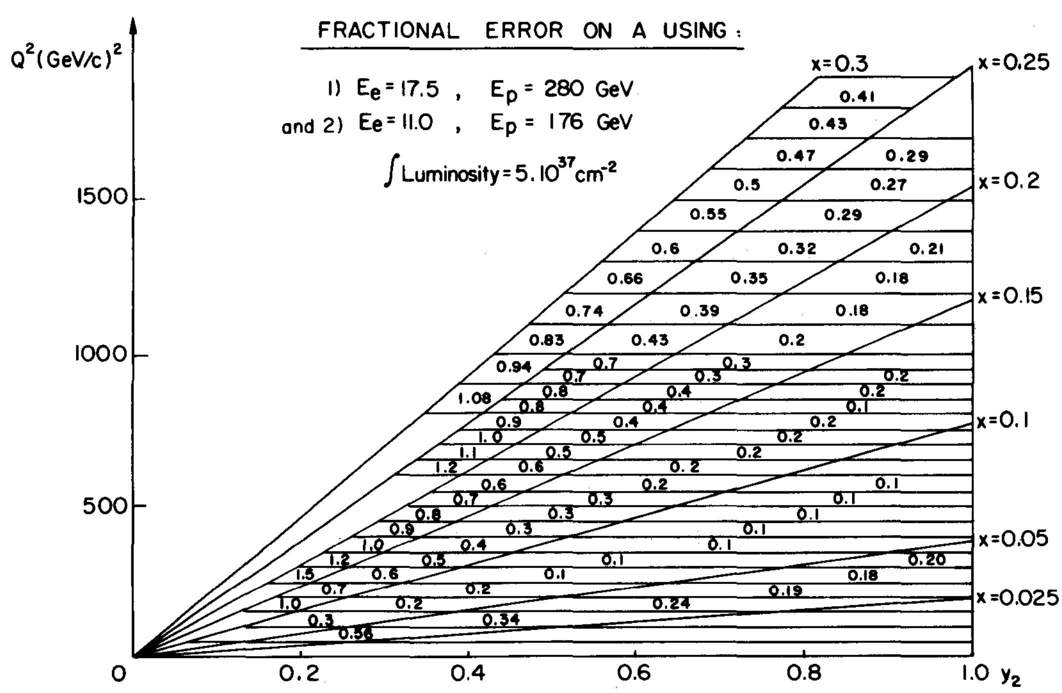

FIG.7

The measurements are most significant at high y_2 , but should be possible even for $y_2 < 0.5$; $Q^2 < 200$ $(GeV/c)^2$ on account of the high yields. A systematic error of ±5% on the cross section measurements at each energy destroys the significance of the measurements for $y_2 < 0.5$.

3. MEASUREMENT OF THE CURRENT JET

The study of the jet structure of the events and its implications on detector design requires a model giving distribution of all particles in momentum and angle, as well as their identity.

3.1 Jet models.

Two models of one photon exchange events have been used for detector design studies:

i) A model in which the current acts on the whole proton. Fragmentation follows QCD ideas, with input from ν-p data.

ii) A model assuming spin ½ partons and a gluon cloud sharing the proton momentum. Fragmentation as in i).

In both cases e^-, p or n and pions are found in the final state. All event generation has been done at 20 + 280 GeV. Both generations have been used for studying detector performance, hence providing a cross check of the results.

Three situations have been retained as showing typical event features:

i) High Q^2 events with $Q^2 \geqslant 3000$ $(GeV/c)^2$ $x \geqslant 0.2$, $y \geqslant 0.2$. An event with two jet structures is given in fig.8.

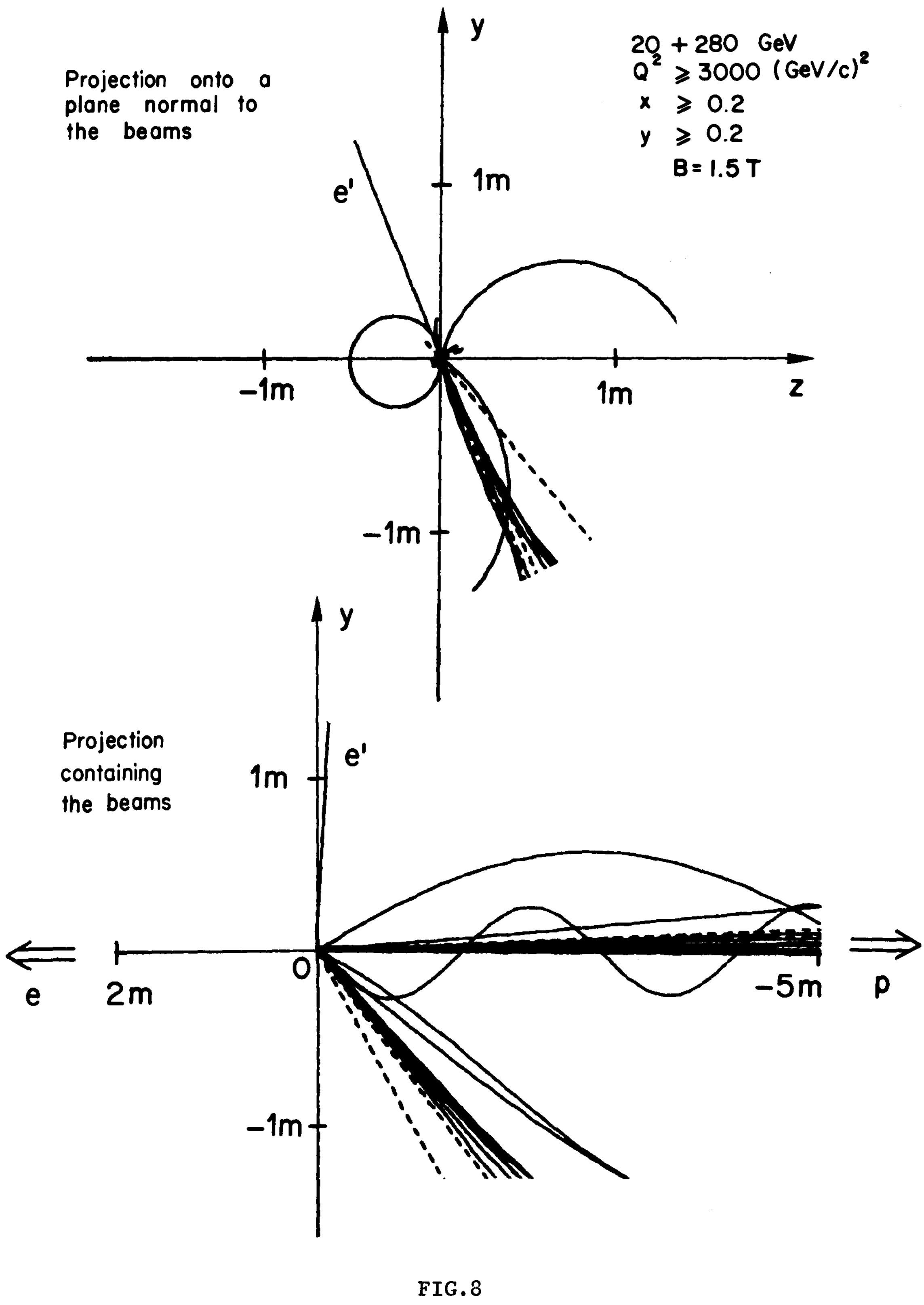

y
Projection onto a plane normal to the beams
20 + 280 GeV
Q² ≥ 3000 (GeV/c)²
x ≥ 0.2
y ≥ 0.2
B = 1.5 T
e'
1m
-1m
1m
z
-1m
y
Projection containing the beams
e'
1m
e
2m
O
-5m
p
-1m

FIG.8

Fig.9 shows a scatter plot of polar angle vs. momentum for all charged particles. The two peak structures of the hadrons is clearly visible, with the current jet making a mean angle of 34° with respect to the proton. The electrons are well separated from the hadrons.

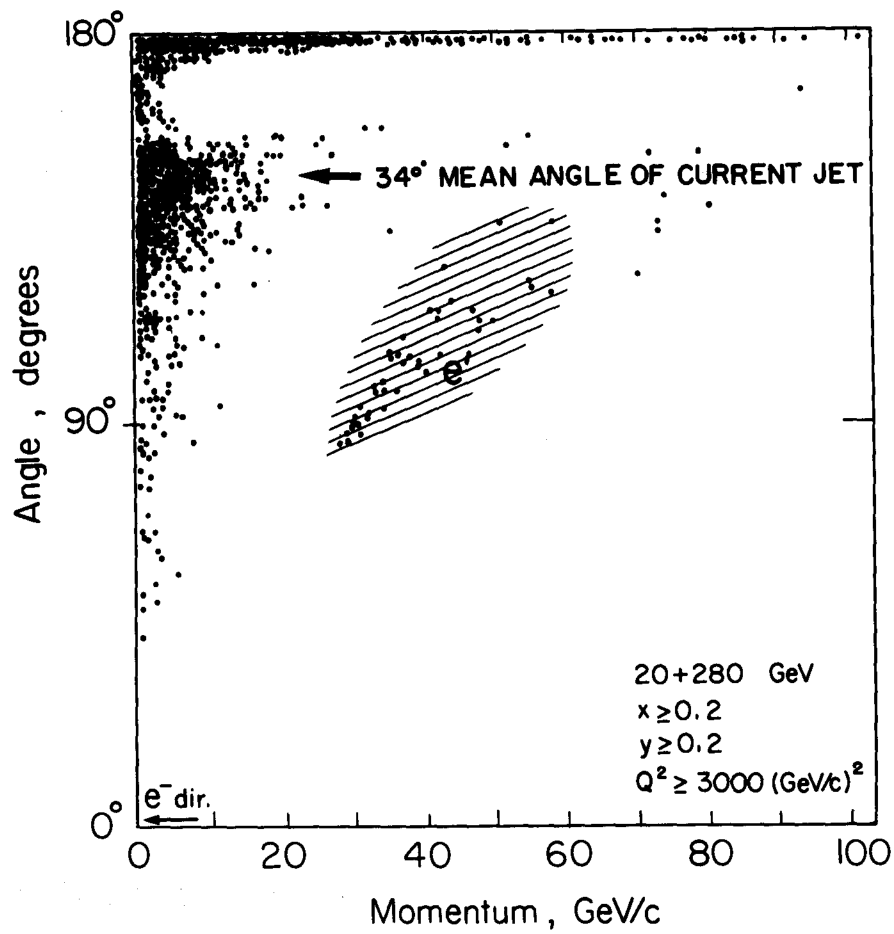

FIG.9

ii) Low Q^2 events with $Q^2 \geqslant 75\ (GeV/c)^2$ $x \geqslant 0.01$, $y \geqslant 0.01$. They represent the common events to be used for normalisation purpose. Fig.10 represents a scatter plot of angle vs. momentum for all charged particles. The two hadron jets are now merged together; the scattered electrons are well separated from the hadrons.

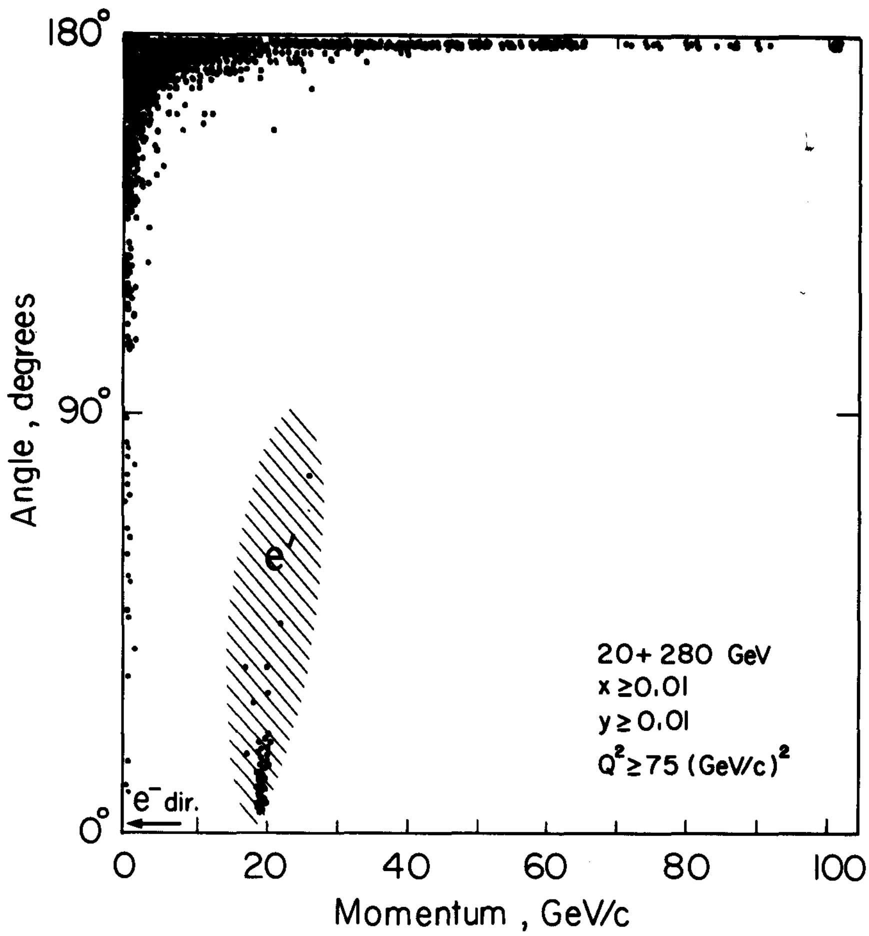

FIG.10

iii) High y events, with $x \geqslant 0.001$, $y \geqslant 0.5$. Fig. 11 shows a scatter plot of angle vs. momentum for all charged particles. A forward jet is accompanied by a uniform low momentum hadron population.

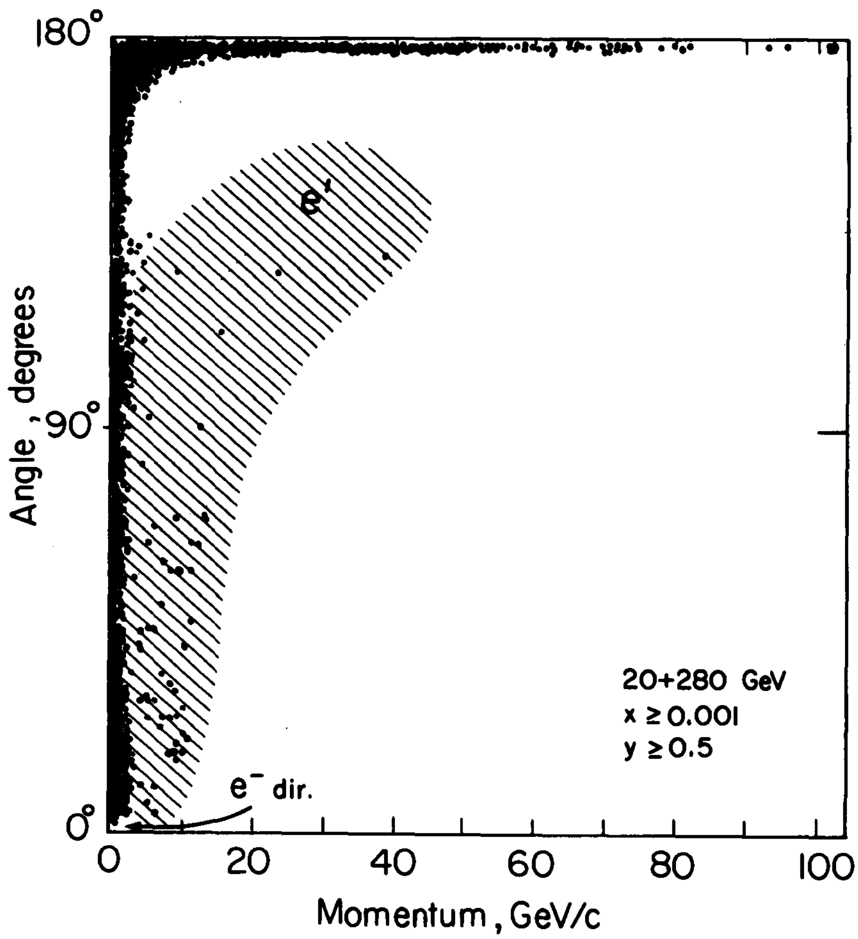

FIG.11

A qualitative conclusion can be drawn from fig.9 to 11. A detector designed to cover all situations outlined above must be capable of measuring the electron over a wide angular range. Moreover, it must measure charged and neutral hadrons in the central and forward (with the proton) regions. This stresses the need for a central detector good for high Q^2 jets and high y events and for a forward detector to limit the loss of particles from the current jet in high Q^2 events and to permit a smooth transition towards intermediate Q^2s.

4. SEARCH FOR HEAVY LEPTONS

The detection of heavy leptons E generated in the reaction $e+p \to E+X$ seams promising in the channels like

$$E^{\pm} \to e^{\pm} e^{+}e^{-}$$

or $$E^{\pm} \to e^{\pm} \mu^{+}\mu^{-}$$

On the other hand the most spectacular events (ref.1) could be 3-jet events originating from

$$e+p \to E + 2 \text{ jets}$$

$$\quad \llcorner\!\!\to e + \text{hadron jet.}$$

The requirements on the detector coming from the study of these channels are similar to those of sec. 2 and 3 as far as electron and hadron jets are concerned. An additional requirement comes from the detection of muons, in particular if charged and neutral heavy leptons are separated in mass and one decays frequently into the other, giving rise to final states with many electrons and muons.

5. DETECTOR LAYOUT

What is attempted in this section is to sketch the requirements of a general purpose detector covering the physics outlined in sec. 2 to 4. Much emphasis is put on the detection and measurement of the scattered electron over a very wide azimuthal region: This is obtained by use of a fine grained electromagnetic shower counter, which also measures photons. A charged particle detector in the form of a large gas volume operating as a drift chamber in a magnetic field is used for charged particle momentum measurement and identification by energy loss. The central detector is complemented by a forward spectrometer, in the proton direction. Hadron calorimetry is desirable for the study of jet structure and can be accomodated by segmenting the iron yoke of the central magnet. The hadron calorimeter can be used also for muon detection, by addition of iron and range chambers. Fig.12 represents a longitudinal cut through the detector in a vertical plane.

5.1 Choice of the magnet configuration

Central Magnet. The usual arguments in favour or against dipole, toroid or solenoid are presented.

In the presence of an electron beam the use of a dipole becomes problematic on account of synchrotron radiation if the beam is not shielded from the field. Power dissipation in the vacuum pipe becomes prohibitive for fields as low as 0.3 T (ref.3). Shielding by ferromagnetic or superconducting channels is possible at the cost of a very thick walled pipe.

The jet structure of the events, with rather open jets, is not matched with the subdivision of detector space imposed by the coils in a toroid, leading to a substantial particle loss. This becomes even more disturbing on account of the low counting rate at high Q^2.

What is left is a solenoid as a central detector magnet, despite its obvious weakness in forward analyzing power. On account of the relatively large dimensions required for momentum analyses and particle identification, the magnet should be superconductive.

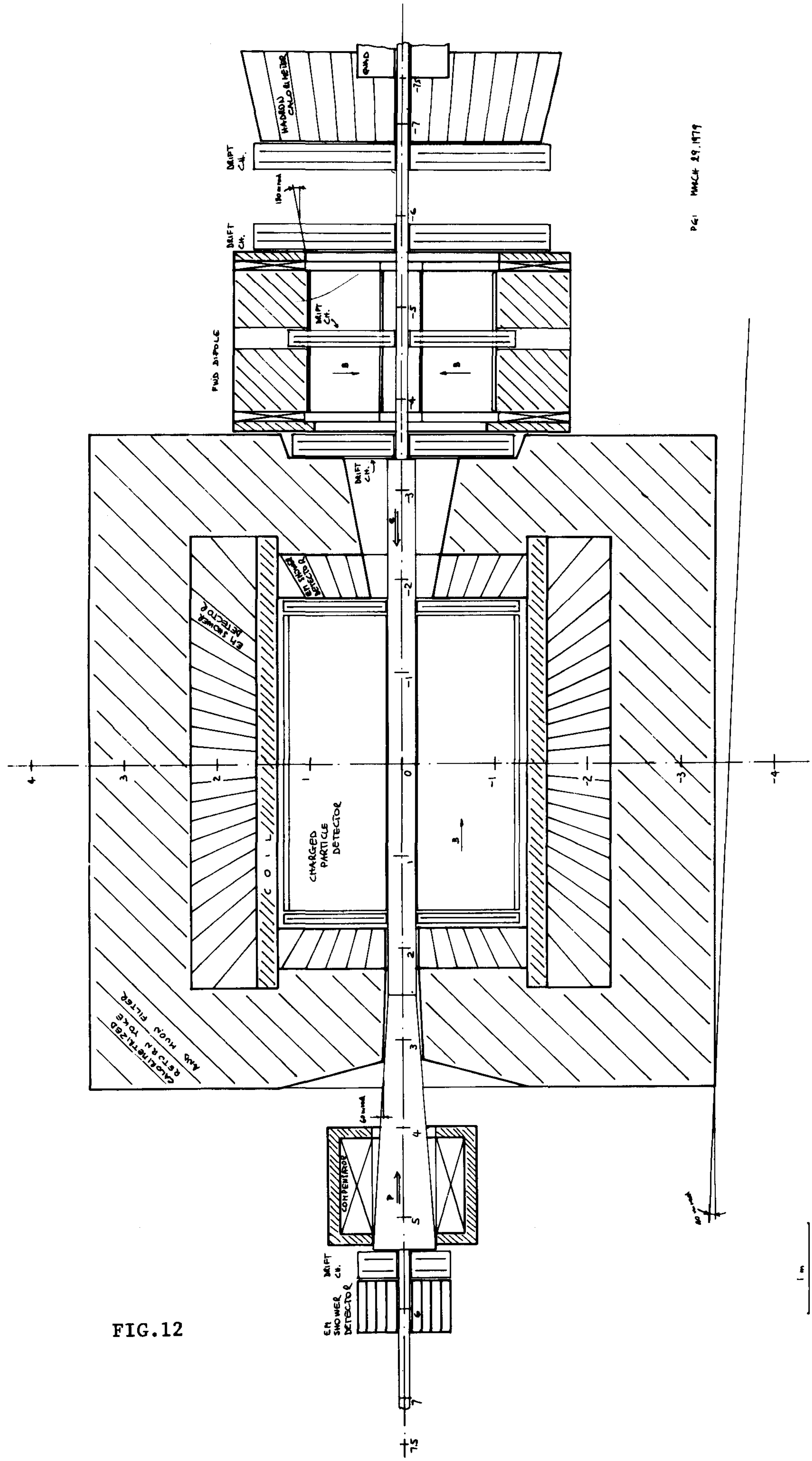
QUAD
HADRON CALORIMETER
DRIFT CH.
FWD DIPOLE
EM SHOWER DETECTOR
COIL
CHARGED PARTICLE DETECTOR
CALORIMETRIZED RETURN YOKE AND MUON FILTER
COMPENSATOR
E.M. SHOWER DETECTOR
PGI MARCH 29, 1979
1 m

FIG.12

Forward magnet. The proton and its fragments are energetic and highly collimated. Their magnetic analyses has to be attempted independently of the central solenoid, by a forward dipole. Because of synchrotron radiation the beam pipe has to be shielded with special care to limit acceptance losses at small angle.

A dipole with an iron septum is proposed. Given the large size, the magnetic field must not exceed 0.5 T on account of acceptance (size of shielding), power limitation and fringe field.

5.2 Electromagnetic shower detector.

In sec.2 the effects of angular and energy resolution on the electron measurement have been investigated. The accuracy assumed there (σ_θ = 10 mrad; $\sigma_E = 0.1\sqrt{E}$ with E in GeV) permits a proper determination of the cross section with the exception of the high x, low y region.

It is proposed to use lead liquid argon shower counters throughout. They consist of a cylindrical counter mounted outside the coil and two end-cap counters inside the field. The required energy resolution should be reached over the full angular coverage. However, special attention has to be given to the influence of the coil and cryostat, particularly away from normal incidence and at the junction of the cylinder with the end-caps. The coil thickness must be kept at half of a radiation length in order to ensure the required energy resolution for all angles (ref.4): This sets an upper limit to the magnetic field strength and superconducting coil diameter. It is felt that a field of 1.5 T with a coil I.D. of 2.6 m should be feasible.

The grain of the shower counter must be optimized with respect to:

a) simultaneous occupation of a cell by the scattered electron and a photon;

b) two photon separation in hadronic events;

c) simultaneous occupation of a cell by a pion and a photon, relevant to the search for events with many electrons.

The most unfavourable situation with respect to requirement a) arises in high Y events. Fig.13 shows the distance of the impact points, on the inner surface of the shower counter, of the scattered electron and any photon in the same event. Approximately 1% of the photons fall within 50 cm of the electron.

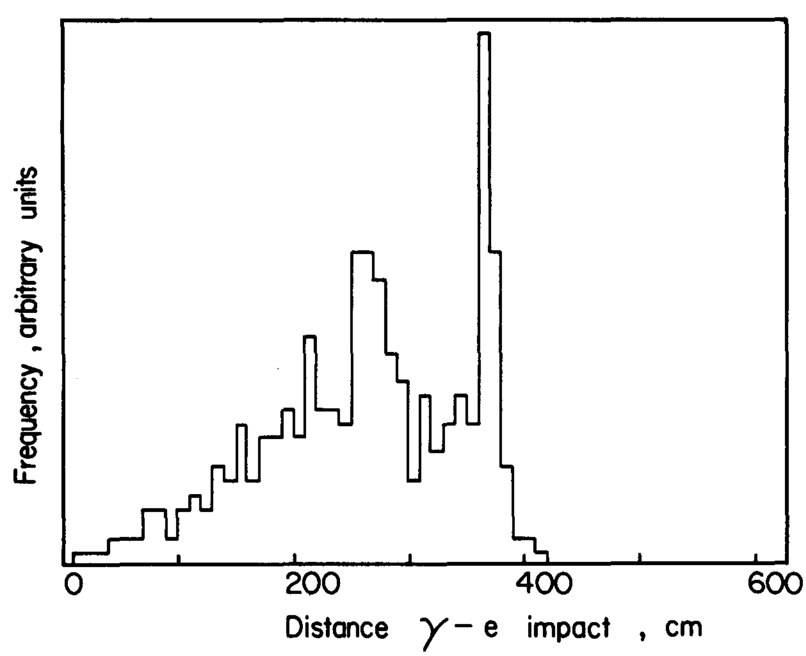

FIG.13

As far as requirement b) is concerned, the most stringent conditions are given by resolving two photons from the same π^0 in jets of high Q^2 events. Fig.14 shows the distribution of the distance between the two γ's from a π^0.

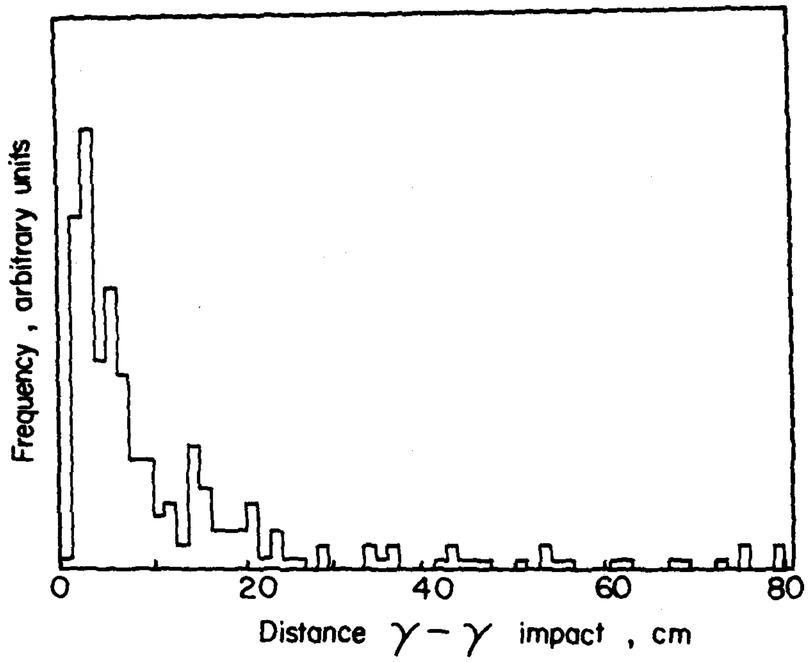

FIG.14

The mean value of the distribution is 18 cm. Alternatively, if one considers all photons in the current jet irrespective of the parent π^0, 20% of all photon pairs fall within 18 cm. On account of the lateral development of the shower, it is unlikely that complete separation of γ pairs can be achieved.

A pion and a photon, hitting the shower counter within a distance which does not permit to resolve them individually, simulate an electron, if the pion momentum and photon energy, measured independently, match within resolution. Fig.15 shows a scatter plot of photon energy E vs. pion momentum p for all combinations hitting the shower counter within 8 cm, in high Q^2 events.

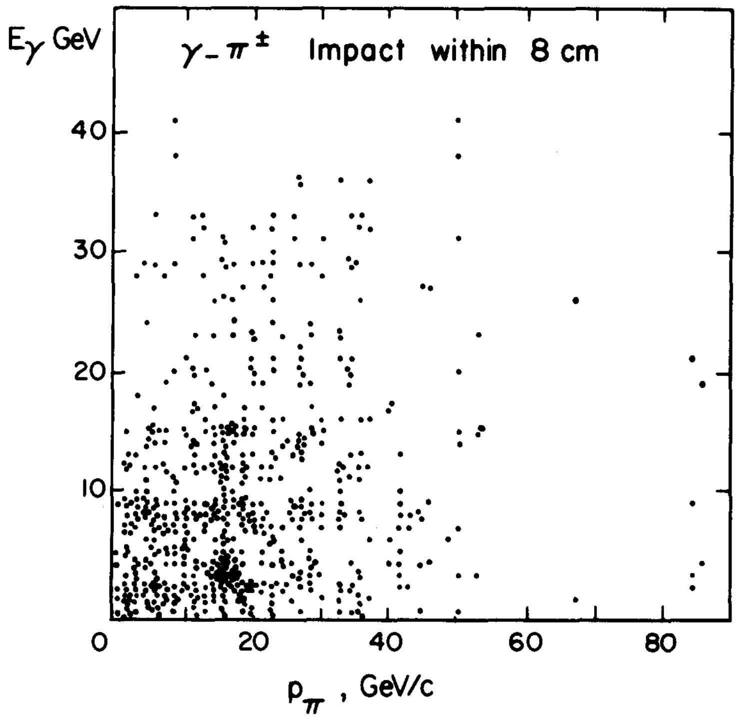

FIG.15

With the energy resolution of $\sigma_E = 0.1\sqrt{E}$ and the momentum resolution given in sec. 5.3 a rejection of better than 1% with 99% electron efficiency should be reached. Further rejection can be obtained by a study of the longitudinal and lateral shower development and by particle identification by energy loss in the gas of the central detector. A word of warning is appropriate, concerning the effect of the coil thickness, most detrimental to the measurement of low energy photons.

5.3 Central charged particle detector

The central charged particle detector must permit simultaneous momentum and energy loss measurements. The detector has not been designed in detail but it is clearly inspired by large cylindrical chambers like JADE (ref.6) or the TPC (ref.7) working in the drift mode and recording pulse height: Some additional features are necessary in the present case

- A chamber layer with high precision in the coordinate along the beams, immediately inside the coil, to improve the electron angle measurement.
- End-cap chambers on both sides, one for angular precision on the electron, the other one as lever arm chamber for forward hadrons.

The detector shown in fig.12 has an outer diameter of 2.6 m and a length of 3.6 m. We assume 1.5 T as the highest manageable field and a precision of 200 μm on each individual track measurement. On account of the jet structure, some fraction of the total track length will not be usable for momentum and dE/dx measurements. We define a "clean" track length as the fraction of the track separated from neighbours by at least 1 cm. A projection of the clean track length onto a plane perpendicular to the magnetic field, gives a quantity useful for estimating momentum resolution: The clean projected track length is shown in fig.16 for high Q^2 events, in a scatter plot vs. momentum.

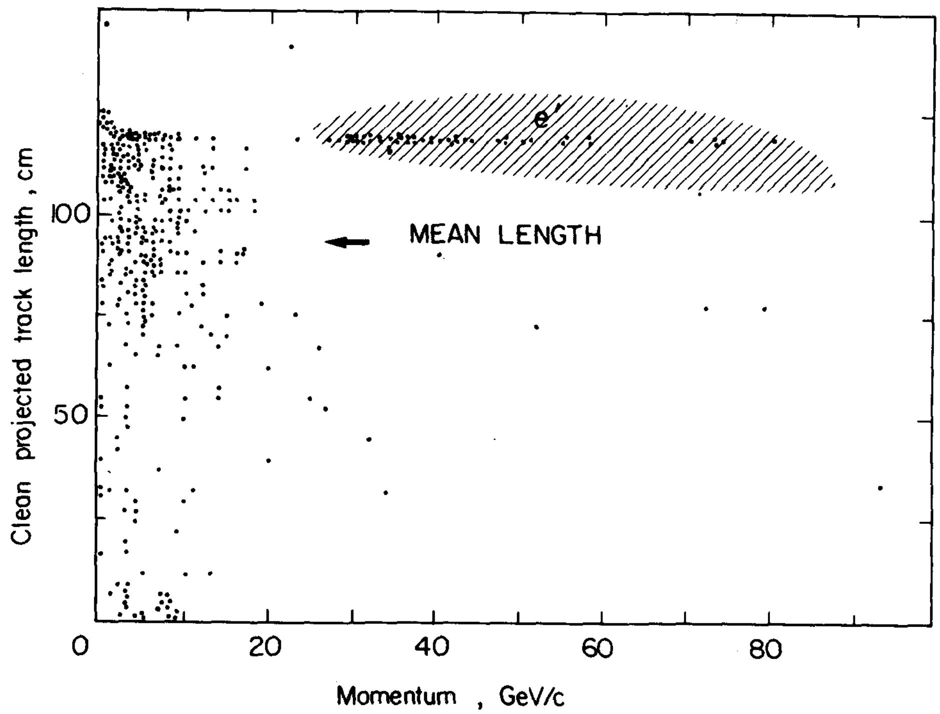

FIG.16

The average clean projected track length with measurements every centimetre has been used to compute the momentum resolution vs. angle to the proton shown in fig.17.

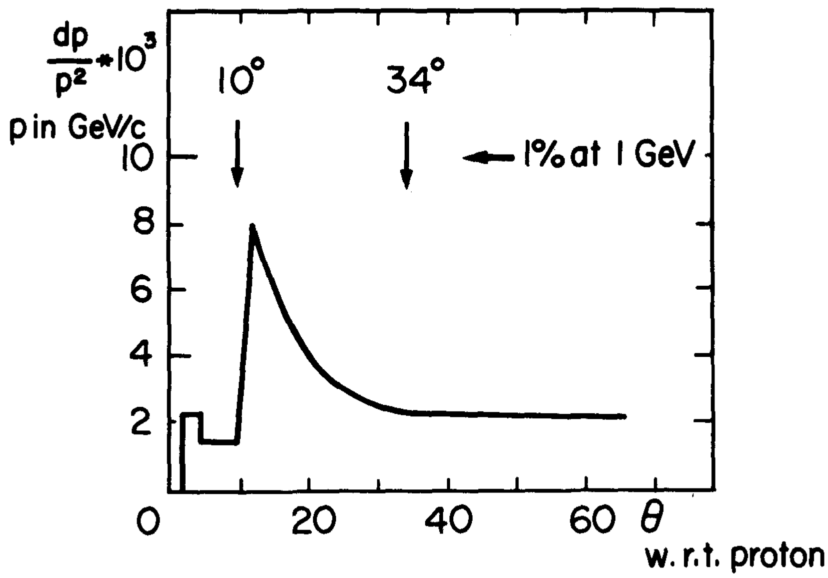

FIG.17

The clean track length has been used to estimate the performance of the energy loss measurement. Sampling is assumed on each centimetre of clean projected track length. A scatter plot of clean track length vs. number of samples is shown in fig.18 for high Q^2 events.

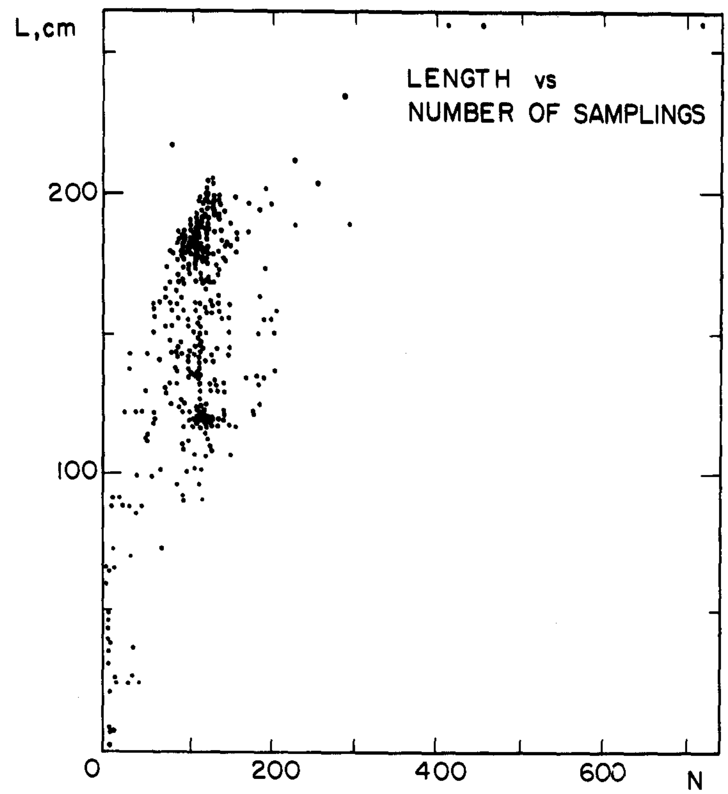

FIG.18

The average number of samples is $\gtrsim$ 100 for 90% of the tracks. If we assume a pressure of 4 atm, the (length)·(pressure) exceeds 4 m of gas at NTP. A resolution on dE/dx measurements better than 7.5% FWHM can be obtained (see ref.8).

In fig.19 the e-π and π-k separation (in units of standard deviations) is shown as a function of momentum.

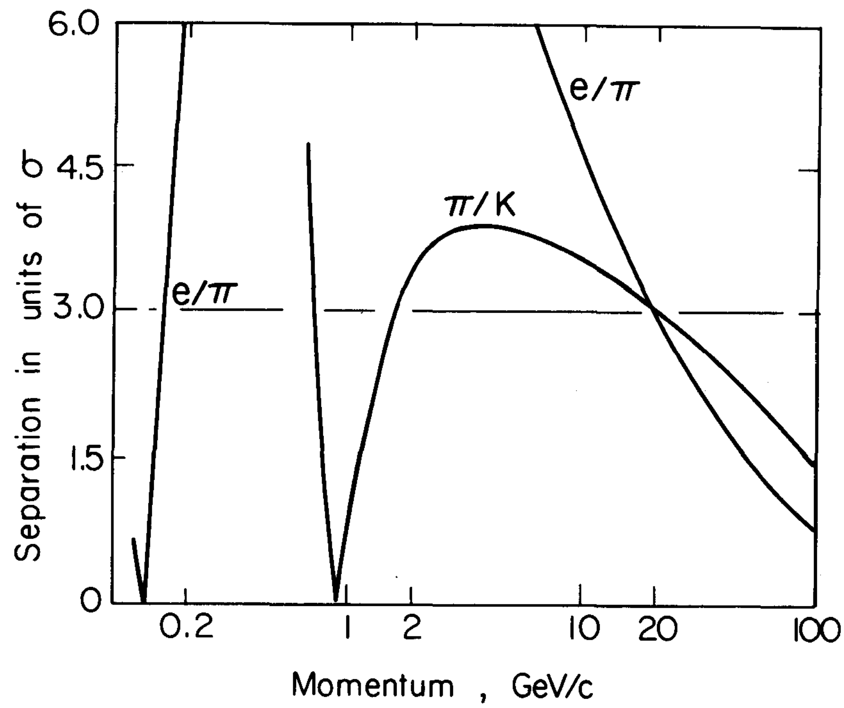

FIG.19

At a 3σ confidence level π-k separation is possible between 1.7 and 20 GeV/c, e-π separation up to 20 GeV/c. It should be noticed that the error on the momentum measurement in the angular region around 34^{o} (with respect to the proton) somewhat shrinks the range of particle separation at the highest momenta (ref.9).

5.4 Forward charged particle detector

A forward dipole with a set of drift chambers allows the measurement of energetic particles travelling near to the proton direction.

The magnet (fig.20) is clearly inspired by PEP-9 (ref.10). The magnetic field runs in opposite directions above and below the beams and returns to the main yoke by two iron wedges in the horizontal plane. The

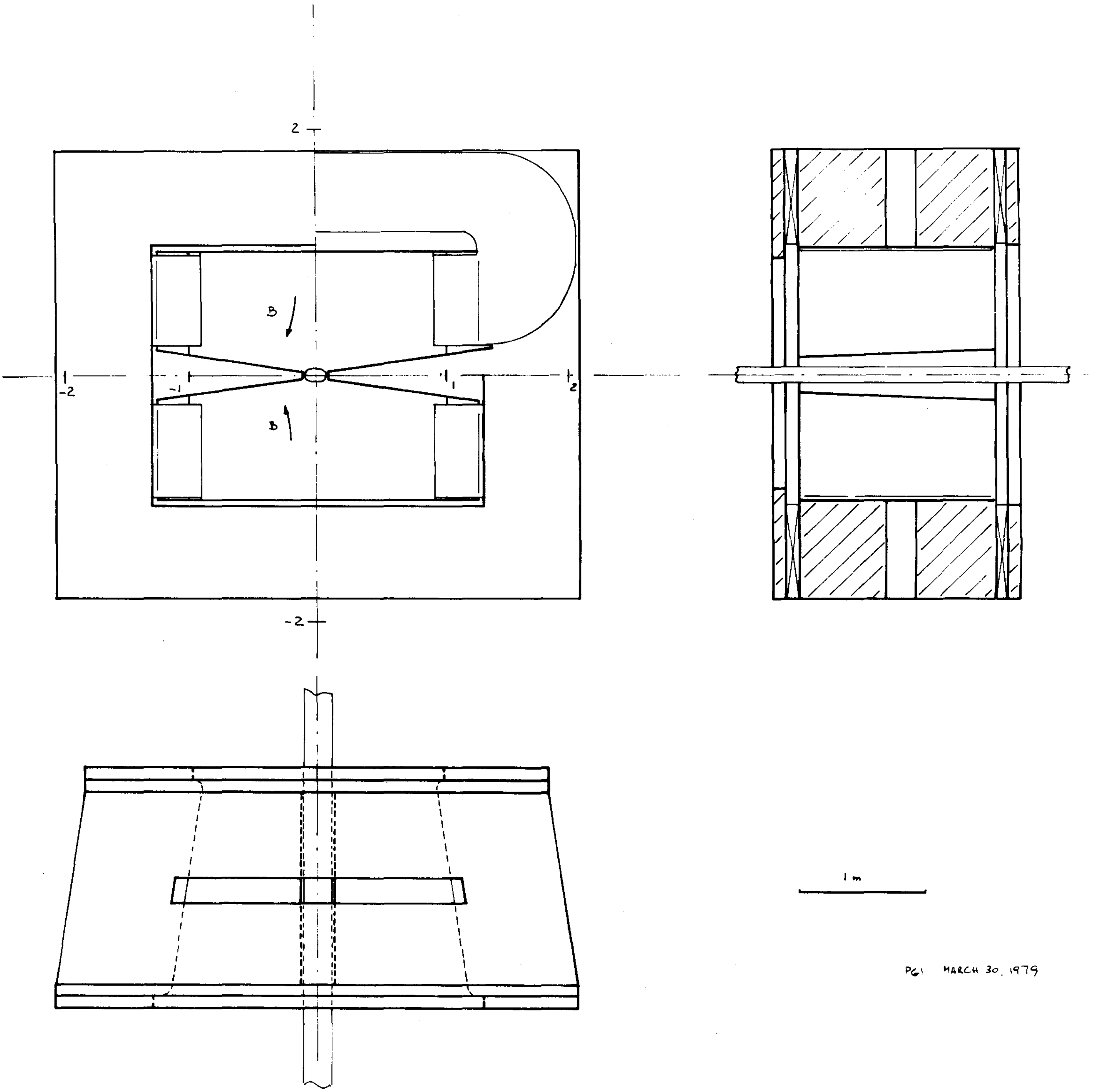

FIG.20

coils are folded back against the yoke and covered by shielding plates. By extrapolating from measurements on the magnet used by ISR experiment R603 (ref.11), the stray field can be kept below 0.01 T at 30 cm from the magnet end, for a central field of 0.5 T, which is possibly the upper limit compatible with adequate acceptance.

If one assumes a measuring error in the drift chambers of 200 μm and $\int Bdl = 0.75\ T{\cdot}m$, with the lever arm allowed by the central solenoid and a half interaction region of 7.5 m, the resolution shown in fig.17 can be obtained. For the smallest angles, the vertex position, known from measurements in the central detector, is used in the calculations.

5.5 Hadron calorimetry and muon detection

Although it is felt that hadron calorimetry by segmenting the magnet yoke represents a desirable feature, one should not neglect other detection possibilities in the central region. The solenoid iron return yoke could be built concentrated at the top and bottom of the central shower counter (fig.21) to allow the installation of other detectors on the open sides. Full calorimetry and muon detection could be added whenever needed, as shown in fig.22.

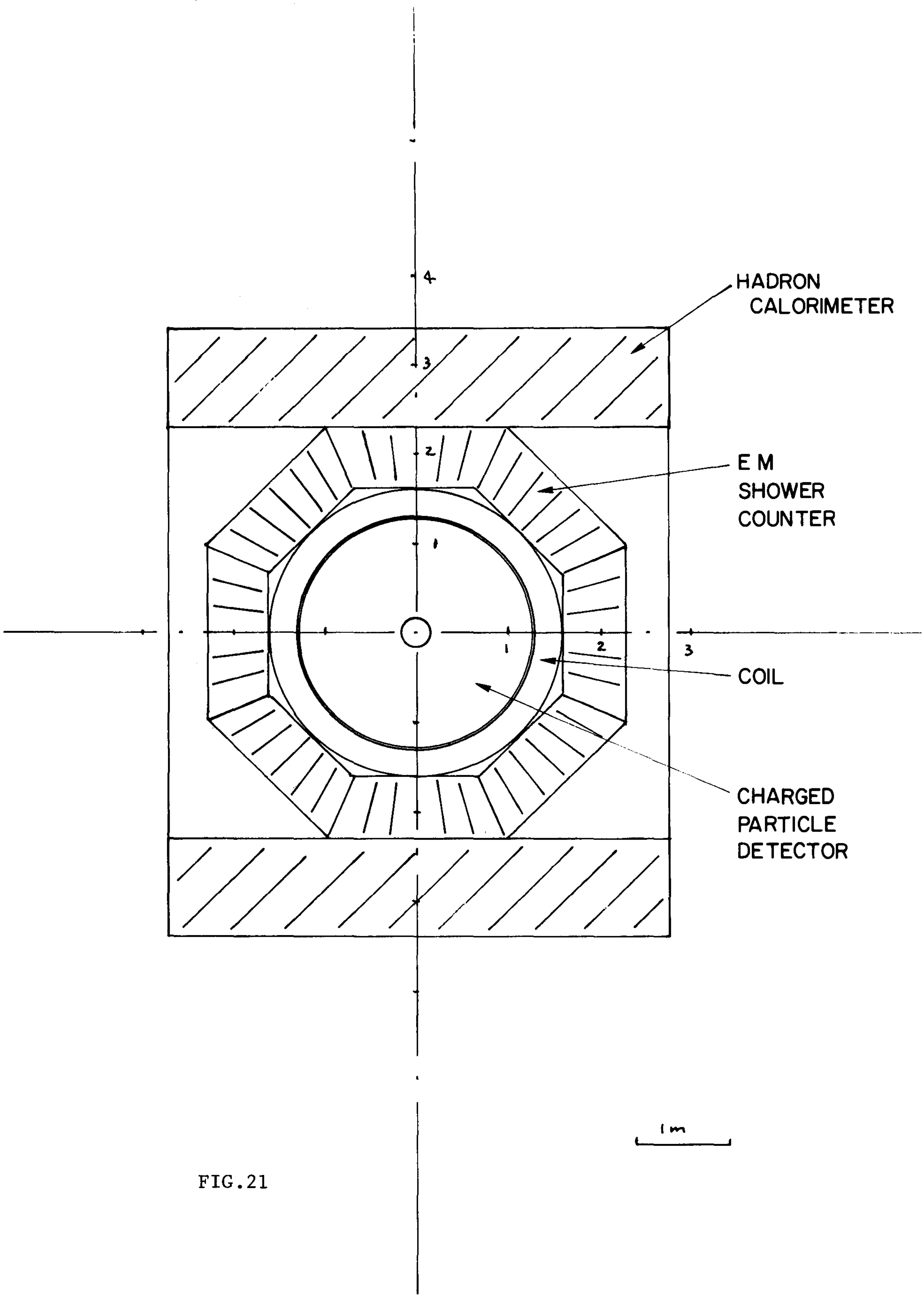
HADRON CALORIMETER
E M SHOWER COUNTER
COIL
CHARGED PARTICLE DETECTOR
1m

FIG.21

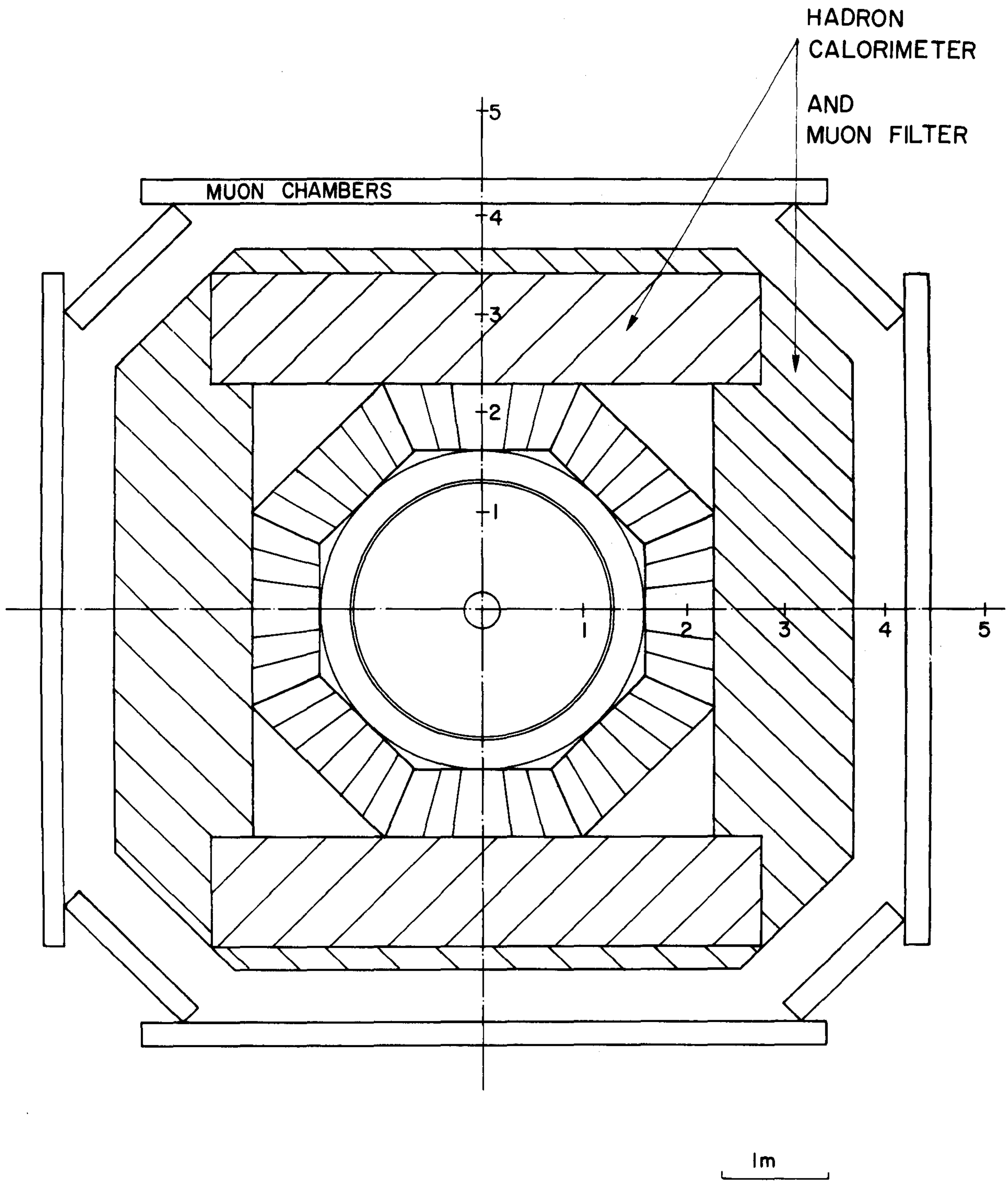
HADRON
CALORIMETER
AND
MUON FILTER
MUON CHAMBERS
5
4
3
2
1
1
2
3
4
5
Im

FIG.22

6. CONCLUSIONS

We have studied the detection problems connected with a variety of particle topologies.

We have ascertained that a magnetic charged particle detector and an electromagnetic shower counter combined permit carrying out a complete physics programme in inclusive measurements of the scattered electron, in the study of jet structure and in the search for new particles.

The detection techniques we have retained are rather conventional and give confidence that the detectors will perform as anticipated. However, a sizeable fraction of the physics of interest is limited by statistics and the quality of the results depends on the assumed luminosity and beam polarization.

REFERENCES

Ref.1 C.H. Llewellyn-Smith and B.H. Wiik; Physics with Large Electron-Proton Colliding Rings
DESY 77/38, June 1977

Ref.2 J. Ellis, B.H. Wiik and K. Hübner (editors); CHEEP; An e-p Facility for the SPS
CERN/78-02 February 1978

Ref.3 L. Camilleri (editor); The Physics Interests of a 10 TeV Proton Synchrotron, 400x400 GeV^2 Proton Storage Rings and Electron-Proton Storage Rings
CERN/76-12 June 1976

Ref.4 D. Hitlin et al.; Test of a Lead/Liquid Argon Electromagnetic Shower Detector
Nucl. Inst. & Meth. 137 (1976) 225-234

Ref.5 J.H. Cobb et al.; A Large Liquid Argon Shower Detector for an ISR Experiment
Nucl. Inst. & Meth. 158 (1979) 93-110

Ref.6 JADE; Proposal for a Compact Magnetic Detector at PETRA

Ref.7 PEP-4; Proposal for a PEP Facility based on the Time Projection Chamber, December 1976

Ref.8 - M. Aderholz et al.; High Resolution Ionization Measurements in the Region of the Relativistic Rise
Nucl. Inst. & Meth. 118 (1974) 419-430

- I. Lehraus; Particle Identification by Ionization Sampling in the Relativistic Rise Region
ECFA/LEP/SSG/11/11, March 1979

- A. Wagner; Particle Identification by Ionization Measurements in the LEP-JET Detector
ECFA/LEP 18, September 1978

Ref.9 B. Esposito; Some Considerations on Momentum Resolution
ECFA/LEP/78-36, September 1978

Ref.10 PEP-9; Proposal for a PEP Forward Detector Facility, December 1976

Ref.11 T.M. Taylor; Analyzing Magnet with Field-Free Channel for Use in the ISR
CERN/ISR-MA/TMT/rh August 1974

Foreword by convener (M. Holder):

I have left the discussion almost literally as it took place.

M. Holder/Hamburg

It looks now like there will be two seperate detectors, one for charged currents and one for neutral currents. I think, George Kalmus has made the remark already that if you would intend to do that, then you lose a nice calibration for the charged current events. In one type of event you have an electron and in the other you have a neutrino, but the remainder of the event should be the same. So eventually those two types of detector may merge into one.

T. Ekelöf/CERN-Uppsala

What is the strength of the magnetic field that you have used in your calculations? In work with the LEP jet detector it has turned out, that there is a great unbalance in the obtainable momentum resolution between charged and neutral particles when using superconducting magnets with a field strength of 15 kg. Did you use values as high as that?

P.G. Innocenti/CERN

I think we have been discussing fields in the level of 5 or 7 kGauss. But eventually we turned out to be rather ambitious.

U. Amaldi/CERN

I would like to comment on the fact that this new algorithm has been found in the other group for measuring x and y without knowing at all where the neutrino goes. That was I think a very big step forward in comparison with the CHEEP report. I think it has been proven by what you have seen in the previous talk, it works, but of course, now this could be used as a constraint when you have on top of that a measurement of electrons, so that you reduce the errors even further, because that will certainly mean that if you add a measurement of the electron, also if the angular resolution is not good, you can make a fit and can get better resolutions on x and y.

J. Rander/Saclay

I would like to comment that the technique to measure x and y only from the hadronic system's $E_H + P_{||}$ and $P_\perp^2$ outlined in the charged current discussion, can also be used here to look for new leptons. In neutral current events you have three ways of determing y, one by measuring the outgoing lepton, one by measuring the current jet direction, and the last from the new CC technique. As Turlay discussed, differences in the latter two methods can probe for heavy quark masses. I would like to point out that differences between the new method and the direct lepton measurement can probe for new lepton masses, even when there are missing neutrinos. It should be clear that if you want to take advantage of this effect, the neutral current detector should also be able to measure well $E_H + P_\perp$ and $P_{||}$ for particles outside of the proton jet.

M. Holder

Yes, I think that is very relevant. The fact that in the neutral current case the events are really overconstrained helps you very much to find out what is going on, especially for things, which you do not expect. You should see if there is something new.

A. Ali/DESY

I would like to make a comment on the comparison of $q\bar{q}$ gluon distribution in thrust with $b\bar{b}$. Somehow I have the impression that the message is being given that e^+e^- is not a good place to test QCD. It is based on a calculation on which I am one of the authors. It is a question which depends on the energy. It is true that near the treshold of the resonance, since the event is spherical, the QCD effect is very much subdued. But if you move away then simply because of the one photon production of all of these quarks, all these quarks and their decay products go in the forward direction. Consequently, if you are sufficiently far away from threshold the distributions from the heavy quarks become very steep and the QCD tail emerges once again. For instance for the case of $b\bar{b}$ it will correspond to a center of mass energy of 25 GeV.

The second point is that this is a calculation in which we have only studied total events in spherocity and thrust. But one could use other cuts e.g. one could look at planar events, because from the weak decays of heavy quarks most of the events are expected to be non planar. One could also look for leptons and exclude those events and look only on the hadronic events. I think these cuts on coplanarity and on the hadronic events would sufficiently suppress the contribution of heavy quarks in e^+e^- and therefore I suggest, sufficiently far away from the threshold e^+e^- is a very good laboratory to test QCD.

M. Holder

I thought that one of the very positive things for an ep machine is that it is a good laboratory for testing QCD. So I would very much appreciate, if some theoreticians could comment on that. If everybody says that QCD-tests are already made in e^+e^- then there is may be not such a big need to do them in ep. Now, I understand that it is not so obvious for the e^+e^- case because there you expect to cross new thresholds whereas in ep you have up and down quarks, and new thresholds are probably much less important.

U. Amaldi

In this connection I think that one should not forget that one of the ideas of e^+e^- is just to use this effect to find new thresholds. So you cannot have the cake and eat it. If you like to cut in sphericity or in thrust so that you find the new threshold, eventually this means that you cannot use same region to measure the quantum chromodynamic effects. Of course, we may hope that there are no masses above, let us say, 20 GeV and then you work so high that you are above this mass but if I remember correctly, calculations done here for the PETRA machine, show that if the mass of the top is 12 GeV and you sit at 15 GeV, which is 20% above, you still get 70% of the events with spherocity above 0.2, and that was the reason for which it has been decided to go to 15 + 15 GeV immediately with the machine here to discover possibly in the next weeks these particles . This means that these effects die very slowly with energy and so not to have to bother about threshold to me is a good argument.

G. Altarelli/Rome

Concerning the usefulness of an ep machine for testing QCD versus e^+e^-, I think it must be kept in mind that testing QCD quantitatively is a very difficult task, because there are many unknowns which come from the difference between partons and hadrons obscuring our way to disentangling the dynamics of the fundamental processes. So I think that confidence in QCD can only arise from a long systematic work that uses all possible sources of information. The information from the e^+e^- and the information from ep experiments are certainly both necessary for eventually getting to some solid statement. I think that there is no doubt that with only one kind of experiment we cannot reach a definite conclusion.

G. Preparata/CERN

I believe that what is very much interesting about these machines is to find new physics. I hope at that time however, problems which are more like aristotelic problems about whether quarks are confined or not, would be solved, and eventually QCD will disappear if it is not right. So I think we should really concentrate on the fact and look in history that this kind of machines have always, whenever they have opened a new regime in energy, opened new physics. We have to be open in finding new things if they are there. To concentrate on this kind of really aristotelian questions what will be the effect of QCD at q^2 equal to 2000 or 20 000 GeV^2, I find it neither interesting nor very much in the spirit of out enterprise.

D. Perkins/Oxford

I only wanted to answer in reply to Giuliano. I think it is the theorists who find QCD interesting. Experimentalists want to find the facts of the highest possible q^2.

J. Ellis/CERN

I would like to come back to the somewhat more mundane debate which we were engaged in earlier on, about whether it is possible to test QCD with e^+e^-. I must say that I agree with what Ahmed Ali said. In coming to this question of trying to distinguish heavy quark production from $q\bar{q}$-gluon production, it is clear you have two things you can cut on, one is a thrust type variable, another is an acoplanarity type variable. I think that the acoplanarity cut which Ahmed mentioned would be a very good way for example of beating down the bottoms. So, that is why I would agree with him. I also very strongly agree with what Altarelli said. It seems to me that the sort of measurements that you do with an ep-facility like this is just so totally different from what you do in e^+e^-. These are all checks that you have to make. If you like, physically, one is tearing apart the vacuum, the other one is tearing apart the proton. This machine would tear apart the proton 10 times more vigourously than anybody else has torn it apart. And this may be a basic physical reason for doing it. Another way of looking at it if you do not like that picture: the total cross section in e^+e^- is R, and the total cross section in ep is two structure functions which are functions of x and q^2. A lot of information is there, which is note quite the same.

DETECTOR IMPLICATIONS
FOR 100 GeV ELECTRONS AND 400 GeV PROTONS

P.G. Innocenti and H. Wahl, CERN

1. DETERMINATION OF STRUCTURE FUNCTIONS

The region accessible to experiments where the rate per day and intervals $\Delta x = 0.1$, $\Delta y = 0.1$ for a luminosity of $10^{32} cm^{-2} s^{-1}$ is still acceptable moves towards high Q^2 and low x by increasing s (see fig.1). The resolution on the cross section measurements improves as a consequence of the higher electron energy $(\frac{\sigma E}{E} \sim E^{-\frac{1}{2}})$, but the relative importance of the error on the scattering angle increases (see fig.2 to 5). An angular resolution better than 10 mrad is therefore desirable in particular in the region of low x and y where the expected rates are high and systematic errors would dominate.

2. OBSERVATION OF THE CURRENT JET

The angle of the current jet with respect to the proton direction becomes larger as the ratio of electron to proton energy increases. For values of $Q^2 \gtrsim 3000\ (GeV/c)^2$ in the x,y region where rates are measurable, the current jet is roughly perpendicular to the proton direction (see table 1). This feature favours an accurate study of the current jet as far as momentum and energy measurements and particle identification is concerned. Higher magnetic field and/or larger charged particle detectors should possibly be envisaged to cope with narrower jets and higher individual particle momenta.

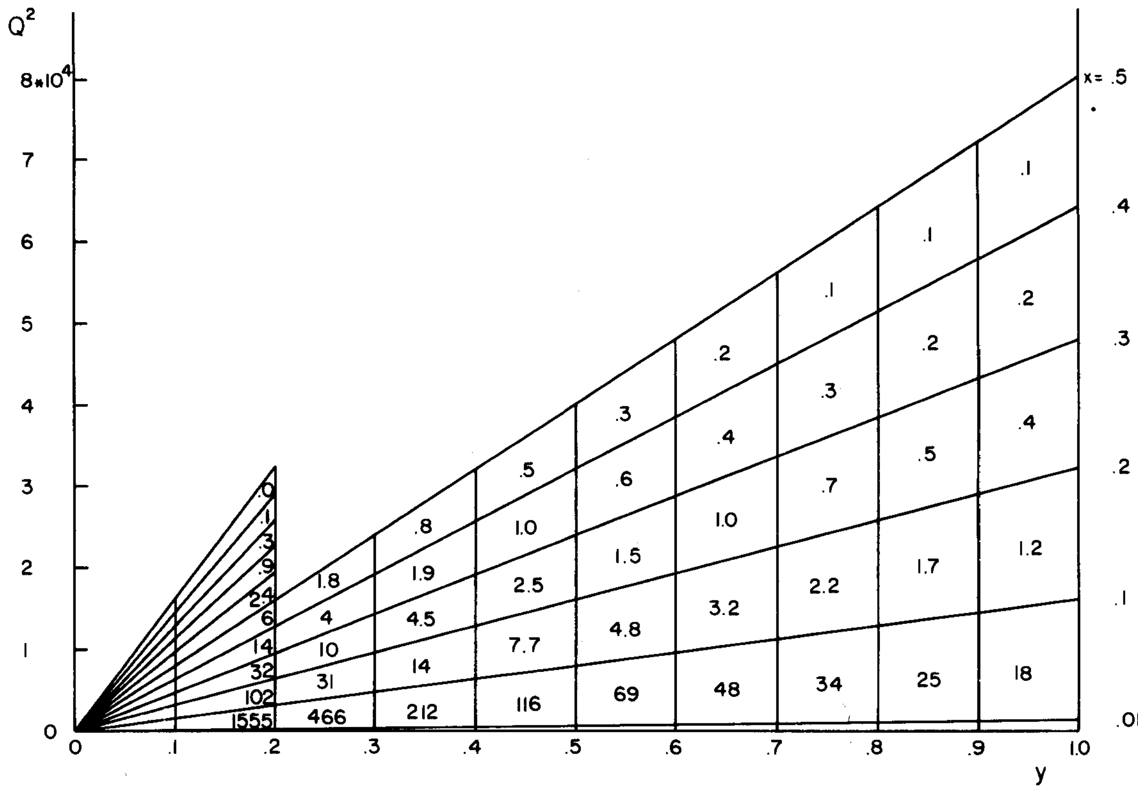

FIG.1

Events per day in $\Delta x \cdot \Delta y = 0.01$ for a luminosity $L = 10^{32} cm^{-2} s^{-1}$ at a CM energy $s = 160000\ (GeV)^2$

100 + 400 GeV

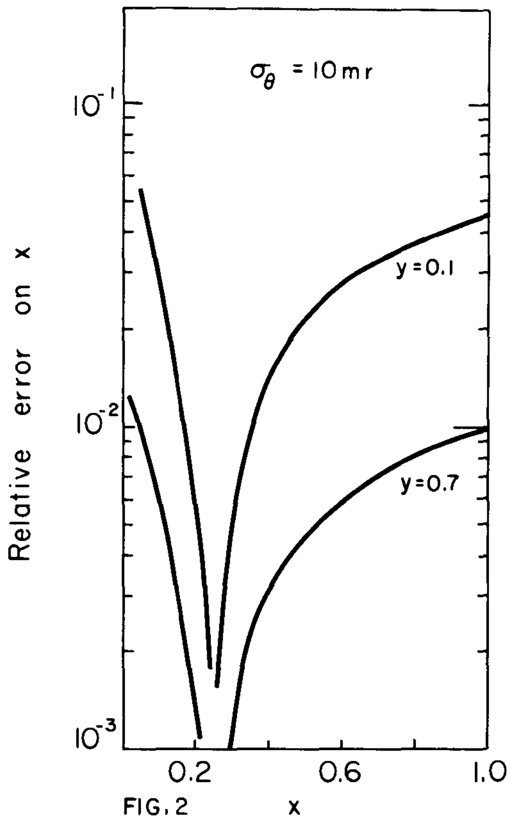

FIG. 2

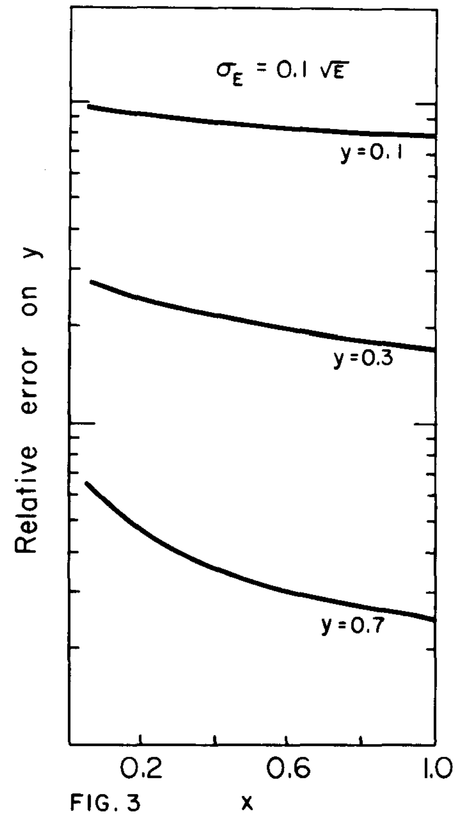

FIG. 3

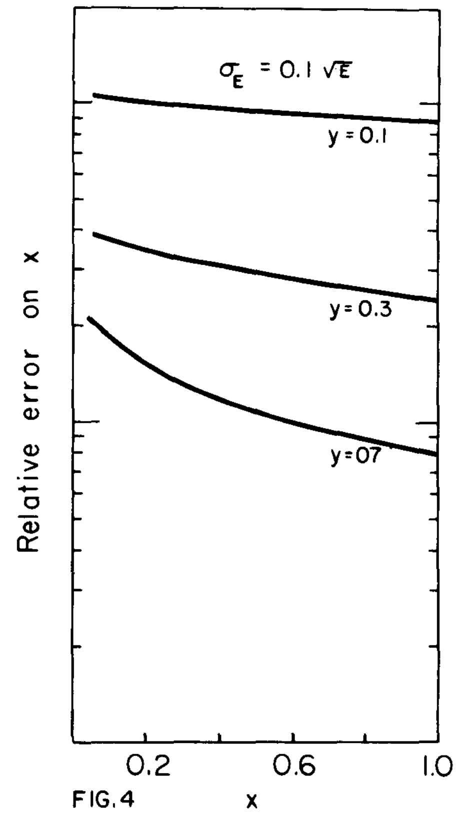

FIG. 4

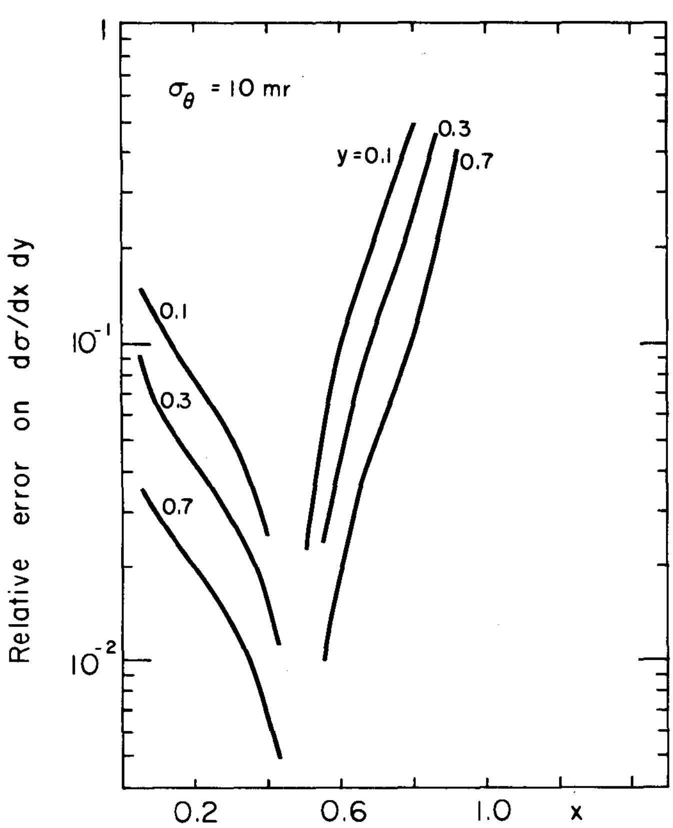

FIG. 5

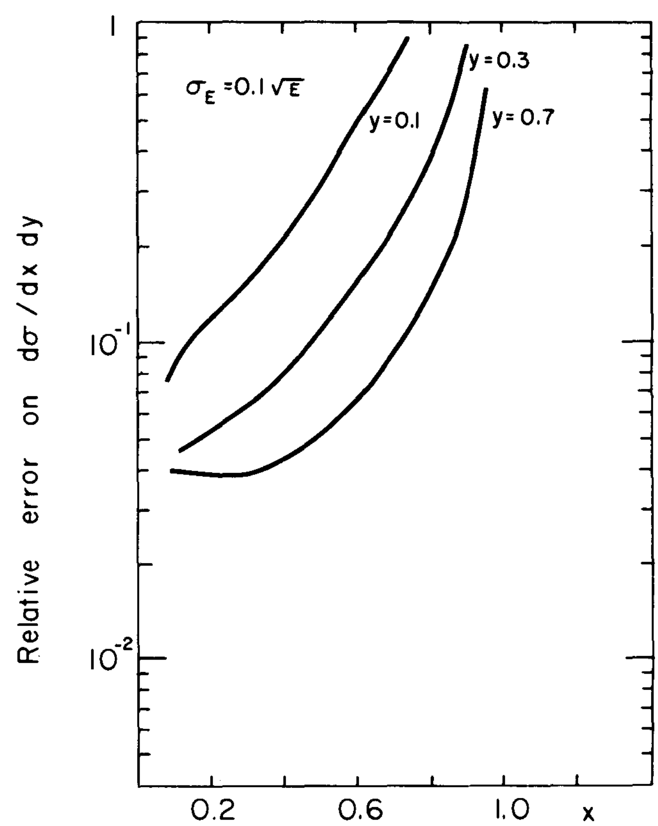

FIG. 6

TABLE I

x \ y		0.1	0.3	0.5	0.7	0.9
0.01	Q^2	160	480	800	1120	1440
	$E_{e'}$	90	71	52	33	14
	$\theta_{e'}$	8	15	23	34	62
	θ_J	62	34	23	15	8
0.05	Q^2	800	2400	4000	5600	7200
	$E_{e'}$	92	76	60	44	28
	$\theta_{e'}$	17	33	48	69	107
	θ_J	107	69	48	33	17
0.1	Q^2	1600	4800	8000	11200	14400
	$E_{e'}$	94	82	70	58	46
	$\theta_{e'}$	24	45	65	88	124
	θ_J	124	88	65	45	24
0.3	Q^2	4800	14400	24000	33600	43200
	$E_{e'}$	102	106	110	114	118
	$\theta_{e'}$	40	71	95	118	146
	θ_J	146	118	95	71	40
0.5	Q^2	8000	24000	40000	56000	72000
	$E_{e'}$	110	130	150	170	190
	$\theta_{e'}$	51	86	110	130	154
	θ_J	154	130	110	86	51
0.7	Q^2	11200	33600	56000	78400	100800
	$E_{e'}$	118	154	190	226	262
	$\theta_{e'}$	58	95	118	137	158
	θ_J	158	137	118	95	58
0.9	Q^2	14400	43200	72000	100800	129600
	$E_{e'}$	126	178	230	282	334
	$\theta_{e'}$	65	102	124	142	160
	θ_J	160	142	124	102	65

$e + p \to e' +$ current jet + proton jet at 100 + 400 GeV.

Kinematics of the scattered electron and the current jet

(Q^2 in GeV^2, $E_{e'}$ in GeV, θ (w.r.t. incoming electron direction) in degrees)

MONTE-CARLO EVENT GENERATION FOR THE e p COLLIDER

A.L. Grant

CERN, Geneva, Switzerland

In the design of any new experimental facility, especially one with the unusual kinematic configuration of the e p collider it is extremely useful to have samples of Monte-Carlo generated events to use to compare the performance of different detector layouts. To be useful the events must be unweighted, conserve all the usual quantities, energy, momentum, etc... and correspond as closely as possible to reality.

To extrapolate from the present experimental data to the energy and Q^2 range of the e p collider can only be done in a model dependent way. However, at present, there is no well defined prescription to define how a current will interact with the quarks of a proton, how these quarks will acquire a real mass as they move apart, and how they will fragment into the final hadrons.

In the present note, an attempt has been made to construct two models which might be expected to correspond to possible extremes of the configuration of the experimental data. The reality of the e p collider might be expected to lie between these two models.

In what follows experimental data taken from the present SPS neutrino experiments in the $Q^2 \sim 50\ GeV^2$ energy range, has been used whenever possible to define the parameters used in the model.

The generation of events is divided into three parts:

(a) Generation of the four vector of the scattered lepton and current.

(b) Fragmentation of the quarks after interaction into the final hadrons.

(c) Interaction of the current with the quarks of the proton to give an intermediate state of massive quarks moving apart prior to fragmentation.

This last part (c) is the least well defined by any theoretical prejudice and gives rise to the different possible models.

1. The method of generation of the direction and energy of the scattered lepton is well defined. The present program allows generation at fixed

$$X = Q^2/2\,m\nu \quad \text{and}$$
$$Y = (E_e - E_h)\,/\,E_T \qquad \text{or by one photon exchange.}$$

In this case the proton structure functions

$$xF_1(x) = F_2(x) = \sqrt{x}\,(1-x)^{3.5} \qquad \text{are used.}$$

This implies valence quarks only with no Q^2 dependence. Scattered leptons are generated according to the one photon exchange form:

$$\frac{d\sigma}{dxdy} = \frac{4\pi\sigma^2}{S.x^2y^2}\left\{ (1-y)F_2(x) + y^2x\;\; F_1(x) \right\}$$

A simple extension of the program would be to add the Buras and Gamers [1] parameterisation of the Q^2 dependence of the structure functions, also including the sea quarks. This already exists in a neutrino version of the same program.

2. In the program, fragmentation of the quarks follows the ideas current in QCD, and allows reasonable confidence in extrapolating the presently measured fragmentation functions D(Z), Z = h.q / p.q to higher values of energy and Q^2. The fragmentation functions used have the scale breaking Q^2 dependence and non factorisation behaviour seen in the present neutrino proton data of WA 21. Extrapolating the Q^2 dependence of the moments of the fragmentation functions of generated events yields a value of $\Lambda^2 = 0.73$ for the parameter in the strong

coupling constant.

In practice the hadron four vectors are generated by sampling experimental distributions in Feynman x_F, $x_F = p^*_{11} / p^*_{max.}$ and not Z, this is simply for reasons of technical convenience.

The tabulated correlation between x_F and $<P_T>$ and the form

$$f(P_T) = P_T / _{<P_T>} e^{-P_T / <P_T>}$$

are used to generate the transverse momentum of the hadrons in the quark direction. The distributions in x_F have a simple Gaussian form for different particle production at fixed charged particle multiplicity (independent of energy). From the WA21 data fits one made to

$$<x_F> = a \; N^{-b}$$
$$\sigma_{x_F} = c \; N^{-d}$$

the only energy dependence comes through the multiplicity, N

$$<N> = a + b \; \log S$$

and dispersion $D = c + d \; <N>$

The multiplicity distribution in N and D are given by a generalised Poisson distribution [2]. The mean number of π^o is taken from the tabulated correlation between N_{ch} and S.

This formalism has the feature that the moments of the x_F distributions and hence also the fragmentation functions D^n have a Q^2 and x dependence

$$D^n(Q^2, x) \; \alpha \; \left(\log \left(\frac{Q^2}{x}\right)\right)^{-b}$$

as expected from QCD.

3. The interaction of the current with the proton is handled by the program in two different ways giving rise to rather different models.

(a) The current acts on the whole proton without any consideration of its quark/parton structure. This method with the features 1) and 2) gives a naïve extrapolation of the present neutrino data to the kinematic region of the e p collider.

The result of the extrapolation is a back to back two jet structure in the CMS of the current-proton interaction which when transformed into the collider laboratory frame gives the expected structure of a target fragmentation jet going down the beam pipe and a well separated current jet.

In general the generated events tend to be rather simple and clear with no confusion at the vertex and two well separated jets.

(b) An attempt has been made to use a second model which introduces the point interaction of the constituants of the proton. The proton is assumed to consist of three valance quarks and a gluon cloud which carries some fraction of the proton momentum.

The quarks are given a small mass, 150 MeV and have a transverse motion, $\langle P_T \rangle \sim 500$ MeV/c. The quark which interacts with the current has momentum $x \cdot p^*$, $x = Q^2/2m\nu$ as before. p^* is the momentum of the proton in the current-proton CMS system. The remaining diquark system has the momentum

$$(1 - x)\ p^* \int F_2\ (x)\ dx$$

where $\int F_2(x)\ dx \approx 0.5$ is a measure of the fraction of the total energy of the proton carried by the valence quarks. The remaining energy of the proton

$(1 - x)\ p^*\ (1 - \int F_2(x)\ dx)$ can be thought of as the energy content of the soft gluon cloud. This energy is shared between the struck quark and the fragments giving these quarks an effective mass as the jet when the quark, diquark system fragments as described in 2). If as in the present program it is required that energy and momentum are conserved locally at each stage, the only freedom in the model is to change the fraction of the energy given to the two quark systems.

The generated events are rather different in character from those of the first model. They tend to be more complex, with higher multiplicity and have more soft hadrons causing confusion round the vertex in the collider system. Because of the high mass given to the jets originally, they tend to be slower in the current-proton CMS and hence after transforming to the collider frame the jets are not so well separated as in the previous model.

REFERENCES

[1] A. J. Buras and K. J. F. Gaemers, Nucl. Phys. B 132 (1978) 249.
[2] O. Czyzewski and K. Rybicki, Nucl. Phys. B 47 (1972) 633.

Report prepared by M. Holder

The members of the working group were:

G. Coignet, J. Drees, A. Grant, H. Grote, M. Holder,+)
P. G. Innocenti, K. Kleinknecht, V. Korbel, K. H. Mess,
H. E. Montgomery, R. P. Mount, P. R. Norton, W. Scott,
D. Schlatter, J. Steinberger, H. Wahl, P. Weilhammer,
H. Wenninger, P. L. Woodworth

The group had three meetings spread between December 1978 and March 1979. Most of its members wanted to concentrate their studies on the topics of structure functions and final states in deep inelastic scattering. The study of a detector for quasi photoproduction events, which also falls in the category of neutral current events, was left to the working group specializing on this subject.

The physics interest of an ep collider is well documented in recent reports[1)]. Some points which were studied in more detail by members of the working group or which may have practical consequences for the machine design are mentioned in the following paragraphs.

A topic of great interest is the interference between weak and electromagnetic interactions, which can only be studied with polarized beams. The Q^2-dependence of the interference term provides probably the most sensitive measurement of the Z_0-mass - if such a particle exists - in this type of experiments. For a complete determination of coupling constants one needs

---

+discussion leader

polarized electrons and positrons of both helicities. If switching from right- to left-handed particles cannot be done without major changes (as e.g. reversal of beam direction), the measurable effect may be reduced to the difference in rate between polarized and unpolarized beams, which is a factor 2 less than the difference between beams of opposite helicities.

Another problem with implications on the machine is the separation between longitudinal and transverse structure functions. It requires running at different beam energies. A study of the accuracy which can be achieved is contained in the talk of P. G. Innocenti. There are various good reasons to anticipate running also with deuterons, as discussed in detail in Ref.3.

The measurement of structure functions is in principle a single arm experiment, and it is conceivable that an experiment which concentrates on a very precise electron measurement, both in energy and angle, is best suited for that purpose. Especially the energy measurement, best done with a calorimeter technique, may suffer from material in the path of the electron.

An important question which has not been settled at the time of this writing, but on which work is in progress at Wuppertal[4)] concerns the radiative corrections. The range in Q^2 accessible to an ep collider is so much extended compared to existing experiments that a careful analysis of the problem is indicated. Eventually there may be consequences for the design of the experiment.

There are various motivations for looking at the particles in the final state. On the one hand one may expect to produce new particles by crossing kinematic thresholds. New quarks, for example, will have a tendency to be produced at small x, where their decay products appear with relatively low energies at large angles to the beams. To measure them one needs a central magnetic detector.

Also the ordinary fragments of the quark involved in the primary collision will appear at relatively large angles, provided the Q^2 is large. Quark fragmentation is a topic which may be important for the understanding of strong interactions, as much as the structure functions in deep inelastic scattering are. Very little is known at present in the region of Q^2 above several GeV^2. The standard theory predicts quite a dramatic increase of the transverse momenta with Q^2 due to gluon bremsstrahlung. In neutral current events the total momentum of the final state is well known from a measurement of the scattered electron; so these events may be the ideal place to study quark fragmentation over the largest possible range in Q^2.

These considerations called for a magnetic detector which measures particles over a large range of angles and momenta. The choice of a central solenoid was made under the assumption that a dipole field is forbidden because of the problems associated with synchrotron radiation.[5)] A toroidal field was not considered because of obstructions in the way of particles. There was, however, not enough time to check the arguments in detail.

No effort was made to detect the so called target fragments which have very small angles to the proton beam. Their total transverse momentum should be close to zero. This can be checked by comparing the transverse momentum of the scattered electron and the sum of the transverse momenta of the hadrons observed at large angles, which should balance. It may be appropriate to recall here, that the kinematics, i.e. Q^2 and ν as given by a measurement of the scattered electron, specifies only the invariant mass of the total hadronic system. The way in which this mass is distributed among the final state particles is a question of dynamics. Various models which are consistent with present knowledge differ in their predictions. The models which have been used in this study are described in Ref.6. The fast that Q^2 and ν can be measured both from the electron and from the hadrons gives an important consistency check on the hadron measurements.

How these constraints can be used in practice is a question of precision and acceptance. A detector was sketched with the idea of maximizing both, but the implications for the physics results could not be worked out in detail in the given time.

On the subject of particle identification no new ideas have emerged. The physics interest is probably chiefly to separate K from π and e or μ from π in the decay of new quarks or new leptons. As already mentioned, this implies particle identification over a large solid angle in a momentum range where the relativistic increase of ionization in gases can be used, as far as e/π or K/π separation is concerned. Of course, particle separation is only possible if the track density is lower than the granularity of the detector. With present day technology one may be able to achieve separation for a major fraction of the particles even in high energy jets.

Open Problems

Apart from physics and detector questions which were left open, and which are mentioned in the previous section, there is an important item which was not covered by the working group: the interaction with the machine. Among the relevant subjects are: schemes for polarized beams, provisions for running at different energies, compensator magnets, minimization of synchrotron radiation problems, size and shape of the vacuum chamber, the vacuum in the intersect and further upstream, luminosity measurements, optimisation of the length of the intersection region, consequences of an eventual asymmetry of the detector along the electron and proton directions.

REFERENCES

1. C. H. Llewellyn-Smith, B. H. Wiik
   Physics with Large Electron-Proton Colliding Rings, DESY 77/38
   J. Ellis, B. H. Wiik and K. Hübner (editors)
   Cheep, An e-p Facility in the SPS, CERN 78-02

2. E. Dasskowski, D. Kohaupt, K. Steffen, G. A. Voss
   An e-p Facility at PETRA, DESY 78/02

3. G. Coignet

4. J. Drees, private communication

5. H. F. Hoffmann
   Interaction of the Synchrotron Radiation with the Proton Beam in the LSR ep Interaction Region, and references therein, in CERN 76-12 ed. by L. Camilleri

6. A. L. Grant, Monte Carlo event generation for the ep collider, p.463